

The Evaluation of Groundwater Resources in the
Crystalline Basement of Northern Nigeria

R. IAN ACWORTH

Thesis submitted for the degree of
Doctor of Philosophy
to the faculty of Science and Engineering
The University of Birmingham

Department of Geological Sciences
May 1981

UNIVERSITY OF
BIRMINGHAM

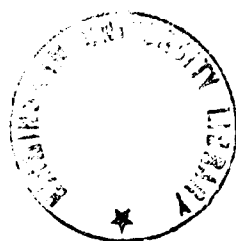
University of Birmingham Research Archive

e-theses repository

This unpublished thesis/dissertation is copyright of the author and/or third parties. The intellectual property rights of the author or third parties in respect of this work are as defined by The Copyright Designs and Patents Act 1988 or as modified by any successor legislation.

Any use made of information contained in this thesis/dissertation must be in accordance with that legislation and must be properly acknowledged. Further distribution or reproduction in any format is prohibited without the permission of the copyright holder.

1272086



ACKNOWLEDGEMENTS

I would like to thank my colleagues at Water Surveys (Nigeria) Ltd., for their help and encouragement during the early part of this work in Nigeria. In particular, Robin Hazell, Bruce Misstear, Richard Carter and Maryla Carter gave much valuable assistance. Much of the field work would not have been accomplished without the assistance of Shade, Sule, Bayo, Nat and Edward.

I would also like to thank in particular, Dr. J.W. Lloyd for his help and constructive criticism throughout the project. Thanks are also due to Professor D.H. Griffiths and Dr. R.F. King for their constructive criticism of the geophysical analysis.

I would like to acknowledge the considerable assistance of the Birmingham University Computer Centre staff throughout the latter part of this study.

Thanks are also due to Mrs. K. Walker for her interpretation of my written script.

I would also like to thank my wife for her help and continuous encouragement throughout a project which has taken a disproportionate amount of my spare time during these last five years.

Synopsis

A methodology of assessment is presented of the groundwater resources available in fracture zones, within the weathered mantle of gneiss, migmatite and granite. A model of weathering is developed, and values of porosity, hydraulic conductivity and electrical resistivity assigned to the different grades of weathering. A geophysical technique is developed, based upon a combination of electrical resistivity profiling and sounding, which allows a volume estimate of the various weathering grades to be made. A finite difference algorithm is used for this estimate which enables the apparent resistivity response of an inhomogeneous resistivity distribution to be calculated. An iterative approach is then adopted, adjusting the resistivity model until the calculated response agrees with the field data.

An analysis of recharge in a savanna climate is developed based upon the Monteith equation for predicting evapotranspiration, and upon a model of unsaturated zone soil moisture movement. The recharge function developed is included in a one dimensional catchment water balance model. The results from this model are compared with observed runoff and groundwater hydrographs.

The estimate of recharge is combined with the estimate of aquifer storage to produce an assessment of available groundwater. Optimal methods for the development of the resource are discussed. While developed in Northern Nigeria, the methodology of assessment is applicable to any similar geological and climatological environment.

CONTENTS

	Page No.
Acknowledgements	
Synopsis	
List of Figures	I
List of Plates	IV
List of Tables	VI
1. INTRODUCTION	1
1.1 Research Location	5
1.2 Savanna Environment	
Introduction	7
Climatic characteristics	7
Savanna vegetation	8
1.3 The Hydrogeological Problem	
Introduction	9
Method of analysis adopted	10
1.4 Previous Research	
General	11
1.5 Available Information	
General	12
Remote sensing data	12
Sidelooking airborne radar	12
Aerial photography	12
Climate data	12
Geological data	13
2. CLIMATIC ENVIRONMENT	
Introduction	14
2.1 Atmospheric Circulation over West Africa	
General	17
The Intertropical Convergence Zone	20
Recent developments	23
2.2 Rainfall	
General	26

Rainfall mechanisms	26
Squall lines	30
Rainfall distribution in space	32
Rainfall distribution in time	38
Energy load of rainstorms	46
2.3 Solar Radiation Balance	
General	48
Solar radiation	49
Dispersion of solar radiation	52
Assessment of albedo	53
Calculation of net radiation	54
Temperature distribution	64
2.4 Evaporation and Evapotranspiration	
General	68
The calculation of evaporation	68
Sensitivity of the evaporation calculation	75
Estimate of evaporation	80
The calculation of evapotranspiration	84
Evapotranspiration results	87
2.5 Summary	94
3. GEOLOGICAL ENVIRONMENT	
Introduction	96
3.1 General Geology	99
3.2 Jointing and Fracturing	
Definitions and method of formation	102
Origin of joints	102
Pressure release joints	103
Depth of jointing	105
3.3 Weathering Gneisses, Migmatites and Granites	
General	107
Weathering processes	107
Chemical weathering	109
Constant volume weathering	114
Deep weathering profiles	117
Groundwater chemistry	122

3.4	Deep Weathering Model	
	General	125
	Definition of terms	125
	Grade I - fresh	128
	Grade II - slightly weathered	128
	Grade III - moderately weathered	129
	Grade IV - highly weathered	130
	Grade V - completely weathered	130
	Grade VI - residual soil	131
3.5	Deep Weathering Examples from N. Nigeria	
	General	133
	Basement evolution	133
	Deep weathering - example A	139
	Deep weathering - example B	139
	Deep weathering - example C	143
3.6	Soil Characteristics	
	General	145
3.7	Summary	148
4.	GEOPHYSICAL INVESTIGATION TECHNIQUES	
	Introduction	151
4.1	Electrical Resistivity Theory	
	Introduction	155
	Electrical conduction in the weathering environment	155
	Theory of current flow	157
4.2	Electrical Resistivity Profiling	
	Introduction	160
	Theoretical considerations	160
	Resistivity profile results	165
	Field method	167
	Data processing	170
	Electromagnetic profiling	170
	Summary	174
4.3	Electrical Resistivity Sounding	
	Introduction	175

	Page No.
Theoretical considerations	175
Resistivity sounding results	176
Summary	181
4.4 Electrical Resistivity Profile Sections	
Introduction	182
Resistivity profile sections	182
Finite difference algorithm	183
Description of algorithm graphical output	185
Description of profile section field method	186
Offset profiling	187
Profile section field data	190
Summary	198
4.5 Seismic Refraction Techniques	
General	202
Weathering grade seismic velocities	203
Seismic refraction results	204
Discussion	212
4.6 Summary	213
5. AQUIFER GEOMETRY AND CHARACTERISTICS	
Introduction	215
5.1 Description of the Aquifer	
General	217
Weathering grade porosities	218
Weathering grade hydraulic conductivities	218
Aquifer boundaries	220
5.2 Groundwater Hydrographs	
General	224
Records available	224
Description of the hydrographs	226
5.3 Recharge Mechanisms	
Introduction	230
Soil moisture characteristics	230
Soil moisture potential	235
Root constants	240

	Page No.
Conventional recharge analysis	243
Assessment of conventional analysis results	244
Model of recharge used for study	249
Assessment of model analysis results	257
5.4 Aquifer Response to Abstraction	
Introduction	260
General	260
Pump test results	261
Example (1)	262
Example (2)	262
Example (3)	263
Example (4)	265
Pump test interpretation	269
Pump test design	270
5.5 Summary	271
6. RESOURCE ASSESSMENT	
Introduction	274
6.1 Resource Distribution	
General	276
Importance of recharge areas	276
Resource location	278
6.2 Size of the Resource	
General	280
Apparent resistivity profiling results	280
Apparent resistivity profile section results	281
6.3 Small Catchment Water Balance	
Introduction	285
Description of the model	285
Initial conditions	288
Observed water balance results	290
Presentation of model results	292
Results for Bauchi during the period 1969-1974	293
Model sensitivity to changes in root constant	298

Model sensitivity to changes in specific yield	299
Specific yield assessment	301
6.4 Assessment of Annual Yield	
Introduction	304
Observed borehole yields	304
Assessment of storage required	304
Assessment of recharge area required	305
Annual yield	306
6.5 Resource Assessment	
Introduction	308
Abstraction by dug well	308
Abstraction by boreholes	309
6.6 Further Research Required	
General	312
Data collection	312
Hydrochemical study	313
Geophysical study	314
CONCLUSIONS	315
REFERENCES	
Appendix A - Evaporation + evapotranspiration algorithm	
Appendix B - Description of borehole samples	
Appendix C - Resistivity profile section algorithm	
Appendix D - Travel time data from seismic refraction surveys	
Appendix E - Description of the water balance algorithm	

List of Figures

Figure Number		Page No.
1.1	Map of Nigeria showing location of towns referred to in the text	2
1.2	Geological map of Nigeria showing areas of crystalline basement + structure	3
2.1	Hadley cell circulation	18
2.2	Schematic cross section of the atmosphere	18
2.3	Diagrammatic vertical section of air circulation within the ITCZ	22
2.4	ITCZ cloud system as observed during GATE - 10 July 1974	22
2.5	Streamline analysis - September 7 - 1974	25
2.6	Streamline analysis - Day 240 - 1974	27
2.7	Cloud cover - Day 240 - 1974	28
2.8	Cloud cover - Day 182, 1974	28
2.9	Streamline analysis - Day 182 - 1974	29
2.10	Rainfall in the Gombe Area - 22 April, 1978	31
2.11	Rainfall stations in the Gombe Area	33
2.12	Annual total rainfall - Gombe Area	39
2.13	Annual rainfall totals at Bauchi	40
2.14	Annual rainfall - Bauchi, normal probability distribution	41
2.15	24 hour rainfall - August 21, 1978, Gombe	44
2.16	24 hour rainfall - October 29, 1978, Gombe	45
2.17	Spectral distribution of incoming radiation	49
2.18	Spectral distribution of outgoing radiation	49
2.19	Rainfall and evaporation summary - Bauchi, 1973	72
2.20	Rainfall and evaporation summary - Bauchi, 1974	73
2.21	Rainfall and evaporation summary - Bauchi, 1979	74
2.22	Evaporation sensitivity to observed sun hours	76
2.23	Evaporation sensitivity to average temperature	77
2.24	Evaporation sensitivity to relative humidity	78
2.25	Evaporation sensitivity to wind speed	79
2.26	Evaporation sensitivity to incoming radiation	81
2.27	Estimates of evapotranspiration	89
2.28	Monteith evapotranspiration	90

Figure No.		Page No.
3.1	Deep weathering profile from the Jos Plateau	11 ^o
3.2	Semi quantitative estimates of minerals in the clay, silt and sand fractions	121
3.3	Weathering grades	127
3.4	Schematic cross section along a weathering trough	140
4.1	Electrode configurations described in the text	162
4.2	Map showing apparent resistivity contours over a part of deep weathering area A	166
4.3	Map showing apparent resistivity contours over a part of deep weathering area B	168
4.4	Tripotential profile data	171
4.5	Alpha profile and EM31 data across deep weathering area A	173
4.6	Tripotential sounding results	177
4.7	Family of sounding curves produced by varying fourth layer depth	180
4.8	Offset profiling electrode configurations	188
4.9	Resistivity profile section - Area A	192
4.10	Resistivity model for profile section - Area A	193
4.11	Resistivity profile section - D	194
4.12	Resistivity model for profile section - D	195
4.13	Resistivity profile section - Area B	196
4.14	Resistivity model for profile section - B	197
4.15	Tripotential profile data produced by resistivity distribution shown in Figure 4.16	199
4.16	Near surface lateral inhomogeneity	200
4.17	Seismic refraction profile 1	206
4.18	Seismic refraction profile 2	207
4.19	Seismic refraction profile 3	210
4.20	Seismic refraction profile 4	211
5.1	Conceptual model showing porosity and hydraulic conductivity changes with depth	219
5.2(i)	Sketch sections showing various hydrogeological environments	219
5.2(ii)		222
5.3	Borehole No. 10 hydrograph (Area A)	225
5.4	Rainfall and borehole hydrographs at Samaru	227
5.5	Dimensions of a uniform soil block	232
5.6	Typical pF curves for a savanna soil	232
5.7	Modification of evapotranspiration when soil moisture is limiting	242
5.8	Soil moisture changes for various drying curves	242

Figure No.		Page No.
5.9	Seasonal changes in soil moisture potential	250
5.10	Flow diagram for water balance algorithm	255
5.11	Pump test recovery data	264
5.12	Pump test drawdown and residual drawdown data for three boreholes in the Bauchi area	266
5.13	Pump test drawdown and residual drawdown data	267
5.14	Drawdown and residual drawdown data for three pumping rates	268
6.1	Isometric diagram to illustrate relationship between recharge areas and a weathering trough	277
6.2	Profile section results over a narrow weathering trough	283
6.3	Development of laterite over section similar to that in Figure 4.9	284
6.4	Water balance model conditions during early dry season	287
6.5	Water balance model conditions during the early wet season	289
6.6	Water balance at Bauchi 1969-1970	294
6.7	Water balance at Bauchi 1971-1972	295
6.8	Water balance at Bauchi 1973-1974	296
6.9	Sensitivity of the predicted groundwater hydrograph to changes in the specific yield value	300
6.10	Water balance at Bauchi 1978-1979	302
6.11	Basement borehole design	311

List of Plates

Plate No.		Page No.
2.1	Nigerian Government Meteorological Station - Bauchi	59
2.2	Gunn Bellani distillator - Bauchi	59
2.3	Crop residue and nearby grass cover burnt surface	66
2.4	Woodland in December showing results of firing	66
2.5	Type A evaporation pan at Bauchi	83
2.6	Dry season land surface close to Bauchi	83
3.1	A typical migmatite from the area of Bauchi	101
3.2	A meta-sedimentary relict within migmatite	101
3.3	Inselberg of migmatite at Gubi, close to Bauchi	104
3.4	Enlargement of 3.3	104
3.5	Spheroidal boulders formed by weathering	108
3.6	Outcrop of grus in road cutting	111
3.7	Grade V weathering material	132
3. ^p	Grade III, IV and V material in road cutting	132
3.9	SLAR image of Bauchi Area	136
3.10	Older granite outcrop	137
3.11	Older granite inselberg	137
3.12	Gneiss showing folding and intrusion	138
3.13	Dyke cutting edge of older granite inselberg	138
3.14	Deep weathering - example A location	141
3.15	Deep weathering - example B location	141
3.16	Drill cuttings from deep weathering area B	142
3.17	Extensive grade V + VI material from deep weathering area C	142
3.18	} Drill samples from deep weathering area C	144
3.19		
3.20	A weathering profile close to Kano	147
3.21	A weathering profile close to Kano	147
4.1	Investigation borehole core in deep weathering area C	209

List of Tables

Table Number		Page No.
1.1	Typical borehole characteristics from a granite area of South Africa	9
2.1	Cross correlation matrix for G.A.D.P. rainfall station - 1978 rainy season	35
2.2	Correlation between daily rainfall at Gombe CAP and other stations - 1978 April-October	36
2.3	Daily rainfall for July 1978 at 17 stations in the Gombe area (mm)	37
2.4	Annual rainfall (mm) 1946-54 for two Tanzanian stations (after Jackson (1978))	36
2.5	Average monthly and 10 day rainfall for Bauchi 1941-1979	38
2.6	Seasonal variations of solar radiation outside the atmosphere at latitude 10° 30' N - Bauchi	51
2.7	Dispersion of solar radiation	52
2.8	Albedo of some typical surfaces	53
2.9	Albedo of maize and millet crops at Samara	54
2.10	Average daily radiation at Samaru	56
2.11	Measured and calculated values of net radiation	58
2.12	Monthly correlations between calculated net radiation and Gunn-Bellani data for Bauchi	60
2.13	Correlation between net radiation, sunshine hours and vapour pressure for 1978	61
2.14	Calculated monthly net radiation for varying albedo	62
2.15	Monthly variation in albedo	62
2.16	Rn for different Angstrom equation values	63
2.17	Average monthly net radiation for Bauchi	64
2.18	Distribution of net radiation components	65
2.19	Evaporation totals for Bauchi	71
2.20	Correlation between Piche data and the aerodynamic term in Penman's equation	82
2.21	Relation between soil cover % and diffusion resistance to water dependent upon fraction of soil covered	86
2.22	Penman evapotranspiration for a surface with constant albedo, compared with an albedo varied to reflect the seasonal changes	
2.23	Modified Penman equation Zo values	87

2.24	Values of Rs used in the Monteith calculation	91
3.1	Selected physio-chemical properties of a deeply weathered profile in Malaysia	120
3.2	Analyses of groundwater from the North Nigerian Basement Complex	123
3.3	Generalised geochronology for the metamorphic rocks of Nigeria	134
4.1	Tripotential profile results over a fracture zone shown in Figure 4.4	169
4.2	Resistivities of weathering grades	178
4.3	Inferred depth of weathering from sounding data	179
4.4	Potentials due to a point source of current	191
4.5	Seismic velocities of weathering grades	204
5.1	Rainfall and hydrograph data	228
5.2	Bulk density and porosity of three soil profiles from Afaka forestry reserve, near Kaduna	233
5.3	Range of available water in two ferruginous soils developed under natural conditions at Afaka	237
5.4	Values of matrix potential at various soil water conditions	238
5.5	Hydraulic conductivity and matrix potential for a soil with varying volume water content	239
5.6	Water budget for Bauchi (1979) using data from Table 2.22	245
5.7	Effects of surface treatment on profile water loss during the dry season	
5.8	Maximum soil moisture deficit for various plant canopies	251
5.9	Comparison of recharge results for 1979	258
5.10	Predicted annual recharge	259
5.11	Geological log of test well	263
6.1	Areas of weathering grades calculated from resistivity profile sections	281
6.2	Water balance for the Samara catchment	291
6.3	Comparison of Samara and Bauchi data	297
6.4	Sensitivity of water balance to changes in the root constant	298
6.5	Sensitivity of water balance to changes in specific yield	299
6.6	Observed and predicted values for the Bauchi groundwater hydrograph shown in Figure 5.3	303
6.7	Recharge for a root constant of 150 mm	

1. INTRODUCTION

The object of this thesis is to make a general assessment of the available groundwater resources from an area of Precambrian and Early Palaeozoic basement complex rocks in Northern Nigeria. The area of particular reference for this study is that of Bauchi in North East Nigeria, however, the analysis is also believed to be generally applicable to any region with a similar geological and climatological environment. In the final section of the thesis the results of the work around Bauchi are summarised and a generalised methodology of approach described for the evaluation of groundwater resources in this environment.

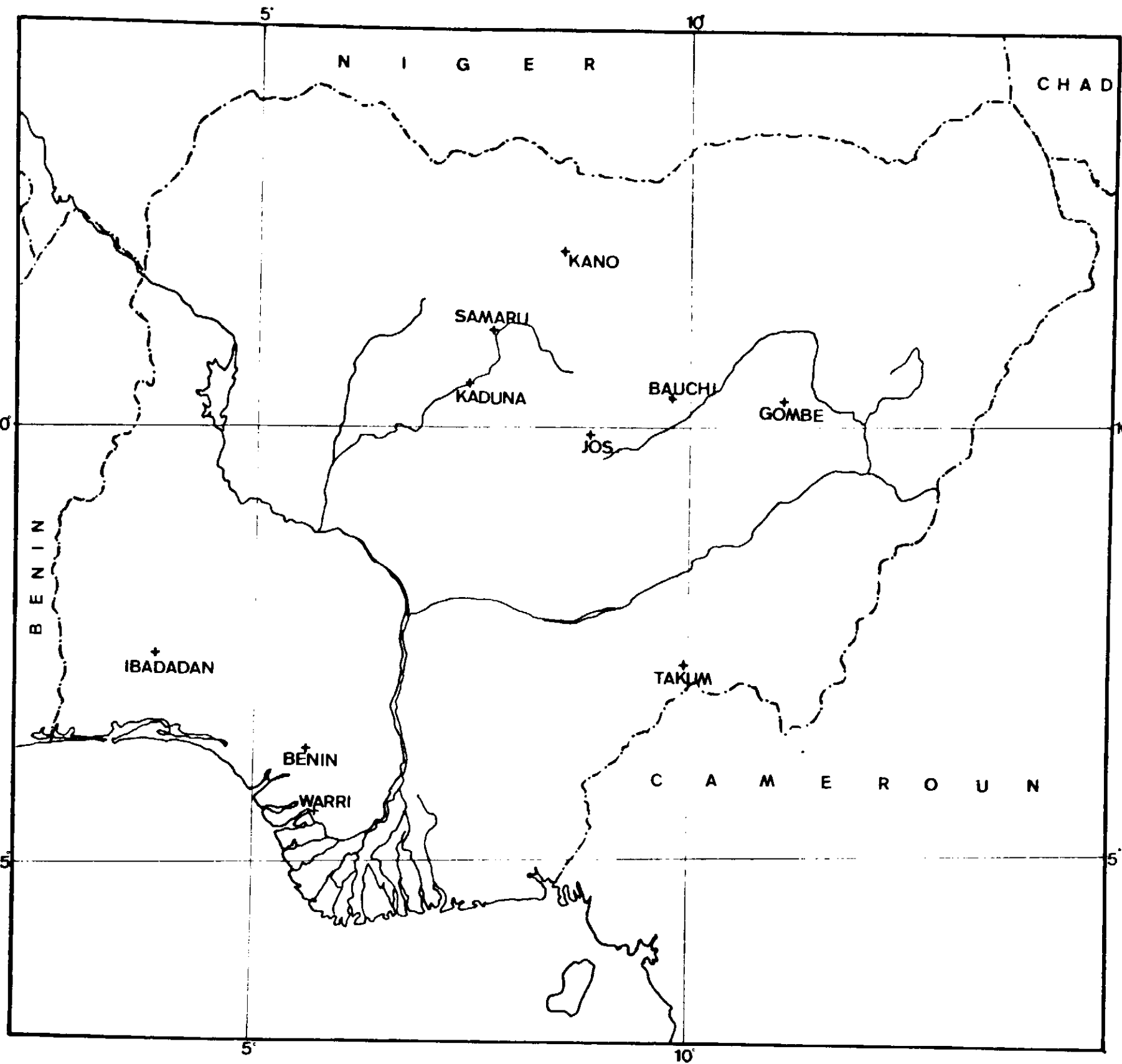
The location of Bauchi, and a number of other towns in Nigeria mentioned in the text, is shown in Figure 1.1.

Bauchi is situated to the east of the Jos Plateau, on a large area of crystalline basement outcrop. The areas of basement outcrop are shown in Figure 1.2. The Basement Complex in Northern Nigeria consists predominantly of an undifferentiated suite of gneiss, migmatite and granite which was mobilised most recently in the Pan African orogeny (ca 600my). Relict meta-sedimentary pendants are widespread throughout the area.

Groundwater is only found in this geological environment where fracturing and weathering have occurred. It is therefore necessary to understand the weathering mechanisms involved before the occurrence and extent of groundwater can be predicted.

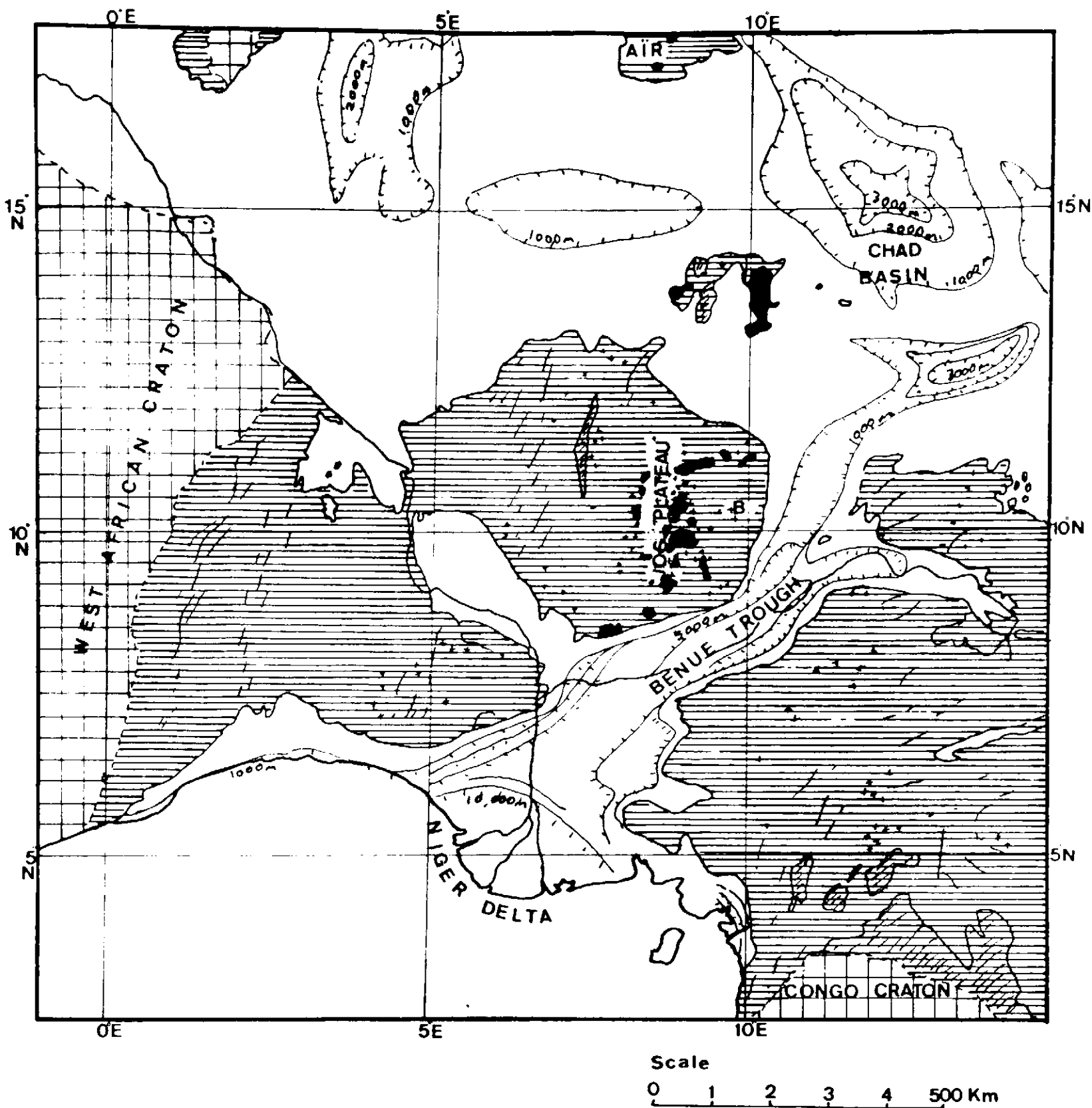
Bauchi lies within the savanna climatic zone. Climatic conditions within this zone have a pronounced effect upon the groundwater resources and are therefore discussed in detail. The socio-economic conditions within the savanna are also of importance as they determine the optimum size of the groundwater supply required. These conditions are briefly described below.

Geophysical methods, such as electrical resistivity and seismic refraction have been used with varied rates of success to locate areas of weathering on the basement. These methods are examined in detail and the reason for their indifferent success rate examined. A new electrical resistivity method is presented which is based upon an interpretational method capable of analysing the complicated geological conditions encountered within the weathering environment.



Scale 1:8,000,000

Figure 1-1 Map of Nigeria showing location of towns referred to in the text.



LEGEND







-  SEDIMENTARY BASINS — Showing basin floor depth below sea level.
-  YOUNGER GRANITES
-  PAN AFRICAN MOBILE BELT
-  Migmatite and gneiss — with granite inselbergs (†+)
-  Metasedimentary belts
-  STABLE CRUSTAL BLOCKS

Figure 1-2 Geological map of Nigeria showing areas of crystalline basement + structure.

A general water balance model for aquifers developed in areas of deep weathering is described as a part of the resource assessment. The results from this model are compared with observations from Bauchi and the results of a small catchment water balance experiment conducted by Kowal at Samaru.

1.1 Research Location.

The field work for this research was carried out during the period commencing in January 1976 and lasting until May 1979. During this time a large number of relatively small hydrogeological investigations were conducted located throughout Northern Nigeria. The majority of the work involved siting boreholes in areas of crystalline basement outcrop. However, a more general resource analysis of groundwater on the basement was also undertaken (Water Surveys, 1978) and several engineering geology investigations for major dam sites on the basement carried out.

More than 50% of the field work was carried out in the general vicinity of Bauchi in Bauchi State, (see Figure 1.1). However, the research that is presented below represents the compilation of a large number of individual investigations, and for this reason is not related to one particular locality. The research represents an appreciation of conditions within a general geological and climatological environment, for which the particular locality of Bauchi is representative. In some of the discussions which follow, data from other areas in Northern Nigeria are analysed and the assumption is also made that these areas are representative of the same general environment.

Wherever possible, the discussion is limited to that of the particular area of reference, however, it is recognised that the method of analysis presented here has a general applicability to any area within the same general geological and climatological environment. Similar areas are found throughout the rest of Africa, in South America, India and Northern Australia. Where information for the particular area of Bauchi is insufficient or unavailable, the discussion is presented in terms applicable to the general environment. For example, in Section 3, the geological environment is discussed first in general terms and a model of weathering developed which is then expressed in terms of examples from the Bauchi area. Similarly, in Sections 5 and 6, the analyses of recharge and the water balance are first made in general terms for the savanna environment and the results then compared with observations from Bauchi and Samaru (see Figure 1.1).

It should also be noted that several components of the analysis are applicable to environments outside those of the general analysis.

In particular, the geophysical methods developed for this study have a general application for any complex geological environment. Similarly, the lumped parameter water balance model developed for this study may be applied, with appropriate modifications, to climates other than the savanna climate.

1.2 Savanna environment.

Introduction.

The savanna environment, in which Bauchi lies, directly affects the groundwater resource analysis in a number of interrelated ways. The most obvious of these is the climatic variability. However, the combination of the climatic factors and the savanna grassland vegetation have far reaching effects upon the hydrological cycle, which in turn determines the availability of recharge to groundwater storage.

Throughout the savanna there is a rapidly increasing demand for small scale ($< 1\text{m}^3/\text{hr}$) supplies of water for individual villages (World Bank, 1976) and for larger supplies ($\sim 10\text{m}^3/\text{hr}$) for schools and hospitals etc. The preferred resource, for both these scales of supply is groundwater (WHO, 1973).

Climatic characteristics.

The dominant climatic characteristic of the savanna is the annual alternation between the wet season and the dry season.

In Bauchi, the wet season lasts for approximately 5 months, from May to September inclusive. During this time, an average quantity of 1075mm rainfall is received from a relatively small number of intense storms. This quantity of rainfall is equivalent to the annual rainfall of large parts of N.W. Europe.

The dry season lasts from October to April. During this time little or no rainfall occurs. Although from the annual quantity of rainfall received, the savanna climate would not be classified as semi-arid, the evaporation and evapotranspiration during the first part of the seven month dry season are sufficiently high that almost all water lying at the surface, or in the soil zone, is exhausted. The availability of water after this time becomes a major restriction to plant growth and human or animal movement. During the latter part of the dry season and the first part of the wet season, groundwater is often the only available source of water.

Although the average rainfall within the savanna is relatively high, a dominant characteristic of the rainfall is its poor distribution, both in time and space. Climatologists used to working in more predictable temperate climates, have used values of mean annual rainfall as representing conditions throughout large parts of the

savanna, however, it is shown in Section 2, that the areal distribution of rainfall for one year, and within a small area, can vary by as much as 40%. Similarly, annual totals vary widely. In a recent 6 year period at Bauchi, the maximum and minimum annual totals varied by 36%.

An accurate assessment of the quantity of rainfall received over a catchment area, together with an assessment of the actual evapotranspiration within the area, form the basic components of a water balance from which recharge to groundwater is usually calculated. Actual evapotranspiration is a function of the available moisture and the vegetation cover throughout an area. A brief description of the vegetation is also therefore required.

Savanna vegetation.

The vegetation around Bauchi corresponds to typical accacia - tall grass savanna which is common throughout a wide belt of Africa which stretches from Gambia in the west through to the south eastern Sudan. The dominant plants are tussock grasses which form an almost continuous cover over the ground, even beneath the trees. During the growing season, the grasses attain a height of between 0.5 and 1.5m. The trees may be either deciduous or evergreen.

During the early part of the dry season, transpiration by the extensive cover of grasses rapidly depletes the moisture held in the upper parts of the soil profile; with the result that the grasses wilt and die. It is the common practice of subsistence farmers throughout the savanna to set fire to the dead grass cover, with the result that extensive bush fires occur each year in December and January. It has been argued (Eyre, 1968) that the practice of burning the grasses has had a dominant effect on the development of savanna vegetation types.

After the burning of dead grass has occurred, the vegetation is dominated by the remaining trees. The ground between the trees remains bare until the following wet season when germination of the grasses occurs rapidly following the first rains.

The changes in both the height and character of the vegetation have a pronounced effect upon the quantity of evapotranspiration which occurs.

1.3 The Hydrogeological Problem.

Introduction.

Groundwater is the preferred type of resource for small scale supplies in the rural and the urban environment, however, it is recognised that only limited supplies of groundwater are available from the weathered profile developed upon gneiss, migmatite and granite. The success rate of boreholes or dug wells in the weathered basement environment varies widely, and the yields of successful boreholes also show a wide variation. Data from South Africa reported by Brown (1975) are shown in Table 1.1. These results are also typical of the Bauchi area but unfortunately no such detailed results exist for Bauchi.

Table 1.1 Typical borehole characteristics from a granite area of South Africa. (Brown, 1975).

Area	Number of boreholes	Total depth (m)	Depth of water (m)	Average yield (m ³ /hr)	Failure rate %
1	62	40	21	5.0	14
2	497	47	34	5.0	25
3	130	61	51	3.9	50
4	404	37	26	5.9	10
5	202	51	35	4.6	35
6	136	48	35	3.7	27
7	16	56	43	1.0	31

21%

Whether a borehole is a success or a failure depends in many cases upon the purpose for which the water supply is required. To this extent, the failure rate of boreholes is partly subjective. However, it is clear that a considerable potential exists for improving the success rate of boreholes.

Although the cost of a dry borehole is far greater than the cost of a dry dug well, the social impact of the latter is probably the greater.

The failure of boreholes or wells is principally caused by siting them where an insufficient depth of weathered material exists. However, in both cases, an initially encouraging yield may later become significantly reduced or may dry up completely.

The hydrogeological problem in this geological and climatological environment is two fold, viz,

1) The groundwater must be located. The occurrence of a large number of dry boreholes and wells indicate that groundwater does not exist everywhere in the weathered profile.

2) Once the presence of groundwater has been established, some estimate of the available quantity of water must be made.

Method of analysis adopted.

The method of analysis adopted for this thesis may be broadly divided into 5 sections. These sections form the subsections of the thesis and are as follows :

- a) A study of the climatic environment of the savanna.
- b) A discussion of the development of the weathered profile on crystalline basement rocks.
- c) The development of geophysical techniques with which to locate areas of deep weathering.
- d) A study of the hydrogeological characteristics associated with areas of deep weathering.
- and e) An analysis of the groundwater resources available on areas of crystalline basement.

In Sections 3 and 4 a method of analysis is developed from which a volume estimate of the aquifer can be made. In Sections 2 and 5, the necessary inputs to a lumped parameter water balance model are analysed. From the water balance model, an estimate of annual recharge is made. In Section 6, the two estimates are combined to produce a value for the safe yield of three weathered zone aquifers close to Bauchi.

1.4 Previous Research.

General.

A multi disciplinary approach is required for the hydrogeological analysis of groundwater in the weathered environment. Previous research in many interrelated disciplines is therefore of significance to the present analysis. However, the author is not aware of any previous attempt to present an analysis along the lines described in this thesis.

Sections 2, 3, 4 and 5 of the thesis each contain references to previous work in the respective fields covered by these sections, and references are given in the text where appropriate.

In Section 2, the recent work by the World Meteorological Organisation has been particularly useful in explaining the distribution in time and space of the rainfall within the savanna. The calculation of evaporation data for Bauchi is based on the original analysis by Penman (194^o), however, the work of Monteith, (1965), has also been used to provide a method of calculating actual evapotranspiration for the climate data from Bauchi.

In Section 3, results from a large number of studies on granite weathering have been consulted. The weathering model detailed by Dearman (1978) and based upon the weathering of granites from the Cornish Peninsular in the U.K. has been used as a basis for the description of weathering profiles on granites + gneiss in general, and around Bauchi in particular.

In Section 4, geophysical research from a number of authors has been consulted, but, by far the most important has been the work of Dey + Morrison (1976b) who have produced a mathematical model for the analysis of the electrical resistivity response over inhomogeneous resistivity ground.

In Sections 5 and 6, the results of work by Kowal (Kowal + Kassam, 1978) at the Institute of Agricultural Research in Nigeria, are generally referred to. In particular, the results from a small catchment water balance study have been invaluable as a comparison for the lumped parameter water balance model developed for this study.

1.5 Available Information.

General.

In general terms very little data are available concerning this environment. In addition, the records which have been kept are often uncorrelated and therefore of little use.

Specific sources of data are described below.

Remote sensing data.

Landsat II and III products are readily available for all areas. Although computer interpretation of these products is not generally available, an examination of the colour and false colour images at a scale of 1:250,000 provides a very useful basis reference for an area. Geological and land use factors can be interpreted from the imagery.

Side Looking Airborne Radar (SLAR).

SLAR images for Nigeria at a scale of 1:250,000 are available for interpretation at the Federal Forestry Research Station at Ibandan. The SLAR products are particularly useful for geological interpretation and fracture analysis. In addition, the products give a clear indication of the geomorphology.

Aerial photography.

Various scales of aerial photography are available for inspection at the State Survey Department. The whole of Northern Nigeria has been flown at a scale of 1:40,000, although larger scale photography is usually available around towns. Bauchi, for instance has been flown at 1:4000, 1:10,000 and 1:40,000.

Contour maps of the majority of the area around Bauchi are available at a scale of 1:50,000, produced from the available aerial photography.

Climate Data.

A meteorological observation station has existed at Bauchi Airport since 1940, and monthly rainfall data is available from 1916. The records of parameters other than rainfall are often incomplete however.

Daily observations of maximum + minimum temperature, relative

humidity, observed sunshine hours, daily wind run and rainfall were obtained for this study, for the period 1969-1974 and 1978-1979 from the Nigerian Government Federal Meteorological Station at Bauchi. During 1978-1979 the station was manned on a 24 hour basis and all measurements, where applicable, are averages of at least 8 daily readings. In addition, measurements of ground temperatures, piche evaporimeter, gunn-bellani radiometer and type A pan evaporation data were obtained.

Geological Data.

Very little published geological information exists for the basement areas. At Bauchi, several occurrences of a fayalite quartz monzonite have been described (Eborall, 1976). However, the majority of the basement is listed as 'undifferential basement complex' on existing geological sheets.

The drillers logs of a large number of boreholes are available from the Government Geological Survey, or from the offices of individual drilling companies, however, these are usually of little direct use as conditions change very rapidly within a small area.

2. CLIMATIC ENVIRONMENT.

Introduction.

In order to assess groundwater recharge within the savanna regions, it is necessary to examine in detail the savanna climate. Most of the research concerning groundwater recharge has been carried out in temperate latitudes and it is important to assess the effects of the more extreme savanna climate upon the models of recharge commonly used in temperate latitudes. The recharge assessment for the savanna is made in Section 5 of this thesis, however, major climate elements such as rainfall evaporation and evapotranspiration are discussed below.

The savanna climate may be divided distinctly into two seasons. During the dry season, which may last from the end of October through until the following March or April, the wind blows predominantly from the NE. The NE Trade over West Africa has a very low humidity and often carries considerable dust south west from the Sahara. The wet season, which characteristically lasts for five months from June to October, is dominated by surface SW winds which have a high humidity. During the wet season, 800-1000mm of rainfall are received, almost entirely from cumulonimbus storm cells. The intervening period at the beginning of the wet season is characterised by an alternation between the two air mass types, which can give rise to false starts to the rainy season. Such false starts to the growing season (wet season) have particular significance to the agricultural industry where early planting is encouraged.

The alternation between the two air masses throughout the year can only be understood in terms of the overall tropical circulation. As the character of the air masses plays such a significant part in determining the various parts of the hydrological cycle within the savanna, the tropical circulation is described in detail below.

The rainfall mechanisms which operate throughout the savanna are a direct result of the tropical circulation. Localised cumulonimbus storm cell activity is generated in the adiabatically unstable SW trades. As tropical storm cells have very intense air circulations within them, and operate within moist air conditions, the energy released by the latent heat of condensation is very large. A result of this is that

rainfall from these cells is intense ($> 40\text{mm/hour}$) and also, poorly distributed both in time and space. This is in complete contrast to the rainfall mechanisms which produce rainfall in temperate latitudes. For this reason it is not possible to extrapolate rainfall totals from point gauge readings in the same way in which the extrapolation is possible at higher latitudes. This basic characteristic of the savanna rainfall has important implications for factors such as interception, infiltration and run off, which become especially significant during recharge calculations. For this reason, the temporal and spatial distribution for a number of stations within the study area are examined in detail below.

The radiation input within the tropics is the main source of energy which drives the tropical circulation. The large amount of input is responsible for the intensity of the storms and also produces high levels of potential evaporation. Characteristically, the potential evaporation is double the annual rainfall. It is this imbalance which enhances the contrast between the wet and dry seasons. The change from moist SW winds to dry NE winds causes a very rapid drying of the soil and vegetation at the beginning of the dry season, and usually within six weeks of the last rains, the crops have been harvested, all shallow rooted vegetation has died and most smaller rivers are reduced to negligible flows.

The quantification of evapotranspiration is essential if a meaningful ground water balance is to be attempted. Therefore, the levels of radiation input and output are examined in detail in the third part of this section, as small changes in radiation input are reflected in reduced potential evaporation.

As soil moisture is almost entirely depleted by the end of the dry season, actual evapotranspiration falls considerably below the potential evaporative demand of the air. The first rains of the wet season fall on dried out ground and shallow rooted vegetation can only become established as the soil moisture produced by these rains percolates downwards. As evaporative demand is also very high at the beginning of the rains, a break of ten days between storms results in a complete drying of the soil again and the death of any crops that have been sown.

These points are made to illustrate the differences between potential and actual evapotranspiration that exist between temperate and savanna latitudes. The differences are highly significant and require

considerable modifications to the methods of computing a water balance that were employed in temperate latitudes.

In the fourth part of this section the Penman (1948) calculation is used to produce values for potential evaporation of the air. The calculation is shown to be particularly sensitive to incoming radiation and albedo variations. Data have also been calculated for the Monteith (1965) evapotranspiration equation and it is suggested that this model is more representative of conditions during the year for the savanna.

Data for a number of years from the Bauchi climate station are used to produce daily values of evaporation and evapotranspiration. An algorithm is presented in Appendix A which performs the calculation based upon the Penman and Monteith equations. This data demonstrates that the actual evapotranspiration is a complex function of the vegetation height and soil moisture deficit and can only be calculated as a part of a larger soil moisture and recharge balance. This balance is described in section six of the thesis.

2.1 ATMOSPHERIC CIRCULATION OVER WEST AFRICA

General.

The atmospheric circulation within the tropics may be approximately represented for a stationary, or non-rotating earth, by the Hadley Cell shown in Figure 2.1. The circulation approaches a simple convective system driven by the unequal heating of the ground surface at the equator. The air rises towards the troposphere and falls away north and south to form the sub-tropical high pressure zones at approximately 30° north and south of the equator.

The rotation of the earth, both about its own axis and around the sun, considerably complicates the simple model. The inclination of the earth's axis of rotation, ($23\frac{1}{2}^{\circ}$) to the plane of the elliptical orbit around the sun, causes the apparent migration of the sun between the tropics of cancer ($23\frac{1}{2}^{\circ}$ N) and capricorn ($23\frac{1}{2}^{\circ}$ S) during the year. This has the result that the axis of greatest heating at the ground surface also moves north and south throughout the year. This axis of heating is known as the thermal equator.

The air which is heated at the thermal equator rises in the ascending limb of the convection cell towards the troposphere. The difference in angular momentum between the ground surface and the troposphere, associated with the easterly rotating earth, causes the rising air to be deflected westwards, giving rise to the band of equatorial easterlies shown in Figure 2.2. This easterly flow of air is dynamically unstable and tends to form waves, moving first slightly north west then south west. The waves have a significant effect on the temporal pattern of rainfall distribution as will be discussed below.

The continued supply of air from low levels at the thermal equator, to the belt of easterlies is compensated by a slow spread of air northwards and southwards at the top of the troposphere. As the air moves away from the equator it is increasingly affected by the coriolis force. The coriolis force is a function of the earth's rotation and may be described mathematically as :-

$$\tilde{F} = 2 \omega \sin \phi$$

————— 2-1

where F = Coriolis force

ω = angular velocity of the earth

ϕ = latitude

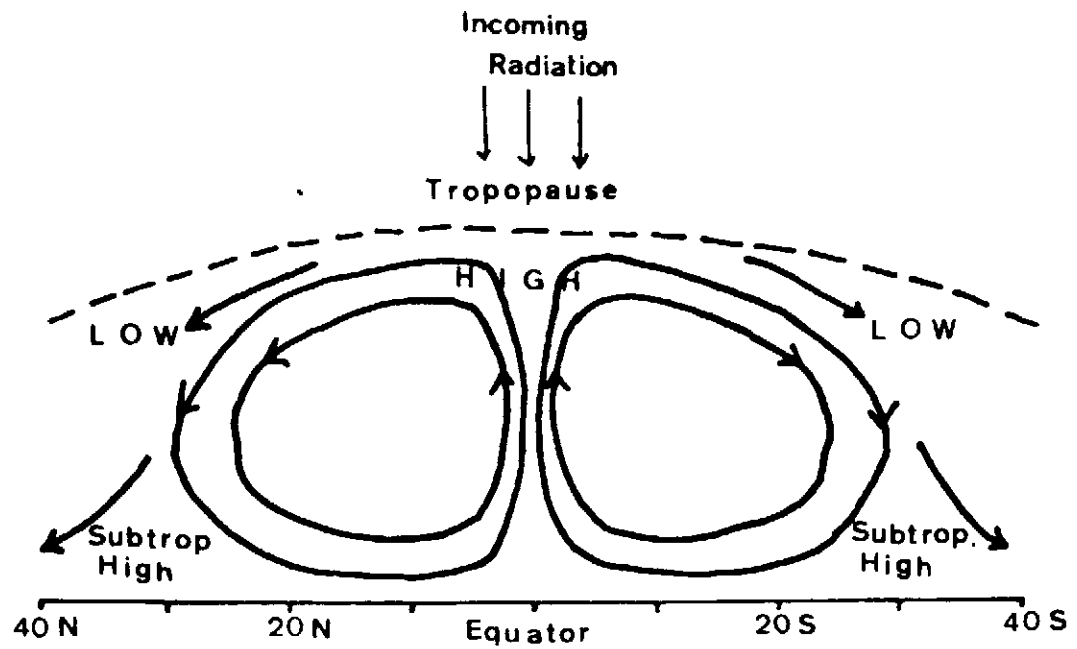


Figure 2-1 Hadley cell circulation

Simplified north south section over the equator — showing the basic transfer of air due to equatorial heating.

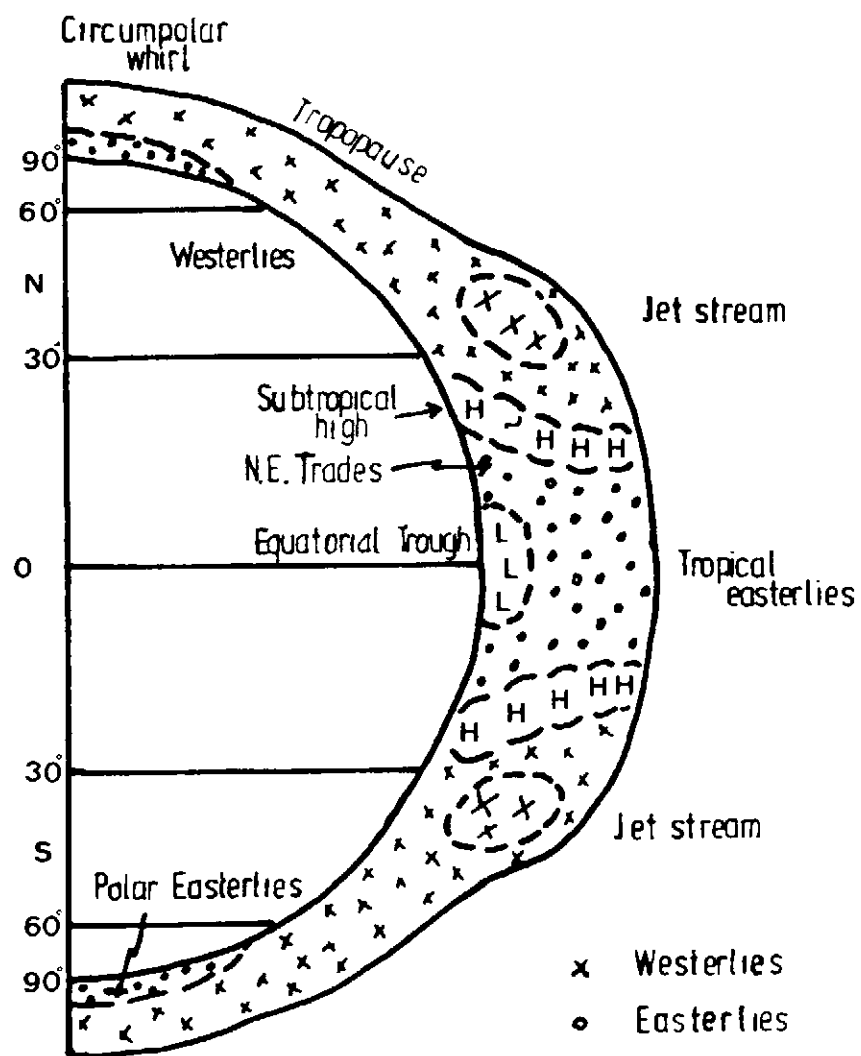


Figure 2-2 Schematic cross section of the atmosphere. (after Strahler, A.N. (1963))

It may be seen from Equation 2.1 that the coriolis force is zero at the equator, increasing to a maximum at the poles. The force acts, in the northern hemisphere, to deflect a northerly moving air mass to the east and a southerly moving air mass to the west. The situation is reversed in the southern hemisphere (Harvey, 1976).

The air moving northwards enters a zone of lower angular velocity, where it tends to accumulate and form a high pressure zone. Air subsides within this zone to form the sub-tropical high pressure zones referred to in Figures 2.1 and 2.2.

In the northern hemisphere, air in the lower troposphere moves outward from an area of high pressure in a clockwise direction, the result of the coriolis force. A component of this circulation moves back at low troposphere levels towards the equator. It is deflected westwards and approaches the equator from the north-east, forming the north-east trade wind. A similar process south of the equator produces the south-east trades. Figure 2.2 depicts a schematic north-south cross section of the troposphere with the easterly and westerly air motions indicated.

The north-east trades and the south-west trades converge at the thermal equator in a zone termed the Intertropical Convergence Zone (ITCZ). Heating within the area of the ITCZ produces uplift and completes the basic pattern of circulation within the tropics.

The distribution of land and sea within the vicinity of West Africa produces a further complication to the patterns described above, which may be thought of as existing over a uniform rotating earth. The north east trade wind originates over the eastern Sahara from subsiding air at the edge of the sub-tropical high pressure zone. As subsiding air is adiabatically stable, no rainfall occurs within this zone and the air that arrives over West Africa has a very low humidity at all levels with a large decrease in temperature with height (lapse rate). The humidity at Bauchi during January is 35% at 06.00 and 10% at 16.00. The low humidity results in a large diurnal temperature range, with an average maximum of 21.6°C and an average minimum of 13.1°C at Bauchi in January. In addition, this air mass often carries dust caused by low level turbulence in the Sahara. Satellite imagery has been used by Martin (1975) to locate several areas of dust origin. The western slopes of the Ahaggar in particular have been isolated as an area where dust tongues are produced, typically in the hours just after sunrise. The local

name for the dusty air in West Africa is the Harmattan, and the air mass is also sometimes referred to as the harmattan. Visibility can be reduced to a few hundred metres with an associated reduction in the net radiation received at the land surface. Plate 2.1 shows the effect of harmattan dust on a day in February, 1980.

By contrast, the south east trade wind originates around the South Atlantic high pressure zone, and has a long ocean path before reaching West Africa. The air mass is deflected to the east, by the change in sense of the coriolis force as it crosses the equator, and approaches West Africa as a south westerly wind. This deflection is well demonstrated by the low level wind stream lines shown in Figure 2.10. The south west air mass is saturated with water vapour, and Warri, in the Niger delta, which lies under this air mass throughout the year, has mean monthly relative humidities at 06.00 of 95-99% and 65-85% at 12.00. The relative humidity remains constant with increasing altitude to about 2000m, but falls off sharply above this level. The decrease in temperature with height (lapse rate) is small in the saturated air, and the air mass is therefore adiabatically unstable. This instability gives rise to cloud formation and rainfall. The cloud cover and high humidity reduce the radiation from the earth and therefore the diurnal temperature range is small compared to that which exists under north east trade wind conditions.

The ITCZ, the zone where the two air masses converge, moves north and south across the geographical equator in response to the sun's zenithal position. The ITCZ lags behind the passage of the overhead sun by a period of from four to six weeks.

The Intertropical Convergence Zone (ITCZ)

The two trade winds converge within the ITCZ which runs around the earth within the tropics. The nature of the meteorological conditions prevailing within the ITCZ is very much determined by the nature of the converging air masses. The ITCZ over the Pacific Ocean is less well defined than that over West Africa, for this reason.

It is only as continuous coverage of the tropical weather conditions has become available from satellite imagery that many of the major features of the ITCZ have become established. Before this time, models of equatorial meteorology were constructed based upon ground observations

from widely separated positions.

From the position of an observer in Northern Nigeria, it was seen that an intermittent belt of localised convective storms moves north into the area during the period April to October, with a maximum of cloudiness in August and September. This belt of storms lies to the south of the savanna for the rest of the year, and hot dry conditions prevail throughout the north. It was recognised from an early date that these conditions could be related to the interaction of the two trade wind belts and the existence of an intertropical front, separating the air masses, or disturbance zone was proposed. The analogy of a front was based on the observed conditions through a warm front in temperate latitudes. The tropical front was thought to move north and south in response to the sun, and as described above.

Figure 2.3 is a schematic vertical section through the Intertropical disturbance, or front after Kowal (1978). A number of zones were thought to exist behind the front, and in gross forms these are still useful concepts.

Zone 1 - At the actual boundary of the air masses on the surface, there is no rainfall because the air being lifted is too dry to cause precipitation. The dry north east trade air mass rides over the heavier moist south west trade to form a wedge which increases in thickness south westwards. No rainfall occurs until the depth of moist air within the wedge is greater than 2000m, some several hundred kilometres to the south of the interface between the air masses at the ground surface. Although no rainfall occurs, the presence of humid air at ground level causes a rise in humidity from dry season values of 20 or 30% up to 70%.

Zone 2 - Further south, a zone of 400-500 kilometres occurs where the humid air is sufficiently deep for the development of localised cumulonimbus cells. Rainfall occurs within the zone with storms of medium intensity but limited extent, leading to widely varied times for the commencement of the rainy season within comparatively small areas.

Zone 3 - A zone of about 1000km occurs to the south of zone two where disturbance lines predominate. These are discussed in section 2.3. Storm cells build to heights of 8000-1000m and occasionally as high as 12000m (Burpee, 1975). These cells are associated with areas of intense rainfall and electrical discharge. It is these storm cells which provide the main convective mechanism for lifting air from ground level towards

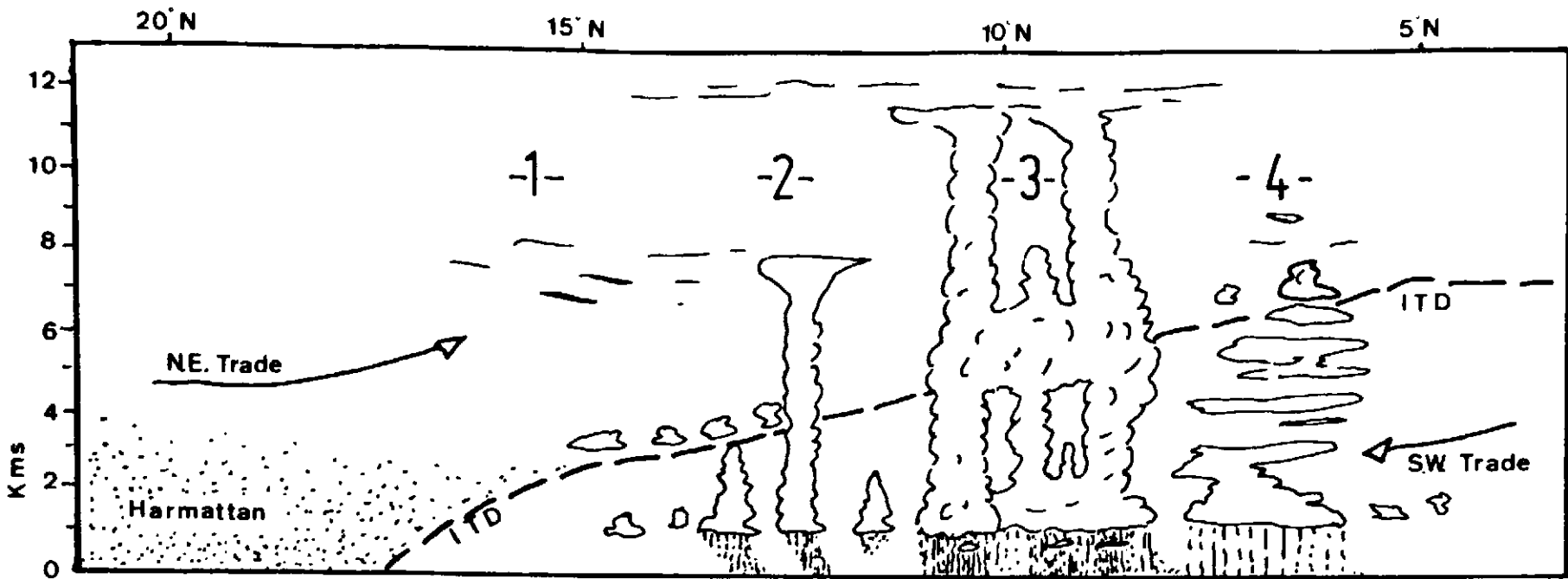


Figure 2-3 Diagrammatic vertical section of air circulation within the I.T.C.Z. (AFTER KOWAL 1978)

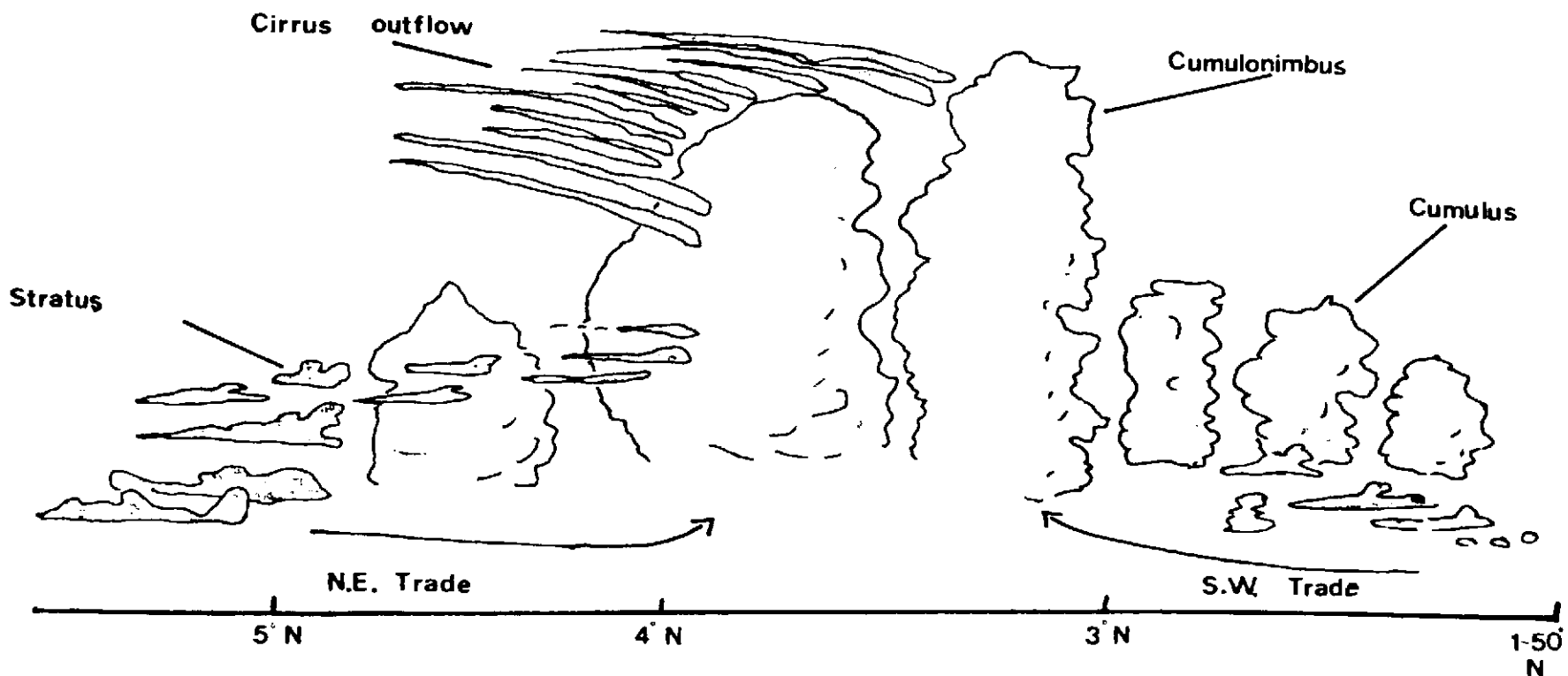


Figure 2-4 I.T.C.Z. Cloud system as observed during G.A.I.E. — 10 July 1974 (AFTER WEICKMAN 1975)

the troposphere, and thus to drive the Hadley cell circulation.

Zone 4 - Lying to the south of zone 3 and beyond the limit of the convergence zone is a belt some 300-400km wide, characterised by more prolonged intermittent precipitation. This zone does not usually extend as far north as the savanna.

Recent Developments

The World Meteorological Organisation (WMO), as a part of its global atmospheric research programme (GARP) carried out an extensive series of observations over West Africa and the Eastern Atlantic in the summer of 1974. The experiment is known as the GARP Atlantic Tropical Experiment (GATE). Although Bauchi lies on the far east boundary of the experimental area (10°E), the results are directly applicable to the savanna as a whole.

During GATE, large numbers of upper air observations were made, and it is the combination of these, along with the satellite imagery, that has enabled a better understanding of the ITCZ.

The principal result of GATE is perhaps a more comprehensive view of the three dimensional processes operating within the tropical atmosphere, and in particular the significance of the upper troposphere easterly winds. Wave disturbances in the easterlies are related in a complex way to shallow cyclonic depressions in the lower troposphere. Where the easterlies do not show wave disturbances, then low level disturbances are also absent. It is the presence of low level cyclonic disturbances which is most at variance with the simple sectional model discussed above. Figure 2.5 shows the satellite infra-red image and a number of wind streamline analyses for September 7th 1974. A shallow cyclonic circulation at 800mb can be seen to exist over the West African coast. Below this are the surface south westerly trades, while above are the upper easterly winds. The shallow disturbance can be seen to lie to the west of the upper easterly wave, which is especially well marked on the 700mb streamline. The SMS image shows the cloudiness associated with this shallow disturbance. Bands of cloud can be seen converging on the disturbance centre, which although would appear discrete to a ground observer, can be seen to represent part of a disturbance covering a large proportion of West Africa from the coast to the sahel.

Satellite pictures sometimes show two or three different shallow cyclonic centres in front of a single wave in the 700mb streamline. The

average period of the easterly waves during the GATE was 3.5 days with an average wavelength of 2500km and a typical speed of 8ms^{-1} . Considerable variation was observed both in the wavelength and the periodicity.

The intensity, amount and latitude of the convective activity was related to the passage of easterly waves. In general, the convection was most intense before or at the time of the trough passage at 700mb. The least amount of convection occurred about one day after the trough passed overhead. This periodicity can be seen in the rainfall totals presented for the Gombe area in Table 2.14. Although the period is in general longer than three days, there is a definite tendency for the grouping of raindays with intervening dry periods.

Figure 2.4, by comparison with Figure 2.3, is a sketch of an actual cloud system associated with the ITCZ on 10 July 1974. The sketch was made by Weickman (1975), flying in an observation aircraft across the ITCZ. The high cirrus outflow to the north represents the flow in the upper troposphere away from the top of the cumulo nimbus towers at the centre of the ITCZ. Smaller cumulus towers flank the two main towers both to the north and to the south. Several different layers of stratus are seen, indicating a complex situation with more than one cloud base layer. This sketch was made in the East Atlantic when the converging air mass conditions were possibly more uniform than over the savanna. However, it does show an example of a cloud vertical section, whereas the satellite imagery only shows the cloud tops. A layer of high cirrus outflow can often mask significant cloud forms below.

Although the GATE data is still being collated and correlated, when the work is completed, it is likely that there will be a significant increase in the understanding of tropical meteorological processes.

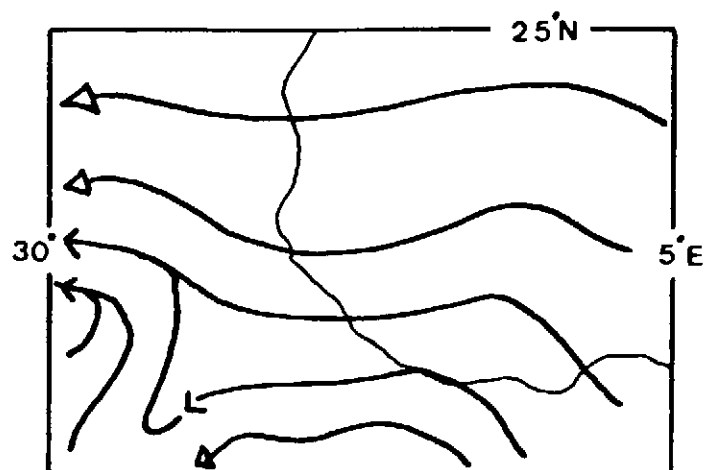
September 7 1974

12.00

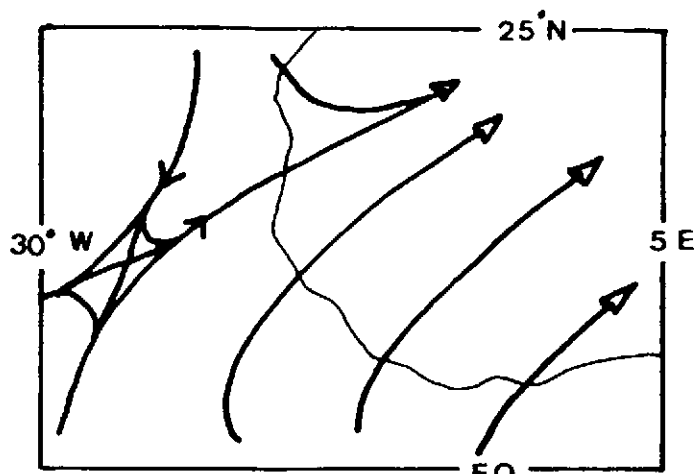


S.M.S. INFRARED IMAGE

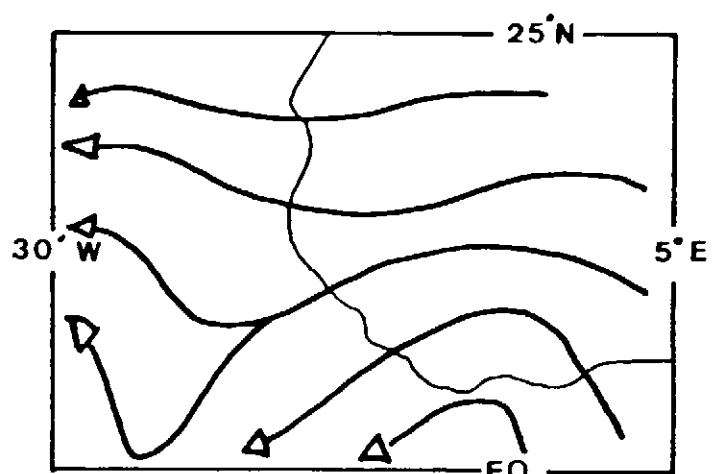
■ Observed high level cloud cover



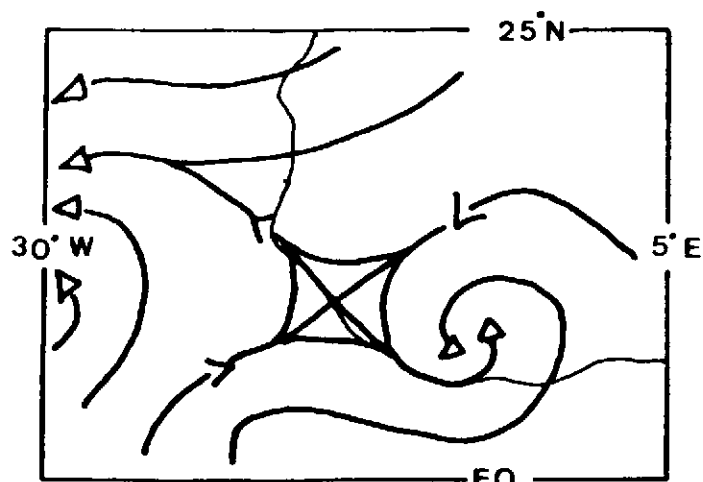
700 Mb



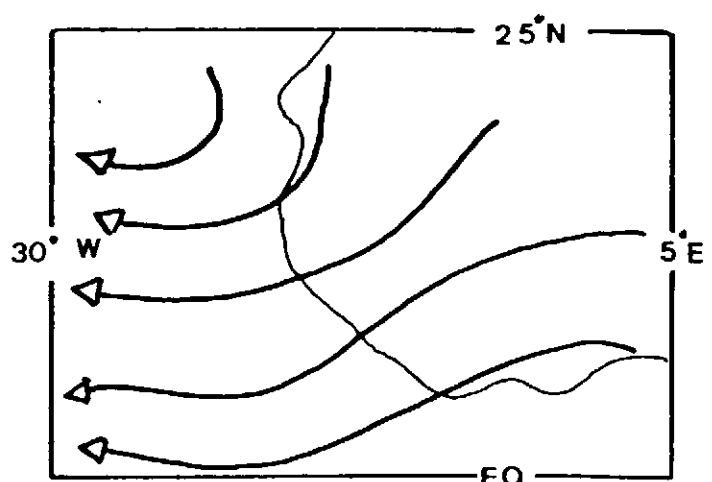
SURFACE



500 Mb



800 Mb



200 Mb

Fig. 2-5 Streamline analysis

(AFTER BURPEE 1975)

2.2 RAINFALL

General.

As discussed in the introduction, the nature of the rainfall mechanisms and the distribution of rainfall vary markedly from those within temperate latitudes. As rainfall is such a basic parameter to any attempted water balance, it is of importance to examine the ways in which tropical rainfall characteristics vary and to assess whether any allowances or adjustments must be made to methods of computing the water balance.

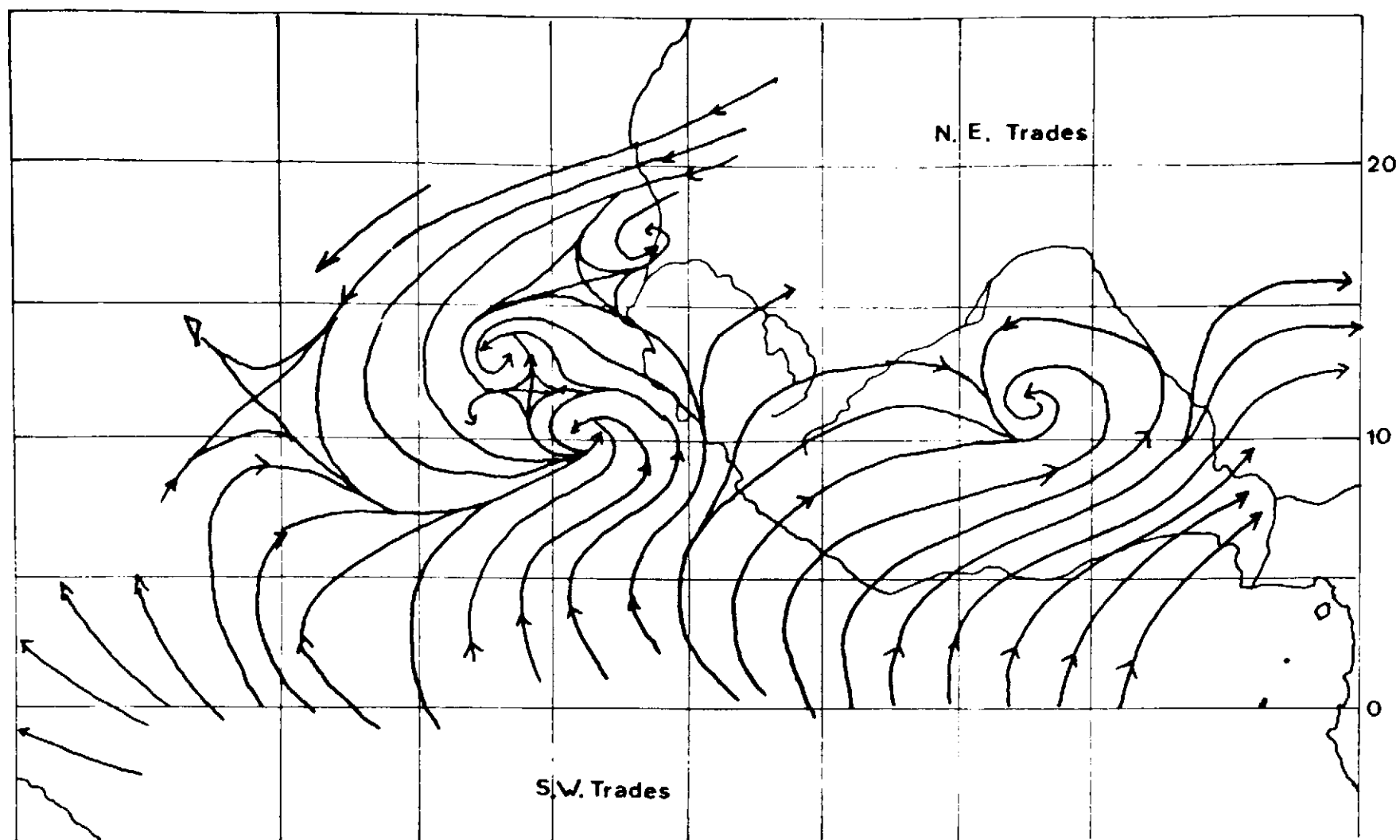
Rainfall Mechanisms.

The most common rainfall producing mechanism is that of thermal instability, produced by intense heating of the ground and near surface air, initiating convective instability in the adiabatically unstable low level south westerlies. The turbulence develops most fully where the depth of saturated air exceeds several thousand metres. The tops of the cumulonimbus storm cells which develop as a result of the adiabatic instability reach 10,000 metres in height, and upper tropospheric conditions influence markedly the development of these cells. If convergent conditions exist in the upper troposphere, the development of the cells is effectively inhibited. If divergent conditions exist, however, then the necessary outflow from the cumulus tower can be accommodated and the storm cell grows to maturity. The upper level conditions are controlled by the waves in the upper easterlies described above. Convergent conditions are created by the upper easterly flow tending towards the north west, while divergent conditions are formed as this upper flow moves towards the south west. The conditions are the result of angular momentum changes and have the opposite sense in the southern hemisphere.

The dependence of storm cell formation upon upper air conditions is shown in the series of Figures 2.6 to 2.9. Figure 2.6 shows the wind streamline analyses for day 240 (August 28, 1974). The ITCZ can be seen, from the surface wind streamline, to lie at approximately 20°N . The 700mb wind streamline indicates a series of well developed waves in the upper easterlies. Shallow cyclonic disturbances can be seen located in front of and at the crests of each wave. The satellite image presented in Figure 2.7, shows a major north south band of cloudiness associated with the first wave, and more diffuse cloudiness associated with the more westward wave.

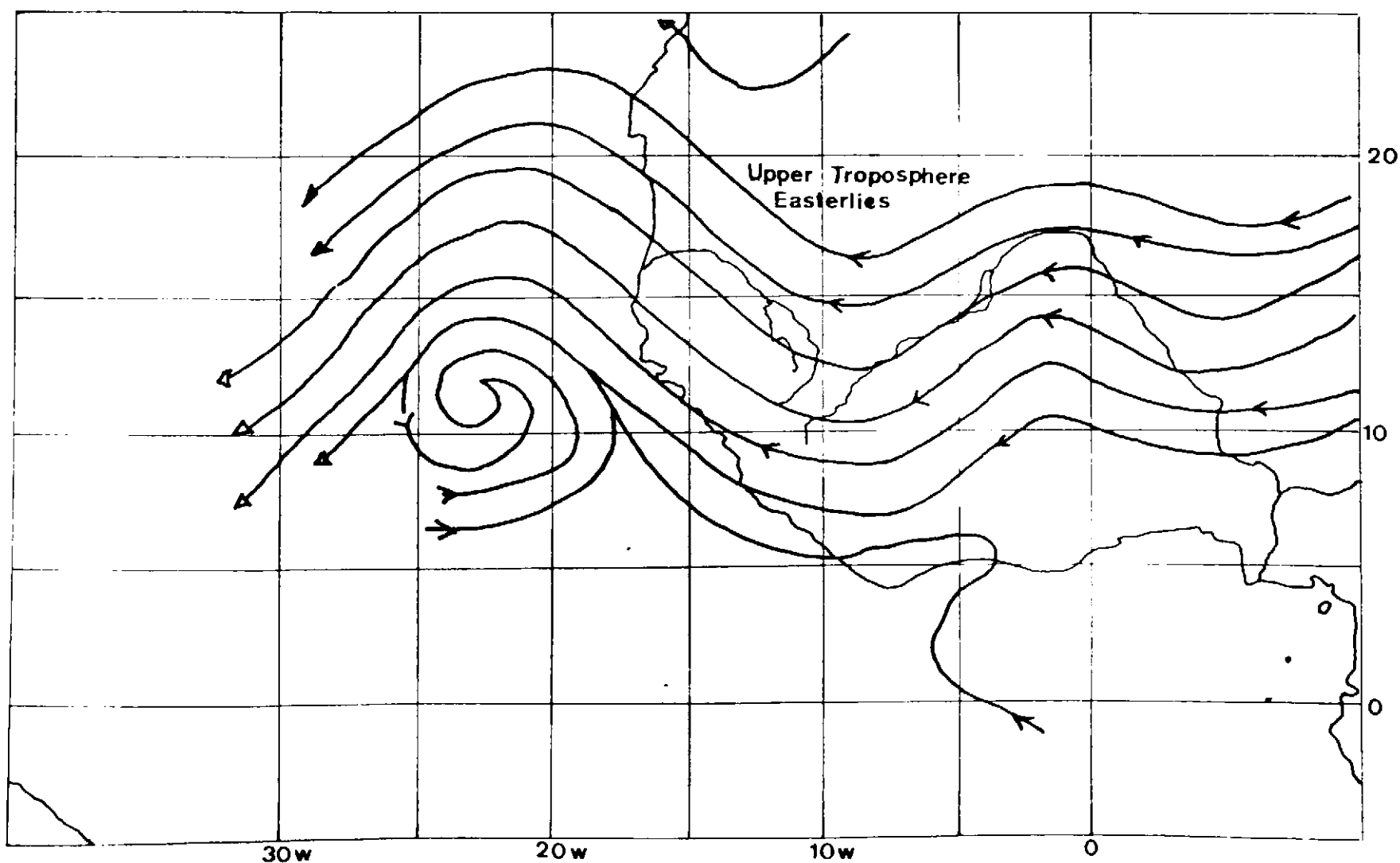
Figure 2-6 Streamline analysis

Day 240



Land 500m ——— Sea surface

Note the eastward movement of the south west trades as they cross the equator.



700 mb

Well developed waves in the upper easterlies that can be correlated with storm cell growth (see text)

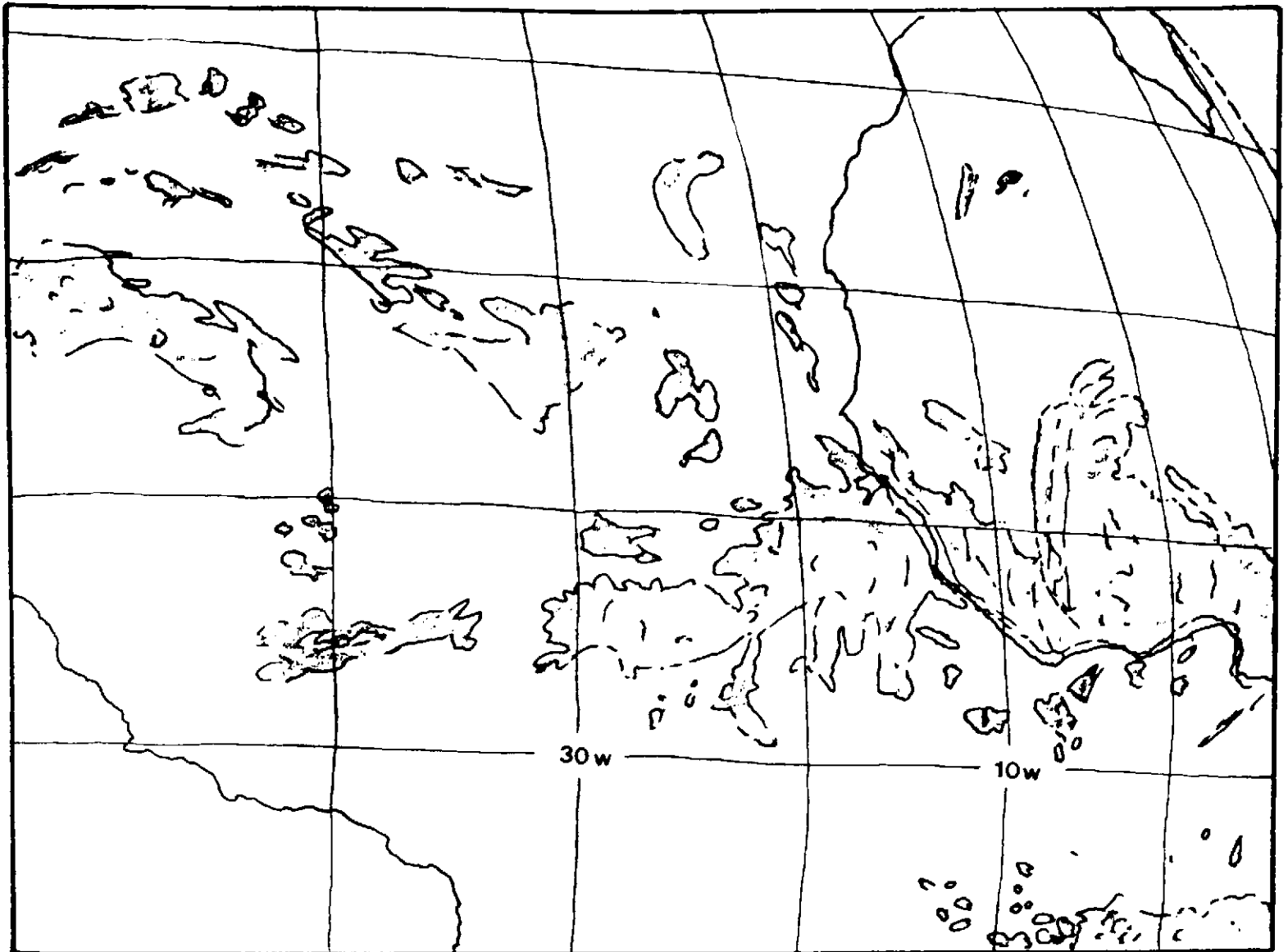


Figure 2-7 Cloud cover Day 240 1974

Cover associated with waves in the easterlies

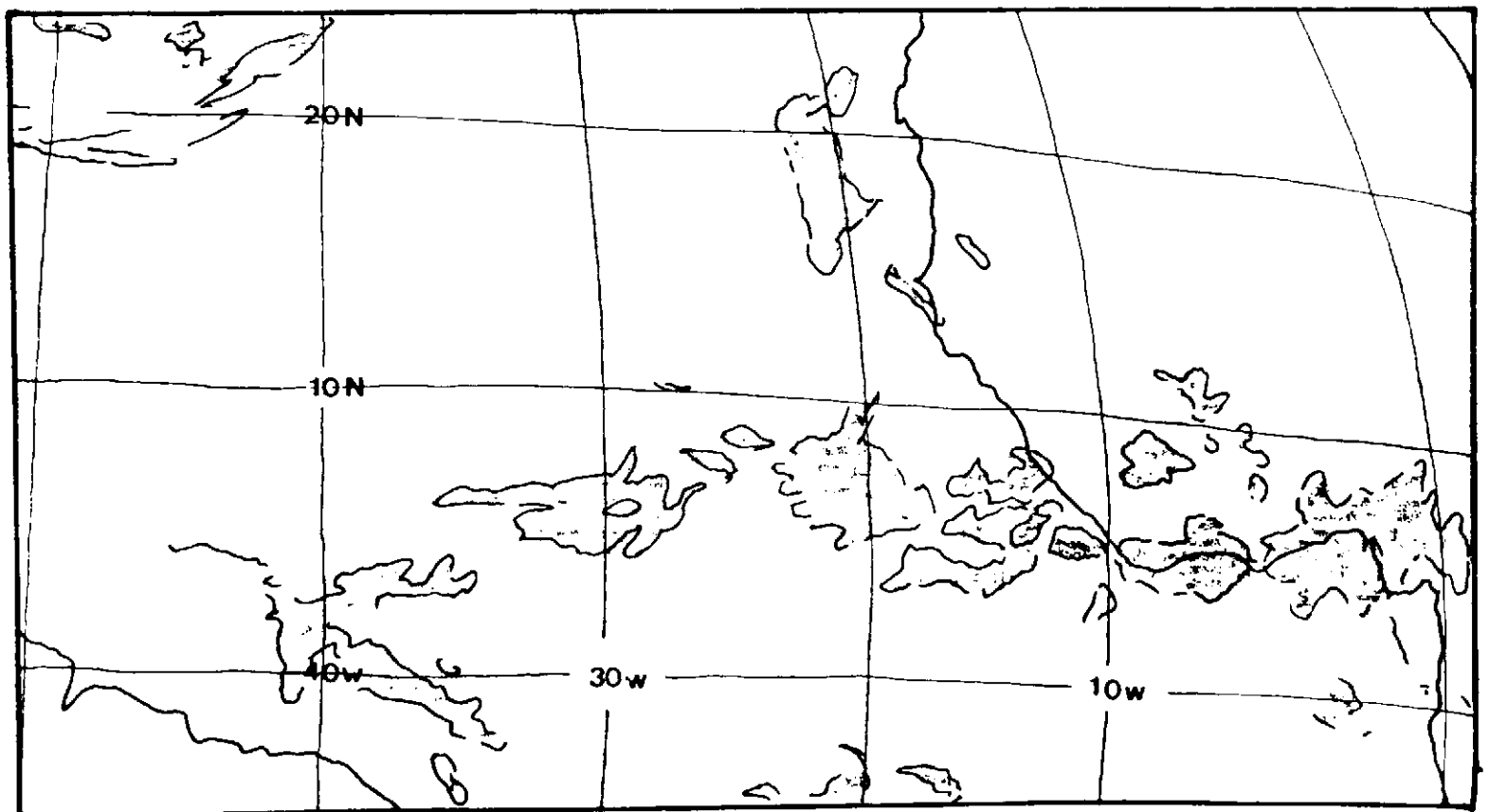


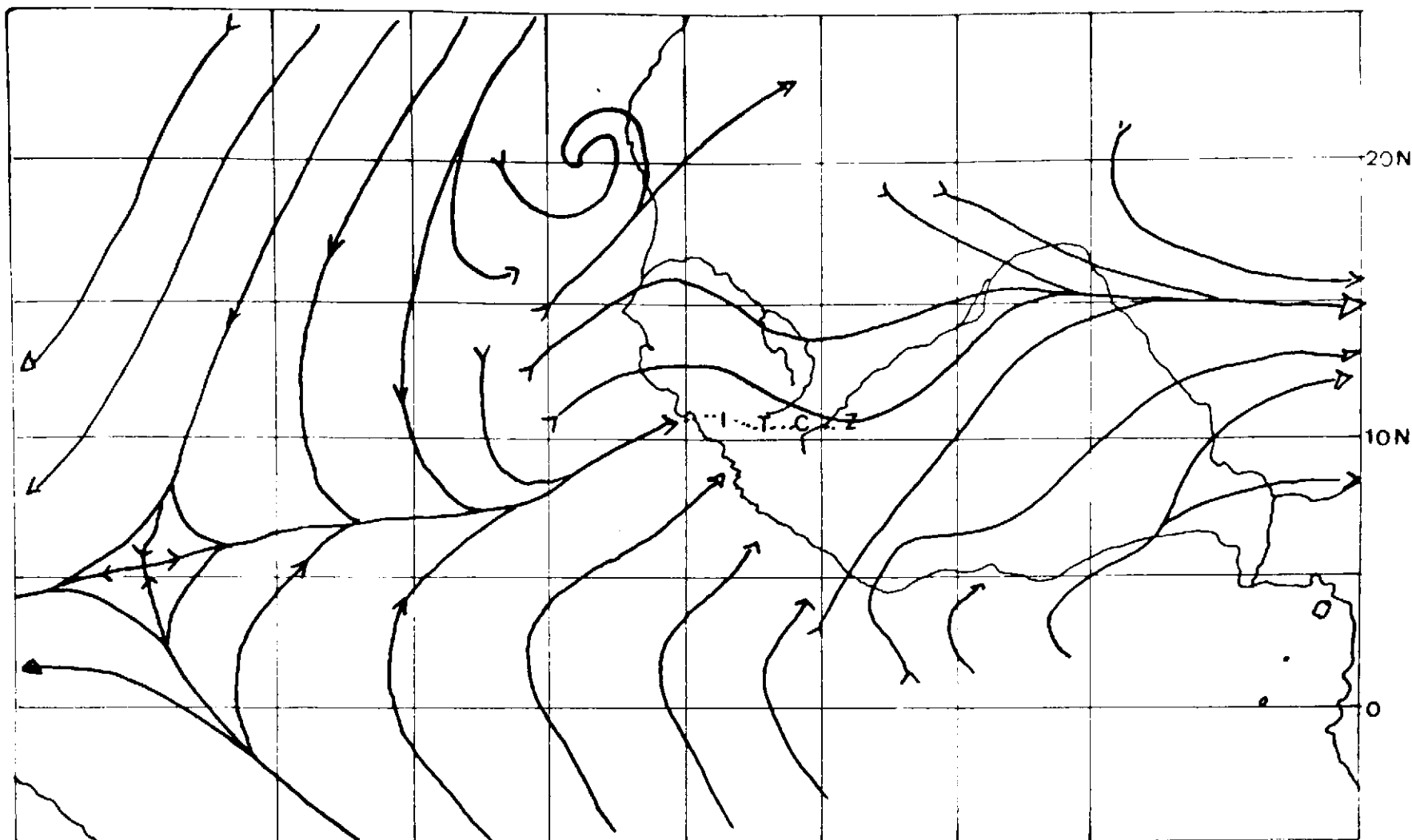
Figure 2-8 Cloud cover Day 182 1974

Cover associated with planar flow in the easterlies

 Cloud cover

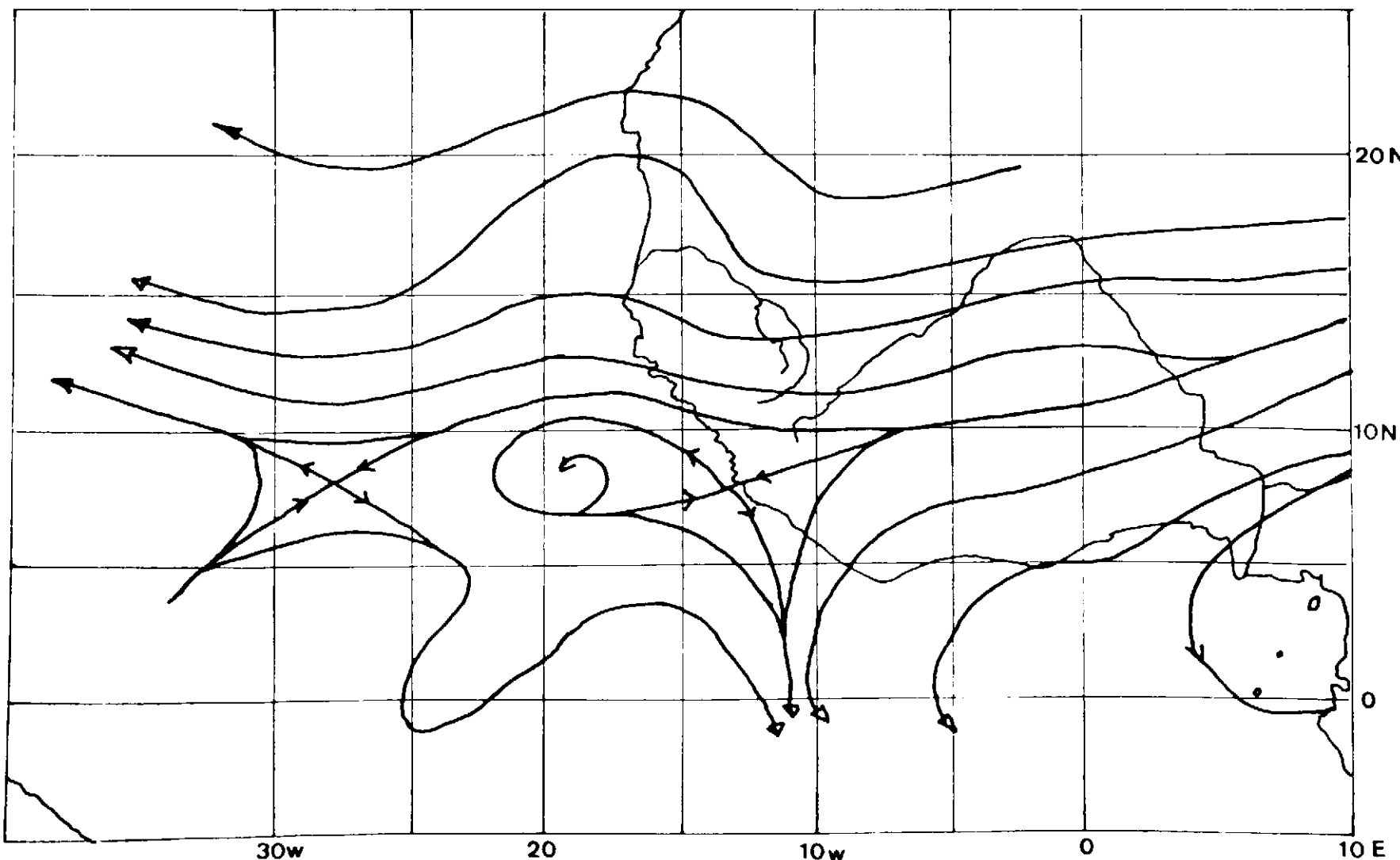
Figure 2-9 Streamline analysis

Day 182



Land 500 m — Sea surface

The I.T.C.Z. is represented by westerly winds over West Africa with no disturbances and little cloud cover.



700 mb

Streamlines show absence of wave disturbances over West Africa

By contrast, Figure 2.9 shows the streamline analysis for an earlier period, day 182 (1st July, 1974). The I.T.C.Z. can be seen at approximately 15°N over Northern Nigeria. The 700mb streamline analysis shows no wave disturbance, while the surface streamline shows no shallow disturbance. Correspondingly, the satellite image indicates very little cloudiness (Figure 2.9).

Figure 2.20 shows a histogram of rainfall at Bauchi during 1974. An examination of this demonstrates that while day 182 and the period of days around that time was also mainly dry, day 240 occurred in a wet spell.

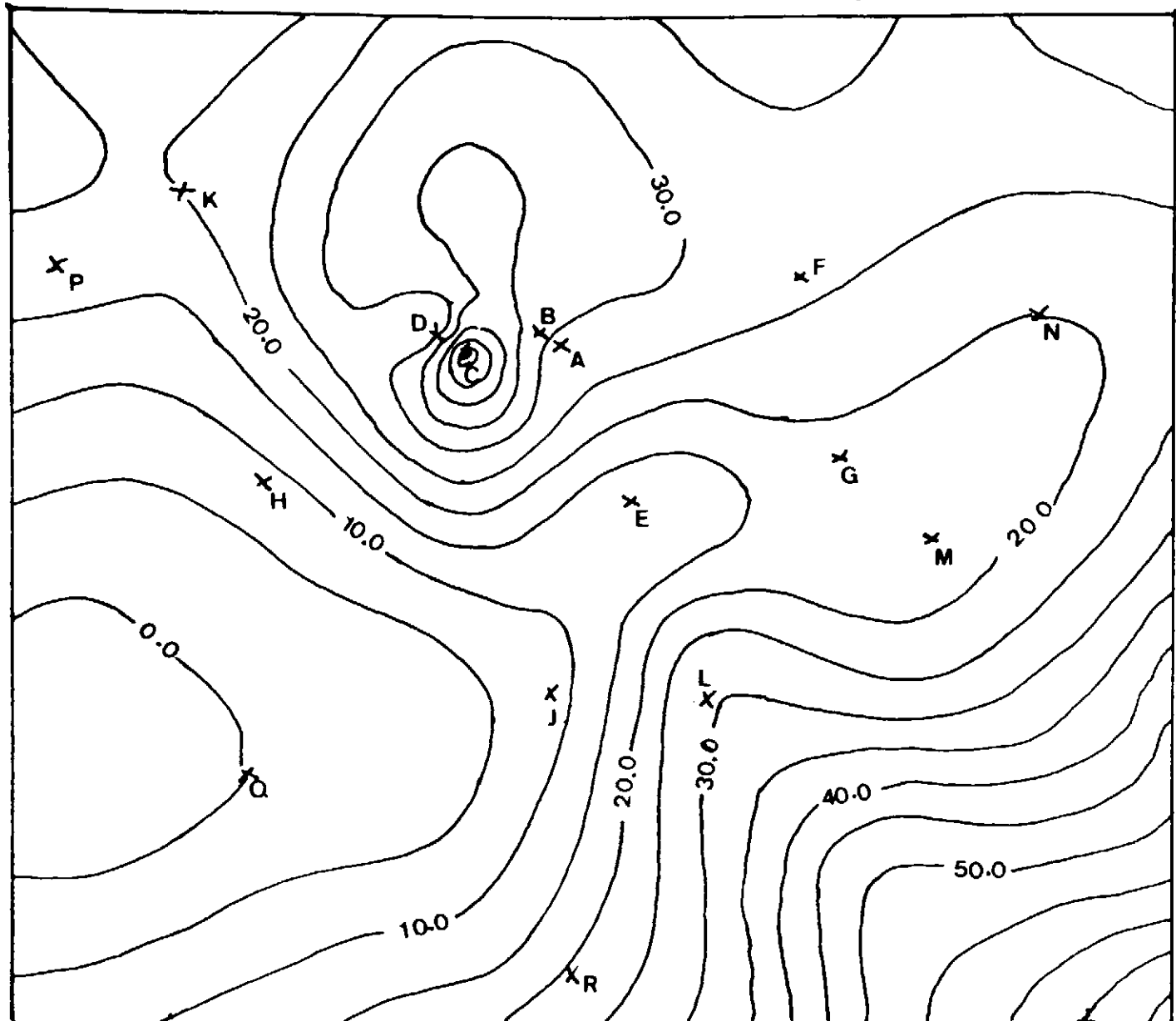
Satellite imagery has been used to demonstrate that the majority of cloud clusters appear between 14.00 and 16.00 local time over West Africa. This represents the time of maximum ground surface heating and associated turbulence. The average lifetime of a cluster is less than 24 hours and frequently, individual areas of active cumulus convection have lifetimes of three to four hours. The analysis of radar echoes under cirrus cloud shields or cloud clusters, indicates that individual areas of rain are limited in extent, and that there is only a slight tendency for the ~~areas~~ areas of rain to move westwards, while all other directions of movement are commonly encountered. Cloud systems which build up from a number of coalescing storm cells frequently contain up to eight stratiform layers.

Squall lines.

The line squall or disturbance line is characterised by violent thunderstorms and squall winds, resembling the phenomena associated with a cold front in temperate latitudes. The squall line is the only rain producing mechanism which brings rainfall to a large area at the same time.

Squall lines are formed between 7° and 17° North and are some 200 to 500 kilometres in length (Burpee, 1975). The life cycle of several squall lines over West Africa was plotted during GATE, using the images supplied by a number of satellites. There appears to be an initial period of very rapid growth of cumulus, often in isolation from the other systems, and often in the late afternoon. Many thunderstorms develop and coalesce with the development of a secondary system some 800km further east. The cirrus outflow from all the convective storms merges into an extensive cirrus shield by late evening. The squall lines have a typical lifetime of 12-24 hours.

24 Hour Total Rainfall (mm.)



Scale 1:300,000

Figure 2-10 Rainfall in the GOMBE
Area 22 April 1978

The rainfall associated with
a squall line

Viewed from the ground, the passage of a squall line is impressive and represents the most extreme weather type experienced in the savanna. Reed (1975) and Ojo (1979) have both described the passage of a squall line.

The squall line approaches from the east. Ahead of the line, the surface winds are normal south westerlies. As the disturbance line approaches, dark heavy cumulus clouds develop, extending up to 1000m. As this low roll of cloud passes rapidly over, there is a very intense fall of rain, associated with a 10°C drop in temperature and a squall wind from the east. The rainfall intensity commences at 1mm per minute. This rate lasts for the first twenty minutes, after which time the rate slowly diminishes. The disturbance line usually has a depth of 50 kilometres.

The passage of a squall line was recorded by the raingauge network in the Gombe area on 22nd April 1978. Although rain fell in most parts for only two hours, the total fall was sufficient to produce early rainy season flooding in many places. Figure 2.10 shows the isohyets for the storm.

Line squalls are thought (Burpee,(1975)) to be generated in some way by wave disturbances in the upper easterlies. If this is so, then they move quickly ahead of the wave away from the area of genesis. The mechanism by which they are formed, and by which they maintain their intensity and linear nature over great distances are not understood.

Rainfall distribution in space.

In March 1977, a report was submitted to the Gombe Agricultural Development Project (GADP) (GADP Water Resources Report, 1977), in which it was recommended that rainfall gauges be set up at as many sites as possible throughout the project area of 6400 sq. km. This was acted upon, and for the 1978 rainy season, rainfall records are available for twenty-five stations within the area. The complete record for 17 stations from April to October 1978 was analysed in detail by the author, in order to examine the spatial variabilities suggested by the rainfall mechanisms described above.

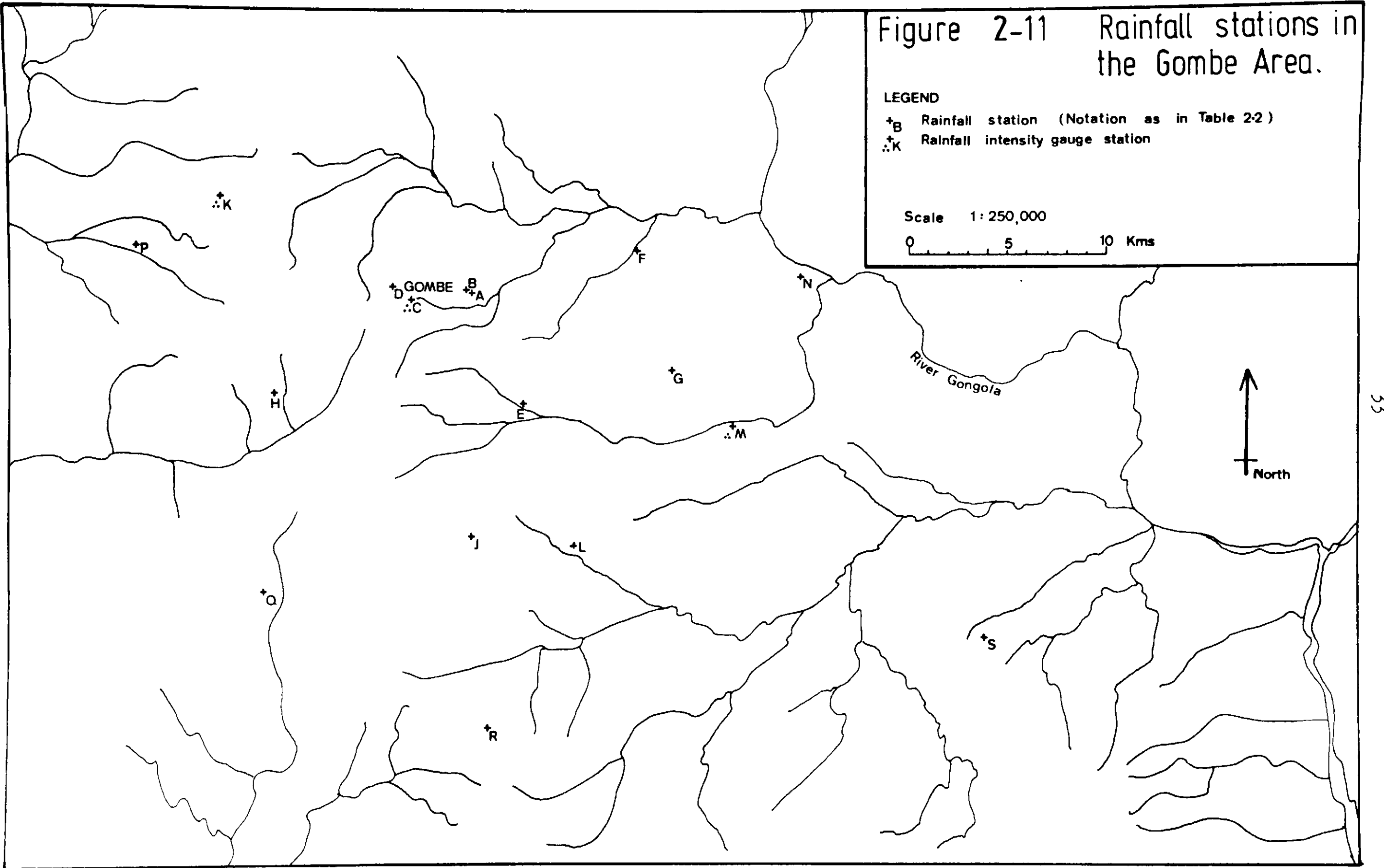
The gauge density, excluding some of the remoter areas, is one gauge per 250 sq. km.

The area and gauge locations are shown in Figure 2.11. Although Gombe lies 150 kilometres to the east of Bauchi and at an elevation some

Figure 2-11 Rainfall stations in the Gombe Area.

LEGEND
+B Rainfall station (Notation as in Table 2-2)
.:K Rainfall intensity gauge station

Scale 1:250,000
0 5 10 Kms



200m lower than Bauchi, the general pattern of rainfall distribution is generally applicable not only to Bauchi, but to the savanna in general.

A cross correlation analysis was carried out for the 17 stations. The results are produced in Table 2.1.

For rainfall area analysis and rain gauge network design, a value of 'r' (the correlation coefficient) between two adjacent stations should be greater than 0.85. To estimate rainfall over an area of 6000 sq. km to an accuracy of 10%, a gauge density of 1 per 250 sq. km. is required (Weisner, ~~et al.~~, 1970). It may be seen from Table 2.1 and Figure 2.11 that this gauge density is entirely insufficient to predict rainfall across the GADP area. Even for a storm event such as the passage of a squall line, the rainfall totals vary markedly as shown in Figure 2.10.

In Table 2.2, the correlations for Gombe CAP are presented against other stations. Although Gombe CAP is some 1000m from an area of hills to the northwest, which are some 200m higher than the surrounding area, the area to the south and east is predominantly flat. Gombe CAP has the highest correlation with nearby stations as might be expected, however, the degree of correlation is very poor.

The correlation coefficients strongly indicate that it is not possible to extrapolate rainfall from one station to a nearby station even less than 1000m away. For the 300 m separation between Bogo FSC and Gombe CAP there is a 15% difference in the annual totals.

Within the comparatively small area of the GADP, the smallest annual total is only 60% of the largest. This wide difference in total rainfall, measured over a small area, and for any period of time from an hour to a year is a dominant feature of the savanna climate. As the period of time increases then the total rainfall over an area does become less poorly distributed. However, for any one rainy season there are very significant departures from long term averages, on a scale which does not appear to have been comprehended previously. The departures from average are so large, that water balance calculations can vary significantly over a small area.

Table 2.3 is a record of the daily rainfall for the 17 stations during the month of July 1978. The tendency for raindays to be grouped into rainy periods of 5 to 6 days followed by shorter dry spells, is well demonstrated, and reflects the fluctuation and intensity of upper easterly waves as discussed above.

Table 2.1 Cross correlation matrix for G.A.D.P. rainfall stations - 1978 rainy season

Station No Fig.2.11	Name																	
1. A	GOMBE C.A.P.	1.00																
9. J	KUMO C.A.P.	0.20	1.00															
11. L	KEMBU F.S.C.	0.25	0.58	1.00														
3. C	GOMBE G.R.A.	0.54	0.43	0.41	1.00													
12. M	KURI F.S.C.	0.17	0.27	0.39	0.23	1.00												
10. K	BULA F.S.C.	0.33	0.22	0.31	0.25	0.12	1.00											
5. E	KALSHINGI F.S.C.	0.09	0.18	0.27	0.14	0.21	0.13	1.00										
8. H	TUKULMA F.S.C.	0.13	0.46	0.28	0.22	0.22	0.19	0.35	1.00									
6. F	ZAMBUK F.S.C.	0.42	0.11	0.01	0.13	0.07	0.29	0.02	0.05	1.000								
15. Q	TUMU F.S.C.	0.02	0.05	0.06	0.08	0.07	0.05	0.08	0.06	0.02	1.000							
4. D	STIRLING A.S.T.	0.21	0.33	0.20	0.29	0.19	0.18	0.22	0.21	0.08	0.03	1.000						
17. S	TALASSE F.S.C.	0.21	0.28	0.40	0.29	0.51	0.12	0.22	0.34	0.04	0.05	0.18	1.000					
2. B	BOGO F.S.C.	0.75	0.29	0.34	0.52	0.35	0.30	0.16	0.25	0.30	0.01	0.25	0.44	1.000				
7. G	DEBA F.S.C.	0.06	0.08	0.18	0.08	0.16	0.05	0.44	0.19	0.02	0.09	0.01	0.14	0.00	1.000			
14. P	LAWANTI F.S.C.	0.17	0.22	0.17	0.18	0.08	0.29	0.04	0.09	0.16	0.04	0.13	0.16	0.23	0.03	1.000		
13. N	DADIN KOWA F.S.C.	0.83	0.25	0.31	0.39	0.33	0.11	0.13	0.08	0.13	0.04	0.14	0.35	0.27	0.13	0.13	1.00	
16. R	BILLIRI F.S.C.	0.11	0.18	0.16	0.10	0.14	0.01	0.34	0.27	0.07	0.09	0.12	0.17	0.22	0.35	0.03	0.01	1.00

Table 2.2 Correlation between daily rainfall at Gombe CAP and other stations - 1978 April-October.

Station	Distance (km)	Correlation (r)	Total annual (mm)
1(A) Gombe CAP	0.0	1.00	1118.8
2(B) Bogo FSC	0.3	0.75	962.1
2(C) Gombe GRA	3.7	0.54	874.3
4(D) Gombe SA	5.6	0.21	1162.8
5(E) Kalshingi FSC	6.2	0.09	890.8
6(F) Zambuk FSC	8.7	0.42	919.7
7(G) Deba FSC	10.7	-0.06	732.3
8(H) Tukulma FSC	11.2	0.13	729.7
9(J) Kumo CAP	12.2	0.20	780.5
10(K) Bula FSC	13.5	0.33	1108.1
11(L) Kembu FSC	13.7	0.25	1061.6
12(M) Kuri FSC	14.7	0.17	710.3
13(N) Dadin Kowa FSC	16.6	0.33	871.2
14(P) Lawanti FSC	17.2	0.17	1051.6
15(Q) Tumu FSC	18.4	0.02	706.4
16(R) Billiri FSC	21.7	0.11	785.1
17(S) Talasse FSC	31.5	0.21	972.1

(Letters refer to later diagrams 2-12, 2-15 and 2-16)

The spatial variation between stations has been reported by other workers in Southern Nigeria (Nwa, 1977) and East Africa (Jackson, 1978). The extent of the variations appears to be more marked in the Gombe area than in either of the other studies. Jackson presents data for two stations 8km apart in Tanzania. This data is reproduced in Table 2.4

Table 2.4 Annual rainfall(mm) 1946-54 for two Tanzanian stations (After Jackson (1978))

Station	1946	1947	1948	1949	1950	1951	1952	1953	1954	Average
A	754.6	973.1	966.5	790.1	1069.6	1188.7	755.1	1108.7	930.7	948.6
B	859.8	1248.4	1420.9	619.8	1127.0	1127.0	564.5	859.8	869.8	966.4
(A + B)	-105.2	-275.3	-454.4	+170.3	+61.7	+61.7	189.7	248.9	+61.0	-17.8

Table 2.3 Daily rainfall for July 1978 at 17 stations in the Gombe area (mm)

Day	Station																
	1	2	3	4	5	6	7	8	9	10	11	12	13	14	15	16	17
1.			13.5						5.1	8.6	16.5	22.8	31.0	44.0	25.4		48.0
2.		17.3		13.0			6.9	28.4					9.4			54.9	38.0
3.			26.0			14.7						33.0					
4.		21.3		21.2	11.9		6.6	12.7	26.7	37.3	19.0	23.6		20.4	41.9		10.0
5.	33.0				15.5	38.6	17.8										20.1
6.																	
7.						36.1						44.2	32.2				
8.		18.8	20.4	20.0	24.6		9.7	23.4	44.9	20.5	70.3			14.0	11.7	43.7	
9.	20.3		9.8	25.2	1.0		10.4						24.4	38.0			
10.									5.6	40.1	29.5	22.8			8.6		34.0
11.							44.9										14.0
12.	40.6	31.7	36.7	27.3		18.0									37.6		
13.	25.4	31.0	27.6	15.7				22.8	23.6	15.0	24.1	20.3		38.0	25.6		10.0
14.					21.8		28.7										28.4
15.		1.8	36.7	20.3		3.0			17.8	33.0	62.7			22.0			
16.		2.3	0.5	20.6	25.6			8.9	6.3	3.5	1.8			8.4	6.3	47.5	
17.					2.3	28.7	28.4	8.4		1.0			29.5	12.0	7.9	0.8	
18.	8.6	4.6	4.1	4.8	10.7		17.3		33.3		17.3	6.8		16.0	33.3		12.5
19.																	4.6
20.																	
21.																	
22.													3.1				
23.		4.3	4.8						40.4				2.8	26.0			
24.		8.6	2.8	80.9		10.7	1.5		26.7	11.2	2.3		4.6	3.0	3.8		
25.		16.8	9.8	8.8				3.3	0.8		1.0	7.6		7.6	33.0	12.2	25.0
26.					4.8		9.4	6.3					2.8		1.3	6.3	
27.			0.8														
28.																	
29.								10.1									
30.																	
31.	64.0	58.9	33.9	16.5					20.3	18.5	34.4	38.1	35.3				22.5

The average of the nine year period for each station in Table 2.4 converges markedly, but marks a very considerable variability.

Figure 2.12 indicates the annual totals for the GADP region and represents clearly the local variability.

Rainfall distribution in time.

The daily rainfall records for the years 1941 to 1979 have been obtained from the Nigerian Meteorological Service. With the exception of the period October 1966 to September 1968, the time of the Nigerian civil war, the record is complete. This period has been completed by a controlled data estimation method.

The data was summed to produce 10 day, monthly and annual totals, of which the average monthly and 10 daily data are presented in Table 2.5.

Table 2.5 Average monthly and 10 day rainfall for Bauchi, 1941-79.

	1-10	0.0			1-10	69.8	
January	11-20	0.0	0.0	July	11-20	82.0	270.1
	21-31	0.0			21-31	118.3	
	1-10	1.1			1-10	109.8	
February	11-20	0.0	1.9	August	11-20	104.6	319.0
	21-28	0.8			21-31	104.6	
	1-10	0.1			1-10	70.9	
March	11-20	1.5	3.8	September	11-20	64.8	177.5
	21-31	2.2			21-30	41.8	
	1-10	4.8			1-10	26.9	
April	11-20	11.0	30.7	October	11-20	8.0	38.7
	21-30	14.9			21-31	3.8	
	1-10	24.4			1-10	1.0	
May	11-20	25.2	85.2	November	11-20	0.0	1.0
	21-31	35.6			21-10	0.0	
	1-10	44.0			1-10	0.0	
June	11-20	49.4	148.0	December	11-20	0.0	
	21-30	54.6			21-31	0.0	

The mean annual rainfall for the period was 1074mm (sd = 165mm). Figure 2.13 shows the annual data, and the data filtered with a five point running mean. There appears to be a declining trend evident although Figure 2.14 indicates the data to be normally distributed.

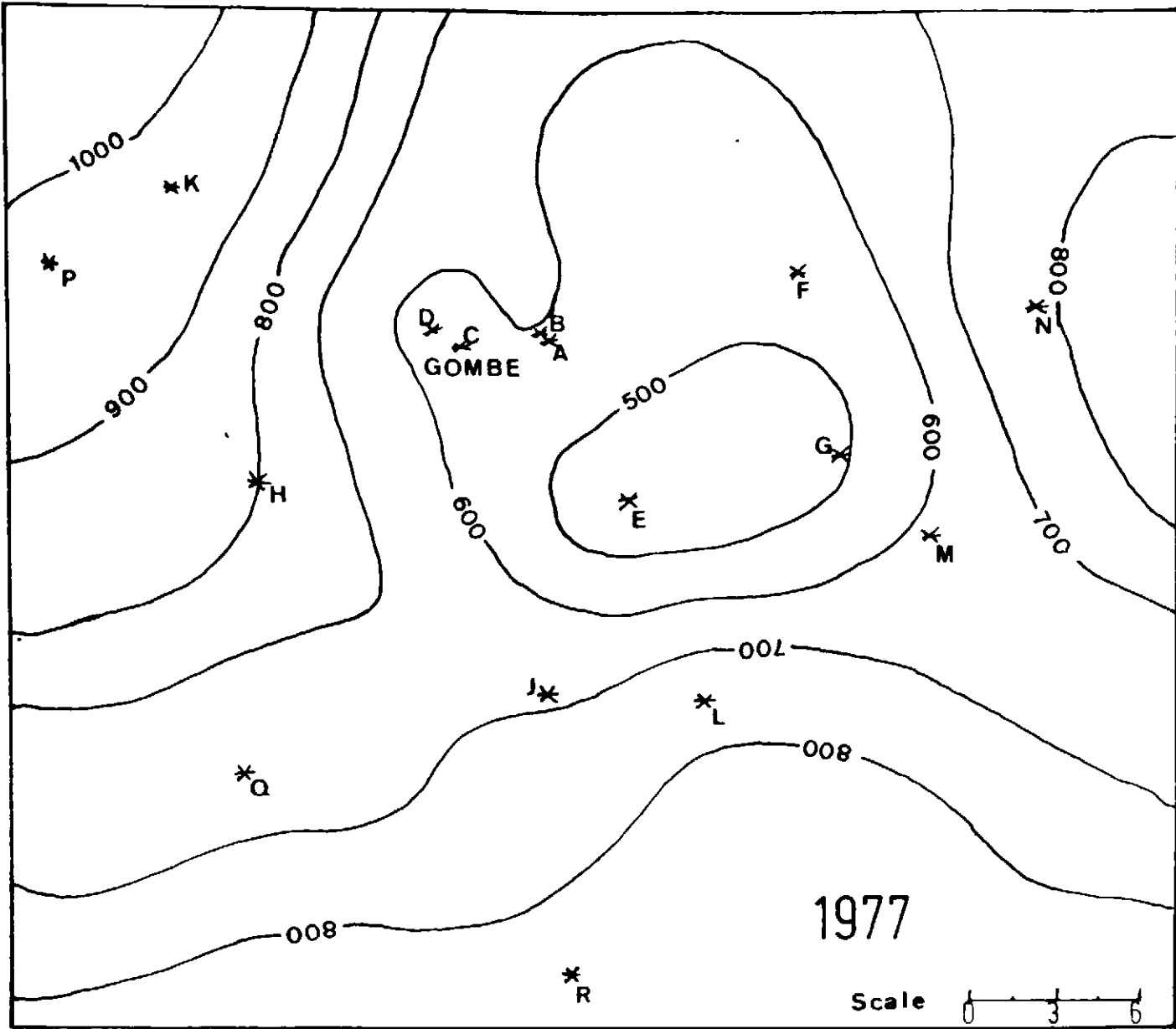


Figure 2-12 Annual Total Rainfall — GOMBE Area

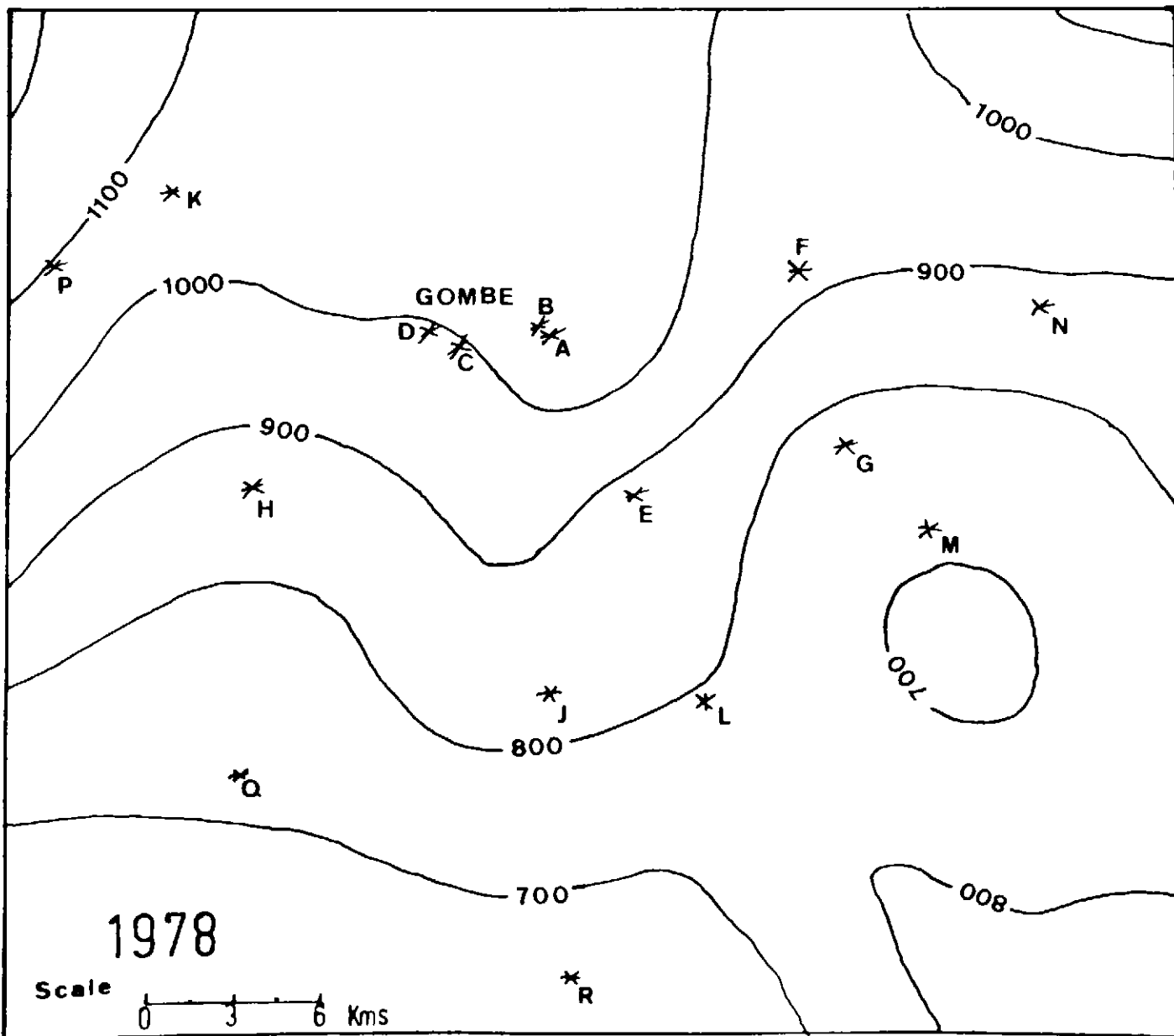
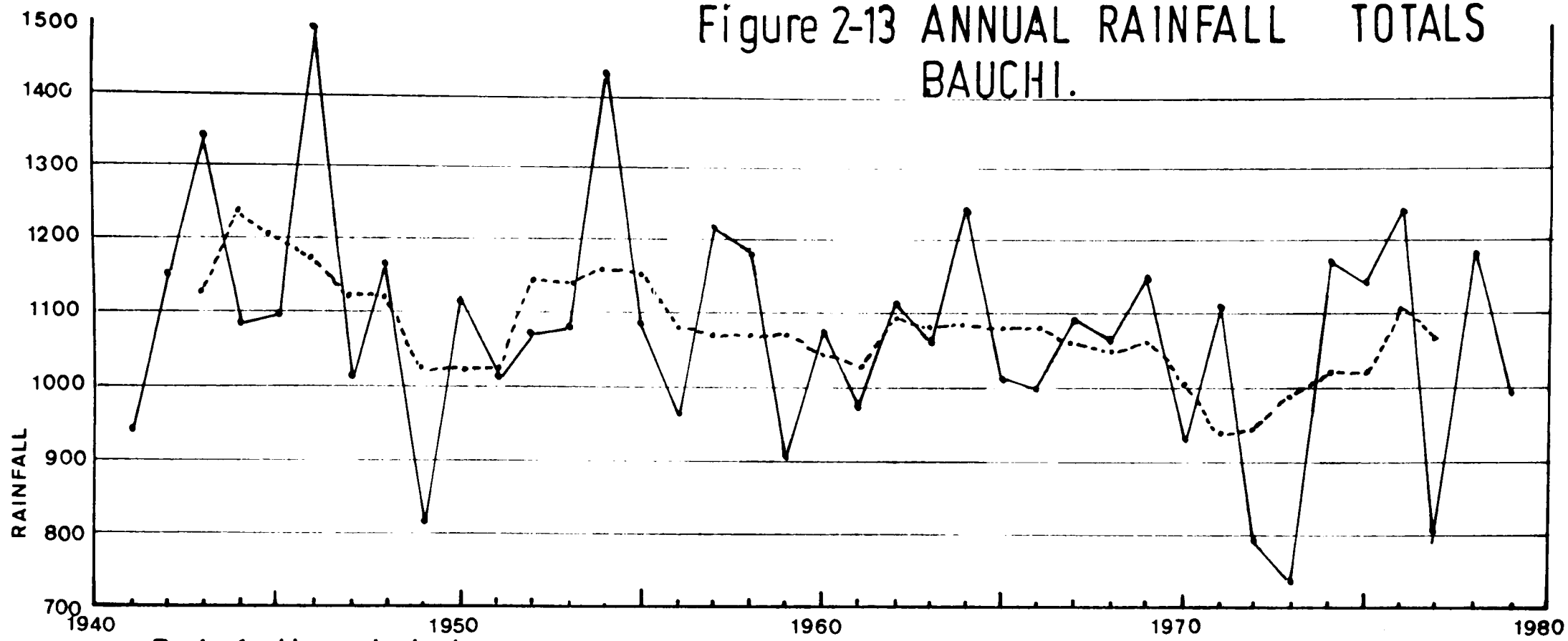
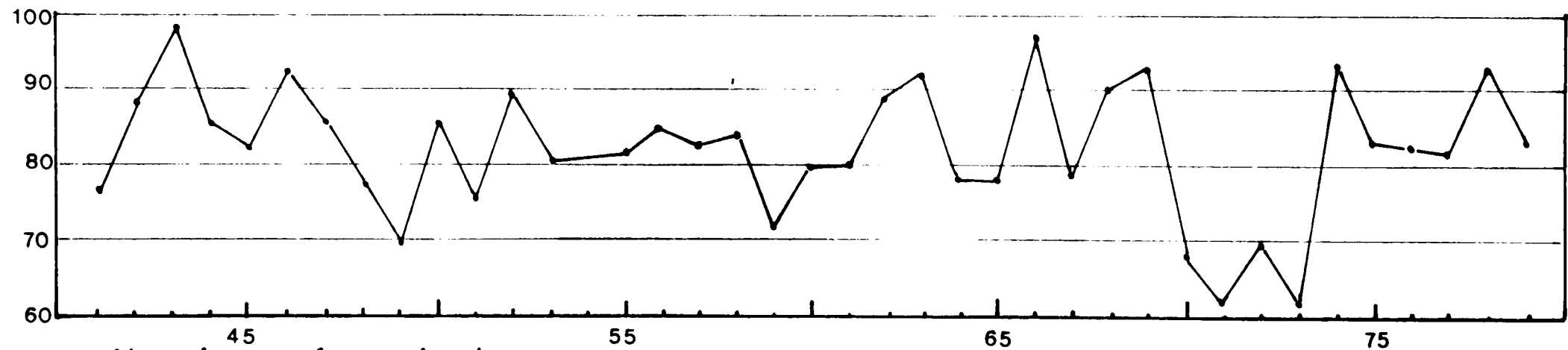


Figure 2-13 ANNUAL RAINFALL TOTALS
BAUCHI.

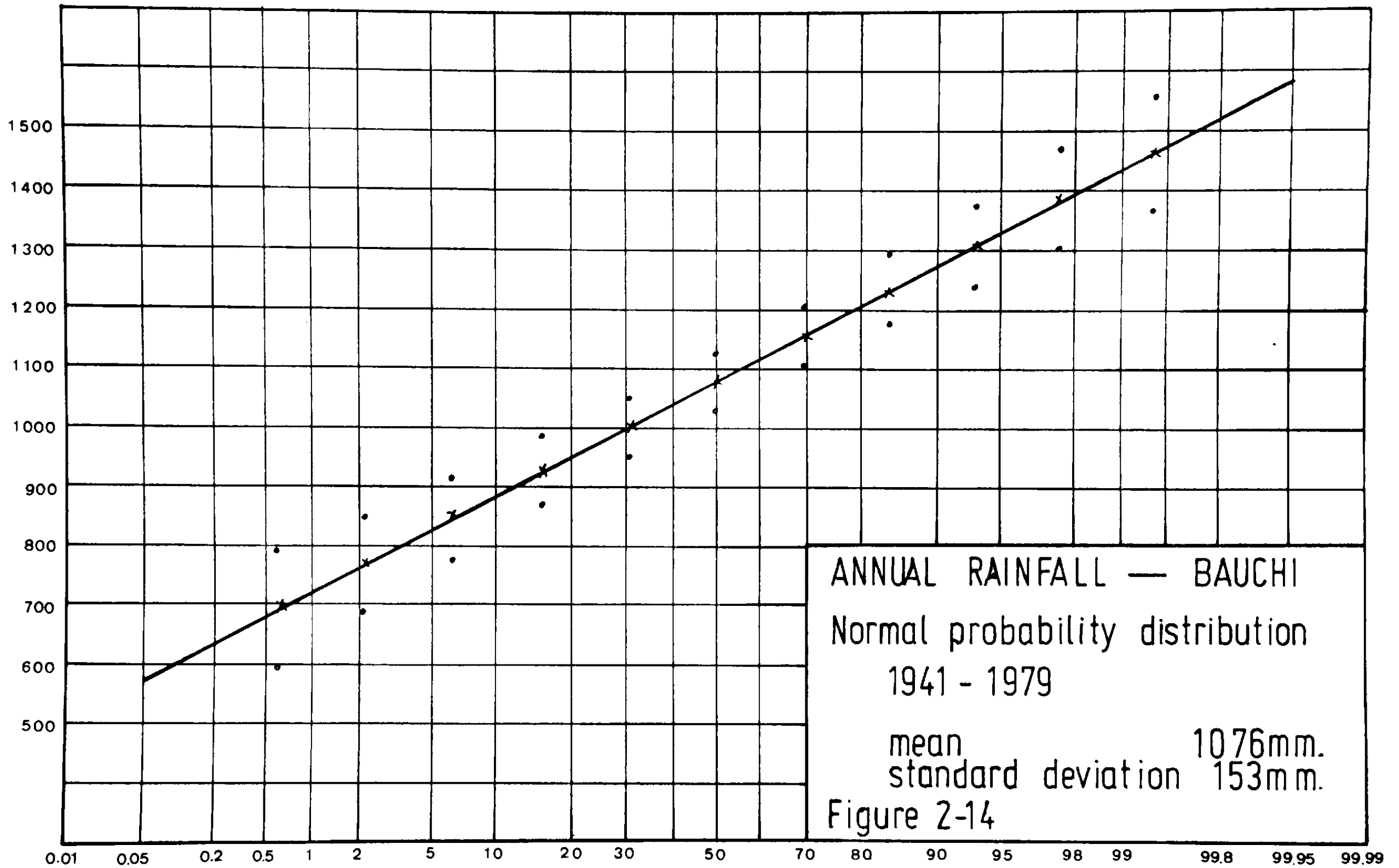


Rainfall totals

--- FIVE POINT MOVING AVERAGE



Number of raindays



Tropical rainfall has been reported (Griffiths, 1960,1966) to have a normal distribution in about 75% of cases and a log normal distribution in the remainder of cases. Kowal and Kassam (1975) report a normal distribution for the 1905-1973 rainfall record at Kano, Northern Nigeria.

The reliability of rainfall expressed in terms of confidence limits or standard deviations about a mean can be in doubt if the observed rainfall pattern is representative of a changing climate (Lamb, 1972). The evidence for the Bauchi rainfall record is in conflict in that the probability plot indicates a normal distribution, while the graph of annual totals shows a declining trend. The 1973 low rainfall total of 730mm had a probability of 12% or a return time of once every 83 years. Extrapolation of the annual rainfall plot suggests that 1984 may have a lower rainfall than 1973, thus indicating a much smaller return time. However, in the aftermath of the sahelian drought of the early seventies, Bunting et al (1976) carried out a statistical analysis of the available long term records of the region. Their conclusion was that the succession of drought years in the early seventies fell within statistical expectation and did not indicate a changing climate in the area. Figure 2.14 tends to confirm this, in that annual totals fall very closely about a normal probability distribution.

Some concern has been expressed, particularly in view of the sahelian drought, that various desertification procedures are causing a change of climate (Howard, W.J., 1976). The lack of firewood in the savanna is resulting in an increased rate of felling of the few trees which do exist. Overgrazing is also leading to a marked deterioration in soil structure. It is argued that both these factors result in a change of the albedo (reflectivity of the surface) and that this results in a changed net radiation budget. The loss of vegetation results in an increased albedo which, in turn produces a decrease in the net radiation received at the surface. This loss of net radiation produces less instability in the lower troposphere and therefore less rainfall. The process is one of positive feedback. These topics are discussed further by Otterman (1974), Charney (1975), and Walker-Rowntree (1976).

The variation of rainfall in the spatial dimension is reflected by an equivalent variation in the time dimension. The Bauchi rainfall record indicates that rain falls on an average for 81 days each year. A rainday is defined as a 24 hour period, (usually 10.00 to 10.00) when

measurable rainfall is recorded. The standard deviation around the mean number of raindays is only 9.6. Years with low annual totals do not necessarily correspond with years when a low number of raindays occurred. In 1976, 81 raindays produced 1238mm rainfall, whereas in 1977, 80 raindays produced only 809mm.

The daily totals for each rainday were ranked and cumulative percentage figures calculated for each year. Fifty percent of the annual rainfall falls on less than 17% of the raindays. Typically some 500mm of rainfall falls in only 14 daily periods. These raindays may occur at any time from April to October.

The poor distribution of rainfall can be traced to a small number of intense bursts associated with individual storm cells. Within the GADP area, two rainfall intensity gauges were set up. The locations of the gauges are shown in Figure 2.11. One gauge was relocated at the beginning of the 1978 rainy season. The gauges were of the 24-hour-tipping bucket type and were operated by GADP staff.

The intensity gauge data correlate poorly with immediately adjacent 24 hour rain gauge measurements. This may represent the extreme variability of tropical rainfall, or considerable observer error. The probability must be that the gauges were incorrectly read on a number of occasions, although it would seem unlikely that observer error is responsible for more than a proportion of the dubious readings.

Two days have been selected from the 1977 and 1978 rainy seasons in which the intensity gauge data is shown alongside the spatial distribution. It is considered that this form of presentation* clearly demonstrates the overall structure of the storm event. Figure 2.15 shows the data for August 21 1978, while Figure 2.16 represents data for October 27 1978. These figures are largely representative of storm events throughout the year.

As the temporal structure of a storm event has considerable significance when calculating infiltration^{and} runoff (see section 5), the structure of a number of storm records was investigated further. The data for a part of the 1978 rainy season was decomposed into fifteen minute totals. Fifty events were recorded with a total rainfall of 710mm. The total time during which rain fell was 93 hours, however, a large proportion of this total time was the result of light rainfall at the end of a

*Note. The contours have been calculated and drawn using a computer centre software package called Ginosurf.

24 Hour Total Rainfall (mm)

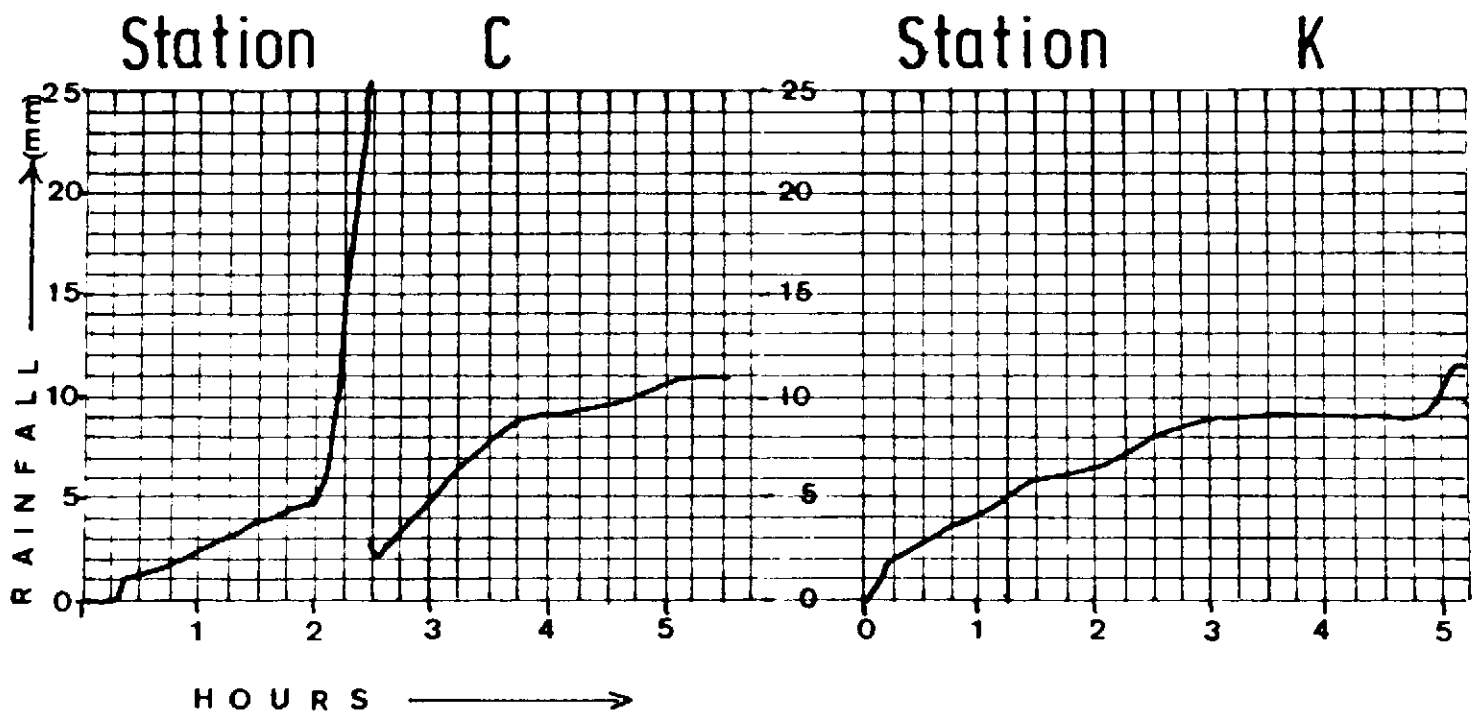
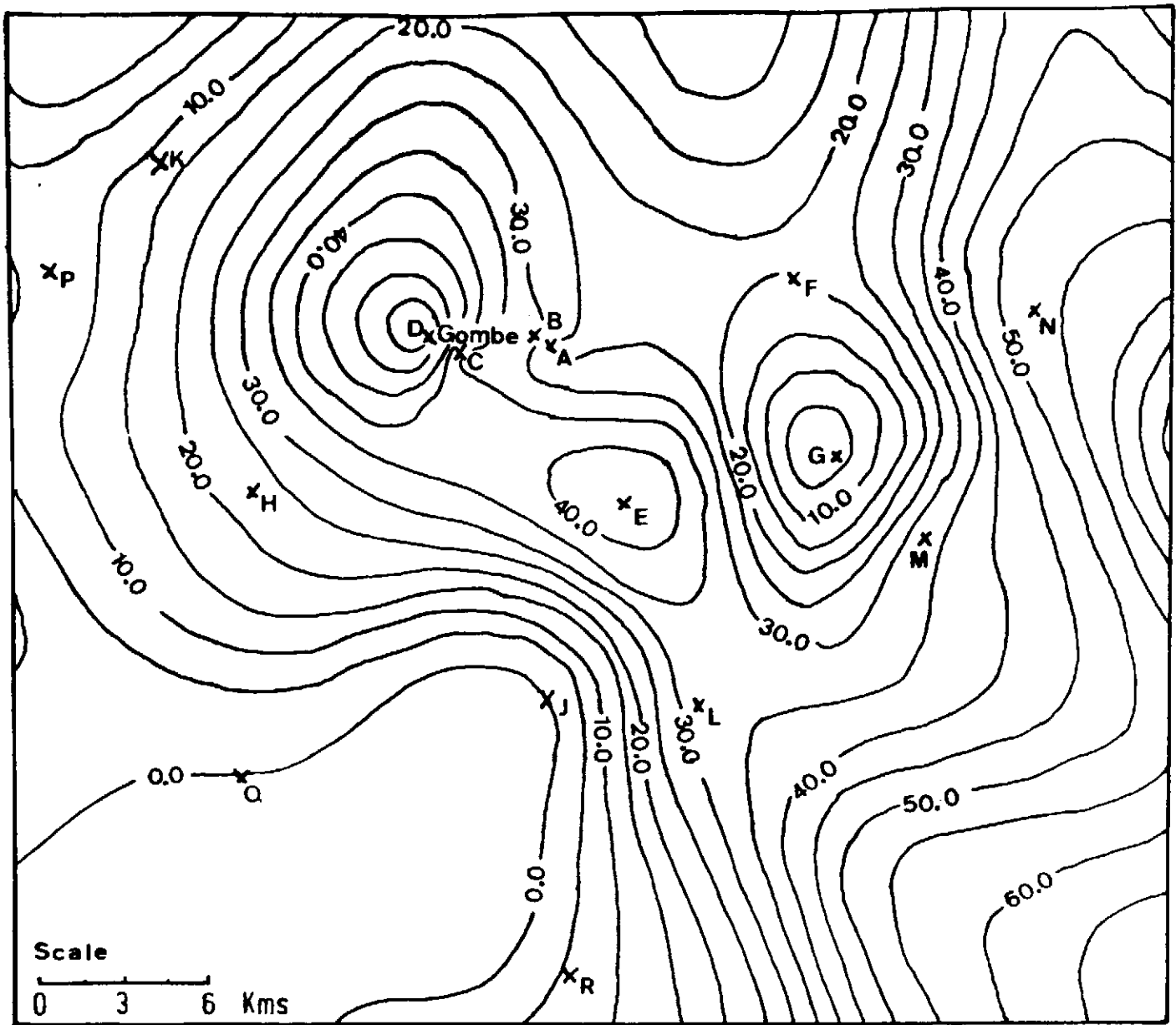


Figure 2-15 GOMBE — Bauchi State

Isohyets of 24 hour rainfall for August 21 - 1978

The station letters refer to Table 2-2

Intensity gauge data for two stations indicates the time structure of the event.

24 Hour Total Rainfall (mm)

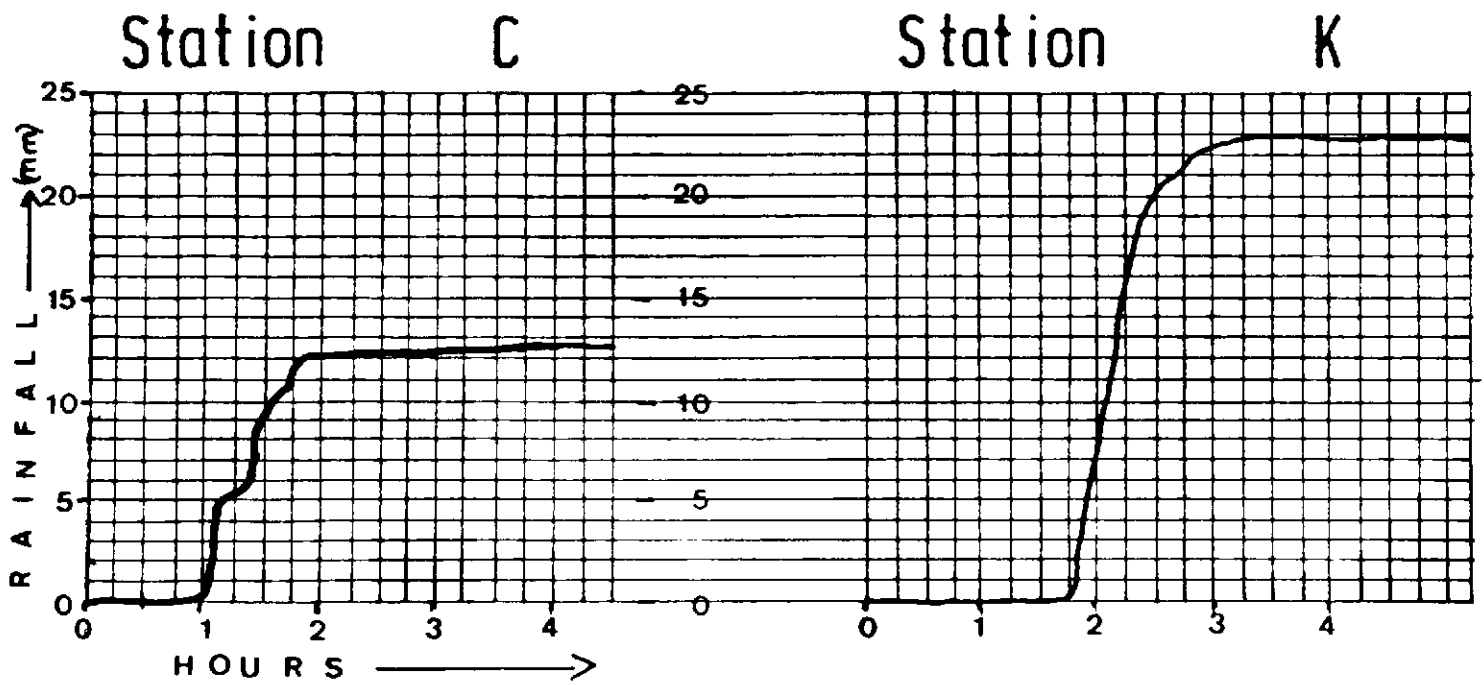
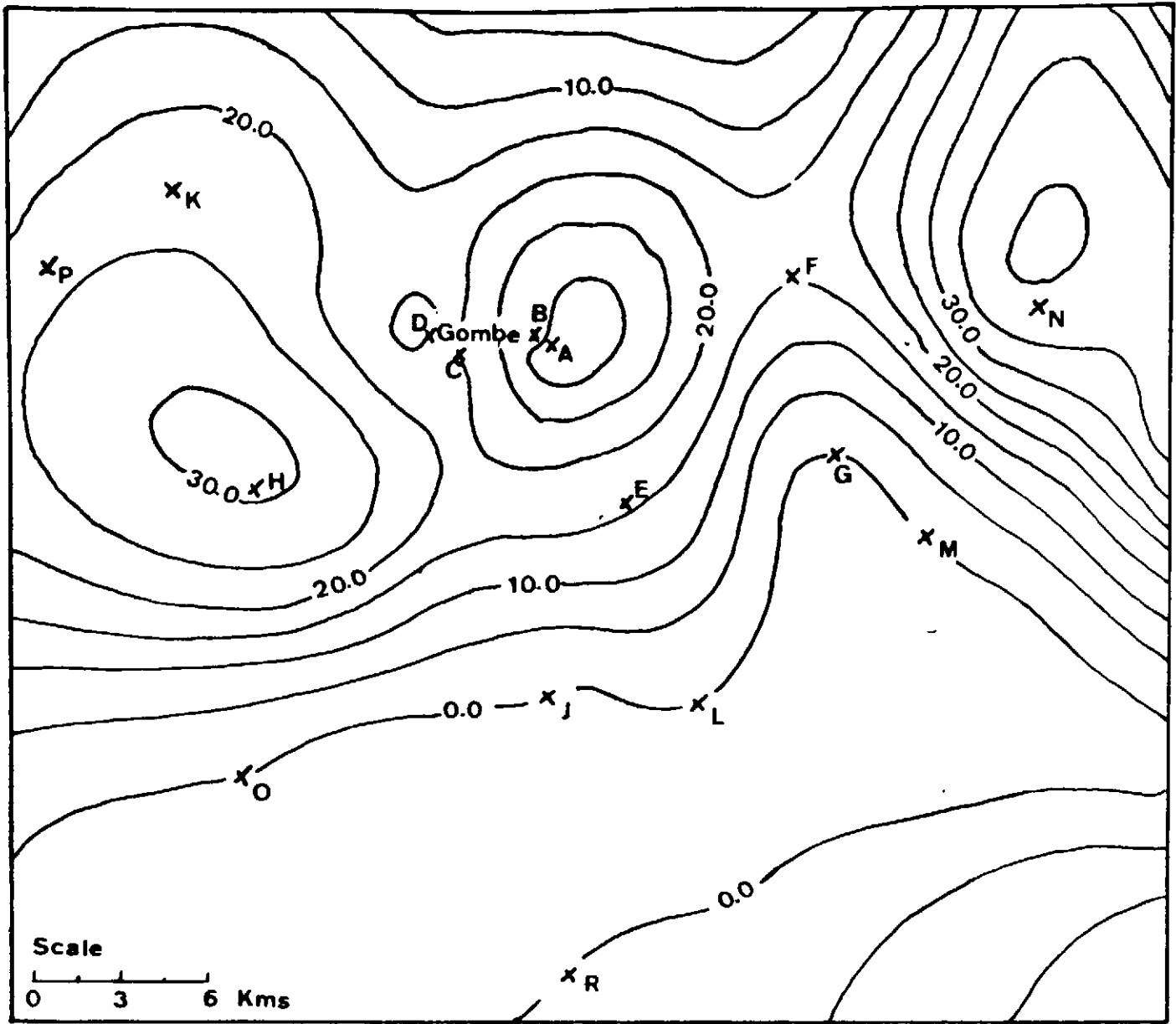


Figure 2-16 G O M B E — Bauchi State

Isolyets of 24 hour rainfall for October 29 1978

storm cell passage. 31% of the total fall occurred in bursts of intensity greater than 10mm in fifteen minutes, with a maximum fifteen minute intensity of 16.3mm. The rainfall intensities shown in figures 2.15 and 2.16 are typical of the total record.

As the rainfall intensity gauge data for GADP headquarters in Gombe was used, a comparison with the GADP rainfall gauge data for 1978 was possible. An examination of the records suggests that only 15 events were missing from the intensity gauge data. Assuming that the sample of recorded data fairly represents the missing data, it may be calculated that rain fell for a total time of 120 hours during 1978.

Energy Load of Rainstorms.

The bursts of high intensity rainfall which characterise the savanna record, as discussed above, are caused by circulation within very large cumulonimbus cells. The energies released by the latent heat of water are sufficient to build up very strong air circulation within the cells. The result of this is that the raindrops can attain a large size before falling out of the system.

Kowal and Kassam (1976) have analysed a number of storms at Samaru, recording parameters such as drop size distribution, instantaneous intensity, energy load and drop number. Ellison (1944) demonstrated the erosive nature of raindrop splashes and the effects of individual large raindrops on the soil surface. These characteristics of tropical rainfall, and particularly the large drop size, result in the breaking up of the soil aggregates, compaction, and the sealing of the soil surface. The sealing effect on the soil surface produces a decrease in infiltration and an increase in runoff and soil erosion.

Kowal (1970c, 1970d) describing the results from a small experimental catchment at Samaru, found that out of an average of 85 rain days, 32 rainstorms (30%) produced runoff. The water from the remaining 53 rainstorms was wholly accepted by the soil. All rainstorms producing more than 20mm of rainfall caused some runoff, although the amount of runoff was a complicated function of rainfall duration, intensity, and antecedent soil moisture conditions.

Kowal reported that natural vegetation had the lowest runoff percentage of total rainfall, due to the more efficient root structure for allowing infiltration to penetrate, and the intercepting qualities of the canopy and ground mat of decaying vegetation.

The Institute of Hydrology (1977) in a regional study of the Congo River, which flows through savanna areas in Bauchi state, suggested the use of a 10% runoff factor for Basement rock types in the savanna.

2.3 SOLAR RADIATION BALANCE

General

Solar radiation is the single most important factor of the savanna environment. The energy input is responsible for causing rainfall and evaporation, and therefore has a dominant influence on the water balance, on crop production and the whole ecology of the savanna. It is important to quantify the radiation and to measure the net radiation which is taken up by the surface as accurately as possible. Unfortunately, measurement of net radiation is very scarce in the savanna and the calculation has to be approached from an empirical manner.

Solar Radiation.

The sun is assumed to act as a black body, with a surface temperature of $6,000^{\circ}\text{k}$ (Harvey, 1976.) The total electro-magnetic radiation, per unit surface area, emitted by the sun is described by Stefan's Law which may be represented mathematically as :-

$$E = \sigma T^4$$

————— 2-2

where σ = Stefan's constant $\frac{5.67 \times 10^{-8}}{\text{Wm}^{-2}\text{K}^{-4}}$

E = Energy $[\text{Wm}^{-2}]$

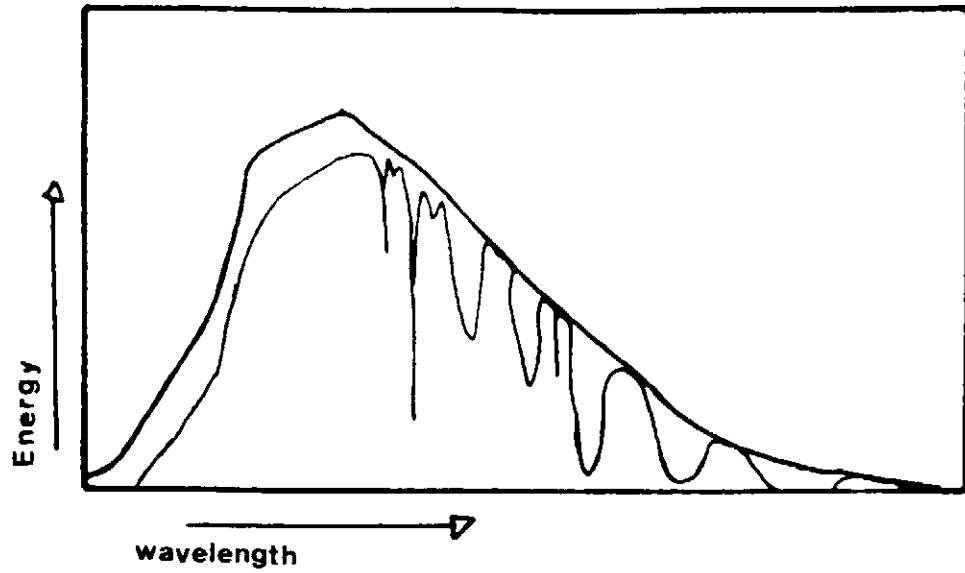
T = Temperature of surface $^{\circ}\text{k}$

The electro-magnetic energy is spread through a wide range of wavelengths and is shown graphically in Figure 2.17. Approximately 99% of the sun's radiation is of wavelengths between $0.15\mu\text{m}$ and $4.0\mu\text{m}$. The maximum emission is of a wavelength of about $0.5\mu\text{m}$ (blue-green light) (Harvey, 1976).

The sun radiates in all directions, and therefore the earth only receives a small fraction of that energy. The amount of energy produced by the sun in unit time is thought to be approximately constant. It may vary slightly due to sun spot activity, however the variation is too small to measure with the techniques currently available. A variation of five percent has been suggested however, and although this seems small, it is demonstrated to have a measurable effect upon evaporation calculations discussed later.

A quantity known as the solar constant has been defined to represent the amount of energy that a surface would receive, which is perpendicular to the sun's rays and, exposed at the mean distance of the earth from the sun, with no atmosphere to cause distortion. This quantity has

Figure 2-17 Spectral distribution of incoming radiation.



SHOWING THE SOLAR BEAM BEFORE AND AFTER
PASSING THROUGH THE EARTH'S ATMOSPHERE

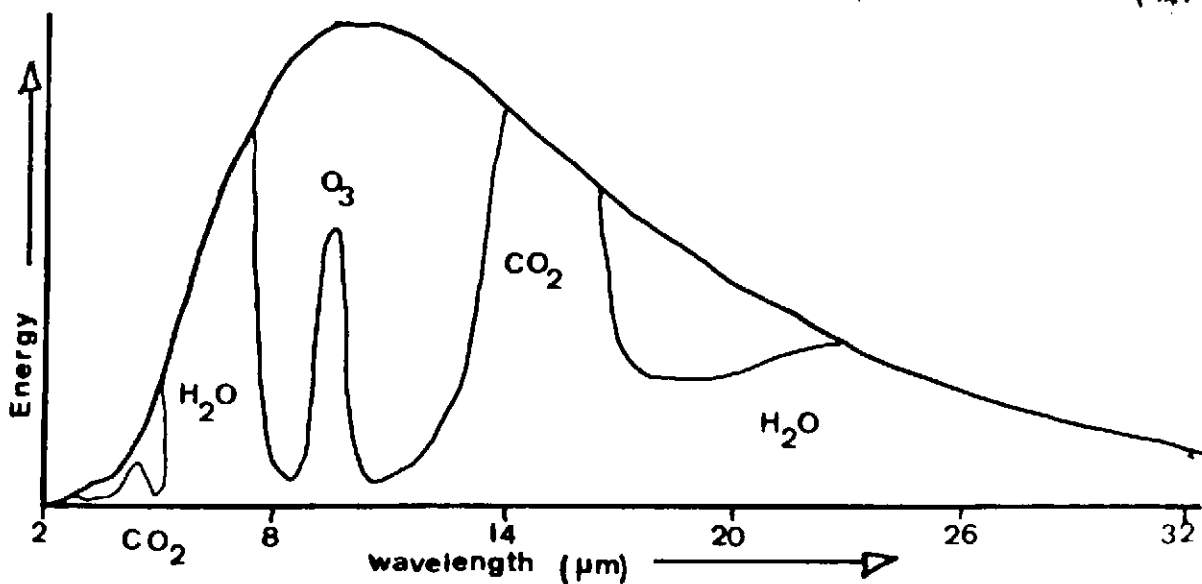
(After LAMB 1972)

Figure 2-18 Spectral distribution of outgoing radiation

BLACK BODY TEMPERATURE 285 K

SHOWING ABSORPTION BANDS OF THE
EARTH'S ATMOSPHERE,

(After HARVEY 1976)



been found (S.M.T.,1958; Harvey, 1976) to be 1.36 k Wm^{-2} .

Three factors modify the amount of radiation actually received at a point on the earth's surface. The first is the position of the earth in its elliptical orbit around the sun. The second is the inclination of the earth's axis of rotation ($23\frac{1}{2}^{\circ}$) to the plane of the elliptic. The third is the latitude of the receiving surface.

The theoretical incoming radiation above the atmosphere may be calculated as follows (S.M.T.,1958; H.M.S.O., 1973).

$$\frac{d(R_a)}{dt} = \frac{J_o}{r^2} \cos z \quad \text{----- 2-3}$$

where R_a = incoming radiation [Wm^{-2}]
 J_o = solar constant 1.36 [kWm^{-2}]
 z = sun's zenithal distance
 r = radius vector of the earth

$$\cos z = \sin \phi \sin \delta + \cos \phi \cos \delta \cos h \quad \text{----- 2-4}$$

where ϕ = latitude of the observer (rads)
 δ = declination of the sun (rads)
 h = sun's hour angle, the angle between the sun's zenith for the observer and the horizon.

replacing 2.4 in 2.3 and rearranging

$$\frac{d(R_a)}{dt} = \frac{J_o}{r^2} \sin \phi \sin \delta + \frac{J_o}{r^2} \cos \phi \cos \delta \cos h$$

Integrating w.r.t. t [$h = f(t)$]

$$R_a = h \left(\frac{J_o}{r^2} \sin \phi \sin \delta \right) + \frac{J_o}{r^2} \cos \phi \cos \delta \sin h$$

$$R_a = \frac{J_o}{r^2} [h \times \sin \phi \sin \delta + \cos \phi \cos \delta \sin h] \quad \text{----- 2-5}$$

The value of h may be found by considering the sun's altitude for a given observer.

$$\sin(a) = \sin \phi \sin \delta + \cos \phi \cos \delta \cos h$$

($\cos z = \sin a$)

Table 2.6 Seasonal variations of solar radiation outside the atmosphere at latitude $10^{\circ}3'N$
 - Bauchi.

Date	Mar 21	Apr 13	May 6	May 29	Jun 22	July 15	Aug 8	Aug 31	Sep 23	Oct 16	Nov 9	Nov 30	Dec 22	Jan 13	Feb 4	Feb 26	Mar 21
Day No	80	103	126	149	173	196	220	243	266	289	312	334	356	13	35	57	80
Longitude of the sun	0°	22.5°	45°	67.5°	90°	132.5°	135°	157.5°	180°	202.5°	225°	247.5°	270°	292.5°	315°	337.5°	360°
Declination of the sun	-0.1°	8.8°	16.3°	21.4°	23.5°	21.8°	16.6°	9.3°	0.1°	-8.6°	-16.3°	-21.5°	-23.4°	-21.6°	-16.4°	-9.0°	-0.1°
Incoming Radiation In [Wm^{-2}]	430	439	437	432	428	422	433	433	426	407	383	364	356	365	387	411	430
Incoming Radiation for U.K. [Wm^{-2}]	259	342	413	460	479	460	409	339	261	181	116	77	64	77	117	179	252

Data computed using algorithm described in appendix A.



When the sun's altitude is zero, $\sin a = 0$
and therefore :

$$h = \cos^{-1}[-\sin\phi \sin\delta / \cos\phi \cos\delta] = \cos^{-1}[-\tan\phi \tan\delta] \quad \text{————— 2-6}$$

From Equations 2.5 and 2.6, R_a may be computed from known terms. The daily value of declination (δ) and the radius vector (r) may be tabulated from observations. Tables of these constants have been produced by the Smithsonian Institute (S.M.T., 1973), and the algorithm that has been written to calculate daily evaporation, uses daily values of these two variables (Appendix A).

Table 2.6 summarises a number of solar variables and includes values of R_a in Wm^{-2} for Bauchi and for comparison, a U.K. station. To convert these values in Wm^{-2} to the more familiar units of mm equivalent evaporation per day, a factor of 3.4979×10^{-2} is employed. This data has been calculated using the algorithm presented in Appendix A.

Dispersion of Solar Radiation.

Only a portion of the incoming radiation is received at the earth's surface as direct radiation, the remainder is reflected, absorbed or scattered by the earth's atmosphere and surface. About one third is usually reflected back to space, mainly from clouds. Table 2.7 after Weisner (1970) indicates the dispersion of solar radiation.

Table 2.7 Dispersion of solar radiation.

	Type of Day		
	Clear	Overcast	Cloudy
Reflected and scattered back to space.	21	75	42
Absorbed by water vapour	11	3	11
Absorbed by gases	2		4
Direct and scattered radiation reaching the earth's surface	66	22	43
	100	100	100

The amount of depletion also depends upon the solar air mass (the length of the beam's path through the atmosphere) since the highest concentration of dispersing and absorbing materials are found near the

ground level (Kowal - 1978).

Water vapour and carbon dioxide, both highly variable components of the atmosphere, absorb varying quantities of radiation depending upon the amounts present in any one day. The radiation during the dry season is more effective, due to the very low humidity of the north east trade wind, than the radiation during the wet season.

Assessment of Albedo.

A proportion of the direct or scattered radiation that reaches the earth's surface is reflected back to space. This proportion is known as the albedo of the earth's surface, and is strongly dependent upon the nature of the surface. Typical albedos for surfaces in Nigeria are reported by Kowal (1978) and are presented in Table 2.8.

Table 2.8 Albedo of some typical surfaces.

	α
Fresh green tropical vegetation	0.20
Dry soil during the dry season	0.35
Wet bare soil	0.10
Water-dependending upon the angle of incidence and colouration	0.04-0.39
Dark forest	0.05
Short grass	0.25

Kowal (1978) reports further significant changes in the albedo of a crop as the crop grows and matures. These measurements are especially important as the radiation balance during the wet season has a particularly marked effect on the evapotranspiration, as discussed later. Kowal's values are presented in Table 2.9.

Table 2.9 Albedo (α) of maize and millet crops at Samaru - Northern Nigeria (After Kowal.(1978))

Period	Maize	Millet
21-31 May		0.26
1-10		0.25
11-20 June	0.26	0.26
21-30	0.21	0.23
1-10	0.19	0.15
11-20 July	0.18	0.15
21-31	0.17	0.13
1-10	0.16	0.14
11-20 August	0.16	0.13
21-31	0.15	0.14
1-10	0.15	0.17
11-20 September	0.14	0.15
21-30	0.14	
1-10 October	0.13	

Calculation of Net Radiation.

There are no measurements of actual incoming radiation at Bauchi, and for the assessment of incoming radiation received at the surface, the Angstrom (1924) empirical formula is used. This takes the form

$$R_c = R_a [1.0 - \alpha] \times [a + b(n/N)] \quad \text{-----} \quad 2-7$$

where R_c = radiation received at surface Wm^{-2}
 α = albedo
 n = observed sunshine hours
 N = maximum possible sunshine hours

a and b are regression constants

The value of observed sunshine hours is taken from measurements made with a Campbell-Stokes sunshine recorder. These measurements are made in Bauchi, and the recorder can be seen in Plate 2.1. The recorder does not measure diffuse light, under cloud cover, or dust haze, and also underestimates sunshine at low solar altitudes, however, the recorder is simple to operate and is widely used throughout the savanna.

The value of N may be calculated from the following relationship :

(Chidley & Pike, 1968).

$$N = \frac{240}{2\pi} \times 2h + 0.11$$

————— 2.8

where h is the sun's hour angle in radians from equation 2.6.

The calculated values tabulated by the Smithsonian Institution are based on the daylight commencing when the disc of the sun first appears above the horizon and ending when it disappears below the horizon. The above Equation (2.8) is based on the sun's centre. It is necessary to add a correcting factor which will vary with latitude. For instance, in the limiting case when the latitude is greater than 66° , the sun's disc may appear over the horizon for several hours without the centre appearing. A figure of 0.11 hours is found to be appropriate for the latitude of Bauchi.

Kowal (1972a) has compared incoming radiation measured by a Kipp solarimeter and integrator with calculated radiation using the Angstrom equation. The results are presented in Table 2.10. Two sets of values of a and b , the regression constants in Equation 2.7 were used. The values $a = 0.15$ and $b = 0.55$ are those recommended for use at Rothampstead in U.K. Until recently, these values have been used in Nigeria to compute the R_c term. As can be seen from Table 2.10, a considerable error is introduced. McCulloch, working in East Africa, proposed a general form for a and b viz :

$$a = 0.29 \cos \phi$$

$$b = 0.55$$

For the latitude of Bauchi the value of a is 0.285.

Kowal (1972a) recommends the use of $a = 0.235$ and $b = 0.535$ for Samaru. These values provide a good assessment of R_c as measured at Samaru. Davies (1966) measured R_c at Ibadan and arrived at twelve different monthly values of a and b . The average values were $a = 0.125$ and $b = 0.733$ (see Table 2.10).

It can be seen from Table 2.10 that approximately half of the solar radiation is absorbed or reflected by the atmosphere. The large error bounds for the mid rainy season month of August are due to the effects of cloudiness on the measured value. Often, after a storm, the atmosphere

has low humidity and the absorption of solar radiation is less than usual. In addition, the atmosphere is less dusty and therefore a greater percentage of the radiation is transmitted.

Table 2.10 Average daily radiation at Samaru (After Kowal, 1972a)

Month	Measured Radiation W_m^{-2}	R_a W_m^{-2}	Calculated Radiation $a = 0.18 \quad b = 0.55$	W_m^{-2} $a = 0.235 \quad b = 0.535$
J	229 \pm 11	367	217	223
F	258 \pm 7	397	245	262
M	265 \pm 5	425	237	256
A	248 \pm 10	437	229	249
M	249 \pm 9	433	228	247
J	235 \pm 24	426	218	237
J	216 \pm 10	427	198	217
A	213 \pm 36	432	175	196
S	230 \pm 13	427	208	227
O	245 \pm 7	405	235	252
N	234 \pm 7	375	230	246
D	222 \pm 21	356	214	229

Note. A value of $\alpha = 0.25$ is assumed although this is not stated by Kowal.

The effect of varying the albedo (α), causes a large change in the calculated R_c term. It is of great importance to estimate the albedo correctly if a reliable value of R_c is to be obtained. In certain circumstances the albedo remains constant throughout the year, notably for a water surface ($\alpha = 0.05$). If R_c is to be estimated for a land surface, then a variation of from 0.10 to 0.35 should be allowed for. Plate 2.1 shows the dry season ground surface at the meteorological station in Bauchi. The dust haze of the North East trade (Harmattan) is evident.

The earth is warmed by the receipt of radiation from the sun and radiates energy itself in much the same way as the sun. The earth is assumed to radiate energy as a black body at its mean air temperature at the surface. The energy emitted from the earth is also at a longer wavelength than that from the sun. The long wave radiation is reflected by cloud cover and to a lesser extent absorbed by water vapour. Figure 2.18, after Harvey (1976), indicates the nature of the back radiation. Apart from low absorption within the $0.8 - 1.4 \mu m$ wavelength, which escapes

freely into space, about 90% of the earth's radiation is absorbed by the atmosphere.

The effective back radiation may be estimated using the empirical equation derived by Brunt (1941).

$$R_b = \sigma T_a^4 [0.56 + 0.08(e_d)^{1/2}] \times [0.1 + 0.9(n/N)] \quad \text{-----} \quad 2-9$$

where σ = stefans constant $5.67 \times 10^{-8} \text{ Wm}^{-2}\text{o}_k^{-4}$
 T_a = air temperature o_k
 e_d = vapour pressure mb
 $\%N$ = ratio of observed sunshine hours to total possible sun hours

Although Equation 2.9 is an empirical relationship, it does estimate the R_b term to a reasonable degree of accuracy and is in general use. The occurrence of the vapour pressure term provides an explanation of why the land surface cools more efficiently on a clear night in the dry season than during the wet season. Frost damage occurs about once every ten years on exceptionally clear dry nights in the dry season.

The net radiation received at a surface is described as the difference between the upward and downward fluxes

$$R_n = R_c (1.0 - \alpha) \pm R_b \quad \text{-----} \quad 2-10$$

The concept of net radiation (R_n) serves as a convenient measure of the energy available for evaporation, evapotranspiration, heating of the soil and rock surfaces, and photosynthesis. The use of the net energy varies throughout the year and is examined in more detail below.

There are few measurements of R_n applicable to the savanna. Kowal (1972a) and Kassam and Kowal (1975) report measurements made with a Funk ventilated radiometer over short grass or crops at Samaru. The results are presented in Table 2.11.

The values of R_n (calculated) overestimate the values of R_n (measured) by varying proportions. No values of R_n were obtained for the dry season. However, as a result of the pronounced aridity and changes in the land cover that produce bare soil or dried grassland with isolated trees, the albedo and the R_b terms increase substantially, resulting in very low dry season R_n values.

Table 2.11 Measured and calculated values of net radiation (after Kowal 1972a)

Month	Measured		Calculated			
	R_c Wm^{-2}	R_n^a Wm^{-2}	R_c Wm^{-2}	R_n^b Wm^{-2}	R_b Wm^{-2}	$R_n^a - R_n^b$
1	229		223	23	144	
2	258		262	37	159	
3	265		256	67	125	
4	248	87	249	105	81	-18
5	249	111	247	117	68	- 6
6	235	119	237	117	60	+ 2
7	216	113	217	114	48	- 1
8	213	101	196	106	41	- 5
9	230	109	227	116	54	- 7
10	245	93	252	107	82	-14
11	234		246	53	131	
12	222		229	31	140	

Notes. The values of R_c calculated have been obtained using $a = 0.235$ and $b = 0.535$ in the Angstrom equation. A value of the albedo for short green grass is used in Equation 2.7 to calculate R_c .

Various instruments have been designed to measure net radiation directly, or in terms of some parameter which can be accurately correlated with net radiation. One such instrument which is widely used in Nigeria is the Gunn-Bellani distillator. Davies (1965) established a good linear relationship between Gunn-Bellani data and flux radiometer data for Ibadan and Benin. Both these stations are at approximately 7° latitude.

The Gunn-Bellani distillator installation at Bauchi is shown in Plate 2.2. The black sphere is heated by incident radiation which passes through the hollow glass sphere. The glass sphere sits on the black metal ring, at ground level. The heating causes water to be evaporated from a reservoir beneath the surface, which is condensed and falls to the bottom of the lower glass tube. A daily measurement of quantity of distillate is correlated with net radiation during an initial calibration. Unfortunately this calibration was not available at Bauchi.

To investigate the relationship between calculated net radiation using equations 2.7 and 2.9 ($a = 0.235$, $b = 0.535$), and Gunn-Bellani distillator measurements for Bauchi, a correlation analysis was carried out



Plate 2.1 Nigerian Government Meteorological Station, BAUCHI.
Note thick harmattan dust haze. No sunshine recorded by Stoke
Campbell recorder.

Plate 2.2 Gunn Bellani distillator - Bauchi.
Note very dry ground surface in early February.
Albedo = 0.35.



between the two variables. The results were unfortunately poor, being significantly better during the rainy season than during the dry season. The results are presented in Table 2.12.

Table 2.12 Monthly correlations between calculated net radiation and Gunn-Bellani data for Bauchi.

Month	1978	1979	α
1	0.47	-0.49	0.35
2	0.45	0.15	0.35
3	0.08	0.19	0.35
4	0.88	0.25	0.15
5	0.89	0.94	0.25
6	0.84	0.82	0.25
7	0.84	0.87	0.20
8	0.73	0.84	0.15
9	0.62	0.83	0.15
10	0.88	0.85	0.25
11	0.47	0.39	0.30
12	0.11	-0.35	0.35

The lack of correlation during the dry season is perhaps indicative of the significance of the albedo term (α). However, considerably greater correlation is required before distillator measurements can be used to accurately reflect net radiation. In the absence of radiometer measurements the theoretical net radiation calculation based on Equations 2.7 and 2.9 is preferred.

Equations 2.7 and 2.9 may be combined to form :

$$R_n = R_c [1.0 - \alpha] \times [a + b(n/N)] - \sigma T_a^4 [0.56 + 0.08(e_d)^{1/2}] \times [0.1 + 0.9(n/N)] \quad \text{--- 2-11}$$

with notation as above.

When α is held constant, the main variables are n , e_d , and T_a . The temperature does not vary greatly throughout the year and therefore the variations of R_n should be explained by changes in n (observed sunshine hours) or e_d (vapour pressure). A cross correlation analysis was performed for data from seven years to investigate the nature of this inter-relationship. The results for 1978 are presented in Table 2.13.

Table 2.13 Correlation between net radiation, sunshine hours and vapour pressure for 1978 ($a = 0.235$, $b = 0.535$)

Month	Rn vs n	Rn vs ($e_a - e_d$)	α
1	-0.05	0.71	0.35
2	0.27	0.05	0.35
3	0.20	0.56	0.35
4	0.98	0.45	0.15
5	0.96	0.54	0.25
6	0.99	0.55	0.25
7	1.00	0.82	0.20
8	0.99	0.87	0.15
9	0.98	0.51	0.15
10	0.93	0.46	0.25
11	0.06	-0.76	0.30
12	0.27	-0.03	0.35

Note. ($e_a - e_d$) represents the vapour pressure deficit and therefore includes a dependence on T_a .

A high correlation between observed sunshine hours and net radiation for the rainy season months April to October is shown in Table 2.13. By contrast, the correlation between net radiation and vapour pressure deficit is low throughout the year.

In Table 2.14, the albedo is varied between 0.07 and 0.35, while the net radiation for each month is calculated. It may be seen that the change of albedo causes a very significant change in the calculated net radiation.

For any particular period over which Rn is calculated, a simple linear relationship between Rn and (α) may be found. For high values of α , the net radiation becomes negative.

For the calculation of Rn over an open water surface, a value of $\alpha = 0.07$ should be used throughout the year. Similarly, for the calculation of Rn over an irrigated crop surface, a value of α between 0.18 and 0.25 should be used depending upon the growing cycle. For the calculation of Rn over a natural vegetation surface, values varying as in Table 2.15 could be used. The annual variation of albedo over a natural vegetation surface is complicated, and the assessment of the change will have a significant effect on evapotranspiration calculations presented below.

Table 2.14. Calculated monthly net radiation for varying albedo $\overline{[Wm^{-2}]}$
 $a = 0.235$, $b = 0.55$

Month	= 0.07	= 0.10	= 0.20	= 0.25	= 0.35
1	75	70	52	44	12
2	88	82	63	53	33
3	104	97	80	71	53
4	125	119	100	91	71
5	127	122	103	94	75
6	138	133	114	105	86
7	131	126	108	100	82
8	120	115	99	91	76
9	118	113	96	88	71
10	122	119	99	91	73
11	101	96	79	70	53
12	75	70	55	46	31
Total	1324	1260	1048	944	716

However, the values shown in Table 2.15 represent a more accurate assessment of the natural situation than holding the albedo fixed throughout the year.

Table 2.15 Monthly variation in albedo (α).

Month	1	2	3	4	5	6	7	8	9	10	11	12
	0.35	0.35	0.35	0.15	0.10	0.25	0.20	0.15	0.15	0.25	0.30	0.35

The values suggested in Table 2.15 reflect the changing ground surface conditions throughout the year. Commencing in January with bare, burnt ground with isolated trees, the change to young vegetation in April and May will be determined by the timing of the early rains. The ground surface changes very rapidly after the first rains, with new grass becoming established within seven days. The albedo of bare wet soil is only 0.10, implying a rapid drying of this surface at the beginning of the rains. The fluctuations of albedo during the wet season are based upon Kowal's work described above. Finally, the change from wet season albedo to dry season conditions is also determined by the timing of the end of the rains, and a fixed monthly discretisation must involve error in any particular year.

The assessment of albedo within the savanna is an area that requires

considerable research. The importance of the correct assessment is demonstrated by the figures presented in Table 2.14.

The choice of the regression values 'a' and 'b' in the Angstrom equation also significantly effect the net radiation calculation, but not as strongly as the choice of albedo. The values that are recommended by the author, are also those presented by Kowal (1972). These values are $a = 0.235$, $b = 0.535$, and are the values used to calculate net radiations presented in Tables 2.10 and 2.11. Various other sets of values have been used and Table 2.16 shows their relative effects on the net radiation value.

Table 2.16 Rn for different Angstrom equation values [Wm^{-2}] Data for Bauchi, 1978. ($\alpha = 0.25$ throughout)

Month	(1) a = 0.180 b = 0.550	(2) a = 0.285 b = 0.520	(3) a = 0.235 b = 0.535	(4) After Davis	(5) a = 0.123 b = 0.732
1	38.3	54.3	46.8	45.2	54.9
2	54.3	72.6	64.0	63.2	74.0
3	63.2	84.6	74.6	76.3	79.2
4	78.3	102.3	90.9	83.5	83.5
5	98.3	120.3	110.0	113.5	113.5
6	86.9	108.6	98.3	98.3	96.9
7	72.5	94.9	84.0	86.3	75.5
8	87.2	108.6	98.6	99.8	96.9
9	90.0	110.9	101.2	100.6	103.2
10	94.3	118.8	104.6	104.1	111.8
11	60.0	76.9	68.9	68.3	78.6
12	44.6	60.0	52.9	58.0	63.2
Totals	867.7	1107.8	994.8	997.1	1031.5

Notes.

1. Constants originally devised for Rothampstead U.K. and used by Penman (1948). These values have been used in a number of studies, notably by Kowal and Knabbe (1972).
2. Constants from McCulloch (1965)
3. Constants from Kowal (1972a)
4. Twelve different monthly sets of constants devised by Davis (1966)
5. Average values from (4).

The two experimentally verified sets of values after Kowal (3) and Davis (4) show very good agreement both in their distribution and in their

annual totals. The values which have previously been generally used, (set 1), show a 12.8% underestimate of net radiation. The values of a and b after McCulloch (set 2) show a 10.2% overestimate. These percentages are calculated assuming set 3 values to be the most accurate.

Using values of 'a' and 'b' as recommended above, values of albedo as shown in Table 2.15 and the sets of daily meteorological data for Bauchi, values of monthly net radiation were calculated for a number of years. This data is presented in Table 2.17. The degree of annual variation is not insignificant.

Table 2.17 Average monthly net radiation for Bauchi (a = 0.235, b = 0.535, distributed as in Table 2.15)

Month	1969 Wm^{-2}	1970 Wm^{-2}	1973 Wm^{-2}	1974 Wm^{-2}	1978 Wm^{-2}	1979 Wm^{-2}
1	27.7	33.2	26.6	31.2	29.7	28.5
2	33.4	34.9	33.7	31.4	44.0	36.0
3	70.6	45.6	43.7	43.7	54.9	54.6
4	117.8	105.5	109.8	115.2	107.2	112.3
5	117.8	116.3	108.1	111.8	119.8	105.8
6	105.8	112.9	104.9	101.8	98.3	106.9
7	107.5	102.9	108.1	91.2	91.2	110.6
8	109.5	94.1	106.1	106.1	115.5	109.5
9	113.2	108.1	122.1	114.3	118.9	106.5
10	105.5	91.5	96.9	101.8	104.6	92.9
11	67.2	57.5	50.0	55.2	60.0	63.5
12	40.6	34.6	32.0	30.0	35.2	32.6
Total	1016.6	940.1	942.0	933.1	979.3	960.1

The average annual net radiation is $962 Wm^{-2}$ with a standard deviation of $31 Wm^{-2}$. The conditions in 1969 appear to have been exceptionally clear, particularly during the dry season months. The incidence of harmattan must have been low.

Temperature Distribution.

The energy available at ground level from the net radiation, is absorbed by a number of different processes which vary significantly throughout the year.

The use of net radiation may be described by the equation

$$R_n = G + H + L + P \text{ [Wm}^{-2}\text{]} \text{-----} 2.12$$

where G = ground heat flux [Wm⁻²]
 H = atmospheric heat flux [Wm⁻²]
 L = evaporation heat flux [Wm⁻²]
 P = photochemical heat flux [Wm⁻²]

Kowal and Kassam (1973a) report seasonal values for the components of the energy balance as follows :

Table 2.18 Distribution of net radiation components.

	Wm ⁻²	% of Rn
Rn	154	100
Transpiration Ep	84	54.5
Evaporation from soil (Es)	35	22.7
Evapotranspiration (Ep + Es)	119	77.2
Airflux (H)	26	16.9
Soil heat flux (G)	6	3.9
Net photosynthesis (P)	3	2.0

This data was gathered over a crop of maize during the period ~~the~~ June to October at Samaru.

It may be seen that during the rainy season, three quarters of the net radiation is required by the processes of evapotranspiration and only 20% is expended by heating the air and the ground. Consequently, the day temperatures during the wet season do not show much fluctuation. There is also little cooling at night because the Rb term is kept small by cloud cover and a relatively low surface temperature, cooled by rainfall.

During the dry season, vegetation dies and is burnt by the local villagers (see Plates 2.3 and 2.4). Therefore little of the net radiation can be expended via evapotranspiration and the majority of the energy is used to heat the air and soil. Since the skies are clear and daytime air and soil temperatures are high, there is a large component of back radiation (Rb) at night with a consequent drop in night temperatures. Plates 2.3 and 2.4 show typical surfaces which exist throughout the dry season. The albedo in each case will be high.

The varying use of net radiation during the year is of practical significance during the calculation of evapotranspiration discussed below. Within temperate climates the values of H, G and P are assumed to be



Plate 2.3 Crop residue and nearby grass has been burnt off in November to reduce the risk of major fire damage to woodland by a fire started at the end of the dry season.

Plate 2.4 Woodland in December showing the results of firing the grass during the early dry season.



zero and all the net radiation is consumed by evapotranspiration. Within the savanna this assumption must cause considerable error, most especially during the dry season.

2.4 EVAPORATION AND EVAPOTRANSPIRATION.

General.

Evaporation and evapotranspiration are usually considered together even though they relate to two distinctly different elements of the climate. The combined effect of the two processes has a dominant influence on the water balance of the savanna. For example, the annual evaporation from an open water surface is approximately double the annual rainfall, and it is this basic imbalance which causes the marked seasonality of the climate throughout the year.

Evaporation, often denoted by the symbol E_o , and synonymous with 'open water evaporation' relates to the evaporative power of the air. E_o serves as a standard yardstick for the comparison of the evaporative power of the air within different regions, and as such is regularly measured or computed during climatological work. The measurement of E_o , particularly in the tropical environment has not been found to be very reliable and as such E_o is calculated from standard meteorological observations.

Evapotranspiration, often denoted by the symbol E_T , is the combined transfer of water by evaporation from the soil and by transpiration from plants. The quantity of evapotranspiration depends upon the availability of water in the soil, evaporative demand of the atmosphere, crop density and cover, and the stage of growth of the crops or vegetation. Evapotranspiration is therefore a difficult quantity to calculate. Lysimeters have been used to measure evapotranspiration from areas of growing crops however, it is more often calculated using a theoretical approach.

The Calculation of Evaporation.

Evaporation commences and continues as long as there is a supply of moisture, a vapour pressure gradient between the water surface and the atmosphere and a supply of energy. The energy required to supply the latent heat is withdrawn from the most convenient source, which may be the sun, the overlying air, the ground, or from the water itself (Weşiner, 1970). The principal independent source of energy for evaporation however is net solar radiation, and the derivation of this quantity has been discussed in detail above. The input of net radiation reaches an equilibrium with an appropriate rate of water diffusion. If the net radiation input changes, for example, if the sun is obscured by clouds,

there is an immediate drop in net radiation received, but the evaporation flux changes more slowly as the existing vapour pressure gradient permits the continued diffusion of water vapour into the air.

Evaporation may also occur when there is no available net radiation, by the turbulent transfer of energy from the airmass. Such evaporation is determined by the humidity and wind speed of the air passing over the water surface. This advective form of evaporation is especially significant during the dry season.

The combined energy-balance vapour-transfer method of Penman (1948) is widely used for the calculation of evaporation. Since 1948, when Penman published the first theoretically sound treatment of the evaporation process, there has been continued research into the subject and a number of significant modifications have been suggested. Thom and Oliver (1977) have reviewed the evolution of the Penman equation and Weisner (1970) gives an analytical treatment of the combined approach derivation.

Penman's original formula may be written as :

$$E_0 = \frac{\Delta \times H}{\gamma + \Delta} + \frac{\gamma \times E_a}{\gamma + \Delta} \quad \text{————— 2-13}$$

- where E_0 = evaporation in mm water per day
- H = net available energy in mm equivalent evaporation per day
- E_a = aerodynamic term (discussed below)
- Δ = slope of the vapour pressure vs temperature curve for water at the air temperature T_a
- γ = thermodynamic value of the psychrometric constant

The equation consists of two terms, the first is commonly referred to as the radiation term, while the second is called the aerodynamic term. The two terms represent the contribution to E_0 from the energy derived from net radiation input and the energy derived from the drying power of the air.

The net available energy consists of the available net radiation (R_n) calculated from equations presented in Section 2.3., less the energy expended in heating the water. The latter term is usually considered to be insignificant.

The aerodynamic term is calculated from a number of formula of the type :

$$E_a = f(u) \times (e_s - e) \quad \text{-----} \quad 2.14$$

where u = windspeed

$(e_s - e)$ = vapour pressure deficit

The original Penman relationship was :

$$E_a = 0.26 (e_s - e) \times (1 + 0.006214 \times u) \quad \text{[mm day}^{-1}\text{]} \quad \text{-----} \quad 2.15$$

where e_s = vapour pressure [mb]

e = saturated vapour pressure [mb]
at T_a the average air temperature [$^{\circ}\text{C}$]

u = wind run per day [km]

The constants have been adjusted to conform to the metric system.

$$\gamma = 6.574 \times 10^{-4} \times \rho \quad \text{-----} \quad 2.16$$

where ρ is the average ambient pressure [mb]

Δ = slope of the saturation vapour pressure curve at T_a .

Appendix A contains detailed notes on the algorithm that has been written to calculate evaporation. The use of a wide range of units has led to some confusion in the literature and recent results (Slabbers, 1977, Bevin, - 1979) have been presented using S.I. Units.

The daily evaporation for a water surface with an albedo of 0.07 has been computed for the years 1969, 1970, 1971, 1973, 1974, 1978 and 1979, based on the daily climate data available at Bauchi. Values of daily wind run at 2 metres height (km), relative humidity (average of 8 daily readings), average temperature (maximum and minimum readings in $^{\circ}\text{C}$) and sunshine hours as measured by a Campbell Stokes recorder, have been used in the analysis. Of these data inputs, only the temperature estimation of a 24 hour average from maximum and minimum data is likely to be in error, and this has been found to be less than 2°C from an examination of hourly measurements. The effect of a 10% error in T_a is described below.

The average monthly totals, calculated by summing daily values are shown in Table 2.19.

Table 2.19 Evaporation totals for Bauchi (mm day^{-1})
 $= 0.07, a = 0.235, b = 0.535$

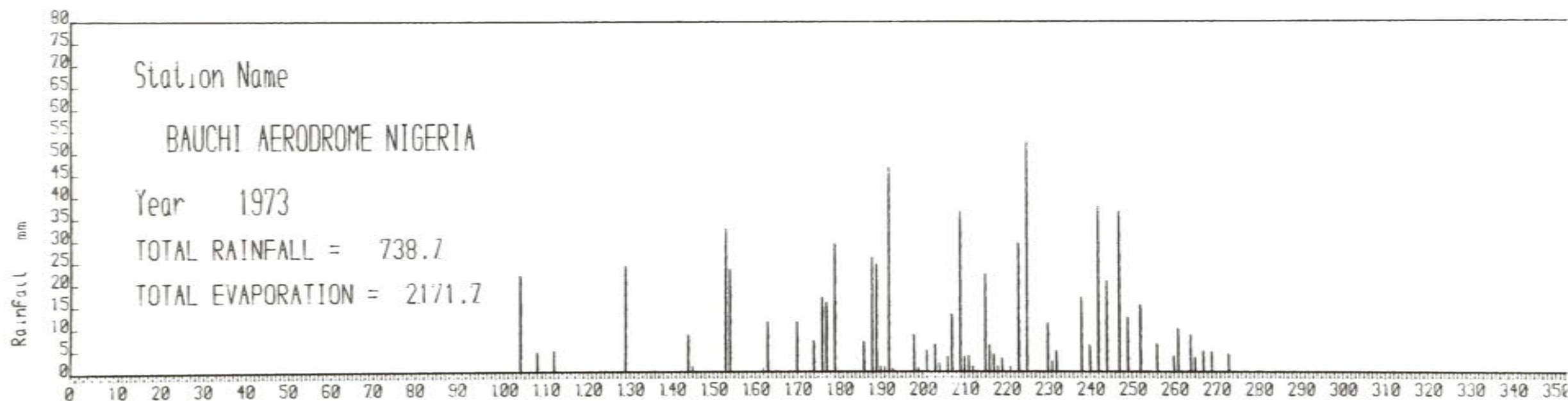
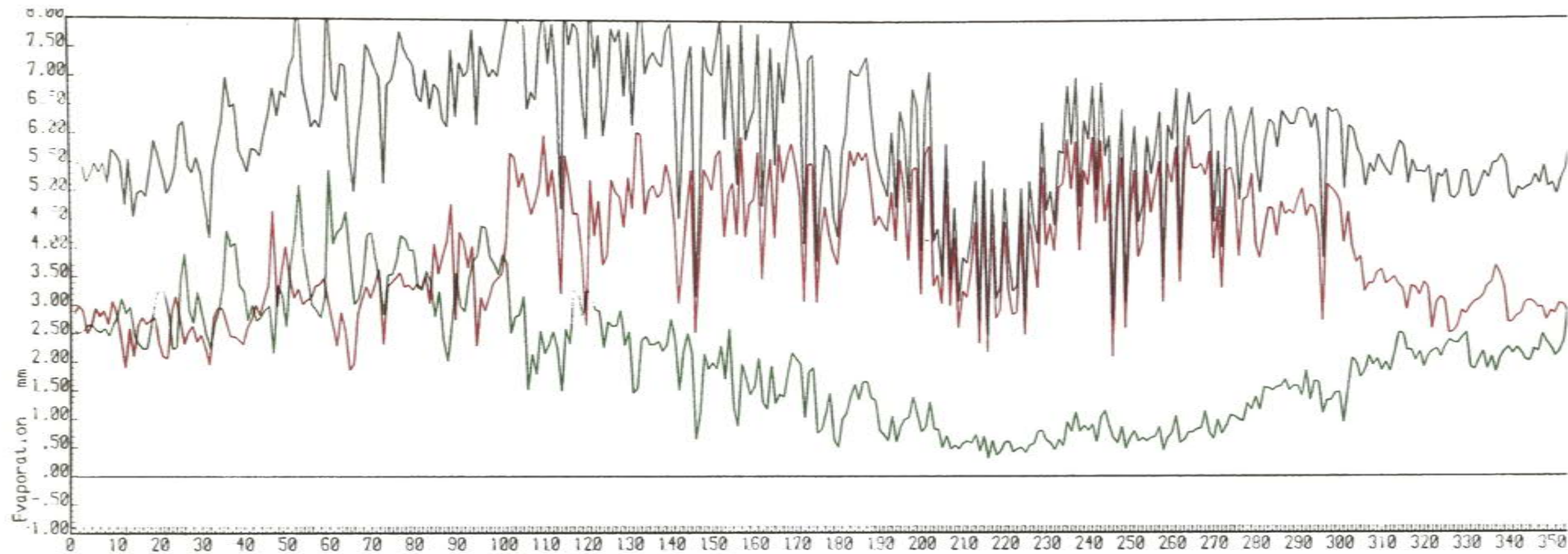
Month	1969	1970	1971	1973	1974	1978	1979	Average
1	161.4	163.8	158.9	166.2	149.5	160.1	161.1	160
2	176.2	169.7	169.5	173.5	164.5	172.2	167.5	170
3	225.6	213.4	214.6	211.4	205.1	213.4	205.3	213
4	208.6	211.3	214.0	220.1	213.8	185.5	207.5	209
5	206.8	213.2	218.0	215.8	197.5	206.4	202.7	209
6	180.7	200.0	180.2	193.7	179.5	163.8	181.2	183
7	162.6	158.8	151.9	171.8	138.9	136.7	165.9	155
8	150.8	128.0	141.8	148.3	144.2	155.5	155.4	146
9	152.1	145.2	159.7	166.3	153.2	158.1	160.9	156
10	178.5	171.6	178.9	184.0	176.5	175.8	167.9	176
11	161.2	163.4	159.8	160.3	163.7	157.8	158.2	161
12	166.0	156.4	153.8	160.5	149.9	153.7	148.3	155
Totals	2124.4	2094.7	2101.1	2171.8	2036.2	2038.9	2082.0	2093

The effect of using the Rothampstead values of $a = 0.180$ and $b = 0.550$ in the Angstrom equation rather than the recommended values is to reduce the total evaporation for the year by approximately 8%.

The proportion of the total evaporation that is contributed by the aerodynamic term varies throughout the year. In general, as the dry season progresses, the vapour pressure deficit increases substantially and therefore the quantity of water that the air can absorb also increases. For the mid dry season months the aerodynamic term contributes more than half of the total evaporation. The radiation term is strongly dependent on the observed sunshine hours. During the wet season, the vapour pressure deficit is very low and the aerodynamic term is correspondingly small. Total evaporation during the wet season is therefore strongly influenced by sunshine hours.

A double peak in the total evaporation graphs is the result of a double peak in the net radiation term corresponding to the sun's zenithal position.

The components of total evaporation and their interrelationship may be best shown diagrammatically. Figures 2.19, 2.20 and 2.21 show total evaporation for the years 1973, 1974 and 1979 respectively. Daily rainfall is shown as a histogram beneath the plots of daily total evaporation,



Station Name

BAUCHI AERODROME NIGERIA

Year 1973

TOTAL RAINFALL = 738.7

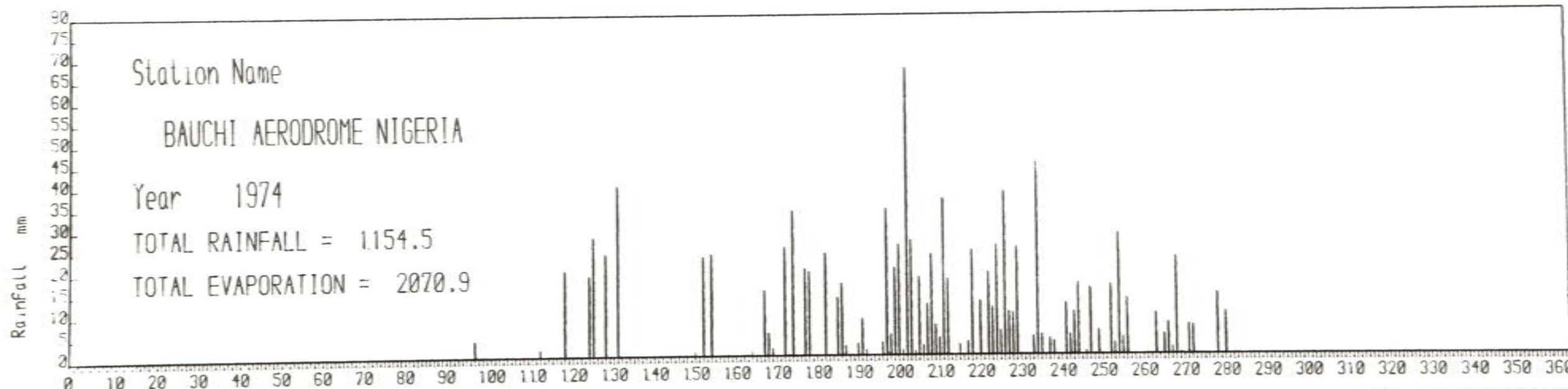
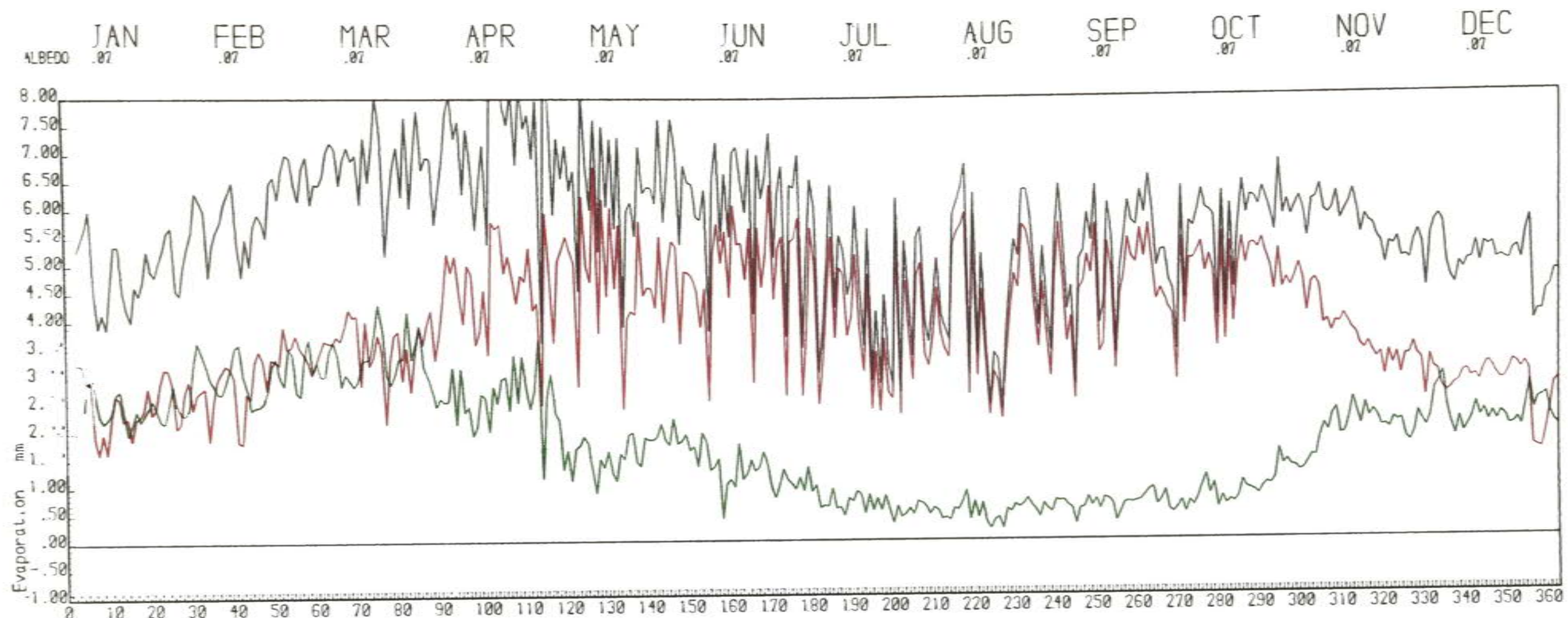
TOTAL EVAPORATION = 2171.7

RAINFALL AND EVAPORATION SUMMARY

PENMAN EQUATION

AERODYNAMIC COMP
RADIATION COMPONE

Figure 2-19



Station Name
 BAUCHI AERODROME NIGERIA

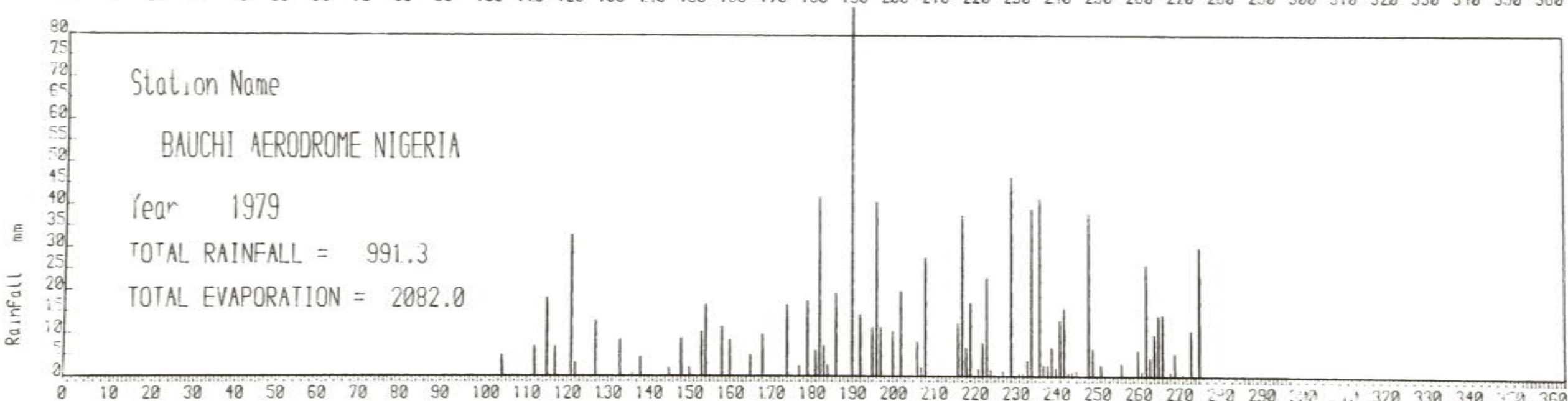
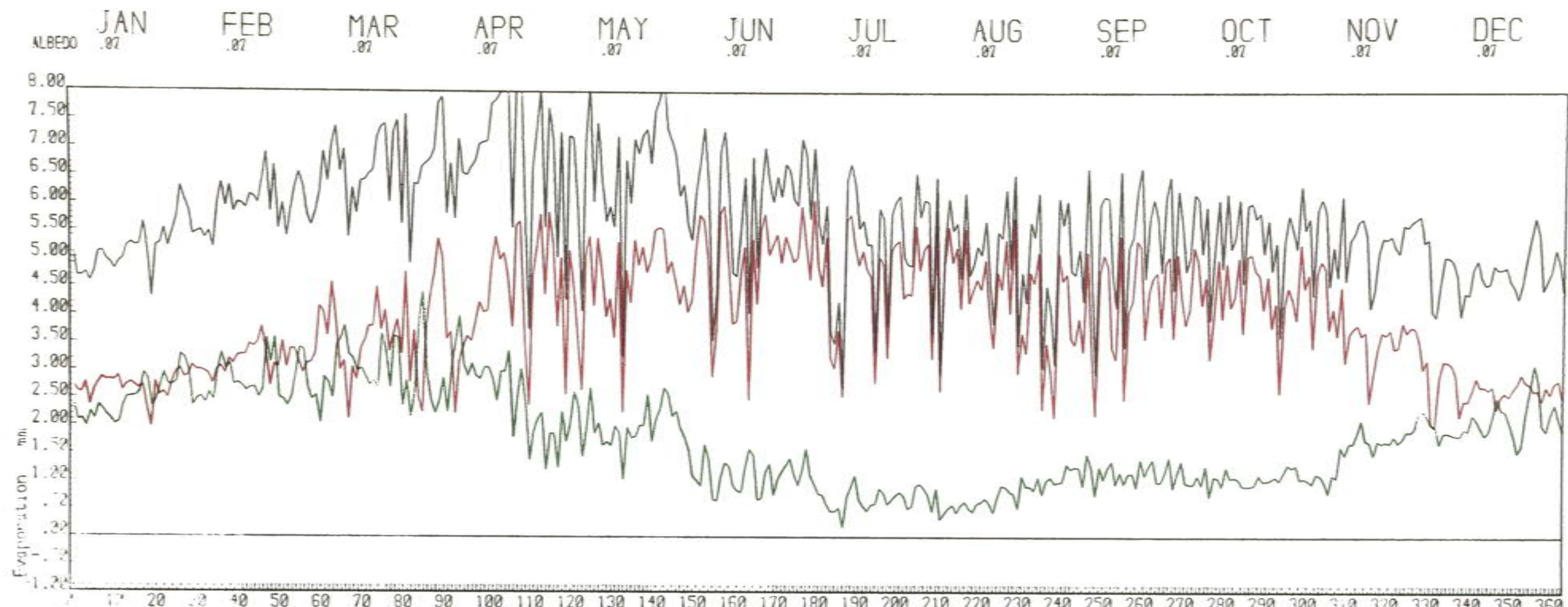
Year 1974

TOTAL RAINFALL = 1154.5

TOTAL EVAPORATION = 2070.9

RAINFALL AND EVAPORATION SUMMARY PENMAN EQUATION AERODYNAMIC COMPONENT RADIATION COMPONENT

Figure 2-20



Station Name
 BAUCHI AERODROME NIGERIA

Year 1979

TOTAL RAINFALL = 991.3

TOTAL EVAPORATION = 2082.0

RAINFALL AND EVAPORATION SUMMARY PENMAN EQUATION AERODYNAMIC COMPONENT RADIATION COMPONENT

Figure 2-21

the aerodynamic contribution, and the radiation term contribution.

The evaporation calculation has been conducted for daily and monthly periods. The results obtained by summing the data calculated on a daily basis and the results obtained by using averaged daily data on a monthly basis show very little variation. An error of less than 1.5% in the monthly total during the dry season months is found to occur. This error is reduced during the wet season. Penman (1948) originally recommended that the evaporation calculation be carried out using data averaged over a ten daily period. This precaution was introduced to compensate for the diurnal variations in evaporation which the empirical form of the equation, especially in the aerodynamic term, may wrongly estimate.

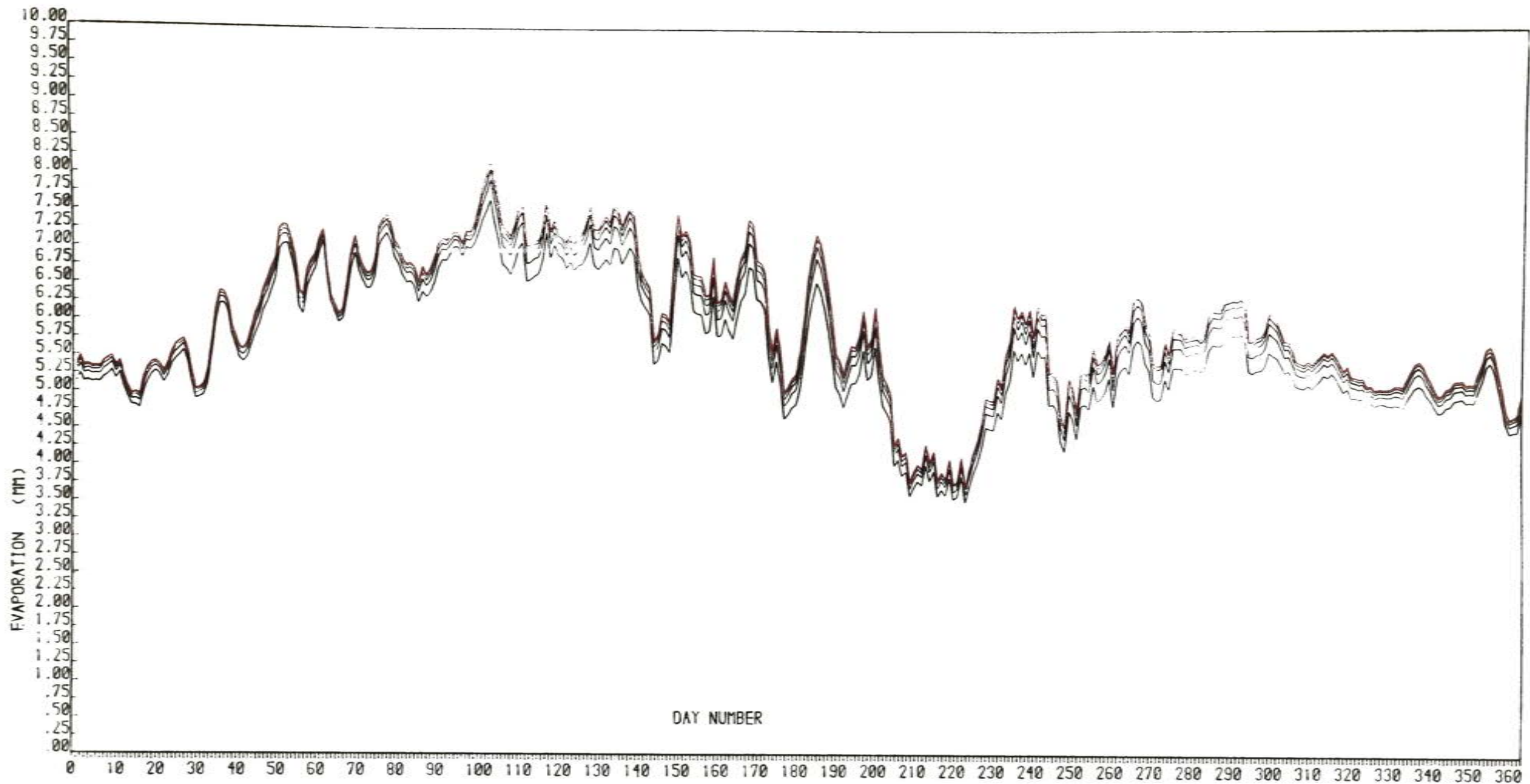
Sensitivity of the Evaporation Calculation.

Equation 2.13 is comprised of a complex association of measured and estimated parameters, all of which affect the accuracy of the evaporation estimate. The estimated parameters are contained wholly within the net radiation term and the highly significant effects of using poor estimates of these parameters has been demonstrated in Section 2.3. The measured parameters consist of sunshine hours (n), wind speed (u), average temperature (T_a) and relative humidity, usually derived from wet and dry bulb measurements.

The effect of errors in the measurement of these parameters has been studied for a U.K. climate by Howard and Lloyd (1979), who reported that calculation of evaporation using the Penman equation is most sensitive to wet bulb data.

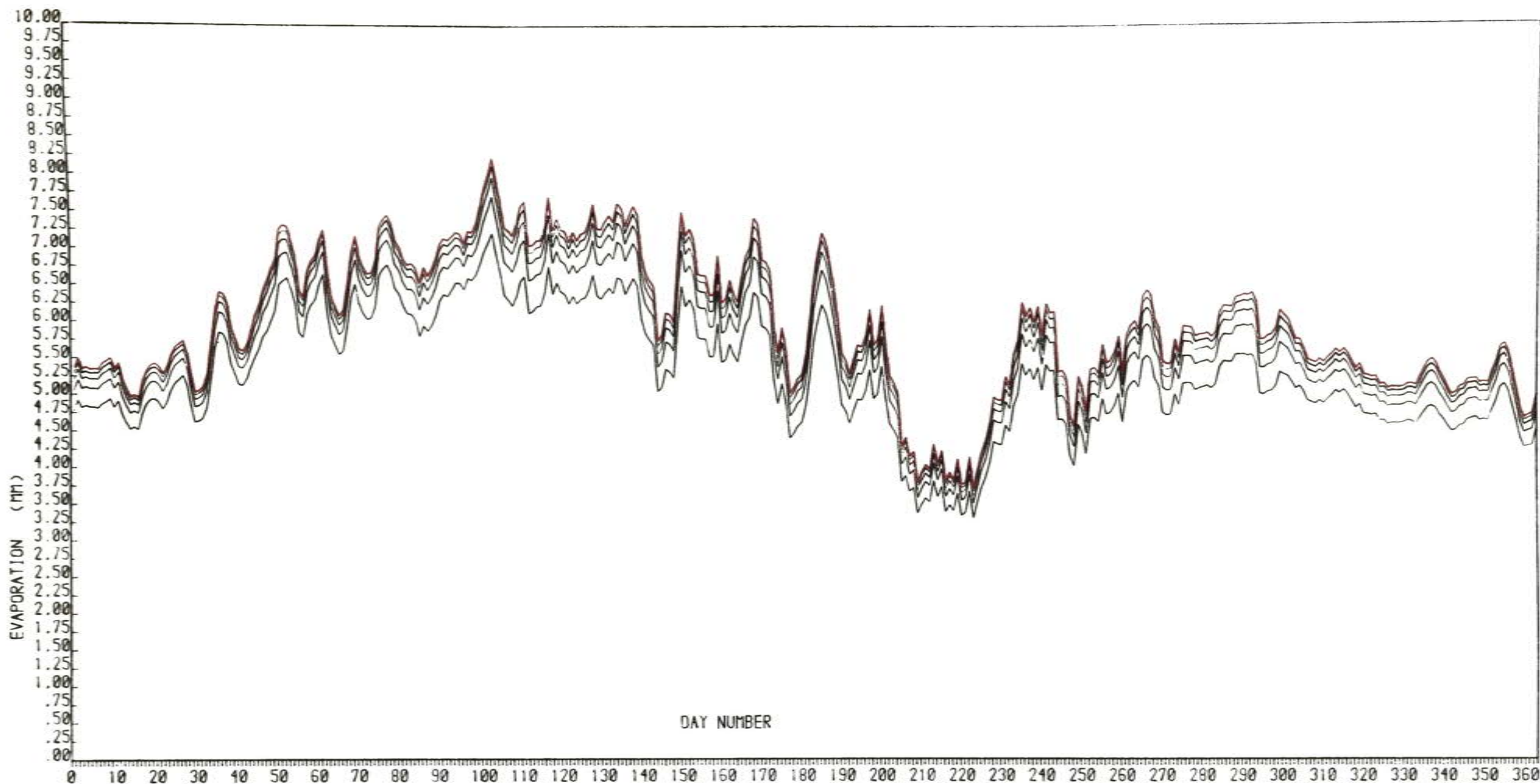
A sensitivity analysis has been carried out for the data available at Bauchi to investigate the effects of errors in measured parameters on the evaporation calculation in a savanna environment. The measured parameters have been varied by 2, 5, 10 and 20%, with the results presented graphically in Figures 2.22 (variation in n), 2.23 (variation in T_a), 2.24 (variation in relative humidity), and 2.25 (variation in windspeed, u). A five point running mean filter has been used to smooth the data so that the considerable daily variations shown earlier do not mask the sensitivities.

It may be seen from Figures 2.22 to 2.25 that the most sensitive measured parameter is the average temperature. The maximum 10% error in average temperature produced by averaging the daily maximum and minimum temperatures, will produce a 5.8% error in the calculated evaporation.



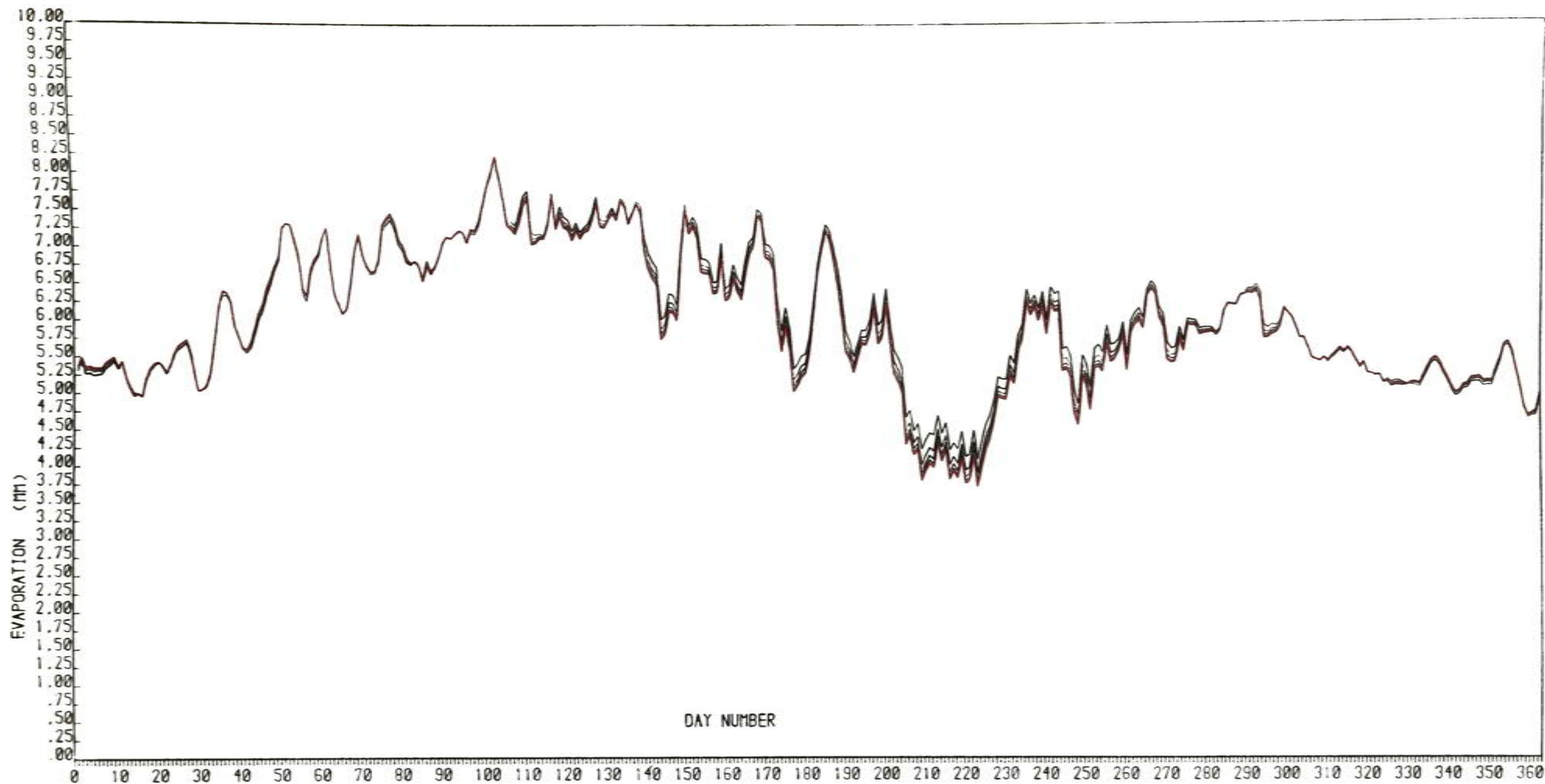
Station Name	YEAR	INPUT PARAMETER MULTIPLIED BY	TOTALS
BAUCHI AERODROME NIGERIA	1973	FACTORS OF 1.00	2171.80
		.98	2158.55
		.95	2138.68
		.90	2105.57
		.80	2039.34
EVAPORATION SENSITIVITY ANALYSIS			
MEASURED INPUT PARAMETER	7		

Figure 2-22 Evaporation sensitivity to observed sun hours.



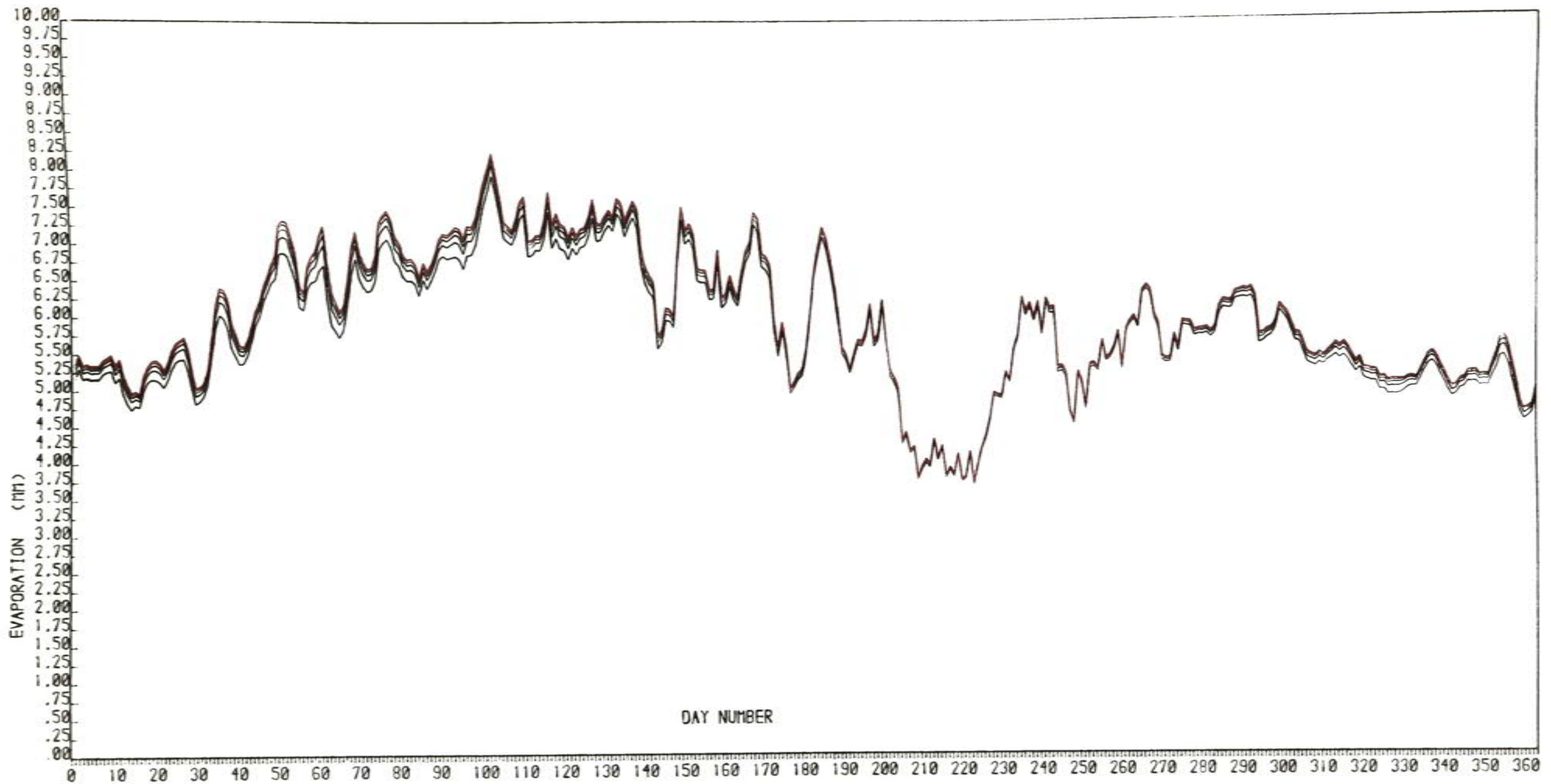
Station Name	YEAR	INPUT PARAMETER MULTIPLIED BY FACTORS OF	TOTALS
BAUCHI AERODROME NIGERIA	1973	1.00	2171.80
EVAPORATION SENSITIVITY ANALYSIS		.98	2146.24
		.95	2108.35
		.90	2046.28
MEASURED INPUT PARAMETER 11		.80	1925.59

Figure 2-23 Evaporation sensitivity to average temperature



Station Name	YEAR	INPUT PARAMETER MULTIPLIED BY	TOTALS
BAUCHI AERODROME NIGERIA	1973	FACTORS OF 1.00	2171.80
		.98	2175.39
		.95	2180.59
		.90	2188.77
		.80	2203.06

Figure 2-24 Evaporation sensitivity to relative humidity



Station Name	YEAR	INPUT PARAMETER MULTIPLIED BY	TOTALS
BAUCHI AERODROME NIGERIA	1973	FACTORS OF 1.00	2171.80
		.98	2165.31
EVAPORATION SENSITIVITY ANALYSIS		.95	2155.56
		.90	2139.33
MEASURED INPUT PARAMETER	4	.80	2106.86

Figure 2-25 Evaporation sensitivity to wind speed

The seasonality of the sensitivity of the other parameters is well demonstrated. The wind run is the most sensitive parameter in the dry season. The relative humidity is by contrast most sensitive during the wet season, when a small change in vapour pressure deficit can cause considerable evaporation to occur. The measured sunshine hours have an even sensitivity throughout the year.

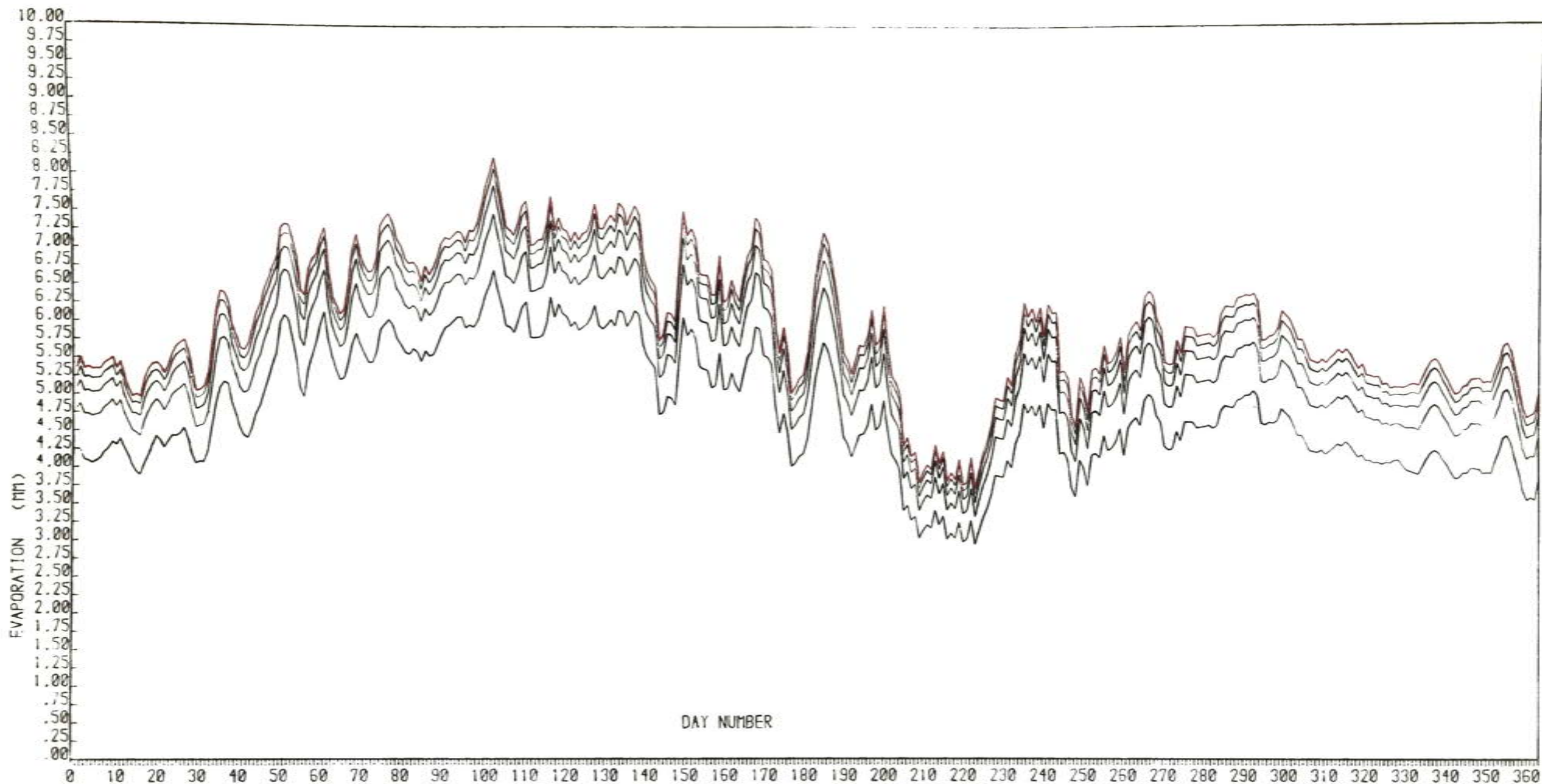
The sensitivity calculations have been worked assuming a constant albedo. It is probable that algal growths during the dry season, and the extensive development of vegetation, both floating and peripheral, will alter the albedo and thus cause significant departures from the estimated values. These effects remain completely unquantified however.

As the radiation input is the controlling factor behind the evaporation, the same sensitivity analysis was run for incoming radiation, the R_a term in Equation 2.5. In the light of the possible 5% error in estimating J_0 (Equation 2.3) (Lamb, 1972), it may be seen from Figure 2.26 that the associated error in evaporation is 5%.

From the above analysis it may be seen that the measurement of temperature is the most significant parameter in which lack of accuracy can lead to error. An average daily temperature computed from three hourly readings at least is required to maintain accuracy. In addition, a variation of R_a is seen to significantly influence the evaporation calculation. If J_0 varies by $\pm 5\%$ as is thought possible (Lamb, 1972), then a variation of evaporation by as much as 220mm between different years could occur. This tends to support the argument that variations of the solar constant can influence climate significantly. However, that subject is treated extensively by Lamb (1972), and will not be entered into here.

Estimation of Evaporation.

Very little direct work has been carried out in savanna regions to measure evaporation losses from surface water bodies. For this reason, there is no direct comparison between actual evaporation loss and the predicted loss based on Penman type calculations. Estimates of evaporation show a variation which mainly reflects the use of different Angstrom equation constants. The lowest estimate of yearly evaporation at Rauchi is provided by Kowal & Knabbe (1972). The Agroclimatological Atlas of Northern Nigeria gives a figure of 1851mm per year. The highest figure suggested in the literature is one of 2443mm per year (Consulint, 1976). The results provided by the above analysis indicate a figure between these



Station Name	YEAR	INPUT PARAMETER MULTIPLIED BY	TOTALS
BAUCHI AERODROME NIGERIA	1973	FACTORS OF 1.00	2171.80
		.98	2128.04
		.95	2062.40
		.90	1953.01
		.80	1734.22
EVAPORATION SENSITIVITY ANALYSIS			
MEASURED INPUT PARAMETER	17		

Figure 2-26 Evaporation sensitivity to incoming radiation.

two extremes of 2093mm per year (Table 2.18).

In temperate latitudes, the evaporation from pans has provided a useful guide to E_o . The Bauchi data for 1978 and 1979 includes evaporation for a class A pan shown in Plate 2.5. Unfortunately the correlation analysis carried out for monthly data indicated very low correlations between E_o and the pan data. It is not clear why these results were so poor.

Piche evaporimeter measurements have been taken for several years at the Bauchi station. The Piche evaporimeter is installed in the Stephenson screen beside the maximum and minimum thermometers. A paper filter is attached to a water reservoir and advection of water occurs through the filter from the reservoir. A daily measurement of water loss from the reservoir provides an estimation of the aerodynamic component of the evaporation. The Piche evaporimeter has been used to estimate E_o for a number of stations in Israel (Stanhill, - 1963), where the data is used in the absence of wind speed measurements. A high correlation between measured evaporation for a large open area of water and calculations of the evaporation based on the use of Piche data to estimate the aerodynamic component is reported. In Table 2.20, the correlations between Piche data and the aerodynamic term for the Bauchi data are shown. It can be seen that throughout the year the correlation is high for a well kept instrument. Low correlations tend to occur due to dust, insects or other material clogging the filter paper.

Table 2.20 Correlation between Piche data and the aerodynamic term in Penman's equation.

Month	1970	1971	1973	1974	1978	1979
1	0.85	0.64	0.78	0.74	0.83	0.91
2	0.76	0.77	0.88	0.75	0.71	0.88
3	0.85	0.83	0.87	0.83	0.62	0.85
4	0.82	0.93	0.82	0.63	0.86	0.87
5	0.88	0.92	0.85	-	0.84	0.71
6	0.90	0.86	0.90	-	0.88	0.58
7	0.93	0.79	0.91	0.92	0.85	0.94
8	0.88	0.91	0.88	0.95	0.92	-
9	0.72	0.92	0.74	0.82	0.92	-
10	0.94	0.88	0.87	0.88	0.81	-
11	0.68	0.63	0.72	0.63	0.70	0.94
12	0.85	0.45	0.90	0.79	0.59	0.86



Plate 2.5 Type A evaporation pan at Bauchi.



Plate 2.6 Dry season land surface close to Bauchi.

The results of work conducted at the Makwaye Lake, Samaru (Kowal & Kassam, 1978) indicate that the average evaporation loss during the dry season is about 7 to 8 mm day⁻¹. The estimated rate of evaporation using the Penman formula and meteorological data collected over the lake was 6.9mm day⁻¹. The additional evaporation is thought to occur as a result of the advective transfer of energy from the adjacent dry, hot land surface. Kowal & Kassam report that a fetch of 60-75m is necessary before the evaporation over the water surface ceases to be influenced by this additional energy input. It is this factor which is also the major cause of error in evaporation pan measurements.

No allowance was made in the above experiment for the loss of energy due to the warming of the lake water. It is assumed that due to diurnal convective transfer within a shallow lake that this energy change is insignificant.

The Calculation of Evapotranspiration.

The original form of the Penman system given in Equation 2.15 was modified by Penman (1956) to give a value known as potential evapotranspiration. This was defined as the following. 'The amount of water transpired in unit time by a short green crop completely shading the ground, of a uniform height and never short of water.' The same equation was used to compute this value but the albedo was altered from 0.05 to 0.25. This modification, assuming all other parameters were held constant, produces a value of evapotranspiration (Et) which is 20% (\pm 1%) lower than Eo.

The definition of the potential evapotranspiration term is too limited for the savanna environment. In particular, the crops are not short green, growing on average to 2 metres in height, and the ground is not often completely covered. Apart from these limitations, a basic incompatibility exists between the energy balance term and the aerodynamic term (Thom & Oliver, 1977) in the Penman equation.

Monteith (1965) showed from first principles that the latent heat flux from an unsaturated surface can be represented more accurately by Equation 2.17.

$$\lambda E = \frac{\Delta \times A}{\Delta + \gamma \times (1.0 + r_s/r_a)} + \frac{\rho \times c_p \times (e_s - e)/r_a}{\Delta + \gamma \times (1.0 + r_s/r_a)} \quad [\text{Wm}^2] \text{-----} 2-17$$

- where
- E = evaporation [$\text{kg m}^{-2}\text{s}^{-1}$]
 - λ = latent heat of vaporisation [$2.47 \times 10^6 \text{ kg}^{-1}$]
 - A = available energy [Wm^{-2}]
($A = R_n - G - H - P$, as in equation 2.12)
 - ρ = density of air [1.2 kg m^{-3}]
 - c_p = specific heat of air [$1.01 \times 10^3 \text{ kg}^{-1}\text{C}^{-1}$]
 - e_s = saturated vapour pressure at T_a [mb]
 - e = vapour pressure [mb]
 - T_a = average air temperature at reference level z [$^{\circ}\text{C}$]
 - Δ = slope of the saturation vapour pressure curve [$\text{mb}^{\circ}\text{K}$]
 - γ = psychrometric constant [$\text{mb}^{\circ}\text{K}^{-1}$]
 - r_a = aerodynamic resistance to the transport of water vapour from the surface to the reference level z [sm^{-1}]
 - r_s = canopy resistance to the transport of water from some region within or below the evaporating surface to the surface itself. Under wet canopy conditions $r_s = 0.0$

It may be appreciated from Equation 2.17 that for wet canopy conditions, the condition for which the Penman equation is limited. This equation resembles the Penman equation as $r_s = 0$. The radiation term becomes identical, but the aerodynamic term is altered somewhat.

The net radiation measured at the reference level has been described previously.

One form in which r_a may be calculated is as follows (Bevin, 1979)

$$r_a = \left[\ln\left(\frac{z-d}{z_0}\right) / k \right]^2 \times u \quad [\text{s m}^{-1}] \quad \text{-----} \quad 2-18$$

- where
- u = mean wind speed [ms^{-1}]
 - z = reference level of the anemometer (2.0m) [m]
 - d = zero plane displacement [m]
 - z_0 = roughness length ($z_0 = h/100$) [m]
 - k = Von Karman's constant 0.41
 - h = vegetation height [m]

This form was originally used by Penman and Long (1960). There is evidence (Bevin, - 1979) that d and z_0 are both functions of the wind speed u . However, for the purposes of the present study, where an accurate assessment of regional evapotranspiration is required, Equation 2.18 has been used as modified by Thom and Oliver (1977). The zero plane displacement is considered insignificant and z_0 is estimated by $h/10.0$ where h is the vegetation height in cms.

The value of r_s represents a complicated interaction of factors, and it is in this term that there is scope for representing the savanna environment more accurately. Slabbers (1979) suggests an equation of the form :

$$r_s = r_l + r_c + r_h \quad [s\ m^{-1}] \quad \text{-----} 2-19$$

where r_l = stomatal resistance $[s\ m^{-1}]$
 r_c = resistance dependent upon the degree of soil cover $[s\ m^{-1}]$
 r_h = resistance dependent upon the availability of soil moisture and on liquid flow in the plant $[s\ m^{-1}]$

Slabbers, working in northern and southern Iran, the Lebanon and Tunisia reports values of r_c as follows

Table 2.21 Relation between soil cover % and diffusion resistance to water vapour dependent upon fraction of soil covered $[sm^{-1}]$

Soil cover %	10	20	30	40	50	60	70	80	90	100
$r_c\ sm^{-1}$	250	180	120	80	50	30	20	10	0	0

The r_c parameter is naturally important in the savanna environment, especially at the beginning of the rains and during the dry season. The value of r_l is difficult to quantify but is thought (Slabbers, 1797) to be of an order of magnitude less than r_c or r_h . Bevin reports r_l to vary diurnally, and Monteith reports values of r_l of only $10^{-2}\ sm^{-1}$ for leaves in contact with moisture and values of $50\ sm^{-1}$ for forest.

It has been found during runs of the evapotranspiration algorithm described in Appendix A, that values of r_s of several thousand are required in Equation 2.19, to reduce dry season evapotranspiration to levels of less than $0.5\ mm\ day^{-1}$, the levels that are probably operative during the dry season.

The complexities inherent in Equation 2.17 were readily recognised by Thom & Oliver (1977) and they suggested a modified form of the aerodynamic term in the Penman equation, viz

$$E_a = 13.8 (e_s - e) \times (1.0 + 0.006214 \times u) / [\ln(z/z_0)]^2 \quad [mm\ day] \quad \text{-----} 2-20$$

Identity with Equation 2.15 occurs for $z = 2m$ when $z_0 = 1.37mm$. This represents a very small value of the vegetation height corresponding to Penman's original emphasis on short green grass. The vegetation height in this case would be 1.37cms.

Evapotranspiration Results.

Penman evapotranspiration, using an albedo of 0.25 in equation 2.13 has been calculated for the year 1979. To investigate the effects of varying the albedo within the context of the more familiar Penman equation, the same algorithm was run with albedos varied as presented in Table 2.15. Although the annual total of evapotranspiration remains almost unchanged, the distribution within the year is significantly altered. Of a total of 1660mm, 75mm extra evapotranspiration occurs during the rainy season, compensated by 75mm less during the dry season. Such a change of balance will naturally effect the ground water balance. The results are presented in Table 2.22.

The figures presented in Table 2.22 represent the potential Penman evapotranspiration, or the evapotranspiration which would occur if the soil moisture held in the root zone was never depleted, and the crops were of a constant, small height.

Use of the modified Penman equation (Thom & Oliver, 1977) for the 1979 data set indicates a figure of E_T that is approximately double the value obtained using the Penman equation. This difference is accounted for by the fact that the vegetation height is always greater than that implied by the Penman aerodynamic term. Using monthly values of Z_0 as indicated in Table 2.23, the annual total E_T is 3093mm.

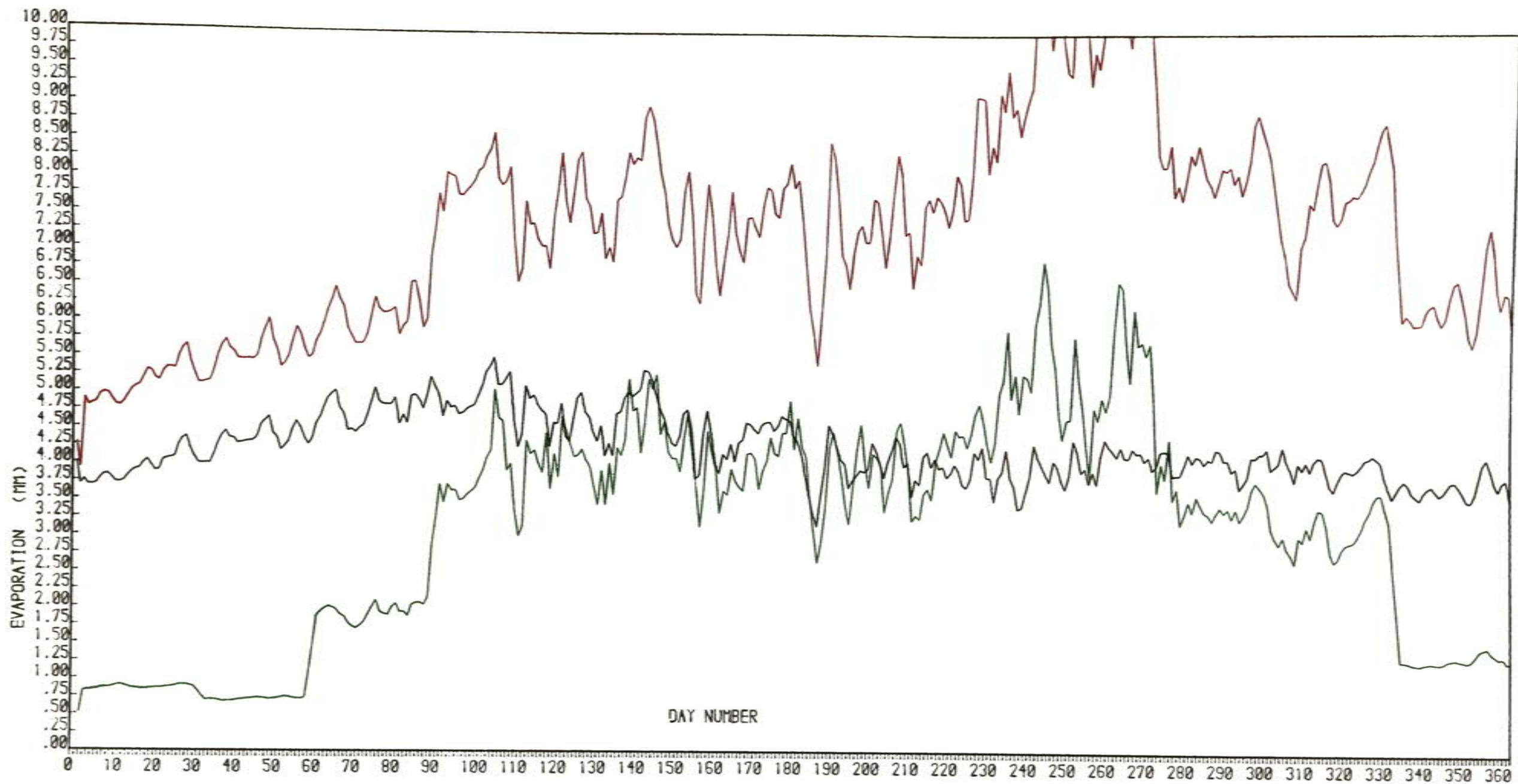
Table 2.23 Modified Penman equation Z_0 values

J	F	M	A	M	J	J	A	S	O	N	D
4.0	4.0	8.0	12.0	20.0	50.0	100.0	150.0	180.0	150.0	70.0	20.0

The values of Z_0 reflect the seasonal vegetation changes. However, as the dry season values are still higher than the Penman values, and the aerodynamic roughness of a dry landscape should still be greater than that of a short grass crop ($z_0 = 1.37mm$), this modification does not provide a useful improvement to the E_T calculation for a savanna environment. The equation is recommended for use in a temperate environment however.

Table 2.22 Penman evapotranspiration for a surface with constant albedo compared with an albedo varied to reflect the seasonal changes.

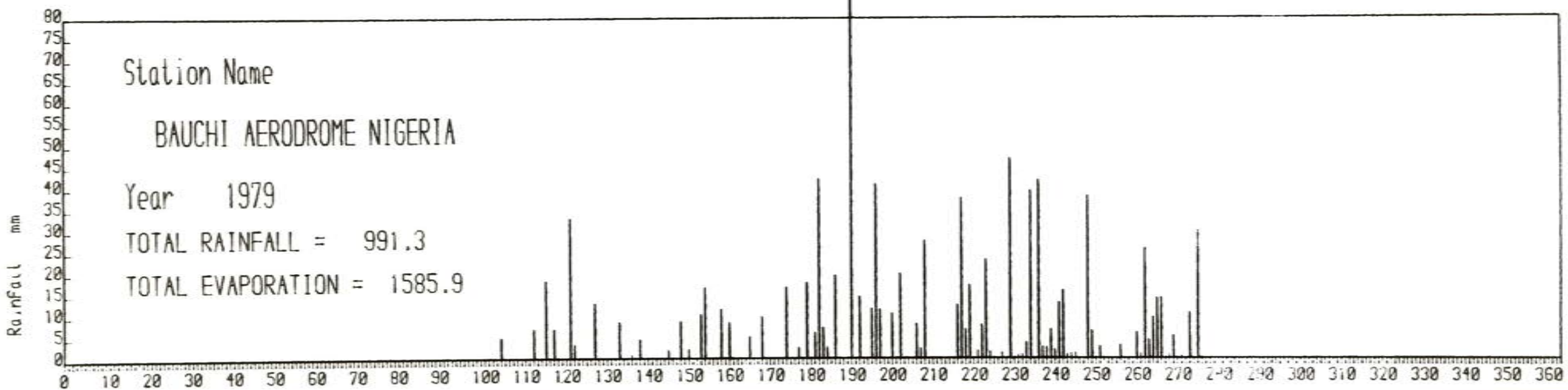
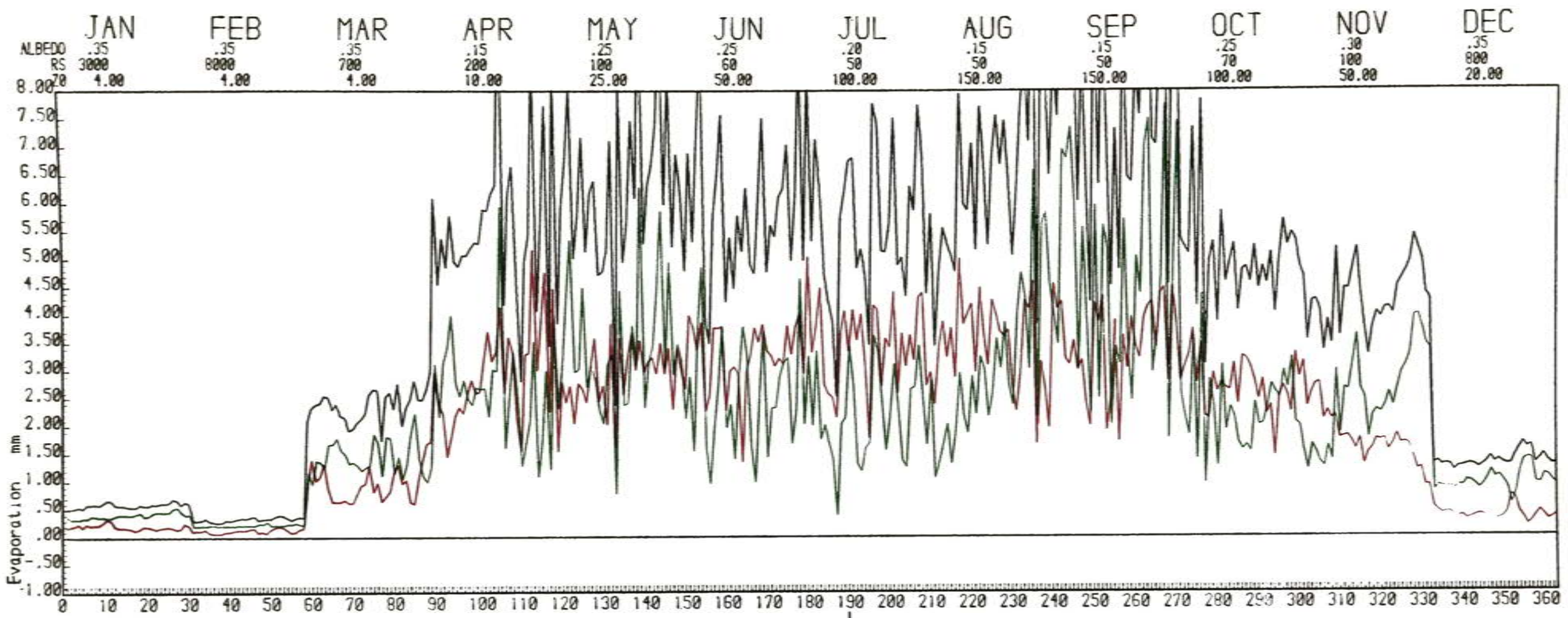
Decade	Albedo α	E_{T_1}	Albedo α	E_{T_2}	$E_{T_2} - E_{T_1}$
1		38.1		32.2	-5.9
2	0.25	40.0	0.35	34.0	-6.0
3		48.6		41.4	-7.2
4		45.6		38.6	-7.0
5	0.25	48.7	0.35	41.6	-7.1
6		38.3		33.0	-5.3
7		54.1		48.0	-6.1
8	0.25	53.4	0.35	45.8	-7.6
9		61.5		55.0	-6.5
10		55.5		61.8	+6.3
11	0.25	62.1	0.15	70.0	+7.9
12		53.2		59.4	+6.2
13		52.5		55.6	+3.1
14	0.25	50.4	0.20	53.6	+3.2
15		62.9		66.9	+4.0
16		42.5		48.5	0.0
17	0.25	45.6	0.25	45.6	0.0
18		51.1		51.1	0.0
19		40.7		43.6	+2.9
20	0.25	41.9	0.20	45.0	+3.1
21		48.9		52.4	+3.5
22		40.6		46.5	+5.9
23	0.25	40.7	0.15	46.6	+5.9
24		42.6		48.3	+5.7
25		41.4		47.0	+5.6
26	0.25	42.7	0.15	48.6	+5.9
27		44.6		51.0	+6.4
28		43.2		43.2	0.0
29	0.25	43.8	0.25	43.8	0.0
30		45.9		45.9	0.0
31		42.8		39.8	-3.1
32	0.25	40.7	0.30	37.6	-3.1
33		41.6		38.6	-3.0
34		37.1		31.6	-5.5
35	0.25	36.4	0.35	30.8	-5.6
36		43.3		37.1	-6.2
Total		1669		1659	



Station Name	YEAR	PENMAN EVAPOTRANSPIRATION	MODIFIED PENMAN EVAPOTRANSPIRATION	MONTEITH EVAPOTRANSPIRATION
BAUCHI AERODROME NIGERIA	1979	1669.13	2915.76	1585.88

EVAPOTRANSPIRATION DATA

Figure 2-27 Estimates of evapotranspiration.
 Data smoothed with a 5 point running mean.



RAINFALL AND EVAPORATION SUMMARY
Figure 2-28

MONTEITH EQUATION

AERODYNAMIC COMPONENT
RADIATION COMPONENT

In a similar manner to the sensitivity analysis of the measured parameters of evaporation, the sensitivity of Equation 2.17 to variations in albedo (α), r_s and z_0 has been investigated. To achieve the low values of E_T in the dry season that are likely from surfaces as indicated in Plates 2.1 and 2.2, the R_h term in Equation 2.19 is increased to several thousand, and completely dominates the calculation of R_s . This is not unreasonable as the resistance dependent upon the availability of soil moisture will approach infinity as the soil becomes completely dry. It is probable that some deep rooted plants tap the water table and that some evaporation occurs direct from this zone even during the dry season. For this reason, it is unlikely that E_T ever becomes zero.

During the wet season, the crops grow to approximately 2 metres in height. The effect of increasing the Z_0 term to reflect this increase in aerodynamic roughness (Table 2.21), and of increasing R_s to 50 ms^{-1} is to indicate considerably greater E_T during the wet season.

To demonstrate these changes, the values of E_T for the Penman and Monteith equations are shown in Figure 2.27. A five point running mean has been used as a smoothing filter to afford a clearer comparison. The Penman value for a fixed albedo of 0.25 is shown on the least variable function (annual total 1669mm). The Penman modified function varies reflecting the changing vegetation height. It is always greater than the Penman function. The Monteith value approaches zero during the dry season months and increases to become greater than the Penman function during the wet season. The values of R_s used are presented in Table 2.24.

Table 2.24 Values of R_s used in the Monteith calculation.

Month	J	F	M	A	M	J	J	A	S	O	N	D
R_s	3000	8000	700	200	100	60	50	50	50	70	100	800

The effect of changing R_s during the wet season when k_0 is large is insignificant. Similarly, the effect of altering k_0 in the dry season when R_s is large is unimportant.

Figure 2.28 shows the contribution of the Monteith aerodynamic and radiation term to the total evapotranspiration function shown in Figure 2.27. The 1979 rainfall is included for comparison.

Considerable error can occur at these transitions between the seasons. The values of albedo, k_0 (vegetation height) and R_s are all dependent

upon the rains or more directly, upon the soil moisture balance. A monthly discretisation of these values is insufficient and a model whereby these functions are in some way linked to the soil moisture balance is suggested. Possible relationships will be discussed in section five.

It is evident from the above that the sensitivity of the E_T calculation to the measured climatic parameters is of an order of magnitude less than that of the estimated parameter, particularly the R_s function.

Lastly in this section, it is worth noting that the calculated E_T function will be reduced further in the dry season as the use of the available net radiation is changed. This point has been discussed in Section 2.3, although no allowance has been made for it in the calculations presented in this section. In temperate latitudes, the complete net radiation is assumed to be available for evapotranspiration, and it is not likely that this causes a significant overestimate of E_T . In the savanna however, it is not reasonable to make this assumption. Equation 2.12 expresses the possible different ways in which net radiation can be absorbed, and Table 2.18 presents the results of experiments at Samaru (Kowal & Kassam, 1973a).

From Table 2.18 it may be seen that even in the wet season, only approximately 75% of net radiation is used to produce evapotranspiration (E), the remainder is used to heat the soil (G), the air (H) and to drive the photosynthesis mechanisms (P). During the dry season, most vegetation is dead and therefore evapotranspiration must be small, although some direct evaporation from the soil still occurs (as discussed in section five). It seems probable therefore that there is a large redistribution of the use of net radiation during the dry season. The increase in albedo causes a higher percentage of incident radiation to be reflected and therefore net radiation will be less in the dry season. Of this reduced net radiation it is suggested here that only 25% is used for evaporation, the remainder is used to heat the ground and the air.

In the water balance algorithm, described in section five, and presented as Appendix E, the net radiation available for evapotranspiration during the year is modified as described above. The change between the 75% available during the wet season, to the 25% available during the dry season is a function of the increasing soil moisture deficit

(see section five). While it is accepted that this is not the conventional approach, it is felt that the error produced by any inaccuracy in the empirically guided choice of conditions, is more than offset by the more realistic approximation of the actual environment.

2.5 SUMMARY

Research in the whole general area of tropical meteorology has received a considerable impetus from the general availability of satellite imagery. Before this time, the network of meteorological stations throughout the tropics was very sparse and the lack of upper troposphere observations was a particular restraint to understanding the tropical circulation. In addition to the general availability of satellite imagery, the results of the world meteorological observation programme directed at the West African and Eastern Atlantic area has provided a wealth of detailed observation of upper and lower troposphere data. When this data is finally completely analysed, it is likely to provide a complete re-assessment of tropical weather systems in general, and perhaps the Inter-tropical Convergence Zone in particular.

It is of use to summarise some of the major ways in which the tropical climate differs from that at temperate latitudes however, as there are direct hydrogeological implications arising from these differences.

1. There are no frontal systems producing fairly uniform rainfall over a wide area.
2. The high net radiation input creates a large number of localised storm cells which are characterised by very high intensity rainfall over limited areas. Lateral extrapolation of rainfall from a recording station is therefore not possible in time scales of less than five years if any order of accuracy of the extrapolation is required.
3. The high net radiation input combined with the very marked seasonality of the climate produces greatly varying albedos throughout the year. A background variation of between 0.10 and 0.35 probably occurs. This variation produces a range of evapotranspiration values which are not experienced in temperate latitudes.
4. The concept of potential evapotranspiration based upon Penman's equation cannot be applied throughout the year. A more sophisticated model based on an analysis after Monteith is required, with particular emphasis being placed on the evaluation of the aerodynamic and canopy resistance terms.

A considerable research programme is required before a systematic method of calculating actual evapotranspiration can be finalised. However, the methods suggested in Section 2.4 indicate a definite path of approach. In section six a groundwater balance is presented which attempts to explain several features of the groundwater hydrograph. The concepts presented in this section are used to control the evapotranspiration function in the general water balance. The effect of the variability of rainfall is also

investigated by using a number of different years of data from the Bauchi record with the same general evapotranspiration function.

It is necessary to describe the nature and evolution of the weathering basins and the rocks which are acted upon by the climate before a water balance can be attempted however, and the next two sections are concerned with this analysis.

3. GEOLOGICAL ENVIRONMENT

Introduction

The Cambrian and Pre-Cambrian gneisses and granites which compose the majority of the Basement Complex of Nigeria are essentially similar to those which occur throughout the rest of Africa, and also over large areas of the continents of Asia, Australia and ~~the~~ ^{South} America~~s~~. In addition, the climatic conditions discussed in section two of the thesis, represent the same general conditions which occur throughout the savanna regions of the world. The geological and climatological environments of Central South America, India, Northern Australia and large parts of Africa south of the Sahara, are sufficiently similar to those of Northern Nigeria that the general discussions in this section are valid throughout these areas. For this reason the first part of this section is discussed in general terms before specific examples from Northern Nigeria are described.

It is the purpose of this section of the thesis to examine the geological environment, and in particular the weathered zone, in order that a simple model of the groundwater resources may be constructed. This model will then serve as a basis for the development of the geophysical techniques designed to locate groundwater reserves in a specific area, and will also be used as a basis for the resource assessment in section six.

Crystalline rocks such as granites and gneisses, when in the unweathered and unfractured state, exhibit very low porosity and are completely impermeable. By contrast, the weathering residues of these rock types are predominantly silty clays and quartz particles. The residue therefore has a high porosity, comprised of a large number of very small interstices between clay laminae, and negligible permeability. At some intermediate stage in the weathering process, a stage is reached whereby the crystalline matrix is completely ruptured and yet chemical weathering reactions have not produced large amounts of clay minerals. These horizons within the weathering profile have porosities of 10-20% and permeabilities of $50 \text{ m}^2 \text{ day}^{-1} \text{ m}^{-1}$. It is the latter horizons which constitute the groundwater resource. Unfortunately, the combination of weathering processes which produce these zones is not well understood. In the majority of locations the weathered profile is only approximately 10m thick, and the zone of higher porosity and permeability is not

sufficiently thick to form a useful resource. In addition, this zone lies often above the dry season water table levels.

The existence of areas of deep weathering, where the depth of the weathered profile exceeds 30 metres, has been recognised for some time (Ruxton & Berry, 1957, Thomas, 1966, Faniran, 1975). However, as information concerning the depth and extent of this deeper weathering is intrinsically difficult to obtain, very little research work has been devoted to the problem. The weathering mechanisms that produce these weathering basins or troughs are not well understood.

Deep weathering in the tropics has played a considerable part in the protracted geomorphological discussion concerning the origin of inselbergs (Ollier, 1975), and has been studied from the civil engineering approach where deep weathering encountered in tunneling may be problematic (Newbery 1971; Irfan & Dearman, 1978). However, no consensus of opinion has been developed, especially with regard to the nature of weathering beneath the permanent water table.

In the following section, various aspects of deep weathering are examined with the aim of identifying the significant hydrogeological processes. It is recognised that the treatment is in no way complete and that a great many questions remain unanswered.

In the first part of the section, the petrographical and chemical nature of the granites and gneisses are described with a discussion of the tectonic setting in which they have been formed. This may seem of little hydrogeological significance, however, the work in Nigeria has concentrated almost entirely on S-type (see section 3.1) granite and surrounding gneisses, and there is some indication that the I-type granites do not weather in quite the same way to produce basins of deep weathering.

The locus of deep weathering is probably a fracture or dyke intrusion related to a fracture system. If the tectonic style of an area can be understood then orientation and location of areas of deep weathering may be predicted. These predictions, usually based upon an analysis of the remote sensing data, are of considerable use in restricting the areas that are investigated using geophysical techniques. For this reason the second part of this section contains a description of the various fracture types which may control deep weathering.

The third part of the section contains a discussion of the weathering processes and reactions that may occur within the deep weathering

environment. A large part of this discussion is conjectural and there is ample scope for more detailed research in this area.

The engineering and petological approaches have been combined in the fourth part to produce a geological model of a typical area of deep weathering. The concept of engineering grades (Dearman et al 1978) are of particular use in this respect.

The application of the geological model to areas of Northern Nigeria is described in the fifth part of the section. The results of diamond core drilling through shallow weathered zones and the logs of a number of water well boreholes are used to substantiate the model.

Lastly, the physical properties of the soil are described in a final section as these are of great importance when the water balance is considered in section six of the thesis.

It is recognised that the development of a water table within the weathered zone is inextricably linked with the chemical reactions which occur within the zone, and that the two cannot be separated for hydrogeological purposes. However, in order to improve the clarity of the discussion, the description of the hydrological and hydrogeological implications are delayed, as much as possible, to section five of the thesis.

3.1 General Geology

The geological environment which is common to the stable cratonic areas consists of a complex association of high grade metamorphic rocks, gneisses, migmatites and granites. The rock associations are generally the result of a number of little understood geosynclinal periods, of Cambrian or Pre-Cambrian age. The last such orogenesis to effect large parts of Africa was the Pan African (650-850 Ma).

As the petrogenesis of these rocks has such a long history, it is not surprising to find a highly complicated association of rock types resulting. The following discussion is restricted to the weathering of migmatites and granites produced by anatectic processes. Such granites are referred to as S-type granites (White & Chappel, 1977), indicating that they have originated from the partial melting of ancient sediments. I-type granites are the products of differentiation of gabbroic magmas. The differentiation is significant in hydrogeological terms as the s-type granites show more compositional irregularity than the I-type and are therefore subject to more variable forms of chemical weathering (see below).

S-type granites have a number of compositional features which it is useful to summarise.

1. They are strongly peraluminous $Al / (Na + k + (Ca/2))$ ~~is~~
2. They have high initial Sr^{87} / Sr^{86}
3. Complex zoned plagioclases

In addition the magmas are more viscous and tend to move as diapirs in such a way that the restite is carried along with the magma producing numbers of xenoliths which are still mostly recognisable as meta-sedimentary types.

The s-type granites have not generally moved very far from the place of origin, and complicated suites of migmatites are seen in close proximity to the granites. A migmatite is simply a mixture of high grade metamorphic rock (gneiss) and granite. Migmatites have light coloured layers with portions composed of quartz and feldspar, often showing euhedral crystal shapes, and dark coloured layers in which biotite predominates (Winkler, 1967). The minerals of the darker coloured layers generally have a preferred orientation. Plates 3.1 and 3.2 show typical outcrops of migmatite from the Bauchi area. In

Plate 3.2 a meta-sedimentary pod has caused a local irregularity.

As mentioned above, the following discussion is limited to that of gneisses, migmatites and granites. Although many of the principles may be extended to less high grade metamorphics, on the one hand, and to mafic intrusives and their derivatives on the other, it is necessary to restrict the scope of the discussion as in particular equigranular crystalline rocks such as the I-type granites fracture and weather in such a way as to generally not produce areas of deep weathering.



Plate 3.1 A typical migmatite from the area of Bauchi. Note the lamination of biotite in the dark zones, compared to the more euhedral crystal development in the light zones. Note also several different phases of granite veining.

Plate 3.2 A meta-sedimentary relict within migmatite. The relict is almost entirely biotite. Note the flow structures strongly implying movement as a semi mobile environment. Note also the slip plane running top right to bottom left.



3.2 Jointing and Fracturing.

Definitions and method of formation.

Joints and faults are structures which result from the brittle failure of blocks of rock which are displaced relative to one another across narrow and approximately planar discontinuities (Hobbs et al, 1976). The discontinuities are called joints if the component of displacement parallel to the structure is zero (or too small to be apparent to the unaided eye) or faults if the parallel component of displacement is larger.

Most joints or faults form by fracturing, that is, the development of cracks across which the original cohesion is lost. Joints are often sealed tight again at a later date by the deposition of secondary minerals or by the recrystallisation of the original minerals.

Joints usually occur as groups in a given rock type.

A joint set is a group of joints, of common origin, which are usually parallel or subparallel to each other. The pattern of stresses which cause joints to form, most often give rise to more than one set of mutually orthogonal joints.

The whole assemblage of joints within an area is referred to as a joint system. Typically, the orientation of joints within a system varies across contacts between different rock types.

Joints which are small enough to require microscopic observation are called microjoints. By contrast, joints which are larger than associated joints of the same set are referred to as masterjoints. The masterjoints observed in remote sensing data can be traced for distances of several kilometres.

Origin of Joints.

Joint systems in granites are often symmetrically related to the contacts of the body, suggesting an origin during emplacement and cooling. Commonly granites are intruded along a particular orientation to produce ellipsoidal bodies with the major axis orthogonal to the direction of stress. The stress pattern causes a lineation produced by feldspar and biotite crystals which in turn acts as a fracture plane when the granite is later subject to stress often in the same sense. For this reason a major set of joints often exists parallel to the principal lineation.

In tabular bodies such as dykes, joints perpendicular to the contacts are formed due to the cooling and contraction of the basalt magma. This joint set may extend to considerable depth and the joints act as a main point of entry for water, which initiates chemical weathering. Dykes are often preferentially weathered out of granites and therefore form a locus of weathering in the surrounding granite. This is clearly demonstrated by Plates 3.3 and 3.4.

The weathering associated with dykes extends below ground surface to form in many cases the axis of an area of deep weathering.

Pressure Release Joints.

An important set of joints forms during the erosional unloading of a granite or migmatite area. As material is removed from an area by the weathering processes, the initial condition of stress within a given volume of rock is changed in that the component of stress orthogonal to the surface is reduced. The rock volume reacts to this change in stress by a strain in the orthogonal, which may not necessarily be the vertical, direction. The strain is accommodated until the point of brittle failure is reached and the rock fractures to produce a joint in the orthogonal plane to the initial release of stress.

Joint sets form which are parallel to the outcrop morphology, and these in turn set up stresses which cause a further pair of vertical and orthogonal joint sets. The result is the exfoliation slab commonly observed on many granite inselberg. The joints which are parallel to the surface outcrop and therefore commonly subhorizontal, often occur separated by as much as 1000mm, whereas the later subvertical joints may be several metres apart.

It is commonly observed that granites and some migmatites, where the percentage of granite is high, occur mainly as inselbergs, whereas gneisses and high grade meta-sedimentary rocks often occupy deeply weathered areas. An explanation for this observation may lie in the different ways in which the rock types react to unloading stress.

Coarse grained rocks are competent as a result of their interlocking crystalline fabric. They react to stresses as homogenous bodies and form joint sets at spacings as described above, separating into a number of coherent blocks or slabs. The individual blocks present a relatively small total area that can be attacked by chemical weathering, and more important, the joint sets are sufficiently wide



Plate 3.3 Inselberg of migmatite at Gubi close to Bauchi. This plate demonstrates the geomorphological effect of a dyke during the weathering process. The increased fracture density within the dyke has been exploited to produce a pronounced modification in the outcrop morphology.

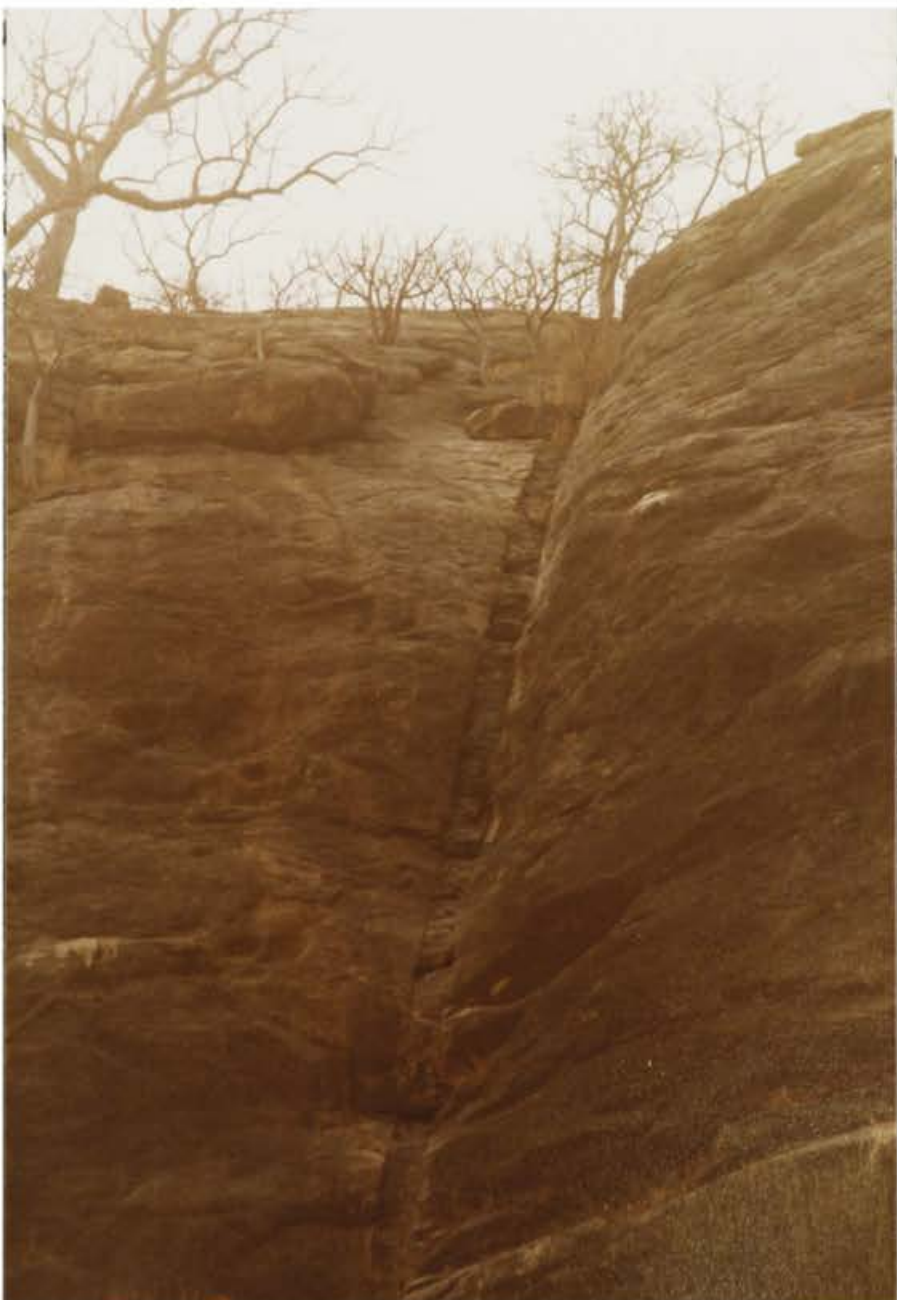


Plate 3.4

Close up of 3.3.

to allow efficient drainage of rainwater. This ensures that the blocks remain dry for the majority of the time.

By contrast, gneisses and amphibolite facies rocks are composed of mineral grains of many different sizes and with often an abundance of mica which gives the rock a schistosity or at least a pronounced lineation. As the rock is very inhomogenous, it reacts to the unloading stress by strain which is accommodated by fracturing, producing microjoints of crystalline dimensions. This density of jointing releases an area of rock of many orders of magnitude greater than that of the granite block, to the attack of chemical weathering. Similarly, the small size of the joints inhibits drainage and the whole rock mass remains damp. The efficiency of the weathering processes is greatly increased by this dampness as is well demonstrated in Plate 3.5.

Depth of Jointing.

The depth of jointing in granite is not known with any accuracy. Sheet joints and radial joints which are the result of unloading probably extend to depths of 10 to 15 metres before becoming tight. In the absence of other jointing, the weathering profile is commonly an average of 10m depth (Water Surveys 1978), and this tends to support the average depth of unloading joint sets.

Sheet like intrusives such as dykes can contain open joints to much greater depths. The joints are caused by contraction of the cooling magma. As the existence of the dyke indicates a condition of tension at depth, at least at the time of intrusion, there is no reason for the joint set to be closed until considerable depths are reached. Often dykes observed in quarry faces made into fresh rock, will exhibit brown staining on contraction joints, indicating the passage of water and the initiation of weathering along the dyke.

Regional joint sets and masterjoints or faults may extend to depths of 50 or 60 metres before becoming closed by the compressional stress of the surrounding rock mass.

As weathering has been recorded in granites in mines at depths of several hundred metres, it appears that major faults may remain open to the extent sufficient for the percolation of water to these depths. Such occurrences are not common however.

A combination of regional joint sets or masterjoints with an area

intruded by several dykes can produce a deeply weathered basin which holds significant groundwater reserves. The prediction of such a location in an area of generally weathered rock is possible in general from a detailed observation of the overall joint pattern within an area of interest. All the available remote sensing data is analysed to provide a structural map of the area of interest. There is generally available 1:40,000 or 1:50,000 photography of most places and this combined with more recent products such as side looking airborne radar (SLAR) imagery (see Plate 3.9) is particularly useful. Areas of deep weathered rock are evident on the photography by the absence of topography or outcrop. Light ~~strong~~ soils usually indicate solid rock at depths of less than five metres. Farming is often carried out on marginal soils and is not a reliable indicator. By contrast, the presence of phreatophytes, such as the mangoe in Nigeria, which fruit late in the dry season, is good evidence of water at depth.

3.3 Weathering of gneisses, migmatites and granites.

General.

The weathering processes that occur above the water table have been investigated in a number of recent studies (Nesbitt, 1979; Ledger & Rowe, 1980) and is also reported in standard texts such as Krauskopf (1967). The end product of the processes is a mixture of clay and quartz grains, with the clay chemistry determined by a number of environmental factors. The clay and quartz sand end product has a low permeability, although the porosity may be high. Such deposits provide good sites for large diameter wells, but are of no use as borehole sites where a higher permeability is required.

In the partially weathered material beneath the water table, a part of the rock fabric is removed by weathering reactions, which leave the matrix of the rock unaltered. In this way, the porosity and permeability of the partially weathered rock is increased markedly. Zones where this process has occurred are referred to by Cornish miners as *grus* zones (Brunsdon, 1964). The reactions which are involved in this process are not understood, however, the results produce areas of sufficiently high permeability that boreholes producing $10\text{m}^3/\text{hr}$ can be successfully completed.

In the following discussion the general weathering processes are described and possible mechanisms suggested to describe the weathering processes beneath the water table.

Weathering Processes.

The weathering processes may be subdivided into three main groups; mechanical, biological and chemical. Although each of the processes does operate individually, their concerted effect is the most efficient.

The mechanical processes act to break up the rock mass. Of these processes, the most effective is the jointing associated with pressure release as discussed above. Rock mineralogy as much as crystal size appears to affect the spacing between joints formed by this process. For example, quartz monzonites which crop out around Bauchi, tend to form three equidistant orthogonal joint sets which produce spheroidal boulders upon weathering. This effect may be seen in Plate 3.5. In another part of Nigeria, the joint pattern is observed to change character as a result of a small change in feldspar chemistry, - (Hazell -



Plate 3.5

Spheroidal boulders formed by weathering of quartz monzonite.
Note the advanced chemical weathering beneath the soil as compared
to the comparatively fresh rock on the surface.

personal communication).

Biological processes are effective in mixing the top soil layer. Termites in particular, transport large quantities of soil towards termite mounds, which can reach 3 metres in height. At the rock face, roots are very effective in loosening the slabs released by jointing. Trees and bushes are commonly seen rooted in joint systems and growing on otherwise bare rock surfaces.

The most important of the three processes is that of chemical weathering. Once the rock is broken by jointing, the high temperature and ready supply of water produce rapid chemical breakdown of the mineral grains within the rock.

Chemical Weathering.

Chemical weathering may be described as an attempt by the rock mass to attain an equilibrium with the environment of the atmosphere and biosphere. Whereas it has been possible to describe the chemical phases within the closed system of a granite melt (Winkler, 1967), the same order of understanding is not possible in the low temperature, open system of the weathering environment.

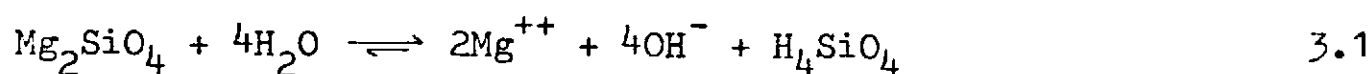
Most weathering reactions which occur are not reversible and therefore do not have equilibrium constants which can be readily calculated. The rates of reaction are determined therefore, by the rate at which the products of weathering are removed from the system. In turn, the rate of removal is determined by the solubility of the various weathering products in water, as percolating groundwater is the principal means of removal. In this respect, the warm (23°C) mildly acidic (pH 5.7) rainwater is efficient as a solvent.

The principal component of granites or gneisses are the silicate minerals. Microcline, plagioclase and quartz form between 80 and 95% of a typical granite with muscovite, biotite and a few minor accessories such as magnetite, ilmenite and sphene forming the rest. The weathering of these rock types is therefore principally the weathering of the silicates.

The basic unit of silicate minerals is the silicon oxygen tetrahedra, where a silicon atom is bonded covalently with four adjacent oxygen atoms. The tetrahedra may be arranged in discrete groups, such as chains (pyroxenes and amphiboles), sheets (micas) or three dimensional structures (quartz and feldspars). In addition, various other

ions of a similar size to silicon may be substituted for the silicon ion in each tetrahedra. In general terms, the simple three dimensional network of silicon and oxygen (quartz) is the most stable mineral. Instability increases both with the degree of isomorphous substitution of alumina for silicon and with the degree of condensation of the silicon oxygen tetrahedra. The subject of silicate weathering is discussed at length in several standard texts (Kraupskopf, 1967; Ollier, 1975), and will not be described in detail.

The principal chemical reaction involved is that of hydrolysis. As an example, the hydrolysis of forsterite by pure water (pH 7.0) may be represented (Kraupskopf, 1967) as:

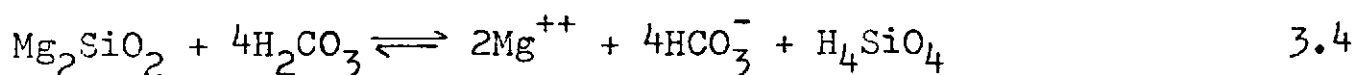


The water disassociates as :

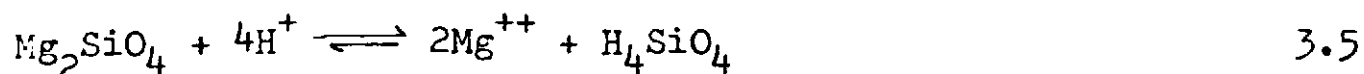


and the hydrogen ion replaces the magnesium in the forsterite to produce the very weak silicic acid. Note that the reaction leaves the solution more basic than before, due to the hydroxyl ion release.

Water in the weathering environment does not have a neutral pH however. As the rain falls through the atmosphere, the water equilibrates with atmospheric carbon dioxide to produce a weak carbonic acid. As the rainwater percolates through topsoil, a further absorption of CO_2 takes place as the soil air partial pressure of CO_2 is considerably greater than that of the atmosphere. With this greater concentration of hydrogen ions the reaction is modified to :



The supply of hydrogen ions is further augmented in the vicinity of plant roots. The roots produce a supply of hydrogen ions which are exchanged for metal ions, and by removing the latter, the reaction is kept in imbalance. This reaction may be represented as :

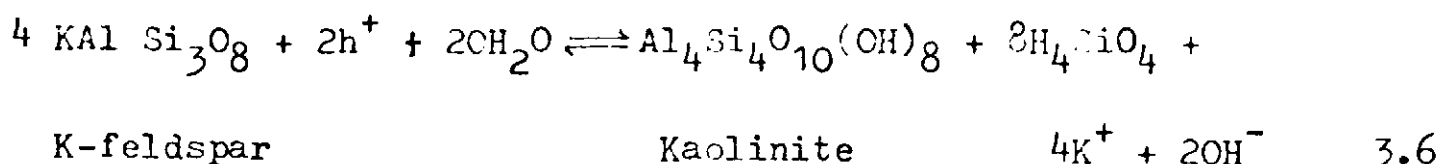


Similar, but more complicated reactions may be written for the more common minerals in the weathering environment, such as :



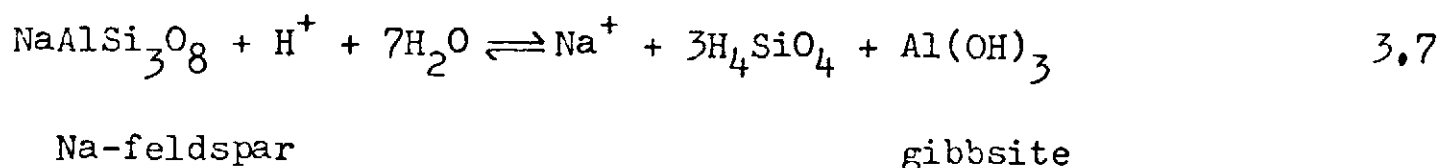
Plate 3.6. This plate shows an example of grus from Northern Nigeria in a recently made road cutting. The cutting face stands at an angle of 60° although it was constructed by repeated passes with a D9 caterpillar excavator.

- Note:
1. The granular disintegration sand of the base of the cutting
 2. The constant volume weathering indicated by the undisturbed quartz stringers (veins)
 3. The basalt dyke weathered to clay within the less weathered granite.
 4. The very thin soil zone with almost no clay development.

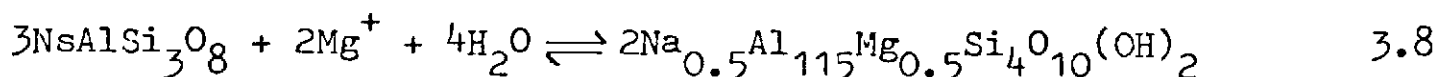


This reaction is a simplification however, and a more complex process occurs in reality. It is possible that the hydrolysis does not take place directly but in a series of steps. The feldspar may first break down to form gibbsite ($\text{Al}(\text{OH})_3$) setting silica free as dissolved silicic acid, and then kaolinite forms by a later reaction between gibbsite and silicic acid.

Berner (1971) has emphasised the importance of water flow as a controlling factor in weathering. At moderate flow rates albite ($\text{NaAlSi}_3\text{O}_8$) is changed to gibbsite as described by Equation 3.7.



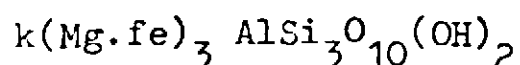
When flow rates are very slow and providing magnesium is present, the product is montmorillonite.



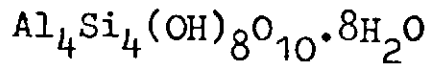
Bauxite minerals such as gibbsite tend to form in areas of high rainfall and high relief. Montmorillonite tends to form in conditions of low rainfall and low relief. The formation of kaolinite is intermediate between the two.

A red brown limonite staining on otherwise fresh joint surfaces is usually the first indication of weathering. As limonite is a complex oxide of iron, the first weathering reaction must involve an iron bearing silicate or oxide. Of the common silicates found in granites and gneisses, only biotite contains appreciable iron. Magnetite and the iron bearing amphiboles or pyroxenes are considerably less common than biotite.

The mica biotite has a sheet like structure, with iron, magnesium and potassium held in octahedral co-ordination sites between the sheets. The chemical formula of biotite may be written :-



The cations in the octahedral sites are only weakly held and may easily be replaced by hydrogen. Although the hydrolysis reaction is complicated, biotite first alters to the clay mineral halloysite which pseudomorphs the biotite. Halloysite has the chemical formula:



The inter sheet octahedral cations are replaced by a layer of orientated water molecules. The cations are released into solution, where iron is oxidised to form limonite and precipitated out to produce the red brown staining.

Ledger and Rowe (1980) have presented results which confirm the early weathering of biotite. Working upon the change of radioactivity in granite weathering associated with the removal of uranium, they found that uranium was held in two principal sites in granite. The first is in small inclusions of zircon. These are held along biotite grain boundaries, or within the inter sheet octahedral co-ordination sites, and are responsible for the pleochroic haloes of biotite (Deer, et al, 1975). The second is within resistant grains such as zircon and sphene adjacent to quartz and feldspar grains. The uranium associated with biotite is lost very early in granite weathering, presumably due to the hydrolysis of biotite. The radio-activity over a weathering profile therefore shows a stepped decrease. There is an initial rapid fall coincidental with the weathering of biotite, and the release of the very small grains of zircon. This is followed by a period of constant radio-activity as the larger zircon and sphene crystals are held in position until the final disaggregation and removal of the completely weathered rock.

The initial replacement of iron by hydrogen in the biotite allows sufficient room for access by water to the surrounding grains so that hydrolysis reactions may continue. Where the rock lies above the water table, the weathering reactions are comparatively rapid. Rain-water percolating downwards provides a constant source of hydrogen ions. The pH may be as low as 4.5 (Eswaran & Bin, 1978). Water also removes the products of hydrolysis. The final breakdown products of all the silicates are clays, principally kaolinite and gibbsite, but often modified by environmental factors as discussed above. These clays can be seen in deeply weathered areas forming the top few metres of the regolith. On exposed sites at outcrop, where weathering is

occurring, there exists a mixture of fresh rock, partially weathered rock and clay, the proportions of which are a function of the original chemistry, fabric and fracturing.

It is suggested here that rocks which do not contain disseminated mica, will not weather as readily as those which contain mica throughout. Without an initial means of access to the rock matrix over a sufficiently large crystal surface area, the weathering reactions slow down or stop. This is because each crystal surface which is being exposed to hydrolysis, becomes coated with a layer of hydrogen ions. These ions tend to repel other ions still in solution, and therefore form a protective coating (Kraupskopf, 1967) around the silicate crystal. The process is particularly evident in coarse grained rocks which have relatively small total crystal surface areas. The result is that coarse grained equigrannular rocks predominantly composed of quartz, feldspar and localised areas of biotite, are more resistant to weathering than gneisses, which are typically fine grained and contain abundant disseminated mica. This suggestion is given strong support by the observation that granites typically occur as inselbergs.

Constant Volume Weathering.

As has been described above, the significant horizon in the weathering profile for hydrogeological purposes is the partly decomposed and fractured zone that occurs above fresh rock and below the high clay content more weathered surface zone. Weathering in this zone is often considered to be constant volume weathering (Ollier, 1975) although the term may be misleading.

The evidence for constant volume weathering is essentially that the fabric of the rock appears to be undisturbed. In particular, small quartz veins and joint orientations are preserved in such a way that any form of large scale movement during weathering is not possible. Plate 3.6 demonstrates a number of these features.

Apart from the apparently undisturbed fabric of this zone, there are two other important modifications. The porosity is increased from zero to approximately 10%, and the crystal grains become loose and parted from each other.

The zones which this stage in the weathering process produces have been given a number of names; grus, or granular disintegration sand

or saprofitite (Ollier, 1975). In outcrops above the water table, individual crystals can be rubbed off the surface, as can be seen in Plate 3.6. When this grade of weathering¹ is encountered in boreholes, the drill cuttings are a disaggregated crystal sand², with no trace of the original intergranular components.

The problem of identifying grus in boreholes is further exacerbated by the common use of down-hole-hammer pneumatic rotary rigs for drilling boreholes in hard rock areas. The hammer action of the drilling bit on the already disaggregated matrix ensures that no trace of any remaining intergranular components remain in the drill cuttings. The drill cuttings often contain perfect crystals showing prism ends and no signs of weathering. However, the penetration rate of a rotary rig through this material is very slow, indicating that the original interlocking crystalline texture is not disturbed. This fact complements that indicated in Plate 3.6 of a stable and steep cutting slope in the road section.

When attempts are made to obtain an undisturbed sample of grus for examination, for example by diamond coring, it is found that the material has no tensile strength and falls out of the bottom of the core barrel, especially if water is used as a flushing agent.

It is difficult to account for the formation of grus within a constant volume weathering environment. The through-put of water essential to continued hydrolysis cannot be sustained within a constant volume, and the weathering reactions would be reduced to the rate at which ionic diffusion could carry away the released cations and supply hydrogen ions. Such a process is considered here to be prohibitively slow within a constant volume environment.

What is required therefore, is a set of processes which appear to leave the fabric undisturbed yet do not rely upon weathering within a constant volume. It is suggested below that pressure release jointing provides the background in which such a set of processes could operate.

Pressure release jointing has been discussed above. However, it

- Notes. 1. Grades of weathering are defined and described in the following section.
2. The mistaken identification of grus as sandstone fragments is common in drill logs from crystalline basement areas.

is important to appreciate that the stress which causes the jointing is continuous, in such a way that the joint will continue to open after the point at which brittle failure causes the joint formation. However, except in coarsely crystalline rocks, widely opened joints are not observed at the surface. Only the trace of these joints remains, helping to give the impression of little disruption.

In medium to fine grained rocks it has been noted above that joint sets are likely to be closely spaced (of the order of 1000mm). In such circumstances, the following sequence of events could lead to grus formation without marked disruption of the fabric.

- (i) Initiation of a joint through which a flow of water may commence.
- (ii) Hydrolysis of biotite and release of iron which forms limonite staining.
- (iii) Conversion of outer part of biotite to halloysite and the release of inter sheet components (e.g. zircons).
- (iv) Disruption of biotite causes loosening of adjacent crystals and further penetration of water.
- (v) Hydrolysis of plagioclases, especially if calcium content is high. The water will be highly undersaturated in calcium and silica if pH is as low as 4.8 (Eswaren & Bin, 1978).
- (vi) Removal of silicon as H_2SiO_4 and calcium, potassium and sodium as hydroxides.
- (vii) Expansion of the weathered rim of the jointed block, due to crystal parting, until flow of water decreases, when reaction rates will also decrease.
- (viii) Joint expands due to further unloading caused by erosion, and the process is regenerated.
- (ix) Complete extinction and solution of cryptocrystalline intergranular phases will occur in the active rim at any time, thus increasing the porosity.
- (x) Process continues until the centre of the jointed block, also referred to as core stone, is finally penetrated.

The genesis and distribution of the clay minerals is described below. However, if the flow of water through the joint becomes sufficient to convert all the mica, plagioclase and some orthoclase to halloysite then an important second stage commences. The halloysite is altered to kaolinite. This change affects the porosity of the zone significantly. The halloysite has formed as pseudomorphs of the original silicate (Eswaren & Bin, 1978) and the original texture is retained. However the kaolinite forms as clay sheets and these block the pathways between grains thus reducing the permeability. Core

stones may thus become isolated and remain intact to a much higher level in the weathering profile.

As much of the weathering within the grus zone produces pseudomorphs of the original crystals, the texture of the zone remains unaltered, thus giving the impression that the weathering has occurred within a zone of constant volume.

The sequence of events described above is by necessity hypothetical. However, there are several implications which it is possible to test by general observation. These are listed and discussed below.

(1) Coarsely crystalline rocks with limited biotite should not form grus zones. Most of the coarse grained granites or granitic migmatites found in Northern Nigeria occur as inselbergs and not as areas of deeper weathering. The converse is equally true, that no gneisses with disseminated biotite are found as inselbergs.

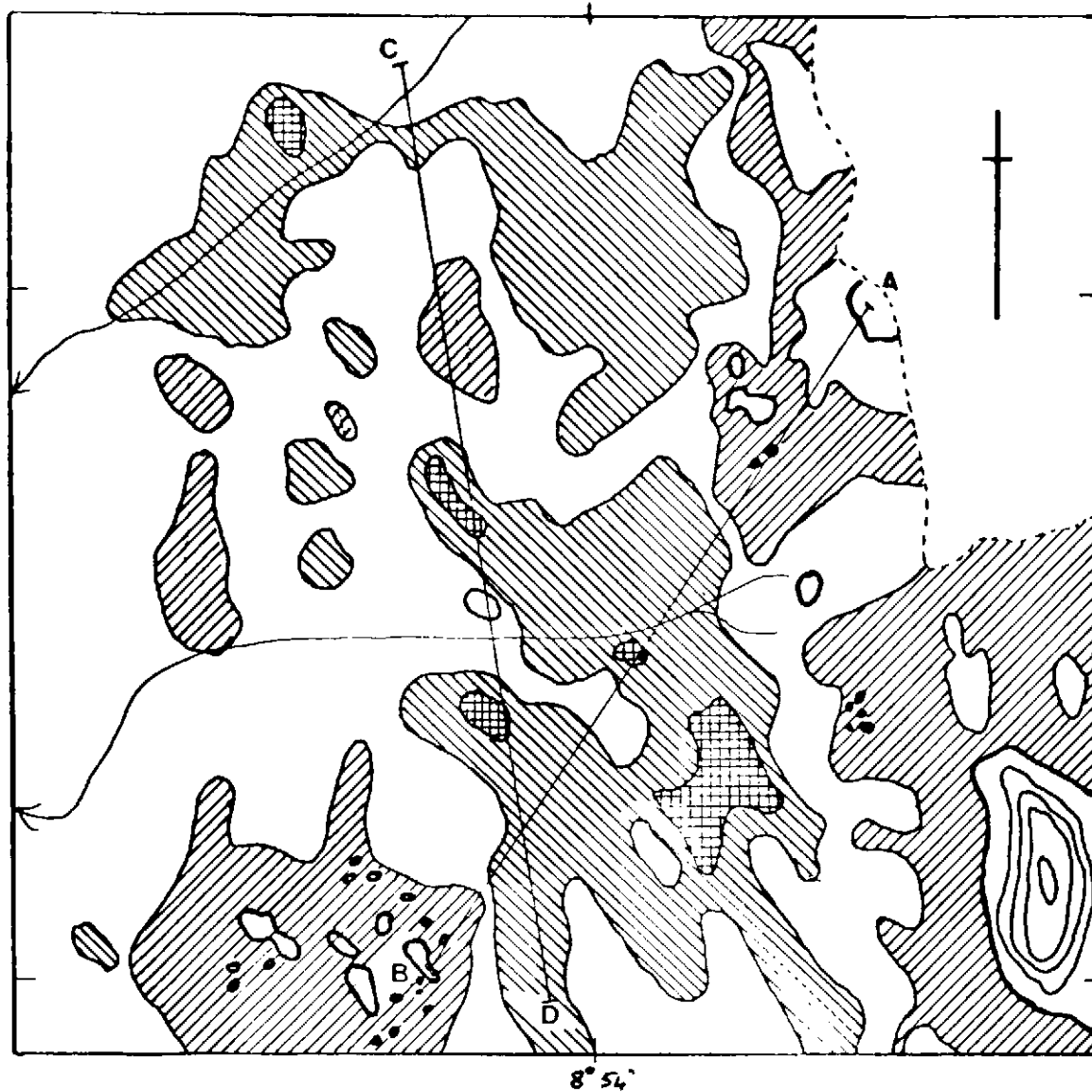
(ii) The distribution of biotite in an s-type granite will be determined by the nature of the original metamorphic material, and will show considerable variation both horizontally and laterally. If grus formation is a function of biotite content then it may be expected to show a similar variation. This appears to be so in Northern Nigeria, the pockets of deeper weathering occur around fault zones with a limited zone of disaggregation in coarse grained rocks, and only develop extensively in areas of gneiss.

It is not possible to prove or disprove the proposed sequence of events with the available data but the proposed model does explain a number of the observed facts.

Deep Weathering Profiles.

The geological practice of mapping from outcrop to outcrop and extrapolating the geology between outcrop has allowed deep weatherings to go undetected in many areas. It is only when mapping has been carried out for soil or sub-surface features that the extent of deep weathering becomes apparent. More recently, a number of deep weathering occurrences have been detailed. (Ruxton & Berry, 1957; Brunsdon, 1964; Thomas, 1966; Newberry, 1971)

Thomas (1966) reported weathering to 90m depth on the Jos plateau of Nigeria, and his sections have been reproduced in Figure 3.1.



Depth to Fresh Rock (METRES)

< 15

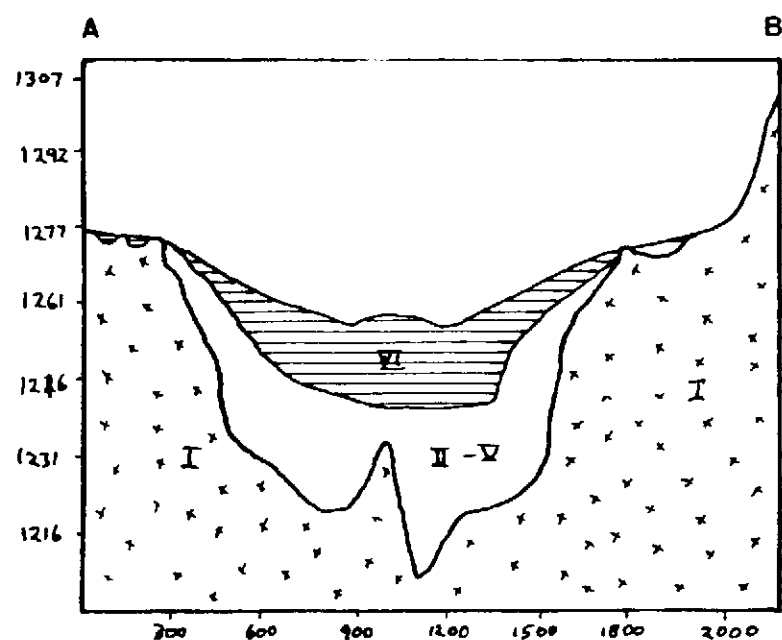
15 - 30

30 - 45

> 45

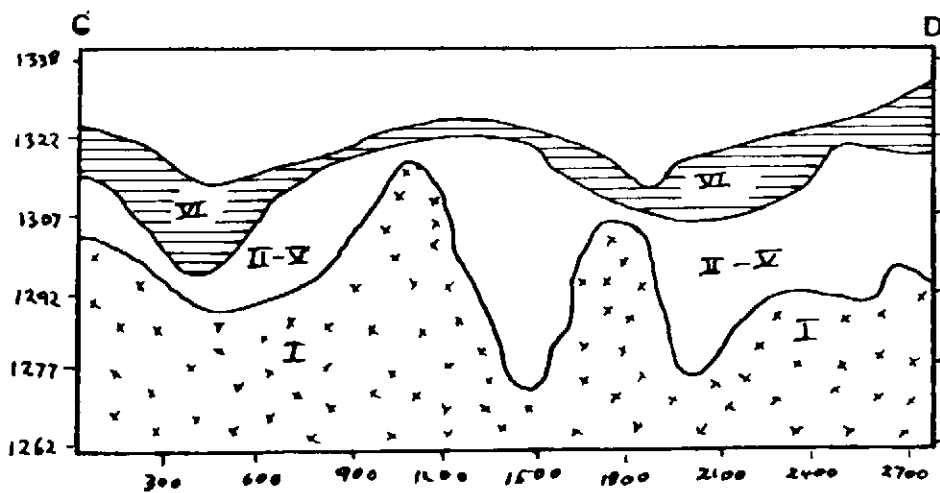
Outcrops of fresh rock contours at 15m intervals

Scale 1:25,000
0 250 500



Section A - B

Showing the depths of weathering grades



Section C - D

Figure 3-1 Deep weathering profile from the Jos Plateau. (After Thomas, 1966)

Ollier (1975) reports weathering to 350m in gneiss encountered during tunneling in Victoria. Such depths of weathering are only associated with fault zones, where the necessary water flow and reactions can be accommodated. The weathering reactions cease in these zones when there is no further expansion about the fault zone, in the way that probably rejuvenates weathering in the pressure release joints described above.

Eswaran and Bin (1978) have used scanning electron microscopy (SEM) techniques to make a detailed physio-chemical and micromorphological study of a 20m deep weathering profile developed on a coarse grained granite in peninsular Malaysia¹. Although the climatic conditions are not savanna type, but tropical rain forest type (see Note 1), the chemical reactions are likely to be similar to those in other parts. The granite has 41% quartz, 10% orthoclase, 32% plagioclase and 13% minor constituents (Niggli Norms), however, no chemical analyses is given.

A number of selected physio-chemical parameters from the profile are listed in Table 3.1. Note in particular the low pH, which can only be maintained by continual removal of cations released by hydrolysis and supply of hydrogen ions.

The detailed results of the study can best be summarised diagrammatically. Figure 3.2 shows the percentage composition throughout the profile of the six basic components viz; quartz, feldspar + mica, goethite + amorphous iron, kaolinite, gibbsite and halloysite. Similarly, the percentage composition of the six components in each of the clay, silt and sand particle sizes is shown.

It may be seen from Figure 3.2 that halloysite is the only clay mineral present in all grades other than V and VI. The SEM studies indicated that halloysite formed pseudomorphs after the principle silicates in these zones, rather than individual clay flakes. The effect of this is to retain the texture of the original rock. Kaolinite only forms in zone V by alteration of halloysite and by primary alteration of silicates. It is suggested (Eswaran & Bin, 1978) that the pH may be a controlling factor in kaolinite and gibbsite formation.

Note 1. The profile is from Kuantan in Malaysia. Annual rainfall of 3257mm and potential evapotranspiration of 1130mm are given. In such a climate, the rock surface will be continually wet and the tendency for the larger joints in the granite to dry out and prevent weathering will be negated.

Table 3.1 Selected physio-chemical properties of a deeply weathered profile in Malaysia (after Eswaran & Bin, 1978)

Soil Horizon	Depth (m)	Weathering Grade	Clay %	Silt %	Sand %	pH H ₂ O	CEC meg/100g	Base Sat %
A1-3	0-0.1	VI	36.7	7.9	55.4	4.36	10.51	6.1
B21ox	0.1-0.4	VI	37.5	10.8	51.7	4.40	9.94	5.0
B22ox	0.4-0.6	VI	36.7	12.2	51.1	4.20	6.58	4.0
B23ox	0.6-1.0	VI	32.5	5.7	61.8	4.20	5.33	3.9
B3	1.0-1.5	VI	37.6	7.9	54.5	n.d	3.86	8.8
C2	1.5-2.8	V	18.1	13.8	68.1	4.40	2.60	1.5
C3	2.8-5.0	V	20.1	27.9	52.0	4.60	4.47	1.6
C4	5.0-8.0	V	10.2	35.5	54.3	4.65	6.18	1.6
C5	8.0-9.5	IV	18.4	32.5	59.1	4.70	8.91	1.2
C6	9.5-12.5	IV	15.5	25.9	58.6	4.84	8.98	1.3
C7	12.5-13.6	IV	11.7	22.5	65.8	4.80	9.10	1.5
C8	13.6-15.0	IV	8.5	21.7	69.8	4.85	8.62	1.5
R1	15.0-16.0	III	10.5	24.7	59.8	4.90	8.29	1.6
R2	16.0-16.6	III	n.d	n.d	n.d	4.90	7.66	1.8

Note The weathering grades refer to terms defined in section 3.4.

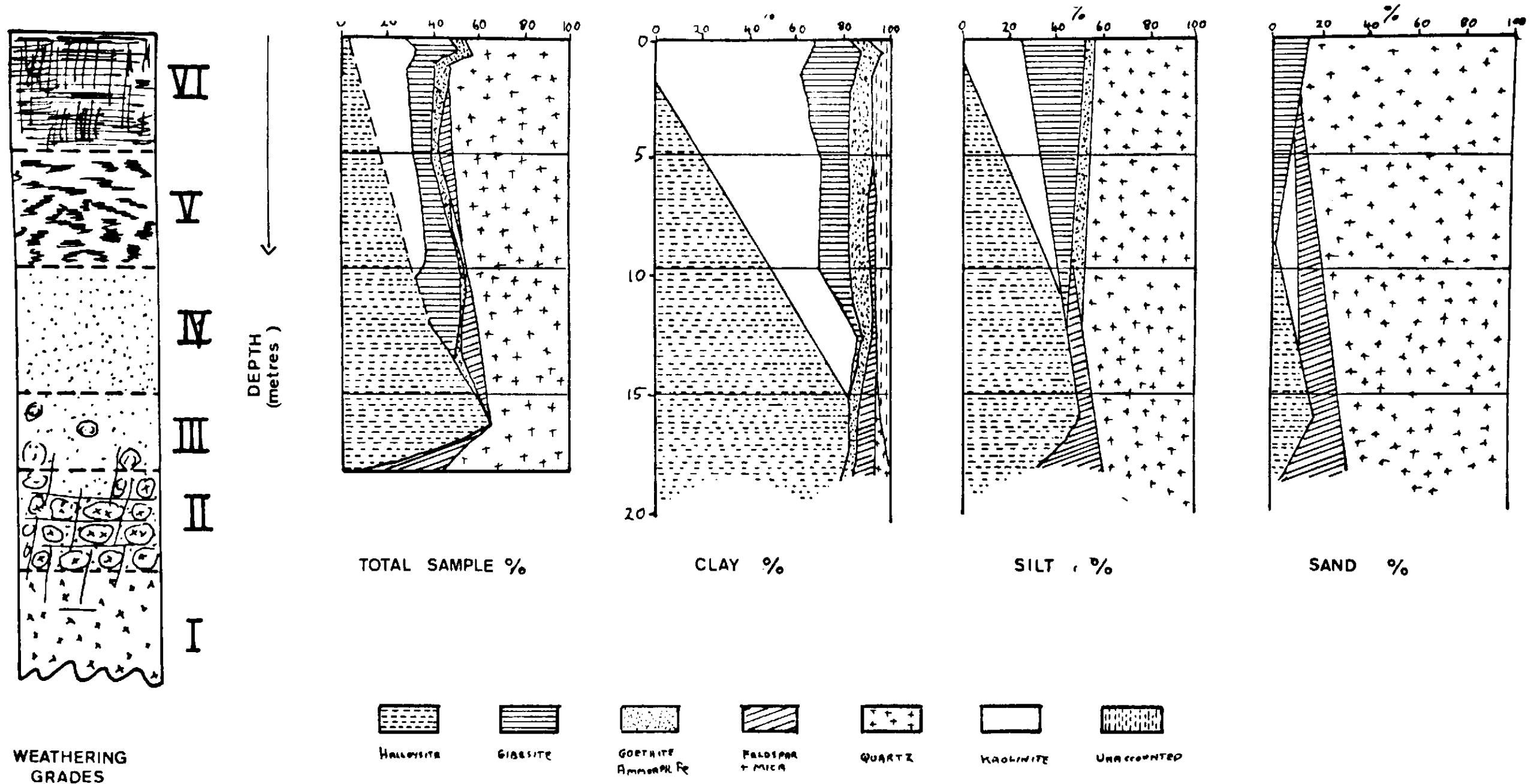


Figure 3.2

Semiquantitative estimates of minerals in the clay, silt, and sand fractions.

(AFTER ESWARAN + BIN, 1978)

The result is that clay plates are formed instead of pseudomorphs and as the clay flakes block the interstitial pores, the permeability is reduced.

Many deep weathering profiles appear to be weathered below the local base level of ephemeral stream channels. The weathering has occurred around fault zones and formed closed basins of weathered material within fresh rock. It has been suggested (Ollier, 1975) that such basins will contain zones of stagnant water with relatively high salinity. This, however, does not appear to be true. Of more than 100 boreholes sunk for water supply purposes in Northern Nigeria, and sited so as to penetrate the deepest part of the weathered zone, there was no record of high salinity. All the boreholes produced good quality potable water. Similarly, without a flow of groundwater at depth, the weathering reactions will stop, and this is contradictory to the evidence of great (> 100m) depths of weathering reported above.

Experiments have recently been made in the Hydrogeological section of the University of Birmingham Geology Department with a Hele-shaw viscosity model. The model has been used to demonstrate that a depth of 300m of saline water lying in an aquifer mostly below current sea level can be flushed out by surface recharge and discharge, as long as a hydraulic head is maintained over the length of the aquifer. A similar run of the model, but without the density contrast between fresh and salt water, indicated that a groundwater flow would be maintained to the bottom of a closed basin of weathering, where the depth of the basin is only 50m and the hydraulic head is approximately 5m. In this way, the hydrolysis reactions described above would be maintained.

Groundwater Chemistry.

The chemical composition of groundwater should provide useful evidence concerning the weathering reactions. Unfortunately, however, very few accurate analyses have been reported. In Table 3.2, data published by the Nigerian Geological Survey is presented. Only two of the analyses, numbers 946 and 1756 show a reasonable balance between the cations and anions which are the major species in water. However, there are a number of points of interest.

Table 3.2 Analyses of groundwater from the North Nigerian Basement Complex (Nigerian Geological Survey).

Average from 30 wells Durosoz (1961)		Bauchi BH 945	Bauchi BH 946	Plateau BH 1501	Plateau BH 1528	Fano BH 1756
0.024	Ammonia (NH_4^+)	0.004	<0.002	0.004	0.012	2.4
0.4	Magnesium (Mg^{++})	NIL	12.75	0.4	0.4	0.4
20.5	Calcium (Ca^{++})	31.43	8.59	6.0	2.0	13.7
0.01	Aluminium (Al^{+++})	NIL	NIL	<0.01	<0.01	<0.01
0.12	Iron ($\text{Fe}^{++} + \text{Fe}^{+++}$)	0.06	0.08	<0.04	<0.02	0.06
0.2	Copper (Cu^{++})	N.D.	NIL	<0.2	<0.2	<0.2
0.1	Zinc (Zn^{++})	N.D.	N.D.	<0.2	<0.2	<0.2
0.02	Manganese (Mn^{++})	N.D.	N.D.	<0.025	<0.025	<0.025
11.0	Sodium (Na^+)	11.0	14.66	NIL	3.2	16.0
6.0	Potassium (K^+)	N.D.	tr.	4.0	4.0	3.2
0.2	Fluoride (F^-)	0.2	0.6	0.2	0.3	0.1
6.0	Chloride (Cl^-)	5.0	NIL	2.0	3.0	7.5
0.06	Nitrite (NO_2^+)	NIL	NIL	0.06	0.06	0.013
10.5	Nitrate (NO_3^+)	NIL	<0.5	2.2	<0.132	24.4
0.1	Phosphate (PO_4^{+++})	N.D.	N.D.	<0.1	<0.1	N.D.
tr	Sulphate (SO_4^{++})	tr	tr	NIL	NIL	NIL
43.0	Bicarbonate (HCO_3^+)	66.0	117.9	3.9	9.2	48.8
NIL	Carbonate (CO_3^{++})	NIL	NIL	NIL	NIL	NIL
50.0	Silica (SiO_2)	60.0	130.0	16.0	24.0	24.0
	Total alkalinity as CaCO_3	N.D.	N.D.	6.5	15.0	40.0
	Total hardness as CaCO_3	N.D.	N.D.	2.5	2.5	33.0
	Σ equivalents Mg, Ca, Na, K	2.05	2.11	0.40	0.37	1.49
	Σ equivalents Cl, SO_4 , HCO_3	1.22	1.93	0.16	0.23	1.40
	Total Solids (180°C/IL)	174.0	252.0	68.0	60.0	N.D.
	pH	7.1	7.4	6.8	6.1	6.9

Note 1. The cation balance between major cations and anions is poor for each of the above analyses and therefore they are not presented graphically.

Note 2. The pH will not represent accurately conditions at the borehole as the determination is made in the laboratory.

(1) The silica content is much higher than in waters from sedimentary rocks. This would be expected in an environment where the predominant chemical reaction is hydrolysis. Silicic acid (H_2SiO_4) is released into solution in all the reactions noted above.

(ii) The level of total dissolved solids is low for any groundwater, indicating that the waters do not have a long residence time, and tending to confirm the idea of rapid and efficient flushing from the base of the basin.

(iii) Aluminium is low in all the samples. It is held in the grade V and IV material as gibbsite.

(iv) Sulphate is low, indicating the very low sulphate concentration in the primary material.

(v) The sample from Kano indicates bacterial pollution with high ammonia and nitrate.

(vi) Although the primary silicates do not contain a high proportion of calcium, it can be seen that the calcium that is available in plagioclases is readily dissolved by the pH 4.5 groundwater. The observation above that plagioclase crystals often show solution pits whereas orthoclase crystals do not, also supports this idea.

Further detailed analytical work combined with tritium dating would provide very useful evidence concerning the weathering reactions. However the chemical data available does support the general model of weathering described above and also suggests a rapid flushing of the active weathering zone. This, in turn, implies that the depth of weathering is controlled primarily by rock chemistry and grain size which is reflected in the nature of the pressure release jointing.

3.4 Deep Weathering Model.

General

Deep weathering has been described by scientists working in the fields of geochemistry, pedology, civil engineering, geomorphology and geology. It is not therefore surprising to find a number of classification schemes proposed to describe the sequence of materials between soil and fresh rock. In general however, six zones or grades can be recognised. As the grades reflect basic geochemical changes, they can be recognised from areas throughout the tropics, and also in areas which have experienced tropical weathering in the past, i.e. Europe in Tertiary times.

Moye (1955) classified weathered granite for civil engineering purposes during investigation for the Snowy Mountains Hydro-electric scheme. Ruxton & Berry (1957) described similar profiles developed upon granite in Hong Kong. These classifications were combined by Little (1969) and also Newberry (1971). The literature has been extensively reviewed recently (Dearman et al, 1978) and a comprehensive classification system proposed. It is this system which will be used as a basis for a model of deep weathering.

Definitions of terms.

Many terms used in the description of weathered rock are used only in a poorly defined manner. The descriptions proposed by Dearman have been adopted for this work and are presented below.

Fresh	No visible sign of weathering of rock material
Discoloured	The colour of the original fresh rock material is changed and is evidence of weathering
Weakened	The rock is weathered to the extent that it is noticeably weakened.
Decomposed	The rock is weathered to the condition of a soil in which the original fabric is still intact, but some or all of the mineral grains are decomposed.
Disintegrated	The rock is weathered to the condition of a soil in which the original material fabric is still intact. The rock is friable, but the mineral grains are not decomposed.

Corestones Relict, usually spherical or elliptical bodies of fresh or discoloured rock found in the soil zone.

The six grades of weathering are shown in Figure 3.3 against some typical particle size analyses after Fitzpatrick (1971). The weathering grades may be defined as follows (Dearman, 1978).

VI	Residual Soil	All rock material is converted to soil. The mass structure and material fabric are destroyed. There is a large change in volume, but the soil has not been significantly transported. Can be divided into an upper A horizon of eluviated soil and a lower B horizon of illuviated soil.
V	Completely weathered	All rock material is decomposed and/or disintegrated to soil. The original mass structure and material fabric are still largely intact.
IV	Highly weathered	Some of the rock material is decomposed and/or disintegrated to a soil. Fresh or discoloured or weakened rock is present either as a discontinuous framework or as corestones within the soil.
III	Moderately weathered	The rock material is discoloured and some of the rock is appreciably weakened. Discoloured but unweakened rock is present either as a discontinuous framework or as corestones.
II	Slightly weathered	Discolouration indicates weathering of rock material and discontinuity surfaces. Some of the rock material may be discoloured by weathering, yet it is not noticeably weakened.
I	Fresh	No visible signs of rock material weathering, perhaps slight discolouration on major discontinuity surfaces.

The degree of alteration of silicates within the weathering profile has a direct influence on porosity, permeability, seismic velocity and electrical resistivity. Irfan & Dearman (1970) have made a detailed petrographic analysis of thin sections of weathered material taken from an s-type granite in Cornwall, U.K. They included as a part of this work a description of the microfracturing and void content of each section. Similarly, Onadera et al (1974) used the number and width of microcracks as an index of granite weathering, and found a linear relationship between effective porosity and density of microcracks defined as :

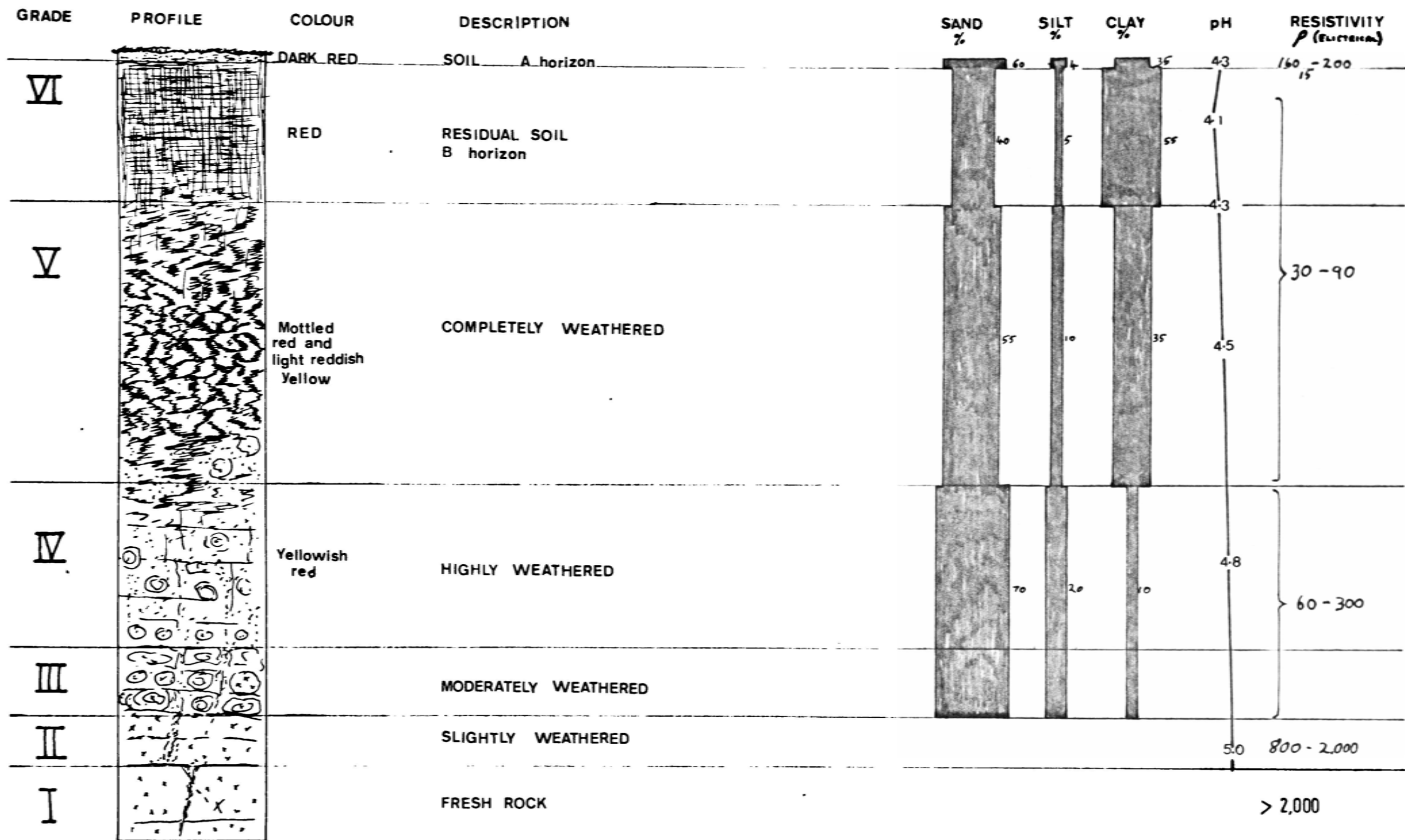


Figure 3-3 Weathering grades (AFTER FITZPATRICK 1971)

$$P_{cr} = \frac{100 \times \text{Total width of cracks}}{\text{length of measuring line}}$$

They found that the mechanical strength of granite decreases rapidly as P_{cr} increases from about 1.5 to 4.0 per cent. Porosity increases with physical weathering by an increase in crack number and openness.

The descriptions of Irfan & Dearman are combined with the SEM analyses below to provide a detailed description of each of the weathering grades. These descriptions may be related back to the general discussion of chemical weathering above.

As the geochemical reactions throughout the profile are progressive from fresh rock to residual soil, the separate grades are discussed in ascending order.

Grade I - Fresh Rock.

Included within this section are all types of alterations which may have occurred post magmatically, but still at depth below the surface. Eggle^r et al (1969) refer for example, to the post magmatic oxidation of biotite which results in a slight expansion and rupturing of surrounding grains.

Plagioclase feldspars often have a cloudy appearance in thin section and show alteration to sericite, particularly at the centre of crystals and along cleavage planes. Potassium feldspars are usually fresh, but often containing a number of inclusions. Quartz is fresh and unfractured except for short hair-like cracks which show no staining. Partial alteration of biotite to chlorite is most likely post-magmatic.

Grade I rock is separated from Grade II rock by the weathering front (Ollier, 1975). This front represents the greatest extent of groundwater percolation in any one direction, and as such is often a complex three-dimensional surface, which encloses grade I rock to form core stones.

Grade II - Slightly Weathered.

Irfan subdivides this zone into three subzones based upon the percentage of microfracturing and staining.

(1) The rock is iron-stained only along the joint faces. No penetration of iron-staining.

(ii) Penetration of iron-staining inwards from the joint faces along microcracks. Formation of simple, branched microcracks; tight and partially stained. Slight alteration of the centres of plagioclases. Occasional staining along quartz-quartz and quartz-feldspar grain boundaries. Grain boundaries are sharp.

(iii) More inward penetration of brown iron-staining along microcracks and partial staining of plagioclases. Micro-fracturing of feldspars and quartz by inter-granular but sometimes trans-granular microcracks.

The only secondary mineral present in this zone is halloysite, as may be seen from Figure 3.3. SEM analyses indicates that after formation the halloysite is not dislodged from the original mineral but forms a pseudomorphic coating around the mineral. Some solution of the feldspars occurs along cleavage planes.

Interlocking corestones of unweathered rock are common in this zone. The size and shape of the core stones is a function of the jointing as discussed above.

Grade III - Moderately Weathered.

In this grade the discolouration of the rock is complete. Partial alteration of the plagioclases has produced solution pores and the formation of complete pseudomorphs of halloysite. Similar alteration of biotite has occurred but orthoclase and microcline feldspars are often unaltered, or with limited halloysite coating. The plagioclase pseudomorphs have a speckled appearance in thin section.

Some alteration of feldspar to gibbsite occurs in the top part of this zone. Similarly alteration to kaolinite also commences in the upper part of this zone and it is not uncommon (Eswaran & Bin, 1978) to find kaolinite flakes in between tubes of halloysite on the surface of the pseudomorph. This suggests a transitional environment, probably dictated by decreased pH, between the formation of halloysite and kaolinite.

Grain boundaries remain tight but stained brown by iron oxides. The rock fabric is highly micro-fractured by complex branched, trans-granular microcracks.

This zone has also been called the pallid zone, due to the incomplete degree of iron staining throughout the matrix, in contrast

to the mottled and stained fabric of grade IV material.

Grade IV - Highly Weathered.

The halloysite content decreases in this zone, presumably as it is converted to kaolinite or gibbsite. Alteration of the smaller grains of feldspar to kaolinite is direct in this zone, although larger grains alter to gibbsite. The biotites alter to a mixture of kaolinite and goethite.

In this section, interconnected pores can be seen to have formed in plagioclases, while orthoclase feldspar only shows slight alteration. Quartz grain boundaries show slight rounding indicating solution of silica. Biotite is bleached to different degrees and altered along grain boundaries.

Intense microfracturing of the rock fabric by a complex branched and dendritic pattern of microcracks is seen. Dearman (1978) reports that this zone has the highest permeability. Although the porosity continues to increase in the higher zones, there is more crystallisation of kaolinite as flakes which tend to block the pores. Similarly, the rock matrix begins to collapse with the alteration of orthoclase.

Grade V - Completely Weathered.

Plagioclases are completely altered to kaolinite and gibbsite, with some residual halloysite remaining. Orthoclase and microcline are highly microfractured and partial alteration to kaolinite has occurred along microcracks and cleavage planes. Quartz is intensely microfractured and has been reduced in grain size by open, branched microcracks. Some biotite still persists in a near fresh state, presumably effectively protected by a thin coating of halloysite or goethite. Some grains of biotite show alteration along grain boundaries and cleavages, and some expansion to vermiculite is noted.

The fabric is highly broken by micro and macrocracks, forming a reticulate pattern; most are open, clean or partially filled; some are wider and parallel sided forming macrocracks (> 1.0mm). The material is very much weakened in strength, and is also highly porous, although the permeability is decreased by the kaolinite formation.

Halloysite is actively replaced by kaolinite as can be seen in Figure 3.3. Once the secondary mineral is reduced to extinction size,

further weathering results in its destruction : silica is lost in the groundwater and alumina precipitates as gibbsite.

Grade VI - Residual Soil.

Orthoclase and microcline feldspars are partially decomposed to gritty aggregates and extremely microfractured. Kaolinite and gibbsite are present throughout the matrix as recrystallised plates or pseudomorphs of the feldspars. Quartz shows extensive microfracturing and some solution. Microfractures and macrofractures are abundant throughout the matrix. The material has lost all cohesiveness and may be dug into with a pick axe.

The permeability of this zone is low. In areas of deep weathering, all trace of rock matrix is removed and the material becomes a silty clay containing relict crystals as a dispersed sand fraction.

Lying above this grade of weathering are the typical A and B soil horizons which are developed on any rock material. The A horizon is particularly coarse, a reflection of the raindrop energy, as all the clay is either carried away as runoff, or illuviated downwards to the B horizon. The base of the B horizon is defined as the limit of bioturbation.

Plate 3.7 shows an example of grade V material where the rock texture can still be clearly seen. The material has a very low permeability as may be seen.

Plate 3.8 shows a further (Plate 3.6) example of grade IV weathering, indicating the effect of different lithology.

It is important to point out that the grades may be truncated in any particular sequence. Either grades II to V may be missing, representing the weathering out of an inselberg, as in Plate 3.20 and Plate 3.21. Or grades IV, V, and VI may be missing at the edge of an area of outcrop. The former occurrence represents an area that may be successfully investigated using seismic refraction techniques and will be returned to in section 4. The latter represents an area of considerable groundwater recharge and will be discussed in Section 5.

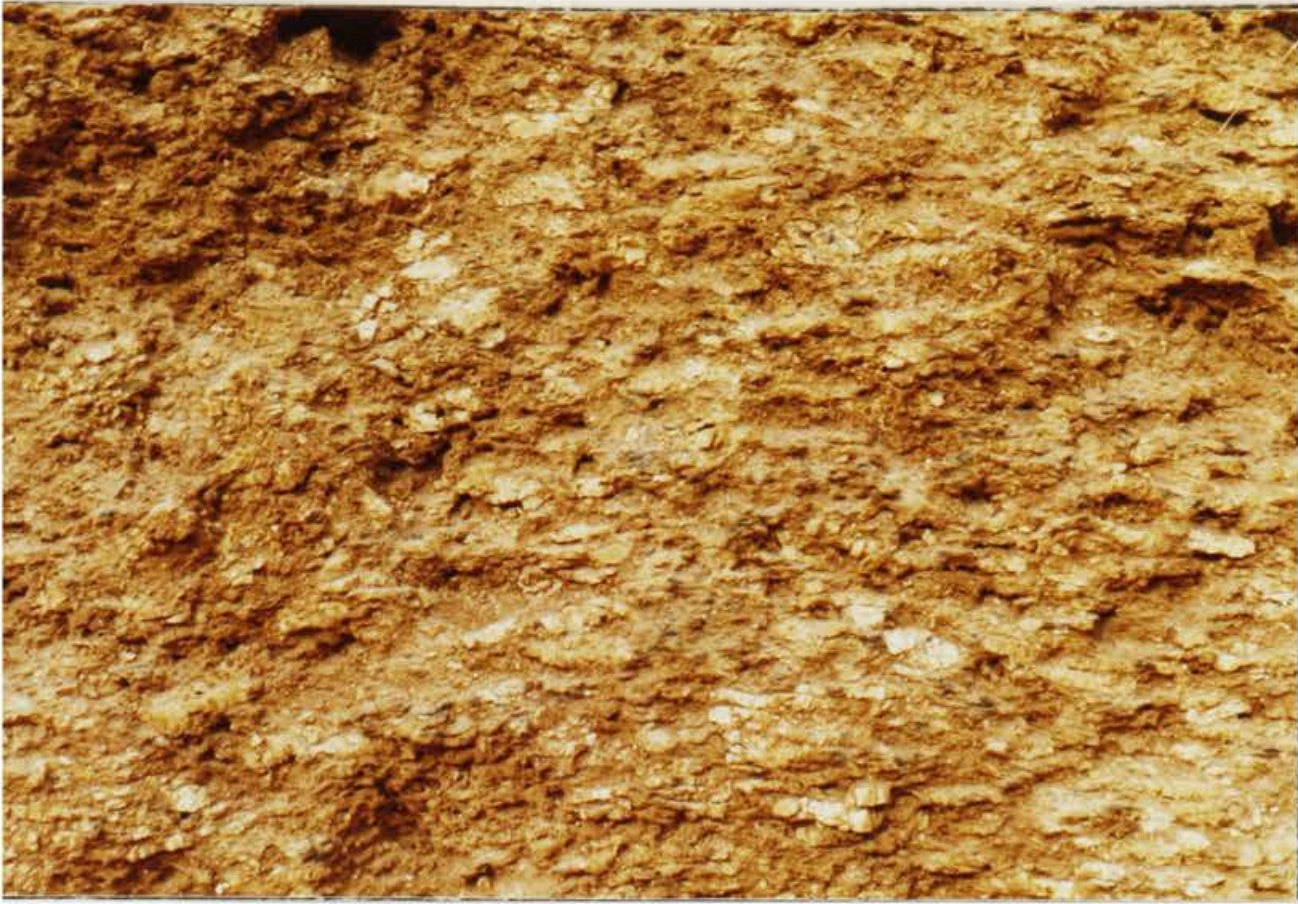


Plate 3.7 Grade V weathering material above the water table in a pit dug for road construction purposes. Note the intact rock texture and kaolinisation of the feldspar.

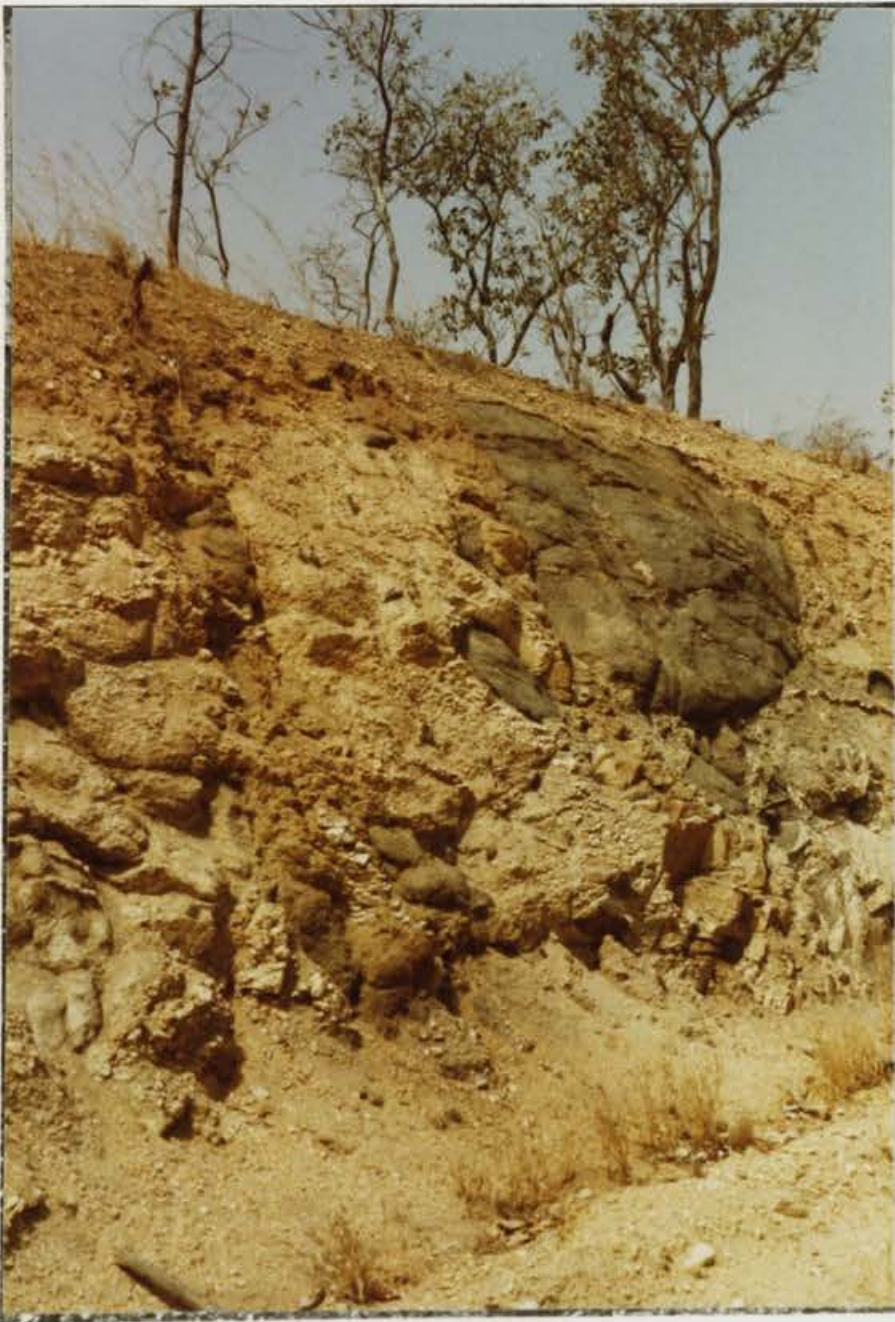


Plate 3.8

Grade III, IV and V weathered material in a recent rock cutting. The difference in grade is the result of differing rock chemistry.

3.5 Deep Weathering Examples from Northern Nigeria

General

The deep weathering observed by Thomas (1966) on the Jos Plateau (see Figure 1.) has been shown diagrammatically in Figure 3.2. In this section, the general geology of Northern Nigeria, and the area around Bauchi in particular, is briefly reviewed. This review includes descriptions of the major fracture trends and petrological descriptions of some of the common rock types, so that the geological background to deep weathering in this area is established.

Basement Evolution.

There has been very little general geological mapping of the basement complex rocks where they crop out to the east of the Jos Plateau. McCurry working in the area around Zaria has established the succession shown in Table 3.3. The Katangan metasediments which crop out in the Zaria area in a wide north-south trough, are not seen to the east of the Jos Plateau, and it seems probable that the basement to the east of the plateau represents a lower level of erosion than that to the west.

Nigeria lies completely within a mobile belt of the Pan African orogeny, with the stable areas of the Congo craton to the south and east, and the West African craton to the west. Figure 1.2 shows a simplified geological map of Nigeria. Bauchi is seen to lie to the east of the line of Jurassic granites which extend through the Jos Plateau area, and to the west of the Benue Trough of Cretaceous sedimentation. An area of Tertiary sandstone deposition masks the boundary between the basement and the Cretaceous deposits in the east. Many of these features can be seen on Plate 3.9, which is a side scan radar image of the Bauchi area.

The structure within the Pan African typically shows a 030° lineation. This can be clearly seen in the older granite inselbergs visible in Plate 3.9, and which are typically ellipsoidal and elongated in this direction. The younger granite shows this lineation, although the line of younger granite intrusions from the Jos Plateau to the Air Massif in Niger, has an orientation of 005° . This later orientation can be seen also in fracture analyses of Landsat products as occurring widely throughout the basement areas. A third lineation with an orientation

Table 3.3 Generalised geochronology for the metamorphic rocks of Nigeria (after McCurry, 1973)

Age m.y	Period/Event	Geologic History	Rock Type
540 [±] 400	Mid Cambrian	uplift, coding, fracturing and faulting	
650-580	Lower Cambrian	granite intrusion, pegmatite and aplite development	Older Granite
850-650	Pan African	orogonesis - deformation, metamorphism, migmatisation and reactivation of pre- existing rocks.	
1000-800	Katangan	geosynclinal deposition	Katangan Metasediments
1900([±] 250)	Eburnian	granite intrusion	Eburnian Granites
		orogonesis-folding metamorphism and reactivation of pre- existing rocks	
2500	Birrimian	geosynclinal deposition	Birrimian Metasediments
2800([±] 200)	Liberian(?)	formation(?) of banded gneiss complex near Ibadan	
>2800	Dahomeyan	Crystalline Basement	

of 80° can be seen controlling valley development and erosion within the older granite outcrop areas.

Both older and younger granites are present in the Bauchi area, and both occur mainly as areas of hills or inselbergs. The large elliptical hill called Zaranda which can be seen in Plate 3.9, lies some 600m above the surrounding plain, and is a younger granite complex which has not been mapped in detail. More typically, older granites occur as smooth sided inselbergs throughout the area and can be seen as the smaller hill areas on Plate 3.9. Plates 3.10 and 11 show typical older granite morphology close to Bauchi.

Eborall (1976) reports the occurrence of an intermediate suite of quartz monzonites developed within older granite intrusions in and around Bauchi. As Bauchi Old Town is situated on this outcrop, the rock type was called bauchite by Oyawoye (1965). Eborall lists four occurrences of this rock type, however a number of other areas of outcrop were identified during water resource investigations, and some of these have been marked on the overlay to Plate 3.9. Bauchite occurs associated with biotite granite and quartz diorite in elliptical areas of outcrop. Fresh specimens of bauchite are dark green due to the green colour of quartz and feldspar, the most conspicuous crystals being twinned alkali feldspars up to 50mm long. Bauchite consists of extremely coarse microperthite and oligoclase, with eulite, ferroaugite, ferrohastingsite and small amounts of quartz, fayalite and ilmenite or magnetite (Eborall, 1976).

The older granites more typically consist of porphyritic microcline and plagioclase (An25) with subordinate quartz. Biotite, hornblende, apatite, sphene and zircon occur as secondary minerals. The feldspar megacrysts are dominantly microcline perthite and usually contain inclusions of the other major rock-forming minerals. The presence of the inclusions strongly suggests a metasomatic origin for the megacrysts, and not crystallisation from a granite melt.

The migmatites commonly occur as pavement outcrops close to the base of inselbergs. Plate 3.12 shows a typical migmatite from an area close to the base of inselbergs. The gneiss can be seen clearly in this plate.

A series of basalt dykes of unknown age were intruded along a strike direction of 080° , and weathering down these dykes is often responsible

Plate 3.9. Side looking airborne radar (S.L.A.R.) image of Bauchi area. (Courtesy, Federal Forestry Office in Ibadan)



Notes.

1. Younger granite ring complexes.
2. Zaranda - Younger granite
3. Bauchi airfield. North south line is reflection from tin roofs in Bauchi old town.
4. Boundary of Tertiary Keri Kuri sediments and crystalline basement rocks.
5. Elliptical intrusions of Bauchite (Older granite)
6. Road and Rail bridges over the River Gongola east of Bauchi.

The image extends from 9° - $10^{\circ}30''$ east and 10° - 11° North.

The approximate scale is 1 : 1,000,000 1cm = 10 kilometres.



Plate 3.10 Older Granite outcrop close to Bauchi.

Note the coarse grained porphyritic texture, the large pressure release exfoliation slabs and the predominant gulleys which are defined by later age (?) basalt dykes.



Plate 3.11

Older Granite inselberg,
north of Bauchi at Gubi.

The sides are almost sheer,
with the formation of
exfoliation slabs of several
hundred square metres extent.

Note - all season water hole
at the base of the inselberg.

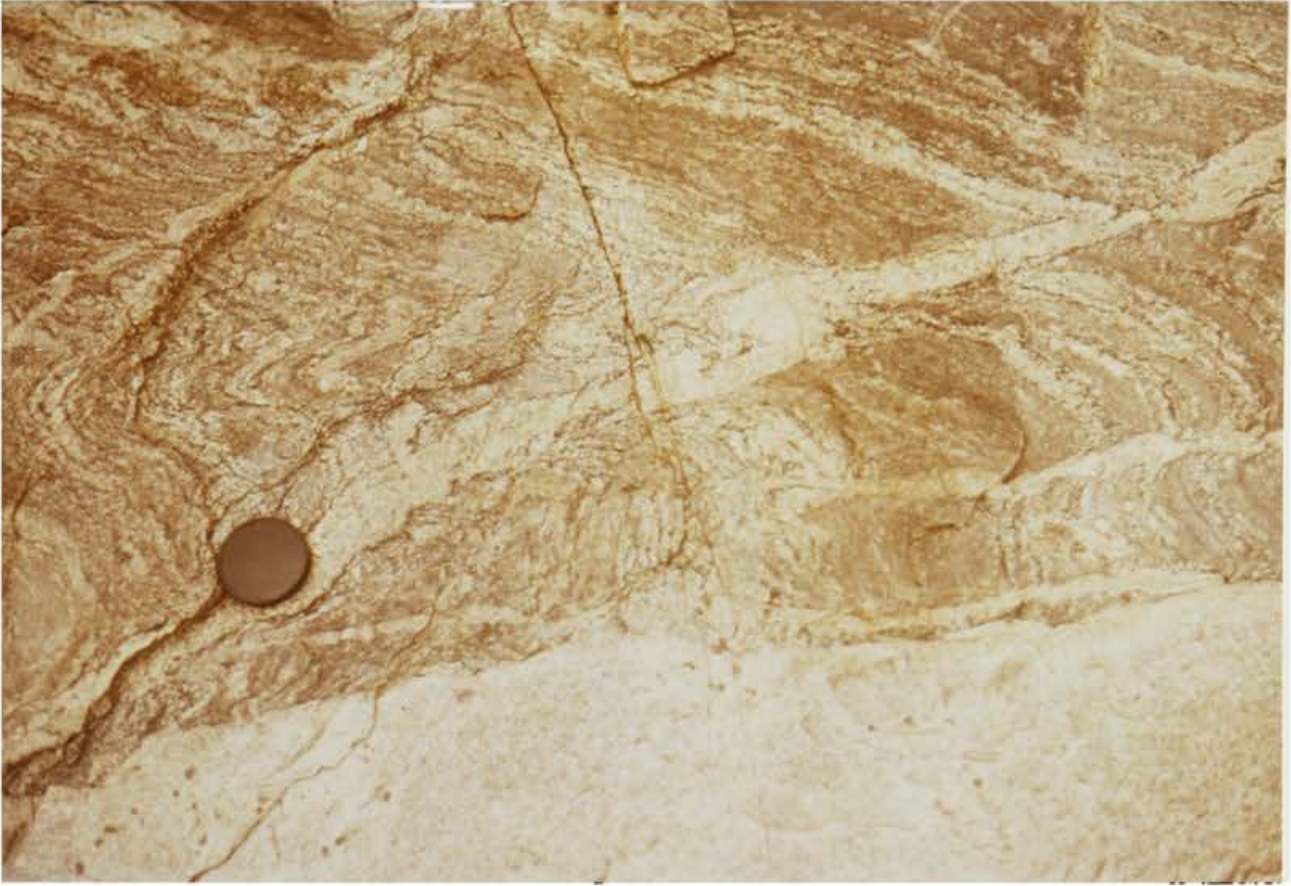


Plate 3.12 Gneiss showing folding and intrusion by aplite veins.
Pavement outcrop close to Bauchi.

Plate 3.13. Dyke cutting edge of older granite inselberg.



for the geomorphological evolution of the older granite inselbergs. The dykes cut cleanly through the granites and cross onto areas of gneiss where they often form the locus for areas of deep weathering. Plate 3.13 shows a basalt dyke cutting through the edge of a granite, close to Bauchi. A borehole producing $10\text{m}^3/\text{hr}$ was sited in an extension of the valley associated with this dyke some 500m onto an area of flat, weathered ground.

Deep Weathering - Example A.

Plate 3.14 shows a part of the trough of weathering discovered by electrical resistivity geophysical techniques to extend for a minimum of ten kilometres in a 005° orientation through Bauchi. A number of boreholes have been successfully sited on this fracture zone where it runs through gneisses. A section compiled from the borehole records and covering 2 km length is shown in Figure 3.4. The section is drawn to show the different grades of weathering, and two of the original geological logs of the boreholes are presented in Appendix B.

The hydrology of this fracture is considered in detail in section five of the thesis, as the borehole location described in Plate 3.14 is the location of the groundwater hydrograph presented in Figure 5.4.

The apparent resistivity anomaly over a part of this fracture zone is shown in Figure 4.7. As can be seen from Plate 3.14, there is no surface indication of the deep weathering profile, and it is thought to have been caused by a combination of faulting and pressure release jointing in an area of biotite gneiss (see Appendix B).

Deep Weathering - Example B.

Plate 3.15 shows a part of a complex area of deep weathering to the south east of Bauchi. The photograph is taken from an older granite inselberg which falls almost vertically to the level of the plain. The weathering appears to be located about a number of fractures, or more probably dykes in gneiss which belong to the 080° orientation set. Seismic refraction was used to locate the boreholes, and this area was then covered again by electrical resistivity profiling techniques. The combined results are discussed in Section 4. The apparent resistivity anomaly over a part of this zone is shown in Figure 4.8

The pits that can be seen in the middle distance have been dug into grade V weathered material using a pick axe. The material is shown in

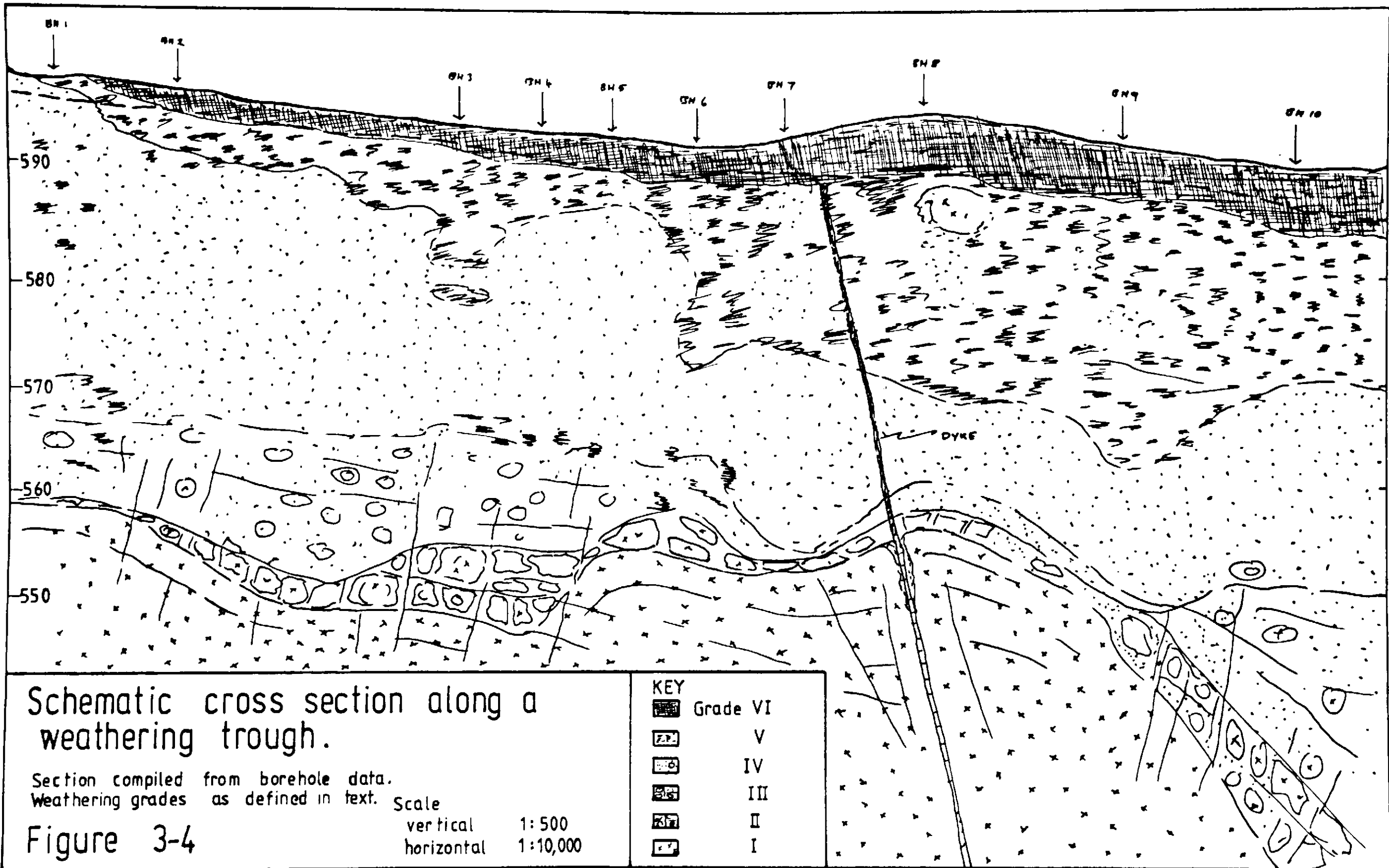




Plate 3.14. Deep weathering - example A location. The weathered zone runs from the direction indicated. The photograph is taken from an inselberg of granite, which can be seen in the right foreground. At centre right, two pavement outcrops of gneiss and migmatite similar to plate 3.12 can be seen. A borehole has been drilled to 60m depth by the tree at left centre (an orange air compressor can be seen under the tree).

Plate 3.15 Deep weathering - example B location. A diffuse area of deep weathering associated with 080° jointing crosses the picture from right to left. The picture of grade V weathering material shown in plate 3.7 was taken in the road construction pits that can be seen in the middle distance.



GRADE
V

GRADE
VI



Plate 3.16. Drill cuttings from deep weathering area B. The hole has been drilled using a pneumatic down-hole-hammer rig, with the result that the more compact the rock, the finer ground is the sample. The rock dust in the final pocket represents fresh grade I material. The samples are arranged 'book fashion'. Note the absence of grade IV and V material, with a very thin grade VI.

Plate 3.17. Extensive grade V and VI material from deep weathering area C. Cores have been obtained using dry drilling techniques. S.W.L. 15.5m.



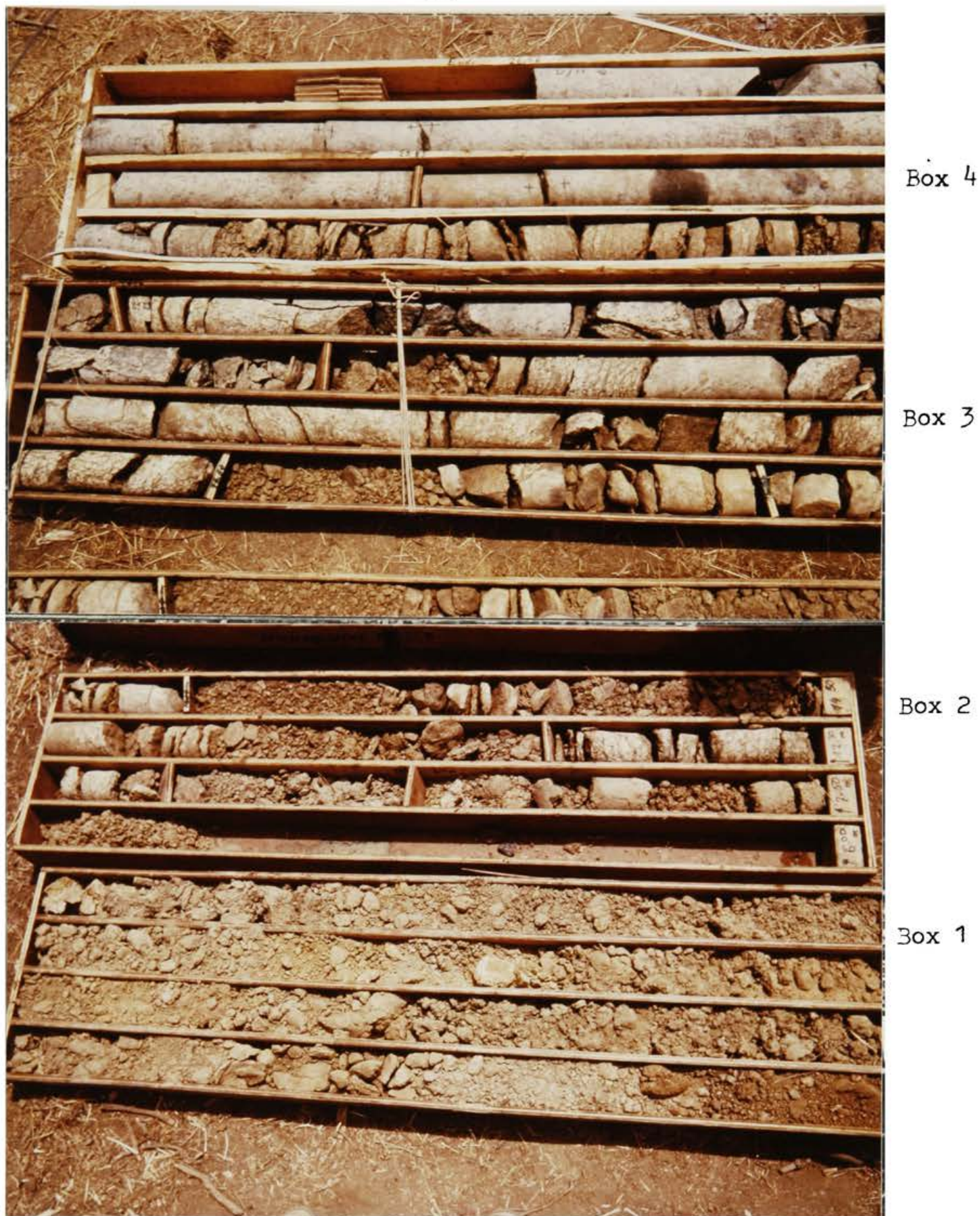
Plate 3.7. Note also the trees rooted into the pressure release joints within the older granite in the foreground of Plate 3.15.

Plate 3.16 shows the drill samples from a borehole at the edge of this area. Only grade I, II and III material is present in any significant quantity, with no evidence of grade IV, V and VI material. The individual boxes hold a composite sample from a 2.7m (9') length of hole, and are arranged 'book fashion'. The particular significance of such areas as recharge zones is further discussed in section 5.2.

Deep Weathering - Example C.

This example is taken from the engineering geology investigations for a major dam site. Resistivity profile data, EM31 data and seismic refraction data were all collected as a part of the centre line survey for the dam. Diamond core drilling at points of interest selected from the geophysical data was later carried out, and good core recovery was obtained from a number of holes. Plate 3.17 illustrates a deep development of grade V and VI material, where the complete alteration of the silicate minerals to clay is well illustrated. The division between grade V and grade VI material is also shown.

Plates 3.18 and 3.19 show an unusually complete section from a borehole on the dam line. The seismic refraction data from this line is shown in Figure 4.23, with the resistivity profile data included for comparison. As the standing water level was at 19m in the borehole, the whole section is usually unsaturated.



Plates 3.18 + 3.19 An almost complete¹ sequence of samples through a weathering profile (deep weathering - example C) obtained using a site investigation rig. Note the clay material (Grade VI) close to the surface, the pressure release sub-horizontal joints and the presence of grade I material above grade III material in the top core box. After drilling, the standing water level was recorded at 19.0m.

¹ The sample box should have 1.5m of core in each run. In box 2 there are 10m of core.

3.6 Soil Characteristics.

General

The grade VI weathered rock represents the C horizon of the soil profile in normal pedological terms. The limit of bioturbation marks the change from C to B horizon, although extensive clay bands found in the upper part of grade VI material may represent fossil B horizons. The change from A to B horizons is marked by the presence of illuviated clay in the normal pedological sense.

The high kinetic energy of the rainfall associated with tropical storms has the effect of breaking up the soil particles, particularly the clay aggregates, and removing them from the profile in suspension, either by infiltration, or by surface runoff. River water in the savanna is never clean, as the clay content carried in suspension is always very high.

The soil which is developed on agricultural land can become very sandy, with a high porosity. Interception is particularly efficient, in reducing the kinetic energy of the raindrops, and the removal of the natural vegetation cover may quickly lead to erosion problems.

The consistency of the surface soil is non-sticky and non-plastic when wet and friable when moist. Savanna soils also show a marked degree of hardening and cementation with decrease in soil moisture. The process of increased cohesion and hardening does not start until about half of the moisture content at field capacity has been lost, but it then continues for as long as evaporation continues (Kowal, 1978).

The ~~clay~~^{clay} fraction of the soil (35%) is either colloidal or colloidal like and is principally kaolinite (78%) with the remainder as goethite and gibbsite. The sand fraction (60%) of the soil is dominantly quartz and relict orthoclase or microcline grains with some mica fragments. The micas are preserved in the weathering environment by a protective goethite sheet (Eswaran, 1976).

The soil profile developed over crystalline rock in a savanna environment is known as a Krasnozem (Fitzpatrick, 1971). A problem associated with the profile development which is not well understood is that of lateritisation. The essential requirements for laterite formation are high rainfall, and intense leaching in an oxidising environment. The result of the process is the formation of an iron oxide rich

layer some 300 - 800mm in thickness at the top of the soil profile. The layer is dominantly pisolithic and may develop to form almost solid iron oxide.

The principle significance of laterite formation to this study is that it produces a shallow, very high electrically resistant layer which causes severe problems during geophysical work described in the following section. A typical occurrence of laterite is shown in Plates 3.20 and 3.21. A sheet of laterite can be seen beneath the A horizon of the soil throughout the section.

Laterite formation has received extensive discussion in the literature (McFarlane, 1976) and the method of formation is not significant within the context of the present study.

The bulk physical properties of the soil, the moisture retention and field capacity are discussed in Section five of the thesis.

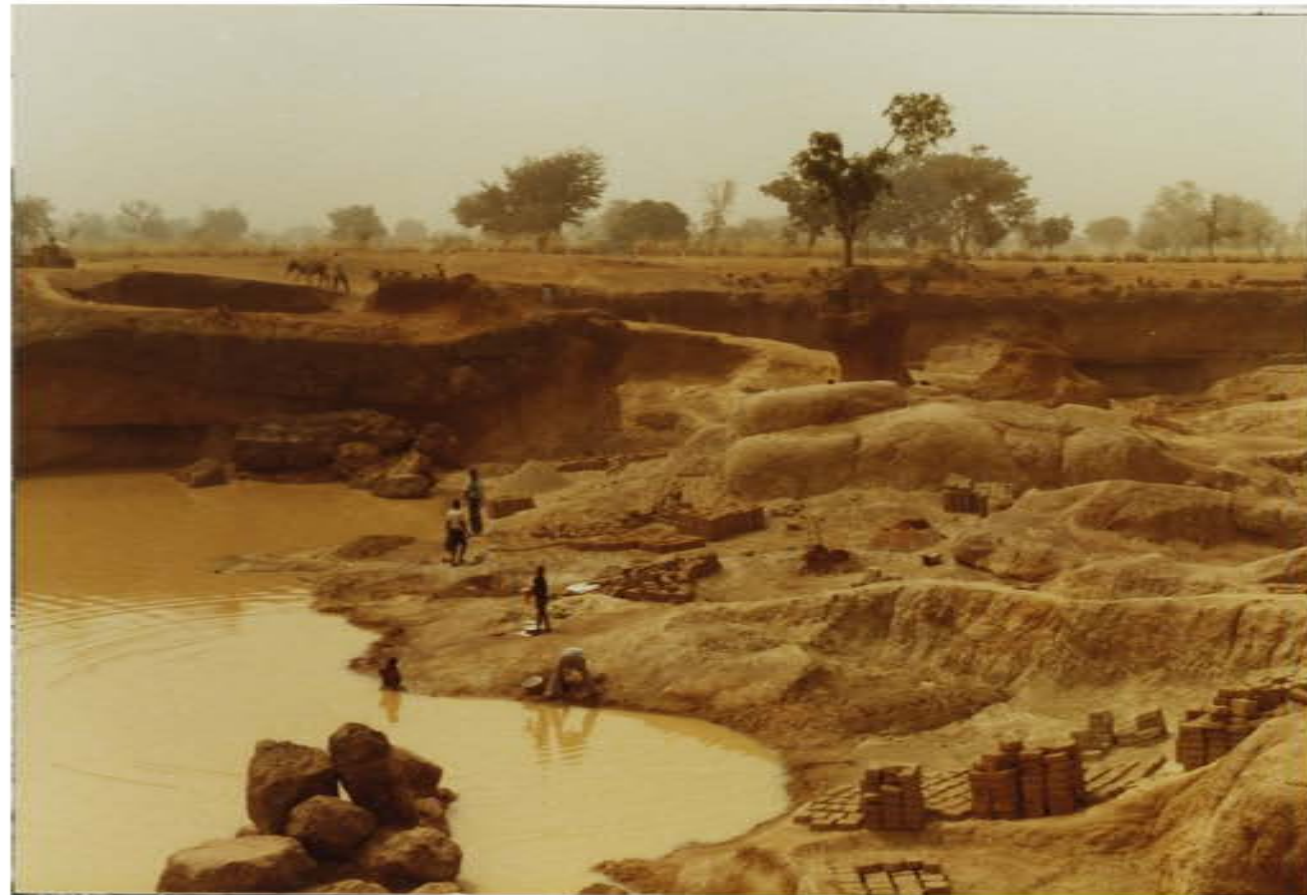


Plate 3.20. A weathering profile close to Kano, Northern Nigeria. Grade I and II weathering can be seen in the 'exhumed' inselberg at centre right. Grade Vi weathering material is being used to make bricks, indicating high clay content, and occurs close to but at the same level as the grade I material. The high porosity and low permeability of the grade V material is well demonstrated by the presence of water slowly released well into the dry season.

Plate 3.21. A weathering profile in a different part of the same location as 3.1. Note the same general features and the 1-1½ metre thick laterite sheet close to the surface.



3.7 Summary

The weathered zone developed upon gneiss, migmatite and granite is the result of interaction between four basic factors, viz:

- 1) Composition of the rock, crystal type and size.
- 2) Joints formed as a result of pressure release.
- 3) Presence of dyke intrusion.
- 4) Presence of faulting or jointing formation at depth.

The most important of these four is the composition of the rock and the size of the various crystal phases present. Although considerable further research is required in this field, it seems probable that coarse grained granites with quartz, orthoclase or microcline and subordinate plagioclase, with only minor biotite, will react to pressure release by forming joints at regular and widely spaced intervals. These joints produce large exfoliation slabs which are only reduced by chemical weathering very slowly. In this way such rocks tend to form inselbergs.

The size and spacing of pressure release joints appears to be a complex interaction between rock chemistry and crystal size. For example, a small change in feldspar chemistry may result in a pronounced change in the density of jointing, and therefore the rate of weathering. In contrast to granite, a medium grained gneiss with usually abundant biotite and a pronounced lineation, appears to react to pressure release jointing by forming a larger number of more closely spaced joints which may be rapidly weathered to produce a grus, or disaggregated crystal sand. At the far end of the scale a schist reacts to pressure release jointing by microfracturing between adjacent crystals, and therefore does not form joint blocks. As the total surface area opened up by microfracturing is very large, chemical weathering is correspondingly more active.

The presence of basalt dykes often forms a locus for a greater depth of weathering. Groundwater percolation down the contraction joints within the dykes allows greater access to the rock walls; if these are gneissic then weathering may extend outwards from the dyke. If the wall rock is granite then the different weathering rate of the basalt may still have a pronounced effect on the morphology of the inselberg.

Where a major fault is present which can allow groundwater access

to a depth of 75m or more, then deep weathering on either side of the fault may occur. If the fault runs through granite the extent of the weathering is likely to be less than that would occur if the fault line runs through a gneiss. In all the above instances, the behaviour of migmatites is somewhat intermediate.

Major joint systems associated with the cooling and contraction of emplaced granite magmas may allow deep weathering in granite, however the older granite suite around Bauchi is most probably predominately formed by metasomatism, and this process does not produce such contraction jointing. The metasomatic origin of at least the major feldspar megacrysts is indicated by the large number of inclusions found within these crystals, and by their zoned nature.

The predominant chemical reaction is hydrolysis. The silicates are hydrolysed by percolating groundwater with a pH of ~5.0 in the grade II weathered material. The hydrolysis reaction increases the pH due to the release of hydroxyl ions. Halloysite is the first clay mineral to be formed and typically plagioclase and biotite are altered to halloysite which forms as pseudomorphs around the original crystal. The calcium contained in plagioclase is dissolved out by the acidic groundwater. The initial alteration causes a microfracturing of the surrounding crystalline matrix. As this microfracturing in turn requires an element of expansion, the amount of weathering is controlled by the space made available by joint formation, or the fracturing associated with faulting.

The products of weathering in the grade II and III material are efficiently removed by groundwater flow, even through closed basins of weathering. This has been indicated by the results of a hele-shaw viscosity model, and is also strongly inferred by the fact that basement groundwaters are invariably very pure with negligible dissolved matter and very low salinity. (Feth, 1964).

The grade IV weathered zone marks a change between predominantly halloysite clay in lower zones, and kaolinite and gibbsite as alteration products in higher zones. It seems probable, although there is no conclusive evidence, that the production of large amounts of kaolinite, begins to reduce the permeability of the higher zones although the porosity continues to increase. This factor is significant for both geophysical and hydrogeological reasons, and is the most important single factor identified in this section.

Three examples of deep weathering are introduced in this section with a number of plates showing the actual areas under study. From these plates it may be seen that there is no reliable surface indication of deep weathering in the savanna, and considerable geophysical effort is required to accurately locate positions for boreholes in order that they may intercept the greatest depth of weathering.

4. GEOPHYSICAL INVESTIGATION TECHNIQUES.

Introduction.

The genesis of weathering basins has been described in Section 3. The development of groundwater reserves contained within these basins is obstructed by the fact that their existence is not reliably indicated by any criteria observable at the surface. Although the existence of basins can be predicted from an examination of the surrounding geology, it is necessary to use geophysical techniques to determine their actual existence and extent.

The sequence of materials encountered within a weathering profile has been described in Section 3. Each of these subdivisions is developed to an increased extent within a weathering basin developed over homogeneous material. However, grades III and IV material may be absent when a change in the lithology has halted the downward progression of the weathering front. Plate 3.20 indicates such an instance.

Significant groundwater reserves are found in the grades II, III and IV weathered material, where the porosity and hydraulic conductivity are relatively high compared to the underlying solid rock or the overlying high clay content material. The variation of hydraulic conductivity within the weathering grades is discussed in detail in Section 5 of the thesis. The geophysical problem is therefore resolved into the development of techniques which can reliably identify the presence of grades II, III and IV weathered material, and subsequently the depth at which this material lies.

Seismic refraction and electrical resistivity techniques are both used at present in geophysical surveys designed to detect weathering basins. For this reason the results obtained by both methods are described below and a critical assessment made of their general applicability. More recently, electro-magnetic (EM) instrumentation and techniques have become available and a combination of electro-magnetic and electrical resistivity methods which greatly decreases the geophysical survey time required is described in this section.

The geological descriptions of the various weathered layers allows the physical properties of both grade I and grade V + VI material to be reasonably identified. Grade I material is unweathered rock with a low porosity and no hydraulic conductivity. Consequently, the electrical resistivity is high ($> 4000 \Omega m$) and the seismic velocity is similarly high (4.0-6.0 m/ms). Grade VI material is completely weathered rock with

no structure intact and a high proportion of the rock components completely converted to clay. The porosity of this material is high, but the hydraulic conductivity is low due to the high clay content. The electrical resistivity of the damp material is low $\sim 200 \Omega\text{m}$, but as the surface material dries out, this increases to above $1000 \Omega\text{m}$. As this material is uncompacted, the seismic velocity is low at 0.4-2.0 m/ms, depending upon the degree of saturation.

Both seismic refraction and electrical resistivity interpretation techniques, in their most generally used form, are based upon an assumption that the subsurfaces may be discretised into sections of homogeneous material separated by abrupt planar interfaces. However, the weathering profile is most often gradational with no easily identified interfaces, (see for example Plates 3.17, 3.18 and 3.19), and it is this gradational characteristic, both in the horizontal and the vertical planes, which is responsible for the interpretation problems which commonly arise in this environment.

During the work in Nigeria, the electrical resistivity and EM method proved to be the most successful for locating areas of deep weathering. Several developments of this technique are described below and therefore in the first part of this section the relevant theoretical aspects of the electrical resistivity method are discussed.

The electrical resistivity method comprises two separate methods of investigation. The continuous separation traverse or profiling technique is used to establish the presence of lateral variations of resistivity. This method is the most useful technique in the basement environment where the depth of weathering is a function of faulting and fracturing and therefore changes over short distances. It is not possible to interpret profile results at a single electrode separation in terms of a depth, however the method was used extensively for this study in Nigeria and is described and discussed in part two of this section.

The electrical resistivity sounding method can be successfully employed where a sequence of plane layered homogeneous media are to be resolved into depths and resistivities of the component layers. The interpretation techniques depend upon there being very little lateral variation along the layering over an area of 500m by 250m necessary for the field measurements. This constraint is seldom satisfied within the weathering environment due to the basic inhomogeneity of the gneiss

and granite material being weathered. Despite this constraint, depth sounding interpretation results are widely reported in the literature, with generally poor correlations between interpreted depths and results from nearby boreholes (Verma, et al, 1980). The attraction of this method is that a value for the depth of weathering is produced by the interpretation, even though it may not be very accurate. In the third part of this section, the resistivity sounding method is discussed.

In the fourth part of this section, the resistivity techniques of profiling and sounding are combined to produce a new method developed for this study. A resistivity profile section comprises the results from a number of profiles conducted at different electrode separations. A finite difference approximation of the potential distribution is used as the basis for a computer based interpretation technique which permits the modelling of field data in terms of a discrete resistivity distribution. The resistivity distribution within the model is varied at a number of nodes (~ 3000) which allows the required lateral and vertical variation of resistivity in the weathering environment to be interpreted. Three examples of the use of this technique are presented.

Seismic refraction methods rely on the presence of an interface between materials of sufficiently contrasting physical properties. The interface generates refracted waves which may be identified on a graph of travel time vs distance as various straight line segments. The assumption is made during the interpretation that the material lying between the interface is of a uniform homogeneous nature. Although plane layering is not required, an increase of seismic velocity with depth is necessary otherwise layers of lower velocity material beneath layers of higher velocity material are not identified.

Within the weathering environment seismic refraction can be used successfully to identify shallow lying grade I or II materials but considerable error occurs when interpretations are made over gradationally weathered sequences. For this reason, the conditions which lead to satisfactory interpretations of seismic refraction data are also those which would not yield supplies of groundwater. In the fifth part of this section the seismic refraction method is discussed and a number of examples presented.

The use of EM techniques are considered here to be an extension of electrical resistivity methods and as such are included in the

discussion in Section 4.2 and 4.4.

4.1 Electrical Resistivity Theory.

Introduction.

Electrical resistivity techniques are shown below to be the most successful method by which weathering basins can be delineated. For this reason, electrical resistivity theory is described in some detail in this section.

The method by which current is propagated through the weathering environment varies significantly in the different weathering grades. Therefore, if a successful interpretation of the resistivity results is to be made, the different methods of electrical conduction require description.

The interpretation of electrical resistivity results is often based upon an analytical solution to the equations which describe electric current flow. The analytical solution is constrained however by the requirement that the subsurface can be divided into plane layered homogeneous media. The weathering environment can rarely be so described and for this reason a finite difference solution to the equation of current flow is also considered.

Electrical conduction in the weathering environment.

Electric current may be propagated through rocks or weathered material in three basic ways; electronic, electrolytic and dielectric conduction (Telford, et al, 1976).

Dielectric conduction takes place in poor conductors and insulators, which have very few free ions to act as carriers. Under the influence of an external varying field, the atomic electrons are displaced slightly with respect to their nuclei, and this slight displacement represents a small current flow. As direct current is used in almost all the following work, the contribution to the total conductivity of the rock mass by dielectric conduction is very small.

Electrolytic conduction occurs through the solution contained within the pore space of a material. If this solution contains a high proportion of dissolved ions, then the ion will move in response to an applied potential difference. The flow of ions, which are either positively or negatively charged, constitute an electric current.

Electrolytic conduction can only occur where the pore space is

interconnected. Grade I and grade VI weathering material have very low hydraulic conductivities and therefore the electrolytic conduction in these weathering grades is also small.

The chemical composition of groundwater obtained from basement boreholes has been described in Section 3.4. From these analyses it may be seen that the waters have a very low dissolved solids level, and are usually very pure. Electrolytic conduction in waters of this type will not be very significant.

Electronic conduction is the normal way in which current flows through metals. As metals are however, relatively rare in the basement environment, the contribution to the bulk conductivity of the rock mass by electronic conduction is very small.

From the above discussion it is clear that the three basic methods of conduction do not produce high values of electrical conductivity within the weathering environment. However, it is commonly observed, and results will be presented below, that weathering troughs produce major conductivity anomalies. A contrast of from $>1000\text{ }\Omega\text{m}^{-1}$ to $<50\text{ }\Omega\text{m}$ is often observed over the weathering trough. Although no experimental evidence is available it is probable that a combination of matrix conductivity and electrolytic conductivity within the secondary clay minerals is responsible for this increase in bulk conductivity.

The process of matrix conductivity is not clearly understood. However, it is probable that, in saturated material, conduction occurs by transfer of charge along the surface of, or along inter-sheet sites of clay minerals. Where clay minerals are linked together to form a network throughout the weathering environment, then conduction by this process can occur widely.

In grade V + VI material, where kaolinite is extensively developed, matrix conduction through the kaolinite will produce a high value of bulk conductivity. The proportions of clay in the weathering environment has been discussed in Section 3.4. Clay content increases from grade II material to grade VI material. On the joint faces of grade II material it is probable that a thin sheet of clay produces the conduction observed. However, the bulk conductivity in grade II material is low as the volume of fracture porosity is low (see Section 5.1).

Note 1. The units of conductivity and resistivity are defined below.

It is probable that a direct relationship exists between the clay content and the electrical conductivity of the weathering material, and that the porosity of the various grades does not of itself affect conductivity, due to the very low electrolyte concentration in the groundwater.

The electrical conductivity (σ) of a material may be defined as

$$\sigma = \underline{j}/\underline{E} \quad 4.1$$

where \underline{j} = current density (amp m⁻²)
 \underline{E} = electric field (Vm⁻¹)

The conductivity is measured in mhos/m. The reciprocal of conductivity is resistivity.

$$\rho = 1/\sigma \quad 4.2$$

where ρ = resistivity (ohm-m)

Although conductivity is probably not related to porosity in the weathering environment, matrix conductivity can only occur in clays which are saturated. Therefore, a high value of conductivity (low resistivity) must also indicate saturation.

Theory of current flow.

Although the previous discussion has been in terms of electrical conductivity, it is more usual to measure in the field, electrical resistivity. In the majority of the discussion below, this convention will be followed, although for the mathematical derivation below, units of conductivity have been used for convenience.

The apparent electrical resistivity of an inhomogeneous half space may be calculated by measuring the electrical potential developed about a current source. The theory is briefly developed so that the main difference between the analytical and the finite difference interpretational methods can be appreciated.

The electric field is the gradient of a scalar potential where the potential (Φ) is measured in volts.

It is probable that a direct relationship exists between the clay content and the electrical conductivity of the weathering material, and that the porosity of the various grades does not of itself affect conductivity, due to the very low electrolyte concentration in the groundwater.

The electrical conductivity (σ) of a material may be defined as

$$\sigma = \underline{j} / \underline{E} \quad 4.1$$

where \underline{j} = current density (amp m⁻²)
 \underline{E} = electric field (Vm⁻¹)

The conductivity is measured in mhos/m. The reciprocal of conductivity is resistivity.

$$\rho = 1/\sigma \quad 4.2$$

where ρ = resistivity (ohm-m)

Although conductivity is probably not related to porosity in the weathering environment, matrix conductivity can only occur in clays which are saturated. Therefore, a high value of conductivity (low resistivity) must also indicate saturation.

Theory of current flow.

Although the previous discussion has been in terms of electrical conductivity, it is more usual to measure in the field, electrical resistivity. In the majority of the discussion below, this convention will be followed, although for the mathematical derivation below, units of conductivity have been used for convenience.

The apparent electrical resistivity of an inhomogeneous half space may be calculated by measuring the electrical potential developed about a current source. The theory is briefly developed so that the main difference between the analytical and the finite difference interpretational methods can be appreciated.

The electric field is the gradient of a scalar potential where the potential (Φ) is measured in volts.

It is probable that a direct relationship exists between the clay content and the electrical conductivity of the weathering material, and that the porosity of the various grades does not of itself affect conductivity, due to the very low electrolyte concentration in the groundwater.

The electrical conductivity (σ) of a material may be defined as

$$\sigma = \underline{j}/\underline{E} \quad 4.1$$

where \underline{j} = current density (amp m⁻²)
 \underline{E} = electric field (Vm⁻¹)

The conductivity is measured in mhos/m. The reciprocal of conductivity is resistivity.

$$\rho = 1/\sigma \quad 4.2$$

where ρ = resistivity (ohm-m)

Although conductivity is probably not related to porosity in the weathering environment, matrix conductivity can only occur in clays which are saturated. Therefore, a high value of conductivity (low resistivity) must also indicate saturation.

Theory of current flow.

Although the previous discussion has been in terms of electrical conductivity, it is more usual to measure in the field, electrical resistivity. In the majority of the discussion below, this convention will be followed, although for the mathematical derivation below, units of conductivity have been used for convenience.

The apparent electrical resistivity of an inhomogeneous half space may be calculated by measuring the electrical potential developed about a current source. The theory is briefly developed so that the main difference between the analytical and the finite difference interpretational methods can be appreciated.

The electric field is the gradient of a scalar potential where the potential (Φ) is measured in volts.

$$\underline{E} = -\nabla \Phi \quad 4.3$$

where E = electric field

$$\nabla = i \frac{\partial}{\partial x} + j \frac{\partial}{\partial y} + k \frac{\partial}{\partial z}$$

Φ = electric potential

From Equation 4.1 it may be seen that

$$\underline{j} = -\sigma \nabla \Phi \quad 4.4$$

The divergence of the current density ($\nabla \cdot \underline{j}$) must be zero everywhere except within volumes enclosing a current source or sink, therefore :-

$$\nabla \cdot \underline{j} = 0 \quad 4.5$$

and from 4.4
$$-\nabla \cdot [\sigma \nabla \Phi] = 0 \quad 4.6$$

Equation 4.6 may be expanded to produce

$$\sigma \nabla \cdot \nabla \Phi + \sigma \nabla^2 \Phi = 0 \quad 4.7$$

If σ is a constant, for example, if the half space is homogeneous, then $\nabla \sigma = 0$

and Equation 4.7 reduces to

$$\sigma \nabla^2 \Phi = 0 \quad 4.8$$

As $\sigma \neq 0$ the equation further reduces to the Laplace equation

$$\nabla^2 \Phi = 0 \quad 4.9$$

The solution to Equation 4.9 has been studied in detail (Koefoed, 1979) and the theory will not be developed further here. The resistivity sounding interpretation methods which are based on an analytical solution to Equation 4.9 have been used extensively in the weathering environment (Palacky, 1980) often with poor results. In Section 4.3 resistivity sounding curves for the basement are presented and discussed.

The electrical resistivity of the weathering environment is a function of the clay content as discussed above. From the geological description of the weathering environment it is evident that the resistivity distribution is unlikely to be homogeneous. In fact any interpretation which is based only on this assumption will produce results which are mostly erroneous.

Therefore, if an interpretational technique which is applicable to the weathering environment is to be developed it must be based upon a solution to Equation 4.6, where the conductivity is a function of the space co-ordinates.

In practise, no analytical solution to Equation 4.6 exists. However, equations of a similar form have been solved using a finite difference approximation, and Dey + Morrison (1979b) report a method for a similar solution to Equation 4.6. In this solution, the assumption is made that the resistivity does not vary in the y direction. This is equivalent to considering ρ_x resistivity distribution which has an infinite extent along its strike. The advantage of this assumption is that the finite difference approximation may be made in two-dimensional space (x-z plane). However, the resistivity distribution within the x-z plane may be varied as finely or as coarsely as the finite difference approximation allows, and therefore the potentials developed over inhomogeneous resistivity distributions can be analysed.

The mathematical treatment of the solution is described by Dey + Morrison (1979a, 1979b), and relevant descriptions of the solution of similar equations may be found in Cheng (1979) and Rushton + Ward (1979).

A computer program which is based upon this method of solution has been written for this study and is presented in Appendix C. The results from the program are described in Section 4.4 where a new investigation method is described.

4.2 Electrical Resistivity Profiling

Introduction.

The electrical resistivity profiling technique is used to identify lateral variations of resistivity. Various electrode configurations have been employed, however, for all the work in Nigeria, a colinear equispaced quadripole of electrodes was used. The profiling method, also known as continuous separation traversing (CST) or resistivity mapping, involves repeated measurements of the potential difference developed between the two central electrodes by a current passed between two outer electrodes, as the electrode set is moved across an area of interest.

More recently, electro-magnetic methods have been developed which produce similar results to the conventional resistivity profiling technique, and which result in a very considerable saving of field time.

From the discussion in Section 3, it may be seen that a resistivity profile, conducted across the edge of a weathering basin, will detect a significant contrast in resistivity associated with the increased clay content in the basin (grades V + VI material) as opposed to the lower clay content in the shallow weathered profile outside the basin. The resistivity profiling method can be used therefore to identify areas of deep weathering.

Theoretical consideration.

It may be shown that (Telford, et al, 1971) the potential measured at some distance (r) from a current source situated over an homogeneous resistivity distribution can be expressed as

$$\Phi = \frac{\rho I}{2\pi r} \quad 4.10$$

where Φ = electrical potential (volts)
 I = current (amps)
 r = distance (m)
 ρ = resistivity of the half space

As the resistivity of an homogeneous half space is constant, it may be seen from Equation 4.10 that hemispherical shells representing

surfaces of equipotential can be constructed around the current source, and that the size of the potential decreases inversely with distance from the current source, becoming zero at infinite distance.

In the more general case of an inhomogeneous half space, where the resistivity is a function of the space coordinates, the surfaces of equipotential are no longer hemispherical, but assume a complicated three dimensional shape which is a function of the resistivity distribution. Similarly, the potential, as defined by Equation 4.10 will therefore also vary as a function of the space coordinates (x,y,z) and it is then necessary to specify the location of the current source and the point at which the potential is measured with respect to the resistivity distribution to define the potential completely. A change in the location of these points over an inhomogeneous resistivity distribution will cause a change in the measured value of potential, even if the separation remains constant.

For a generalised set of four electrodes at the surface of an inhomogeneous half space, as shown in Figure 4.1.a, the potential difference between P_1 (at electrode 1) and P_2 (at electrode 2) may be expressed as

$$\Delta\Phi_{0123} = (\phi_{10} + \phi_{13}) - (\phi_{20} + \phi_{23}) \quad 4.11$$

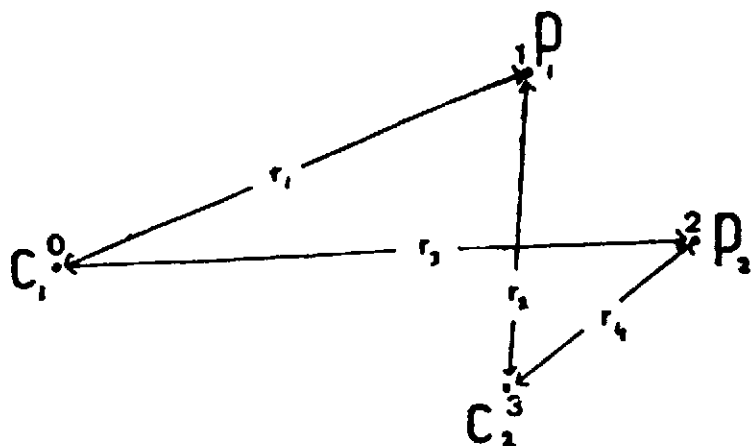
In Equation 4.11, the first suffix refers to the potential electrode and the second suffix to the current electrode. By measuring $\Delta\Phi_{0123}$ and I and knowing the electrode configuration, Equations 4.10 and 4.11 may be combined as shown in Equation 4.12.

$$\rho_a = \frac{2\pi\Delta\Phi_{0123}P}{I} \quad 4.12$$

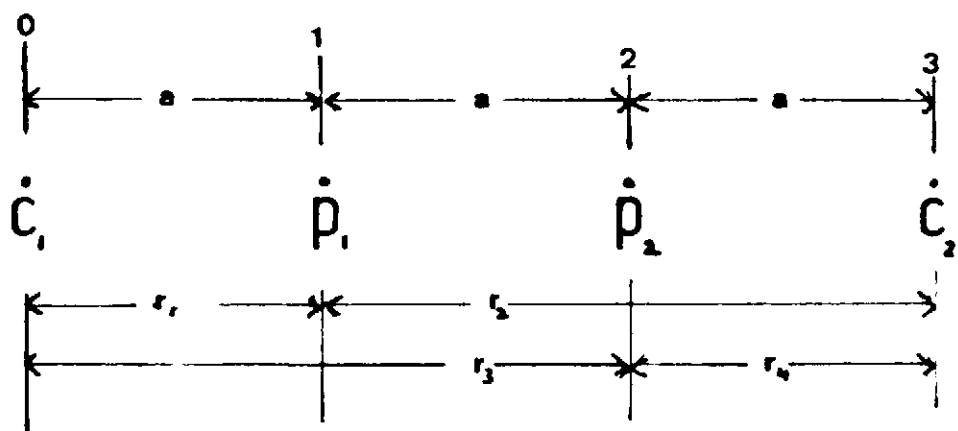
where ρ_a = apparent resistivity

$$\text{and } P = \frac{1}{[(1/r_1 - 1/r_2) - (1/r_3 - 1/r_4)]}$$

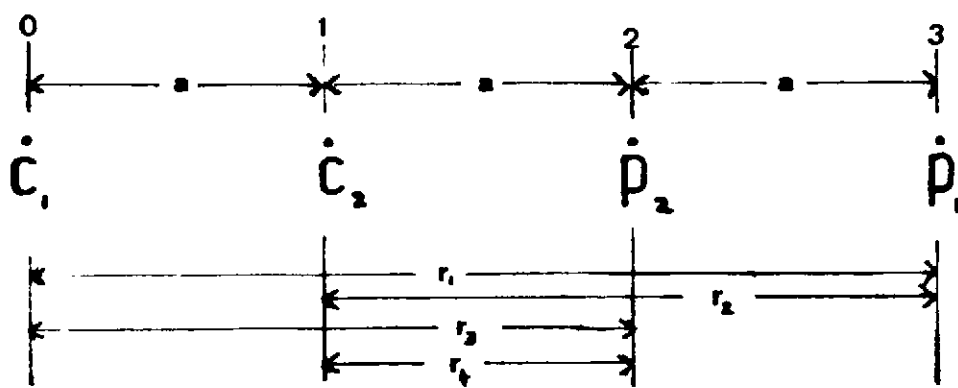
The apparent resistivity term in Equation 4.12 will be clearly a function of the electrode configuration and the measured value of potential difference between electrodes at points 1 and 2. This latter term, as discussed above is a function of the resistivity distribution throughout the half space. The measured value of apparent resistivity is therefore diagnostic, to some extent, of the actual



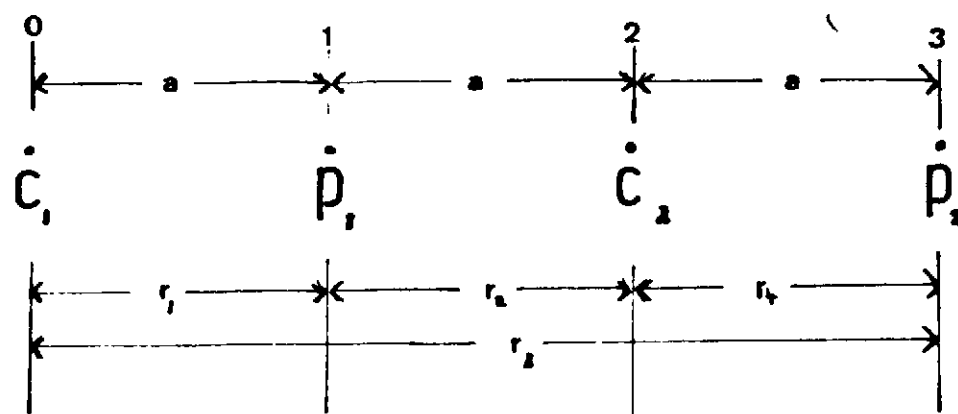
a Generalised set of four electrodes



b Wenner Alpha configuration



c Wenner Beta configuration



d Wenner Gamma configuration

Figure 4-1 Electrode configurations described in the text.

resistivity in the vicinity of the electrode array, but is also affected to a lesser extent by the resistivity distribution remote from the array.

During resistivity profiling, it is convenient to arrange the electrode configuration as an equispaced colinear array. A number of equispaced electrodes can then be placed in the ground prior to the survey. Four electrodes of such a set are shown in Figure 4.1.b, numbered 0,1,2 and 3. If the spacing between the electrodes is 'a' metres, then the spacing parameter (p) in Equation 4.12 reduces to 'a' and the measured value of apparent resistivity becomes

$$\rho_a = 2\pi a \frac{\Delta\Phi}{I} \quad 4.13$$

In many sets of field equipment the ratio $\Delta\Phi/I$ is measured directly as a resistance and then Equation 4.13 becomes

$$\rho_a = 2\pi a R \quad 4.14$$

$$\text{where } R = \Delta\Phi/I \quad (\text{ohms})$$

In any configuration of four electrodes, a change in the order of the current and potential electrodes without a change in the electrode positions, can only produce three independent values of potential difference. The same value of potential is obtained if the current and potential electrodes are reversed. Therefore $\phi_{10} = \phi_{01}$ in Equation 4.11.

The three independent values of $\Delta\Phi$ are shown in Figures 4.1, b,c and d.

The potential differences measured for these three configurations, the Wenner alpha, beta and gamma configurations, will always have the relationship that the sum of the beta and gamma potentials is equal to that of the alpha potential. This may be shown mathematically as

$$\Delta\Phi_\alpha = (\phi_{10} - \phi_{13}) - (\phi_{20} - \phi_{23})$$

$$\Delta\Phi_\beta = (\phi_{30} - \phi_{31}) - (\phi_{20} - \phi_{21})$$

$$\Delta\Phi_\gamma = (\phi_{10} - \phi_{12}) - (\phi_{30} - \phi_{32})$$

$$\Delta\Phi_\beta + \Delta\Phi_\gamma = \phi_{30} - \phi_{31} - \phi_{20} + \phi_{21} + \phi_{10} - \phi_{12} - \phi_{30} + \phi_{32} = \Delta\Phi_\alpha \quad 4.15$$

This simple relationship may be used in the field as a check of equipment and wiring. If the three readings obtained do not agree within 1% accuracy, then an observation error has occurred and its cause should be investigated before proceeding with the survey.

It may be shown from Equations 4.11 and 4.15 that if the resistivity distribution is homogeneous, the alpha, gamma and beta readings vary as the ratios $\alpha : \gamma : \beta = 3 : 2 : 1$. Over inhomogeneous ground the departure from this ratio, for a fixed set of electrodes, provides information on the resistivity distribution. It has been demonstrated by Barker (1979), that the three configurations react to a near surface lateral variation in resistivity in a characteristic manner. The presence of near surface lateral inhomogeneity can be detected therefore if measurements of the three configurations are made at each position occupied by the electrode set.

It has been noted above that the measured apparent resistivity is both a function of the electrode configuration and the resistivity distribution within the volume of material beneath the electrodes. A complicating factor in the interpretation of any investigation method based upon measurements of a potential field, is that it is not possible to relate the measurement to a specific location. For convenience, measurements of apparent resistivity are assumed to refer to a volume of ground beneath the mid point of the electrode array, although it is appreciated that all the material within the vicinity of the array will have contributed to the measured value. The depth of investigation of a particular configuration is similarly subject to this uncertainty.

Roy + Apparo (1971) have defined the depth of investigation of a colinear electrode configuration as that depth at which a thin horizontal layer of ground contributes the maximum amount to the total measured signal at the ground surface. For a Wenner alpha array, this depth of penetration, in homogeneous ground, is given by Roy + Apparo as $0.11 \times L$, where L is the distance between the current electrodes. For example, if the electrode spacing is 30m, then the depth of penetration is approximately 10m.

Over inhomogeneous ground, the concept of penetration depth is more complicated. Current will preferentially flow through low resistivity (high conductivity) material and therefore if low resistivity

material is present at depth, the signal contribution from that depth will be more significant than in the case of homogeneous ground. Therefore, in the weathering environment where low resistivity material occurs at depth, often adjacent to high resistivity material, the depth of penetration will increase over a weathering trough. Similarly, although it is convenient to think of the depth of penetration in terms of a definite figure, the material both below, to the side, and above this level, also contributes significantly.

The overall depth of penetration increases as the electrode separation is increased, although in some resistivity distributions this effect is limited. For example, a low resistivity layer close to or at the surface will cause the current to be more confined in this layer, and increasing the electrode separation will not materially increase the depth of penetration. In Section 4.4 an algorithm is presented based upon a finite difference solution to the equations of current flow discussed in Section 4.1. Using this algorithm, it is possible to change the resistivity distribution by a known amount and to then observe the change in apparent resistivity predicted by the algorithm. In this way a clearer idea of the depth of penetration concept can be achieved.

Resistivity Profile Results.

The electrical resistivity profiling technique with measurements of Wenner alpha apparent resistivity was used to obtain in excess of 100km of profile data during the period 1976 to 1979. The data was gathered either as a part of a water well site investigation or as a part of a dam site investigation. In both cases, the geophysical data was supported by the results obtained from later drilling investigations.

There is no point in cataloging all the data for this thesis: rather, a number of examples are presented which demonstrate the nature of the results. The results which are presented have been taken from investigations carried out in the three areas discussed in Section 3.5.

Figure 4.2 shows the results of a large number of profiles carried out over area A and shown in Plate 3.14. Values of equal apparent resistivity have been extrapolated and contoured, based upon the

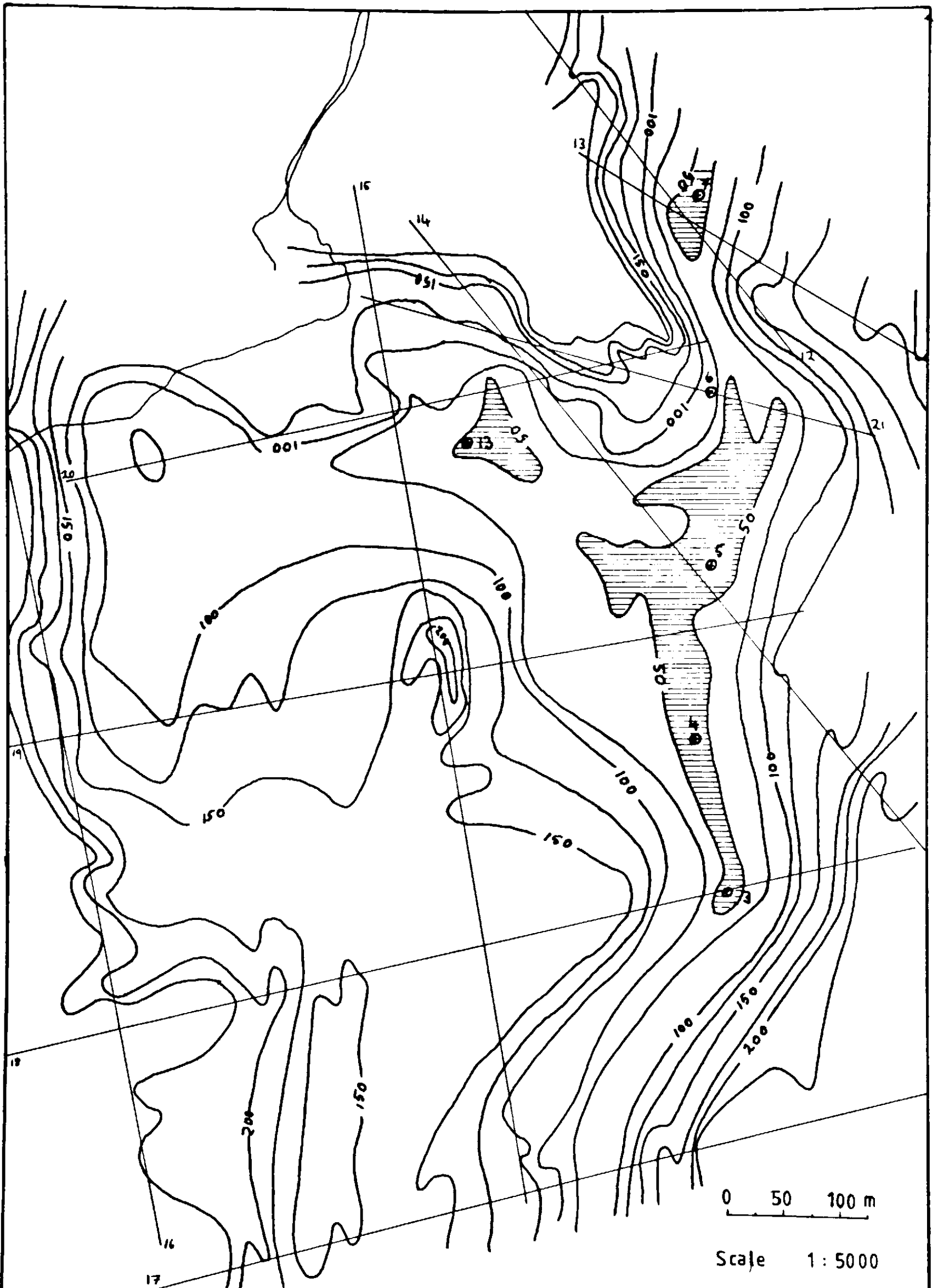


Figure 4-2 Map showing apparent resistivity contours over part of deep weathering area—A

Electrode separation 30m (wenner configuration)

Resistivity contours in Ohm metres, Lines show profile positions.

profile data, to produce an iso-resistivity map, for an electrode separation of 30m, over an area of approximately 3 km². Ten successful boreholes were drilled into the apparent resistivity low anomaly and the drill cuttings obtained have been used to prepare the section shown in Figure 3.4. The low anomaly continued both north and south of the area shown in Figure 4.2 for a proven length of 10 km.

The resistivity anomaly passes within 100m of an inselberg where the boundary between grades I and II + III weathering are as steep as those shown by Thomas (1966) and presented in Figure 3.1.

Figure 4.3 shows iso-resistivity contours from a part of area B shown in Plate 3.15. The anomaly is seen to be considerably wider than that shown in Figure 4.2, and is related to weathering along what is probably an older fracture trend. The boreholes sited close to the offset in the resistivity anomaly gave higher than average yields ($> 15\text{m}^3/\text{hr}$) for the area, although boreholes sited on the broad anomaly to the south-west dried up after several months of pumping (see Section 6.3).

Readings of Wenner alpha, beta and gamma resistivity (also known as tripotential readings) were obtained for all the profile lines shown in Figure 4.2. The data for one of these lines is shown in Figure 4.4 and tabulated in Table 4.1. According to Barker (1979) the beta and gamma profiles show a characteristic response as the electrode set passes over a shallow resistivity inhomogeneity, such as a shallow buried boulder. The beta profile shows a negative movement whereas the gamma profile shows a similar positive displacement. Several such fractures are marked by the letters 'LI' on Figure 4.4, indicating near surface lateral inhomogeneities.

The resistivity profile results show clearly that the method successfully delineates weathering troughs.

Field method.

A GTE Rhometer was used for the majority of the profiling work. This push button, digital display instrument produced results in a quick and convenient manner.

Between 70 and 100 short (75cms) steel electrodes were placed in the ground at measured intervals of 15 or 30 m along the profile line

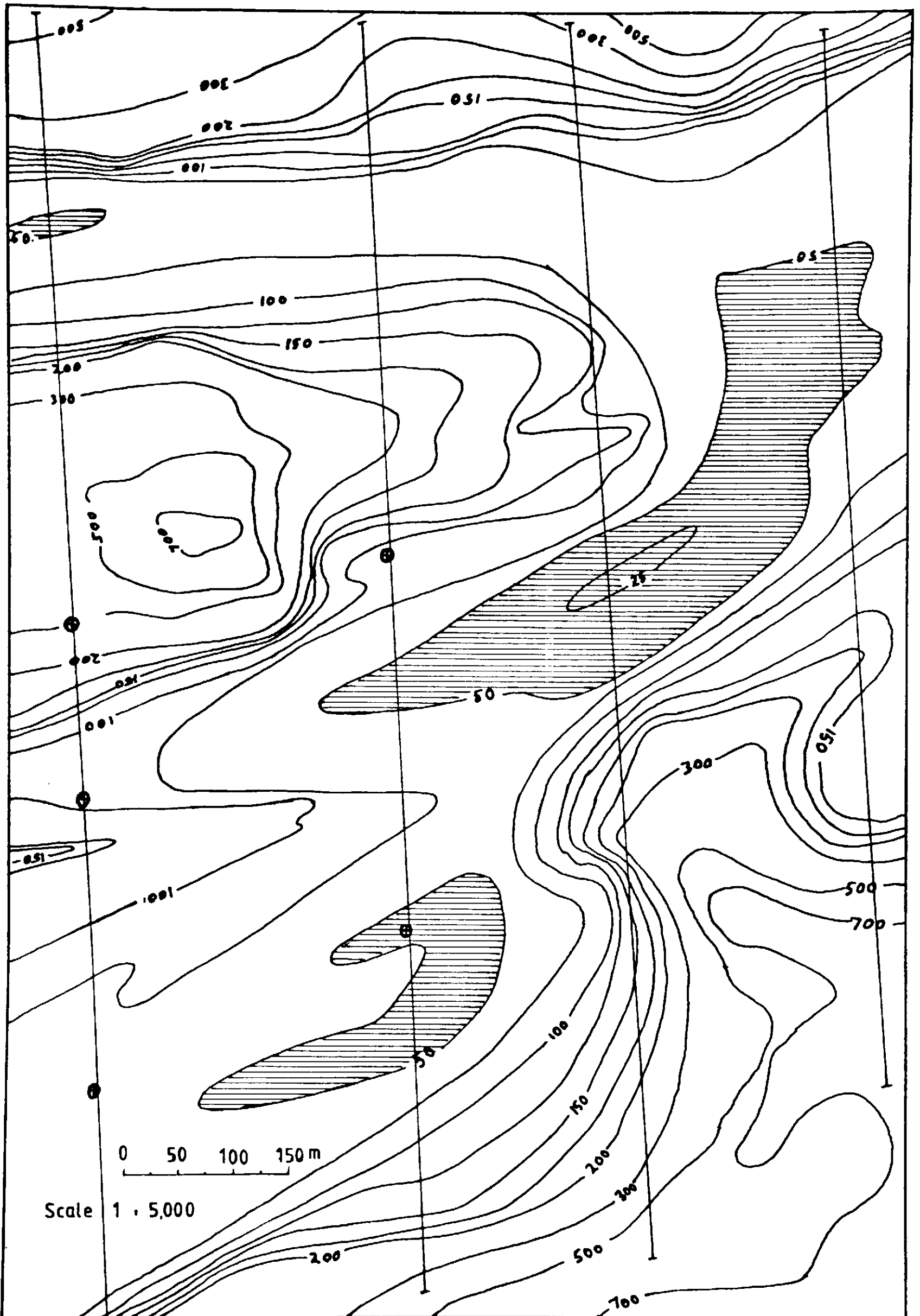


Figure 4-3 Map showing apparent resistivity over a part of deep weathering area B

⊕ Borehole

Contours in Ohm metres

Electrode separation $a = 30$ m

Table 4.1 Tripotential profile results over a fracture zone shown in Figure 4.4. (Data in ohm metres)
Electrode spacing = 30m. Station spacing = 15m.

Station	α	β	γ	Offset α	Station	α	β	γ	Offset α
0					35	121	85	111	111
1					36	102	73	90	96
2					37	93	56	81	86
3	150	28	122		38	99	45	83	82
4	150	45	115	101	35	102	40	83	75
5	119	45	81	81	40	82	40	68	83
6	65	23	47	65	41	124	51	83	92
7	76	23	49	49	42	187	51	117	100
8	82	45	51	55	43	135	73	117	110
9	98	28	62	64	44	110	107	104	111
10	93	45	77	85	45	119	79	105	104
11	130	62	109	96	46	121	68	104	97
12	147	90	115	120	47	113	51	89	95
13	127	130	132	137	48	107	45	87	88
14	172	130	160	158	49	107	45	87	79
15	206	141	185	173	50	87	39	72	131
16	200	147	187	186	51	237	51	175	123
17	142	164	187	183	52	178	102	175	156
18	181	158	179	197	53	144	107	138	285
19	240	147	207	196	54	452	277	396	399
20	249	136	213	194	55	933	124	660	414
21	153	187	181	204	56	480	350	433	451
22	189	181	196	207	57	367	136	243	376
23	283	181	234	205	58	283	339	320	329
24	243	141	215	203	59	481	209	415	358
25	181	158	173	189	60	452	198	396	424
26	161	147	164	175	61	557	271	434	432
27	212	119	177	177	62	537	339	471	471
28	237	107	190	178	63	537	401	509	546
29	195	141	179	172	64	678	463	622	574
30	147	164	154	166	65	792	418	640	641
31	141	170	153	152	66	763	447	660	602
32	175	130	151	155	67	622	447	565	565
33	192	102	158	141	68				
34	153	96	132	134	69				
					70				

Table 4.1 Tripotential profile results over a fracture zone shown in Figure 4.4. (Data in ohm metres)
Electrode spacing = 30m. Station spacing = 15m.

Station	α	β	γ	Offset _{α}	Station	α	β	γ	Offset _{α}
0					35	121	85	111	111
1					36	102	73	90	96
2					37	93	56	81	86
3	150	28	122		38	99	45	83	82
4	150	45	115	101	35	102	40	83	75
5	119	45	81	81	40	82	40	68	83
6	65	23	47	65	41	124	51	83	92
7	76	23	49	49	42	187	51	117	100
8	82	45	51	55	43	135	73	117	110
9	98	28	62	64	44	110	107	104	111
10	93	45	77	85	45	119	79	105	104
11	130	62	109	96	46	121	68	104	97
12	147	90	115	120	47	113	51	89	95
13	127	130	132	137	48	107	45	87	88
14	172	130	160	158	49	107	45	87	79
15	206	141	185	173	50	87	39	72	131
16	200	147	187	186	51	237	51	175	123
17	142	164	187	183	52	178	102	175	156
18	181	158	179	197	53	144	107	138	285
19	240	147	207	196	54	452	277	396	399
20	249	136	213	194	55	933	124	660	414
21	153	187	181	204	56	480	350	433	451
22	189	181	196	207	57	367	136	243	376
23	283	181	234	205	58	283	339	320	329
24	243	141	215	203	59	481	209	415	358
25	181	158	173	189	60	452	198	396	424
26	161	147	164	175	61	557	271	434	432
27	212	119	177	177	62	537	339	471	471
28	237	107	190	178	63	537	401	509	546
29	195	141	179	172	64	678	463	622	574
30	147	164	154	166	65	792	418	640	641
31	141	170	153	152	66	763	447	660	602
32	175	130	151	155	67	622	447	565	565
33	192	102	158	141	68				
34	153	96	132	134	69				
					70				

selected. The ground around the electrodes was moistened with a dilute saline solution when conditions warranted this treatment. In practise, this was necessary for the entire dry season commencing within 10 days of the last rains of the wet season.

Domestic 3 core 13 amp flex was found to be a convenient cable for profiling. As the cable is continuously dragged along the ground it does not last for more than 6-8 weeks of work, and a continuous supply of cable is therefore required.

The members of a four man team move synchronously along the profile line connecting the required conductor of the three core cable to an electrode. A switch box carried alongside the measuring instrument allows the required configuration of electrodes to be selected.

Data processing.

Due to the uncertainty associated with establishing the response of the potential field to variations in resistivity, it is sometimes possible to confuse the response created by a small near surface inhomogeneity with that of a deeper and more important lateral variation in resistivity. The suppression of 'noise' associated with near surface effects is therefore important. Barker (1981) has recently shown that the average of two adjacent alpha readings efficiently suppresses near surface effects.

A two point running mean of the field data collected during a resistivity profile exercise can significantly improve the data quality. In Figure 4.4, the offset filter has been applied to the original data and can be seen to be particularly efficient at suppressing the effects created by the areas of near surface lateral inhomogeneity discussed above.

Lateral resistivity variations at depth cannot produce short wavelength anomalies in the profile data. Therefore if a profile does show extensive wavelength noise, this is due to conditions within the top 1-2m of ground.

Electromagnetic profiling.

Many of the problems arising from poor contact or excessive near surface variation can be overcome using electromagnetic methods which

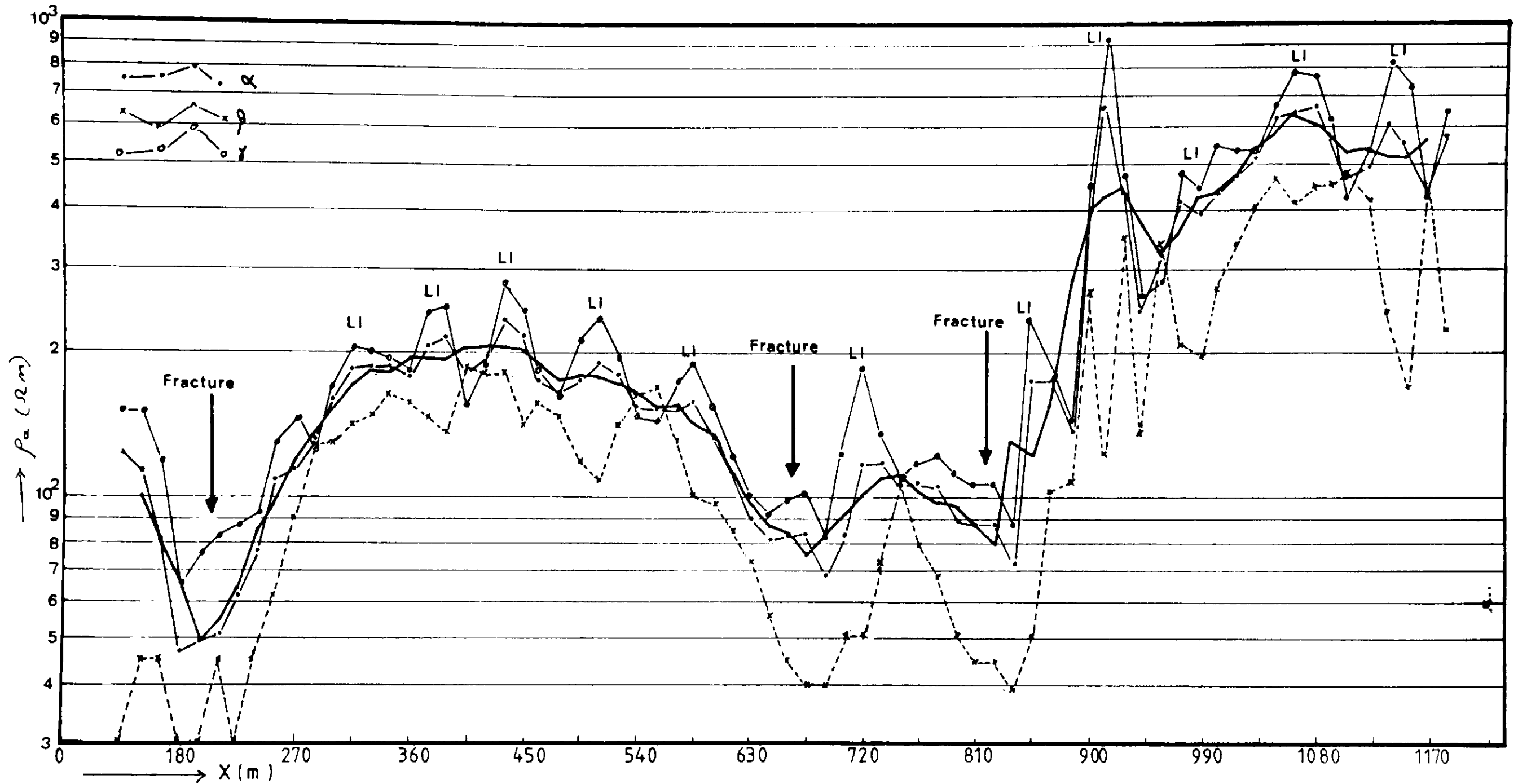


Figure 4-4 Tripotential profile data

Areas showing pronounced lateral variation are marked LI
 The effect of using an offset filter to smooth the data is shown by the red line.

do not require ground contact. McNeil (1980) describes two new instruments, the EM31 and the EM34-3, which can be used to obtain resistivity profile data over a range of exploration depths. The EM31 is a one man portable device with a nominal depth of penetration of 6m, while the EM34-3 has four penetration depths, 7.5, 15, 30 and 60m, although two men are required to operate the system.

An EM31 was used extensively in Nigeria to obtain resistivity profile data. It was found that this instrument could be used very quickly to delineate areas where grade I rock lies close to the surface.

The EM31 consists of a transmitting coil and a receiving coil separated from each other along a boom 3.7m in length. The time-varying magnetic field arising from the alternating current in the transmitter coil induces small eddy currents in the earth. These currents generate a secondary magnetic field, which is sensed, together with the primary field at the receiver coil. Under certain conditions, satisfied in the design of the EM31 (McNeil, 1980), the ratio of the secondary to the primary magnetic field is linearly proportional to ground resistivity. The EM31 gives a continuous readout in millimhos per metre, which may be converted directly to ohm metres.

This instrumentation provides a method by which profile data may be accurately and rapidly collected by one man rather than by four.

The depth of penetration of an alpha array ($a = 30\text{m}$) has been given above as 10m. The EM31 penetration depth is reported as 6m and the two systems should provide broadly comparable data. This hypothesis was tested by operating the two systems over approximately 10 km of profile line with measurement intervals every 5 or 10m.

In general the two profiles parallel each other when plotted on semi log paper, and no features identified on the alpha profile data were missed on the EM31 results. In Figure 4.5 the results over borehole 10 on Figure 3.4 and also corresponding to the profile section discussed in Section 4.4 in area A (Figure 4.9) are presented. The EM31 profiles always showed lower values of apparent resistivity. This corresponds with the slightly lesser depth of penetration which would therefore be affected to a greater degree by the low resistivity

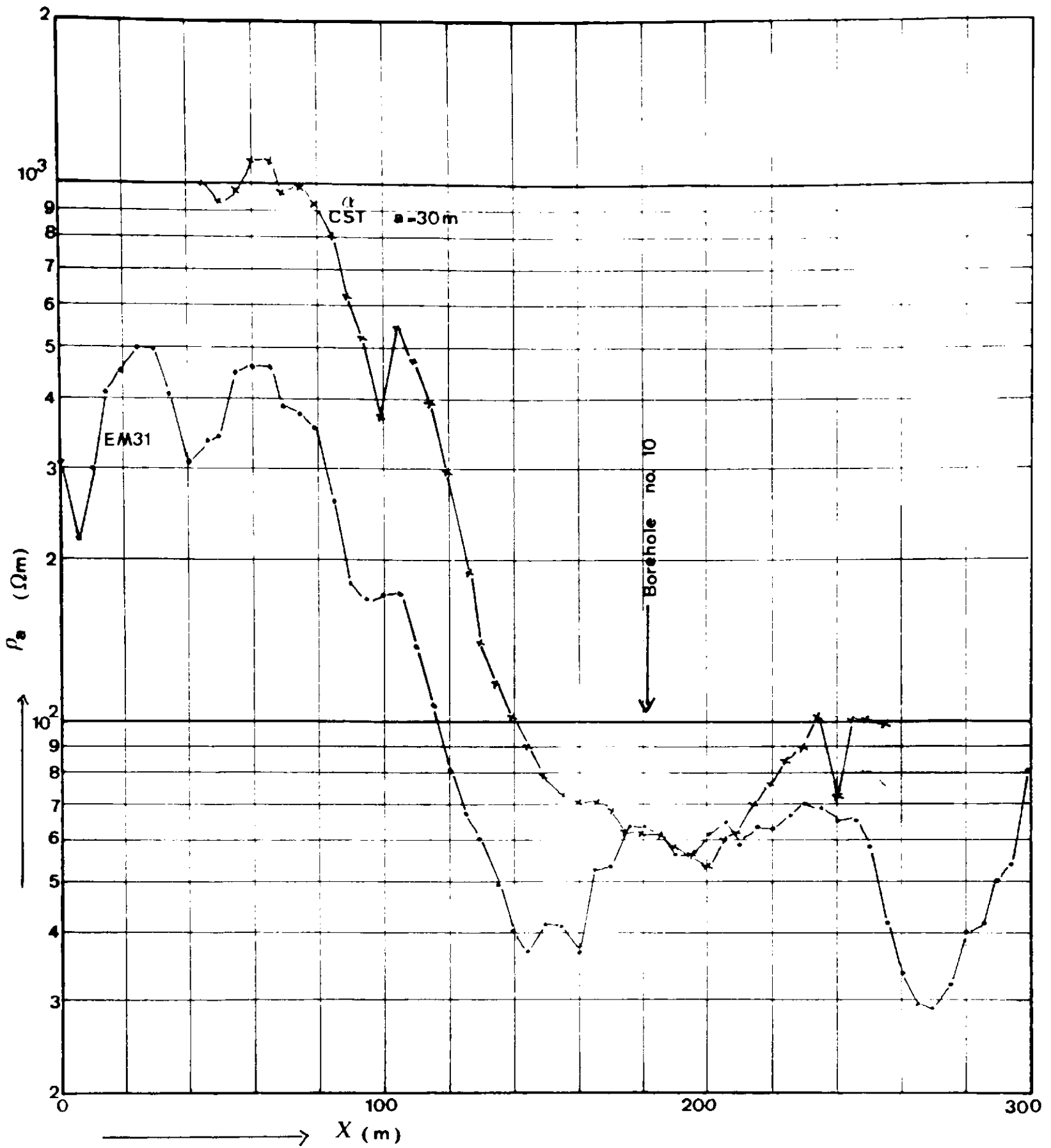


Figure 4-5 Alpha profile and EM31 data across deep weathering area A.

clay materials closer to the surface.

Summary.

The apparent resistivity profiling method provides a rapid method of establishing the presence of areas of deep weathering. However, due to the complexities involved in interpreting potential field data, it is not possible to make a quantitative interpretation of weathering depths, or weathering grade thicknesses from a single profile line. In any particular area however, it is possible to select an electrode spacing from experience and interpret profile data qualitatively. For example, in the area around Bauchi, and in several other similar areas, it was found that a resistivity anomaly similar to those shown in Figures 4.2 and 4.3 could be loosely correlated with a depth to fresh rock of between 40 and 50 metres.

4.3 Electrical Resistivity Sounding.

Introduction.

The electrical resistivity sounding technique is used to resolve a series of plane layered homogeneous resistivity layers into the individual resistivities and thicknesses which comprise the layering. A number of electrode configurations have been proposed to achieve this end (Telford, et al, 1976), although the method used for this work in Nigeria was based upon a colinear set of four equispaced electrodes. This configuration, which is the same as that used for the profiling method discussed in Section 4.2, has been called the Wenner sounding method.

A set of four electrodes are expanded about a common centre in such a manner that the spacing between the electrodes remains equal. A sounding curve is obtained by plotting the log of the spacing (a) against the log of the alpha apparent resistivity (ρ_a) obtained at that spacing. This method has been described in the literature (Griffiths + King, 1965; Telford, et al, 1976; Koefoed, 1979). The interpretation procedure, described in detail by Koefoed, is based upon an analytical solution to the Laplace equation discussed in Section 4.1.

Theoretical Considerations.

As the interpretation procedure for a resistivity sounding is based upon an assumption of plane layering, it is useful to be able to establish that this condition exists over an area in which a sounding is to be carried out. This can be effectively and rapidly achieved by the use of one of the EM instruments described in Section 4.2.

The assumption of plane layering implies that the resistivity distribution is not a function of the x and y space co-ordinates, i.e.

$$\frac{\partial \rho_{xyz}}{\partial x} = 0 \quad \text{and} \quad \frac{\partial \rho_{xyz}}{\partial y} = 0$$

Therefore, for a colinear set of electrodes, as shown in Figure 4.1.b, the potential developed at electrode 1 (P_1) due to a current at electrode 0 (C_1) will be equivalent to the potential developed at electrode 2 (P_2) due to a current at electrode 3 (C_2). This may be expressed as :

$$\phi_{10} = \phi_{23} \quad \text{and similarly} \quad \phi_{13} = \phi_{20}$$

The dependence of the potential term upon the x and y co-ordinates is released by an assumption of plane layering, and the potential term then depends only upon the electrode spacing (a) and the resistivity distribution with depth ($\rho_{x,y,z} = f(z)$). For any given spacing (a) the results from a resistivity profile will therefore show no change.

It is important to note therefore that resistivity soundings can only be successfully and accurately interpreted if they have been carried out in areas where resistivity profile results would show no change in value of measured apparent resistivity. In practice, such areas are uncommon in the basement weathering environment as discussed above.

Resistivity sounding results.

Whatever restrictions are placed upon the accuracy of the interpretation by the assumptions discussed above, the resistivity sounding method remained the principal method for obtaining formation resistivities which can be associated with the different weathering grades. Also, as it has been long recognised that the most successful boreholes are usually located where the greatest depth of weathering is developed, the sounding method has been used to produce a value for the depth of weathering. In many instances (Verma, et al, 1980), the predicted depths of weathering have not agreed with borehole results and the error in interpretation can be ascribed to the lack of plane layering.

In Figure 4.6 three soundings are shown from the area around Bauchi. Tripotential measurements have been made at each electrode separation and in sounding O2 these measurements in particular show the presence of lateral variations.

Sounding O1 shows an area of almost homogeneous ground: although the latter part of the curve rises at a rate which cannot be analysed assuming plane layering. Sounding O2 shows typical data from an area where grade III weathering is close to the surface, with grades IV to

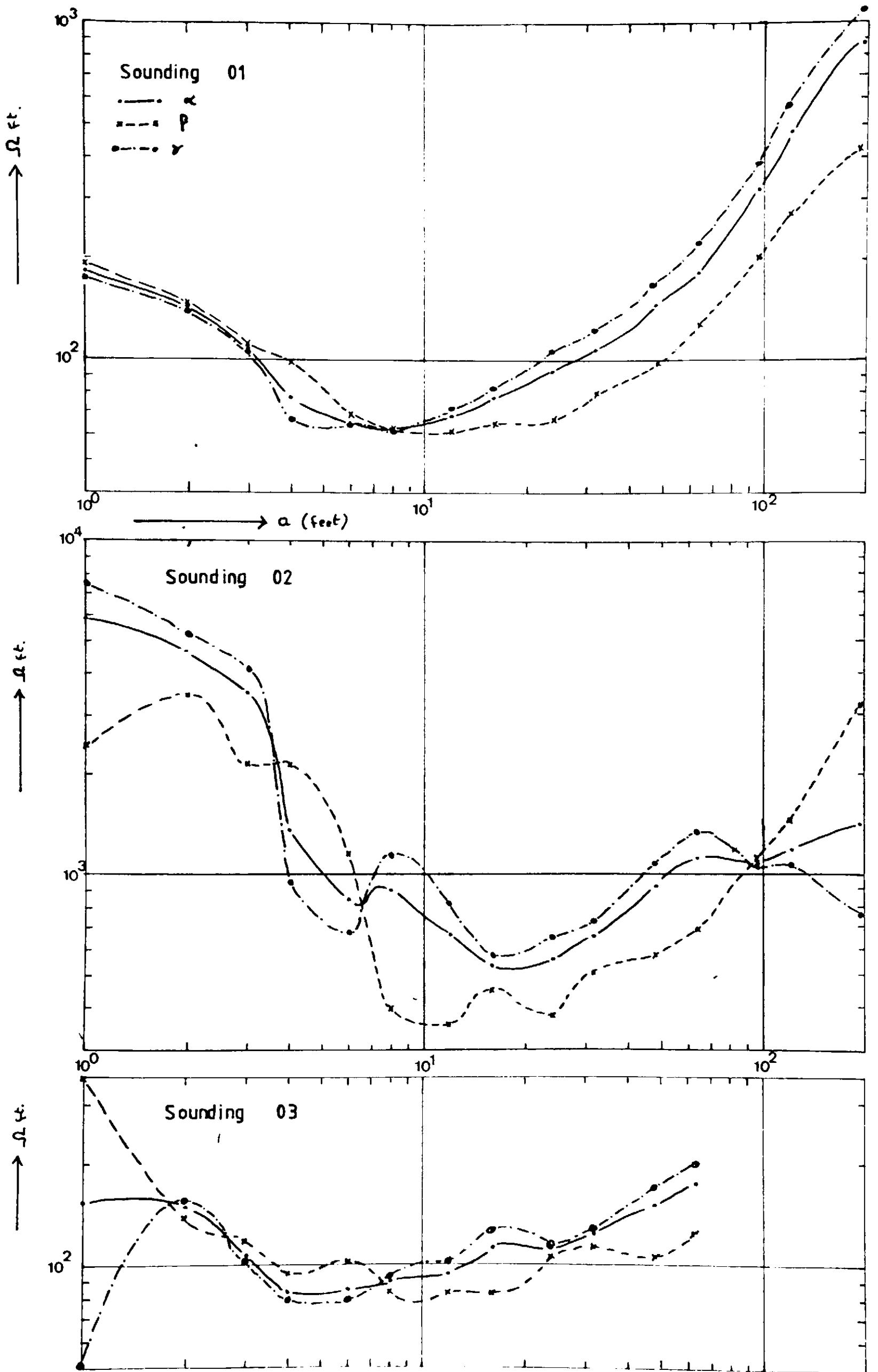


Figure 4-6 Tripotential sounding results.

VI weathering missing. The 'B' soil horizon is also poorly developed. Sounding 03 is from an area of deep weathering where zones V and VI weathering are well developed. The depth of penetration of this sounding is not sufficient to produce data on the deeper grades of weathering.

The three sounding curves are basically all of a similar shape, and are also similar to those described by Palacky (1979) in Brazil and Vermar et al (1980) from India. Plane layer interpretations (Koefoed, 1979) give resistivities as shown in Table 4.2.

Table 4.2. Resistivities of weathering grades.

Layer	Resistivity (Ωm)		Weathering Grade
1	160-200 (wet)	2000-4000 (dry)	Soil 'A' horizon
2	15 (if present)		Soil 'B' horizon
3	30-90 (usually damp)		V + VI
4	60-300 (wet)	300-800 (dry)	III + IV
5	600-3000		II
6	2000-6000		I

In areas where laterite has been formed the 'A' horizon resistivity may exceed $5000\ \Omega\text{m}$. In these areas, electrode contact is very difficult to establish successfully, and the sounding, or profile data is often uninterpretable due to excessive lateral variation near surface (but see also Figure 6.4).

The 'A' horizon resistivity may change substantially during the year as a result of the reduction in soil moisture throughout the dry season.

The resistivity data presented in Table 4.2 and derived from a number of sounding curves in addition to those presented in Figure 4.6, is similar to that described by Palacky, but includes a greater number of layers. This increased number of layers is required by the weathering model described in Section 3.4. It is probable that they have not been previously recognised because their resistivities are intermediate between those of the high clay content grade V + VI material and the fresh grade I rock.

Zones with resistivities intermediate between two others form suppressed layers on a sounding curve, and their detection and accurate interpretation becomes very difficult. To illustrate this point, a family of curves have been generated, using methods described by Koefoed (1979) with resistivities as described by Table 4.2 and layering thicknesses derived from a typical borehole section. The thickness of the fourth layer, representing the aquifer material, is varied between 5 and 30 m in increments of 5m. The resistivity sounding curves are presented in Figure 4.7.

From the curves shown in Figure 4.7 it may be seen that, in the presence of lateral variations as shown in Figure 4.6 an accurate interpretation of the section would not be possible.

A large number of curves have been generated using the resistivities in Table 4.2 as a form of standard. These values are only approximate, however, the range of values represents a reasonable approximation, given the data and quality of the data available. Making the further generalising assumption that plane layering does exist, a sensitivity analysis of the depth of each layer was carried out, in order to assess the combination of layers which would produce the apparent resistivity low anomaly, at a = 30m, observed in the profile data. From this work a minimum depth of weathered section is suggested for such an anomaly as shown in Table 4.3.

Table 4.3 Inferred depth of weathering from sounding data.

Layer	Resistivity (Ω m)	Thickness (m)	Depth (m)	Weathering Grade
1	175	0.5	0.0	Soil A
2	15	2.5	0.5	Soil B
3	40	27.0	3.0	V + VI
4	100	20.0	30.0	III + IV
5	800	10.0	50.0	II
6	4000	-	60.0	I

It is apparent from this work that unless the fourth layer has a low resistivity, indicating saturation, the required anomaly may not be produced. Similarly, therefore, if the fourth layer is absent this anomaly is not possible.

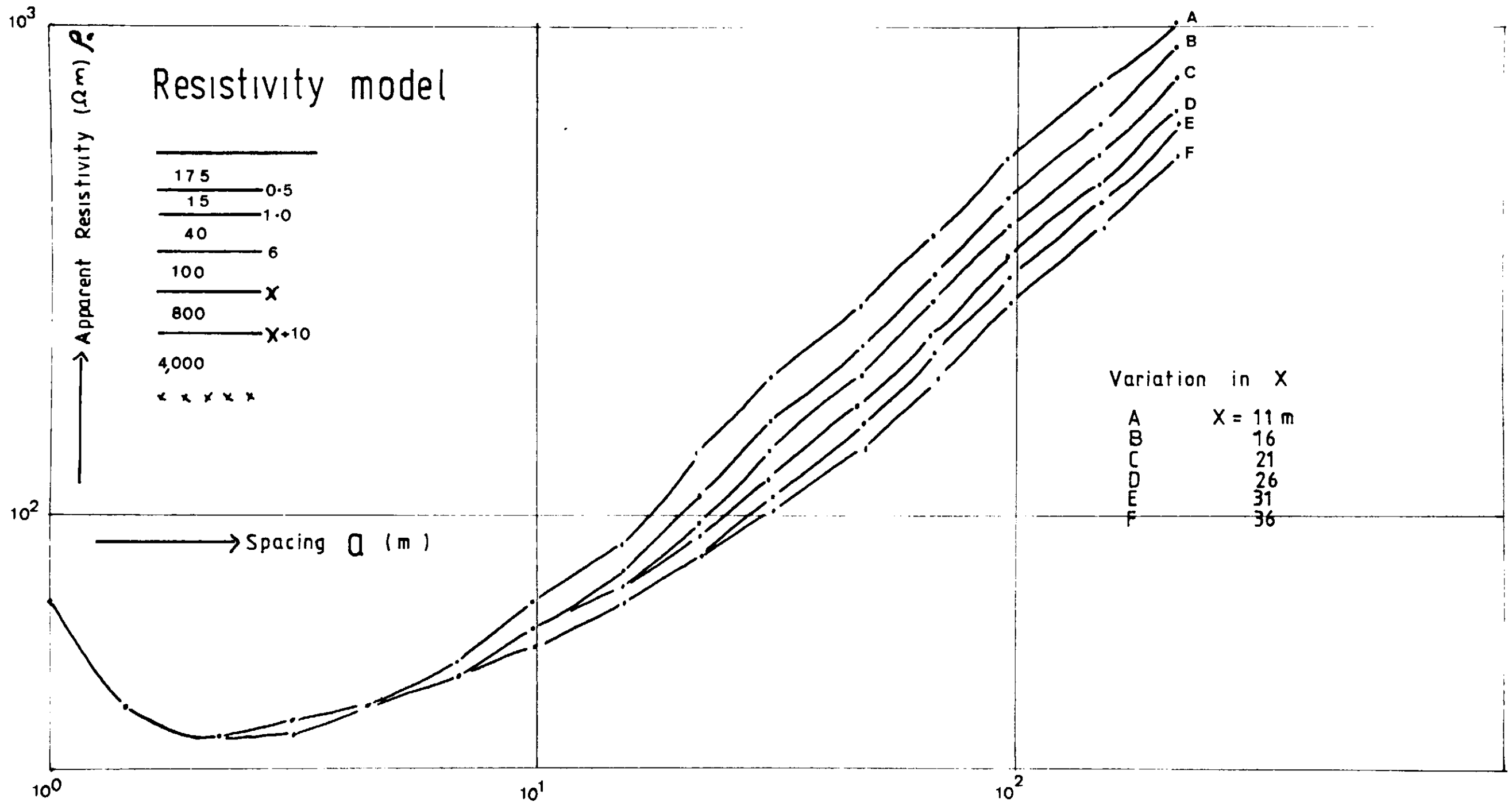


Figure 4-7 Family of sounding curves produced by varying forth layer depth.

Summary.

The resistivity sounding technique has been widely used in basement areas with mixed, and often poor results. These results may be explained in terms of the presence of lateral variations in resistivity which depart from the basic theoretical interpretation assumption of plane layering. Despite this fact, the resistivity sounding method can provide useful information, although it cannot be recommended for siting boreholes.

The presence of lateral variation can be detected by a profile across the area in which a sounding is to be conducted. A resistivity sounding should be orientated so that the minimum possible lateral variation is crossed by the line occupied by the sounding.

4.4 Electrical Resistivity Profile Sections.

Introduction.

Resistivity profiling is used to examine lateral variations in resistivity. However, only profile results produced by simple two dimensional anomalies have been calculated analytically (Telford, et al, 1976) and in more complicated resistivity distributions, the quantitative interpretation of the profile results becomes impossible using the analytical approach. Similarly, resistivity soundings can be used to investigate changes in resistivity with depth, as long as there is no lateral variation. As has been discussed above, the weathering profile varies both laterally and vertically, and therefore both the generally used techniques are unsatisfactory in a number of ways.

The main drawback of the conventional methods of analysis is that insufficient data is produced by the interpretation. In the case of profiling, the presence of lateral variation is established, but not the depth or variation within the weathered section. By contrast, the sounding method produces information on the changes of resistivity with depth, at the expense of the assumption that there is no lateral variation. A combination of the two methods would enable a more complete interpretation to be made.

Resistivity Profile Sections.

During resistivity profiling, the value of apparent resistivity for a particular position of the electrode array is, by convention, plotted at the mid point of the electrode array. The exact depth of penetration for a given electrode spacing is not known, however, if the electrode spacing is increased and measurements repeated along the same profile, then the value of apparent resistivity associated with the same mid point as before relates to a greater depth of penetration and can be plotted below the initial value.

If measurements are repeated along the same profile line with a number (> 4) of electrode spacings, and the apparent resistivity results plotted as described above, a section of readings is obtained. This section represents both lateral and vertical changes in resistivity. The section is called a 'profile section' here to differentiate it from the pseudo section results produced by the dipole dipole

method, although the prefix 'pseudo' could be equally applied to either section.

The distance between the plotting positions of the different profile lines is entirely arbitrary, as to assign an actual position, beneath the ground, to any reading of apparent resistivity is itself unwarranted.

Figures 4.9, 4.11 and 4.13 are examples of resistivity profile section data obtained around Bauchi. The figures are referred to here only as examples of the method results and will be discussed below. The electrode spacings used are shown in the figures.

From the sensitivity analysis shown in Figure 4.6, it may be seen that the significant part of the data for a sounding carried out over an area of deep weathering is contained within the spacing (a) log cycle of from 10-100m. It is only the resistivity distribution which produces a response in this range which is significant for the purposes of interpreting the depth of weathering. Therefore the spacings for the profile section should be chosen between 10 and 100m.

The profile sections can be interpreted qualitatively as they stand, however, the major advance provided by the finite difference discretisation method of Dey + Morrison (1979b) is that the sections can also be modelled, and a model resistivity distribution changed until the model produces results similar to the field data.

Finite Difference Algorithm.

Equation 4.7 in Section 4.1 represents the potential distribution in an inhomogeneous half space. This equation may be written for the most general case as

$$-\nabla \cdot (\sigma \nabla \Phi) = \frac{dI}{dt} \delta(x_s) \delta(y_s) \delta(z_s) \quad 4.16$$

where $\frac{dI}{dt}$ — is the differential of the current density with time at the point defined by the dirac delta functions $\delta(x_s) \delta(y_s) \delta(z_s)$

The inclusion of a right hand side term enables the equation to represent volumes of space which enclose a source or sink of current, that is, volumes where the divergence of the vector field is not zero.

It is possible to draw a three dimensional grid through the resistivity distribution and to assign an independent value of resistivity to each volume element of the grid. The finite difference approximation to Equation 4.16 may then be made as accurate as is required by defining the grid in the area of interest as finely as necessary. Although this method is the simplest to write an algorithm for, the quantity of computer storage rapidly becomes prohibitive, and the time to arrive at a stable solution to the potential field similarly becomes excessive, even for a comparatively advanced machine such as the CDC 7600.

Dey + Morrison (1979b) have reported a modification of the three dimensional approach. It is worth outlining this approach here, as the algorithm presented in Appendix C is based on this method. However, for details, the reader is referred to the original reference.

The electric potential, unlike the hydraulic potential (Rushton+ Redshaw, 1979) cannot be modelled in two dimensions. A two dimensional representation of a point source of current becomes a line source, and this produces an entirely different potential field to the point source.

As a compromise between computing resources and accuracy of the three dimensional solution, the assumption is made that the resistivity does not vary in the one dimension. The justification for this assumption is discussed in Section 6.2.

$$\frac{\partial}{\partial y} [\sigma(x,y,z)] = 0 \quad 4.17$$

with this assumption, Equation 4.16 may be written

$$-\nabla \cdot [\sigma(x,z) \nabla \Phi(x,y,z)] = \frac{dI}{dt} \delta(x_s) \delta(y_s) \delta(z_s) \quad 4.18$$

The algorithm presented by Dey (1976) involves a fourier transform of the potential in 3D space to 2D wave number space where the finite difference approximation to the equation is made. The 3D potential distribution $\Phi(x,y,z)$ due to a point source of current at (x_s, y_s, z_s) over a 2D conductivity distribution $\sigma(x,z)$ is reduced in this way to a 2D transformed potential $\Phi(x,ky,z)$.

The fourier transform of Equation 4.18 subject to these constraints is given by Dey as

$$-\nabla \cdot [\sigma_{(x,z)} \nabla \tilde{\Phi}_{(x,y,z)}] + k_y^2 \sigma_{(x,z)} \tilde{\Phi}_{(x,ky,z)} = \bar{\alpha} \delta(x_s) \delta(z_s) \quad 4.19$$

where $\bar{\alpha}$ is defined as the constant steady state current density in (x,ky,z) space.

Equation 4.19 is solved for a number of source positions in (x,ky,z) space using a finite difference approximation.

The solution is repeated for a sufficient number of values of ky so that the reverse fourier transformation of the potentials can be made from x,ky,z space to x,y,z space, with sufficient accuracy (Dey + Morrison, 1979b).

A matrix inversion technique is used to invert the capacitance matrix which results from the finite difference discretisation.

The algorithm which has been written for this study is presented in Appendix C.

The algorithm produces the values of the potential at a number of pre-selected nodes on the surface of the half space, due to a current source of each of the selected surface nodes. A symmetric matrix of potentials is thus created whose order is determined by the number of surface nodes selected. Since these potentials are scalars, they may be combined in exactly the same manner as described in Section 4.2 for resistivity profiling.

Graphical routines have been used to output a profile section computed over a given resistivity model section.

Description of algorithm graphical output.

For general use in modelling profile sections obtained in the field, a 185×16 array of nodes is used. This allows a control area of the mesh to be modelled linearly, and the potential at 41 nodes, due to a source at each of the 41 nodes in turn is calculated by the algorithm. A 41×41 matrix of potentials is thus obtained with the potential in the node surrounding the source position in each case

The fourier transform of Equation 4.18 subject to these constraints is given by Dey as

$$-\nabla \cdot [\sigma(x,z) \nabla \hat{\Phi}(x,y,z)] + \kappa_y^2 \sigma(x,z) \hat{\Phi}(x,ky,z) = \bar{\alpha} \delta(x_s) \delta(z_s) \quad 4.19$$

where $\bar{\alpha}$ is defined as the constant steady state current density in (x,ky,z) space.

Equation 4.19 is solved for a number of source positions in (x,ky,z) space using a finite difference approximation.

The solution is repeated for a sufficient number of values of ky so that the reverse fourier transformation of the potentials can be made from x,ky,z space to x,y,z space, with sufficient accuracy (Dey + Morrison, 1979b).

A matrix inversion technique is used to invert the capacitance matrix which results from the finite difference discretisation.

The algorithm which has been written for this study is presented in Appendix C.

The algorithm produces the values of the potential at a number of pre-selected nodes on the surface of the half space, due to a current source of each of the selected surface nodes. A symmetric matrix of potentials is thus created whose order is determined by the number of surface nodes selected. Since these potentials are scalars, they may be combined in exactly the same manner as described in Section 4.2 for resistivity profiling.

Graphical routines have been used to output a profile section computed over a given resistivity model section.

Description of algorithm graphical output.

For general use in modelling profile sections obtained in the field, a 185×16 array of nodes is used. This allows a control area of the mesh to be modelled linearly, and the potential at 41 nodes, due to a source at each of the 41 nodes in turn is calculated by the algorithm. A 41×41 matrix of potentials is thus obtained with the potential in the node surrounding the source position in each case

occupying the principal diagonal element of the matrix.

Data input to the algorithm includes scaling information which sets the source/potential position nodes at 10m apart. The profile section is thus 400m long in this scaling mode.

The apparent resistivity response for electrode spacings of 10, 20, 30, 40, 50, 60 and 70m is shown in the graphical output. The resistivity value is shown plotted at the mid point of the electrode (source/potential position) configuration and approximately 1cm below the previous reading, although this distance is arbitrary as discussed above.

The vertical scaling information for the model is shown at the lower right hand side of the graphical output. A non-linear scaling is adopted, with the lower boundary effectively representing infinity in the z-direction.

The resistivity distribution shown in the lower part of the output represents coded data. Each code element represents an area of resistivity between four nodes. The area is 2.5m long in the x-direction, a varied length in the z-direction as shown in the scaling information on the right, and an infinite length in the y direction. Note therefore that an element in the coded distribution close to the base represents a larger area than one close to the surface. The reason for such a grading of the mesh may be explained in terms of potential theory as discussed in Section 4.1.

Each element of the resistivity distribution may be assigned one of 10 coded values of resistivity. The code values are shown in the middle right of the output. These ten values may represent any value of resistivity, however, the code values used in the analysis below are those shown in Table 4.2, and therefore refer to specific grades of weathering.

Examples of the graphical output are shown in Figures 4.10, 4.12 and 4.14 below.

Description of profile section field method.

The field technique for the collection of profile section data is very similar to that of ordinary profiling.

An area of interest is selected from a study of the remote sensing data and an appropriate number of electrodes placed in the ground

at 10m intervals. The area of ground around the electrodes is moistened with a dilute saline solution if necessary.

A four man team makes repeated traverses up and down this line of electrodes varying the electrode spacing each time, until sufficient data has been collected. A maximum separation of 70m was used in the results presented below.

The majority of field time is expended travelling to an area and establishing the line of electrodes in the ground, and therefore the collection of the extra data does not represent the equivalent of five or six new profile lines.

At the smallest spacing adopted, the collection of tripotential data is advised, as this will provide valuable information on the near surface lateral variation, as discussed above. However, there is no point in repeating these measurements at larger spacings.

An EM31 can be usefully employed when the line of electrodes is laid out. An EM survey over the area of interest will delineate the basin of weathering and the results can be used to orientate the line so that it is orthogonal to the strike direction. It is good field practice to number the electrodes (beginning with zero) and to note any features of interest or points which may help with later location during the initial stage.

Offset profiling.

The collection of the extra field data can take a considerable time. In Nigeria it was found that approximately 100 minutes was required to measure one profile line along 40 electrodes. The total time can be reduced, and the quality of the overall data set improved if the offset profiling method is used. This has the disadvantage that an extra field man is required, but the advantages that by one pass along the line of electrodes, two electrode separations are collected, thus reducing the total number of passes required.

It is suggested here that the offset profiling method be used where ever profiling is carried out as for little extra effort, the data output is doubled. In the savanna environment, there is usually no problem in finding an extra field crew for the day.

The offset profiling configuration is shown in Figure 4.8. The method recommended here is a development of the tripotential method

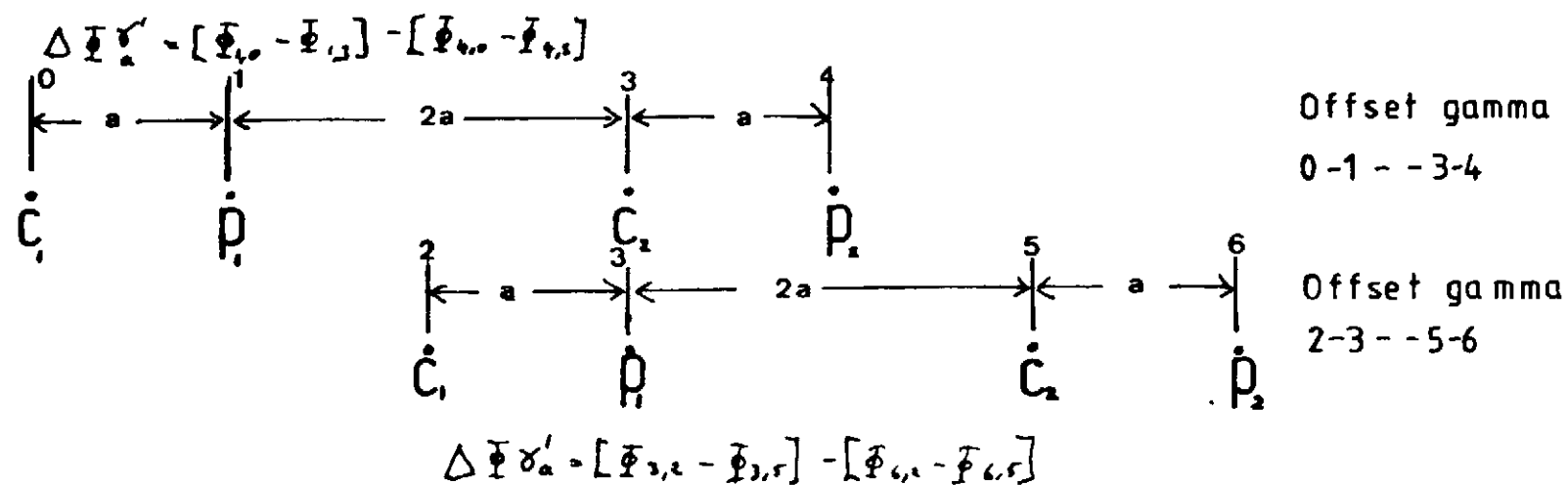
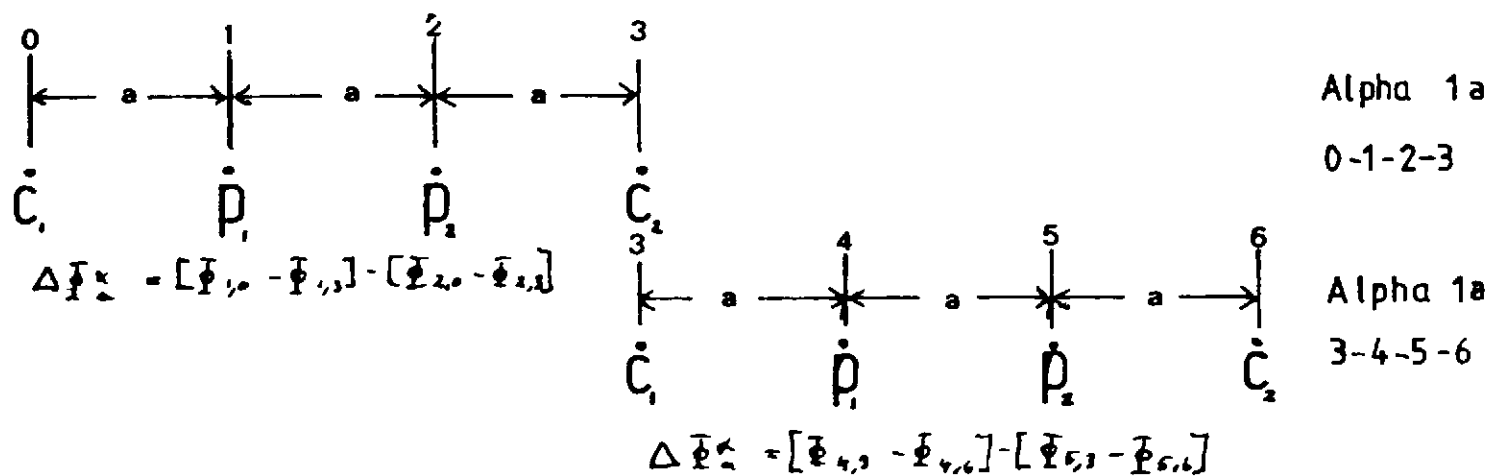
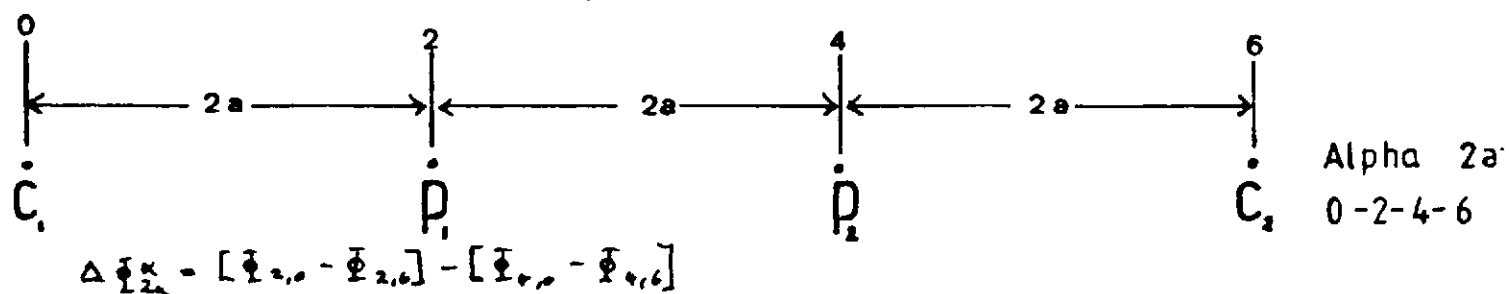
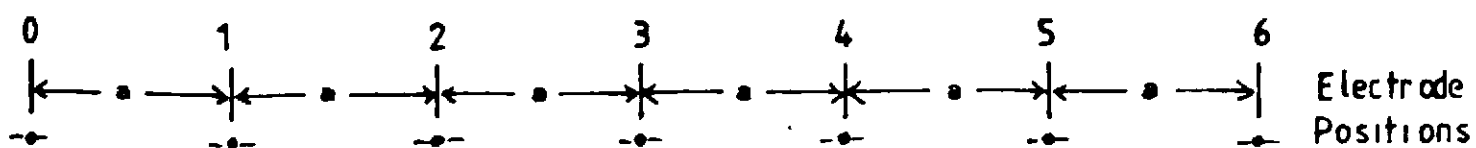


Figure 4-8 Offset profiling electrode configurations.

discussed in Section 4.2 where a simple summation of measurements was used as a field check.

For a set of 7 equispaced electrodes as shown in Figure 4.8 the apparent resistivity at $2a$ for the electrode set 0-2-4-6, may be measured as

$$\Delta\Phi_{\alpha 2a} = (\varphi_{20} - \varphi_{26}) - (\varphi_{40} - \varphi_{46}) \quad 4.20$$

This potential difference can also be measured by a combination of alpha (C-P-P-C) and offset gamma (C-P- - C-P) measurements as shown in Figure 4.7. The advantage gained is that the cable length is only increased from $3a$ to $4a$, instead of to $6a$ as would be required for the alpha $2a$ measurement, and that by taking two measurements at each electrode during one traverse, the measurements alpha 'a' and alpha '2a' are collected.

The potentials for the calculation are shown in Equations 4.21, 4.22, 4.23 and 4.24, viz

$$\text{Alpha a} \quad 0-1-2-3 \quad \Delta\Phi_{\alpha a}^1 = (\varphi_{10} - \varphi_{13}) - (\varphi_{20} - \varphi_{23}) \quad 4.21$$

$$\text{Alpha a} \quad 3-4-5-6 \quad \Delta\Phi_{\alpha a}^2 = (\varphi_{43} - \varphi_{46}) - (\varphi_{53} - \varphi_{56}) \quad 4.22$$

$$\text{Offset gamma} \quad 0-1- - 3-4 \quad \Delta\Phi_{\gamma a}^1 = (\varphi_{10} - \varphi_{13}) - (\varphi_{40} - \varphi_{43}) \quad 4.23$$

$$\text{Offset gamma} \quad 2-3- - 5-6 \quad \Delta\Phi_{\gamma a}^2 = (\varphi_{32} - \varphi_{35}) - (\varphi_{62} - \varphi_{65}) \quad 4.24$$

By adding Equations 4.23 and 4.24, then subtracting from the sum, Equations 4.21 and 4.22, the required potentials for Equation 4.20 are produced.

$$\Delta\Phi_{\gamma a}^1 + \Delta\Phi_{\gamma a}^2 - \Delta\Phi_{\alpha a}^1 - \Delta\Phi_{\alpha a}^2 = \varphi_{10} - \varphi_{13} - \varphi_{40} + \varphi_{43} + \varphi_{32} - \varphi_{35} - \varphi_{62} + \varphi_{65} -$$

$$(\varphi_{10} - \varphi_{13} - \varphi_{20} + \varphi_{23} + \varphi_{43} - \varphi_{46} - \varphi_{53} + \varphi_{56}) = (\varphi_{20} - \varphi_{62}) - (\varphi_{40} - \varphi_{46}) = \Delta\Phi_{\alpha 2a}$$

The accuracy of the predicted value of alpha $2a$ is controlled by the accuracy of the four measurements used to produce this value. However, it should be noted that the value of alpha $2a$ is not an estimate based upon any assumption of plane layering, or an extrapolation from the measurements at smaller electrode spacings. The

discussed in Section 4.2 where a simple summation of measurements was used as a field check.

For a set of 7 equispaced electrodes as shown in Figure 4.8 the apparent resistivity at $2a$ for the electrode set 0-2-4-6, may be measured as

$$\Delta\Phi_{\alpha 2a} = (\varphi_{20} - \varphi_{26}) - (\varphi_{40} - \varphi_{46}) \quad 4.20$$

This potential difference can also be measured by a combination of alpha (C-P-P-C) and offset gamma (C-P- - C-P) measurements as shown in Figure 4.7. The advantage gained is that the cable length is only increased from $3a$ to $4a$, instead of to $6a$ as would be required for the alpha $2a$ measurement, and that by taking two measurements at each electrode during one traverse, the measurements alpha 'a' and alpha '2a' are collected.

The potentials for the calculation are shown in Equations 4.21, 4.22, 4.23 and 4.24, viz

$$\text{Alpha a} \quad 0-1-2-3 \quad \Delta\Phi_{\alpha a}^1 = (\varphi_{10} - \varphi_{13}) - (\varphi_{20} - \varphi_{23}) \quad 4.21$$

$$\text{Alpha a} \quad 3-4-5-6 \quad \Delta\Phi_{\alpha a}^2 = (\varphi_{43} - \varphi_{46}) - (\varphi_{53} - \varphi_{56}) \quad 4.22$$

$$\text{Offset gamma} \quad 0-1- - 3-4 \quad \Delta\Phi_{\gamma a}^1 = (\varphi_{10} - \varphi_{13}) - (\varphi_{40} - \varphi_{43}) \quad 4.23$$

$$\text{Offset gamma} \quad 2-3- - 5-6 \quad \Delta\Phi_{\gamma a}^2 = (\varphi_{32} - \varphi_{35}) - (\varphi_{62} - \varphi_{65}) \quad 4.24$$

By adding Equations 4.23 and 4.24, then subtracting from the sum, Equations 4.21 and 4.22, the required potentials for Equation 4.20 are produced.

$$\Delta\Phi_{\gamma a}^1 + \Delta\Phi_{\gamma a}^2 - \Delta\Phi_{\alpha a}^1 - \Delta\Phi_{\alpha a}^2 = \varphi_{10} - \varphi_{13} - \varphi_{40} + \varphi_{43} + \varphi_{32} - \varphi_{35} - \varphi_{62} + \varphi_{65} -$$

$$(\varphi_{10} - \varphi_{13} - \varphi_{20} + \varphi_{23} + \varphi_{43} - \varphi_{46} - \varphi_{53} + \varphi_{56}) = (\varphi_{20} - \varphi_{26}) - (\varphi_{40} - \varphi_{46}) = \Delta\Phi_{\alpha 2a}$$

The accuracy of the predicted value of alpha $2a$ is controlled by the accuracy of the four measurements used to produce this value. However, it should be noted that the value of alpha $2a$ is not an estimate based upon any assumption of plane layering, or an extrapolation from the measurements at smaller electrode spacings. The

information contained in the four measurements represented by Equations 4.21 to 4.24 includes the exact potentials necessary to calculate alpha 2a over an inhomogeneous distribution. The potential differences measured at the smaller spacings, are also larger than those that would be measured at the larger spacing and may be therefore more easily measured.

In Table 4.4, the potentials calculated by the finite difference algorithm over an area of near surface lateral inhomogeneity, and for a 7 electrode set are shown. Note that the matrix (7 x 7) is symmetric and that therefore potential $\varphi_{ab} = \varphi_{ba}$ etc. From this matrix the potential difference calculated by the method described can be shown to be exactly equivalent to that measured. The figure of 20.90 is obtained by both methods.

The method has been tested in the U.K. and found to be accurate to within 5%, which is a sufficient accuracy in profiling over large resistivity contrasts.

By choosing an initial electrode separation of 10m, profile data at 10, 20 and 40, and 30 and 60m can be obtained by three passes along the electrodes.

Profile section field data.

Three resistivity profile sections are presented in Figures 4.9, 4.11 and 4.13. Each section represents an area of deep weathering close to Bauchi. The section in Figure 4.9 is from weathering area A and passes through borehole No. 10 on Figure 3.4, but at 90° to the line of the trough. Figure 4.11 shows an area of weathering where grade V material occurred to a depth of 28m in a borehole. The groundwater was confined by this clay and had a final standing water level of only 3m. Figure 4.13 shows a section from a part of weathering area B and also corresponds to the seismic refraction line shown in Figure 4.20. The drill samples shown in Plate 3.16 are from a borehole drilled into this anomaly.

The three profile sections each show a trough of weathering against a higher resistivity shoulder. Each section also shows pronounced lateral variations which would produce anomalous sounding results.

The finite difference algorithm has been used to model these

Table 4.4 Potentials due to a point source of current, at seven equispaced electrodes, over near surface lateral inhomogeneity. Value in volts.

Source	0	1	2	3	4	5	6
0	1395	75.03	62.07	55.53	51.66	47.51	44.86
1	75.03	2453	111.41	66.59	58.56	52.35	48.79
2	62.07	111.41	1384	93.62	65.50	55.92	51.49
3	55.53	66.59	93.62	1383	104.69	62.94	56.05
4	51.66	58.56	65.50	104.69	2319	80.81	61.98
5	47.51	52.35	55.92	62.94	80.81	1385	94.23
6	44.86	48.79	51.49	56.05	61.98	94.93	1393

- Note 1. The electrodes are equispaced with a separation of 'a' metres.
 2. That potential 5 - 6 = potential 6 - 5 etc.
 3. The values are in volts
 4. The principle diagonal of the matrix contains the values of potential close to the current electrodes.
 5. The values for 41 source terms are shown in a 41 x 41 matrix in the results presented in Appendix C.

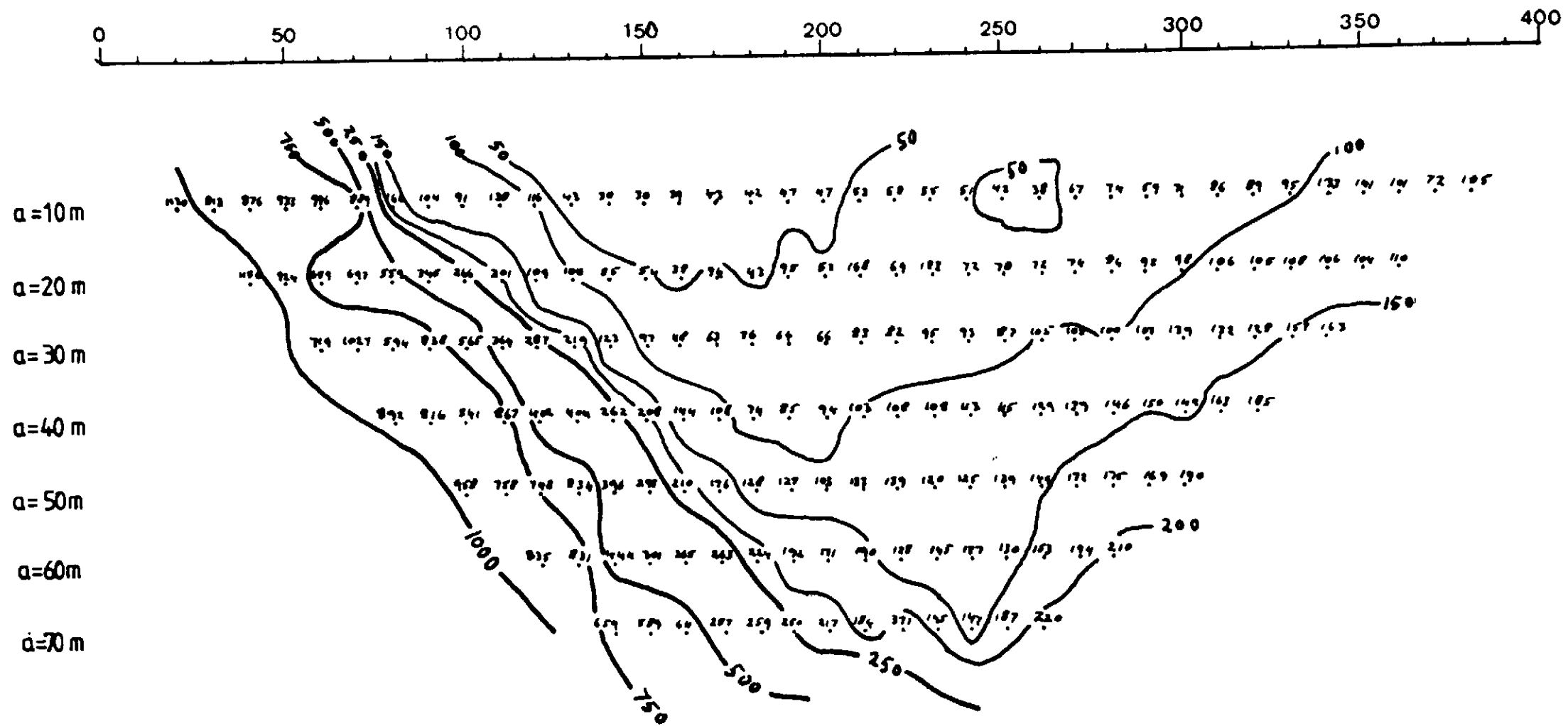


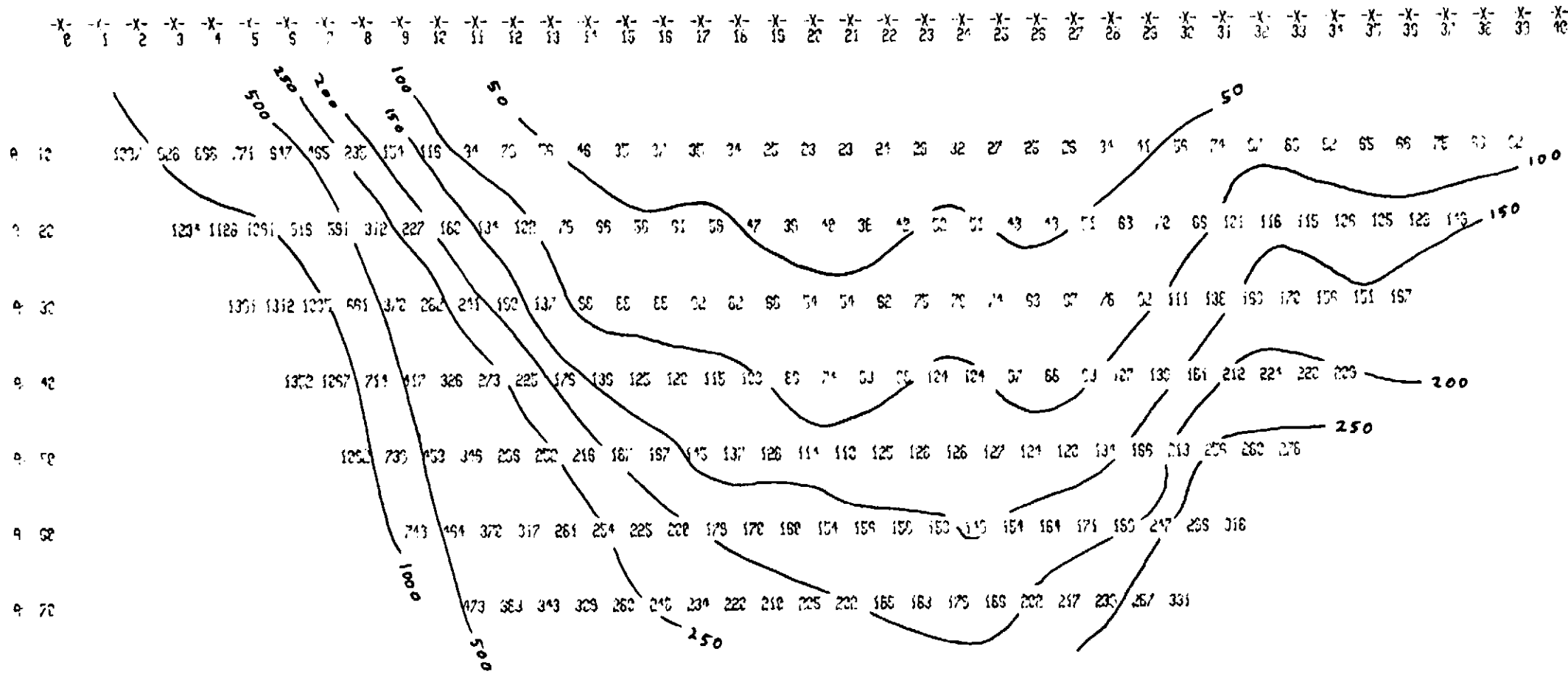
Figure 4-9 Resistivity profile section - Area A

RESISTIVITY PROFILE SECTION

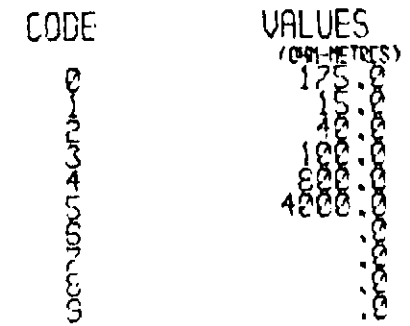
Calculated from the model resistivity distribution shown below

ELECTRODE POSITIONS

10 METRES APART



MODEL RESISTIVITY DISTRIBUTION



DEPTHS (METRES)

CODED RESISTIVITY DISTRIBUTION

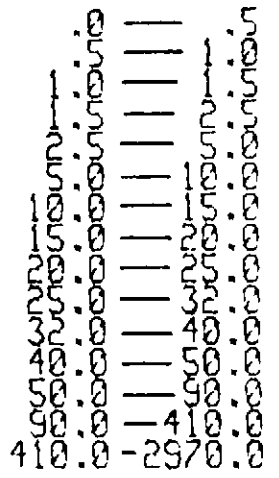
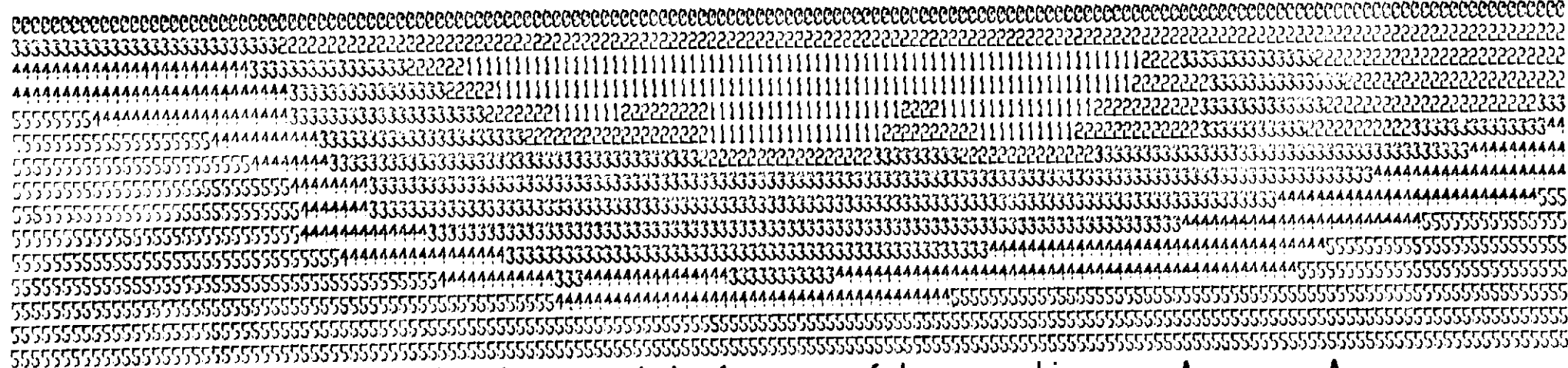


Figure 4-10 Resistivity model for profile section - Area A

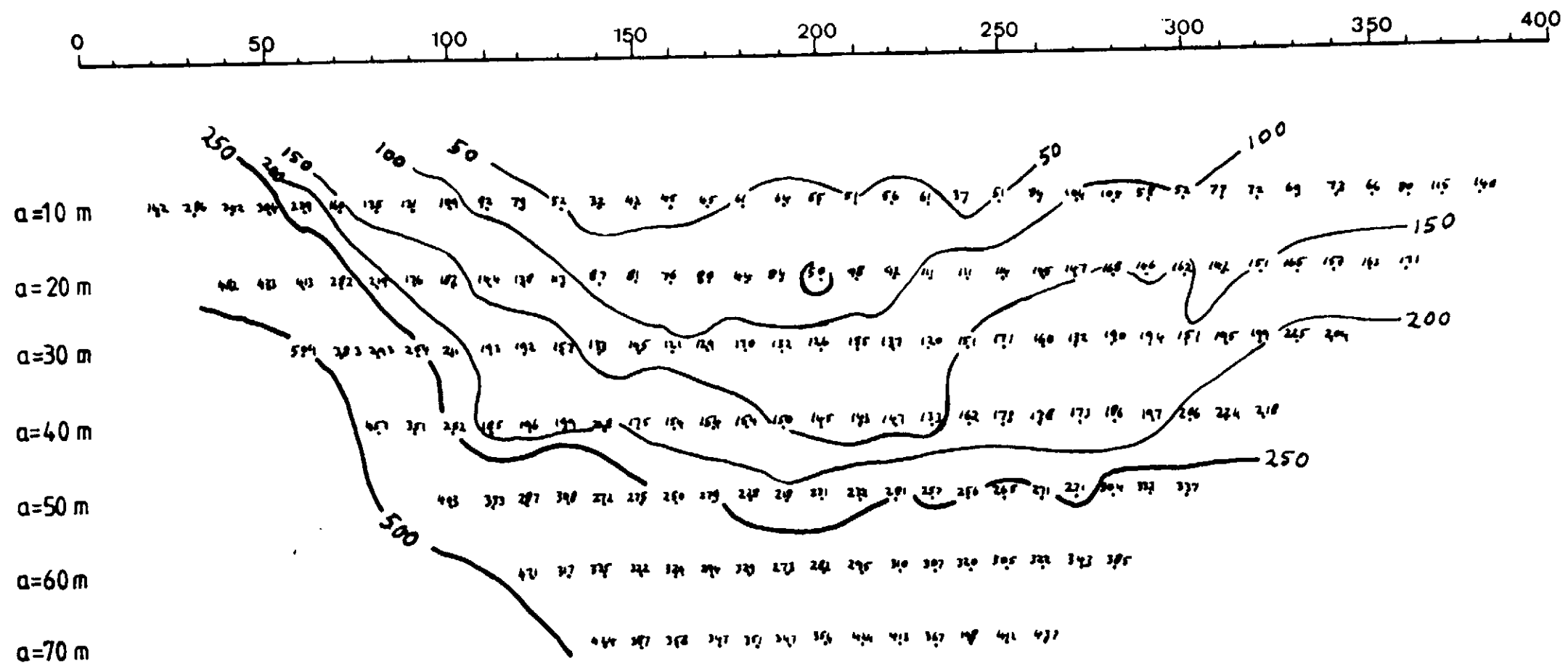


Figure 4-11 Resistivity profile section — D

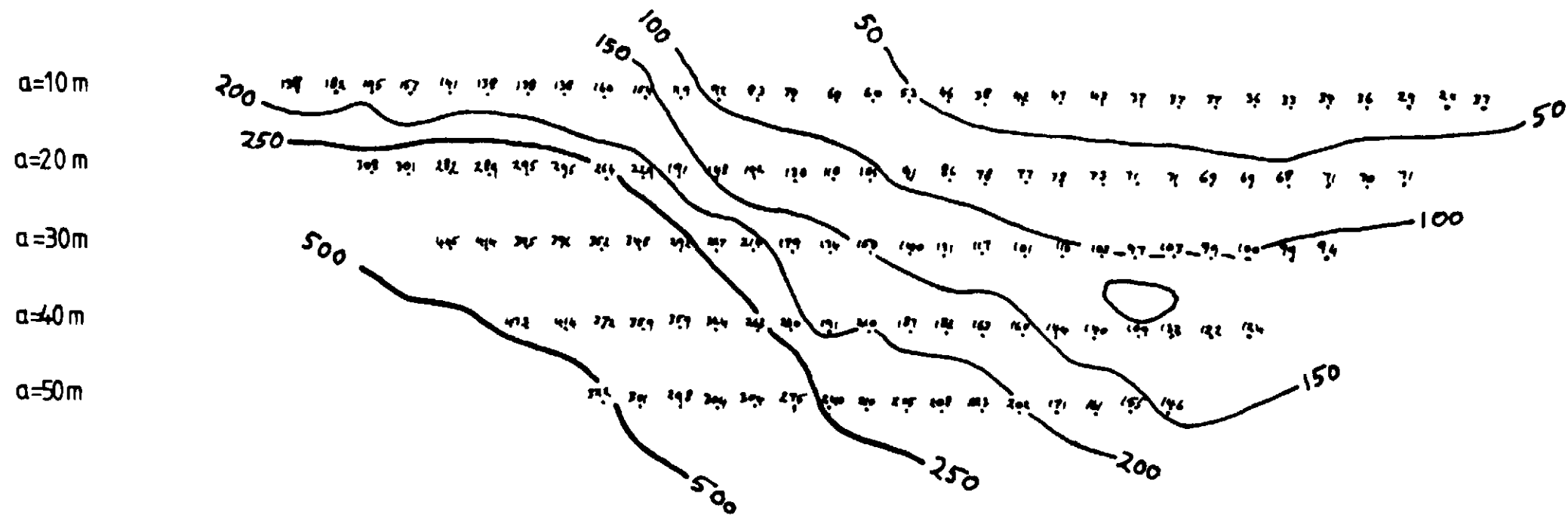


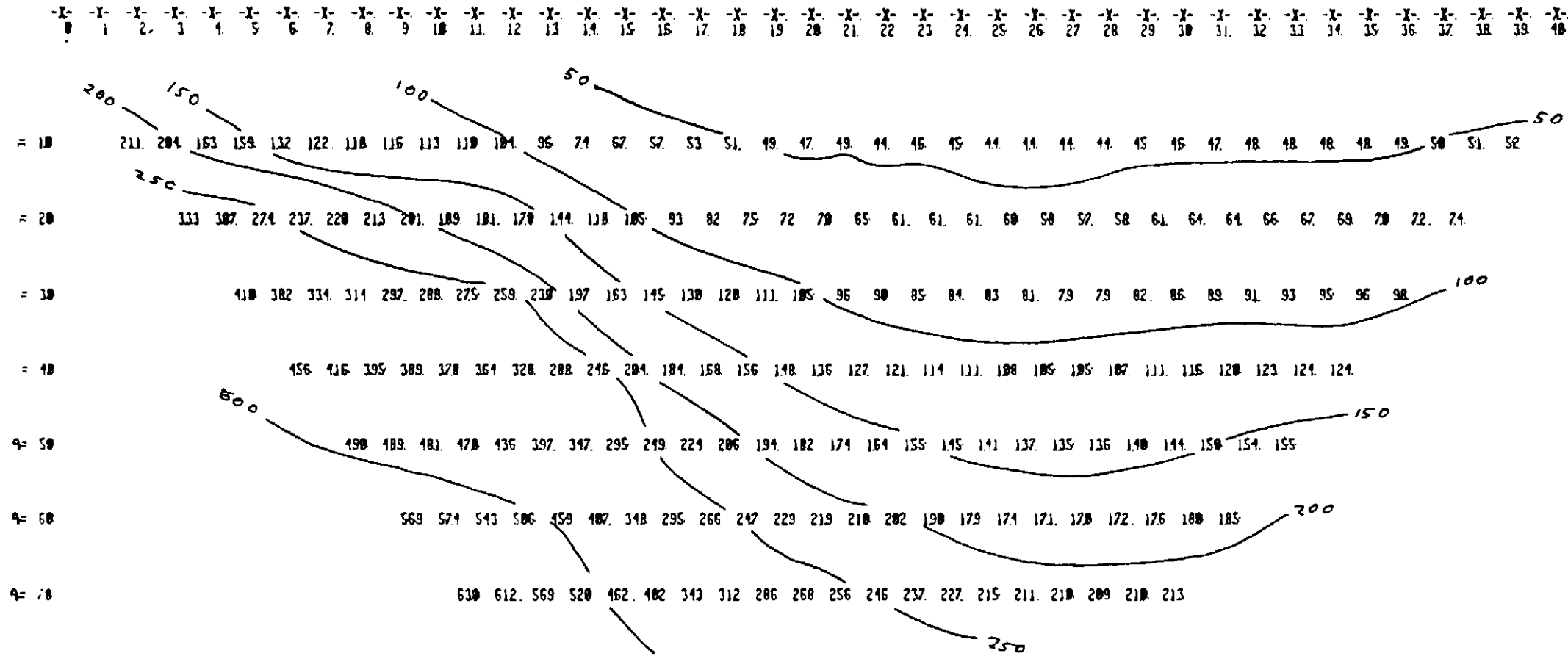
Figure 4-13 Resistivity profile section Area B

RESISTIVITY PROFILE SECTION

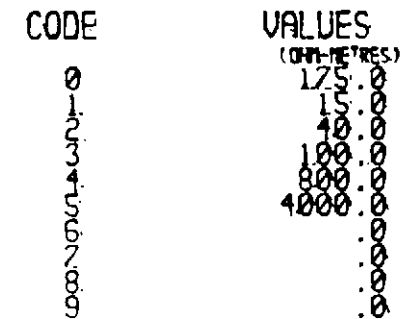
Calculated from the model resistivity distribution shown below

ELECTRODE POSITIONS

10 METRES APART



MODEL RESISTIVITY DISTRIBUTION



DEPTHS (METRES)

CODED RESISTIVITY DISTRIBUTION

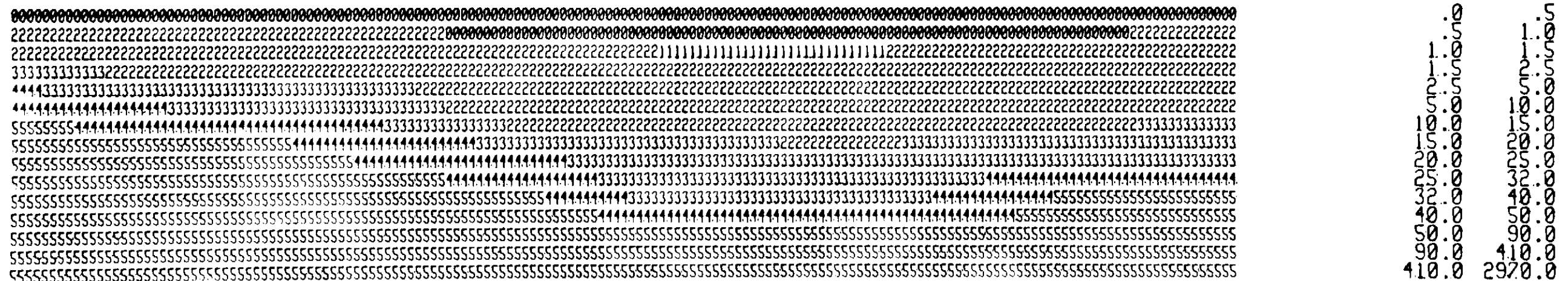


Figure -4-14 Resistivity model for profile section - B

three profile sections in terms of the resistivities shown in Table 4.3. The best results are shown in Figures 4.10, 4.12 and 4.14. This graphical output gives a good impression of the extent of the weathering basins in each case. The results are also further used in Section 6.2.

Without the benefit of the computed model sections, the resistivity profile section provides a good qualitative impression of the depth of weathering which is a significant improvement upon a single profile line, or a number of soundings, the interpretation of which would be highly suspect over such an area.

Summary.

The resistivity profile section method is a useful extension of conventional resistivity techniques and is particularly suitable to the basement weathering environment where the resistivity varies extensively both laterally and vertically.

A new method of collecting the required profile data has been described. Although this has had only limited trials at present, it seems that a considerable improvement in the quality of field data can be achieved using this method.

EM techniques could also be possibly used to collect resistivity profile section data. The EM 34-3 would appear to be well suited to the task, however no trials have been carried out with this equipment.

The major interpretational advance that has been achieved is the ability to model the resistivity profile section in terms of an inhomogeneous 2D resistivity distribution. This advance means that the collection of the extra field data is worthwhile, whereas possibly before, it was not. The algorithm presented in Appendix C represents a versatile interpretational method. In Figures 4.15 and 4.16, the profile results produced over an area of near surface lateral inhomogeneity are presented to demonstrate the potential that the algorithm has to improve understanding of the apparent resistivity response to a given resistivity distribution.

One run of the program on a fast computer such as the CDC 7600 requires 60 seconds. Therefore it is not reasonable to use such a model to calculate the response for a single profile line. However,

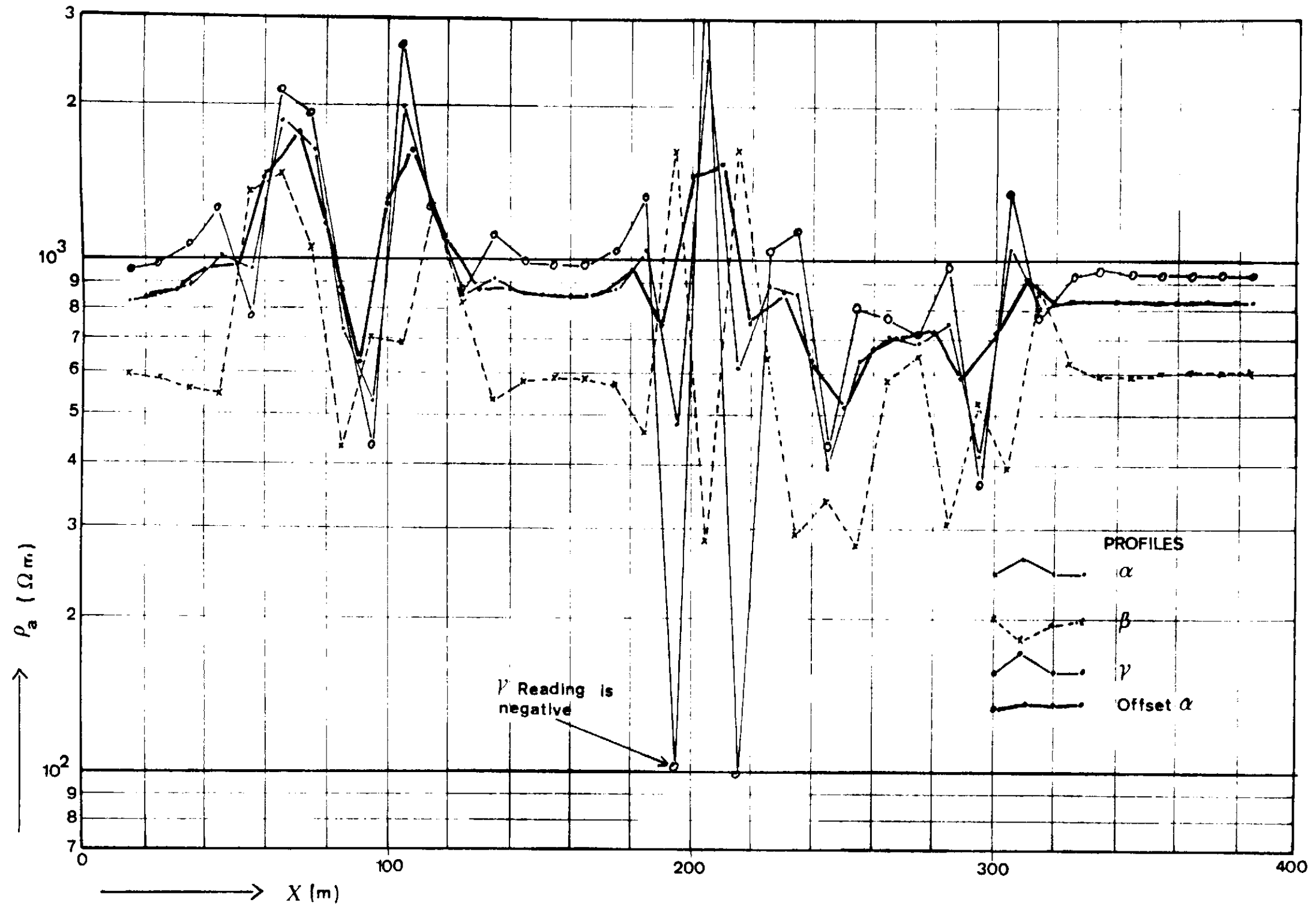


Figure 4-15 Tripotential profile data produced by resistivity distribution shown in Figure 4-16

it is envisaged that a limited library of such solutions could be built up and an extrapolation of field data between these models used in the field.

4.5 Seismic Refraction Technique.

General.

The seismic refraction investigation technique may be used to delineate areas within the earth which have different seismic velocities. The different velocities may then be associated with rock types, either by comparing the seismic section with local borehole control, or by laboratory studies of rock samples.

The basic technique consists of generating seismic waves in a controlled manner, and then measuring the time taken for these waves to reach a line of geophones. A plot of travel time against distance of the geophone from the source (T-X graph) is then prepared. Straight line segments on the T-X graph may then be interpreted in terms of velocities and depths.

The seismic refraction method is described in detail by Telford et al (1976), and a number of engineering geology applications have been described in the literature (Allen, 1960, Burke, 1967). Depth to bedrock surveys have been successfully carried out in many areas and it is this type of application that most resembles the granite weathering problem. The plus-minus method of interpretation (Hagedorn, 1959; Cummings, 1979) is most often used to analyse the data from this type of investigation, where an undulating bedrock is overlain by variable depths of less compacted, lower velocity material.

The seismic refraction interpretation is constrained by a number of theoretical limitations. It is of use to summarise these before proceeding to a description of the field technique and the results obtained.

In the simplest form of interpretation the ground is assumed to consist of homogeneous and isotropic layers, which have a uniform seismic velocity, separated by planar horizontal or dipping interfaces. This model seismic section produces a straight line segmented T-X graph.

Layers which have a lower seismic velocity, lying beneath layers with a higher seismic velocity cannot be resolved and the presence of such layers leads to considerable error in interpreted depths. This difficulty is known as the blind layer problem.

Thin layers of material with seismic velocity intermediate between two thicker layers, and lying between these layers are suppressed on the T-X graph, and an interpretation that does not take account of such

layers also produces incorrect depth estimates. This difficulty is known as the hidden layer problem.

A gradational increase in velocity throughout a layer can be resolved. However, the layer must extend laterally over the length of the investigation. If a depth of 30m is being investigated, then the maximum source to geophone distance will be approximately 300m, and uniformity over this distance is required.

A large number of shallow seismic investigations were carried out in the North of Nigeria, principally for dam site investigation work, although, as will be described below, some refraction lines were carried out for hydrogeological purposes. A six channel Bison signal enhancement seismograph was used for the majority of this work. Due to the administration difficulties associated with using explosives on a large number of small, highly dispersed, surveys, a hammer was used as the energy source. The signal enhancement facility was used to stack successive signals until a satisfactory seismic signal was obtained. A chart recorder was then used to produce a permanent copy of the signal.

The hammer source proved sufficient to generate a satisfactory signal at distances between 50 and 150m from the source. Depending upon the source distance and the subsurface material, a maximum number of 20 hammer blows was most often required. This maximum distance was insufficient to receive refracted waves from the base of a weathered trough some 40m deep. For studies of this type overlapping profiles were obtained with source positions every 50 or 75m, the overlapping sections of the T-X plot were then used to complete a reversed refraction line of up to 300m length (see Appendix D4 and D5).

Weathering Grade Seismic Velocities.

The limitations of the refraction technique have been briefly discussed above, and it is evident from this discussion and that presented in section three, that the weathering environment does not often produce uniform layers which may be simply interpreted. However, in general, four velocity layers may be recognised, although the interface between them is rarely sharp (see example 2). Table 4.5 lists the seismic velocities that may be assigned to the different grades of weathering.

Table 4.5 Seismic velocities of weathering grades.

Weathering Grade	Seismic Velocity (m/ms)	Notes
Soil	0.25-0.8	
VI		
V	0.5 - 2.0	Velocity may be higher if saturated
IV		
III	1.5 - 4.0	
II	3.0 - 5.0	Velocity depends upon degree of fracturing.
I	4.0 - 6.0	

A distinct velocity contrast is often found between grades II and III weathering. The disaggregation caused by micro-fracturing of the crystal fabric, the increase in velocity and the alteration of clay minerals, all act to reduce the seismic velocity. In areas where grades II, III and IV weathering are very thin or absent, such as in the area shown by Plate 3.20, the interface is abrupt and produces an easily identified range of slope on the T-X graph. The plus-minus method may then be used to obtain the depths to fresh rock along the profile line (as in example 1).

In areas of deeper weathering, such as those shown in Plates 3.17, 3.18 and 3.19, the interfaces between the various grades are not abrupt and do not therefore give rise to straight line segments on the T-X graph; instead, a continuous curve is produced. It is not possible to interpret this data if the rate of change of velocity with depth is not constant over the profile line. The interface between grade II and grade III weathering can be seen in core box No 4 in Plate 3.18. This interface lies at approximately 23.5m depth. Above this depth the changes are gradational.

Seismic Refraction Results.

Examples of refraction data from four localities are presented below. In each case, borehole evidence is available to gauge the accuracy

of the seismic interpretation, where an interpretation has been attempted. The examples are presented in order of increasing depth of weathering. The travel time data is presented in Appendix D.

Example 1. This data was obtained as a part of a long profile line, with shot (hammer) points every 50m. Plate 4.1 shows the core taken from an investigation hole drilled into this line.

The travel time data, the \bar{T} -X data (Hagedorn, 1959) and the interpreted seismic section are shown in Figure 4.17.

In this example, the boundary between grade II and grade III material can be seen approximately at 3.2m in Plate 4.1. Grade II weathering continues to a depth of approximately 9.2m with zones of grade I material separated from the completely unaltered rock by a number of subhorizontal fractures where grade III weathering has occurred. The lack of an absolutely clear boundary is demonstrated by the considerable scatter of the points shown on the \bar{T} -X plot.

The plus-minus interpretation shows a depth of approximately four metres to the main refractor at the borehole site. While this figure is a reasonable measure of the depth to Grade II weathering it should be noted that important fractures which would contain water, occur below this level.

Example 2. This data was obtained over a dry river bed. The geophones were placed in clay to hold them firm, just above the water table in the saturated coarse sand alluvium. The travel time data is presented in Appendix D 2, and Figure 4.18 shows the \bar{T} -X data, and the depth interpretation. Borehole investigation proved this profile to be accurate within 5'. A varying depth of coarse sand alluvium combined with grade IV and V weathered material was found to have a velocity varying between 1.3 and 1.7 m/ms. Grade III weathered material, encountered in the boreholes as the first horizon from which core would be taken, was found to have a velocity of 3.8m/ms. The travel time distance plot shows segments representing a fourth velocity layer at approximately 6m/ms although it was not possible to obtain a depth for this layer. A borehole in the centre of the section was drilled to 35m depth without encountering grade I material.

The accuracy of this profile was possible only because the top layer of coarse alluvium was homogeneous, completely unlike the top

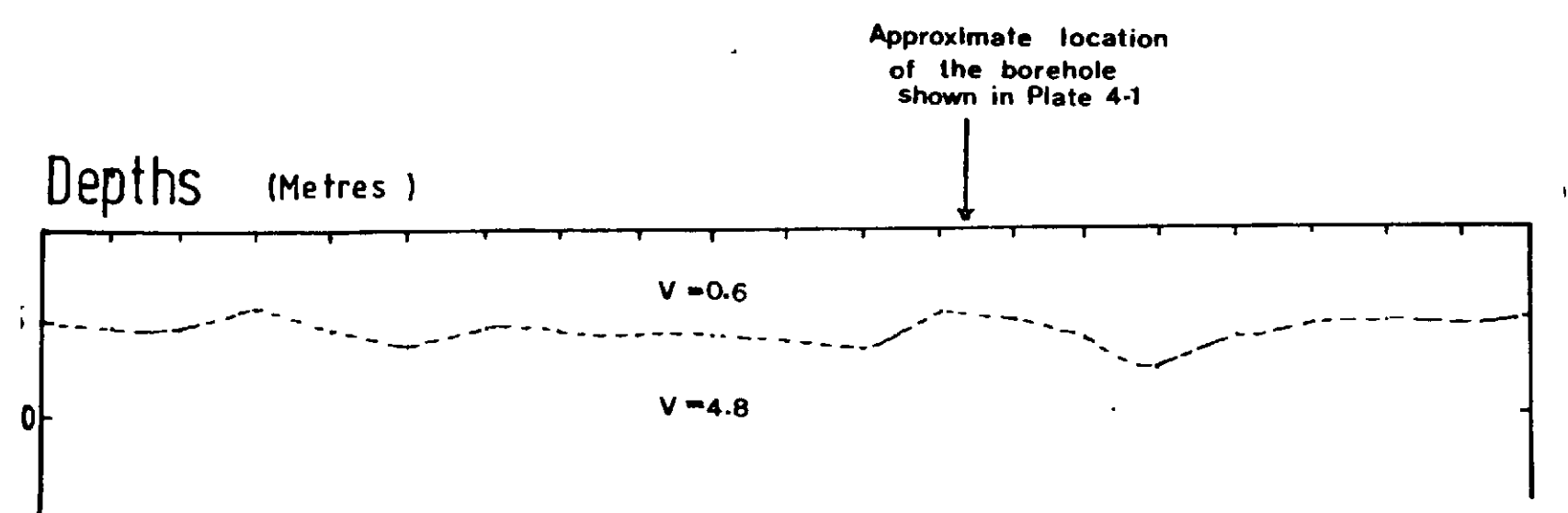
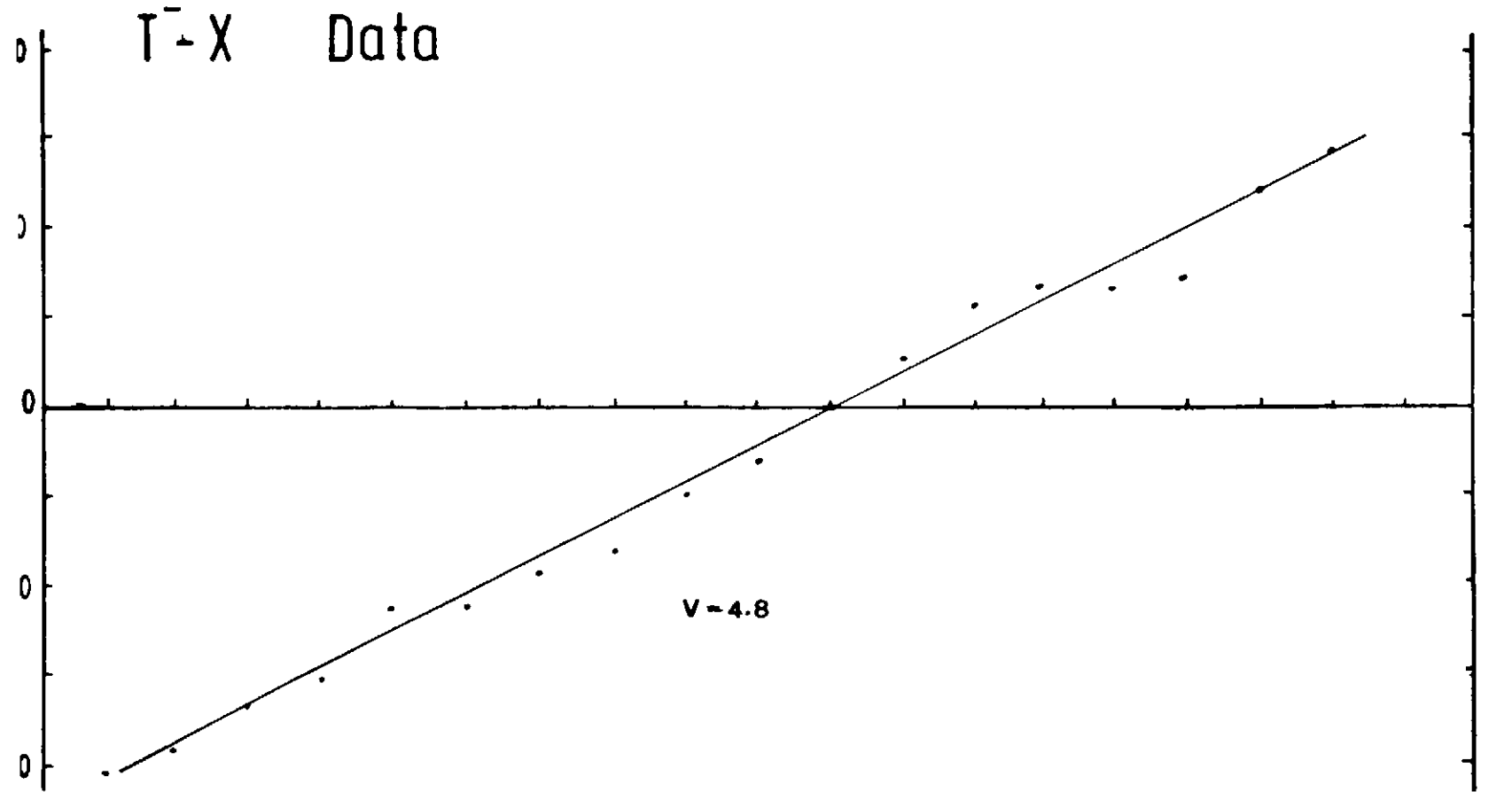
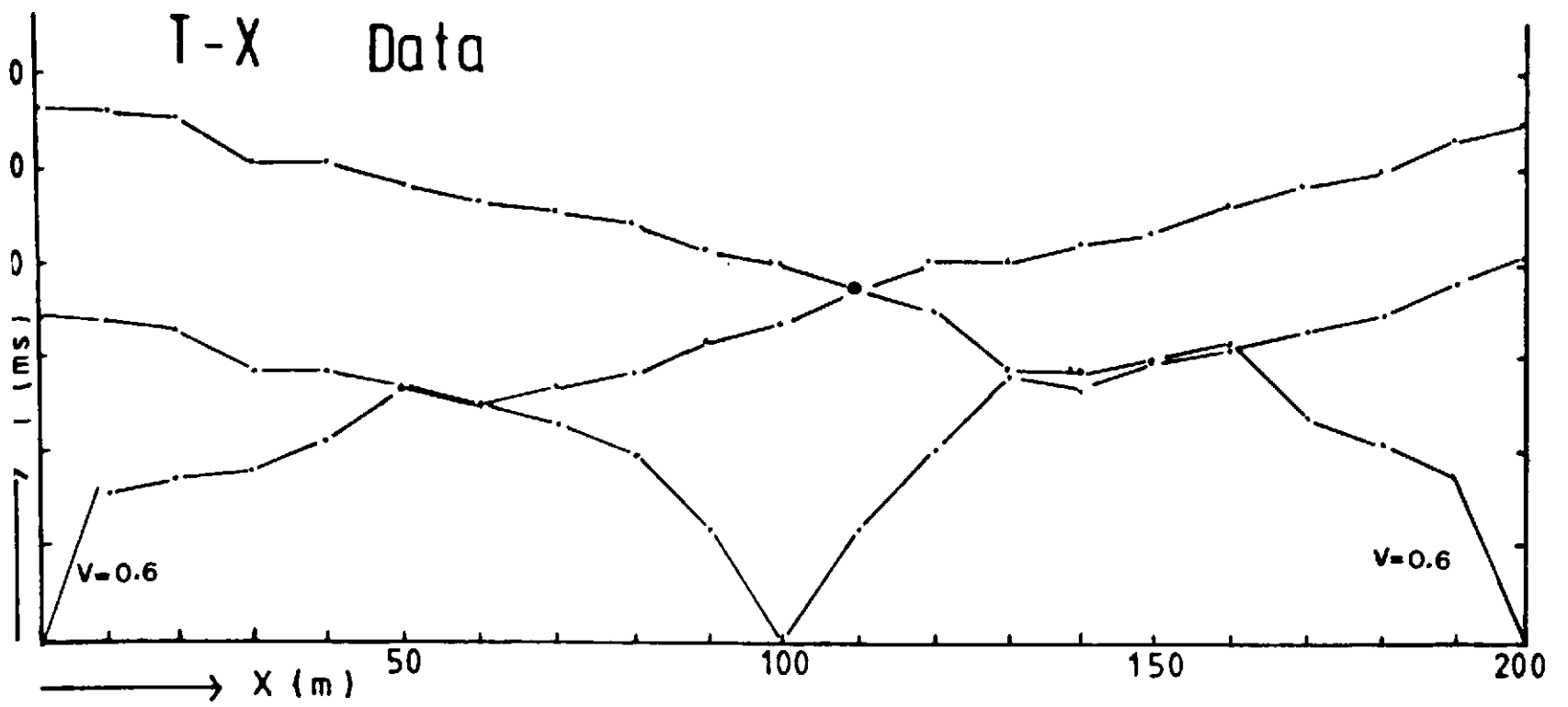


Figure 4-17 Seismic refraction profile 1

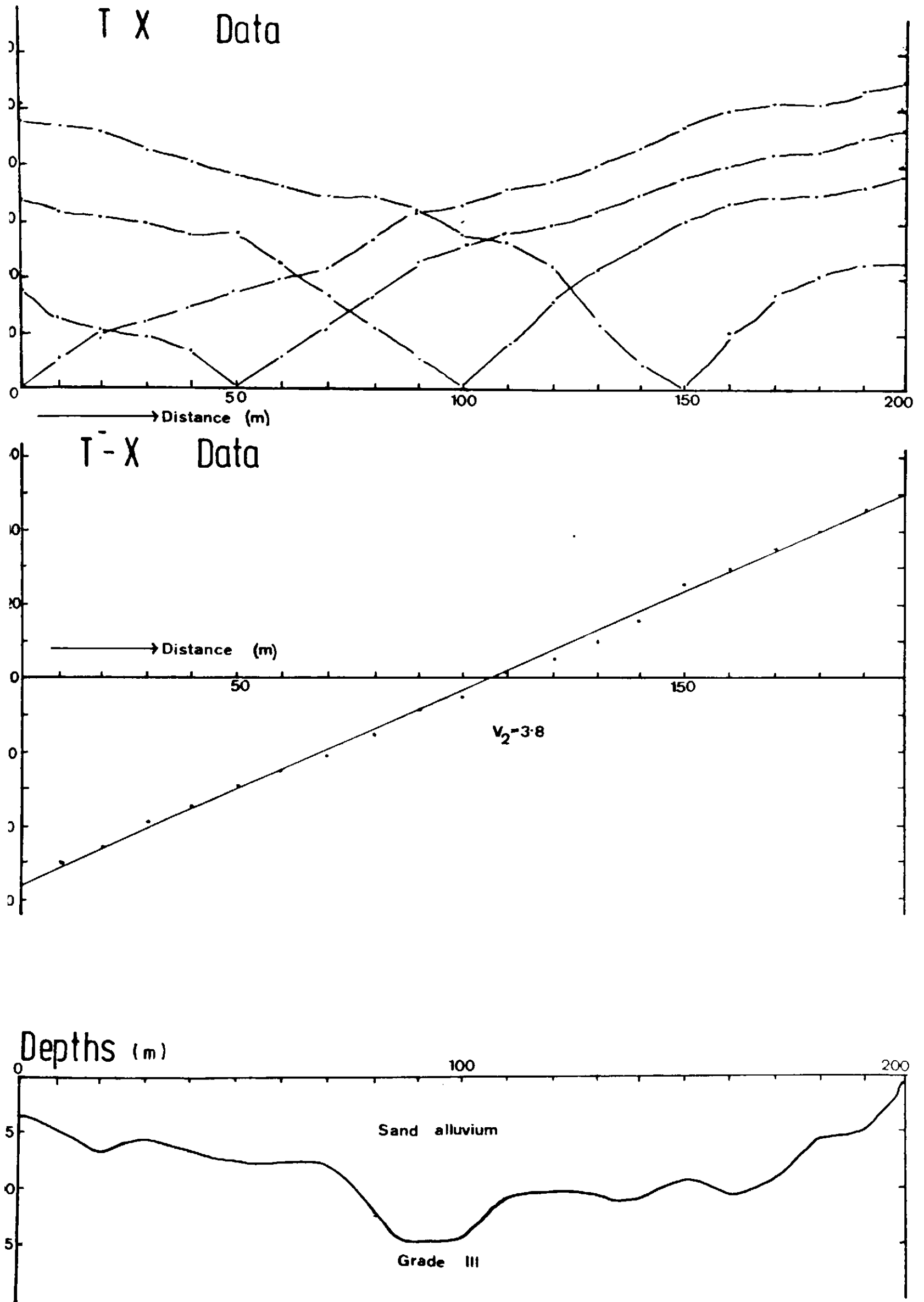


Figure 4-18 Seismic refraction profile 2

weathered layer. However, the data is presented here as an example of the use of the technique under good conditions. The data in example 3 indicates the problems caused by a deep low velocity layer at the surface.

Example 3. In contrast to the data shown in the previous example, this data has been taken from a profile carried out over the borehole section shown in Plates 3.18 and 3.19. The water table in this borehole was recorded at 19m and the majority of the material above the water table can be seen to be loose. The thick low velocity layer produced by this dry grade IV, V and VI weathering, and the considerable variability within the zone has obscured any arrivals from lower refractors, although it is doubtful from the plates whether a clear refractor exists in this situation.

The T-X data is listed in Appendix 4.3 and the travel time distance plot is shown in Figure 4.19. From the interpretation which was possible from this data set, it was found that the low velocity layer was some 5 to 8 metres thick, overlying material with a velocity of 2.1m/ms.

Example 4. Despite the difficulty encountered with the interpretation of the data from the previous example, it was thought probable that seismic refraction represents one of the few methods available from which an estimate of the volume of material occupied by grade III and IV material may be made. For this reason, a refraction profile was carried out using a 5m geophone separation over parts of deep weathering areas A and B. The profiles were along the same lines as those of the resistivity profile sections shown in Figures 4.9 and 4.11.

The travel time data for these two profiles are listed in Appendices D 4 and D 5 respectively.

Although it was possible to complete the travel time data set for deep weathering area A, it was not possible to interpret the data in terms of a coherent seismic section. Borehole 10 in Figure 3.4 passes through this section and encountered grade II and III weathering to a depth of 60m with no well defined interface present throughout the section. By contrast, the data set for deep weathering area B was more readily interpretable, and the data is presented in Figure 4.20. It is significant that the samples from this borehole, shown in Plate 3.16 show a very sharp interface between grade II and grade III weathering, and it is the presence of this interface that has given rise to the straight



Plate 4.1 Investigation borehole core in deep weathering area C.

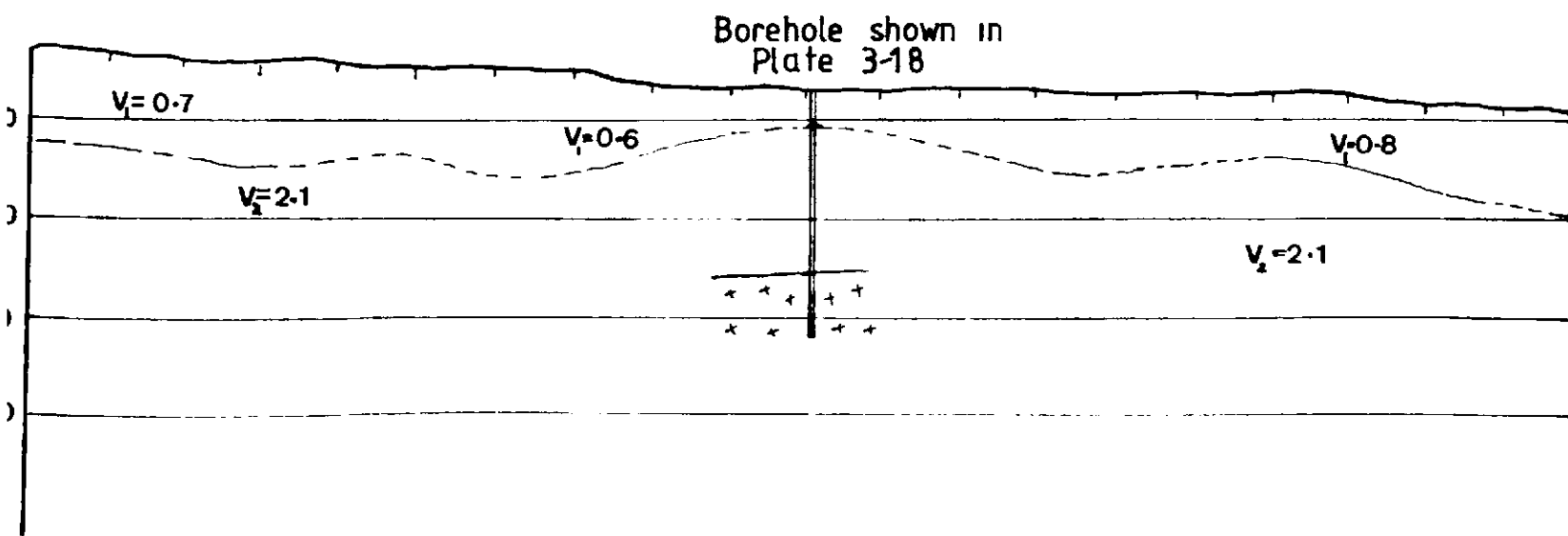
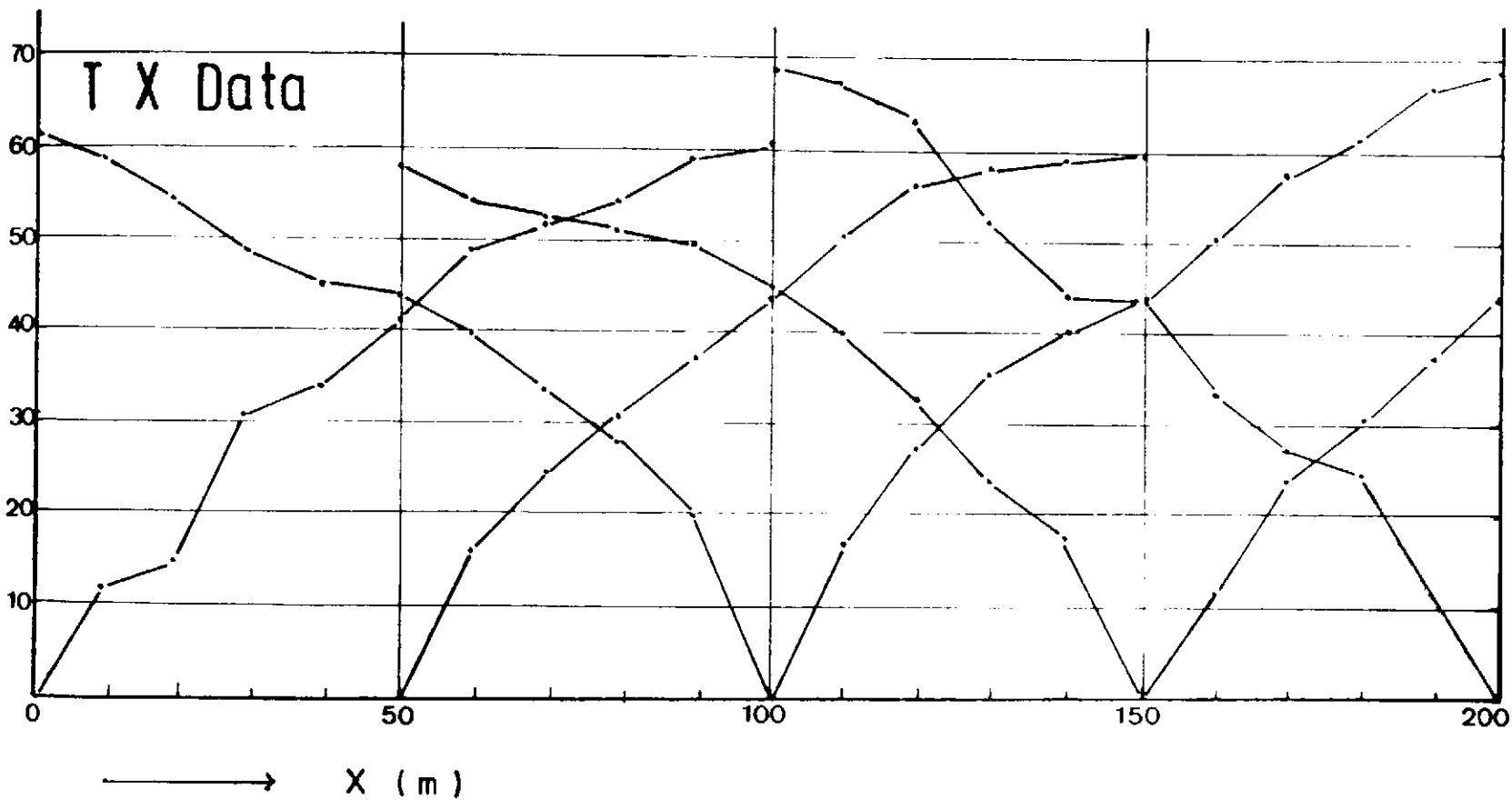
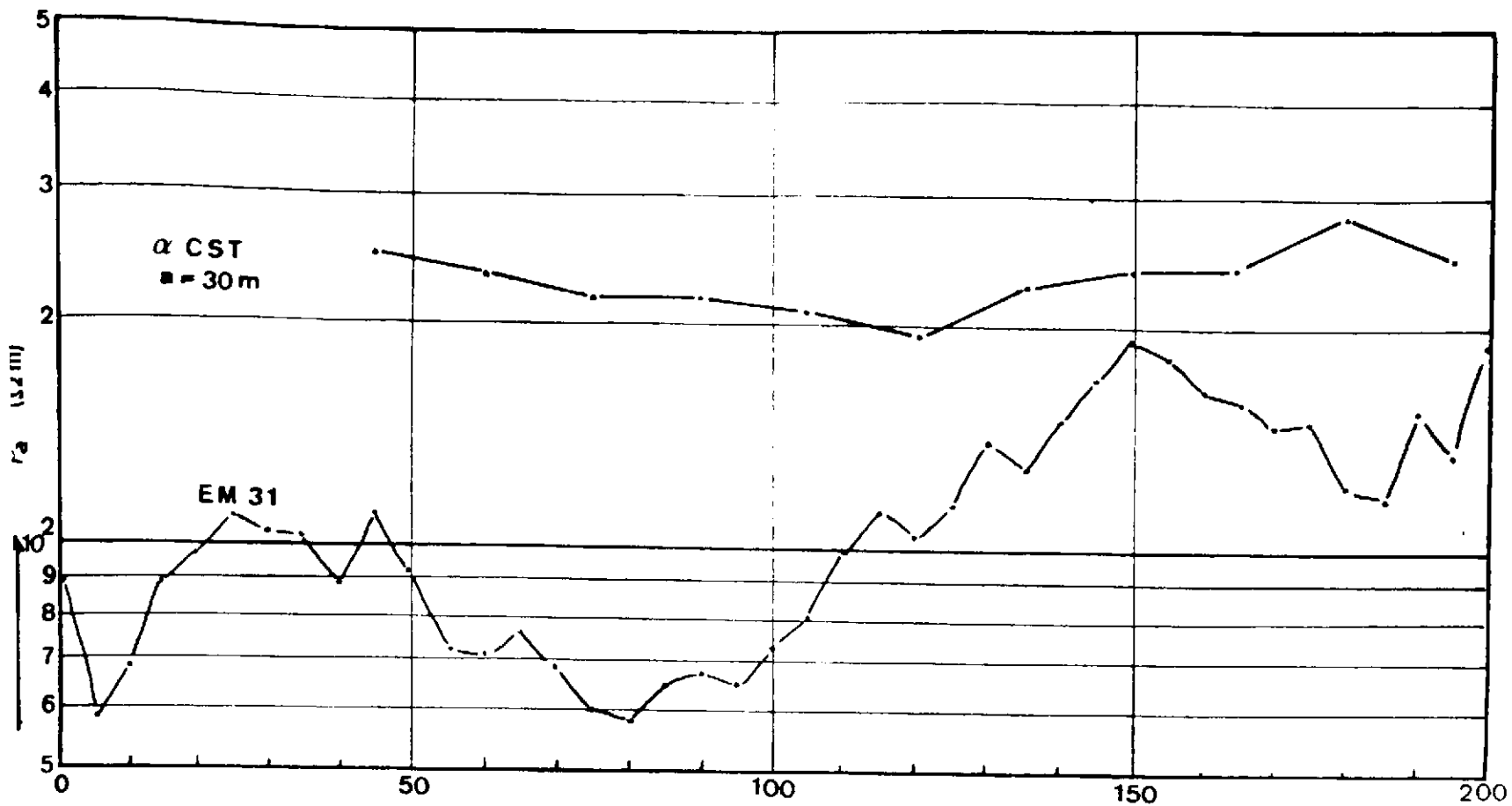


Figure 4-19

Seismic refraction profile 3

Showing apparent resistivity profile results for comparison

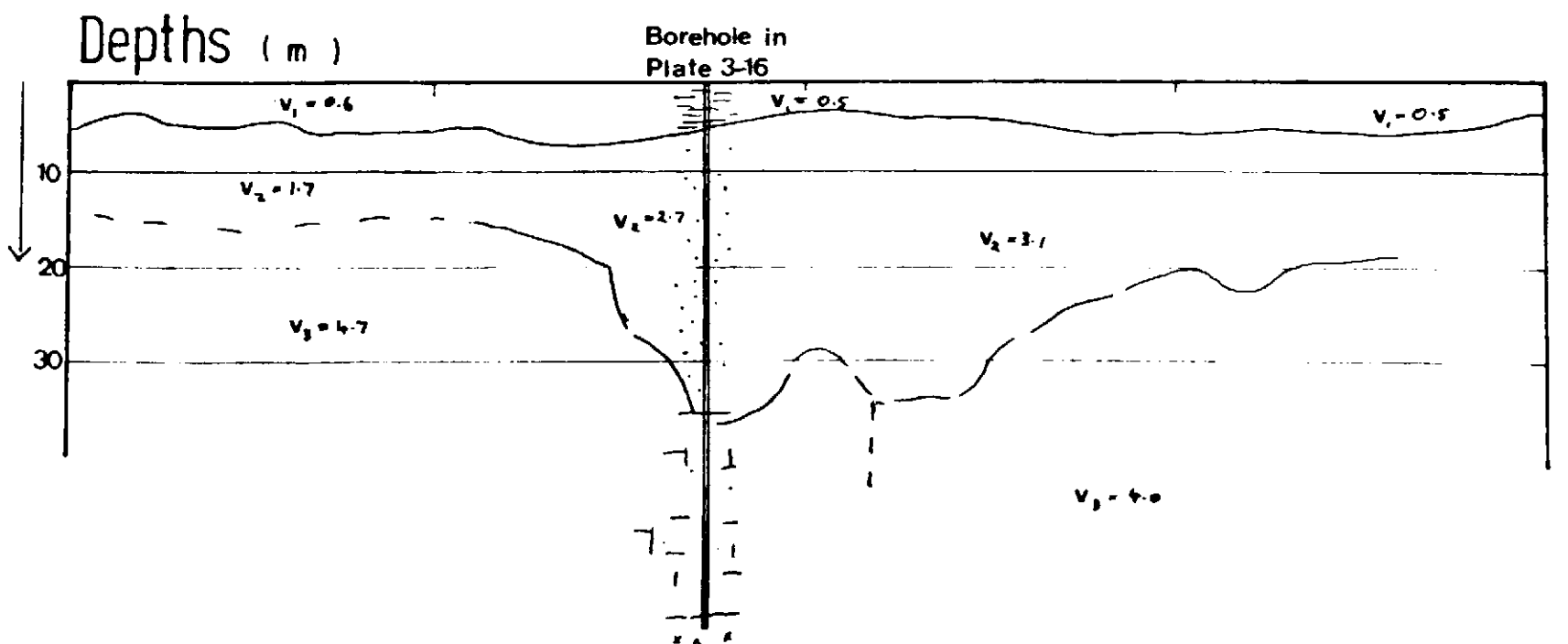
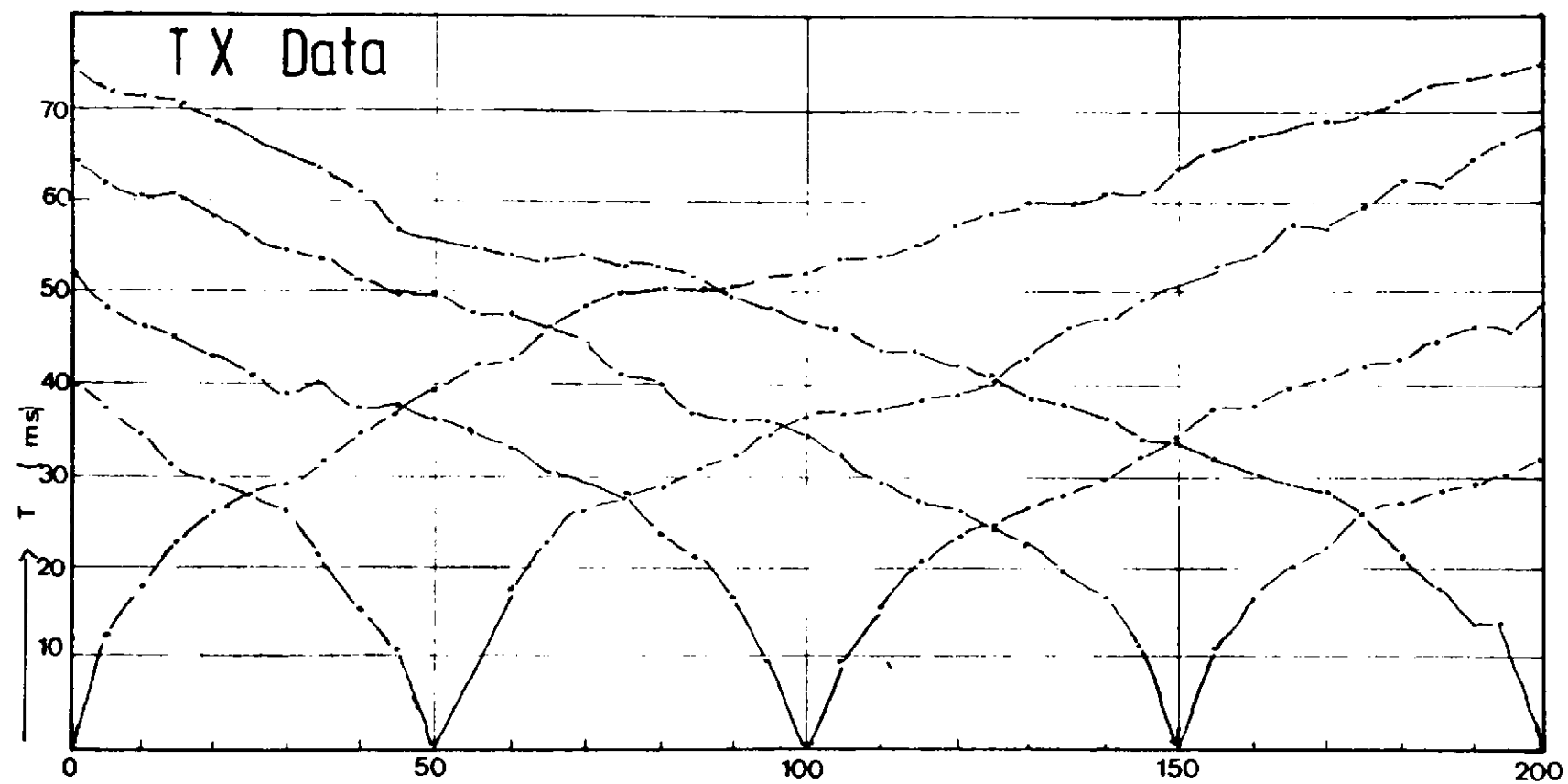
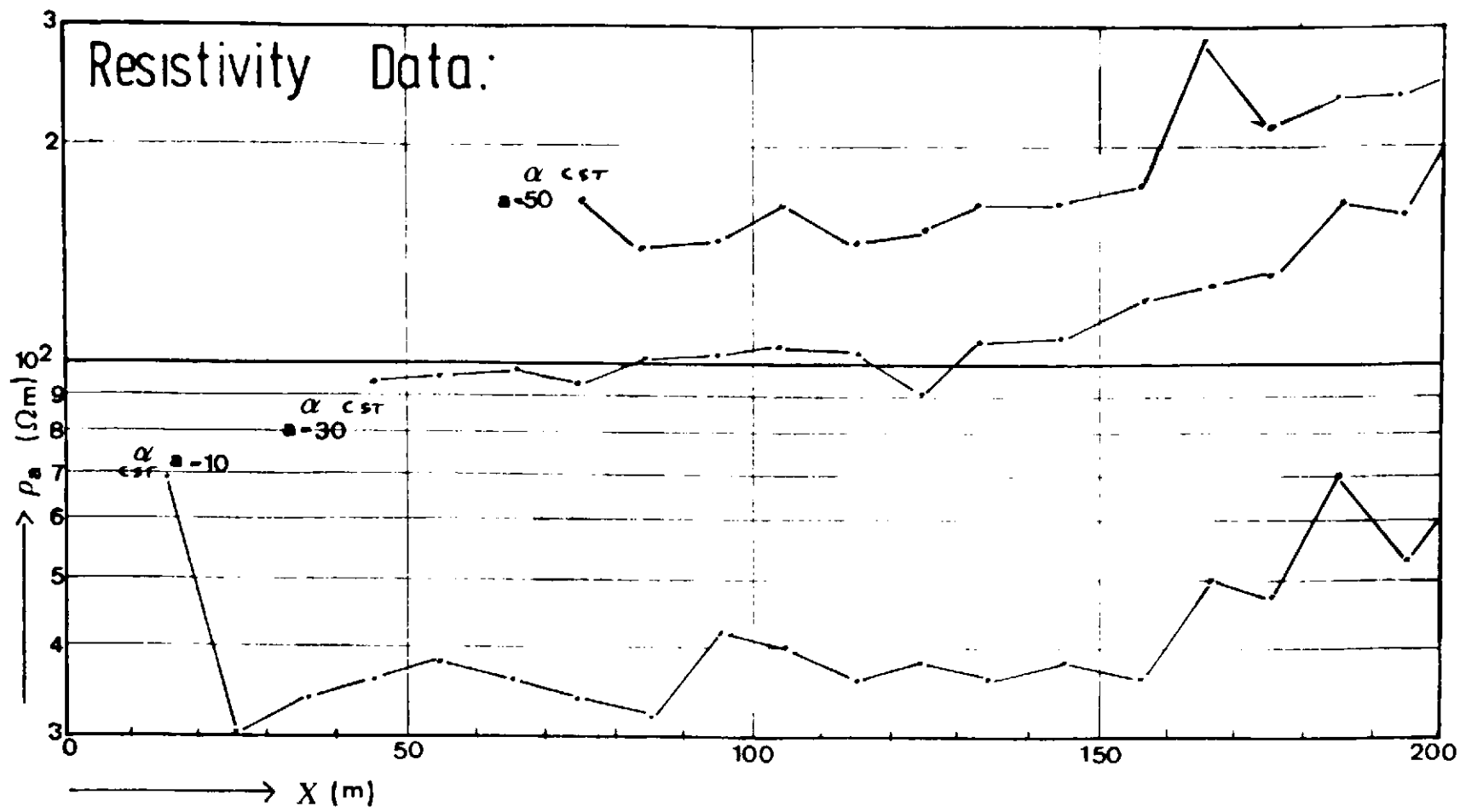


Figure 4-20 Seismic refraction profile 4

line portions on the T-X graph.

The interpretation of the travel time data shows that the grade III material has a velocity varying between 2.7 and 3.1 m/ms, with the grade II material showing a velocity variation between 4.0 and 4.7 m/ms. The higher velocity may represent grade I material. The three layer plus-minus interpretation gave depths to grade II rock in reasonable agreement with the borehole results.

Discussion.

A number of relevant points arise from a consideration of the examples described above, viz.

1) It is evident that the lateral and horizontal variations within the weathering profiles are as difficult to resolve using the seismic method as the resistivity sounding method. In particular, the lack of definite interfaces within the profile, make a layered velocity interpretation impossible, even in terms of an undulating boundary. While methods exist to model these conditions (such as ray tracing), they have not been applied to small scale problems such as those under consideration.

2) To investigate areas of deep weathering, it is necessary to use explosives to produce a sufficient seismic signal at distances up to 400m. The use of explosions would also overcome the problem of the very low velocity top soil, which can absorb a large proportion of the hammer blow energy. Signal enhancement combined with the use of detonators placed 15-20 cms beneath the soil is also a possible alternative.

3) With the exception of the detailed profile described in example 4 from deep weathering area B, the seismic method was not successful in providing data on the thickness of the grade II, III and IV material. It is possible that the use of more sophisticated techniques, using explosives, signal recording and later digital analysis would produce more satisfactory results, although such an investigation represents a vastly increased investment in resources and interpretational effort.

4.6 Summary.

In the introduction to this section it was stated that the use of geophysics was necessary for two purposes, viz,

- 1) To establish the presence of deep weathering.
- 2) To quantify the volume of grade III and IV material present at depth.

It is of use therefore to summarise the extent to which these two objectives have been satisfied.

Both electrical resistivities and seismic velocities have been successfully assigned to each of the weathering grades listed in Section 3.4, and these are shown in Tables 4.2 and 4.5 respectively. However, a basic difficulty to both the electrical resistivity and the seismic refraction techniques is the lack of a clearly defined interface, or interfaces, between the various grades of weathering.

The electrical resistivity method, or a derivative of this method, may be used to very quickly establish the presence or absence of deep weathering. An electromagnetic survey using a one man portable EM31 can delineate areas where grade I material lies close to the surface. Within a few hours, data covering an area of a square kilometre can be produced. This reconnaissance survey can immediately satisfy the first of the two objectives, and in the situation where only a limited groundwater supply ($1\text{ m}^3/\text{hr}$) is required, it is not necessary to proceed to the second objective. It should be noted that the seismic method can equally well be used to establish the presence of near surface grade I material, and can in addition provide depths and velocities of this section. However, if the criteria is simply to establish areas where grade I material is not near surface, then the seismic method provides data which is not required and is in addition very much more time consuming to acquire.

The second objective is very much more difficult to satisfy and it should be said that there is no entirely satisfactory method available. While the resistivity technique provides information of a qualitative nature very rapidly, it is not possible in the field to produce accurate data representing the depth to which a borehole should be drilled. The use of the offset profiling technique and the preparation of resistivity profile sections overcomes many of the previously experienced difficulties with this method, such as noise due to near surface

inhomogeneity and distortions produced by deep lateral resistivity contrast. Furthermore, the availability of a computing algorithm to model resistivity profiles provides the possibility of discretising the profile section data into a realistic model which completely satisfies the second objective. However, the availability of the computing power required for this process is strictly limited and not yet at all available to field crews, although this restriction will probably be removed in the future. The preparation of resistivity profile sections is however not as time consuming as the preparation of seismic refraction sections covering the same area and with the use of a limited library of computed solutions it is considered that this method is the most effective available.

The seismic refraction method can in many instances be used to resolve the layering, if present, within the weathering profile. However, over comparatively narrow and deep troughs, the amount of data collation and interpretation required to resolve the layering begins to approach that required for the resistivity modelling. In addition the time required for the data collection is several times that for a resistivity profile section; the equipment required is substantially more complicated and prevalent to breakdown; and, lastly, the field data available as a travel-time distance plot may not be qualitatively interpreted in the same way that a resistivity profile section allows.

In the absence of resistivity profile sections, where resistivity profile data is available for only one separation, considerable ambiguity remains in the qualitative interpretation. Where an apparent resistivity of less than $60\Omega\text{m}$ occurs in a well defined trough, then a substantial ($>30\text{m}$) thickness of weathered material was found to be present in all the surveys carried out in Northern Nigeria. Therefore, if this value of apparent resistivity is used as a criteria for drilling (see also Section 6), the number of dry boreholes will be kept to a minimum. However, this method relies on the presence of substantial grade V and VI material, with well developed soil B horizons to provide low resistivity material which will combine to produce a low apparent resistivity. If this material has been removed by erosion in recent times, then there is the possibility that deep weathering, represented by thick grade III and IV material, exists which will not be located if all areas with an apparent resistivity of $>60\Omega\text{m}$ are discarded. It is necessary to carry out a full profile section to detect these areas.

5. AQUIFER GEOMETRY AND CHARACTERISTICS

Introduction.

The development of areas of deep weathering has been discussed in the third section of the thesis. The location of deep weathering zones using geophysical techniques has been described in Section 4. It is the purpose of this section to identify those parts of the weathering profile which may be considered as aquifers or aquicludes and to demonstrate as fully as possible the hydrogeological parameters associated with each part.

The identification of grades II, III and IV material as potential aquifers has been necessarily anticipated in previous sections. In the first part of this section, a more detailed description of the aquifer and its boundaries is given. The presence or absence of various grades of weathering may then be seen to give rise to confined or unconfined conditions, and also to lead to an identification of areas where recharge to the aquifer is possible.

In order to achieve an understanding of the aquifer response to recharge or abstraction, it is essential to obtain a borehole hydrograph. Unfortunately, due to the socio-economic conditions discussed in the general introduction, boreholes are invariably developed as abstraction sites, and no water level measurements are taken after the initial pump test; which itself is often unsatisfactory. In recognition of the deficiency of this type of data, water level measurements from deep weathering area A were collected for 14 months, at intervals which were as regular as possible. In addition, Kowal (Kowal + Kassam, 1978) has produced wet season hydrographs for three years from an area close to Samaru. These two sets of data represent the only groundwater hydrographs available to the author.

The hydrographs are all basically similar and indicate a number of distinct phases within the annual hydrological balance of the savanna. These phases are described and discussed in the second part of this section.

From the groundwater hydrograph in Bauchi, a small component of direct recharge is seen to occur early in the wet season, although the major recharge must occur by infiltration into the unconfined parts of the aquifer. The quantity of such indirect recharge is controlled by

the balance between rainfall and evapotranspiration in the soil zone.

The estimation of annual recharge is an important part of any hydrogeological study. In the savanna zone, and upon basement rocks, this estimate is particularly important as many of the weathering aquifers have only limited storage, probably only capable of supporting abstraction, in the absence of recharge, for one or two years.

In the third part of this section two methods of calculating recharge are described. The first method corresponds to the conventional analysis used in previous studies (Lloyd, 1966; Kowal + Knabbe, 1972). However, the results predicted by this analysis do not satisfactorily explain the observed conditions within the savanna, and for this reason a second method has been developed for this study.

Lastly in this section, the response of weathering zone aquifers to abstraction is assessed. Pump testing techniques are commonly used for this purpose, however, the pronounced lateral and vertical variations in hydraulic conductivity produce similar problems for pump test interpretation to those already described for the geophysical interpretation. The general methods of pump test interpretation are based upon analytical solutions to the equations describing laminar flow in an aquifer of constant depth and possessing intergranular porosity. The weathering aquifers are not of a constant depth, and more significantly, the porosity varies between predominantly fracture controlled in grade II weathering to predominantly intergranular controlled in grade IV weathering. For these reasons, the general methods of pump test interpretation are not applicable to this environment.

The combination of fracture and intergranular controlled hydraulic conductivity produces a characteristic drawdown response. Several examples of this response are described and discussed.

5.1 Description of the aquifer.

General.

The following discussion refers in general terms to any area of basement where the progression of weathering grades can be recognised. Recent evidence (Ternan + Williams, 1979; Moore + Gribble, 1980) indicates that weathering of granites is occurring in temperate climates at the present time and that therefore, deep weathering features are not necessarily only relicts of weathering from previous warmer climatic periods. However, the area of particular reference remains that of the Nigerian savanna.

An aquifer has been defined (Brown, et al, 1975) as a water-bearing formation having a porous or fissured structure that permits water to move through it under ordinary field conditions. While it is evident that weathered material may permit water to move through it, the depth of weathering is nowhere sufficient to produce large uniform areas which can be considered as aquifers in the sense that a sedimentary sandstone forms an aquifer. As the weathering processes are primarily controlled by the presence of jointing or fracturing, it follows that the aquifers produced by weathering are only developed in zones where jointing or fracturing have a higher than normal incidence. Therefore, aquifers produced by weathering are normally developed as isolated zones, often completely hydraulically isolated from one another.

In general, only the topographically low areas contain aquifers. Although an inselberg may contain a complex and interconnecting set of exfoliation joints which give rise to perennial springs or seepages at the base of the inselberg, quantities of groundwater which are sufficient to support abstraction by pumping from boreholes, are only found in the low lying areas.

If the area of basement outcrop is considered as a whole, then probably in excess of 90% of the basement does not contain weathering sufficiently deep to form an aquifer. Over the majority of the area, the depth of weathering is either insufficient, or the water is lost as baseflow to ephemeral streams at the end of the dry season. The remaining 10% of the total area however, is composed of a large number of highly dispersed zones of deeper weathering which do form aquifers. It is these zones which are considered in detail below.

Weathering grade porosities.

The chemical reactions and physical processes by which fresh rock is altered to residual soil have been described in Section 3.3. The porosity of the profile increases from zero to approximately 50% in the 'A' horizon of the soil. This increase represents a complex interaction of pressure release jointing and chemical solution as described above. It is not possible to quantify the changes in porosity through the weathering grades exactly, mainly because it is difficult to obtain an undisturbed sample. However, the generalised changes are presented in Figure 5.1.

In grade II weathered material, the porosity is almost entirely represented by the open areas between joint faces. The intervening material still has zero porosity. In coarse grained rocks, the joints are usually widely spaced, but have a joint width which varies from <1mm to >50mm depending upon the depth of burial.

The porosity steadily increases upwards as first the micro-crystalline components of the matrix are removed, and then the major crystalline components. The effectiveness of this process is reflected in the very high silica content of the groundwater.

The rapid increase in porosity between the 'A' and 'B' soil horizons reflects the almost complete removal of clay from the soil 'A' horizon by leaching caused by the intense rainfall.

Weathering grade hydraulic conductivities.

It is possible to measure the weathering grade hydraulic conductivities by a number of indirect methods, such as packer testing (Pearson + Money, 1977). Dearman (1978) has collated all the published values and these have been included in Figure 5.1. There are a number of important implications arising from the hydraulic conductivity variations.

The hydraulic conductivity in the grade II weathered material is more anisotropic than that in the higher weathering zones. Brown (1975) reports a value of 60 m/day hydraulic conductivity for a rock containing a 1mm wide fracture occurring every metre (bulk porosity of 0.1%). However, this value is representative of conditions in the plane containing the fracturing. The hydraulic conductivity in a direction orthogonal to this plane would be zero. Considerable anisotropy in hydraulic conductivity will result from the orientation of fractures in

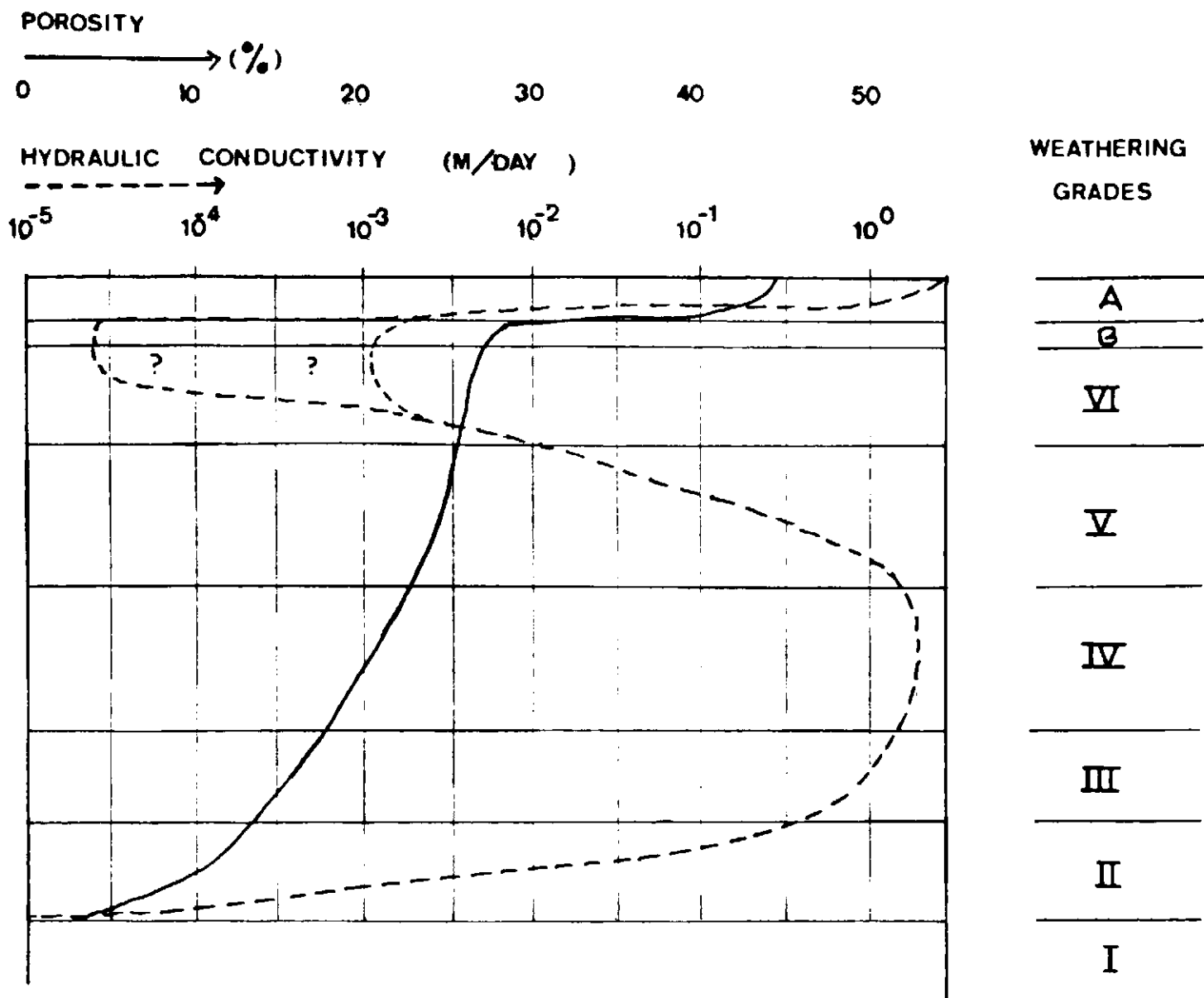


Figure 5-1 Conceptual model showing porosity and hydraulic conductivity changes with depth.

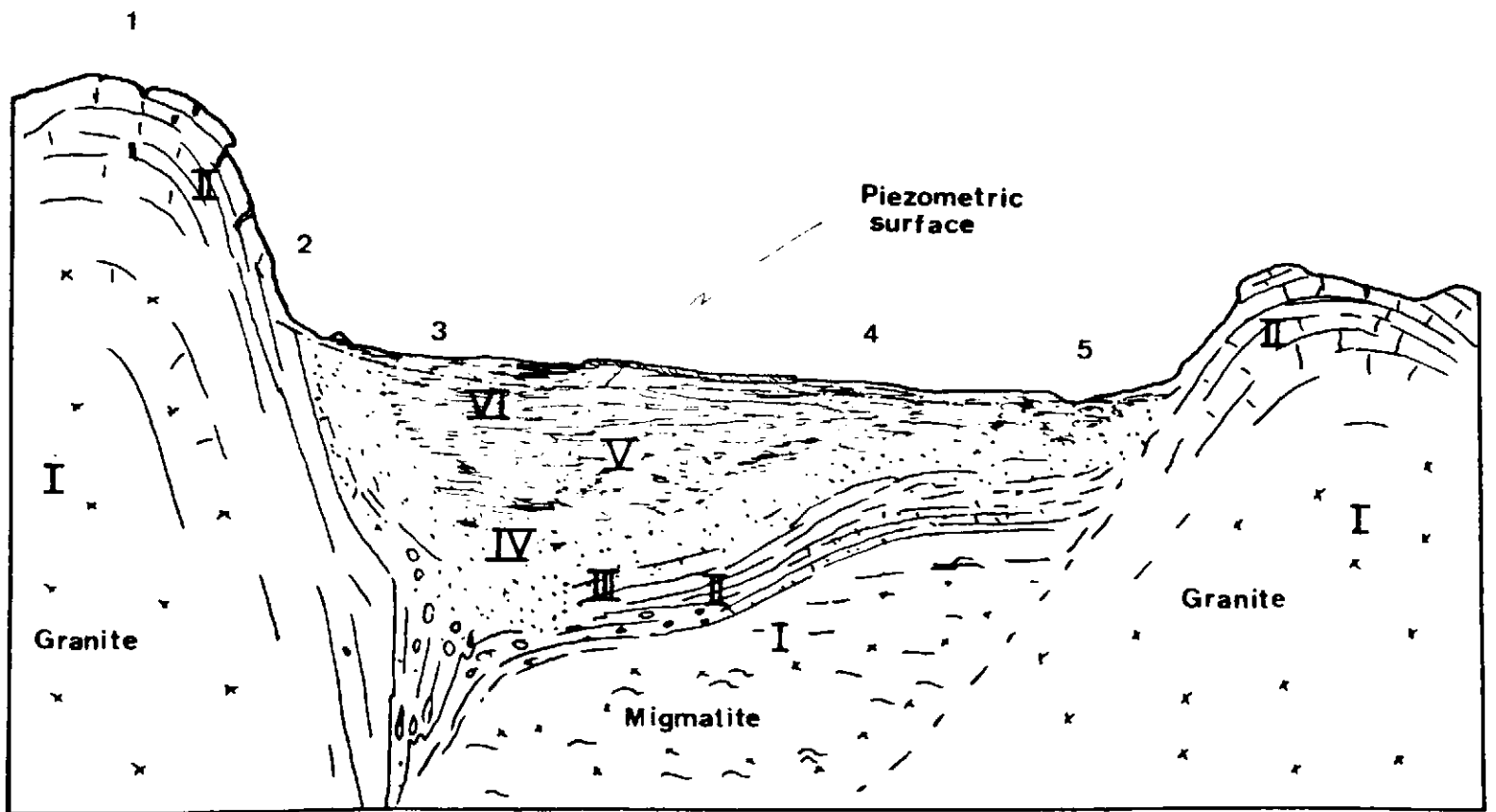


Figure 5 2(i) Sketch sections showing various hydrogeological environments.

Numbers refer to notes in section 5.1

the grade II material, and the bulk value of hydraulic conductivity will depend principally upon the degree of interconnection between the various joint systems. As the predominant jointing should be sub horizontal, caused by pressure release, it is probable that the value of hydraulic conductivity in the plane parallel to the surface will be considerably higher than in the orthogonal planes.

The hydraulic conductivity becomes less anisotropic as the weathering processes remove more material in solution. By the time grade IV weathering has been reached the conditions most nearly resemble an intergranular sand conductivity. This is the *grus* zone referred to above.

Recent evidence (Eswarian + Bin, 1978) indicates that the change in the formation of the predominant clay mineral from halloysite to kaolinite, which occurs in grades V and VI of the weathering profile, is responsible for the general reduction in hydraulic conductivity towards the top of the profile. The clay bands developed in grade VI material have a very low hydraulic conductivity and form an aquiclude.

The aquifer within the weathered profile exists where grade II, III and IV material remain permanently saturated.

Aquifer boundaries.

As the term implies, aquifer boundaries are used to define the flow conditions at the boundaries of the aquifer. As such, aquifer boundaries may be constant head, recharge, leaky or zero flow boundaries.

The lower boundary of the weathering aquifer is always formed by the interface between grade I and grade II weathering. It has been noted above that this interface is usually a complicated three dimensional surface and as such, flow will occur in the grade II material often completely around an isolated block of grade I material. The lower boundary, and often the side boundaries of the aquifer are therefore zero flow boundaries.

The upper boundary is usually formed by the grade V and VI material. As this material has a very low hydraulic conductivity it may also become effectively a zero flow boundary and produce confining conditions.

In the majority of the boreholes drilled into areas with considerable (>10m) thickness of grade V + VI material, the piezometric head was often within four metres of the surface and in a few instances, was artesian. The drilling records for two typical boreholes drilled into deep weathering area A are presented in Appendix B. These records show that water was first encountered during drilling at the top of grade IV material.

To illustrate the various ways in which the weathering processes may combine to form an aquifer, and to produce confining conditions, two sketch sections are presented in Figure 5.2. The purpose of these sketch sections is to provide a graphical illustration of the aquifer location and in particular the importance of lateral variations in weathering grades in controlling flow within the aquifer.

The significance of the various combinations of weathering grades is discussed below, and relates to the numbers shown in Figure 5.2, viz;

(1) The soil cover on inselbergs is either limited or absent, therefore the high intensity rainfall collects as sheet run off and flows down the surface of the rock. As there are exfoliation joints occurring every few metres, which are often several centimetres wide, a proportion of the run off enters the joint system and percolates towards the base of the inselberg, within the shell of grade II weathering. The majority of the run off flows over the surface until the base of the inselberg is reached, where it infiltrates into the grade III weathered material at the base, or enters ephemeral drainage channels.

(2) A proportion of the water contained in the grade II weathering zone fractures issues as seepages and springs from the base of the inselberg. Plate 3.11 shows such a seepage which has been artificially deepened. The storage within the fracture zone is sufficient to maintain these seepages often throughout the dry season.

(3+4) Although the ground surface is approximately flat in the area between points 3 and 4, the two locations would provide completely different borehole results. Point 3 marks the location of an apparent resistivity anomaly which would be created by the deep fracture zone. A borehole drilled at this location would encounter water at the top of the grade IV weathering. The quantity of water would continue to increase

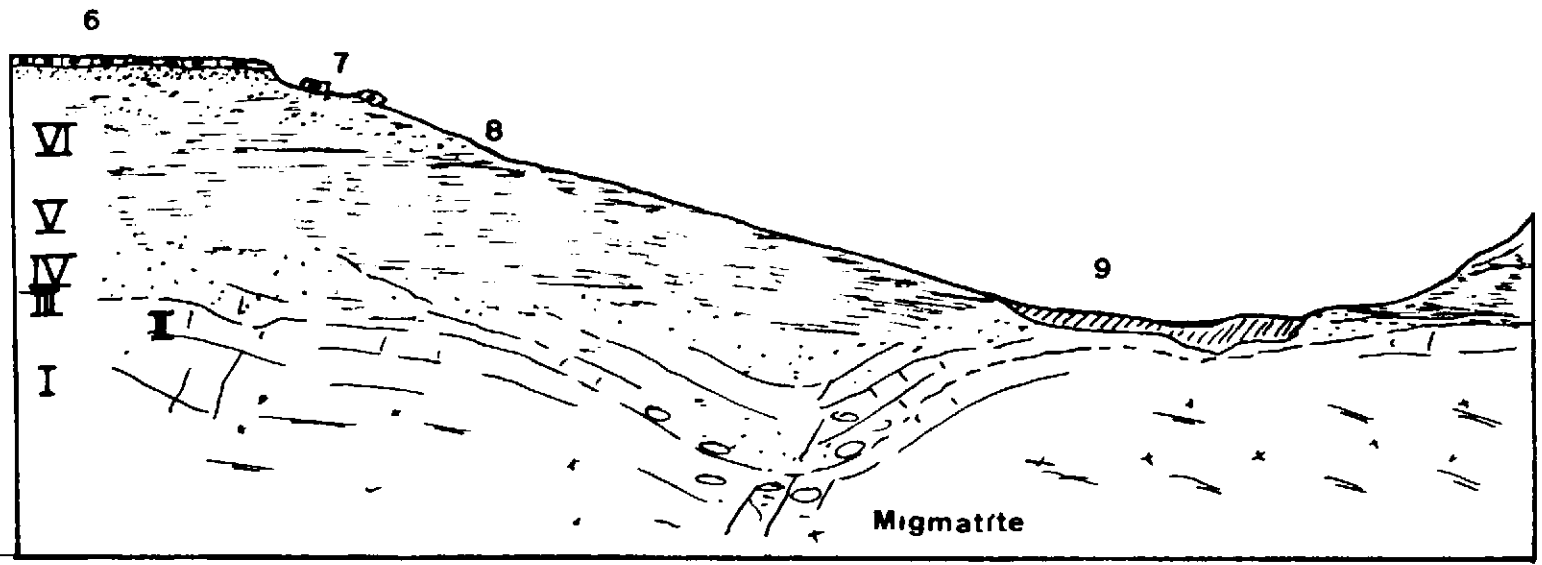


Figure 5 2 (ii)

until fresh rock was encountered. The final standing water level would show a sub artesian rise to the piezometric surface. By contrast, a borehole sited at location 4 would encounter water at a shallow depth and then soon pass into grade I material. The depth of aquifer would be insufficient to maintain abstraction.

(5) A stream at this location would be maintained by groundwater seepage until the piezometric surface fell below the base level of the stream during the dry season. This characteristically occurs sometime in December.

Locations 6 to 9 are on Figure 5.2 (ii).

(6) Where there is little outcrop, an extensive laterite capping is often formed on a deep weathered profile. Grade V and VI material is laterally continuous over the surface. In several areas of Northern Nigeria, particularly around Kaduna, mature, flat erosion surfaces are now being actively eroded. The eroded section is often of the general form shown in Figure 5.2 (ii). A laterite capping forms the flat, often mesa like, hill top, with eroded blocks of laterite scattered below the scarp.

(7) Under the extensive laterite there often exists a thick zone 'A' soil profile. This may form a small aquifer of limited extent.

(8) Spring discharge occurs at the interface between the soil A and B horizons. Streams flow from these springs throughout the dry season as the low hydraulic conductivity material only slowly releases water. The streams do not increase in size as they flow towards the flood plain, as the thick grade V + VI material is effectively impermeable.

(9) The rivers often have a large flood plain due to the high runoff caused by the low hydraulic conductivity surface material. Grade I material often occurs in the river beds or at a shallow depth beneath the flood plain.

5.2 Groundwater hydrographs.

General.

Measurements of the groundwater level in a well or borehole, plotted against time, form a groundwater hydrograph. Changes in the level of the hydrograph throughout the year reflect gross changes in the water flow to the aquifer in the area around the observation point.

The change in flux is caused by changes in flows into or from the aquifer. Input to a small and discrete aquifer can only be recharge as a result of infiltration from rainfall. Output from such an aquifer is composed of losses by transpiration and or evaporation, and losses by seepage to the local surface drainage.

The groundwater hydrograph provides a valuable measurement of the response of the aquifer to recharge, and to losses by seepage and evapotranspiration. Therefore, if the fluctuation of the hydrograph can be reproduced mathematically, by a consideration of the balance between these flows, it is possible to quantify the individual flows.

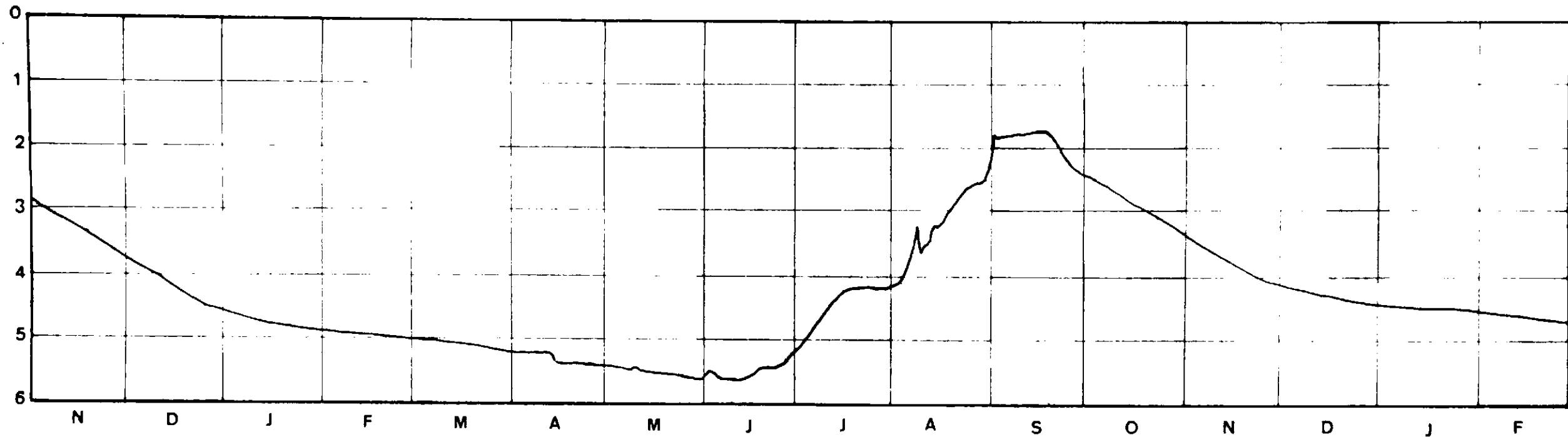
Records available.

Although an extensive search was carried out, no records of groundwater levels were found for the Bauchi area. A number of observation wells were drilled as a part of an urban groundwater development plan for Bauchi Town. However, it was found that several production boreholes either dried up, or their yields dropped substantially soon after they were completed, and in order to maintain the combined yield of the boreholes, the observation boreholes were converted to production boreholes.

The boreholes drilled into deep weathering area A in Bauchi (see section 3.5 and Plate 3.14), were not used for production for some time after their completion, and the opportunity was taken to measure groundwater levels in this area over a period of 14 months. The boreholes were monitored as often as possible using an electric water level indicator. In practice the regularity achieved was two measurements per week during the wet season, and one per month during the dry season.

The borehole hydrograph presented in Figure 5.3 is taken from the record of borehole 10 (see Figure 3.4). The geological log of this borehole is given in Appendix B, and from the log it can be seen that a sub artesian rise in water level was recorded during drilling, and that

Hydrograph



Rainfall BAUCHI AERODROME

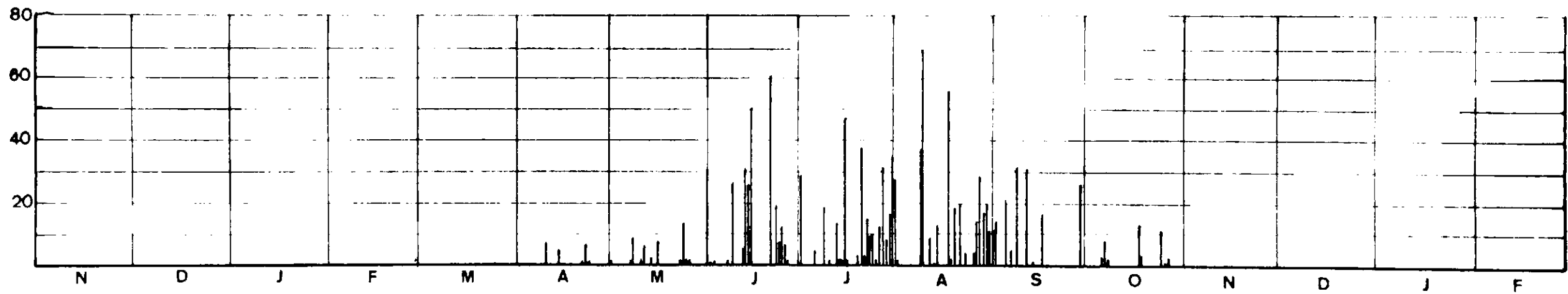


Figure 5-3 Borehole No 10 Hydrograph (Area A) and Bauchi 1978 Rainfall.

therefore the aquifer at this location is confined. However, the resistivity profile section given in Figure 4.9, which also passes through this borehole, shows that the grade V and VI material which confines the aquifer at the borehole is not laterally continuous.

Kowal + Omolokun (1970) have published groundwater hydrographs for three boreholes from the small catchment basin study at Samaru. The hydrographs represent boreholes at three positions on a slope above the valley bottom of the catchment.

The catchments at Bauchi and Samaru are broadly comparable, they are of a similar size, slope, vegetation cover and also receive the same seasonal rainfall.

In the original presentation (Kowal + Omolokun, 1970), only the wet season hydrographs were shown, however, in Figure 5.4, the hydrographs have been rearranged and plotted over a full twelve month period. The dry season part of the hydrograph has been extrapolated from December to June.

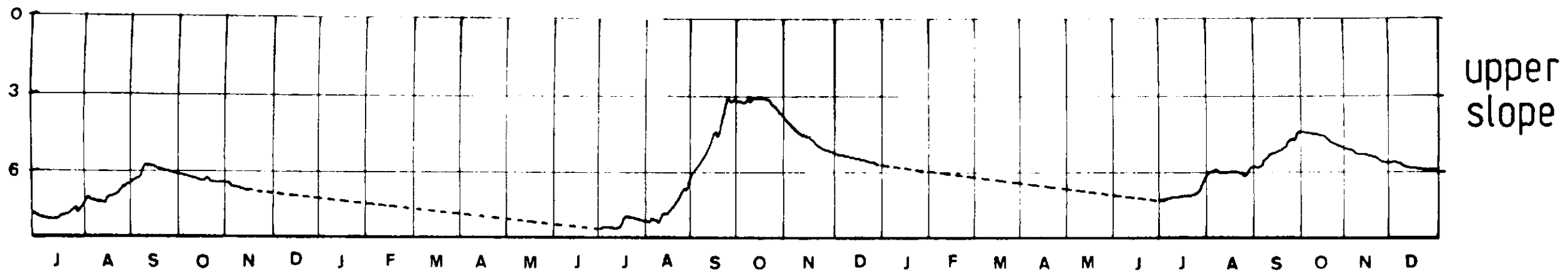
In Figure 5.3, the rainfall data shown has been taken from the record at Bauchi aerodrome. This measurement station is not on the catchment, but lies some 5 km away. For the reasons discussed in Section 2.2, the rainfall over the catchment is likely to have varied significantly from that at the aerodrome. By contrast, the rainfall shown plotted on Figure 5.4 is an average of 5 rain gauges on the catchment, and must therefore be more representative of conditions within the catchment.

Description of the hydrograph.

The three hydrographs are very similar and may be conveniently subdivided into four stages, viz;

- (1) A rising stage
- (2) A constant level stage
- (3) A rapidly declining stage
- (4) A gradually declining stage

The four stages are described below, and an assessment of the implied changes in recharge, seepage and evapotranspiration is made.

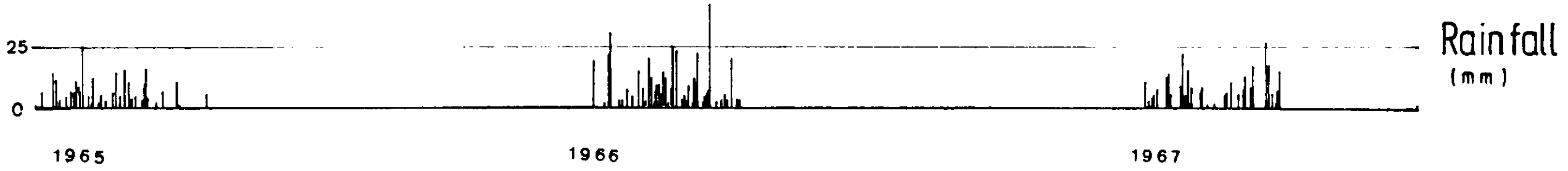


upper slope

HYDROGRAPHS SHOW DEPTH OF THE WATER TABLE BELOW GROUND LEVEL (IN METRES)



lower slope



Rainfall (mm)

Figure 5-4 Rainfall and borehole hydrographs at Samaru

After Kowal + Omolokun (1969)

(1) The rising stage. The rise in the hydrograph marks the beginning of recharge to the water table. This occurs some time after the beginning of the rains, depending upon the frequency and intensity of the early wet season storms. Kowal + Omolokun (1970) report the rise in the water table at Samaru to occur some time during July. Their observations are reproduced in Table 5.1.

Table 5.1 Rainfall + Hydrograph Data.

Year	Annual Rainfall (mm)	Date of rise on hydrograph	Cumulative rainfall before rise (mm)
1964	1054	198 (17-7)	389
1965	978	207 (26-7)	457
1966	1333	192 (11-7)	503
1967	967	196 (15-7)	404
1968	998	208 (22-7)	515

This data confirms that the rise in the water table does not simply occur after a given amount of rainfall has been received over the catchment. For example, during 1968, more than half the total rainfall had fallen before the water table began to rise. The implication is that recharge is controlled by a complicated interaction between rainfall and evapotranspiration.¹

After the initial rise in the water table, the hydrograph shows a continued rise in response to the increasing frequency and intensity of rainfall.

(2) The constant level stage. With the exception of the 1965 hydrograph at Samaru, a constant level stage is reached at the peak of the rains. This is particularly well marked at Samaru during 1966, an exceptionally wet year.

During this time, the groundwater level is close to the surface, the soil above the water table is close to saturation and further rainfall is rejected as surface runoff. Seepage is occurring at this time so that the baseflow component of the stream is also at a maximum.

Note 1. Kowal reports (1970b) that very little runoff occurs before the dry season rise in the water table.

(3) The rapidly declining stage. As soon as the rains begin to diminish, the hydrograph shows a rapid fall in the water table. Water is being lost from the aquifer both to seepage and to continuing high evapotranspiration. Transpiration continues at a high level until the moisture within the rooting depth of the vegetation becomes limiting; after this time much of the vegetation begins to wilt, and later, die.

Depending upon the height reached by the groundwater table during the wet season, which in turn reflects the annual rainfall received, the baseflow to streams ceases at some time between mid-October and mid-December. There is no further surface flow in the streams from this time until, usually, the following July. The cessation of seepage causes the hydrograph to show a definite change of slope, and this marks the end of this stage.

(4) The gradually declining stage. This stage lasts from December until some time in June or July as discussed above. It is important to note that the hydrograph shows a continuing fall at approximately the same rate up to the time the first recharge is received. The water table continues to fall during the early part of the wet season.

The water table falls between one and three metres depending upon the position of a borehole on the slope and the extent of the preceding rains and recharge. For example, the fall is considerably more marked at Samaru after the limited rains of 1965, than after the above average rains of the following year.

The loss of water from the aquifer during the dry season, as measured in a borehole at the bottom of the slope and close to a dry stream bed, can only be attributed to the effects of evaporation from the water table. This is clear evidence that evaporation, rather than transpiration occurs direct from the water table even when it lies at a depth of 6 m. The fact that this evaporation continues at depth after saturated conditions are again established at the surface at the beginning of the rains is of significance in the discussion of recharge which follows.

5.3 Recharge Mechanisms.

Introduction.

In the small and often isolated aquifers that occur within the weathering environment, two factors control the quantity of water available for abstraction by pumping. These are the volume of available storage within the aquifer and the quantity of recharge that occurs, or which may be induced to occur each year.

It is probable that the volume of available storage is less than that of available recharge in many areas. In such cases there is the possibility that the aquifer can be used as a storage reservoir and overpumped each dry season with the assumption that sufficient recharge water is available the following wet season to completely replace the abstraction and other losses. It is also probable that very few basement aquifers are of a sufficient size to support continual abstraction without recharge, for more than two or three years. The quantity of available recharge is therefore a basic parameter in the determination of any development policy, and therefore deserves considerably more attention than it has so far received.

In the following section, two methods of calculating recharge are examined. The first is the conventional analysis based upon the work of Penman (1948, 1949, 1950) and Grindley (1967, 1969) and developed for use in temperate latitudes. The results of this analysis, when used to estimate recharge in the savanna, are described, and it is demonstrated that the method leads to considerable inaccuracy, mainly caused by the extreme climatic variation between the seasons. The second method of analysis has been developed for this study and is based upon the Monteith (1965) method of calculating evapotranspiration.

A major component of both recharge analyses is the balance between rainfall and actual evapotranspiration which occurs within the soil zone. It is therefore necessary to examine and define the moisture retention characteristics of the savanna soils before proceeding to the recharge analysis.

Soil moisture characteristics.

A number of parameters have been used to define the quantity of moisture held in the soil. Concepts such as wilting point, field capacity or soil moisture deficit have been defined specifically in order

that soil moisture conditions can be related to the moisture requirements of plants. However, they do not have a strict physical basis and their use has led to some confusion. In the discussion which follows, a number of these terms are critically assessed.

The ability of a soil to store water is a function of the fraction of the total soil volume that is occupied by solid, the fraction occupied by pore space and the size and distribution of the pores. The ability of a soil to release water is a function of the pore size and shape. If the pores are very small, then a high proportion of the water held within the soil is retained, held in position by capillary forces.

Soil water, porosity and density terms can be most readily defined by considering the soil as a reservoir, with the soil, air and water volumes separated out as shown in Figure 5.5. In terms of the dimensions shown in Figure 5.5, the following parameters may be defined.

Soil bulk density ρ_b

$$\rho_b = \frac{\text{mass dry soil}}{\text{bulk volume of soil}} = \frac{\rho_p c A}{A D} \quad [\text{kg m}^{-3}] \quad 5.1$$

where ρ_p = soil particle density
 c = depth of soil
 A = area of soil
 D = total depth of sample

Volume water content θ_v

$$\theta_v = \frac{\text{volume water}}{\text{bulk volume of soil}} = \frac{b A}{A D} \quad 5.2$$

where b = depth of water [m]

The soil porosity may be defined as

$$E = 1 - (\rho_b / \rho_p) \quad 5.3$$

The values of bulk density are widely used for converting moisture percentage by weight to moisture content by volume and for then

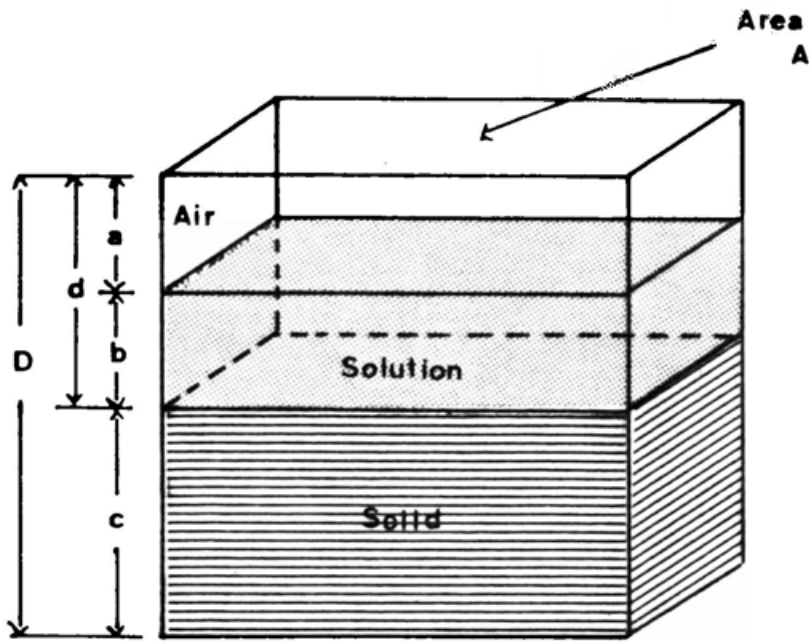


Figure 5-5 Dimensions of a uniform soil block.

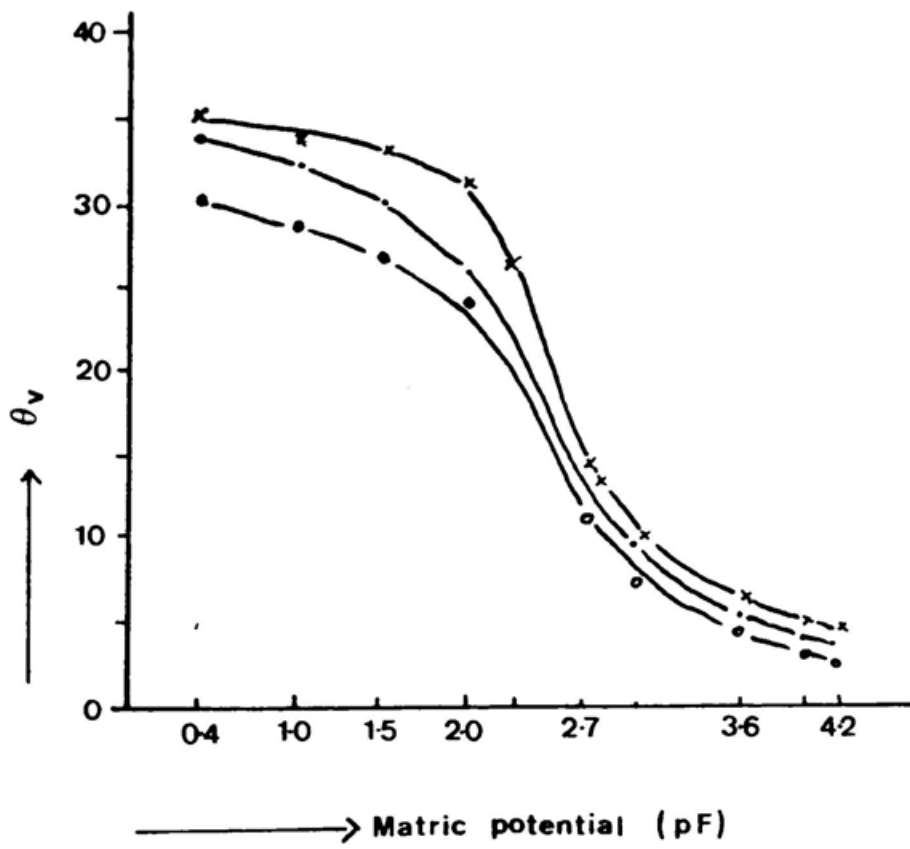


Figure 5-6 Typical pF curves for a savanna soil. (After Kowal 1978)

calculating the soil porosity when the particle density is known. The technique has been recently reviewed by Hanks & Ashcroft (1980).

In the savanna soils, poor structure, compaction and a small total volume of pore space are reflected by high values of bulk density. Kowal + Kassam (1978) present data from several soil profiles taken from uncultivated land close to Kaduna. The data for bulk density and porosity is shown in Table 5.2. A figure of 2.65 g cm^{-3} has been used for the soil particle density in equation 5.2 to give values of soil porosity (Kowal + Kassam, 1978).

Table 5.2 Bulk density and porosity of three soil profiles from Afaka forestry reserve, near Kaduna.

Profile Depth (mm)	Bulk density (gm cm^{-3})			Porosity E		
	1	2	3	1	2	3
0-150	1.53	1.61	1.52	0.42	0.39	0.43
150-300	1.49	1.69	1.48	0.44	0.36	0.44
300-450	1.43	1.62	1.59	0.46	0.39	0.40
450-600	1.46	1.56	1.54	0.45	0.41	0.42
600-750	1.45	1.53	1.57	0.45	0.42	0.41
750-900	1.39	1.77	1.44	0.47	0.33	0.46
900-1050	1.39	1.74	1.44	0.47	0.34	0.46
1050-1200	1.35	1.73	1.48	0.49	0.35	0.44
1200-1350	1.41	1.66	1.42	0.47	0.37	0.46
1350-1500	1.48	1.74	1.43	0.44	0.34	0.46
1500-1650	1.63	1.75	1.57	0.38	0.34	0.41
1650-1800	1.65	1.64	1.55	0.38	0.38	0.41
1800-1950	1.77	1.68	1.55	0.33	0.37	0.41
1950-2100	1.61	1.65	1.53	0.39	0.38	0.42
2100-2250	1.65	1.68	1.69	0.38	0.37	0.36
2250-2400	1.67	1.65	1.72	0.37	0.38	0.35
2400-2550	1.65	1.55	1.79	0.38	0.41	0.32
2550-2700	1.66	1.65	+	0.37	0.38	
2700-2850	1.73	1.67	+	0.35	0.39	
2850-3000	-	1.57	+	-	0.41	

Note. + denotes a laterite layer with values ranging from 2.05-2.37

The high values of bulk density affects the rooting depth of crops adversely. It has been found at Samaru that 75-80% of maize roots have depths of less than 300mm and approximately 90% have rooting depths of less than 450mm.

Water is retained in the soil by physical absorption on surface and by capillary forces as noted above. The effective porosity may be defined therefore as the ratio of the volume of water released by drainage from a soil to the volume of the total sample. This value of porosity may be significantly lower than that of the total bulk porosity, and is also difficult to measure, as any disturbance of the sample will change the pore geometry.

The field capacity of a soil is defined as a unique water content that a given soil reaches and maintains after it has been thoroughly wetted and allowed to drain freely for two days. This value will vary for soils of different textures. The field capacity represents the moisture content of a soil after the water which is held in the volume defined by the effective porosity, has been removed by drainage. A soil at field capacity therefore contains moisture equivalent to the difference between the bulk porosity and the effective porosity of the soil.

A soil which is at field capacity is considered to be freely draining. Therefore, if any extra moisture is added to the top of the soil, an equivalent volume will be released from the base of the soil.

The permanent wilting point of the soil is the unique moisture content that the soil reaches when plants are no longer able to abstract water from the soil by suction. The plants therefore wilt due to water deficiency.

The available water in a soil profile is defined as the difference between the water content at field capacity and the water content at the permanent wilting point, and represents the water available for transpiration by the plant canopy.

A soil moisture deficit (SMD) exists in the soil if it is necessary to add water to the soil before it becomes freely draining. Plant life therefore creates an SMD by transpiration. The quantity of water which it is necessary to add to the soil to replace that lost by transpiration is the SMD. If soil moisture is reduced to the extent that plants wilt, then the SMD is equal to the available moisture

within the soil.

These concepts explain in a qualitative manner the effects of soil moisture changes caused by transpiration. However, implicit in all the definitions is an assumption of the depth of soil from which the transpiration is occurring, or the depth of soil to which the SMD refers. This aspect of the discussion is returned to later.

Soil moisture potential.

The concepts defined in the preceding section are based upon observation of moisture changes within the soil profile, and they lack a physical basis. More recently, attempts have been made to explain the changes in moisture content in physical terms, and a useful description of this approach is given by Hanks & Ashcroft (1980).

The availability of water to the plant canopy corresponds to the work which the plant must expend to move water from the soil to the plant. This can be expressed as a difference in hydraulic potential between the plant roots and the soil.

The hydraulic potential within the soil may be expressed as a sum of a number of potentials as described by equation 5.4.

$$\Psi_h = \Psi_z + \Psi_m + \Psi_p \quad 5.4$$

where Ψ_h = hydraulic potential¹
 Ψ_z = gravitational potential
 Ψ_m = matric potential
 Ψ_p = pressure potential

The gravitational potential is independent of soil properties and only depends upon the vertical distance between the reference point and the data point.

The pressure potential applies to saturated soils. If the quantity of water is expressed as a weight, then Ψ_p is the vertical distance from the data point to the water surface.

Note 1. If the quantity of water is expressed as a mass, the units of potential are Joules kgm^{-1} . If expressed as a pressure, the units are Pascals (nt m^{-2}). If expressed as a weight, the units of potential are metres (or centimetres) of water.

The matric potential is related to the adsorptive forces of the soil matrix and hence is a function of the pore size and distribution within the soil. In saturated soil the matric potential is zero. If the unit of potential is expressed as a weight, the matric potential of the data point is the vertical distance between that point in the soil and the water surface of a manometer filled with water and connected to the data point in the soil by a ceramic cup.

Measurements of soil water potential are useful in that they indicate the potential a plant must overcome to remove water from the soil. They also indicate the direction of movement of water in the unsaturated zone. A negative potential gradient indicates water movement upwards, whereas a positive gradient represents downward movement of water. A zero flux plane exists where the gradient of the potential is zero. There is no flux of water either upward or downward. These concepts are employed below in the discussion of the second recharge model.

Measurements of matric potential may be made by a number of methods (Milburn, 1979). The permanent wilting point and the field capacity may therefore be expressed in terms of matric potential for any given soil.

A partial vacuum equivalent to 0.34 atmospheres is approximately equivalent to the matric potential of a soil at field capacity (Hanks + Ashcroft, 1980). Similarly, a partial vacuum of approximately 15 atmospheres represents the matric potential at the permanent wilting point. The difference in the quantity of water abstracted from a soil at these two different suctions is a convenient measure of the available water in the soil.

Based upon the concept of available water at different matric potentials, experiments have been performed to find the water held in soils at different tensions. The results of this work for two soils, beneath uncultivated land, developed upon basement rocks in Northern Nigeria are given by Kowal + Kassan (1978) and reproduced here in Table 5.3.

Table 5.3 Range of available water in two ferruginous soils developed under natural conditions at Afaka, Nigeria (Data from Kowal + Kassam, 1978).

Depth of Profile (mm)	Bulk Density (gmcm^{-3})	Water content at tension		Available Water (mm)
		0.34 atm (mm)	15 atm (mm)	
0-150	1.52	29	18	11
150-380	1.52	61	45	16
380-1220	1.48	277	197	80
1220-1520	1.43	93	67	26
1520-1780	1.56	77	57	20
1780-2560	1.62	249	180	69
2560-3050	1.79	168	122	46
Total				268
0-120	1.73	26	14	12
120-400	1.64	66	45	21
400-910	1.59	146	107	39
910-2340	1.78	485	384	101
2340-3040	1.68	257	181	76
Total				249

The range of available water for two typical soil profiles, shown in Table 5.3, may be approximated as 80mm of water for each 1000mm soil. A relatively high proportion of the total water content of the soil, represented by the bulk porosity, is still held in the soil at a tension equivalent to 15 atmospheres.

In Table 5.4, values of matric potential for a typical soil at various soil water conditions are shown. A number of different parameters have been used to measure soil matric potential and these are listed in Table 5.4. It should be stressed however that these values represent one particular soil, and that they will change for soils of different textures. However, they do illustrate the approximate conditions for all soils.

Table 5.4 Values of matric potential at various soil water conditions
(Data after Hanks + Ashcroft, 1980)

Soil water condition	Matric Potential ψ_m			
	(cm)	(Joules kg^{-1})	(pF)	(Atmospheres)
Saturation (approximate)	-1	-0.098	0	-1×10^{-3}
Field capacity (approximate)	-100	-9.8	2.0	-0.1
Wilting point of many plants	-1.5×10^4	-1470	4.2	-14.9
Air dry (relative humidity = 0.85)	-2.2×10^5	-2.16×10^4	5.4	-218

Notes. pF refers to the log of the matric potential expressed as centimetres of water.

The hydraulic conductivity of the soil is a function of the matric potential. As the matric potential decreases, hydraulic conductivity also decreases (Hanks + Ashcroft, 1980). To illustrate this effect, the change in hydraulic conductivity with matric potential is shown for a soil at various water contents in Table 5.5. These values refer to a soil of a particular texture, and will vary for soils of different textures.

Table 5.5 Hydraulic conductivity and matric potential for a soil with varying volume water content. (Data after Hanks + Ashcroft, 1980).

Volume water content	Hydraulic conductivity K_w (cm/day)	Matric Potential Ψ_m (cms)	Soil Moisture State
0.05	4.5×10^{-5}	-6,975	wilting point
0.06	6.7×10^{-5}	-3,365	
0.08	4.1×10^{-4}	-1,255	
0.10	4.8×10^{-3}	-447	
0.12	2.6×10^{-2}	-330	
0.14	5.2×10^{-2}	-259	
0.16	7.8×10^{-2}	-209	
0.18	1.1×10^{-1}	-168	
0.20	2.7×10^{-1}	-134	
0.22	7.4×10^{-1}	-106	field capacity
0.24	1.6	-78	
0.26	3.6	-64	
0.28	4.7	-53	
0.30	7.4	-43	
0.32	11	-34	
0.34	19	-26	
0.36	34	-18	
0.38	69	-10	
0.40	1.1×10^2	-3	
0.41	1.2×10^2	0	Saturation

The results presented in Table 5.5 are important as they have an effect upon infiltration rates. For a soil with volume water content close to the wilting point, the hydraulic conductivity of the soil is greatly reduced. When infiltration commences therefore, at the beginning of the wet season, a wetting front is produced which only moves slowly down through the profile. Above the wetting front the volume water content is close to saturation, below this level the soil is still dry. Kowal + Kassam (1978) report that savanna soils

have hydraulic conductivities between 720 cm day^{-1} and 2900 cm day^{-1} for values of matric potential close to zero.

Root constants.

To quantitatively assess the soil moisture deficit it is necessary to estimate the depth of soil from which transpiration and or evaporation has occurred. As plants abstract moisture from the soil via their root networks, it is therefore necessary to measure or make an assumption regarding the depth of rooting beneath the plant canopy in question. A second, and major, complicating factor is that plants encounter difficulty in abstracting water from a soil some time before the permanent wilting point is reached. Plant growth is then slowed and transpiration correspondingly reduced.

The assessment of the actual transpiration of a plant canopy requires a comprehensive overview of biological factors. For example, crop water requirements differ throughout the growth cycle of the crops, and the requirements of one crop differ from those of another. However, there is strong evidence that crop growth is directly related to net radiation, assuming that there is no restriction in the quantity of soil water available. As an approximation therefore, Penman (1956) suggested that for a short green crop, completely shading the ground and not short of water, evapotranspiration is determined by the capacity of the atmosphere to accept water by evaporation, also known as the evaporative demand of the atmosphere (see Section 2.4). This concept is applicable to temperate latitudes where the crop growth cycle corresponds to the evaporative demand of the atmosphere, both being controlled by net radiation. However, in the savanna environment, the plant growth cycle is not determined by net radiation as considerable quantities are received throughout the year. In this environment the limiting factor is the availability of soil moisture.

Rooting depth varies considerably between plant types. Maize in Kenya was observed to root to a depth of 2m, kikuya grass to a depth of 6m and evergreen forest to more than 13m (Jackson, 1977). The water available to each of these plant canopies will vary considerably. Where moisture is limiting, xerophytes develop root systems which extend to 20 or 30m depth (Milburn, 1979). Mangoes in Northern Nigeria have rooting systems which extend to the permanent water table and thus are able to fruit towards the end of the dry season. Faced with such a

diversity of rooting depths it is necessary to assume an average depth for a natural plant canopy. If a specific area of one crop is under study then the rooting depth may be more accurately specified.

The available moisture within the profile under the plant canopy may be defined therefore as the total available moisture above the rooting depth selected. This value of available moisture also represents the maximum soil moisture deficit that may be created by transpiration. The maximum SMD has also been called the D value (Lloyd et al, 1966).

Although the available moisture within a certain rooting depth may be determined for a particular soil type, this quantity of water is not equally available to a plant canopy. At some moisture content between field capacity and the D value, transpiration by the plant becomes restricted by the availability of water.

At high potential evapotranspiration rates, transpiration falls below the potential rate at an earlier stage of moisture tension than in the case of low potential evapotranspiration rates. Similarly, as root density increases, the potential evapotranspiration rate is maintained until much greater soil moisture tensions are reached (Jackson, 1977). In an area where little information is available upon plant physiology, rooting depths, or rooting densities, it is necessary to assume a proportion of the available moisture, below which evapotranspiration becomes reduced due to moisture deficiency. This level has been defined as the C value, or the root constant. Lloyd et al (1966) working in the semi arid environment of Jordan recommended a value of C equivalent to 50% of the available moisture.

The rate at which the actual evapotranspiration falls beneath the level of potential evapotranspiration as the SMD increases from the C value to the D value is a controversial issue and a number of models have been proposed. In Figure 5.7, the ratio of potential evapotranspiration (E_{tp}) to actual evapotranspiration (E_{ta}) is shown plotted against water content (θ_v). Much field work has shown (Hanks + Ashcroft, 1980) that the most correct field situation lies between the extremes of Thornthwaite + Mather, and Veihmeyer + Hendrickson as shown by Penman + Pierre (Refer to Figure 5.7). In reality, this simplification is complicated in a number of ways as discussed above.

Figure 5.8 shows the data in Figure 5.7 expressed in an alternative

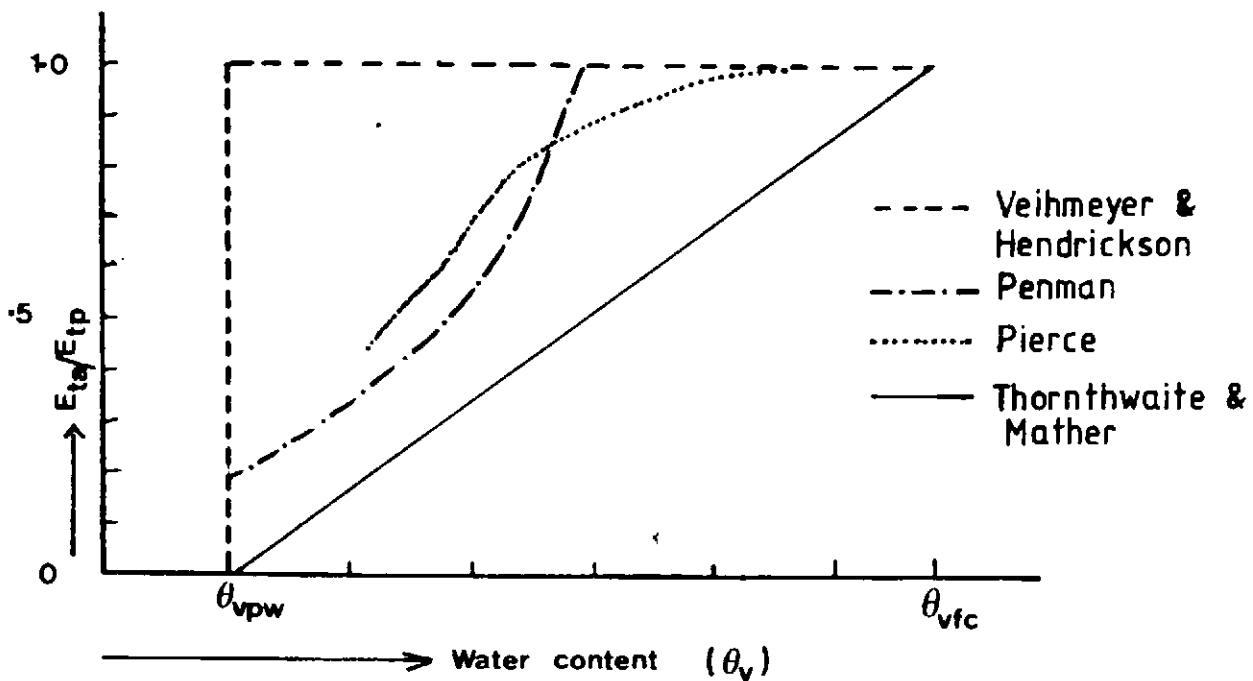


Figure 5-7 Modification of evapotranspiration when soil moisture is limiting.
 (After Hanks and Ashcroft, 1980)

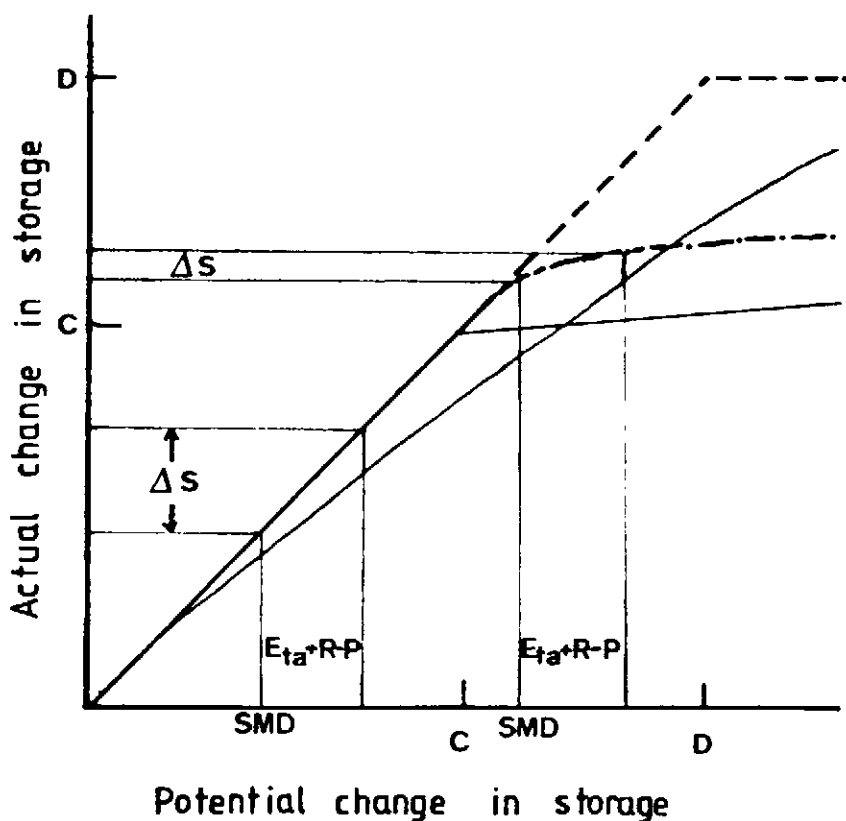


Figure 5-8 Soil moisture changes for various drying curves.
 (After Rushton and Ward, 1979)

form (Rushton + Ward, 1979) which includes the concepts of C and D values and the probable changes in soil moisture storage which result.

Conventional recharge analysis.

Recharge is usually calculated as the balance between input, in the form of rainfall, and output, in the form of losses to runoff, seepage and evapotranspiration. The relationship may be expressed mathematically, viz:

$$\Delta S = P - E_{ta} - R$$

5.5

where P = precipitation (mm)
 E_{ta} = actual evapotranspiration (mm)
 R = Runoff, expressed as (mm)
depth over the catchment
 ΔS = increase in stored water (mm)

A negative value of ΔS represents an increase in the SMD, while a positive value indicates water available for reducing the SMD, or, if the soil is at field capacity (SMD = 0), water available for recharge to the permanent water table.

The conventional method assumes that no recharge can occur unless the soil moisture level is above the field capacity. Similarly, it is assumed that no further reduction in soil moisture can occur when the permanent wilting point is reached.

The accuracy of the estimate of ΔS is determined by the accuracy with which the inputs and outputs can be assessed. Of these three functions, the estimate of E_{ta} is the most difficult to assess accurately. The choice of C and D values, and the choice of the function describing the change of E_{ta}/E_{tp} between C and D may be seen from Figure 5.8 to significantly affect the estimated value of E_{ta} .

Kowal + Knabbe (1972) have produced a water budget for Bauchi using rainfall and E_{tp} averaged over a period of six years and grouped into decades. For this analysis they have used the relationship between E_{tp} and E_{ta} after Veihmeyer and Hendrickson (see Figure 5.7). In effect, this relationship does not specify a C value but assumes evapotranspiration continues at the full rate until the D value is reached, after which evapotranspiration ceases. For the sandy savanna soils,

this relationship is reasonable. Figure 5.6 indicates that the moisture content up to a matric potential of $< 500\text{cms}$ is lost very easily, after which little extra moisture is lost.

The results produced by Kowal + Knabbe form a part of their Agro-climatological Atlas of the Northern States of Nigeria (1972), and as such, have been widely quoted and used by various organisations, (see for example Land Resources Division, 1976). The calculation for Bauchi is reproduced in Table 5.6 using data from Table 2.22. The presentation of the results has been modified to reflect the previous discussion.

Assessment of conventional analysis results.

The estimate of Etp by the Penman method will cause considerable error when used in the savanna environment, if no modification is included to account for the differing savanna conditions from those in the U.K. It is not possible to include the effects of the pronounced seasonality of the savanna climate in the standard analysis. A number of factors in particular lead to errors in the assessment of Etp and these are briefly discussed below, viz;

- 1) The albedo changes between 0.15 and 0.35 during the year in the savanna. The effects of such a change have been described in Section 2.3.
- 2) When soil moisture becomes limiting, the use of net radiation changes. In the wet season Kowal + Kassam report that 75% of net radiation is used for evapotranspiration. During the dry season this quantity must decrease substantially, although no experimental evidence is available. However, to assume that 100% of net radiation is available for evapotranspiration throughout the year will cause a substantial overestimate of Etp. Figure 2.26 indicates the sensitivity of Etp to this parameter.
- 3) The Penman equation is designed to estimate potential evapotranspiration from a short crop. During the wet season the crops grow to between two and three metres in height, and this will cause considerable loss of moisture due to turbulence, and an underestimate of Etp at the time.
- 4) The Penman equation assumes that the surface is covered by the crop. During the early part of the wet season, the

Table 5.6 Water Budget for Bauchi (1979) using data from Table 2.22.

Decade	Etp (mm)	Rainfall (mm)	Eta (mm)	Δs (mm)	SMD (mm)	Percolation to groundwater (mm)
1	38.1	0.0	0.0	0.0	-100.0	
2	40.0	0.0	0.0	0.0	-100.0	
3	48.6	0.0	0.0	0.0	-100.0	
4	45.6	0.0	0.0	0.0	-100.0	
5	48.7	0.0	0.0	0.0	-100.0	
6	38.3	0.0	0.0	0.0	-100.0	
7	54.1	0.0	0.0	0.0	-100.0	
8	53.4	0.0	0.0	0.0	-100.0	
9	61.5	0.0	0.0	0.0	-100.0	
10	55.5	0.0	0.0	0.0	-100.0	
11	62.1	4.9	4.9	0.0	-100.0	
12	53.2	32.3	32.3	0.0	-100.0	
13	52.5	49.3	49.3	0.0	-100.0	
14	50.4	10.0	10.0	0.0	-100.0	
15	62.9	15.8	15.8	0.0	-100.0	
16	42.9	40.9	40.9	0.0	-100.0	
17	45.6	23.4	23.4	0.0	-100.0	
18	51.1	19.2	19.2	0.0	-100.0	
19	40.7	95.3	40.7	+54.6	-45.4	
20	41.9	165.5	41.9	+123.6	0.0	78.2
21	48.9	68.6	48.9	+19.9	0.0	19.7
22	40.6	74.7	40.6	+34.1	0.0	34.1
23	40.7	83.2	40.7	+42.5	0.0	42.5
24	42.6	100.8	42.6	+58.2	0.0	58.2
25	41.4	77.4	41.4	+36.0	0.0	36.0
26	42.7	12.0	42.7	-30.7	-30.7	
27	44.6	76.3	44.6	+31.7	0.0	1.0
28	43.2	41.7	43.2	-1.5	-1.5	
29	43.8	0.0	43.8	-43.8	-45.3	Total Etp = 1669.1
30	45.9	0.0	45.9	-45.9	-91.2	Rainfall = 991.3
31	42.8	0.0	8.8	-8.8	-100.0	Eta = 721.6
32	40.7	0.0	0.0	0.0	-100.0	Groundwater=269.7
33	41.6	0.0	0.0	0.0	-100.0	

Decade	Etp (mm)	Rainfall (mm)	Eta (mm)	Δs (mm)	SMD (mm)	Percolation to groundwater (mm)
33	41.6	0.0	0.0	0.0	-100.0	
34	37.1	0.0	0.0	0.0	-100.0	
35	36.4	0.0	0.0	0.0	-100.0	
36	43.3	0.0	0.0	0.0	-100.0	

- Notes
- 1) Etp calculated using values of $\alpha = 0.25$, $a = 0.235$
 $b = 0.535$ in equation 2.7
 - 2) An initial SMD of 100mm is assumed, equivalent to a
rooting depth of 60cm (see Table 5.3)
 - 3) No allowance is made for runoff ($R = 0$ in equation 5.3)

surface is not covered completely, and during the dry season the majority of the surface is bare. This will cause an overestimate of E_{tp} .

The combined effect of these errors is that the Penman equation overestimates E_{tp} considerably during the majority of the year, and underestimates it during the wet season. The balance between these two sets of errors may produce an approximately accurate figure for the year as a whole however.

Further errors are encountered when computing the soil water balance. In particular, as the rainfall events are both intense and of short duration, and as the infiltration rate of the soil is in general high, the practice of using ten daily data periods to compute the balance will cause a significant underestimate of recharge. This will be particularly marked during the early part of the wet season when much of the ground is still bare. Evaporation from bare soil quickly dries out the top soil thus reducing significantly the subsequent rate of evaporation. Rainfall that can pass below the top soil therefore becomes protected from later evaporation.

Although all the factors described above can cause errors in the recharge calculation, the most severe restriction on the general use of the method in calculating a catchment water balance is that of the prediction of no evapotranspiration when the soil moisture deficit is equal to or greater than the permanent wilting point. Whatever modifications are made to the Penman analysis, the soil moisture balance indicates that the D value is reached some time during the dry season. After this time no evapotranspiration is predicted.

Transpiration by plants stops when the soil moisture is reduced to the permanent wilting point, however, there is evidence that evaporation continues from the soil. As described in Section 5.2, the groundwater level continues to fall throughout the dry season and the only process by which water can be lost from the water table during this time, after seepage has stopped, is by direct evaporation. Further evidence is also forthcoming from an experiment conducted by Jones (1975) at Samaru. The results are particularly relevant and are reproduced in Table 5.7.

Jones calculated the losses of soil moisture that occurred from

beneath three soil profiles at Samaru, between mid-October 1973 and mid-March 1974. The three surfaces each carried a crop of maize during the wet season, then in mid-October the soil profiles were sampled and the three plots treated as follows:

- 1) left undisturbed
- 2) covered with a paraquet based weed killer
- 3) ploughed to a shallow depth - producing a mulch

The moisture profiles beneath the three plots were again measured in mid-March

Table 5.7 Effects of surface treatment on profile water loss during the dry season (after ~~January~~ ^{Jones}, 1975).

	Sampling Depth (mm)				
	150-300	300-450	450-600	600-750	Total
Total moisture content October 1973	33.4	42.9	46.1	45.5	167.8
Total moisture content March 1974	A 15.0 B 19.6 C 22.3	23.1 21.8 34.7	27.2 31.8 39.1	27.5 38.9 38.1	92.8 130.1 134.2
Moisture loss	A 18.4 B 13.8 C 11.1	19.7 11.0 8.1	18.9 7.2 7.0	18.0 5.7 7.4	75.0 37.7 33.6

Note 1) Plot A = weed growth on a natural surface
 B = surface with weeds killed by paraquet
 C = ploughed

It may be seen from Table 5.7 that a significant soil moisture loss is recorded for all three treatments at a time when the conventional analysis predicts no evapotranspiration for plots B and C. The C and D values for these plots would both be zero as the rooting depth was zero.

A proportion of the inaccuracy in the recharge estimate may be rectified by computing the soil moisture balance on a daily basis

(Howard + Lloyd, 1979). However, the major source of error lies in the use of potential evapotranspiration and some form of root constant to estimate actual evapotranspiration. An improved method of calculating actual evapotranspiration would allow a more accurate assessment of recharge. In the following discussion, the Monteith equation (equation 2.17) is used to calculate Eta and it is demonstrated that this method provides an improved estimate of recharge.

Model of recharge used for study.

The recharge model used for this study forms a part of the 'black box' model of a catchment water balance which is described in Section 6.3. The validation of the recharge model is only possible therefore in the context of the larger model, however, in this section the derivation of recharge is described in detail and some model results presented.

Actual evapotranspiration in a savanna environment is controlled by the availability of moisture within the soil. In order to predict the Eta therefore, a detailed understanding of soil moisture availability throughout the year is necessary. It is also necessary to understand the soil moisture distribution within the profile and the way in which this changes throughout the year. If a satisfactory model of moisture availability can be constructed, then the Monteith equation (equation 2.17) can be used to calculate Eta and the two combined to form a predictive system.

Soil moisture potentials have been discussed above. If measurements of the soil moisture potential were available for a savanna profile it would be possible to predict the movement of moisture within the profile and to assess when soil moisture becomes limiting to evapotranspiration. In the absence of such measurements however, it is necessary to construct a model of soil moisture movement based upon observed data from the environment.

In the following discussion, the probable changes in soil moisture potential, and the implications for the measurement of Eta, are described based upon the profiles presented in Figure 5.9. In this discussion it is assumed that the water table remains at a constant depth, although in the description of the catchment water balance in Section 6.3 this restriction is removed, allowing a prediction of runoff.

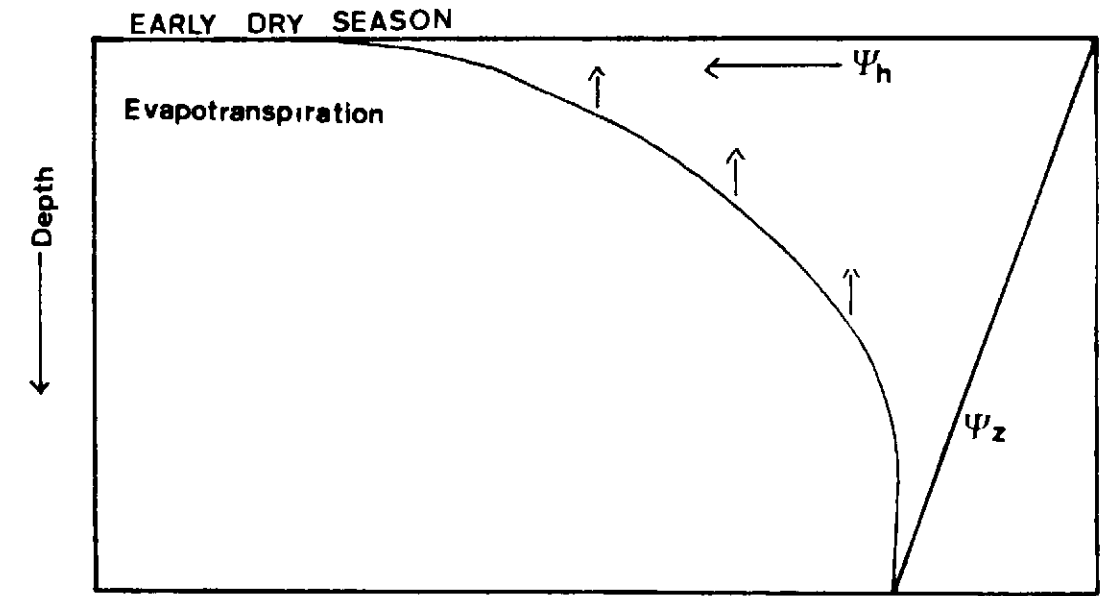
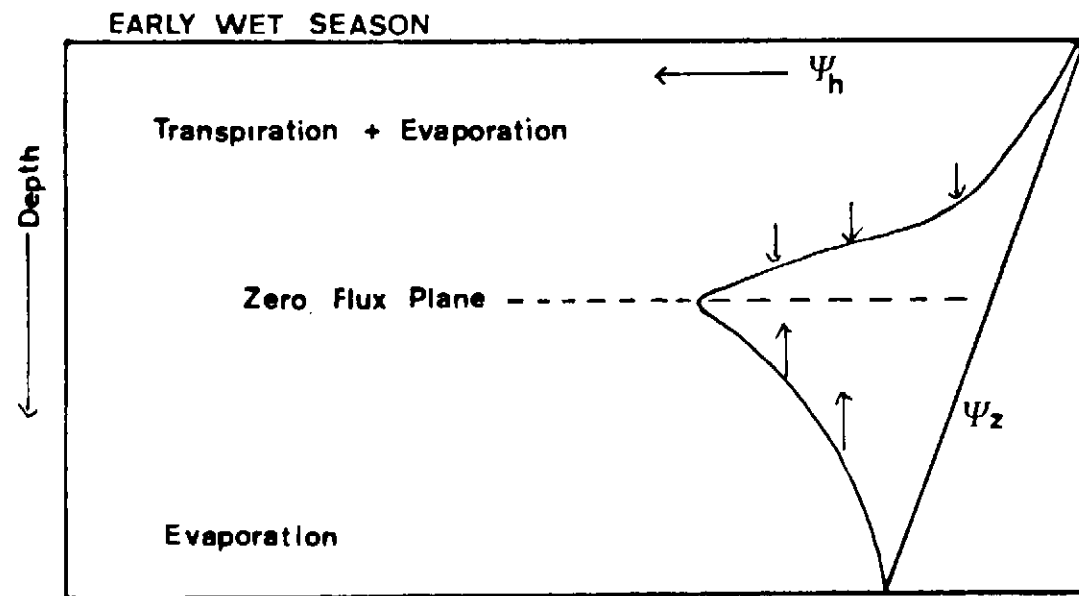
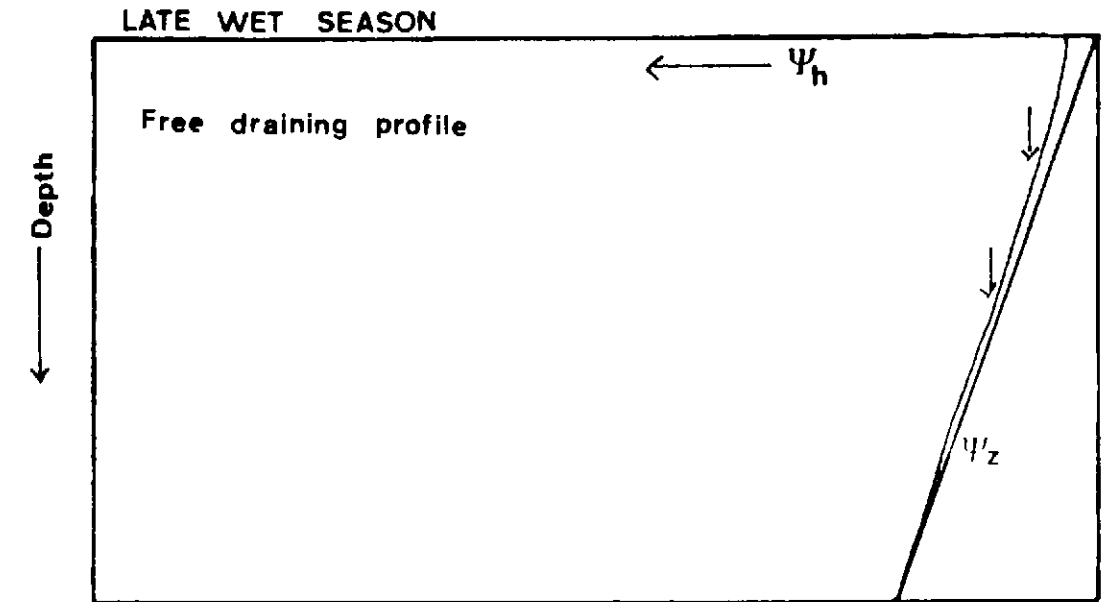
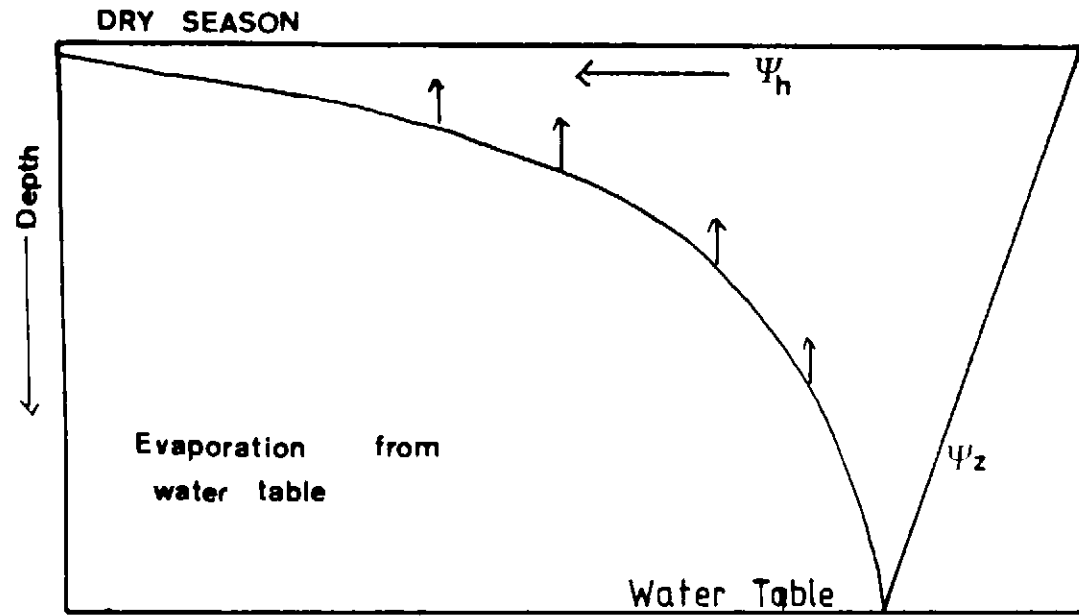


Figure 5-9 Seasonal changes in soil moisture potential. (ψ_h)

1) Dry season - During the dry season, an SMD is developed which reflects the combined evaporation and transpiration that has occurred since the previous wet season. The size of this SMD is a function of the rooting depth of the plant canopy, as discussed above. Kowal + Kassam report the following maximum SMD values for savanna profiles.

Table 5.8 Maximum soil moisture deficit for various plant canopies (after Kowal + Kassam, 1978).

Crop Type	SMD (mm)
Bare fallow	100
Sorghum	140
Groundwater	160
Cotton	200
Grass	240
Natural vegetation	270

Conditions at the end of the dry season indicate the following, viz:

- a) An albedo of approximately 0.35 (Kowal + Kassam, 1978)
- b) A substantially decreased proportion of net radiation available for evapotranspiration. The ground flux component probably increases to approximately 75%
- c) That no transpiration is occurring
- d) That the gradient of the soil moisture potential is negative throughout the profile (Figure 5.9)

The negative soil moisture potential gradient implies that moisture is moving upwards throughout the profile and being lost at the surface, or beneath the surface by evaporation. The soil close to the surface at this time approaches air dryness (refer to Table 5.4). Ground temperature profiles provide a useful confirmation of this prediction. From approximately November to February there exists a daily average positive ground temperature gradient at Bauchi. The temperature at a depth of 300mm is consistently less than that at 1200mm by approximately 2°C. This indicates an upward flow of heat, and therefore water movement from the water table to the atmosphere.

2) Early wet season. The rains which fall at the beginning of the wet season, fall on bare ground, or upon dead vegetation. With the exception of very heavy storms (\rightarrow 40mm), no runoff occurs, and the rainfall infiltrates into the soil. Downward percolation in the soil is very slow due to the low hydraulic conductivity of the dry soil discussed above. A wetting front is formed therefore with conditions close to field capacity in the soil above the wetting front, and dry beneath it.

The soil moisture profile indicates the presence of the wetting front by a zero flux plane (ZFP). There is no moisture movement at the ZFP.

As conditions above the ZFP are close to field capacity, plant seed germination occurs and grasses in particular, rapidly begin to grow. Transpiration and evaporation therefore commence, at a rate which is determined by the degree of plant cover and the transpiration requirement of the vegetation. Evaporation from the bare soil initially is high after a storm, but the reduction of soil moisture in the top few centimetres of soil immediately causes this component of evapotranspiration to fall below the evaporative demand of the air.

If evapotranspiration completely exhausts the moisture held above the ZFP, then dry season conditions are again initiated. Such a failure of the early wet season rains is a commonly encountered problem in the savanna, and due to the rainfall distribution described in Section 2.2, it is probable that this condition varies very widely.

Beneath the ZFP, the soil moisture potential gradient remains negative, in effect, isolated from conditions above. Although moisture can no longer escape to the surface there is a continued redistribution of moisture from the water table to the soil profile in response to this gradient. The soil moisture deficit beneath the ZFP is therefore reduced marginally.

As the ZFP becomes established, the quantity of net radiation used in heating the ground decreases sharply. A similar reduction in albedo is also initiated as the grass cover extends widely.

3) Mid wet season. As the frequency of rain-storms increases, the ZFP moves downward. Transpiration at the surface increases due to the increased leaf area available from growing plants. Evapotranspiration also increases due to the extra turbulence caused by the growing

plant canopy. Deeper rooted plants and trees begin to transpire and grow as moisture becomes available to their root systems.

At some point in the middle of the wet season, determined by the frequency and quantity of the preceding rainfall, the quantity of moisture held above the ZFP becomes greater than the dry season soil moisture deficit. At this time, recharge to the water table occurs, and any subsequent excess of rainfall over evapotranspiration passes through the high hydraulic conductivity soil to the water table.

4) Early dry season. Evapotranspiration continues at a high level determined by the plant requirements, and the evaporative demand of the atmosphere until soil moisture becomes limiting. At this time, which will vary for different root constants, the transition to dry season conditions commences. During a range of moisture contents, which span the root constant, albedo will change, ground flux will increase, transpiration will cease and evaporation from the soil profile will increase. It is probable that evaporation commences from the soil profile at some considerable time before the root constant is reached, especially in areas where the water table is close to the surface. The evaporative demand of the atmosphere during this time is met both by transpiration and by evaporation from the soil profile.

It is clear from the preceding discussion that the presence of a zero flux plane modifies E_a . It is therefore necessary to construct a model which takes account of this, and the various other changes identified above.

The following list represents the assumptions made in the construction of a soil water balance over a period of one calendar year. A flow diagram representing the logic in a form convenient for the construction of a computer algorithm is shown in Figure 5.10.

1) The albedo, the percentage net radiation available for evapotranspiration and the r_h term in the Monteith equation (see below) are all assumed to change from their wet season values to their dry season values over a range determined by the root constants. The changes commence as the SMD approaches a value of the root constant, $(RC - X)$ and are completed as the SMD passes the root constant (as $RC + X$). The constant X is < 35.0 .

2) A maximum soil moisture deficit, equivalent to a D value, is assumed equal to $RC + 35$. The value of 35mm is taken from the data in

Table 5.7 and represents the amount of evaporation that occurs from a bare surface with no transpiration. The maximum soil moisture deficit is composed therefore of two components, a transpiration component and an evaporation component.

3) If the SMD is greater than half the root constant, any moisture available after subtracting E_t from rainfall is assumed to enter a soil moisture store (SMS), representing the presence of a ZFP. On the following day E_t is calculated assuming moisture is not limiting, and with values of albedo and ground flux adjusted accordingly. A second soil moisture deficit (SMD 2 in Figure 5.10) is allowed to build up within the soil moisture store. If on subsequent days, there is no further rainfall, the moisture in the SMS is depleted, and eventually removed, signifying a return to dry season conditions.

4) The SMS is added to ^{by} any subsequent rainfall. A balance is computed for the zone above the ZFP, while the original SMD (SMD1 in Figure 5.10) remains unchanged by conditions at the surface.

5) When the moisture contained in the SMS is equal to the moisture deficit represented by SMD1 the ZFP is assumed to have reached the water table. After this time the soil moisture store ceases to exist, the original SMD returns to zero and the soil profile above the water table is at field capacity.

6) Any further rainfall in excess of E_t is transferred directly to the water table.

7) As the dry season commences, a soil moisture deficit is formed. However, this does not affect transpiration rates until the SMD approaches the root constant as described above.

8) When the SMD reaches a percentage of RC ($\sim 50\%$) a part of the evaporative demand is assumed to be met by evaporation from the water table. This increases until all the demand is met by evaporation when the SMD is equal to the D value. This condition anticipates the discussion in Section 6.3 and is not explained further here.

The changing moisture conditions can be included in the calculation of E_t by the Monteith equation described in Section 2.4. Apart from the measured climatic parameters assessed in Section 2.4, two resistance terms are included in this equation. These resistance terms are defined again here, viz;

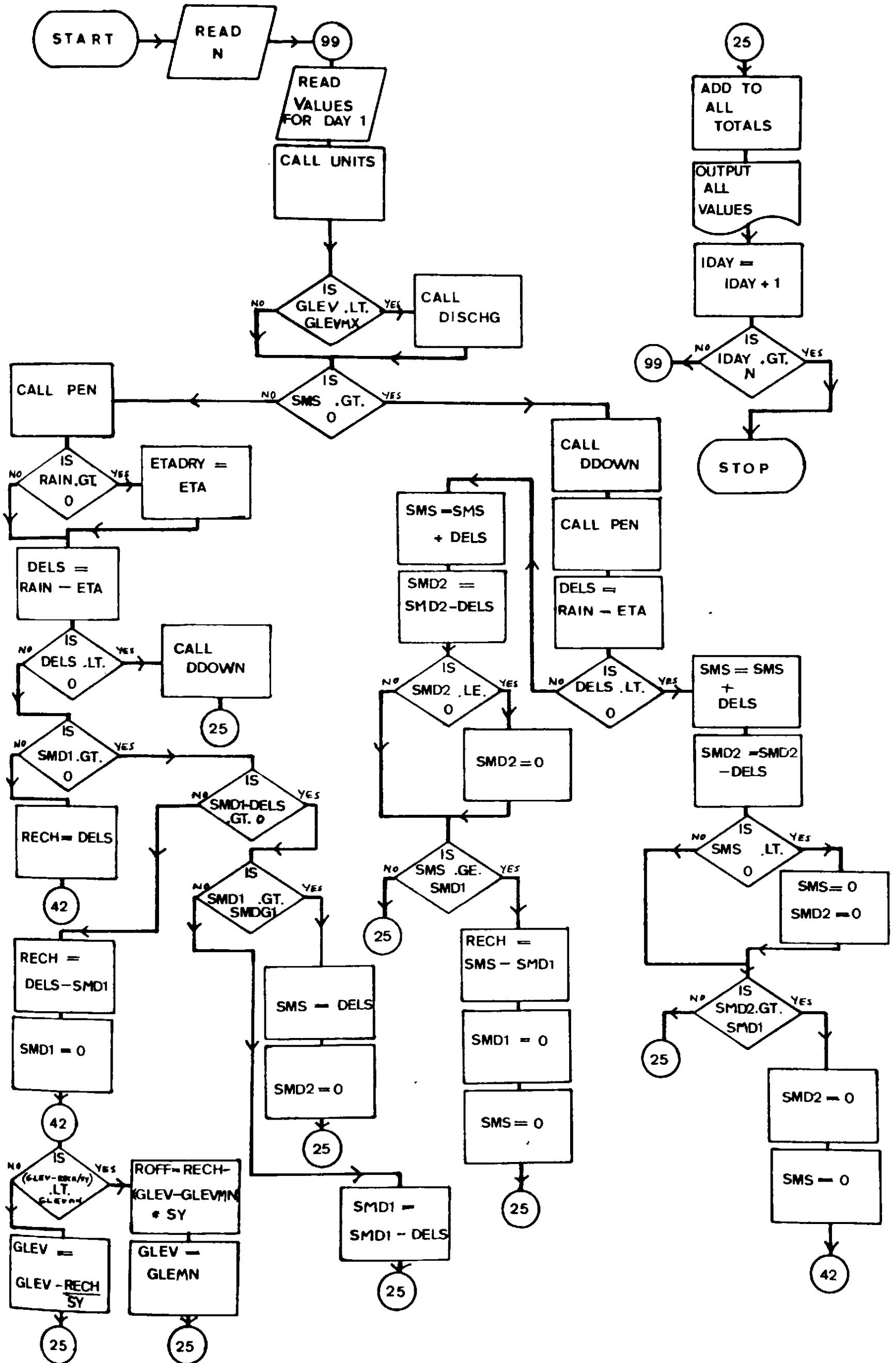


Figure 5-10 Flow diagram for water balance algorithm. Details of subroutines in Appendix E)

$$r_s = r_L + r_c + r_h \quad 5.6$$

where r_L = resistance due to moisture flow within the plant
 r_c = resistance due to soil cover
 r_h = resistance due to moisture content of the soil

$$r_a = \ln((z-d)/Z_0)^2 / k^2 u \quad 5.7$$

where z = reference level of anemometer
 d = zero plane displacement
 Z_0 = roughness length = $h/100$
 k = Von Karman's constant
 L = vegetation height

The terms in Equation 5.6 have been discussed in Section 2.4. The r_L term is approximately 50sm^{-1} and the r_c term is given in Table 2.21. The r_h term represents the resistance dependent upon the availability of soil moisture. From the sensitivity analysis presented in Section 2.4, it was found that if r_s approached 5000sm^{-1} during the dry season, then the estimated value of Eta was approximately 0.5mm day. In the recharge analysis therefore, the value of r_h is allowed to change from 0 to 5000 as the SMD passes between $RL - x$ and $RC + x$ as discussed above.

At the beginning of the rains, the r_h term again becomes zero, but the r_L term only decreases slowly as the ZFP advances, as described by the values in Table 2.21. In this manner, the actual evapotranspiration is modified to represent the slowly increasing moisture demand of the growing plants.

Equation 5.7 specifies the relation between the wind speed, and the vegetation height. A sensitivity analysis has also indicated the significance of Z_0 to the Eta value; as Z_0 increases, then Eta increases. This parameter represents the increasing roughness of the canopy and the aerodynamic transfer of water vapour produced. The size of the Z_0 term can be empirically related to the length of the growing season, which itself is a function of the number of days that moisture has been available at the top of the profile. The Z_0 term is allowed to increase to a limiting value before decreasing again at the end of the wet season.

Although the recharge model described above may seem complicated it provides an assessment of recharge which requires only the daily values of rainfall, observed sunshine hours, wind speed, relative humidity, and average temperature as input. The remaining parameters may be estimated and their sensitivity to the calculation established as necessary.

Assessment of model analysis results.

The recharge model forms a part of the catchment balance model which is described¹ in Section 6.3. The recharge results calculated by the model can therefore be verified as a part of the overall balance. However, to facilitate a comparison of the results with those of the conventional analysis, the data for 1979, summed on a ten day basis are presented in Table 5.9. The results for the conventional analysis listed in Table 5.6 are shown combined with the results produced by the water balance algorithm.

The model predicts a value of Eta which is 17% higher than the conventional analysis. Approximately half the estimated increase is accounted for by evaporation occurring during the dry season, however, the remainder arises from the changed assumption made about the soil moisture balance during the wet season. Column 4 of Table 5.9. shows the complicated variation during the wet season between the two predicted values of Eta.

In general terms, a redistribution of actual evapotranspiration is predicted by the model, with less occurring during the early part of the wet season, and more in the later part of the season than is predicted by the conventional analysis.

The value of recharge predicted by the model is approximately 15% lower than that of the conventional analysis.

In Table 5.10 the recharge results predicted by the model for the years 1969, 1970, 1971, 1972, 1973, 1974, 1978 and 1979 are presented. A root constant of 100m has been used in these calculations so that a comparison can be made with the average value predicted for Bauchi by Kowal + Knabbe (1972). The sensitivity of the calculation to the root constant is presented in Section 6.3.

Note 1. Figure 5.10 illustrates a flow diagram for the water balance algorithm. In Figures 6.4 and 6.5 the variations in the parameters which control recharge in the water balance algorithm are presented.

Table 5.9 Comparison of recharge results for 1979
Root constant = 100m.

Decade	Rainfall	Eta ¹	Eta ²	(Eta ² -Eta ¹)	Recharge ¹	Recharge ²
1	0.0	0.0	4.8	4.8		
2	0.0	0.0	4.5	4.5		
3	0.0	0.0	5.2	5.2		
4	0.0	0.0	4.9	4.9		
5	0.0	0.0	5.1	5.1		
6	0.0	0.0	4.0	4.0		
7	0.0	0.0	4.9	4.9		
8	0.0	0.0	5.0	5.0		
9	0.0	0.0	5.3	5.3		
10	0.0	0.0	4.7	4.7		
11	4.9	4.9	11.6	6.7		
12	32.3	32.3	14.8	-17.5		
13	49.3	49.3	38.6	-10.7		
14	10.0	10.0	37.9	27.9		
15	15.8	15.8	17.1	1.3		
16	40.9	40.9	26.1	-14.8		
17	23.4	23.4	28.5	5.1		
18	19.2	19.2	34.3	15.1		
19	95.3	40.7	29.8	-10.9		
20	165.5	41.9	37.2	-4.7	78.2	56.4
21	68.6	48.9	46.7	-2.2	19.7	23.0
22	74.7	40.6	37.9	-2.7	34.1	31.8
23	83.2	40.7	42.9	2.2	42.5	40.3
24	100.8	42.6	54.7	12.1	58.2	50.6
25	77.4	41.4	54.1	12.7	36.0	24.0
26	12.0	42.7	54.8	12.1	0.0	
27	76.3	44.6	59.7	15.1	1.0	
28	41.7	43.2	52.8	9.6		
29	0.0	43.8	44.7	0.9		
30	0.0	45.9	33.2	-12.7		
31	0.0	8.8	25.1	16.3		
32	0.0	0.0	13.2	13.2		
33	0.0	0.0	8.7	8.7		
34	0.0	0.0	5.3	5.3		
35	0.0	0.0	5.1	5.1		
36	0.0	0.0	5.4	5.4		
Total	991.3	721.6	869.0	+147.4	269.7	228

Notes. Eta¹ and recharge¹ are data produced by the conventional analysis. Eta² and recharge² are produced by the model described above.

5.10 Predicted annual recharge (Root constant = 100m)

	Kowal	1969	1970	1971	1972	1973	1974	1978	1979
Rainfall (mm)	1131	1067	946	1102	929	739	1154	1182	991
Eta (mm)	701	835	652	676	795	729	766	777	869
Recharge (mm)	400	348	405	531	257	128	485	498	228

The average of the calculated recharge values is 40mm less than that reported by Kowal + Knabbe. Given the uncertainty which is associated with both analyses the degree of agreement between the means is good. The conventional analysis predicts an extra 15% recharge.

The major advantage of the recharge analysis presented above is that it can be incorporated in a model of the water balance which is valid for the whole year. The inaccuracy of the conventional analysis during the early and late parts of the wet season is clearly shown in Table 5.9.

The recharge results are not greatly different as the inaccuracy in the calculation of Eta by the conventional analysis is for the most part offset by the concentration of rainfall in the two months that recharge occurs. The distribution and timing of the rainfall clearly has a very significant effect upon the recharge. The standard deviation about the mean of recharge in Table 5.10 is 145mm, with a maximum value of 531mm in 1971 and a minimum of 128mm in 1973. These figures represent 48% and 17% of rainfall respectively.

The timing between rain storms in any one wet season has a significant effect upon recharge. For example, 1970 and 1972 received similar quantities of rainfall, yet the recharge for 1972 was only 62% of that predicted for 1970. This degree of variation is significant as a basic parameter in the resource evaluation presented in Section 6.

5.4 Aquifer response to abstraction.

Introduction.

From the analysis of recharge presented in the preceding section, an estimate of the annual quantity of water available as recharge may be made. Similarly, from the geophysical work discussed in Section 4, an estimate may be made of the aquifer volume. However, before the yield of the system can be analysed, it is necessary to consider the response of the aquifer to abstraction.

In Section 5.1, the hydraulic conductivity of the grade II, III and IV material was described. The change of hydraulic conductivity from fracture controlled in the grade II material to intergranular flow controlled in the grade IV material produces a characteristic drawdown response, the implications of which are described below.

General.

For an aquifer formed from alluvial or sedimentary deposits, the pump test is the accepted method for establishing values of transmissivity and specific yield. If the aquifer can be considered as homogeneous, then the general differential equations of unsteady flow in an unconfined environment may be represented by Equation 5.8.

$$\frac{\partial}{\partial x} (K_x h \frac{\partial h}{\partial x}) + \frac{\partial}{\partial y} (K_y h \frac{\partial h}{\partial y}) = S_y \frac{dh}{dt} \quad 5.8$$

where K_x = hydraulic conductivity in x (m day⁻¹)
 K_y = hydraulic conductivity in y (")
 h = hydraulic head (m)
 S_y = specific yield

The specific yield S_y is defined as the ratio of the volume of water that the aquifer yields by gravity drainage to the volume of its dewatered part. The specific yield has a value very close to that of the effective porosity.

If the hydraulic conductivity of the aquifer is assumed to be homogeneous and isotropic, Equation 5.8 reduces to :

$$T \left(\frac{\partial^2 h}{\partial x^2} + \frac{\partial^2 h}{\partial y^2} \right) = T \nabla^2 h = S_y \frac{dh}{dt} \quad 5.9$$

where T = transmissivity ($h \times k$)

$$\nabla^2 = \text{Laplacian Operator} = \frac{\partial^2}{\partial x^2} + \frac{\partial^2}{\partial y^2}$$

Solutions to Equation 5.8 may be found in analytical terms subject to the restriction that the aquifer may be considered isotropic and inhomogeneous. However, as has been discussed above this degree of uniformity is seldom found in weathering aquifers.

In Section 4, a finite difference discretisation was used to solve the equations of current flow in an inhomogeneous electrical conductivity distribution. Equation 5.6 may be solved in a similar manner, however, for three reasons this was not attempted here. These reasons may be summarised briefly as :

- 1) No detailed knowledge of the boundary conditions.
- 2) Probability of turbulent flow in grade II material close to the abstraction well (Uhl + Sharma, 1978)
- 3) A lack of good quality pumping test data (Rushton, 1978).

Streltsova + Adams (1970) have produced a summary of analytical techniques for heterogeneous aquifer formations, where the hydraulic conductivity is a combination of fracture and intergranular flow. However, these analytical techniques all assume a constant value of transmissivity and therefore may not be used here.

Pump test results.

The difficulties of analysing weathering environment aquifers has been described briefly above. However, it is still necessary to carry out a pump test upon a successful borehole in order that the pump setting may be determined and an operating regime for the borehole specified. It is important that this pump test should adequately reflect the operating conditions required of the borehole.

The results of four pump test are described below. In the following section, these results are qualitatively interpreted.

Three of the four tests are from the area around Bauchi. Examples 1 and 2 are from boreholes sited using the apparent resistivity profiling techniques described in Section 4. Example 3 shows the results from three boreholes sited using seismic investigations. Example 4 is from the area of Takum in Eastern Nigeria. The geological conditions are similar to those around Bauchi.

Example (1)

A number of boreholes were drilled into the weathering trough delineated in Area A. Borehole 5 (Figure 3.4) was air lifted with a continuous yield of approximately $10\text{m}^3/\text{hr}$ for 12 hours with no sign of any fall in yield. Drawdown measurements were not available. The success of this borehole prompted the possibility of carrying out a longer term test using boreholes on either side of the abstraction borehole as observation boreholes.

In June 1976, borehole 5 was tested for 36 hours at a constant rate of $12.5\text{ m}^3/\text{hr}$. The pumped water was carried away by pipes to a stream some 300m distant and to the side of the weathering trough. The water level in the pumped well 16 days before the test was 2.60m below datum, while on the morning of the test, this had risen to 2.31m. From the discussion in Section 5.3 it may be seen that these water levels indicate that recharge to the aquifer had begun for this wet season, and that therefore there was no soil moisture deficit.

Measurements of drawdown were made in boreholes 4 and 6 during the test, and initially at boreholes 3 and 7 in addition. As the pumping was carried out by the air lift method, it was not possible to measure drawdown in the abstraction boreholes. The observation boreholes were situated approximately 100m uphill (no 4) and 100m downhill (no 6) from the abstraction borehole. The gradients may be seen on Figure 3.4.

Although approximately 450m^3 of water was removed from the abstraction borehole. No drawdown was observed at the observation boreholes.

Both borehole No 4 and borehole No 6 showed a slight rise during the test, of 120mm and 60mm respectively. Although a number of theories may be proposed to explain the lack of response, the only clear implication is that this borehole is capable of producing greater than $12.5\text{ m}^3/\text{hr}$.

Example (2)

A borehole was sited on a resistivity low anomaly adjacent to deep weathering Area B. The geological log is shown in Table 5.10 The standing water level in the borehole was 2.65m, and the test was carried out during February.

The borehole was air lifted at a rate of $6.3\text{ m}^3/\text{hr}$ for 330 minutes.

At the end of air lifting, the hose was disconnected as quickly as possible and measurements were then made of the water table recovery (residual drawdown). The maximum drawdown in the borehole measured at three minutes after the end of pumping was 1.16m.

Table 5.1) Geological log of test well.

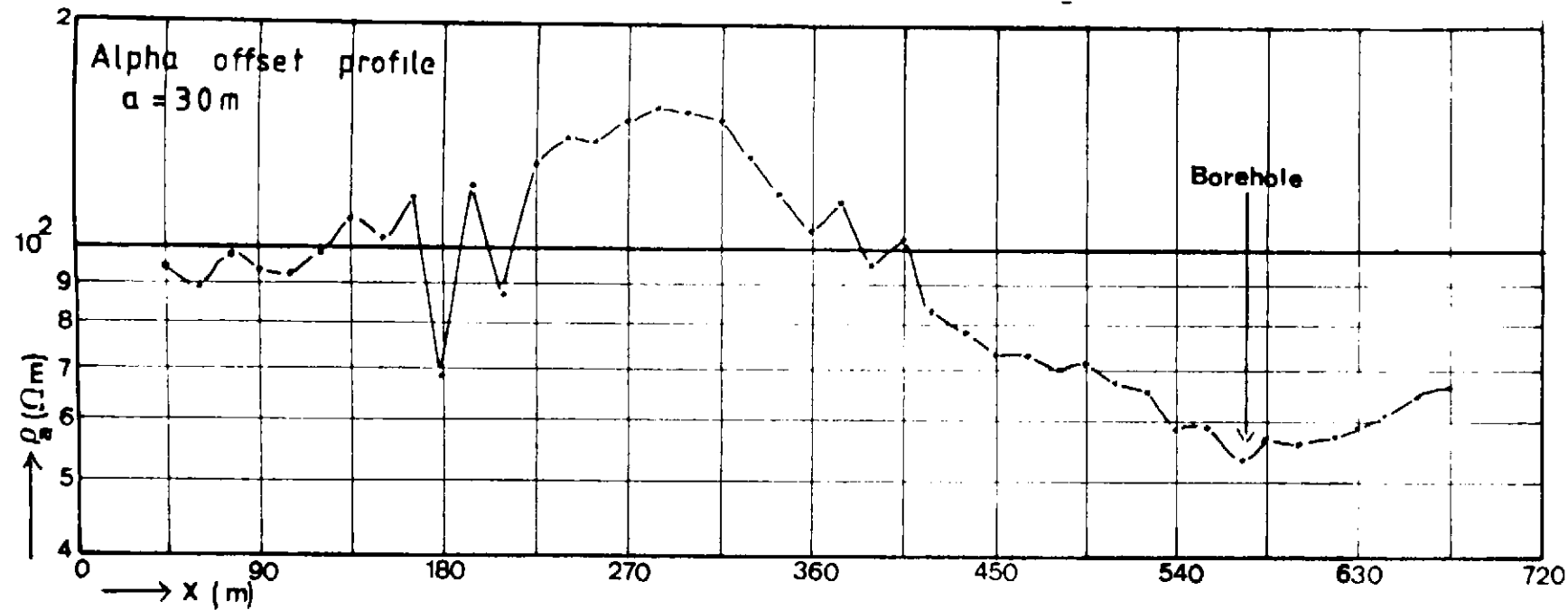
Depth (m)	Description	Weathering Grade
0-2.7	Top soil + clay	VI
2.7-5.5	Clay loam	VI
5.5-8.2	Silty clay	V
8.2-10.9	Fine sand/silt	V
10.9-13.7	Fine sand	IV
13.7-16.4	Medium sand	IV
16.4-19.1	Sand with granite chipping and some basalt fragments	III
19.1-21.9	Coarse gravel with large granite chippings	III
21.9-24.6	Coarse gravel/sand with basalt + granite chippings	III
24.6-27.4	Compact medium sand	III
27.4-35.6	Basic dyke material	II

The resistivity anomaly and the recovery data are shown in Figure 5.11. From this figure it can be seen that at this low pumping rate, the recovery data shows a linear relationship when plotted against the log of time. This indicates that within the area of response, the analytical solution may be used, and a value of transmissivity of $80\text{m}^2\text{day}^{-1}$ has been calculated from the data.

The quantity of water pumped from the borehole was only 35m^3 and this was not sufficient to effectively test the aquifer for boundary conditions. However, the test does show that the transmissivity of the aquifer in the immediate vicinity of the borehole is quite high.

Example (3)

A number of boreholes were sited around Bauchi by the Bauchi State Water Board during 1977 and 1978. Upon completion, each borehole was pump tested for a period of three hours using a submersible pump.



Pump test data
 $Q = 6.25\text{ m}^3/\text{hr}$ for 330 minutes
 $T = 76\text{ m}^2/\text{day}$

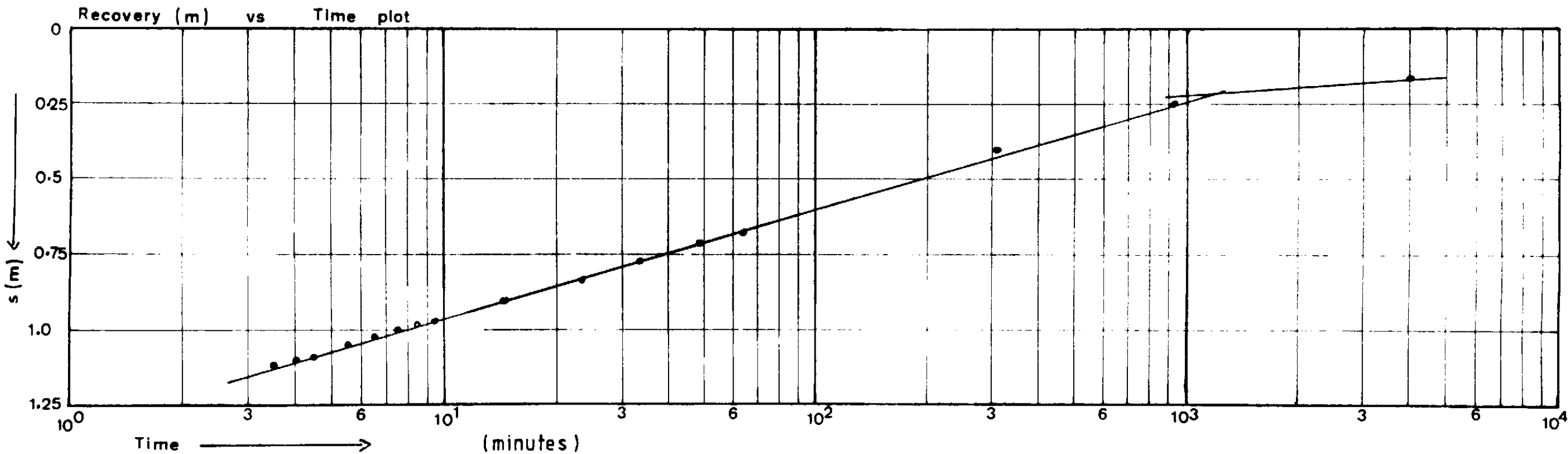


Figure 5-11 Pump test recovery data — with resistivity profile data showing borehole location.

Drawdown and recovery measurements were made in each borehole.

Each borehole was constructed with 6 $\frac{5}{8}$ " casing and 6" Johnson stainless steel screen. The more productive boreholes were gravel packed.

The drawdown and recovery measurements from three of these boreholes are shown in Figure 5.12.

The yields of the boreholes vary considerably, although they are sited within a few hundred metres of each other. The first test indicates dewatering of the complete borehole, to what was probably a fracture at depth. The flow from this fracture was then sufficient to maintain the yield of the borehole.

The second and third tests indicate high yielding boreholes.

Example (4)

Many of the boreholes around Bauchi, drilled as a part of the above exercise, later either dried up, or showed a substantial decrease in yield. This is not surprising if their flow is, in some cases, dominated by a single fracture.

To investigate the longer term pumping response of aquifers of this type, a series of tests was carried out in another area. The geological conditions in this area are similar to those around Bauchi.

In Figure 5.13 the resistivity profile data is shown above the drawdown and recovery data for a borehole pumped at 15 m³/hr for a period of 6500 minutes (4.5 days).

In Figure 5.14 and by contrast to the previous data set, three drawdown and recovery plots are shown for a borehole some 200m distant from the former borehole. A pumping rate of 11.4 m³/hr was first used to test this borehole, and after 200 minutes the drawdown in the borehole became excessive. A rate of 9.1 m³/hr was then tried and after 300 minutes the drawdown again became excessive. A pumping rate of 6.8 m³/hr produced a drawdown which tended to stabilize after 1000 minutes.

The lack of a regular drawdown response at the higher pumping rates is typical of a large number of pump tests from basement weathering aquifers. Similarly, a high yielding initial stage is also characteristic. The pump test are qualitatively interpreted below.

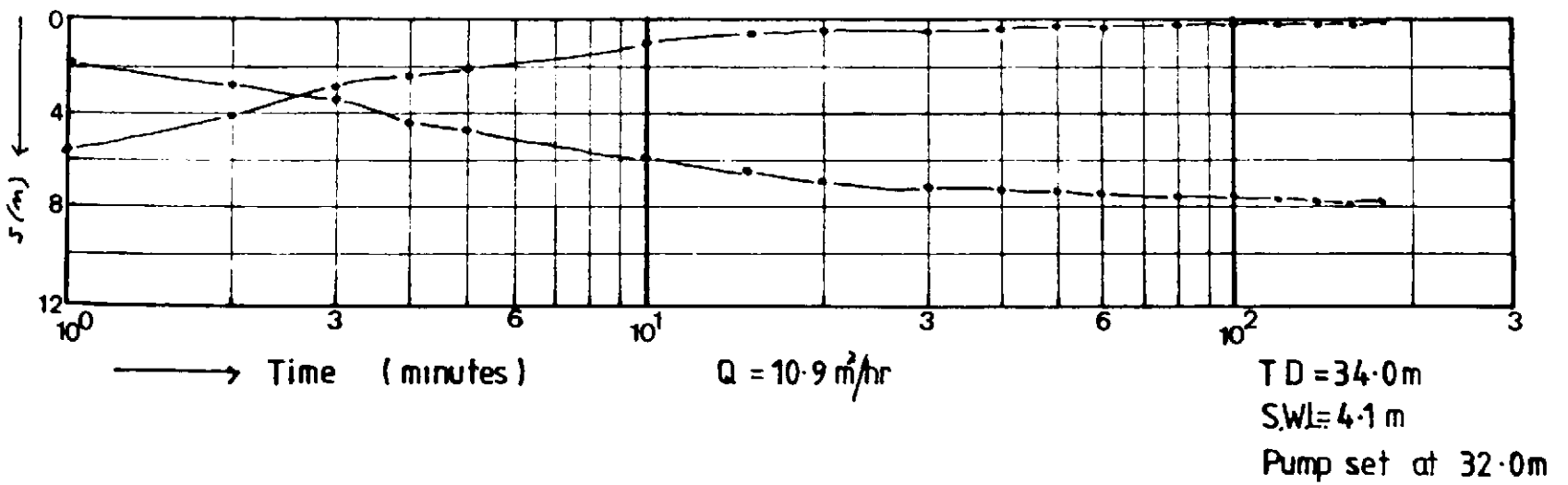
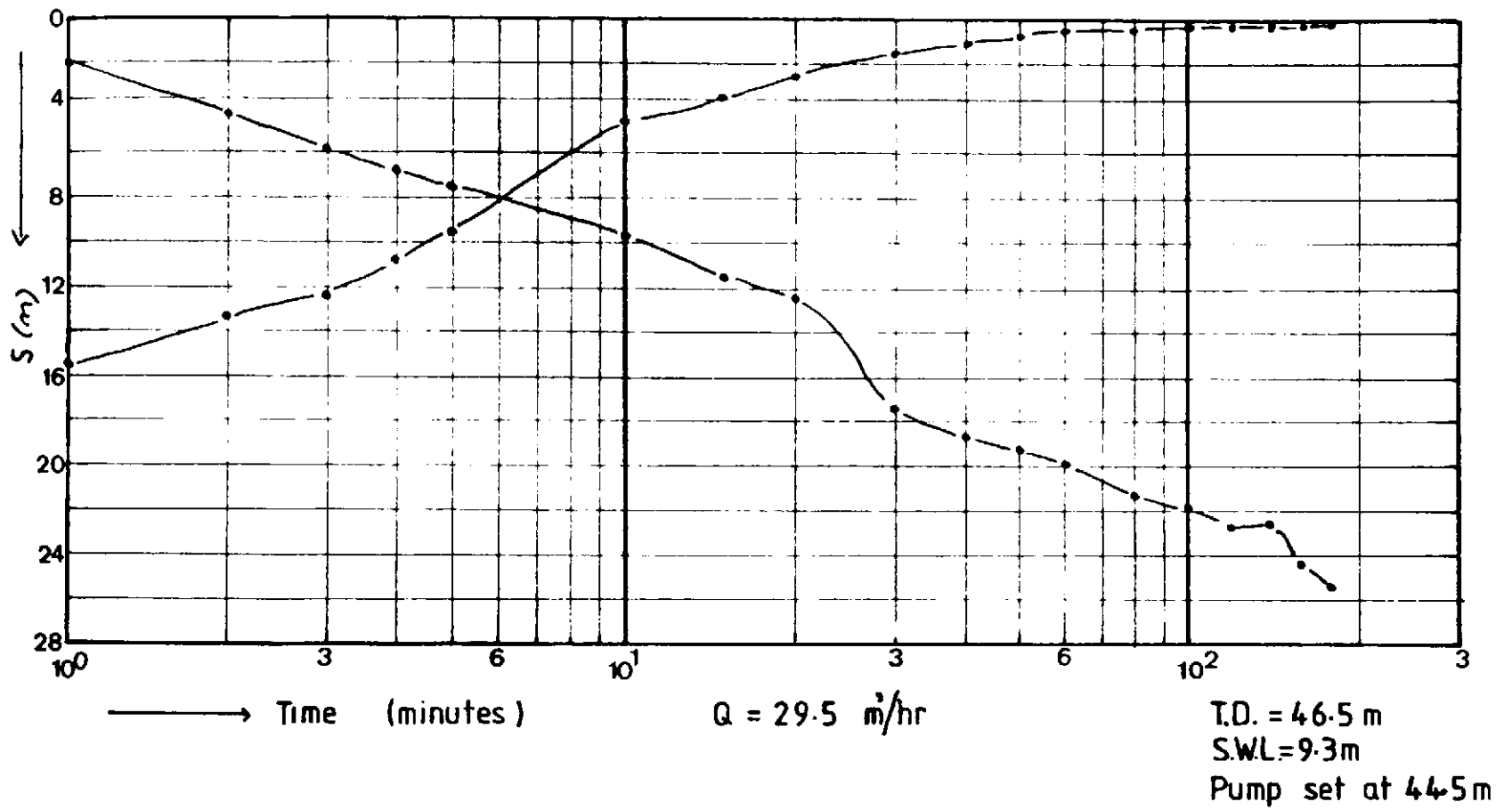
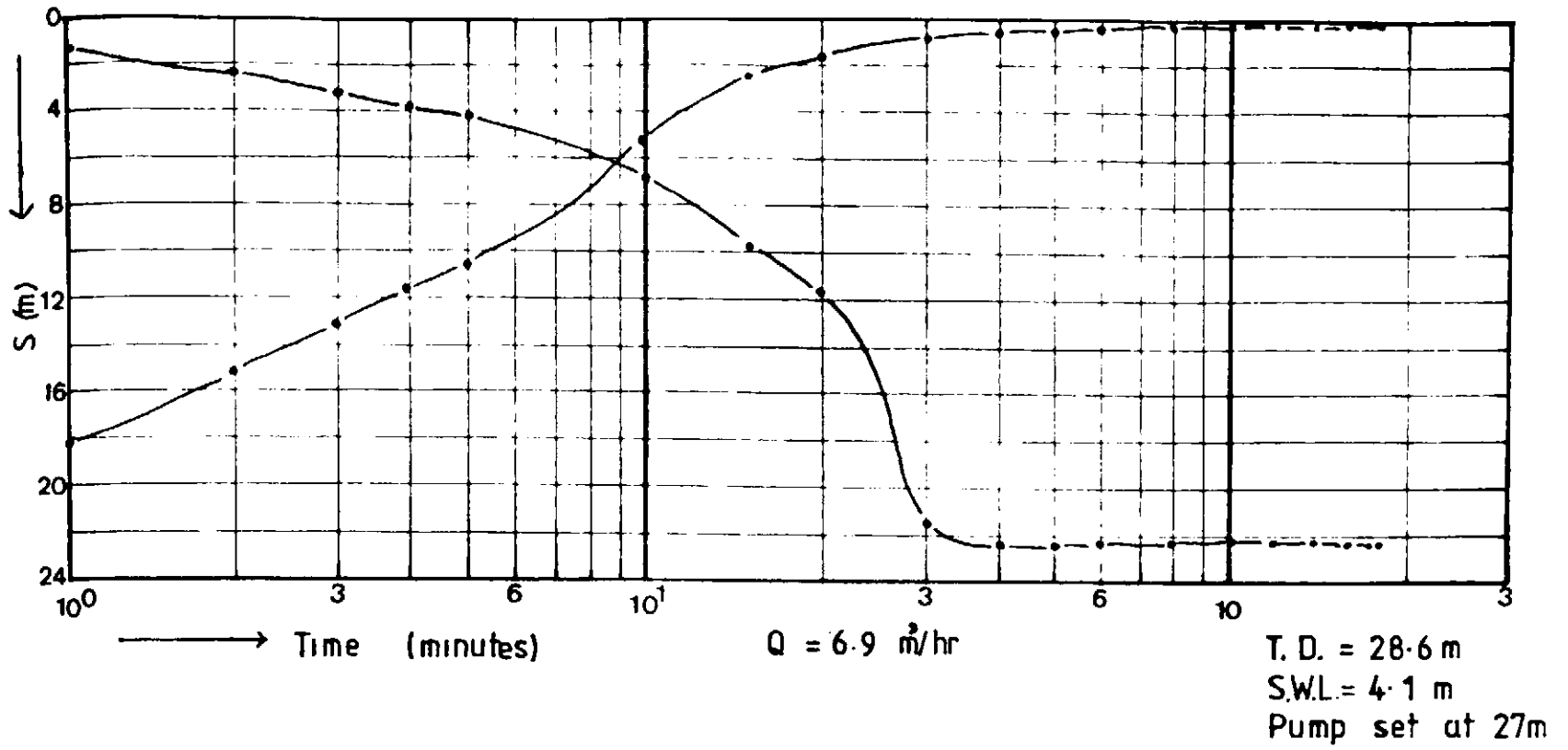
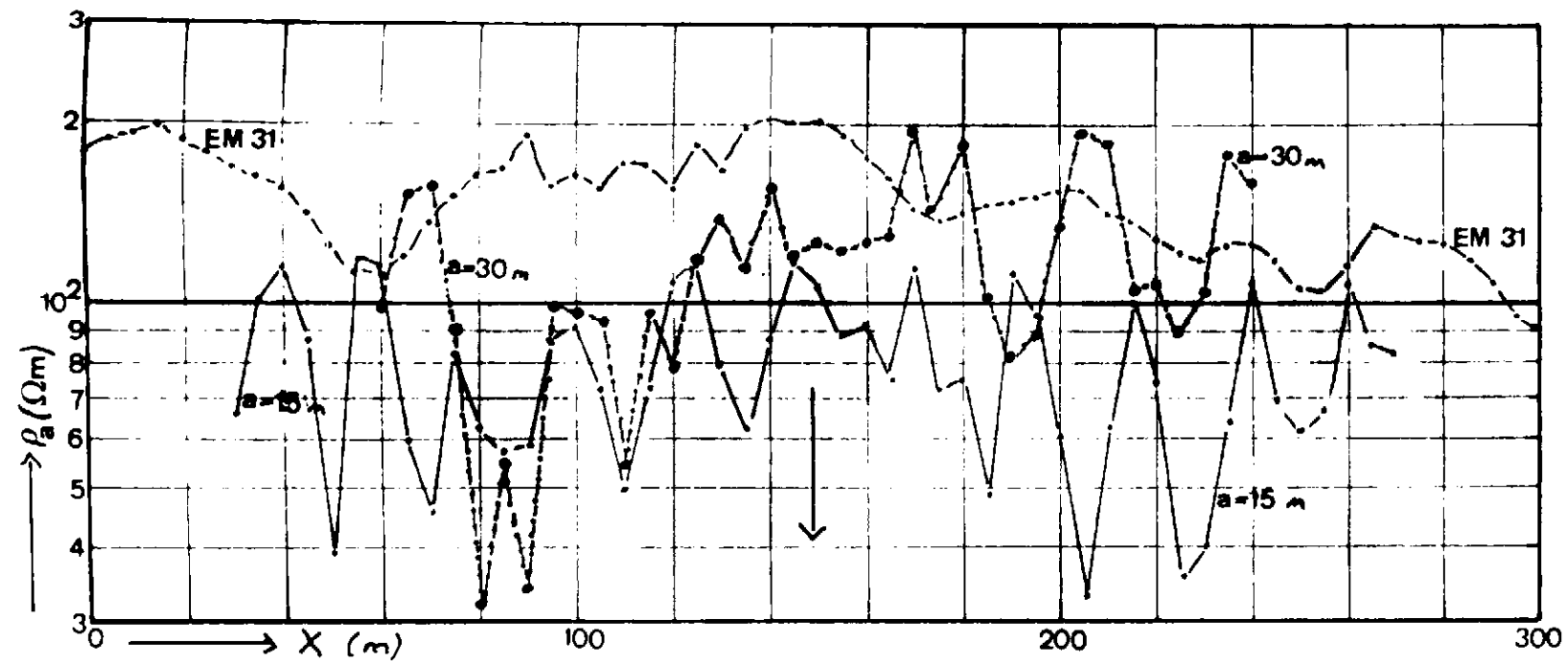


Figure 5-12 Pump test drawdown and residual drawdown data for three boreholes in the BAUCHI area. (Data from Edok Eter Mandilas Nig. Ltd.)



$Q = 18.18 \text{ m}^3/\text{hr}$

T.D. = 61.7 m

S.W.L. = 6.25 m

Pump set at 57 m

$T = 35 \text{ m}^2/\text{day}$

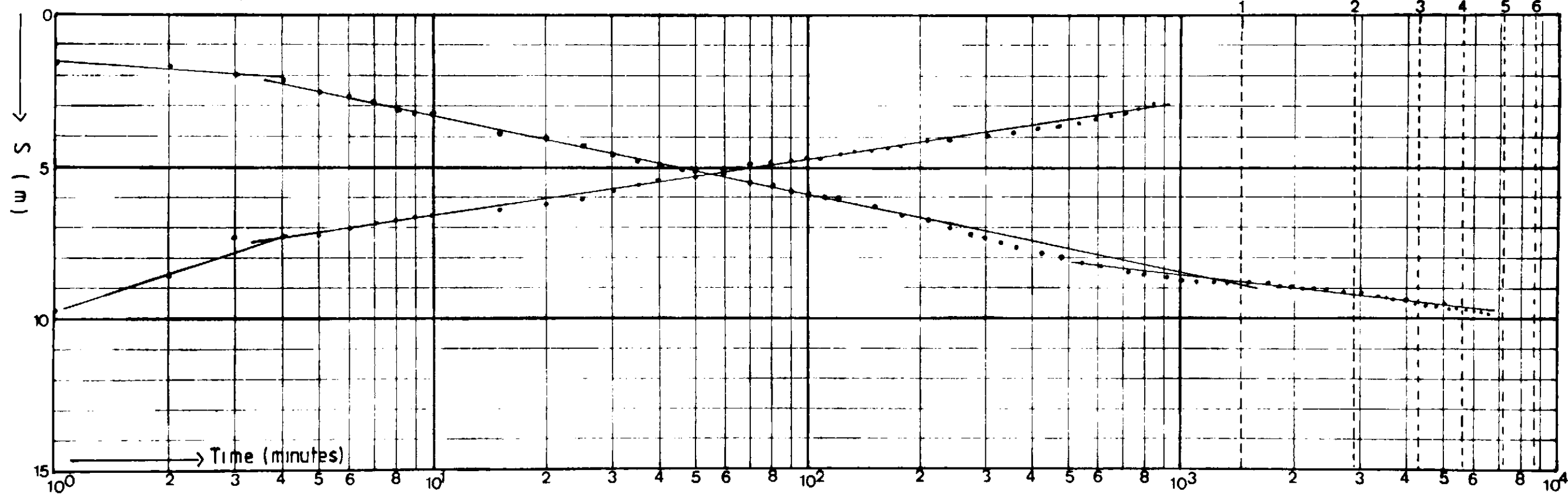


Figure 5-13 Pump test drawdown and residual drawdown data showing borehole location resistivity profile data.

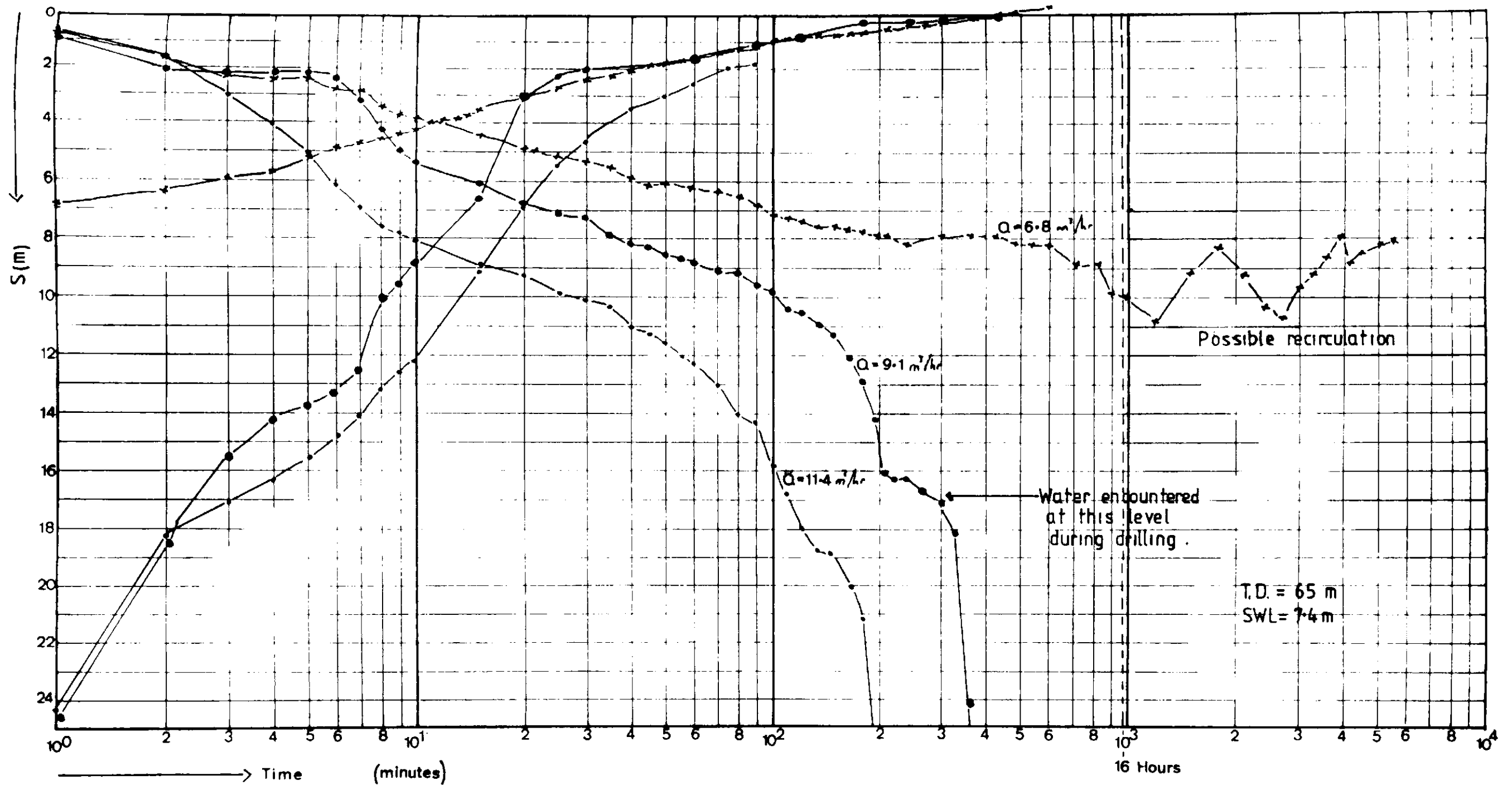


Figure 5-14 Drawdown and residual drawdown data for three pumping rates.

The 16 hour maintainable yield is $7 \text{ m}^3/\text{hr}$

Pump test interpretation.

A number of dominant characteristics may be identified from the pump test results presented above, viz;

- 1) Borehole yields are very variable within a small area.
- 2) For a wide range of pumping rates, the initial drawdown response is small, although this response may only last for 10 or 20 minutes.
- 3) The time drawdown response when plotted on a semi log scale shows a complicated response. This is particularly well marked in Figure 5.12 and 5.14.
- 4) The recovery at the same borehole from different pumping rates is often very similar. Figure 5.14 indicates this feature, and results from several other boreholes not described here showed a similar response.

As all the boreholes which were pump tested were sited using either resistivity or seismic refraction techniques it is probable that they all passed through a full succession of weathering grades and were terminated in grade I material. The difference in drawdown response and yield can therefore only be explained by differences in the extent of the weathering grades and by different values of hydraulic conductivity encountered.

It has been noted above that the grade II material will have predominantly fracture controlled hydraulic conductivity. Although the fracture porosity is less than that of the intergranular porosity, the fracture hydraulic conductivity is several orders of magnitude greater than the intergranular hydraulic conductivity. For boreholes which penetrate the grade II material therefore, a limited quantity of water, contained in the fractures, can flow rapidly into the borehole. When this quantity of water has been abstracted however, the drawdown increases reflecting the lower rate at which water is released from the intergranular material.

This dual response may be identified on several of the drawdown and recovery plots.

Although further work could be carried out to analyse the response at a particular site, the variability of conditions within a very small distance means that the extra work is not justified. However, if the volume of grade II material is limited, then it is possible that

a short pump test of 3 or 4 hours will not cause dewatering of the fracture zone. If an operating regime of 12 hours pumping and 12 hours rest is recommended, the dewatering may occur after 8 hours, causing the yield to fail and the pump to stop. A pump testing sequence related to the operating regime is therefore required.

Pump test design.

It has been demonstrated above that the weathering aquifers have a variable response to abstraction. The dual nature of the hydraulic conductivity produces typically a complicated drawdown response, which generally shows a rapid drawdown and dewatering of the borehole after a varied time period. Recovery is often rapid however, indicating the complexity of the system.

For such a heterogeneous system, there is little purpose in carrying out a detailed analysis of pump test results. Values of transmissivity obtained only represent very localised conditions. However, there is a danger that a short pumping test will only produce a response from the fracture part of the system, which cannot be maintained for more than a few hours.

The maintainable operating yield is in general considerably less than the initial, higher yield.

The operating regime of the borehole is likely to be 12 or 16 hours pumping with 12 or 8 hours rest when demand is low. The pump test therefore should be designed to produce the maximum pumping rate which corresponds to a reasonable drawdown over the pumping period. To achieve this objective in a reasonable period of time, a reverse form of step test is suggested here. The borehole should be first pumped at a high rate. If excessive drawdown occurs within 12 or 16 hours, then the borehole should be allowed to recover and a reduced pumping rate attempted. This process should be repeated until an acceptable drawdown yield relationship is maintained for the recommended operating period.

The recovery rate after the breakaway, or successive drawdown occurs is usually very rapid, indicating seepage from the overlying grade IV material. Therefore this method of testing does not entail a long period of time between phases. The results of such a test are shown in Figure 5.14.

5.5 Summary.

From a consideration of the porosity and hydraulic conductivity of the various weathering grades, a potential aquifer has been identified in the grade II to IV weathering zones. In areas where these grades of weathering are developed below the base level of local drainage, an aquifer exists which retains groundwater throughout the dry season.

The aquifer may be locally confined where grade V and VI weathering is developed. In the limiting case where an unbroken cover of these weathering grades extends for a distance of several kilometres, recharge to the underlying zones will be very small. It follows therefore, that outcrop areas of grade II to IV weathering are necessary in the vicinity of a weathering trough to act as recharge zones. Annual recharge is required to support abstraction as the total volume of each aquifer is limited to the area of deep weathering. The storage is therefore limited and the aquifer hydraulically isolated.

Groundwater hydrographs were presented which indicated a number of important features viz:

- 1) No recharge occurs to the water table before the dry season soil moisture deficit is eliminated.
- 2) The groundwater level continues to fall until the SMD is eliminated, at some time after the beginning of the rains.
- 3) The groundwater level continues to fall after local drainage channels have completely dried up.

An assessment of the annual quantity of recharge to the aquifer forms an essential part of the aquifer evaluation. Traditional methods of calculating the recharge based upon 'C' and 'D' values were assessed, and rejected as they do not adequately represent the savanna environment. In particular, the complete drying out of the near surface soil, to soil moisture values below the permanent wilting point implies that no further evapotranspiration occurs during the dry season, if the conventional model is assumed. However, the continued fall of the dry season water table after base flow to streams has ceased suggests that evaporation continues, albeit at a reduced rate, throughout the dry season.

Four conceptual soil moisture profiles were presented which represent soil moisture changes throughout the year. These profiles were

described in detail and used as the basis for the construction of a one dimensional model of recharge.

A description of the model is given in Appendix E where the algorithm is presented.

A number of the more important features of the recharge model are listed below.

- 1) The Monteith equation in calculating Eta is used.
- 2) The resistance terms r_s and r_a in this equation are predicted based upon a soil moisture deficit model.
- 3) Net radiation, albedo and the r_h term in the Monteith equation are all modified as the SMD increases from a value of $RC - x$ to $RC + x$, where RC represents the root constant and x is approximately equal to 20mm.
- 4) A maximum SMD equivalent to $RC + 35$ is assumed.
- 5) Evaporation occurs from the water table at an increasing rate commencing when the SMD is equal to half the rooting depth. The evaporation demand is completely satisfied by losses from the water table when the SMD reaches the maximum value.
- 6) A zero flux plane at the beginning of the wet season is represented by accumulating excess rainfall over evapotranspiration in a soil moisture store. A soil moisture deficit is allowed to develop in the soil moisture store, which controls the prediction of the r_h and r_L terms in the Monteith equation. When the quantity of water held in the soil moisture store is greater than the dry season deficit, then this deficit is eliminated and recharge occurs to the water table.

Lastly in this section, a review of available pump test data was made. The response to abstraction indicates a variation of hydraulic conductivity between fracture flow and intergranular flow.

The highly variable conditions around each borehole make any assessment of transmissivity meaningless. For this reason, no detailed pump test interpretation was attempted. However, a testing regime designed to establish the greatest rate of abstraction that can be maintained for the operational pumping period (12 or 16 hours) is recommended.

A period of pump testing of this type would identify those boreholes which were unable to maintain their initial pumping rates and would therefore result in a great reduction in the number of boreholes which are reported to dry up some time after pump installation.

6. RESOURCE ASSESSMENT.

Introduction.

The purpose of this final section of the thesis is to draw together the various aspects of the groundwater resource discussed in the preceding four sections, and to present both an overall assessment of the resource and a simple methodology for the development of that resource.

In the first two parts of this section, the groundwater resource distribution and size are discussed.

To obtain an assessment of the resource yield, an approximate value of specific yield is required. This may only be obtained in practise by observing the fall in groundwater level that is caused by a known abstraction or loss of water. It was demonstrated in the preceding section that the pump testing method could not be used due to the extensive variation in hydraulic conductivity within weathering aquifers. A second possibility exists if the groundwater hydrograph response can be modelled by a sufficiently accurate assessment of the inputs and outputs as discussed in Section 5.3. The prediction of recharge has been discussed above. In the third part of this section, the recharge assessment is used as a part of a simple black box model of a small catchment water balance. The sensitivity of this water balance to changes in root constant and specific yield is assessed. From this assessment a method for adjusting the values of root constant and specific yield so that a match is achieved between the model data and the observed data is suggested.

The values of resource size and specific yield are combined in the fourth part of this section to produce an assessment of the annual yield of the resource. The order of accuracy of such an assessment is discussed and the implications for a resource development policy analysed.

In the fifth part of this section a generalised methodology for the location and development of the resource is discussed. Two levels of development are appropriate. The lower level ($\leq 0.5 \text{ m}^3/\text{hr}$) corresponds to that of abstraction by simple means from hand dug wells, while the second ($> 5 \text{ m}^3/\text{hr}$) represents abstraction by mechanical pumps from boreholes.

A number of the aspects of the resource assessment analysis presented in this thesis require further research, therefore in the penultimate part of this section a number of research priorities are discussed.

Finally, in the last part of this section, the various aspects of the complete work are summarised.

6.1 Resource Distribution.

General.

It has been found in the study area that two conditions must be satisfied before an area of weathering may be considered as a potentially useful resource, viz;

- 1) The area of weathering must extend for a considerable (> 15m) depth below that of the local drainage base level, and
- 2) An area where grade II and III weathering occurs at the surface must be in hydraulic continuity with the more deeply weathered zone.

The first condition represents the fact that an area of storage must be available to satisfy dry season abstraction. The second condition represents the important conclusion that, as basement weathering aquifers are of limited extent, a means of recharging them annually is required.

These two preconditions significantly restrict the areas of basement outcrop in which groundwater resources are located. Of the two conditions however, it is the second which has the widest implications.

Importance of recharge areas.

It has been noted above, and has been commented upon by a number of authors (Brown, 1975; Uhl + Sharma, 1978; Ternan + Williams, 1979), that the highest hydraulic conductivity and the greatest yields, occur in grade II and III weathered material, towards the base of the weathered profile. In addition, in the great majority of boreholes drilled into the centre of weathered zones, a considerable sub-artesian rise is encountered, typically of the order of 10-15m. In a limited number of occurrences, a small artesian flow is noted.

These observations strongly imply that no recharge is possible through the overlying more weathered zones.

Recharge must therefore occur laterally, where the grade II and III material outcrops around the edge of the weathered trough. Similarly, it is in these areas that the recharge model, described in Section 5, is operative. In Figure 6.1, this principle is illustrated

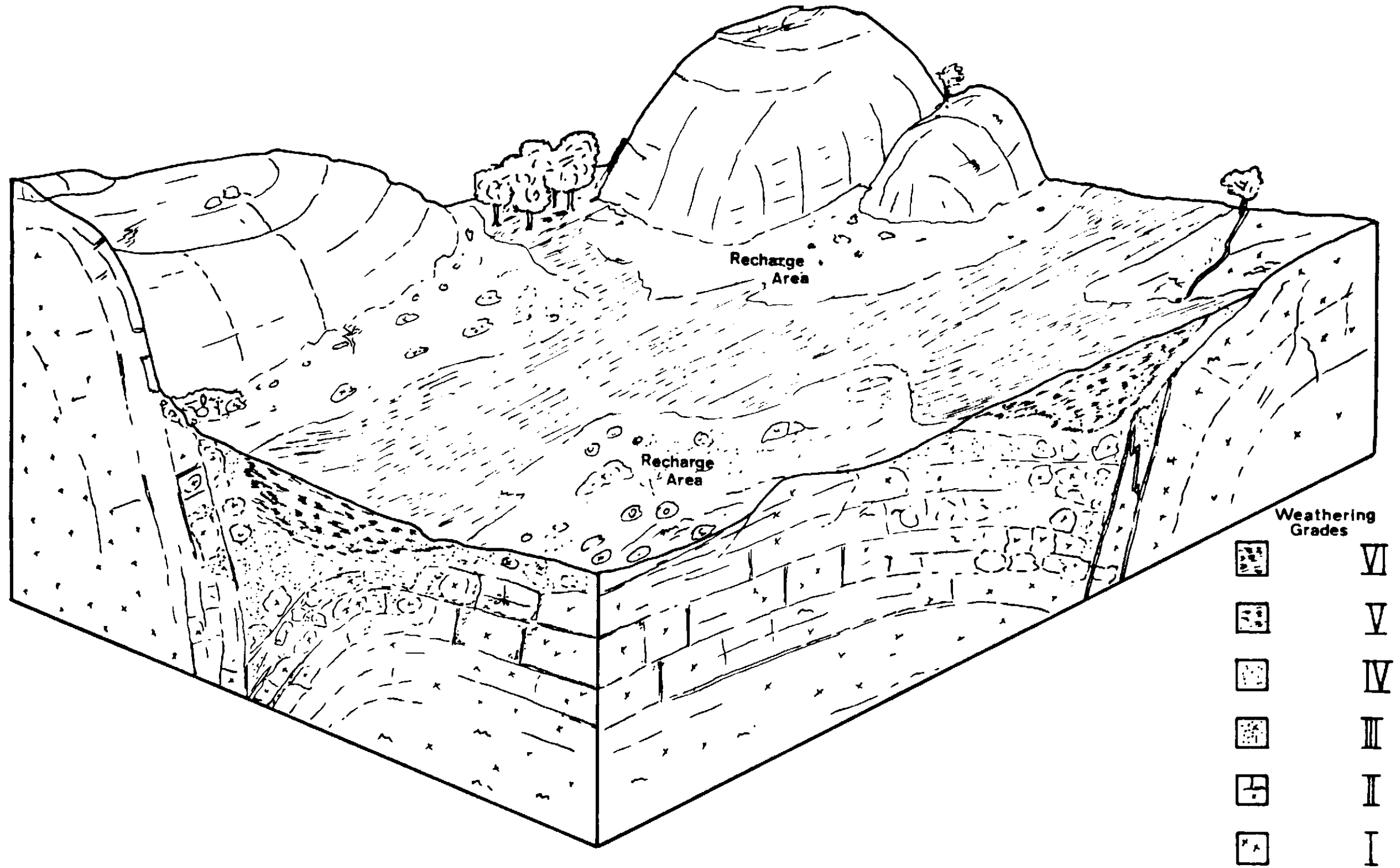


Figure 6-1 Isometric diagram to illustrate relationship between recharge areas and a weathering trough.

diagrammatically. Recharge areas can be seen in a number of the Plates included above, but are best illustrated in Plates 2.6, 3.6 and 3.14.

If it is accepted that recharge must occur laterally, then it must also be accepted that where grade V and IV weathering grades (of low hydraulic conductivity) become laterally extensive, then little or no recharge is possible to the underlying more hydraulically conductive horizon.

Over large areas of the basement outcrop, a mature erosion surface, or peneplain, has been formed as a result of stable conditions over long periods of time. In these areas, the weathering is often deep ($> 20\text{m}$) with the grade V and VI material laterally extensive over large areas ($> 10^2\text{km}$). Extensive lateritisation has occurred (see Figure 5.2(ii)) with often an inversion of topography occurring (Ollier, 1975). The deep weathering encountered in these areas is often considered to have occurred in the geological past, and the profiles have been thought of as fossil weathering profiles. The area around Kaduna in Northern Nigeria is a typical example of such conditions. In these areas, few successful boreholes have been drilled and the yields of these boreholes are usually very small.

Possible weathering reactions were discussed in Section 3, and it was concluded there that a flow of water was necessary at depth to remove the products of hydrolysis formed during weathering. It was further suggested that in the absence of any groundwater flow, these reactions would attain a state of equilibrium and effectively, stop. In areas where no recharge is possible therefore, it seems that active weathering is also not possible. The weathering in such an area will continue, guided by faulting, fracturing and rock mineralogy, until the weathering products (grade V + VI material) accumulate in sufficient depth at the surface to cut off recharge (and discharge).

One important implication of the above analysis is that recharge areas, and therefore, groundwater resources, are only to be found on basement rocks which are undergoing active erosion.

Resource Location.

From an examination of the remote sensing data, areas of basement

which are being actively eroded may be readily identified. In particular, from the SLAR products (see Sections 1 and 3), it is possible to rapidly identify areas of outcrop, fracture traces and drainage lines controlled by fracturing. Many examples of these features may be identified on Plate 3.9, indicating that the Bauchi Plains area is being actively eroded.

In general terms, it is therefore possible to restrict the area of probable groundwater occurrence from an informed study of the remote sensing data. Large areas may be discarded if there is no indication of shallow weathering profiles, however, the notes relating to Figure 5.2(ii) are also relevant in this respect.

Localised areas of deeper weathering within regions which are being actively eroded, may be identified on remote sensing data as usually having an even tone. It is in these areas that further investigation should be concentrated.

There is some evidence to indicate that areas of deeper weathering developed about fractures of a specific orientation are likely to produce better yields of groundwater. Both in the Bauchi and Takum areas of Northern Nigeria, an orientation of approximately north south ($0^{\circ} \pm 10^{\circ}$) produced high yielding zones. Bourguet + Camerlo (1980) report a similar orientation from the Cote d'Ivoire. In either case it is probable that the fracture orientation formed by the most recent deformation is likely to produce the most extensive recent weathering. The weathering associated with fractures formed by older deformations is more likely to have been removed by erosion, or to have reached a point where no further weathering is occurring. The removal of the weathering products associated with older fractures leaves them more clearly visible on aerial photography or SLAR, however, for the reasons outlined above, the most clearly visible fracture set is not necessarily likely to be associated with the greatest depth of recent weathering.

6.2 Size of the Resource.

General.

Groundwater resources have been associated in the previous part of this section with areas of basement undergoing active erosion. Within these areas, small localised aquifers are likely to be widely distributed, and fairly common. For reasons discussed above, each area of deeper weathering is isolated hydraulically, and it is important therefore to obtain an estimate of the size of these zones, before their usefulness as a separate resource can be assessed.

With the exception of a detailed programme of site investigation drilling, geophysical techniques provide the only available means for obtaining a measure of the size of an individual area of weathering.

Apparent resistivity profiling results.

Electrical resistivity profiling methods have been described in Section 4. Profiles obtained with the EM-31 electromagnetic system can very rapidly establish the limits of an area of weathering.

For the siting of hand dug wells (see Section 1) or improved wells (Water Surveys, 197^o), the results from the EM-31 are sufficient.

In Figures 4.7 and 4.8, which show apparent resistivity contours over two areas, the extent of weathering may be clearly seen. The area contained within the 150 Ω m apparent resistivity contour approximately represents the extent of the aquifer. The predominant linearity of the anomaly is clearly seen and is further evidence of the influence of fracturing on the development of weathering zones.

The width of the anomaly is typically 250m (\pm 150), and is bounded laterally by a rapidly increasing apparent resistivity. The ratio of the length to width of the anomaly is generally >5 and may exceed 15.

Hand dug wells can be sited anywhere within the anomaly, although sites towards the margins are likely to encounter water at shallower depths than those in the centre of the anomaly.

Sites for boreholes, where a yield of 5-10m³/hr is required, need to be selected with greater care as it is possible that the

total annual abstraction may exceed the quantity of water contained within the aquifer. It is advisable therefore, to compile profile section data for the investigation of such sites.

Apparent resistivity profile section results.

The three resistivity profile sections presented in Figures 4.9, 4.11 and 4.13 provide an indication of the cross sectional area of the weathering trough. The model (see Appendix C) represents an infinitely long trough with no resistivity variation in the y or strike direction. This approximation will not lead to significant error if the trough is of an order of magnitude longer in the y direction than in the x direction, and as has been shown above, this is generally the case. The models therefore provide a method of assessing the cross sectional area per unit length of trough.

Code values 3 and 4 represent weathering grades (III + IV) and II respectively. As the grade II material represents fractured rock, the porosity of this zone will be lower than the grade II + IV zones, however the permeability will be several orders of magnitudes greater (Streltsova-Adams, 197^o). The two areas may not therefore be amalgamated, as the combination of fracture flow and intergranular flow is responsible for a number of the characteristic features of the aquifer.

The depth of each model element of the completed resistivity profile section is shown in each of the figures. The width of each element is 2.5m. From these measurements the areas occupied by the various grades of weathering may be evaluated. In Table 6.1, these areas are listed, obtained from Figures 4.18, 4.19 and 4.20.

Table 6.1 Areas of weathering grades calculated from resistivity profile sections.

	Area A(m ²)	Area B(m ²)	Area D(m ²)
Grade III+IV weathering (Code 3)	6.0 x 10 ³	4.3 x 10 ³	2.0 x 10 ³
Grade II weathering (Code 2)	8.9 x 10 ³	4.1 x 10 ³	3.2 x 10 ³

The markedly greater size of the grade II material in Area A is the result of the weathering extending to the greater than usual depth

of approximately 90m.

It is appreciated that the values shown in Table 6.1 are based upon a number of assumptions¹, however the models do represent a possible solution which may be supported by other data and therefore the average values are used in the following analysis of yields, viz $5.0 \times 10^3 \text{ m}^2$ for grade II weathering and $4.0 \times 10^3 \text{ m}^2$ for the grade III + IV weathering.

The approximate volume of weathering per metre of weathering trough is therefore $5.0 \times 10^3 \text{ m}^3$ of grade II material and $4.0 \times 10^3 \text{ m}^3$ of grade III + IV material. The margin of error of these estimates is difficult to quantify, but $\pm 1.5 \times 10^3 \text{ m}^3$ seems probable.

Two further examples of resistivity profile sections for situations of hydrogeological importance are shown in Figures 6.2 and 6.3. Figure 6.2 represents the profile produced over a relatively narrow fracture zone with little grade III + IV material present. This situation may correspond to a fracture in granite with little additional weathering. Figure 6.3 corresponds to a more extensive weathering development with some development of laterite in the top of the soil profile. The section is very similar to that shown for deep weathering area A and the two may therefore be compared to analyse the effect of a discontinuous 0.5-1.0m layer of laterite developed at the surface.

The results shown in Figure 6.3 indicate that the presence of a thin layer of laterite does not have a significant effect upon the resistivity profile results. The poor readings that are often obtained in this situation must therefore be the results of high contact resistances at the surface.

Note 1. In particular no allowance has been made for the effects of equivalence (Koefoed, 1979) in the profile sections. It is probable that several solutions could be constructed to fit the field data by varying the apparent resistivities selected.

RESISTIVITY PROFILE SECTION

Calculated from the model resistivity distribution shown below

ELECTRODE POSITIONS

10 METRES APART

X- 0 1 2 3 4 9 8 7 6 5 4 3 2 1 19 16 17 18 19 20 21 22 23 24 25 26 27 28 29 30 31 32 33 34 35 36 37 38 39 40

A= 10 653 654 654 653 652 649 644 635 615 543 511 299 189 184 113 101 95 91 85 65 56 51 51 57 64 85 122 203 329 361 404 417 423 426 428 428 429 429

A= 20 1045 1042 1035 1022 997 952 852 820 843 698 384 320 298 182 154 151 139 109 87 82 84 90 104 136 178 268 445 542 541 567 630 659 674 682 686

A= 30 1328 1294 1231 1113 1001 1103 1098 967 762 507 393 356 269 234 216 195 156 126 123 138 159 183 223 325 529 670 744 726 719 749 825 866

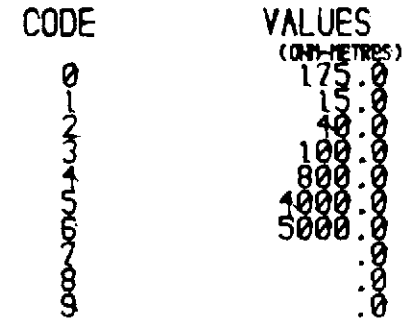
A= 40 1311 1281 1302 1290 1331 1228 1096 865 559 444 418 341 327 286 249 214 185 189 197 223 268 371 593 756 871 932 898 875 869

A= 50 1450 1487 1530 1448 1300 1148 920 613 507 489 411 383 362 321 279 250 242 261 306 417 650 832 963 1060 1107 1064

A= 60 1708 1631 1507 1394 1219 978 676 578 558 466 435 417 390 338 299 310 348 457 699 893 1045 1156 1237

A= 70 1691 1609 1466 1277 1041 746 648 611 514 474 448 427 395 369 394 503 746 947 1103 1232

MODEL RESISTIVITY DISTRIBUTION



DEPTHS (METRES)

CODED RESISTIVITY DISTRIBUTION

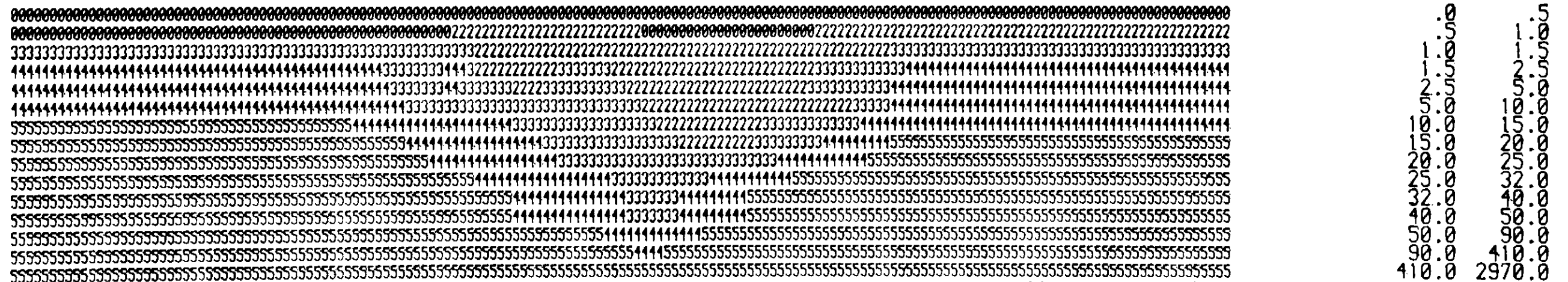


Figure 6-2 Profile section results over a narrow weathering trough.

6.3 Small catchment water balance.

Introduction.

A method for predicting daily evapotranspiration and recharge has been described in Section 5.3. In this section a lumped parameter model of a water balance is presented and the results predicted by the model, compared with those of a small catchment study at Samaru (Kowal, 1970b).

Description of the model.

The analysis of the water balance is based on the assumption that all rain received over the catchment basin leaves the catchment either by evaporation, transpiration, or by the combined flow of seepage and surface runoff. The weathering profile has been discussed in detail above, and from this description it may be seen that there is no loss of groundwater flow at depth. The water balance at the catchment can therefore be estimated from the equation

$$R - Q - S - W - \text{Eta} = 0 \quad 6.1$$

where

- R = rainfall
- Q = surface runoff
- S = seepage to streamflow
- W = change in soil moisture
- Eta = evapotranspiration

Rainfall is measured by a rain gauge on a 24 hour, or less, basis, and a description of this parameter has been given in Section 2.2.

The estimation of evapotranspiration by the Monteith equation has been described in Section 5.3.

The remaining parameters in Equation 6.1 can be estimated from the recharge and Eta predicted by the analysis described in Section 5.3, in the following manner.

Recharge which occurs when the soil profile above the water table is at field capacity passes through the soil to the water table. The water table will rise by an amount which depends upon the specific yield of the aquifer and the hydraulic gradient at this horizon. To simplify the analysis, the specific yield is assumed to be a

constant value, and the hydraulic gradient across the area to be negligible.

As the water table continues to rise it will pass the elevation at which discharge occurs by seepage to stream flow. The quantity of this discharge will depend upon the hydraulic conductivity of the material, and upon the elevation difference between the water table and the stream base level. The quantity of seepage will increase therefore as the water table rises.

During years with average rainfall, the recharge will be sufficient to bring the water table close to the surface. As further recharge would raise the water table above the surface, any recharge in excess of that required to bring the water table close to the surface is assumed to be lost as surface runoff. A storm producing 30-40mm of rainfall on a catchment which already has a high water table produces an almost immediate flood spate in the local drainage.

During the dry season, it is assumed that evaporation occurs directly from the water table, and that the process does not alter the soil moisture deficit created by previous evapotranspiration in the soil profile. The water table falls therefore by an amount controlled by the predicted evapotranspiration and the specific yield.

A complicated situation occurs as the wet season conditions change to dry season conditions. For the purposes of this study, the variables are assumed to change as shown in Figure 6.4. The change in albedo, ground flux of net radiation and the R_s term have been described in Section 5.3, however, it is the partition of evaporation between the soil profile and the water table which is of significance here.

It is assumed that evapotranspiration, represented entirely by transpiration, occurs at a rate unrestricted by soil moisture until the SMD is greater than 80mm. This level of deficit represents loss of all the available moisture within the top metre of soil, and therefore the wilting of a number of short rooted plants. After this time evaporation commences from the soil profile as a large area of the soil is no longer covered by vegetation. Also at this time it is assumed that the soil moisture potential gradient becomes negative throughout the profile and a loss of water is induced from the water table. The proportion of E_t which is assumed to be replaced by loss of moisture from the water table changes as shown in Figure 6.4. ,

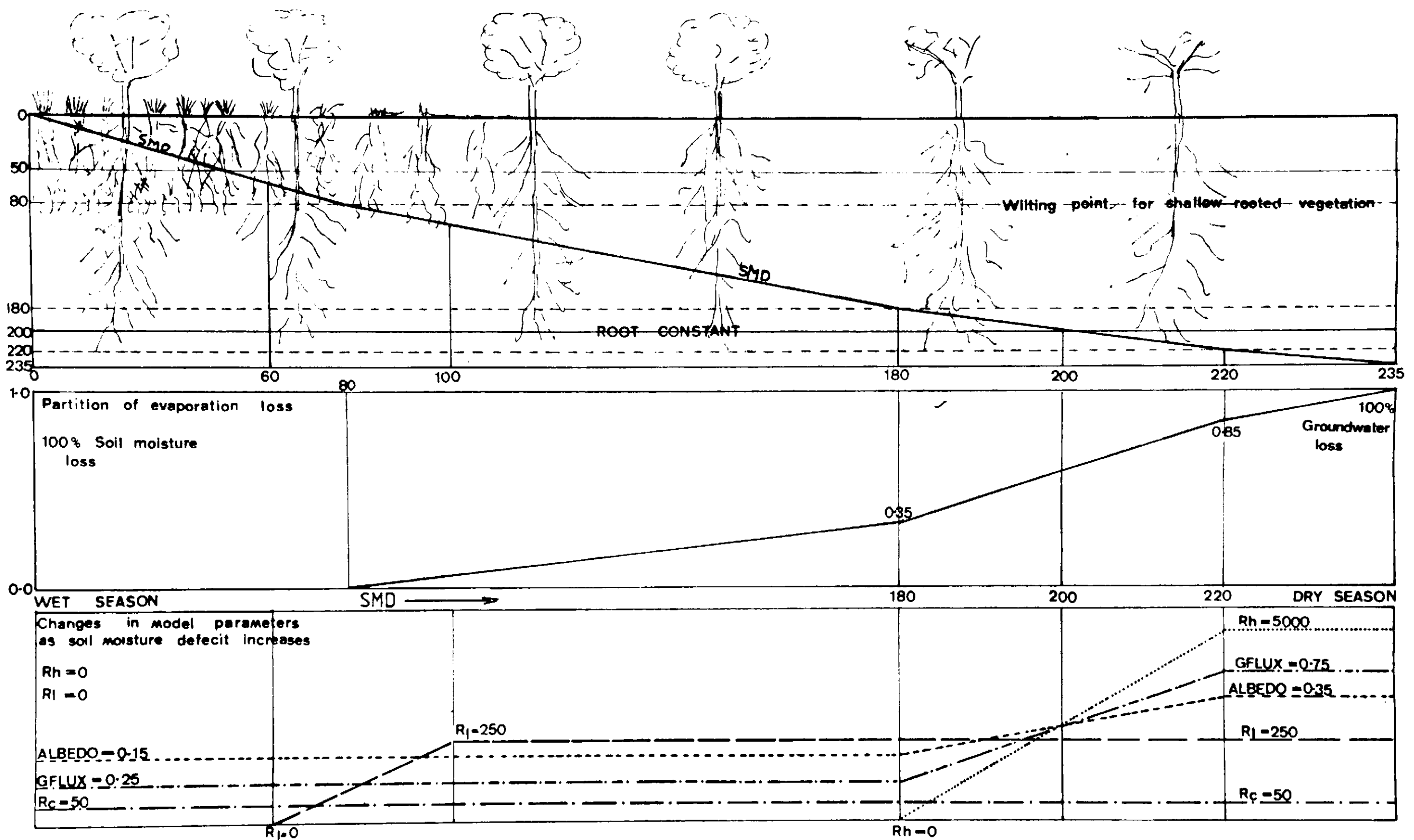


Figure 6-4 Water balance model conditions during early dry season.
 Root constant = 200mm.

When the SMD reaches the maximum value permitted (root constant + 35mm), all the predicted Eta is assumed to be represented by moisture loss from the water table. It should be noted that as the SMD passes through the range of values about the root constant, the predicted value of Eta is greatly reduced, therefore the quantity of evaporation from the water table remains approximately the same.

The partition of Eta between the SMD and the water table has the result that the maximum soil moisture deficit is only very slowly approached, and may not be reached in some years.

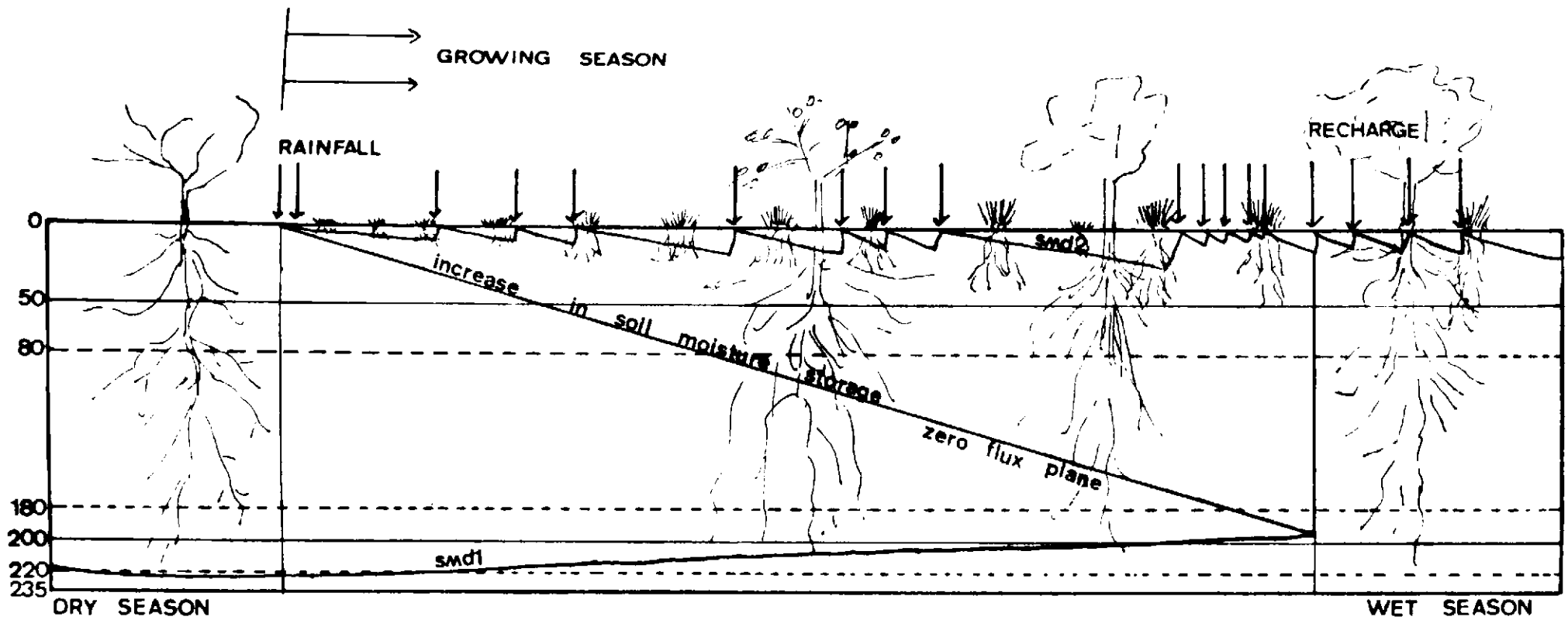
From the end of the dry season and during the period before recharge reaches the water table, the soil moisture potential gradient remains negative beneath the zero flux plane (ZFP). Moisture continues to move from the water table until the ZFP reaches the water table. It is assumed here that the rate of movement continues at a value predicted by the lowest Eta estimated during the dry season. In this way the water table continues to fall until recharge is received. Moisture cannot however pass through the ZFP and therefore the moisture loss from the water table is redistributed in the soil above the water table. In effect the SMD below the ZFP is reduced marginally at this time.

The conditions which occur during the early wet season are illustrated in Figure 6.5.

An algorithm has been written to perform the catchment water balance, based upon daily input of the climatic variable, wind speed, rainfall, relative humidity, observed sun hours and average temperature. The algorithm is presented in Appendix E. A part of this algorithm uses a library of graphical subroutines (GINQ-F) to produce the data for the balance in the form of a diagram. Some examples of this output are included below.

Initial conditions.

In model studies of the kind outlined above, it is necessary to start the model from a set of known conditions. There is only one time during the year when all the conditions can be stipulated, and that is after a rainfall event which has produced runoff. At this time the SMD is known to be zero, and the height of the water table is also known. However, without working the balance it is not possible to say when exactly it will occur. It is also possible that if there

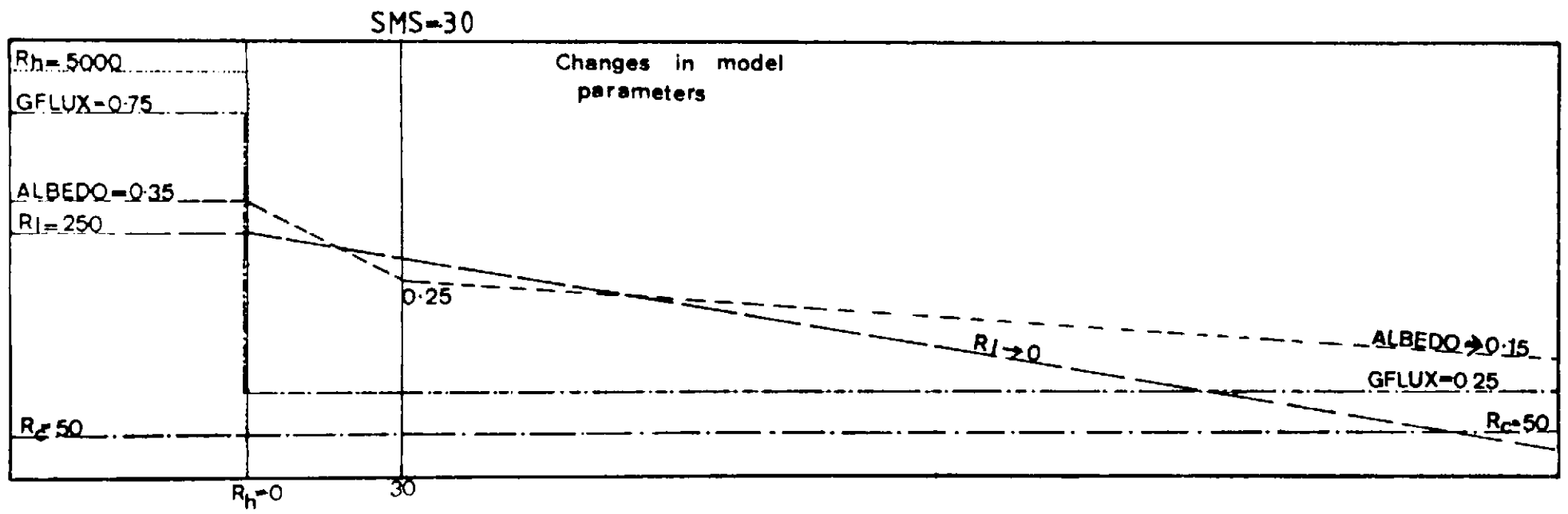


Comments

Growing season progresses unless SMD 2 becomes greater than SMS

When moisture held above the zero flux plane, in the soil moisture store, is greater than SMD1, recharge begins.

SMD1 Decreases beneath zero flux plane.



Albedo and Rf parameters increase as growing season progresses.

Figure 6-5 Water balance model conditions during the early wet season.

is insufficient rainfall in a particular year then no runoff will be produced.

As there is a large measure of uncertainty in specifying the wet season conditions, the balance has been started for each of the following studies on January 1st. At this time it is assumed that the SMD is approximately 10mm greater than the root constant, and that the water table is at a level similar to those observed on the groundwater hydrograph at this time. Although the predicted water balance for the initial year may be in error due to these initial condition assumptions, as long as runoff occurs during the first year the model conditions are set correctly for the second and subsequent years of data.

Observed water balance results.

Before presenting the results of the model analysis, it is of use to present the observed data from a small catchment. In this manner the predicted results may be compared with the observed results.

Kowal (1970b) has presented the results from six years of observations at Samaru. A small dam was built at Samaru and a curved venturi flume weir installed into the dam crest. In this manner, the quantity of runoff + seepage lost from the catchment was measured. Rainfall was measured from 25 gauges installed over the catchment (640 ha), and evapotranspiration was estimated from an equation of the form shown in Equation 6.1.

The results from this experiment are reproduced in Table 6.2.

From Table 6.2 a number of points of importance should be noted viz;

1) The results for individual years show considerable variation. To adopt the mean value as representative of the catchment response disguises the underlying variability. This is also the case for years with similar rainfall. The years 1967 and 1968 illustrate this point well.

2) Seepage commences approximately 1 month after the rise in the dry season water table, and lasts for 60 to 120 days.

3) Runoff varies widely and is not highly correlated to rainfall ($r = 0.81$).

Table 6.2. Water balance for the Samaru catchment, (after Kowal, 1970b)

	1966	1967	1968	1969	1970	1971
Duration of water year ¹	377	350	371	390	330	360
Rainfall over the catchment	1382	990	998	1196	884	775
Number of rainy days	95	83	77	88	77	70
Date of rise in dry season water table (Day Number)	192	196	203	180	212	200
Cumulative rainfall (CP) at the time of the rise in water table	506	419	516	381	460	391
Start of flow over spillway (Day Number)	223	198	227	206	237	238
End of flow over spillway (Day Number)	346	315	289	319	292	293
Total runoff + seepage	459	269	160	480	305	287
Runoff	259	168	8	180	81	49
Seepage	200	101	152	300	224	238
Eta	923	721	838	716	599	488

Note.1. The water year is taken as the time between the last rainfall of each season.

2. Seepage calculated from water table observations.

3. The lake required 30mm of runoff before flow over the spillway commenced.

- 4) Between 40 and 50% of the annual rainfall occurs before the rise in the dry season water table.
- 5) Kowal reports a root constant for the catchment of 100mm.
- 6) The groundwater hydrographs for two wells within this catchment are presented in Figure 5.4.

The daily climate data for the Samaru catchment is not available to the author, and therefore the model balance algorithm results cannot be compared directly with the observed data. However, the catchment size, land use and rainfall parameters are similar to those around Bauchi and therefore the results are broadly comparable.

Presentation of model results.

The results from a comparatively complex computer model are often difficult to present in a concise form. For this reason, a graphical package (GINO-F + GINOGRAF) has been used to present the results for two years data in a convenient form. As several sets of model results are presented below it is of use to briefly summarise the salient points on these diagrams.

- 1) All results are presented on a daily basis.
- 2) Rainfall is shown as a histogram with the scale shown on the left hand axis.
- 3) Evapotranspiration is shown listed as a daily variable with the scale indicated on the right hand axis.
- 4) Combined seepage and runoff are shown in the middle of the figure with a scale on the left hand side (y +ve).
- 5) The groundwater hydrograph is shown plotted below (y -ve), the middle x-axis with a scale shown on the left hand side.
- 6) Recharge is shown on the same x-axis and shown as a histogram plotted with a -ve y-axis, the scale of which is shown on the right hand side.
- 7) The soil moisture deficit which exists beneath a zero flux plane (SMD1), if present, and throughout the rest of the year is plotted with a -ve y-axis at the top of the figure.
- 8) The existence of a ZFP is shown by the quantity of moisture in the soil moisture store (SMS). This is depicted by the red line

plotted on the same axes as SM1.

9) The S¹D which is developed above the ZFF is also shown plotted on the same axes as S¹D2.

In this manner the relative changes between the model parameters can be readily comprehended, and in addition the dates of the groundwater table rise, the beginning and the end of seepage can be displayed.

The totals for each year are shown displayed above the position of 'January' for each year.

The values for the root constant and the specific yield are shown at the top of the diagram. The sensitivity of the balance to these parameters is discussed below.

Results for Bauchi during the period 1969-1974.

The results for Bauchi climate station data are shown in Figures 6.6, 6.7 and 6.8. A root constant value of 100mm has been used for this model run to coincide with the value interpreted for the Samaru catchment by Kowal + Kassam (1970). The only difference therefore lies in the daily variation of the rainfall and evapotranspiration for the two stations. As discussed above, they represent similar areas within the same climatic belt. The average rainfalls for the two areas during the six year periods are 1039mm for Samaru and for Bauchi, 990mm.

In Table 6.3, two sets of data from Samaru, representing observed results, and two sets of data from Bauchi representing the model results are compared. All four sets of data have very similar annual rainfall totals.

The results predicted by the model are very similar in most respects to those observed at Samaru. The only major difference is seen in the quantity of rainfall received before the groundwater begins to rise, and this factor is the result of the difference in regional location between the two stations in as much as Bauchi does not receive as many early season storms as Samaru due to the blocking action of the Jos Plateau (see Section 1 for location maps).

The major cause of variability in water balances computed for areas within the savanna is the distribution of rainfall. The results presented in Table 6.3 clearly indicate this point. The data

SOIL MOISTURE DATA

ROOT CONSTANT = 100

SPECIFIC YIELD = .050

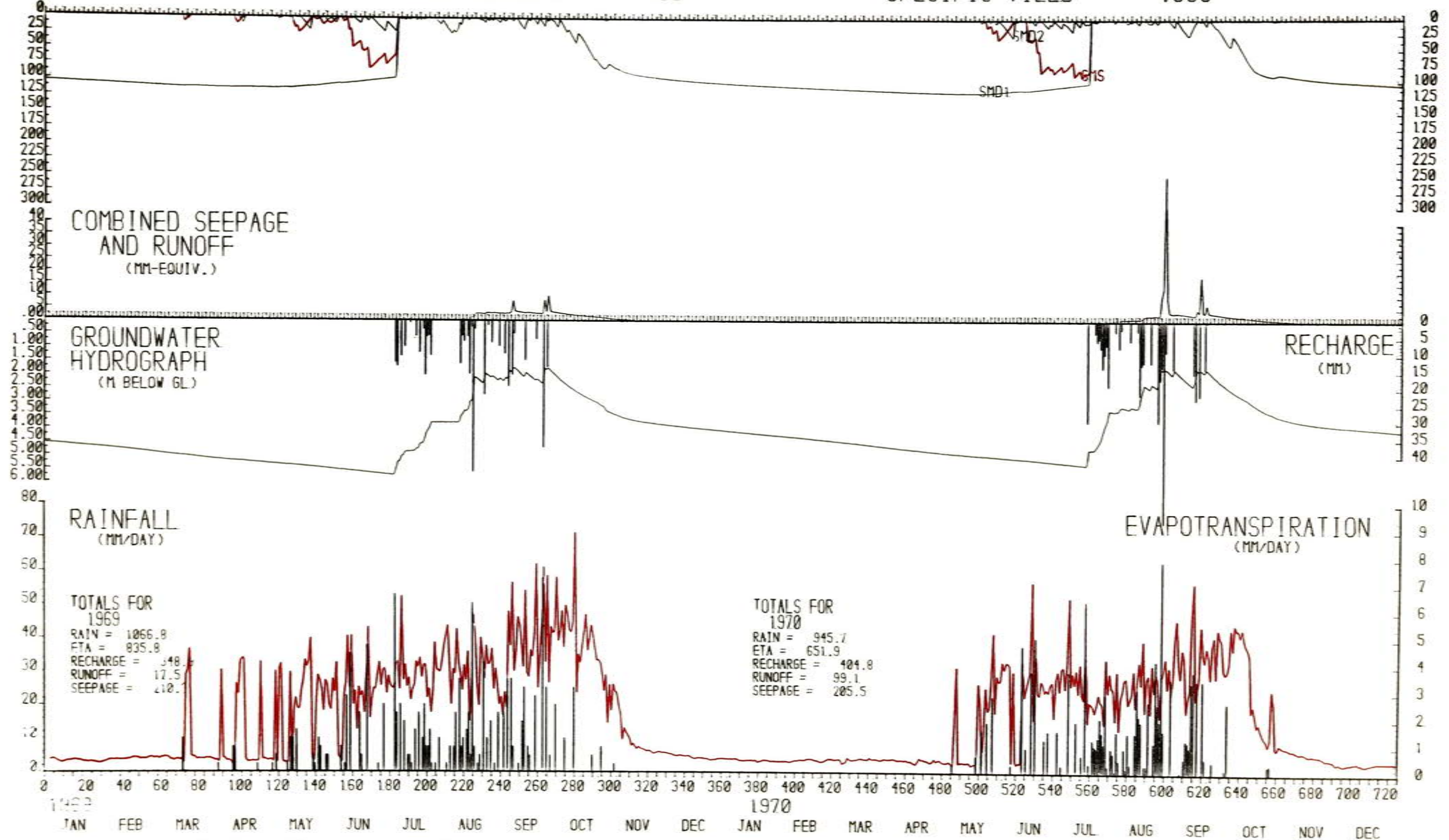


Figure 6-6 Water balance at Bauchi 1969 - 1970

SOIL MOISTURE DATA

ROOT CONSTANT = 100

SPECIFIC YIELD = .050

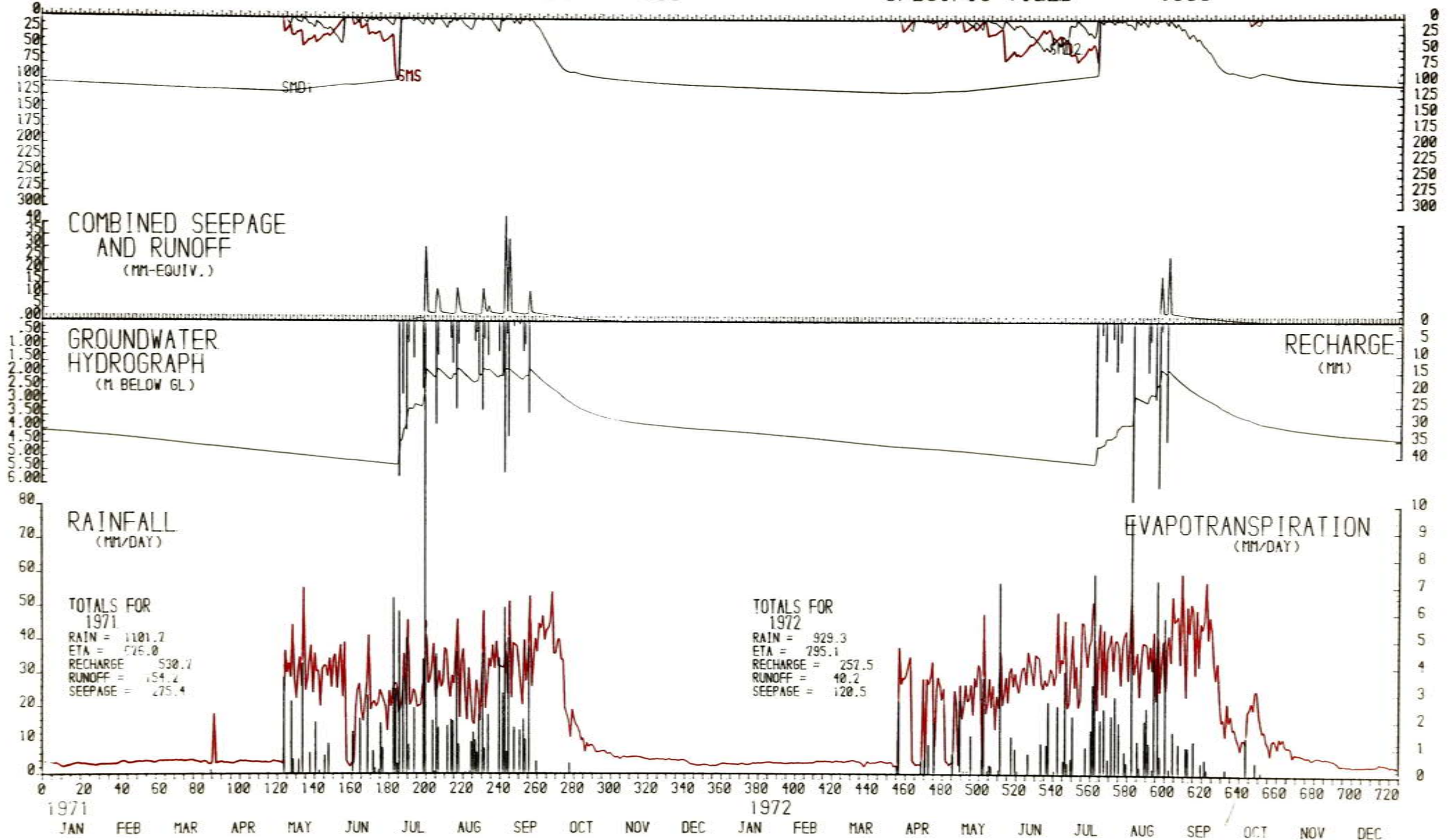
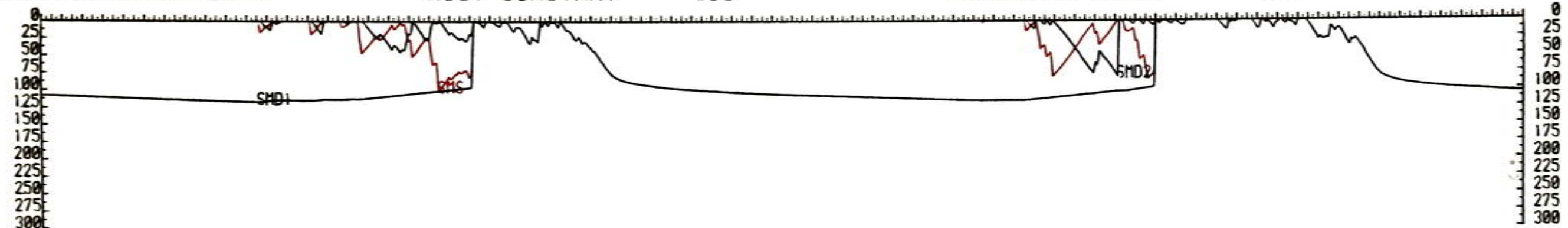


Figure 6-7 Water balance at Bauchi 1971 - 1972

SOIL MOISTURE DATA

ROOT CONSTANT = 100

SPECIFIC YIELD = .050



COMBINED SEEPAGE AND RUNOFF (MM-EQUIV.)

GROUNDWATER HYDROGRAPH (M BELOW GL)

RECHARGE (MM)

RAINFALL (MM/DAY)

EVAPOTRANSPIRATION (MM/DAY)

TOTALS FOR
1973
RAIN = 738.7
ETA = 729.3
RECHARGE = 127.8
RUNOFF = .0
SEEPAGE = 21.9

TOTALS FOR
1974
RAIN = 1154.5
ETA = 765.7
RECHARGE = 484.8
RUNOFF = 132.6
SEEPAGE = 250.1

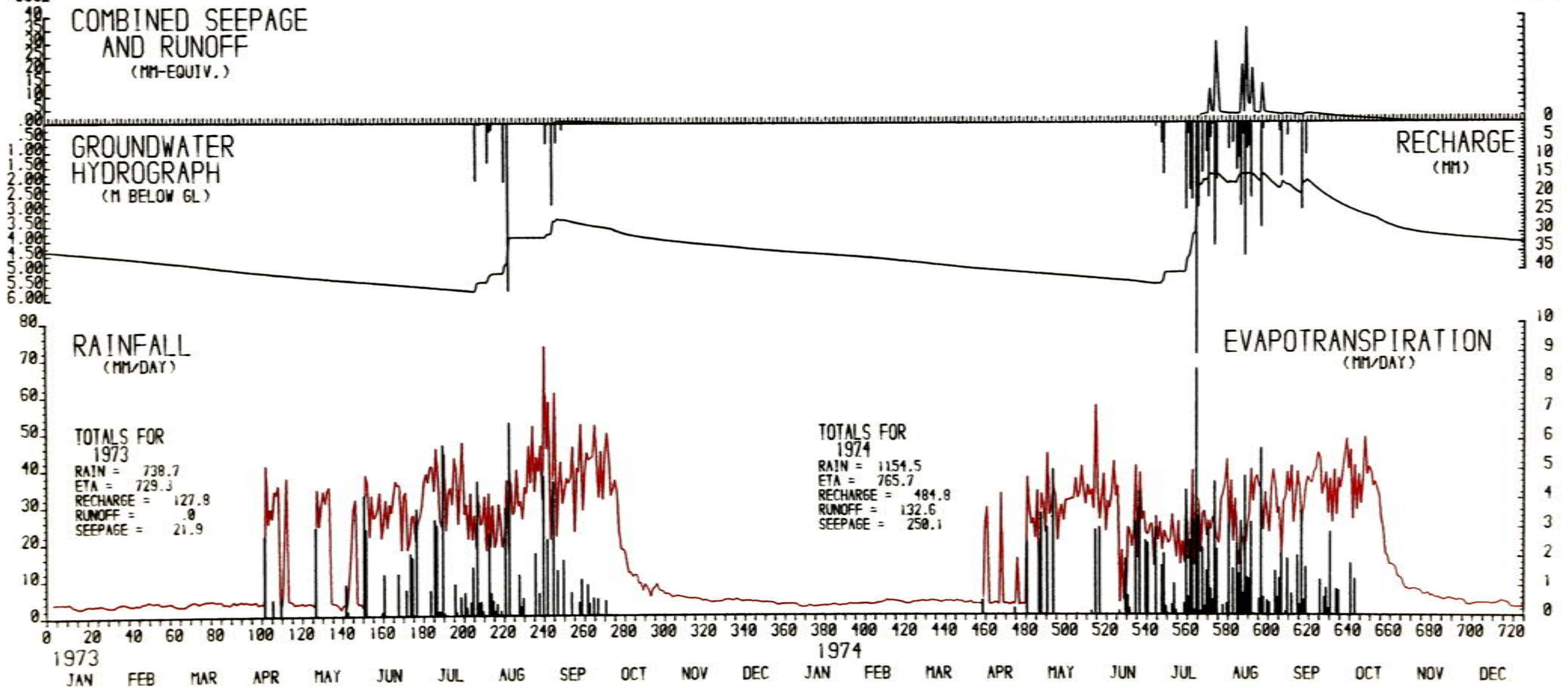


Figure 6-8 Water balance at Bauchi 1973 - 1974

Table 6.3 Comparison of Samaru and Bauchi data.

	1967	1968	1970	1979
	Samaru	Samaru	Bauchi	Bauchi
Rainfall	990	998	946	991
Number of rain days	83	77	67	83
Date of rise in water table	196	203	198	193
Cumulative rainfall before rise	419	516	262	391
Start of seepage flow	198	227	209	200
End of seepage flow	315	299	321	323
Total runoff + seepage	269	160	305	174
Runoff	168	8	205	4
Seepage	101	152	99	170
Eta	721	838	652	825

for 1967 and 1968 at Samaru, although for almost identical annual rainfall totals show considerable differences in the quantity of Eta, and the distribution of runoff and seepage.

The similarity between the observed and predicted results, even though they do refer to different areas, confirm that the assumptions made in the water balance model are broadly correct.

The model may be used to investigate a number of important features of savanna hydrology and water resources. The data shown in Figures 6.4, 6.5 and 6.6 represents the period of the sahelian drought. In particular, during 1973 a number of wells dried up and the drops failed over large areas. A contributory cause of this drought was the distribution of rainfall in 1972. Although 930mm of rain fell at Bauchi during this year, the rains commenced early, and carried on intermittently. Recharge was therefore low and Eta high. The early rains soil moisture is seen to dry out several times during 1972 causing the loss of crops which were sown at the beginning of the rains. A similar event occurred during 1973, and the occurrence of two years crop failure was sufficient to produce local food shortages.

Model sensitivity to changes in root constant.

The value selected for the root constant will affect the water balance in a number of ways. As the root constant increases, the following changes occur, viz;

- 1) Eta is increased.
- 2) Recharge is decreased.
- 3) Runoff is decreased.
- 4) Seepage is decreased.
- 5) The groundwater table shows a later rise.

In Table 6.4 these changes are shown for six different values of the root constant.

Table 6.4 Sensitivity of water balance to changes in the root constant (Data from Bauchi during 197^o)

	Root Constant (mm)					
	<u>50</u>	<u>100</u>	<u>150</u>	<u>200</u>	<u>250</u>	<u>300</u>
Eta (mm)	727	751	777	842	874	936
Recharge (mm)	595	546	498	455	412	767
Runoff (mm)	189	174	149	110	77	48
Seepage (mm)	277	259	247	232	216	196
Day number of water table rise	164	166	173	182	196	206
Start of seepage	174	183	203	209	213	214
End of seepage	296	306	318	319	324	326
Maximum depth to water table (mm)	5365	5593	5592	5803	5965	6058
Groundwater level day 121 (mm)	5354	5310	5270	5357	5377	5377

Note Rainfall = 1182 mm.

Specific yield = 0.05

Balance presented here for 197^o, and therefore the groundwater levels are sensitive to the assumed initial condition for SMD1.

The data in Table 6.4 illustrates clearly the effects of a root constant change caused by a large land clearance scheme such as has been recommended by various international agencies to promote agriculture by mechanisation. The root constant beneath a natural

plant canopy is approximately 250mm as shown by the maximum soil moisture deficits presented in Table 5.8. The effect of large scale vegetation clearing will be reduce this value below 100mm, representing that for a cropped surface. From Table 6.4 such a change in root constant will approximately double recharge, thus producing saturated conditions more quickly. Runoff is therefore increased and also the incidence of water-logging in the top soil. Runoff will also increase as a result of the reduced rate of infiltration. Under bare fallow conditions therefore the incidence of soil erosion will increase.

Model sensitivity to changes in specific yield.

A sensitivity analysis was also performed for the 197^o-1979 data set, of the water balance calculations to changes in specific yield. The results of this analysis are presented in Table 6.5.

Table 6.5 Sensitivity of water balance to changes in specific yield (Data from Bauchi during 1978).

	Specific Yield					
	<u>0.03</u>	<u>0.04</u>	<u>0.05</u>	<u>0.06</u>	<u>0.08</u>	<u>0.10</u>
Eta (mm)	751	751	751	751	751	751
Recharge (mm)	546	546	546	546	546	546
Runoff (mm)	210	193	174	153	108	66
Seepage (mm)	253	255	259	264	282	29 ^o
Dry number of water table rise	166	166	166	166	166	166
Start of seepage	178	183	183	197	197	197
End of seepage	291	294	306	318	352	18
Maximum depth to water table (mm)	6291	5851	5593	5440	5220	5088
Watertable depth Day 121 (mm)	5811	5498	5310	5200	5040	4944

Notes. Rainfall = 1182

Root constant value used = 100mm

Balance presented here for 1978.

Changes in the specific yield do not alter the date upon which the water table rises. However, the slope and response of the water table to recharge are altered considerably. To illustrate this point further, the groundwater hydrographs produced by the model for the

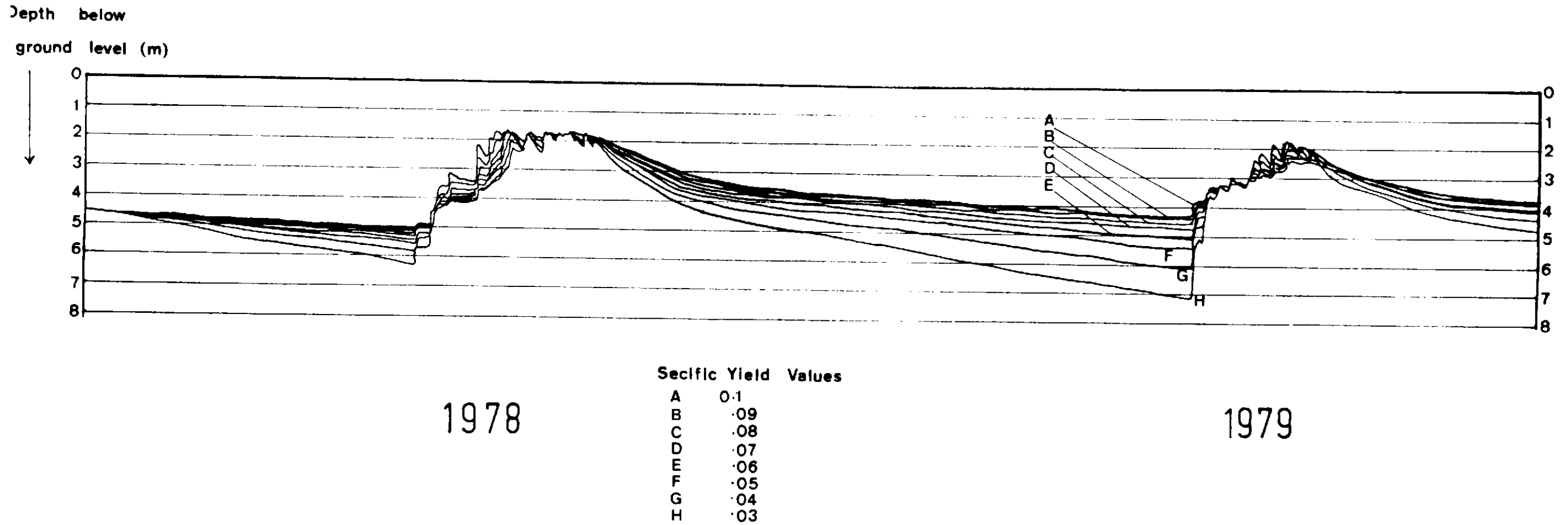


Figure 6-9 Sensitivity of the predicted groundwater hydrograph to changes in the Specific Yield value.

specific yields shown in Table 6.5 are presented in Figure 6.9.

The sensitivity of the model response diminishes markedly as the specific yield is increased.

Specific yield assessment.

From the sensitivity analyses described above, a method for estimating the specific yield of a basement aquifer is suggested. If a groundwater hydrograph and the required climate data are available it is possible to model that hydrograph by varying the values of root constant and specific yield in the model, until the model reproduces the observed hydrograph. This analysis is presented below for the Bauchi hydrograph shown in Figure 5.3.

The groundwater hydrograph response is partially controlled by the elevation at which seepage commences and the level at which further recharge appears as runoff. If the objective of the analysis is to model a particular hydrograph then the values at which these occur on the observed hydrograph may be used in the model. Changes in these values will have a constant effect upon the model. From Figure 5.3 it may be seen that seepage finishes when the groundwater level falls below approximately 3000mm. In practice, this is the elevation of the sand bed of an adjacent river course. The hydrograph peaks at an elevation of approximately 1750mm. These values are used in the following model runs.

The first step in the analysis is to determine the value of the root constant which corresponds with a rise in the water table on the same day as the observed data. When this has been established, the specific yield is varied until a response similar to that of the observed data is achieved.

In Table 6.6, the observed data and the best fitting model data are presented.

In Figure 6.10 the graphical output for these values of root constant and specific yield is shown. The data presented in Tables 6.4 and 6.5 are also for the year beginning January 1st 1978. From this data the range of sensitivity can be established.

A value of specific yield can therefore be given for the aquifer material, in which the water balance operates, which is 0.05 ± 0.005 .

SOIL MOISTURE DATA

ROOT CONSTANT = 100

SPECIFIC YIELD = .050

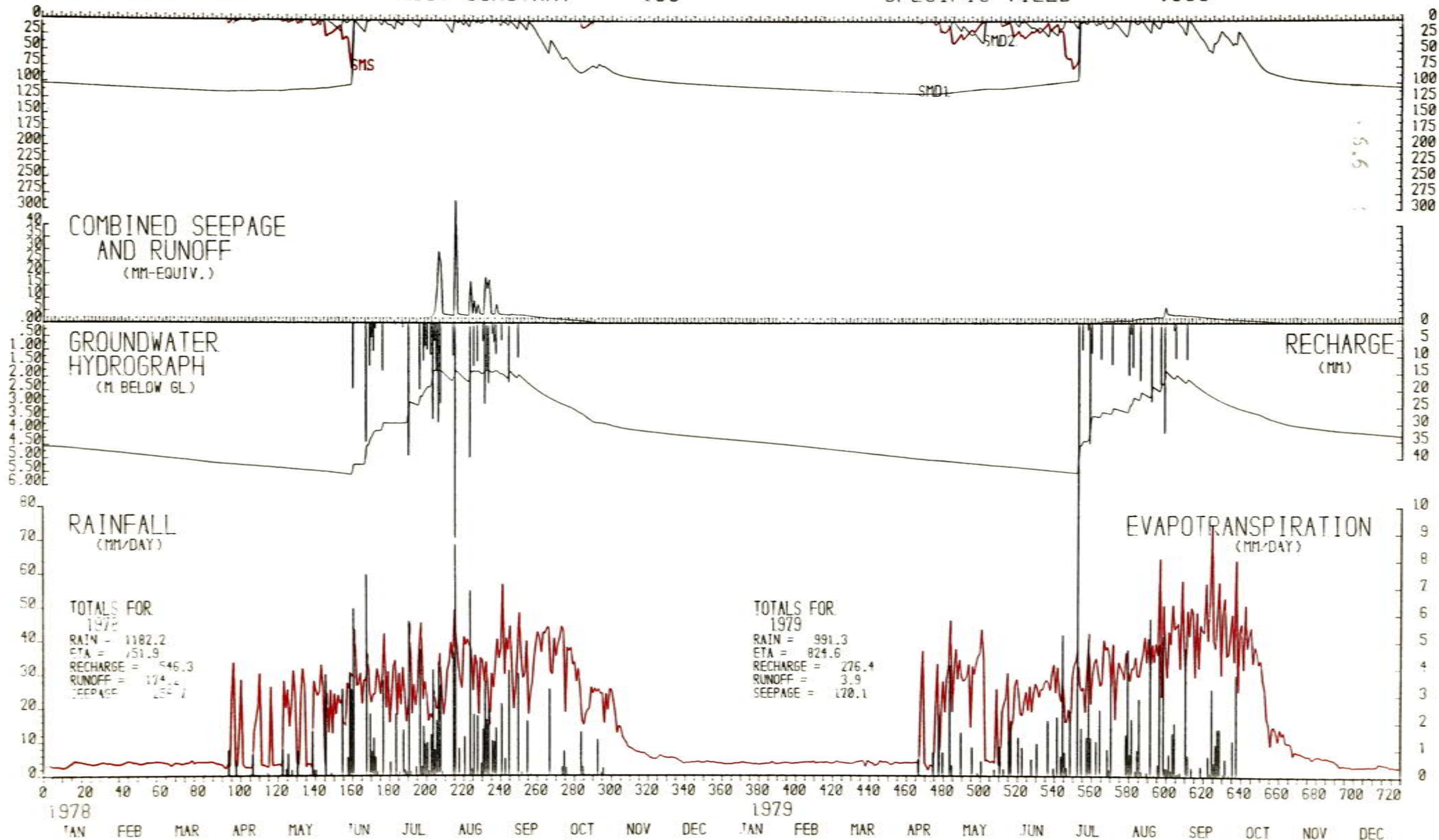


Figure 6-10 Water balance at Bauchi 1978-1979

Table 6.6 Observed and predicted values for the Bauchi groundwater hydrograph shown in Figure 5.3.

Model parameters - Root constant = 100

Specific yield = 0.05

	Observed	Predicted
Level of hydrograph on January 1st 1978 ¹	4650	4650
Maximum groundwater depth (mm)	5600	5592
Rise occurred on day	166	166
Peak level attained on day	243	212
Peak level of groundwater ¹ (mm)	1750	1750
Beginning of rapidly falling stage	263	243
Beginning of gradually falling stage	326	320
Seepage ended at a level of ¹ (mm)	3800	3800
Level of hydrograph on January 1st 1979	4450	4172

6.4 Assessment of annual yield.

Introduction.

There is little available data from which to estimate the annual yield of weathering zone aquifers. Although a large number of boreholes are in operation on basement areas, the total abstraction per year from such boreholes is not recorded. Borehole pumps are in general operated as water is required and no record kept of the quantity of water pumped. The lack of abstraction data is compounded by the lack of abstraction well drawdown data with the result that the long term yield and response of a borehole are unknown.

Despite the lack of detailed data, it is clear that a number of boreholes fail at some time after their commissioning, as a result of complete dewatering of the aquifer. As there are no direct observational data available to assess the annual yield of a basement borehole, it is of use therefore to attempt a prediction of the available yield based upon the analyses presented above.

Observed borehole yields.

Although a limited number of boreholes in the Bauchi area produce $20\text{m}^3/\text{hr}$ for 12 hours per day, throughout the year, such instances are unusual. A more typical yield is perhaps $5\text{m}^3/\text{hr}$ (see also Table 1.1), however, the majority of the boreholes sited around Bauchi on the axis of weathering troughs, produced yields of $10\text{m}^3/\text{hr}$. In the analysis which follows therefore, a design yield of $10\text{m}^3/\text{hr}$ for 12 hours pumping per day is assumed.

Assessment of storage required.

The design yield of $10\text{m}^3/\text{hr}$ represents an annual demand of approximately $4.5 \times 10^4\text{m}^3$ of water.

The estimate of aquifer size listed in Table 6.1 represents the best available estimate of the extent of weathering in a well developed weathering trough. Although the data is from the Bauchi area, it is probable that it represents a good estimate, representative of the environment as a whole. The data from Table 6.1 can therefore be used to assess the typical groundwater storage.

The average volume of grade II material is $5.0 \times 10^3\text{m}^3 (\pm 1.5 \times 10^3\text{m}^3)$

and of grades III + IV material is $4.0 \times 10^3 \text{m}^3$ ($\pm 1.5 \times 10^3 \text{m}^3$). If a fracture porosity of 0.005% is assumed (Strettsova + Adams, 1978) for the grade II material, and 0.05% for the grade III + IV material, then the average quantity of water per metre length of weathering trough in the grade II material is 25m^3 ($\pm 7.5 \text{m}^3$).

As the grade II material everywhere underlies the grade III + IV material, and as the hydraulic conductivity of the fracture zone is high, it will act as an efficient drain to the overlying intergranular porosity material. For this reason it is suggested here that a high percentage ($\sim 80\%$) of the water in the grade III + IV material can be extracted by pumping from the fracture zone. A volume of available water per metre of weathering trough of approximately 180m^3 ($\pm 60 \text{m}^3$) is predicted by the analysis.

The annual groundwater storage requirement is approximately $4.5 \times 10^4 \text{m}^3$ of water. If 180m^3 is available for each metre of weathering trough, then a 250m length of weathering trough is required to support abstraction at the design yield. The figure of 250m therefore represents a minimum spacing of boreholes along a weathering trough.

Assessment of recharge area required.

Where grade III + IV material crops out, only a poor soil development is likely. A restricted vegetation cover is probable on such poor soil, and therefore the possible recharge should be calculated using a short root constant. A root constant value of 150mm is used in the calculation which follows.

The average recharge predicted by the water balance model for a root constant of 150mm is 342mm (sd 138mm). To replace abstraction of $4.5 \times 10^4 \text{m}^3$ would require recharge over an area of 526 x 250m. For example, for each 250m length of weathering trough, a width of recharge zone of approximately 250m on either side of the trough is required to replace abstraction.

The rainfall which falls upon the central low hydraulic conductivity part of the trough, and upon surrounding inselbergs, will runoff without infiltrating. When such runoff crosses a recharge zone it will infiltrate and will add to the volume of direct recharge. The effect of recharge from intercepted runoff may possibly decrease the recharge area required by as much as 50%.

Annual yield.

Although the calculation presented above is based upon a large number of approximations, a number of significant results are evident from the analysis. These are discussed below.

1) A weathering trough 250-300m wide and not less than 400m long contains sufficient water to support abstraction for one year, with pumping at a rate of $120\text{m}^3/\text{day}$ (2.8l/s for 12 hours each day). Weathering troughs of this size are not unusual around Bauchi; they occur with a frequency of approximately one for every four square kilometres. At the end of this period of pumping, the available storage within the trough will be reduced to a minimum.

2) Complete recharge to a trough of this size is probable in most years from a combination of direct infiltration and intercepted runoff. A recharge area of approximately $250 \times 500\text{m}^2$ is required to replace abstraction based upon calculated average recharge.

3) Recharge is very variable. A dependence both upon the quantity of annual rainfall, and the frequency of rain storms has been demonstrated in this study. In Table 6.7, the calculated recharge for the 8 years of available data are shown.

Table 6.7 Recharge for a root constant of 150mm.

	1969	1970	1971	1972	1977	1974	1978	1979
Rainfall	1067	946	1102	929	739	1154	1182	991
Recharge	335	385	440	220	109	462	521	264
% average	99	112	128	64	32	135	152	77

Note. Mean recharge = 342mm (s.d. = 138mm).

The data in Table 6.7 indicates that in three of the eight years, recharge would be less than sufficient to replenish abstraction in the previous dry season. Recharge in excess of that required to replace dry season abstraction is lost as runoff, and therefore it is not possible to draw on water held in storage from a previous higher than average recharge year. The situation which developed in the drought years of 1972 and 1973 is clearly indicated.

4) As approximately a 250m long section of weathering trough in a well developed weathering area is required to support abstraction at $120\text{m}^3/\text{day}$, the borehole spacing along a weathering trough should not be less than 250m.

5) A borehole can produce yields of greater than $10\text{m}^3/\text{hr}$ for considerable periods of time. However, it is the overall quantity of available storage which determines the annual yield, and not the yield of the borehole. There is therefore no reason to construct a borehole which is capable of pumping at rates of greater than $10\text{m}^3/\text{hr}$.

6.5 Resource Development.

Introduction.

In the following discussion, optimum methods of development are described for the development of groundwater on basement complex rocks and within a savanna climate. It is envisaged that although the techniques have been developed for use around Bauchi, they also have a wider application, as discussed in Section 1.1.

The method of resource development is determined by the planned abstraction rate for the resource. This in turn is determined by the purpose for which the groundwater is required. Groundwater requirements within the savanna were discussed in Section 1.2.

Two levels of development were discussed in Section 1.2, viz;

1) Rural supplies with a maximum yield requirement of $1\text{m}^3/\text{hr}$ ($220\text{ gallons hr}^{-1}$ or 0.28 l/s).

2) Institutional supplies for schools (boarding), hospitals, industry, etc, with a yield requirement of $10\text{m}^3/\text{hr}$ or greater.

The first level of development can be met by abstraction by non mechanical means from a dug well. Dug wells have many advantages in the rural context (Water Surveys, 1978), and should be used wherever possible.

The second level of development can only be met by a borehole. As the construction and operation of a borehole requires an investment of > 5 times that of a dug well (Water Surveys, 1978), a significantly increased investigation programme is justified in order that the success of the borehole can be better assured.

The two development strategies are briefly discussed below.

Abstraction by dug well.

It is necessary that a well penetrates below the level of the dry season water table. This implies a typical depth of a well of 10-15m, 6m above the dry season level and 4-9m saturated well beneath this level. A saturated depth of 5.6m in a 1.5m diameter well represents a storage of 10m^3 of water, sufficient water for a day's abstraction. The hydraulic conductivity in the vicinity of the well does not have to be high therefore as any drawdown in the well during the day can be replaced by seepage during the night.

As the yield for a well is low, and the hydraulic conductivity of the aquifer can also be low, it is only necessary to sink wells to the top of Grade IV weathering in a fairly shallow basin of weathering.

The location of suitable sites for wells can be carried out efficiently using an EM-31. Subject to the restrictions concerning recharge discussed above, any area with an apparent resistivity of less than 150Ωm would indicate a possible dug well site.

The construction of dug wells has been extensively reviewed recently (Water Surveys, 1978).

Abstraction by boreholes.

It is necessary that a borehole penetrates the greatest possible thickness of weathered material, and that it passes through fractures in the grade II weathered material. To maximise the quantity of available storage to the borehole, grade II material at a depth of $\approx 40\text{m}$ is required, with at least 20m of grade III + IV material above the grade II material. An average overall depth of weathering of 50m is therefore required.

The location of areas of weathering in which the grade I rock lies at a depth greater than 50m is best achieved by the use of electrical resistivity techniques. It is recommended that the resistivity profile techniques, described in Section 4, be used to obtain profile data at more than one separation over an area of interest delineated by an initial study of the remote sensing data and the use of an EM-31. The borehole should be sited at the point corresponding to the lowest apparent resistivity value obtained with the largest electrode spacing.

The borehole should be designed to produce a maximum of $10\text{m}^3/\text{hr}$, unless it can be demonstrated that the particular area of weathering is of greater than usual extent. This quantity of water may be obtained readily from a 100m ID cased borehole (Johnson, 1972), and the use of 200mm ID or larger cannot be justified on basement weathering areas.

The boreholes can be efficiently constructed using a down hole hammer rig. As it is necessary to drill through grade II + III weathering, it is not practical to use a rotary mud flush rig, or a percussion rig. Modern compressed air techniques utilising down

hole hammers enable a borehole to be constructed in 48 hours in Bauchi.

Many boreholes drilled in basement areas are very considerably over designed, with long runs of stainless steel screen installed into holes drilled for 30 metres through grade I rock. As the borehole yield is only designed to be of a maximum of $10\text{m}^3/\text{hr}$, the use of sophisticated screens is not warranted. For example, one metre of Johnson screen No60 slot at 75mm nominal diameter has sufficient transmitting capacity to exceed $10\text{m}^3/\text{hr}$. If only one metre of screen is to be installed in the borehole, a major problem arises as to the best part of the section to install the screen against.

The grade V + VI material should be cased off and grouted. No groundwater is contained in this material and the grout serves as an efficient protection against pollution. The grade II material is sufficiently competent to not require casing, and this can be left as open hole. A possible design for a typical basement borehole is shown in Figure 6.11. Such a design can be constructed using a 150mm OD down hole air hammer, producing a 100 LD cased finished hole.

The use of a positive displacement borehole pump is recommended. The yield of these pumps can be adjusted at the surface, and there are similarly no submersed electrical or mechanical elements. The pump element consists of a helical metal rotor which rotates inside a fixed sleeve whose internal shape is also helical but with half as many windings in a given length as the rotor. As the rotor turns, water enters the pump element and is carried forward at a uniform speed to the outlet. A pump size which would produce $10\text{m}^3/\text{hr}$ can operate within a 100mm LD bore.

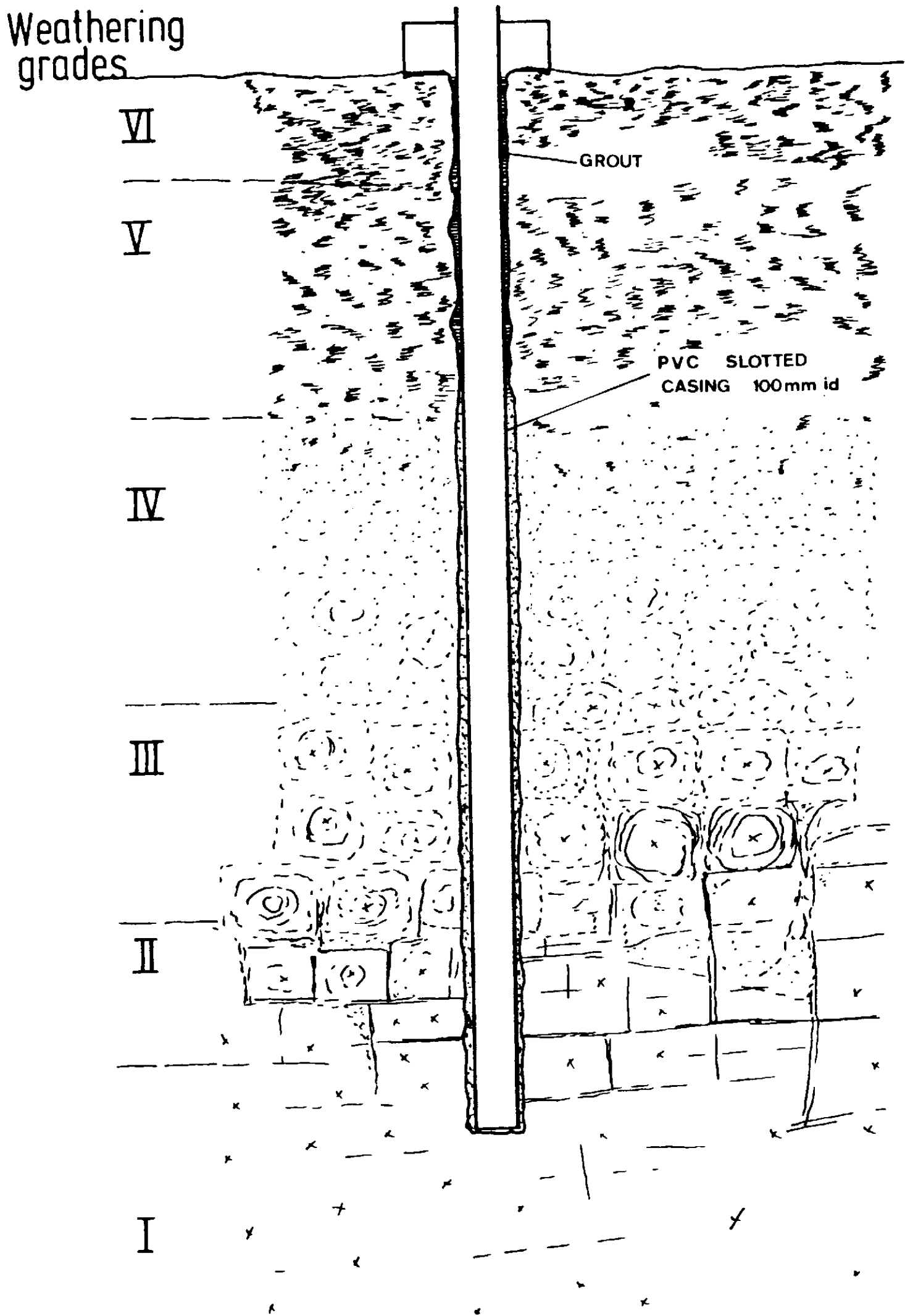


Figure 6-11 Basement borehole design

6.6 Further research required.

General.

The complexity of the hydrogeological environment within the savanna made it impossible to concentrate the subject matter of this thesis on one particular aspect, as had been the initial intention. It was not possible, for example, to develop geophysical techniques without first establishing the physical properties of the aquifer. This in turn led to a detailed consideration of possible mechanisms for granite weathering. Similarly an understanding of the weathering mechanisms became essential if an attempt was to be made to explain the distribution and type of the hydraulic conductivity, and the recharge to the system.

Inevitably, in a study of this nature, where published research is conspicuously absent, a number of hypotheses have been constructed based upon limited data. The lack of basic observational data has been a particular constraint, and has meant that many of even the simplest assumptions cannot be tested.

A programme of further research is described below which, if carried out, will markedly improve the understanding of this environment.

Data collection.

Data is lacking in practically all fields.

To test the adequacy of the recharge model, a detailed study based upon Kowal's (1970) work at Samaru is required. In particular, observations of the following parameters are required for several small trial catchments, viz;

- 1) Rainfall intensity + distribution
- 2) Stream hydrographs
- 3) Seepage
- 4) Evaporation + evapotranspiration
- 5) Groundwater hydrographs

Perhaps the simplest and cheapest observation to make would be of groundwater levels, and days during the wet season when surface runoff caused peaks in stream hydrographs. This simple addition to the data base would be of immense value.

A record of the quantity of water pumped from boreholes, and measurements of the drawdown in pumping boreholes could also be acquired at very little extra cost and would allow a prediction of reduced borehole yields, before the condition became serious. Some idea of the actual quantity of abstraction is also necessary if an assessment of safe yield is to be made.

The results from the water balance algorithm indicate that the hydrological balance is markedly affected by changes in vegetation. A reduction in the rooting depth both allows greater recharge, causing higher groundwater levels, and a considerable increase in surface runoff, which in turn increases the soil erosion risk. All the indications are that the savanna ecosystem is finely tuned to intercept and retain the maximum quantity of rainfall for the maximum time each year. With the advent of large mechanised farming schemes in savanna areas, the impact of clearing large areas of bush should be investigated in detail. It seems probable that water logging and soil erosion will be a serious risk in these schemes.

Hydrochemical study.

A hydrochemical study of the weathering mechanisms and the state of weathering in the weathering grades would be invaluable in increasing the knowledge of the weathering system. If possible, undisturbed samples from beneath the water table should be examined using SEM techniques in an attempt to identify the chemical phases which are removed in the grade III + IV weathering, and which result in the increased porosity of these zones. If for instance, as seems likely, calcic plagioclase is preferentially removed, then rocks containing this feldspar are likely to produce higher yielding aquifer material.

The hydrochemical analysis of seepage water, runoff water, and borehole water from different levels would also improve understanding of the environment. In particular, tritium dating of borehole water would give an indication of the flushing time for water to pass through the weathering trough. This study would confirm, or otherwise, the Hele-shaw model results which indicate a rapid flushing.

If it could be proved that water flushed the products of hydrolysis reactions rapidly from the grade II and III weathering zone, if for example, water from this zone was very recent, then the indications strongly infer that deep weathering is the result of a continued flushing of water in a warm climate. There are a number of interesting geomorphological implications of such a process which would resolve the continuing controversy concerning the formation of inselbergs.

Geophysical Study.

The resistivity profile section technique described in Section four was only used at three sites. The acquisition and interpretation of further sections would increase the data base for this technique and provide more confident extrapolation between a given set of model resistivity distributions.

Electromagnetic EM systems appear to provide a means of gathering resistivity profile sections quickly and inexpensively. The EM 34.3 system is particularly versatile.

Without the use of EM systems, then the offset profiling technique should be used to gather profile section data.

A major complication to the interpretation of profile sections, is the equivalence between the various layers. Recent advances in induced potential (IP) techniques indicate that the hydraulic conductivity can be predicted from a measurement of IP. This method could therefore provide a means of resolving the best parts of the grade III and IV material before drilling a borehole.

CONCLUSIONS

In the introductory section to this thesis it was stated that the object of the research was to make an assessment of the groundwater resources available on crystalline basement rocks within a savanna climate, and to develop a methodology for that assessment. It was further stated that although the general methodology developed was considered to be applicable to all similar geological and climatological environments, the area of particular reference for this research was that of Bauchi, in Bauchi State, Nigeria.

Two levels of resource development were described. The first, and lower level, corresponds to abstraction at a maximum rate of $1\text{m}^3/\text{hr}$ from a dug well, for the purposes of village water supply. The second level corresponds to abstraction at a rate sufficient to satisfy the requirements of a school, hospital, or local small scale industry. These requirements are often greater than $10\text{m}^3/\text{hr}$ and can only be obtained by abstraction from a borehole drilled into an area of deeper weathering. Three such areas of deeper weathering were investigated in the vicinity of Bauchi.

In the Bauchi area, a combination of geological and geophysical evidence was used to justify the assumption that the deep weathering areas were only of limited extent. They could therefore be treated as individual and unrelated compartments which fill up and overflow due to recharge in the wet season, and from which water may be drawn in the dry season. The volume of groundwater storage in such a compartment is simply the volume of water contained in the aquifer below the base level of the local surface drainage.

In Sections 3 and 4, the weathering processes were analysed and a geophysical method developed for determining the volume of the aquifer. From an assessment of the savanna climate in Sections 2 and 5, a value of recharge was calculated for a range of root constants. These two estimates were combined in Section 6 to provide a value of the safe yield from the three weathering troughs which were investigated in Bauchi. From this analysis, the following conclusions concerning the yield at the three sites may be made, viz:

- 1) The maximum design yield for a borehole drilled into the centre of a weathered trough should be $10\text{m}^3/\text{hr}$.
- 2) Pumping should only be carried out for 12 hours each day.
- 3) The minimum spacing between boreholes should be 250m.
- 4) For an average rainfall year, a recharge area of 500 x 250m is required to replace the design yield abstraction by direct infiltration (root constant of 150 mm assumed).
- 5) A substantial quantity of recharge caused by the interception of runoff is probable. This will reduce the area stated in 4 above.
- 6) The quantity of annual recharge will vary substantially within short distances, caused by the great aerial variability in rainfall.
- 7) The quantity of annual recharge will increase significantly due to bush clearance within the catchment.

As the maximum design yield is $10\text{m}^3/\text{hr}$, the borehole design yield should be adapted accordingly. The use of 100mm slotted PVC casing is adequate for this purpose. A larger diameter, or the use of stainless steel screen and gravel pack are not required.

The electrical resistivity, or EM methods, are the most successful for locating deep weathering areas. The electrical resistivity profile section method described in Section 4, is best suited to making a volume estimate of the aquifer within the weathering zone.

A large proportion of the analysis described in this thesis is applicable only if the second level of resource development is anticipated. At the lower level, it is sufficient to locate, perhaps using EM methods, areas of moderate depth of weathering. Dug wells sunk into these areas will usually encounter sufficient supplies of water in the shallow weathered zones where extensive grade V and VI material is often absent.

Where an extensive and thick cover of grade V and VI weathered material has developed it is unlikely that sufficient recharge to an underlying area of deeper weathering can occur to enable abstraction to be replaced. Such areas are therefore of little use for groundwater development.

In areas similar to Bauchi, where inselbergs and surface outcrops are common, groundwater reserves must also be limited in extent, and can be treated as isolated compartments as discussed above. The general analysis as described for Bauchi is applicable throughout these areas. For such limited compartments it is not possible to calculate a groundwater balance based upon measurements of discharge, abstraction and a groundwater flow analysis.

In areas where a more extensive pediplan exists and outcrop areas are less common, groundwater flow can occur over a wider area with measurable discharge to base flow throughout the year. In these areas, a water table will exist throughout the area and it is therefore possible to calculate the movement of groundwater, from water table observations. The water balance analysis described for the Bauchi area will require modification to account for the groundwater flow over an extensive pediplan. However, the geophysical methods may still be used to locate areas of deeper weathering for the location of boreholes and the recharge analysis may similarly be used to describe the infiltration to the system. Recharge on these areas will be at a maximum where grade III or IV weathering material is close to the surface.

It is not possible with the data presently available to assess the accuracy of the analysis. The water balance results predicted for the Bauchi area were shown to be broadly comparable to those observed for a similar area at Samara, however, further detailed observations are essential before the analysis may be finally evaluated.

REFERENCES.

- ALLEN, A., 1960. Seismic refraction investigations of the Pre-glacial Valley of the River Teifi, near Cardigan. *Geol. Mag.* 97, p.276.
- BARKER, R.D., 1979. Signal contribution sections and their use in resistivity studies. *Geophysics. J.R. Astr. Soc.*, 59, 123-129.
- , 1981 The offset system of electrical resistivity sounding and its use with a multicore cable. *Geophysical Prospecting* 29 128-143
- BERNER, A.R., 1971. Principles of Chemical Sedimentology. McGraw Hill, London.
- BEVIN, K., 1979. A sensitivity analysis of the Penman Monteith actual evapotranspiration estimates. *J. Hydrology* 44. 169-190.
- BROWN, R.H., KONOPLYANTSEV, A.A., INESON, J., KOVALEVSKY, V.S., 1975. Groundwater studies No.7. The Unesco Press, Paris.
- BRUNSDEN, D., 1964. The origin of decomposed granite on Dartmoor. In Simmons, I.G. (ed) Dartmoor Essays. Devonshire Association. 97-116.
- BRUNT, D. 1941. Physical and dynamical meteorology. Cambridge University Press.
- BURKE, K.B.S., 1967. A review of some problems of seismic prospecting for groundwater in surficial deposits. In Mining and Groundwater Geophysics. *Geol. Soc. Can. Econ. Geol. Report No. 26*.
- BUNTING, A.H., DENNETT, M.D., EISTON, T.F., MILFORD, J.R., 1976. Rainfall trends in the West African Sahel. *Quart. J. R. Met. Soc.* 102. 59-64.
- BURPEE, R.W., DUGDALE, G., 1975. A summary of weather systems affecting Western Africa and the Eastern Atlantic during GATE. GARP Atlantic Tropical Experiment Report 15. World Meteorological Organisation.
- CHARNEY, J.G., 1975. Dynamics of deserts and drought in the Sahel. *Quart, J. R. Met. Soc.* 101 193-202.
- CHENG, R.TA-SHUN, 1978. Modelling of hydraulic systems by finite-element methods. In *Advances in Hydro-science, Vol. 11*.
- CONSULINT, 1976. Water Resources of NE Nigeria. Unpublished report to Nigerian Government.
- CUTTINGS, D., 1979. Determination of depths to an irregular interface in shallow seismic refraction surveys using a pocket calculator. *Geophysics* 44.
- DAVIES, J.A., 1965. The use of a gunn-bellani distillator to determine net radiation flux in West Africa. *J. Applied Meteorology* 4.

- DAVIES, J.A., 1966. The assessment of evapotranspiration for Nigeria . *Geografiska Annaler* 48 139-156.
- DEARMAN, W. ., BAYNES, F.J., IRFAN, T.V., 1978. Engineering geology of weathered granite. *Engineering Geology* 12 345-374.
- DEER, W.A., HOWIE, R.A., ZUSSMAN, J., 1966. An Introduction to the Rock forming Minerals. Longman.
- DEY, A., 1976. Resistivity modelling for arbitrarily shaped two dimensional structures. Part II. User's guide to the fortran algorithm RESIS2D. Engineering Geosciences and Lawrence Berkeley Lab. Univ. Calif.- Berkeley California 94720.
- , MORRISON, H.F., 1979a. Resistivity modelling for arbitrarily shaped three dimensional structures. *Geophysics* 44 753780.
- 1979b. Resistivity modelling for arbitrarily shaped two dimensional structures. *Geophysical Prospecting* 27.
- EBORALL, M.I., 1976. Intermediate rocks from Older Granite Complexes of the Bauchi area, Northern Nigeria. In *Geology of Nigeria* (Ed) KCGBE, C.A., Elizabethan Publishing Co. Nigeria.
- EGGLER, D.H., LARSON, E.E., BRADLEY, W.C., 1969. Granites, gneisses and the Sherman erosion surface. Southern Laramic Range, Colorado, Wyoming. *Ari. J. Sci.* 267. 510-522.
- ELLISON, W.D., 1944. Studies of raindrop erosion. *Agric. Eng.* 25 131-136.
- ESWARAN, H., YEOW YEW HENG, 1976. The weathering of biotite in a profile on gneiss in Malaysia. *Geoderma* 16 9-20.
- , WONG CHOW BIN, 1978. A study of a deep weathering profile on granite in Peninsular Malaysia. *Soil Sci. Soc. Amer. J.* 42.
- EYRE, S.R., 1968. *Vegetation and Soils. A world picture.* Edward Arnold (Publishers) Ltd.
- FANIRAN, A., 1975. Rural water supply in Nigeria's Basement Complex. A study in alternatives. (In) *Proceedings of the Second World Congress on Water Resources, New Delhi, India. Water for Human Needs Vol. III.*
- FETH, J.H., ROBERTSON, C.E., POLZER, W.L., 1964. Sources of mineral constituents in water from granitic rocks U.S.G.S. Water Supply Paper 1535-I.
- FITZPATRICK, E.A., 1971. *A Systematic Approach to Soil Science.* Oliver + Boyd, London.
- GRIFFITHS, D.H., KING, R.F., 1965. *Applied Geophysics for Engineers and Geologists.* Pergamon.

- GRIFFITHS J.F., 1960. Bioclimatology and the meteorological services. (In) Tropical Meteorology in Africa ed BARGMAN D.T., 283-301.
- , 1966. Applied Climatology - an introduction. Oxford University Press.
- GRINDLEY, J., 1967. The calculation of soil moisture deficits. Meteorol. Mag. 96 97-108.
- , 1969. The calculation of actual evapotranspiration and soil moisture deficits over specified catchment areas. Meteorol. Office, Bracknell. Hydrol. Mem. No. 38.
- HAGEDOORN, J.G., 1959. Plus-minus method of interpreting seismic sections. Geophysical Prospecting 7 158.
- HANKS, R.J., ASHCROFT, G.L., 1980. Applied Soil Physics. Advanced Series in Agricultural Sciences 8. Springer Verlag, New York.
- HARVEY, J.G., 1976. Atmosphere and Ocean - Our fluid Environments. Artemis.
- H.M.S.O. 1973. Admiralty manual of navigation. Vol.2. Revised edition. M.O.D. (Navy).
- HOBBS, B.F., MEANS, W.D., WILLIAMS, P.F., 1976. An outline of Structural Geology. Wiley Internat. Ed.
- HOWARD, K.W.F., LLOYD, J.W., 1979. The sensitivity of parameters in the Penman evaporation equations and direct recharge balance. J. Hydrology 41.
- HOWARD, W.J., 1976. Land Resources of Central Nigerian Forestry. Land Resources Report No. 9. Land Resources Division, M.O.D.
- I.O.H., 1977. Gongola Basin Study. Unpublished report of the Institute of Hydrology, Wallingford, U.K.
- IRFAN, T.Y., DEARMAN, W.R., 1978. The engineering petrography of a weathered granite in Cornwall, England. Q.J.Eng.Geol. 11 233-244.
- JACKSON, I.J., 1977. Climate, Water and Agriculture in the Tropics. Longman.
- , 1978. Local differences in the patterns of variability of Tropical Rainfall: some characteristics and implications. J. Hydrology 38 273-287.
- JOHNSON, 1972. Groundwater and Wells. Johnson U.D.P.
- JONES, M.J., 1975. Observations on dry season moisture profiles at Samaru - Nigeria. Samaru Misc. Paper 51. Inst. Agric. Res. Samaru, Nigeria.
- KASSAM, A.H., KOWAL, J.M., 1975. Water use, energy balance and growth of Gera millet at Samaru, Northern Nigeria. Agric. Met. 15 333-342.

- KOEFOED, O, 1979. Geosounding Principles, 1, Resistivity Sounding Measurements, 14a. Elsevier Scientific Publishing Co.
- KOWAL, J.M., OMOLOKUM, 1970a. The hydrology of a small catchment basin at Samaru - Nigeria, Seasonal fluctuations in the height of the groundwater table. Nigerian Agric.J. 7
- KOWAL, J.M., 1970b. The hydrology of a small catchment basin at Samaru - Nigeria. Assessment of the main components of the water budget. Nigerian Agric.J. 7
- , 1970c. The hydrology of a small catchment basin at Samaru - Nigeria, Assessment of the surface runoff under varied land management and vegetation cover. Nigerian Agric. J. 7.
- , 1972a. Radiation and potential crop production at Samaru - Nigeria. Savanna 1 (3).
- , 1972b. Study of soil surface crusts in the loess plain soils of Northern Nigeria. Samaru Res. Bull. 220. Inst. Agric. Res. Samaru.
- , KNABBE, D., 1972. An Agroclimatological Atlas of the Northern States of Nigeria. Ahmadu Bells University Press.
- , KASSAM, A.H., 1973. Water use, energy balance and growth of maize at Samaru, Northern Nigeria. Agric. Met. 12 391-406.
- , -----, 1975. Rainfall pattern in the Sudan-Savanna region of Nigeria. Weather 30. 24-28.
- , -----, 1976. Energy load and instantaneous intensity of rainstorms at Samaru, Northern Nigeria. Trop. Agric., Trinidad, 53 185-197.
- , -----, 1978. Agricultural ecology of Savanna-A study of West Africa. Clarendon Press.
- KRAUSKOPF, K.B., 1967. Introduction to Geochemistry. McGraw-Hill Book Co.
- L.R.D., 1976. The Land Resources of Central Nigeria. M.O.D. Land Resources Division.
- LAMB, H.H., 1972. Climate - Present, Past and Future. Volumes 1 and 2. Methuen.
- LEDGER, E.B., ROWE, M.W., 1980. Release of uranium from granitic rocks during in situ weathering and initial erosion (Central Texas) Chemical Geology 29 227-248.
- LITTLE, A.L., 1969. The engineering classification of residual tropical soils. Proc. Int. Conf. Soil Mech. found. Eng. 7th - Mexico 1 1-10.

- LLOYD, J.W., DRENNAN, D.S.H., BENNELL, B.M.H., 1966. A groundwater recharge study in NE Jordan. Proc. Inst. Civ. Eng., 35 615-631.
- McNEIL, J.D., 1980. Electromagnetic Terrain Conductivity Measurement at Low Induction Numbers. Geonics Limited, Technical Note TN-6.
- McCULLOCH, J.S.G., 1965. Tables for the rapid computation of the Penman estimate of evaporation. East African Agriculture + Forestry Journal 30. 286-294.
- McFARLANE, M.J., 1976. Laterite and Landscape. Academic Press, London, 151.
- McCURRY, P., 1973. Geology of Degree Sheet 21 Zaria, Nigeria, Overseas Geology + Mineral Resources, 45 NERC - IGS.
- MARTIN, D.W., 1975. Identification, tracking and sources of Saharan dust - An enquiry using SMS. G.A.R.P., G.A.T.E Report No. 14. World Meteorological Organisation.
- MILBURN, J.A., 1979. Water Flow in Plants, Integrated themes in Biology. Longman.
- MOORE, I.C., GRIEBLE, G.D., 1980. The suitability of aggregates from weathered Peterhead granites. Quart. J. Eng. Geol. 13.
- MONTEITH, J.L., 1965. Evaporation and Environment, Symposium. Soc. Exp. Biol, 19 205-234.
- MOYE, D.G., 1955. Engineering geology for the Snowy Mountains scheme. J. Inst. Eng. Aust. 27 281-239.
- NESBITT, H.W., 1979. Mobility and fractionation of rare earth elements during weathering of a granodiorite. Nature 279 206-210.
- NEWBERRY, J., 1971. Engineering geology in the investigation and construction of the Batang Padang hydro electric scheme, Malaysia. Quart, J. Eng. Geol. 3. 151-181.
- NWA, E.U., 1977. Variability and error in rainfall over a small tropical watershed. J. Hydrology 34. 161-169.
- OJO, G., 1979. The Climate of West Africa. Heinemann.
- OLLIER, C.D., 1975. Weathering. Longman.
- ONODERA, T.F., YOSHINAKA, R., ODA, M., 1974. Weathering and its relation to mechanical properties of granite. Proc. 3rd Congress Int. Soc. Rock. Mech. Denver.
- OTTERMAN, J., 1974. Baring high albedo soils by overgrazing. A hypothetical desertification mechanism. Science 186. 531-533.
- OYAWOYE, M.O., 1965. Bauchite - a new variety in the quartz monzonite series. Nature 205. 689
- PALACKY, C.J., KIYOSHI, K., 1979. Effect of tropical weathering on electrical and electromagnetic measurements. Geophysics 44.

- PEARSON, R., MONEY, M.S., 1977. Improvements in the Lugeon or packer permeability test. Quart. 3. Eng. Geol. 10.
- PENMAN, H.L., 1948. Natural evaporation from open water, bare soil and grass. Proc. of the Royal Society, 193.
- , 1949. The dependence of transpiration on weather and soil conditions. J. Soil.Sci. - 74-89.
- , 1950. The water balance of the Stour catchment area J. Inst. Water Eng., 4. 457-469
- , 1956. Discussions of evaporation. Netherlands. J. of Agric. Science. 4. 87-97.
- , LONG, I.F., 1960. Weather in wheat. Quart. J.R. Meteorol. Soc. 86, 16.
- ROY, A., APPARO, A., 1971. Depth of investigations in direct current methods. Geophysics 36. 943-959.
- RUSHTON, K.R., REDSHAW, S.C., 1979. Seepage and Groundwater Flow, Numerical Analysis by Analog + Digital Methods, John Wiley + Sons.
- , WARD, C., 1979. The estimation of groundwater recharge J. Hydrology 41.
- RUXTON, B.P., BERRY, L., 1957. Weathering of granite and associated erosional features in Hong Kong. Bull. Geol. Soc. Am. 68 1263-1292.
- SLABBERS, P.J., 1977. Surface roughness of crops and potential evapotranspiration. J. Hydrology 34 181-191.
- S.M.T., 1958. Smithsonian Meteorological Tables.
- STANHILL, G., 1963. Evaporation in Israel. Bull, Res. Counc. of Israel. Vol. 11G.
- STRELTSOVA-ADAMS, T.D., 1978. Well hydraulics in heterogeneous aquifer formations (in) Advances in Hydroscience Vol.11. Ed. Ven Te Chow 357-418.
- TELFORD, W.M., GELDART, L.P., SHERIFF, R.E., KEYS, D.A., 1976. Applied Geophysics. Cambridge University Press.
- TERNAN, J.L., WILLIAMS, A.G., 1979. Hydrological pathways and granite weathering on Dartmoor. (In) Geographical approaches to fluvial processes. Geo Books.
- THOM A.S., OLIVER, H.R., 1977. On Penman's equation for estimating regional evaporation. Quart. J.R. Met. Soc. 103. 345-357.
- THOMAS, M.F., 1966. Some geomorphological implications of deep weathering patterns in crystalline rocks in Nigeria Trans. of the Inst Brit. Geographers. 40. 173-193.

- UHL, V.W., SHARMA, G.K., 1978. Results of pumping tests in crystalline rock aquifers. Groundwater 16.
- VERMA, R.K. RAO, M.K., RAO, C.V., 1980. Resistivity investigations in metamorphic areas near Dhanbad-India. Groundwater 18.
- WALKER, R.J., ROWNTREE, P.E., 1976. The effect of soil moisture on circulation and rainfall in a tropical model. Tech. Note No. 11/62. Met. Office, Bracknell.
- WATER SURVEYS, 1977. GADP Water Resources Report. Unpublished report to the World Bank.
- , 1978. A limited investigation of rural water supplies and land use in Bauchi State. Unpublished report to the World Bank.
- WEICKMAN, 1975. Observations on convective clouds over the Tropical Atlantic GATE Report No. 14. World Meteorological Organisation.
- WEISNER, C.J., 1970. Hydrometeorology. Chapman and Hall.
- WHITE, A.J.R., CHAPPELL, D.W., 1977. Ultrametamorphic and granitoid genesis. Tectonophysics 43. 7-22.
- WINKLER, H.G.F., 1967. Petrogenesis of metamorphic rocks (revised second ed). Springer Verlag, New York.
- WORLD BANK, 1976. Village Water Supply, World Bank.
- W.H.O., 1973. Community water supply and sewage disposal in Developing countries. World Health Statistics Vol. 26 No.11., World Health Organisation.
- W.M.O., 1975. Meteorological Atlas, Global Atmospheric Research Programme in GATE Report No. 17. W.M.O.

APPENDIX A

Evaporation + evapotranspiration algorithm.

A1 Description of algorithm.

General

The generalised algorithm has been written in FORTRAN-4 to perform a daily calculation of evaporation and or evapotranspiration for a station at any locality. The algorithm has been designed to produce data for various different methods of calculation, as described in Section 2 of the thesis. To facilitate comparison of the various parameters, a cross correlation matrix is calculated for up to 14 variables on a monthly basis.

Method of calculation.

Three different daily values are calculated. The first represents a normal Penman (1948) calculation; the second represents a modified (Thom + Oliver, 1977) calculation, while the third represents a Monteith (1965) calculation.

Daily values of net radiation are calculated for a station at any latitude in units of Watts M^{-2} . Values of albedo, observed sunshine hours, average temperature and humidity are required as INPUT for the calculation. Daily values of the sun's declination and the sun's radius vector are supplied by DATA statements within the algorithm, while a value of the station latitude must be INPUT.

A2 Algorithm structure.

The Main Program.

The main program contains a description of INPUT data required, the units in which the INPUT can be specified and the required FORMAT of that INPUT. Daily values of the required radiation parameters are specified in DATA statements.

Although the calculation is performed on a daily basis, it is

represented on a decade and monthly basis using data averaged over the required period. The lunar structure of the calendar is preserved with monthly totals reflecting the actual number of days in the month rather than a nominal thirty day month. It is assumed that the data run starts on the first day of any specified month. A provision for leap years is included.

Summations of the data are printed for ten day, monthly and annual periods.

The main program completes the data checking and sets up the correct calendar timing, performs the required summation, and prints out the final totals. The remaining parts of the calculation are performed by SUBROUTINES called from the main program. In this manner, the structure of the calculation is preserved and may be altered more easily if required.

SUBROUTINE STATS.

This routine is called from the main program at the end of every month. The routine performs a cross correlation analysis, between 14 variables specified in the main program and prints out the cross correlation matrix. The call to the routine may be suppressed by an appropriate choice on INPUT card 4.

SUBROUTINE PEN.

This routine performs the three calculations of evaporation or evapotranspiration. As the net radiation calculation is common to all three, a separate routine performs this calculation.

The units used in the PEN routine are mm equivalent evaporation.

SUBROUTINE RADIAT.

The calculation of net radiation is performed from first principles and as discussed in Section 2. The units used are $W M^{-2}$.

Two values of net radiation are calculated - the first represents an albedo corresponding to the first value specified on INPUT card 5, while the second represents a varying monthly value of albedo as specified by the remaining 12 values on card 5.

SUBROUTINE ROUGHS.

This routine is called when the Monteith evapotranspiration is calculated. The purpose of the routine is to return values of the

two resistance terms in the Monteith equation viz r_s and r_a . The values of r_s , discretised on a monthly basis are INPUT on data card 7. The values are passed through to this routine as it is envisaged that further theoretical developments may allow a more accurate specification of the resistance, and that this may conveniently be performed within this routine without disruption of the overall program structure.

The value of r_a is calculated using twelve monthly values of Z0 as specified on INPUT card 6.

A3 Specification of variables.

General.

Throughout the algorithm, individual variable names are given which readily allow identification of their purpose, however, the various arrays are described below.

ALBEDO (14)	Holds 14 values of the surface reflection coefficient.
RADNET (3)	Holds 3 values of net radiation.
Y (9)	Holds values of empirically evaluated constants in the Penman equation.
EVAP (3)	Holds the three calculated values of evaporation or evapotranspiration.
AERO (3)	Holds the three values of the aerodynamic term.
MONTH (12)	Holds the number of days in each calendar month.
NAME (12)	Holds the names of the months.
RADIUS (366)	Holds the daily values of the sun's radius vector.
DECLIN (366)	Holds the daily values of the sun's declination (in radians).
Z(600,16)	Holds up to 600 daily values of 16 variables, which are printed out on a separate file for use by plotting routines etc.
X (35,14)	Holds the 14 daily values used to perform the monthly cross correlation analysis.
AZ (14,14)	Holds the cross correlation matrix.
RAD1,RAD2,RAD3 DEC1,DEC2,DEC3	Are dummy arrays necessary by the limitations of machine language on the number of continuation lines in DATA statements.
Z0 (12)	Holds the monthly values of vegetation height in cms.
RS (12)	Holds the monthly values of the r_s resistance parameter.

DAT (3,20)	Is a working array holding various variables as specified below. The array contains the values for daily, ten daily and monthly calculations.
DAT (I,1)	Maximum temperature or daily average temperature.
DAT (I,2)	Minimum temperature.
DAT (I,3)	Rainfall.
DAT (I,4)	Wind run.
DAT (I,5)	Piche evaporation.
DAT (I,6)	Average relative humidity or wet bulb temperature.
DAT (I,7)	Observed sun hours.
DAT (I,8)	Pan evaporation.
DAT (I,9)	Gunn Bellani evaporimeter data.
DAT (I,10)	Sun's radius vector value.
DAT (I,11)	Average temperature.
DAT (I,12)	Vapour pressure.
DAT (I,13)	Saturated vapour pressure.
DAT (I,14)	Aerodynamic term.
DAT (I,15)	Maximum possible number of sunshine hours.
DAT (I,16)	Back radiation term.
DAT (I,17)	Incoming radiation term.
DAT (I,18)	Sun's declination.
DAT (I,19)	Relative humidity.
DAT (I,20)	Ra resistance term.
IDAY	Day number
ELEV	Station elevation.
RLAT	Latitude in radians
HR	Sun's hour angle.
AMBPRS	Average ambient pressure.
GAMMA	Psychrometric constant.
DELTA	Slope of the saturation vapour pressure curve calculated by the ROUTINE DEL after Bevin (1979).

A 4 Listing of the Fortran 4 program.

A listing of the program is given below.

MASTER MAIN

DIMENSION DAT1(3,20),X(35,14),A7(14,14),ALBEDO(14),RADNET(3),
 1 Y(9),EVAP(3),MONTH(12),NAME(6),RADIUS(366),DECLIN(766),
 2 Z(600,16),MNAME(12)
 DIMENSION RAD1(133),RAD2(133),RAD3(170),DEC1(133),DEC2(133),
 1 DEC3(150),Z0(12),RS(12),AERO(3)

PROGRAM FOR THE EVALUATION OF EVAPORATION USING
 THE COMBINED EQUATION OF PENMAN/MONTEITH.

A DAILY VALUE OF EVAPORATION IS CALCULATED FOR THREE VALUES
 OF ALBEDO. DECADE AND MONTHLY TOTALS ARE PRINTED SUMMED
 FROM THE DAILY DATA. AVERAGED DECADE AND MONTHLY DATA ARE
 ALSO COMPUTED.

THE CALCULATION IS WORKED IN THE FOLLOWING UNITS;
 DEGREES CENTIGRADE, MM PRESSURE, KM WIND RUN, MM RAINFALL AND
 W/M**2 RADIATION.

A CORRELATION MATRIX IS CALCULATED FOR EACH MONTH BETWEEN
 EVAPORATION AND A SELECTION OF INPUT DATA.

THE PROGRAM CALCULATES THREE VALUES OF EVAPORATION OR
 EVAPOTRANSPIRATION. THE FIRST VALUE REPRESENTS
 EVAPOTRANSPIRATION CALCULATED USING THE PENMAN EQUATION DESCRIBED
 IN THE TEXT (EQN. 2-12).
 THE SECOND VALUE REPRESENTS A SHORT GRASS EVAPOTRANSPIRATION
 CALCULATED USING A VARYING ALBEDO ON A MONTHLY BASIS
 AND WITH THE AERODYNAMIC TERM MODIFIED AFTER THOM + OLIVER
 (1977). USE OF DIFFERENT Z0 VALUES IS POSSIBLE. A VALUE
 OF 1.37MM GIVES EQUIVALENCE WITH PENMAN SHORT GRASS DATA.
 THE THIRD VALUE REPRESENTS EVAPOTRANSPIRATION CALCULATED
 USING THE MONTEITH EQUATION (EQN 2-16). THE VALUES OF Z0
 AND RS ARE VARIED MONTHLY. VARYING ALBEDOES ARE ALSO POSSIBLE.
 A VALUE OF 0.0 FOR RS GIVES THE EVAPOTRANSPIRATION FOR
 A PLANT SURFACE THAT IS WET.

THE RADIAT SUBROUTINE CALCULATES THE DAILY RADIATION BALANCE
 AT THE EARTH'S SURFACE, IN WATTS /METRE**2. IN PUT TO THIS
 SUBROUTINE MUST BE LATITUDE ,AND SUNSHINE HOURS.
 AN OPTIONAL FACTOR OF 0.95, Y(1) OF THE PENMAN CONSTANTS,
 IS USED TO MODIFY THE BACK RADIATION TERM TO ALLOW FOR
 VEGETATION NOT RADIATING AS A BLACK BODY.

AN ELEVATION DEPENDENCY TERM AFTER MC CULLOCH IS INCLUDED
 IN THE PEN ROUTINES.

THE PROGRAM OUTPUTS DATA ONTO TWO FILES. THE FIRST IS FOR
 RECORDING THE RESULTS, THE SECOND TO BE USED AS DATA INPUT

FOR THE PLOTTING ROUTINES.

DESCRIPTION OF THE DATA CONTROL CARDS

=====

CARD 1 (I3,I4,6A6)

I3 NO. OF RECORDS
I4 YEAR IN WHICH TO START DATA RUN
6A6 STATION NAME - UP TO 36 CHARACTERS

CARD 2 (5F6.0,2F5.0)

THE STATION ELEVATION, AVERAGE AMBIENT PRESSURE (MR)
LATITUDE (DEGREES), VALUES OF A AND B, AND PENMAN
CONSTANTS Y(1), Y(9) IN THE FIRST SEVEN FIELDS.

CARD 3 (6I1,1I2,1I1)

THIS CARD DETERMINS NATURE OF DATA INPUT
A 1 IN COL 1 CONVERTS FARENHEITE TO CENTIGRADE
A 1 IN COL 2 CONVERTS MILES TO KILOMETERS
A 1 IN COL 3 CONVERTS INCHES TO CM
A 0 IN COLS 1-3 GIVES DEFAULT VALUES FOR THE
CALCULATION
A 1 IN COL 4 IF DATA IS NET RADIATION IN CAL/CM/MIN
A 0 IN COL 4 IF RADIATION VALUES TO BE
CALCULATED FROM FIRST PRINCIPLES
A 1 IN COL 5 IF TEMP IS AN AVERAGE OR DRY RULE
A 0 IN COL 5 IF DATA IS MAX AND MIN
A 1 IN COL 6 IF HUMIDITY DATA IS WET RULE TEMP
A 0 IN COL 6 IF RELATIVE HUMIDITY DATA ONLY
COLS 7-8 OF THE THIRD CARD HOLD THE MONTH TO
START THE DATA RUN IN. IT IS ASSUMED THAT RUN
BEGINS AT START OF THE MONTH

CARD 4 (2I1)

THIS CARD CONTROLS OUTPUT.
A 1 IN COL 1 SUPPRESSES THE DAILY OUTPUT
A 1 IN COL 2 SUPPRESSES THE STATISTICS ROUTINE

CARD 5 (14F5.0)

THIS CARD HOLDS THE THIRTEEN VALUES OF ALBEDO
THE VALUE OF 0.07 IS USED WITH TWELVE
DIFFERENT MONTHLY VALUES.

CARD 6 (12F5.0)

THIS CARD HOLDS THE TWELVE MONTHLY VALUES OF Z0.
THE ROUGHNESS LENGTH.
Z0 = APPROX H/10, WHERE H IS VEGETATION HEIGHT

CARD 7 (12F5.0)

THIS CARD HOLDS THE TWELVE MONTHLY VALUES OF
RS, THE CANOPY RESISTANCE TERM.

DESCRIPTION OF DATA CARDS

=====

ANY NUMBER OF CONSECUTIVE DAILY RECORDS MAY BE INPUT UP

TO A MAX OF 600.

THE DATA CARD FORMAT IS (I3,2X,3F5.0,F7.0,5F5.0)

THE FIRST FIELD HOLDS THE DAY NUMBER
 THE 2 FIELD HOLDS MAX TEMP OR AVERAGE TEMP IN DEG F OR DEG C
 THE 3 FIELD HOLDS TMIN IN DEG F OR DEG C
 THE 4 FIELD HOLDS RAINFALL IN INS OR MM
 THE 5 FIELD HOLDS DAILY WIND RUN IN MILES OR KILOMETRES
 THE 6 FIELD HOLDS THE PICHE DATA
 THE 7 FIELD HOLDS RELATIVE HUMIDITY OR WET BULB DATA
 THE 8 FIELD HOLDS THE OBSERVED SUN HOURS
 THE 9 FIELD HOLDS THE PAN DATA
 THE 10 FIELD HOLDS GUNN BELLANI DATA IN MM OR INCOMING
 RADIATION IN CALS/CM**2/DAY

IF ANY DATA IS NOT AVAILABLE THE FIELD IS LEFT BLANK

SUN'S RADIUS VECTOR VALUES

DATA RAD1/0.98324,

1 0.98324, 0.98324, 0.98324, 0.98324, 0.98326, 0.98329,
 1 0.98331, 0.98333, 0.98338, 0.98342, 0.98347, 0.98352, 0.98359,
 1 0.98365, 0.98371, 0.98378, 0.98386, 0.98394, 0.98402, 0.98410,
 1 0.98419, 0.98429, 0.98438, 0.98449, 0.98459, 0.98471, 0.98482,
 1 0.98493, 0.98503, 0.98513, 0.98523, 0.98548, 0.98567, 0.98579,
 1 0.98593, 0.98610, 0.98627, 0.98645, 0.98662, 0.98681, 0.98707,
 1 0.98719, 0.98738, 0.98759, 0.98788, 0.98799, 0.98819, 0.98840,
 1 0.98861, 0.98882, 0.98903, 0.98925, 0.98947, 0.98969, 0.98991,
 1 0.99014, 0.99037, 0.99061, 0.99084, 0.99118, 0.99133, 0.99157,
 1 0.99182, 0.99208, 0.99234, 0.99261, 0.99287, 0.99314, 0.99341,
 1 0.99369, 0.99369, 0.99424, 0.99452, 0.99480, 0.99508, 0.99537,
 1 0.99563, 0.99591, 0.99619, 0.99647, 0.99675, 0.99703, 0.99731,
 1 0.99759, 0.99787, 0.99815, 0.99843, 0.99871, 0.99899, 0.99928,
 1 0.99956, 0.99985, 1.00014, 1.00043, 1.00072, 1.00101, 1.00131,
 1 1.00160, 1.00189, 1.00218, 1.00247, 1.00276, 1.00304, 1.00333,
 1 1.00361, 1.00390, 1.00417, 1.00445, 1.00472, 1.00500, 1.00526,
 1 1.00553, 1.00579, 1.00606, 1.00631, 1.00657, 1.00682, 1.00708,
 1 1.00734, 1.00759, 1.00784, 1.00809, 1.00834, 1.00859, 1.00883,
 1 1.00908, 1.00932, 1.00957, 1.00980, 1.01004, 1.01027, 1.01051/

DATA RAD2/ 1.01073,

1 1.01094, 1.01116, 1.01138, 1.01158, 1.01178, 1.01198,
 1 1.01218, 1.01236, 1.01254, 1.01273, 1.01291, 1.01307, 1.01324,
 1 1.01341, 1.01358, 1.01372, 1.01387, 1.01405, 1.01420, 1.01435,
 1 1.01450, 1.01465, 1.01478, 1.01491, 1.01505, 1.01518, 1.01529,
 1 1.01541, 1.01552, 1.01564, 1.01573, 1.01583, 1.01592, 1.01602,
 1 1.01609, 1.01616, 1.01623, 1.01630, 1.01635, 1.01639, 1.01644,
 1 1.01649, 1.01652, 1.01656, 1.01659, 1.01662, 1.01664, 1.01667,
 1 1.01668, 1.01669, 1.01670, 1.01671, 1.01670, 1.01670, 1.01669,
 1 1.01669, 1.01666, 1.01664, 1.01661, 1.01659, 1.01654, 1.01649,
 1 1.01644, 1.01639, 1.01632, 1.01624, 1.01617, 1.01610, 1.01601,
 1 1.01591, 1.01582, 1.01573, 1.01562, 1.01551, 1.01540, 1.01530,
 1 1.01518, 1.01506, 1.01494, 1.01481, 1.01468, 1.01455, 1.01442,
 1 1.01427, 1.01413, 1.01398, 1.01384, 1.01367, 1.01351, 1.01334,
 1 1.01318, 1.01299, 1.01281, 1.01262, 1.01244, 1.01223, 1.01203,
 1 1.01183, 1.01163, 1.01141, 1.01119, 1.01097, 1.01076, 1.01053,
 1 1.01031, 1.01008, 1.00986, 1.00963, 1.00940, 1.00917, 1.00893,

1 1.00869, 1.00846, 1.00822, 1.00797, 1.00772, 1.00748, 1.00723,
 1 1.00697, 1.00671, 1.00645, 1.00619, 1.00592, 1.00564, 1.00537,
 1 1.00510, 1.00482, 1.00453, 1.00425, 1.00387, 1.00368, 1.00340/
 DATA RAD3/ 1.00311,
 1 1.00283, 1.00255, 1.00226, 1.00198, 1.00170, 1.00141,
 1 1.00114, 1.00088, 1.00062, 1.00036, 1.00010, 0.99972, 0.99944,
 1 0.99916, 0.99888, 0.99859, 0.99831, 0.99802, 0.99774, 0.99745,
 1 0.99716, 0.99688, 0.99659, 0.99630, 0.99601, 0.99574, 0.99544,
 1 0.99516, 0.99488, 0.99461, 0.99433, 0.99406, 0.99379, 0.99353,
 1 0.99326, 0.99306, 0.99275, 0.99249, 0.99224, 0.99199, 0.99175,
 1 0.99150, 0.99126, 0.99102, 0.99078, 0.99054, 0.99030, 0.99007,
 1 0.98983, 0.98960, 0.98937, 0.98914, 0.98892, 0.98869, 0.98848,
 1 0.98826, 0.98805, 0.98784, 0.98764, 0.98745, 0.98725, 0.98706,
 1 0.98688, 0.98671, 0.98653, 0.98636, 0.98620, 0.98604, 0.98589,
 1 0.98575, 0.98560, 0.98546, 0.98533, 0.98520, 0.98507, 0.98494,
 1 0.98482, 0.98470, 0.98458, 0.98446, 0.98435, 0.98425, 0.98415,
 1 0.98405, 0.98397, 0.98388, 0.98380, 0.98372, 0.98366, 0.98360,
 1 0.98354, 0.98348, 0.98344, 0.98341, 0.98337, 0.98334, 0.98331,
 1 0.98329, 0.98326/

C SUN'S DECLINATION VALUES

DATA DEC1/-0.40259,
 1-0.40099, -0.39939, -0.39739, -0.39619, -0.39439, -0.39197,
 1-0.38986, -0.38775, -0.38513, -0.38251, -0.37999, -0.37729, -0.37415,
 1-0.37152, -0.36799, -0.36477, -0.36121, -0.35764, -0.35408, -0.35052,
 1-0.34645, -0.34237, -0.33830, -0.33423, -0.32979, -0.32586, -0.32192,
 1-0.31649, -0.31164, -0.30651, -0.30223, -0.29721, -0.29219, -0.28718,
 1-0.28216, -0.27671, -0.27125, -0.26580, -0.26034, -0.25467, -0.24930,
 1-0.24333, -0.23766, -0.23169, -0.22573, -0.21976, -0.21380, -0.20762,
 1-0.20144, -0.19526, -0.18907, -0.18274, -0.17642, -0.17009, -0.16377,
 1-0.15677, -0.14978, -0.14278, -0.13759, -0.13089, -0.12421, -0.11752,
 1-0.11083, -0.10407, -0.09730, -0.09054, -0.08377, -0.07693, -0.07010,
 1-0.06327, -0.05643, -0.04952, -0.04261, -0.03570, -0.02879, -0.02196,
 1-0.01512, -0.00829, -0.00145, -0.00076, 0.01381, 0.01999, 0.02618,
 1 0.03302, 0.03985, 0.04669, 0.05352, 0.06031, 0.06709, 0.07388,
 1 0.08057, 0.08726, 0.09395, 0.10065, 0.10727, 0.11388, 0.12050,
 1 0.12712, 0.13359, 0.14006, 0.14653, 0.15301, 0.15929, 0.16552,
 1 0.17177, 0.17802, 0.18405, 0.19009, 0.19613, 0.20217, 0.20806,
 1 0.21395, 0.21984, 0.22573, 0.23133, 0.23693, 0.24253, 0.24813,
 1 0.25351, 0.25889, 0.26412, 0.26936, 0.27459, 0.27983, 0.28470,
 1 0.28957, 0.29445, 0.29932, 0.30380, 0.30827, 0.31275, 0.31734/
 DATA DEC2/ 0.32156,
 1 0.32578, 0.33001, 0.33423, 0.33808, 0.34194, 0.34379,
 1 0.34915, 0.35307, 0.35648, 0.35990, 0.36332, 0.36580, 0.36828,
 1 0.37076, 0.37324, 0.37626, 0.37929, 0.38232, 0.38535, 0.38764,
 1 0.38986, 0.39212, 0.39386, 0.39560, 0.39735, 0.39909, 0.40040,
 1 0.40170, 0.40302, 0.40433, 0.40520, 0.40607, 0.40695, 0.40782,
 1 0.40818, 0.40855, 0.40891, 0.40928, 0.40913, 0.40899, 0.40884,
 1 0.40870, 0.40812, 0.40753, 0.40695, 0.40637, 0.40573, 0.40483,
 1 0.40302, 0.40171, 0.40041, 0.39910, 0.39735, 0.39561, 0.39386,
 1 0.39212, 0.38986, 0.38761, 0.38535, 0.38310, 0.38048, 0.37786,
 1 0.37524, 0.37263, 0.36950, 0.36637, 0.36325, 0.36012, 0.35663,
 1 0.35314, 0.34965, 0.34616, 0.34230, 0.33845, 0.33459, 0.33074,
 1 0.32657, 0.32240, 0.31823, 0.31372, 0.30921, 0.30470, 0.30019,
 1 0.29539, 0.29059, 0.28580, 0.28100, 0.27584, 0.27067, 0.26551,
 1 0.26035, 0.25479, 0.24958, 0.24420, 0.23882, 0.23315, 0.22747,
 1 0.22180, 0.21613, 0.21024, 0.20435, 0.19846, 0.19257, 0.18653,

1 0.18040, 0.17446, 0.16842, 0.16222, 0.15601, 0.14981, 0.14341,
 1 0.13701, 0.13061, 0.12421, 0.11766, 0.11112, 0.10457, 0.09803,
 1 0.09141, 0.08479, 0.07818, 0.07156, 0.06487, 0.05817, 0.05148,
 1 0.04479, 0.03806, 0.03126, 0.02450, 0.01774, 0.01103, 0.00432/

DATA DEC3/ 0.01141,

1 0.00931, -0.11614, -0.02298, -0.02981, -0.03665, -0.04492,
 1-0.05132, -0.05708, -0.06385, -0.07061, -0.07738, -0.08407, -0.09076,
 1-0.09745, -0.10414, -0.11076, -0.11737, -0.12399, -0.13061, -0.13708,
 1-0.14355, -0.15002, -0.15649, -0.16282, -0.16914, -0.17547, -0.18180,
 1-0.18798, -0.19416, -0.20034, -0.20653, -0.21249, -0.21845, -0.22442,
 1-0.23038, -0.23610, -0.24182, -0.24754, -0.25307, -0.25859, -0.26412,
 1-0.26965, -0.27481, -0.27998, -0.28514, -0.29031, -0.29518, -0.30005,
 1-0.30492, -0.30979, -0.31437, -0.31895, -0.32353, -0.32812, -0.33226,
 1-0.33641, -0.34055, -0.34470, -0.34814, -0.35211, -0.35582, -0.35953,
 1-0.36280, -0.36608, -0.36935, -0.37263, -0.37553, -0.37844, -0.38099,
 1-0.38352, -0.38608, -0.38863, -0.39050, -0.39300, -0.39500, -0.39706,
 1-0.39858, -0.40009, -0.40161, -0.40317, -0.40419, -0.40520, -0.40622,
 1-0.40724, -0.40768, -0.40811, -0.40850, -0.40899, -0.40891, -0.40884,
 1-0.40876, -0.40869, -0.40799, -0.40730, -0.40661, -0.40592, -0.40481,
 1 -0.40373, -0.40300/

DATA Y/0.05, 0.56, 0.08, 0.10, 0.90, 1.26, 1.00, 1.00, 1.00/

DATA MONTH/31, 28, 31, 30, 31, 30, 31, 31, 30, 31, 30, 31/

DATA NAME/7HJANUARY, 8HFEBRUARY, 5HMARCH, 5HAPRIL, 3HMAV,
 14HJUNE, 4HJULY, 6HAUGUST, 9HSEPTEMBER, 7HOCTOBER, 9HNOVEMBER,
 2HDECEMBER/

READ (1, 100) N, IYEAR, (NAME(I), I=1, 6)

100 FORMAT (I3, I4, 6A6)

READ (1, 200) ELEV, ANPPRS, ALAT, A, P, Y(1), Y(0)

200 FORMAT (5F6.0, 2F5.0)

READ (1, 300) L1, L2, L3, L17, L18, L19, L4

300 FORMAT (6I1, 1I2)

RYEAR=FLOAT(IYEAR)

RY=RYEAR/4.0

IRY=IFIX(RY)

PIRY=FLOAT(IRY)

IF((RY-PIRY).LT.1.0E-5) MONTH(2)=29

READ (1, 700) L20, L21

700 FORMAT(2I1)

READ (1, 400) (ALPEDO(I), I=1, 13)

400 FORMAT(13F5.0)

READ (1, 500) (Z0(I), I=1, 12)

500 FORMAT(12F5.0)

READ (1, 600) (RS(I), I=1, 12)

600 FORMAT(12F5.0)

DO 60 I=1, 366

IF(I.GT.133) GO TO 61

DECLIN(I)=DEC1(I)

RADIUS(I)=RAD1(I)

GO TO 60

61 IF(I.GT.266) GO TO 62

DECLIN(I)=DEC2(I-133)

RADIUS(I)=RAD2(I-133)

GO TO 60

62 RADIUS(I)=RAD3(I-266)

DECLIN(I)=DEC3(I-266)

60 CONTINUE

```

C
C
      DO 10 I=1,18
        DO 11 J=1,3
          DAT1(J,I)=0.0
10 CONTINUE
      DO 11 I=1,35
        DO 11 J=1,12
          X(I,J)=0.0
11 CONTINUE
      KOUNT=0
      KL=0
      EVAPX1=C.0
      EVAPX2=C.0
      EVAPX3=C.0
      EVAPY1=C.0
      EVAPY2=C.0
      EVAPY3=C.0
      EVAPZ1=C.0
      EVAPZ2=C.0
      EVAPZ3=C.0
      JCOUNT=0
      RTOT=C.0
      RAIN10=C.0
      RAIN50=C.0
      WRITE(3,1000)(NAME(I),I=1,6),ELEV,AMPPRC,ALBT
1000 FORMAT(1H0,10X,20HCLIMATE STATION NAME/12X,6A6/
111X,17HSTATION ELEVATION,3X,F6.2,2X,6HMETRES/
211X,24HAVERAGE AMBIENT PRESSURE,2X,F6.2/
3 11X,16HSTATION LATITUDE,2X,F6.2)
      WRITE(3,3000) A,R,(Y(I),I=1,9)
3000 FORMAT(1H0,16HPENMAN CONSTANTS/1X,2HA=,F5.3,5X,2HB=,F5.3/
1 1X,3HY1=,F4.2,2X,3HY2=,F4.2,2X,3HY3=,F4.2,2X,3HY4=,F4.2/
2 1X,3HY5=,F4.2,2X,3HY6=,F4.2,2X,3HY7=,F4.2,2X,3HY8=,F4.2,2X,
3 3HY9=,F4.2)
      WRITE(3,3050)(Z0(I),I=1,12)
3050 FORMAT(1H0,35HMONTHLY AERODYNAMIC ROUGHNESS IN MM/1X,12F8.2)
      WRITE(3,3051)(RS(I),I=1,12)
3051 FORMAT(1H0,31HMONTHLY CANOPY RESISTANCES S/M /1X,12F8.2)
      IF(L4.EQ.0) L4=1
C
C
C
C
      USE DATA IN MONTH ARRAY TO SET UP AVERAGING TIMES
C
C
      PROGRAM ASSUMES RUN STARTS IN JANUARY IF L4 IS EMPTY
98 DO 13 KK=L4,12
      L5=MONTH(KK)
      DO 14 KJ=1,3
        IF(KJ.EQ.1) L6=10
        IF(KJ.EQ.2) L6=10
        IF(KJ.EQ.3) L6=(MONTH(KK)-20)
      DO 15 KA=1,L6
C
C
      READ RECORD CARD AND INCREMENT COUNTER
      JCOUNT=JCOUNT+1
      IF(JCOUNT.EQ.(N+1)) GO TO 99

```

```

      READ(1,600) IDAY, (DAT1(1,I), I=1,9)
600  FORMAT(I3,2X,3F5.0,F7.0,5F5.0)
C
C   CHECK AND CORRECT UNITS IF NECESSARY
      IF(L1.EQ.1) DAT1(1,1)=(DAT1(1,1)-32.0)*5.0/9.0
      IF(L1.EQ.1) DAT1(1,2)=(DAT1(1,2)-32.0)*5.0/9.0
      IF(L2.EQ.1) DAT1(1,4)=DAT1(1,4)*1.6129
      IF(L3.EQ.1) DAT1(1,3)=DAT1(1,3)*25.400
      DAT1(1,4)=DAT1(1,4)*Y(9)
      IF(L18.EQ.0) GO TO 31
      DAT1(1,11)=DAT1(1,1)
      DAT1(1,1)=0.0
31  IF(L19.EQ.0) GO TO 32
      IF(L1.EQ.1.AND.L19.EQ.1) DAT1(1,5)=(DAT1(1,6)-32.0)*5./9.
32  CONTINUE
      IF(L18.EQ.1) GO TO 50
      DAT1(1,11)=(DAT1(1,1)+DAT1(1,2))*0.5
50  CONTINUE
      DAT1(1,12)=SVP(DAT1(1,11))
      IF(L19.EQ.3) GO TO 51
C   COMPUTE VALUE OF ED FROM WET BULB TEMP
C   UNASPIRATED VALUE OF GAMMA USED
      EW=SVP(DAT1(1,6))
      IF(DAT1(1,6).LT.0.0) GO TO 52
      DAT1(1,13)=EW-7.99E-4*A*PRRS*(DAT1(1,11)-DAT1(1,6))
      GO TO 53
52  DAT1(1,13)=EW-7.2E-4*A*PRRS*(DAT1(1,11)-DAT1(1,6))
      GO TO 53
51  DAT1(1,13)=(DAT1(1,6)*DAT1(1,12))/100.0
53  CONTINUE
      DAT1(1,19)=DAT1(1,13)/DAT1(1,12)*100.0
      LMN=0
      IF(DAT1(1,8).LT.1.0E-5) GO TO 77
      DAT1(1,8)=DAT1(1,3)+0.51*DAT1(1,3)
77  CALL PENCEVAP,DAT1,RADNET,LMN,IDAY,Y,ALBEDO,A,B,ELEV,AMRPRS,
1  ALAT,RADIUS,DECLIN,L17,KK,Z0,RS,AERO)
      RAIN=DAT1(1,3)
      JL=ML+1
      IF(L20.EQ.1) GO TO 12
      CALL DATOUT(DAT1,EVAP,IDAY,IYEAR,LS,L6,ALBEDO,KCUNT,ML,RADNET,
1  KK,NAME,JL,L0,AERO)
C   ADD TO ALL SUMS
12  CONTINUE
      RTOT=RTOT+RAIN
      DO 16 I=1,18
          DAT1(2,I)=DAT1(2,I)+DAT1(1,I)
          DAT1(3,I)=DAT1(3,I)+DAT1(1,I)
16  CONTINUE
      EVAPX1=EVAPX1+EVAP(1)
      EVAPX2=EVAPX2+EVAP(2)
      EVAPX3=EVAPX3+EVAP(3)
      EVAPY1=EVAPY1+EVAP(1)
      EVAPY2=EVAPY2+EVAP(2)
      EVAPY3=EVAPY3+EVAP(3)
      EVAPZ1=EVAPZ1+EVAP(1)
      EVAPZ2=EVAPZ2+EVAP(2)

```

```

EVAP73=EVAP73+EVAP(3)
X(JL,1)=EVAP(1)
X(JL,2)=EVAP(2)
X(JL,3)=EVAP(3)
X(JL,4)=DAT1(1,1)
X(JL,5)=DAT1(1,4)
X(JL,6)=DAT1(1,5)
X(JL,7)=DAT1(1,12)-DAT1(1,13)
X(JL,8)=DAT1(1,7)
X(JL,9)=AERO(2)
X(JL,10)=AERO(3)
X(JL,11)=RADNET(1)
X(JL,12)=DAT1(1,13)
X(JL,13)=DAT1(1,9)
X(JL,14)=DAT1(1,8)
Z(IDAY,1)=EVAP(1)
Z(IDAY,2)=EVAP(2)
Z(IDAY,3)=EVAP(3)
Z(IDAY,4)=RADNET(1)
Z(IDAY,5)=RADNET(2)
Z(IDAY,6)=RADNET(3)
Z(IDAY,7)=AERO(1)
Z(IDAY,8)=AERO(2)
Z(IDAY,9)=AERO(3)
Z(IDAY,10)=RAIN
Z(IDAY,11)=FLOAT(IDAY)
Z(IDAY,12)=DAT1(1,1)
Z(IDAY,13)=DAT1(1,2)
Z(IDAY,14)=DAT1(1,4)
Z(IDAY,15)=DAT1(1,12)-DAT1(1,13)
Z(IDAY,16)=DAT1(1,7)
RAIN10=RAIN10+DAT1(1,3)
RAIN30=RAIN30+DAT1(1,3)

```

```

C INCREMENT KOUNT AND TEST FOR AVERAGE PERIOD

```

```

KOUNT=KOUNT+1
IF(KOUNT-L6) 18,19,19
19 KDAY=IDAY-L6+1
COUNT=FLOAT(KOUNT)
DO 22 I=1,18
    DAT1(1,I)=DAT1(2,I)/COUNT
    DAT1(2,I)=0.0

```

```

22 CONTINUE

```

```

L=N=1

```

```

CALL PEN(EVAP,DAT1,RADNET,LIN,IDAY,Y,ALBEDO,A,B,ELEV,A*BPRES,
1 ALAT,RADIUS,DECLIN,L17,KK,ZO,RS,AERO)
CALL DATOUT(DAT1,EVAP,IDAY,IYEAR,L5,L6,ALBEDO,KOUNT,RL,RADNET,
1 KK,FNAME,JL,LO,AERO)

```

```

WRITE(3,2000)KDAY,IDAY,ALBEDO(1),EVAPY1,ALBEDO(KK+1),
1 EVAPY2,ALBEDO(KK+1),EVAPY3,RAIN10

```

```

2000 FORMAT(1H0,6X,26HTOTALS FOR PERIOD FROM DAY,17,3X,6HTO DAY,
117/7X,32HPENMAN EVAPORATION FOR ALBEDO OF,FR.2,3H = ,FR.1/
27Y,41HMODIFIED PENMAN EVAPORATION FOR ALBEDO OF,FR.2,3H = ,FR.1/
37X,34HMCNTEITH EVAPORATION FOR ALBEDO OF,FR.2,3H = ,FR.1/
47X,17HTOTAL RAINFALL = ,FR.1)

```

```

C
      KOUNT=0
      RAIN10=0.0
      EVAPY1=0.0
      EVAPY2=0.0
      EVAPY3=0.0
C
18      PL=PL+1
      IF(PL-L5)23,24,24
24      KDAY=IDAY-L5+1
      ACCOUNT=FLOAT(PL)
      DO 26 I=1,18
          DAT1(1,I)=DAT1(3,I)/ACCOUNT
          DAT1(3,I)=0.0
26      CONTINUE
      LMN=1
      CALL PEN(EVAP,DAT1,RADNET,LMN,IDAY,Y,ALBEDO,A,B,ELEV,AMBPPS,
1 ALAT,RADIUS,DECLIN,L17,KK,ZO,RS,AERO)
      CALL DATOUT(DAT1,EVAP,IDAY,IYEAR,L5,L6,ALBEDO,KOUNT,PL,RADNET,
1 KK,NAME,JL,L0,AERO)
      WRITE(3,2000) KDAY,IDAY,ALBEDO(1),EVAPZ1,ALBEDO(KK+1),
1 EVAPZ2,ALBEDO(KK+1),EVAPZ3,RAIN30
      PL=0
      RAIN30=0.0
      EVAPZ1=0.0
      EVAPZ2=0.0
      EVAPZ3=0.0
C
      IF(L21.EQ.1)GO TO 23
      CALL STATS(L5,IDAY,X,A7,KK,NAME)
C
23      CONTINUE
15      CONTINUE
14      CONTINUE
13      CONTINUE
      IF(N-JCCUNT)54,54,55
55      L4=1
      IYEAR=IYEAR+1
      RYEAR=FLOAT(IYEAR)
      RY=RYEAR/4.0
      IRY=IFIX(RY)
      RIRY=FLOAT(IRY)
      IF((RY-RIRY).LT.1.0E-5) GO TO 56
      MONTH(2)=28
      GO TO 57
56      MONTH(2)=29
57      GO TO 98
54      CONTINUE
C
      WRITE OUT OVERALL TOTALS FOR COMPARISON
99      WRITE(3,5000)RTOT,ALBEDO(1),EVAPX1,ALBEDO(2),EVAPX2,EVAPX3
5000      FORMAT(140,5X,23HTOTAL RAINFALL FOR YEAR,F8.1/
16X,49HPENMAN TOTAL EVAPORATION FOR VARYING ALBEDO OF = ,
2F8.2,3X,3H = ,F8.1/
36X,58HMODIFIED PENMAN TOTAL EVAPORATION FOR VARYING ALBEDO OF =

```

```

4F8.2,3X,3H = ,F8.1/
56X,45HMONTEITH EVAPORATION FOR VARYING ALBEDO OF = ,
6 F8.1)
L25=1
WRITE(6,1001) N,IYEAR,L25
1001 FORMAT(1X,I3,2X,I4,I1)
WRITE(6,1002)(NAME(I),I=1,6)
1002 FORMAT(1X,6A6)
WRITE(6,9000)((Z(NZ,MZ),MZ=1,16),NZ=1,N)
9000 FORMAT(1X,16F6.2/(1X,16F6.2))
STOP
END

```

```

FUNCTION DEL(T)
DEL=(0.012*(T/5.0-3.0)**3+0.189*(T/5.0-3.0)**2+
1 1.55*(T/5.0-3.0)+5.487)/5.0
RETURN
END

```

```

FUNCTION SVP(T)
SVP=0.003*(T/5.0-3.0)**4+0.063*(T/5.0-3.0)**3+
1 0.776*(T/5.0-3.0)**2+5.487*(T/5.0-3.0)+17.044
RETURN
END

```

```

SUBROUTINE ROUGHS(Z0, KK, RS, DAT1, RA)
DIMENSION Z0(12), RS(12), DAT1(3, 20)

```

```

C
C
C SUPROUTINE CALCULATES THE VALUE OF RA, THE AERODYNAMIC
C RESISTANCE TO THE TRANSPORT OF WATER VAPOUR FROM THE
C SURFACE TO 2 METRES, THE REFERENCE LEVEL Z.
C THE VALUES OF RS, THE CANOPY RESISTANCE ARE READ FROM DATA
C CARDS. A MONTHLY VARIATION IS ALLOWED FOR.
C

```

```

RA=(ALOG((Z-0)/Z0))**2/K**2*U
K IS VON KARMAN'S CONSTANT = 0.41
D IS THE ZERO PLANE DISPLACEMENT--ASSUMED INSIGNIFICANT

```

```

C
C
C U=DAT1(1,4)*1000.0/8.64E4
C IF(DAT1(1,3).GT.1.0E-2) RS(KK)=0.0
C RA=(ALOG((2.0E3-0.0)/Z0(KK))**2/(0.41**2*U)
C RETURN
C END

```



```

SUBROUTINE STATS(L5, IDAY, X, AZ, KK, MNAME)
  DIMENSION X(35, 14), AZ(14, 14), MNAME(12)
  DO 10 I=1, 14
    SX=0.0
    SXX=C.0
    DO 11 J=1, L5
      SX=SX+X(J, I)
      SXX=SXX+X(J, I)**2
11    CONTINUE
    A=FLCAT(L5)
    XM=SX/A
    SD=SQRT((SXX-SX*SX/A)/(A-1.0))
    DO 12 J=1, L5
      IF(SD.LT.1.0E-10) GO TO 16
      X(J, I)=(X(J, I)-XM)/SD
      GO TO 12
16    X(J, I)=0.0
12    CONTINUE
10  CONTINUE
  DO 13 I=1, 14
    DO 14 J=1, 14
      SX1=0.0
      SX2=0.0
      SX1X1=C.0
      SX2X2=C.0
      SX1X2=C.0
      DO 15 K=1, L5
        SX1=SX1+X(K, I)
        SX2=SX2+X(K, J)
        SX1X1=SX1X1+X(K, I)**2
        SX2X2=SX2X2+X(K, J)**2
        SX1X2=SX1X2+X(K, I)*X(K, J)
15    CONTINUE
      ABC=(SX1X1-SX1*SX1/A)*(SX2X2-SX2*SX2/A)
      IF(ABC.LT.1.0E-10) GO TO 17
      R=(SX1X2-SX1*SX2/A)/SQRT(ABC)
      GO TO 18
17    R=0.0
18    AZ(I, J)=R
      AZ(J, I)=R
14    CONTINUE
13  CONTINUE
  LDAY=IDAY-L5
  WRITE(3, 1000) LDAY, IDAY, MNAME(KK)
1000 FORMAT(1H0, 29X, 34HMATRIX OF CORRELATION COEFFICIENTS/
  150X, 28HPERIOD FOR DATA SUMMATION IS, I6, 3X, 2HTO, I6, 3X, 4HDAYS,
  25X, 48/15X, 35HFIRST ROW IS OPEN WATER EVAPORATION/
  315X, 55HSECOND ROW IS EVAPORATION WITH VARYING ROUGHNESS LENGTH/
  415X, 56HTHIRD ROW IS EVAPORATION CALCULATED BY MONTEITH EQUATION/
  515X, 32HFORTH ROW IS MAXIMUM TEMPERATURE/
  615X, 17HFIFTH ROW IS WIND/
  715X, 30HSIXTH ROW IS PICHE EVAPORATION/
  815X, 38HSEVENTH ROW IS VAPOUR PRESSURE DEFECIT/
  915X, 31HEIGHTH ROW IS OBSERVED SUN HOURS/
  115X, 36HNINTH ROW IS PENMAN AERODYNAMIC TERM/
  215X, 38HTENTH ROW IS MONTEITH AERODYNAMIC TERM//

```

```

515X,36HELEVENTH ROW IS NET RADIATION (D.07)/
415X,32HTWELTH ROW IS INCOMING RADIATION/
515X,34HTHIRTEENTH ROW IS GUNN BELLANI RHO/
615X,38HFURTEENTH ROW IS PAN EVAPORATION)
DO 19 J=1,14
19 WRITE(3,2000) J,(AZ(J,JZ),JZ=1,14)
2000 FORMAT(1H0,4Y,I2,6X,14F7.2)
RETURN
END

```

```

SUBROUTINE PEN(EVAP,DAT1,RADNET,LIN,IDAY,Y,ALBEDO,A,P,ELEV,
1AMBPRS,ALAT,RADIUS,DECLIN,L17,KK,Z0,RS,AERO)
DIMENSION Y(9),ALBEDO(14),RADIUS(366),DECLIN(366),EVAP(3),
1RADNET(3),Z0(12),RS(12),AERO(3),DAT1(3,20)
ZFACT=8.64E04/2.47E06
GAMMA=AMBPRS*6.574E-4
DELTA=DEL(DAT1(1,11))
IF(L17.EQ.0) GO TO 10
DO 11 J=1,3
11 RADNET(J)=DAT1(1,9)/(59.3*ZFACT)
GO TO 12
10 CALL RADIAT(DAT1,IDAY,RADIUS,DECLIN,ALAT,LIN,Y,ALBEDO,A,P,
1RADNET,KK)
12 RADNET(1)=RADNET(1)*ZFACT
RADNET(2)=RADNET(2)*ZFACT
DO 13 IP=1,3
IF(IP.EQ.2) GO TO 14
IF(IP.EQ.3) GO TO 15
FACT1=GAMMA/(DELTA+GAMMA)
FACT2=DELTA/(DELTA+GAMMA)
AERO(IP)=FACT1*(Y(6)*(DAT1(1,12)-DAT1(1,13))*
1(Y(7)+ELEV*5.0E-5)*(Y(8)+0.006214*DAT1(1,4)))
RADNET(IP)=RADNET(IP)*FACT2
EVAP(IP)=RADNET(IP)+AERO(IP)
GO TO 13
14 AERO(IP)=FACT1*13.8*(DAT1(1,12)-DAT1(1,13))*
1(Y(7)+ELEV*5.0E-5)*(Y(8)+0.006214*DAT1(1,4))/
2(ALOG(2.0E03/Z0(KK)))**2
RADNET(IP)=RADNET(IP)*FACT2
EVAP(IP)=RADNET(IP)+AERO(IP)
GO TO 13
15 DAT1(1,16)=DAT1(1,16)*ZFACT*FACT2
DAT1(1,17)=DAT1(1,17)*ZFACT
RHOCF=1.2*1.01E03
CALL ROUGHS(Z0,KK,RS,DAT1,RA)
X=2.47E06*(DELTA+GAMMA*(1.0+RS(KK)/RA))
FACT2=RHOCF*8.64E04/X
FACT1=3.64E04*DELTA/X
AERO(IP)=FACT2*(DAT1(1,12)-DAT1(1,13))/RA*(Y(7)+ELEV*
15.0E-5)
RADNET(IP)=RADNET(IP)*FACT1
EVAP(IP)=RADNET(IP)+AERO(IP)
DAT1(1,20)=RA
13 CONTINUE
RETURN
END

```



```

SUBROUTINE DATOUT(DAT1, EVAP, IDAY, IYEAR, L5, L6, ALBEDO, KOUNT, ML,
1 RADNET, KK, MNAME, JL, LO, AERO)
DIMENSION DAT1(3, 20), EVAP(3), ALBEDO(14), RADNET(3), MNAME(12)
DIMENSION AERO(3)
IF(ML-L5) 12, 13, 13
13 JDAY=IDAY-L5
GO TO 16
12 IF(KOUNT-L6) 14, 15, 15
15 JDAY=IDAY-L6
C
16 WRITE(3, 1000) IYEAR, JDAY, IDAY, MNAME(KK)
1000 FORMAT(1H0, 1X///1X, 4HYEAR, I4, 3X, 32HDATA AVERAGED BETWEEN DAY NUMBE
1R, 15, 16H AND DAY NUMBER, 15, 10X, A8)
GO TO 17
14 WRITE(3, 2000) IYEAR, IDAY, MNAME(KK), JL
2000 FORMAT(1H0, 1X///1X, 4HYEAR, I4, 3X, 10HDAY NUMBER, 2X, I3, 10X, A8, I3)
17 WRITE(3, 4000)
4000 FORMAT(1X, 6HALBEDO, 2X, 5HTOTAL, 3X, 5HTOTAL, 3X, 5HTOTAL, 3X,
15HTOTAL, 3X, 4HTEMP, 2X, 4HTEMP, 2X, 3HSUN, 5X, 4HWIND, 4X,
23HVAP, 5X, 3HSVP, 5X, 2HIN, 5X, 5HTOTAL, 2X, 5HPICHE, 2X,
33HPAN, 4X, 4HRAIN)
WRITE(3, 5000)
5000 FORMAT(9X, 5HEXRAD, 3X, 6HNETRAD, 2X, 4HAERO, 4X, 4HEVAP, 4X, 3HMAX,
13X, 3HMIN, 3X, 3HOBS, 5X, 3HRUN, 5X, 4HPRES, 12X, 3HRAD, 4X, 3HSUN,
24X, 4HEVAP, 3X, 4HEVAP)
DO 10 I=1, 3
IF(I.GT.1) GO TO 11
WRITE(3, 6000) ALBEDO(I), DAT1(1, 16), RADNET(I), AERO(I),
1EVAP(I), DAT1(1, 1), DAT1(1, 2), DAT1(1, 7), DAT1(1, 4), DAT1(1, 13),
2DAT1(1, 12), DAT1(1, 17), DAT1(1, 15), DAT1(1, 5), DAT1(1, 8), DAT1(1, 3)
6000 FORMAT(2X, F5.2, 2X, F5.2, 2X, F5.2, 3X, F5.2, 3X, F5.2, 4X, F5.2, 1X, F5.2,
11X, F5.2, 3X, F5.1, 3X, F4.1, 4X, F5.2, 3X, F5.2, 2X, F5.2, 2X, F5.2, 2X, F5.2,
22X, F5.2)
GO TO 10
11 IF(I.EQ.3) GO TO 18
WRITE(3, 7000) ALBEDO(KK+1), RADNET(I), AERO(I), EVAP(I)
7000 FORMAT(2X, F5.2, 9X, F5.2, 3X, F5.2, 3X, F5.2)
GO TO 10
18 WRITE(3, 7002) ALBEDO(KK+1), RADNET(I), AERO(I), EVAP(I), DAT1(1, 11),
1 DAT1(1, 19), DAT1(1, 20), DAT1(1, 9)
7002 FORMAT(2X, F5.2, 9X, F5.2, 3X, F5.2, 3X, F5.2, 4X, SHTAV =, F5.2, 5X,
14HRH =, F5.1, 5X, 4HRA =, F5.1, 5X, 11HGUN R RAD =, F5.1)
10 CONTINUE
RETURN
END

```

APPENDIX B

Description of the samples from two boreholes¹ drilled into deep weathering area A.

Notes 1. The boreholes were drilled using a 'Halco-400' pneumatic hammer rig with a 6" bit. The action of the drill bit completely disrupts the sample, which is then carried to the surface by the return air flow. The sample divisions represent a proportion of the returns collected during drilling a depth equivalent to one drill pipe (9').

Borehole No. 5 - Sample Description.

Depth
(m)

- 0 -2.7 Clays-sands. When washed, the medium grained sands contain 40-50% rounded quartz grains with various feldspars, some grains of laterite. The red clay fraction gives the whole sample a red colour, similar to that of the top soil throughout the area.
- 2.7-5.5 The dry sample contains more large aggregates bound by clay. When washed, the sample is seen to be 60-70% quartz sand with 15% larger aggregates of clay (sometimes blue) and sand. The wash water is a fawn colour rather than the lateritic red of the first sample.
- 5.5-8.2 A small (<10) percentage of clay bound aggregates. Mostly sand with 80% quartz (rounded grains), 10% white (kaolinitised?) feldspar. The sample contains much less clay and when dry will run freely through a sieve.
- 8.2-10.9 First sample that was damp when drilled. The sample consists of clay and sand. When washed the sample showed no fines present.
- 10.9-13.7 Clay, wet when drilled. The sample was a gritty clay. When the sample was washed, the remaining portion was 60% sand, mostly red feldspar and rounded quartz grains (1mm size), 40% rock fragments of an intermediate fine grained biotite granite.
- 13.7-16.4 As above - clay was a yellow brown colour.
- 16.4-19.6 Clayey sand with some rock fragments. 40% quartz grains, 50% rock fragments, 10% biotite.
- 19.1-21.9 Sand. Water entering borehole during drilling. Clay now less than 10%. Biotite 15%. When sample is washed, the biotite flakes are carried away by the water. The remaining portion of the sample comprised of rock fragments, quartz and feldspar grains.

- 21.9-24.6 Mostly sand sized particles. Rock fragments formed 15% of the sample. The maximum size of the crystal grains was 5mm. Some plagioclase and quartz grains present. These are subrounded, some showing crystal faces - but not freshly cracked.
- 24.6-27.3 As above - water continuing to increase.
- 27.3-30.1 As above. Fragments of muscovite, quartz, plagioclase, orthoclase and biotite noted.
Water continuing to increase.
- 30.1-32.8 The sample becomes more coarse.
- 32.8-35.5 Very fine grained sample. Free biotite in abundance throughout sample.
- 35.5-38.3 The sample becomes more coarse.
- 38.3-41.0 Coarse sand size sample passes into fine rock dust.

Notes.

The standing water table at the end of drilling was 3.65m.

Yield on airlift = $9.1\text{m}^3/\text{hr}$
drawdown = 3m

Borehole No. 10 - sample description.

Depth
(m)

- 0-2.7 A reddish brown clayey sand size sample containing approximately 20% clay. When the sample is washed, a fine to medium grained, sub-angular to sub rounded, clear quartz sample remains, with a small quantity of a cream coloured feldspar and some biotite.
- 2.7-5.5 As above - but more of an olive brown colour. Clay content increases to 30%.
- 5.5-8.2 An olive brown clayey sand size sample, which when dry congeals together as small clay pellets. When washed, the clay pellets remain discrete. The sand size fraction is dominantly a clear quartz sand with some iron staining on the grain rims. The grains are sub-angular to sub rounded. Orthoclase forms approximately 10% of the sample - showing some quite fresh appearing cleavage faces. A small quantity of biotite is present.
- 8.2-10.9 An olive brown, slightly clayey sand size sample. When washed the sample has a grain size varying between fine sand to gravel. Larger particles are fresh cleavage fragments of a cream to white coloured feldspar. The remaining sample is half a clear angular quartz sand, and half orthoclase feldspar.
- 10.9-13.7 An even textured medium to coarse grained sand size sample with a few larger orthoclase fragments. The orthoclase is partly decomposed. Some biotite is present.
- 13.7-16.4 A fine gravel to coarse sand size sample of cream to yellow coloured fresh orthoclase cleavage fragments and angular to sub rounded clear quartz grains. Very little biotite. The whole sample is bound together with a little yellow brown clay.
- 16.4-19.1 As above.
- 19.1-21.9 Water begins to enter borehole. An even textured fine to medium grained sand sized sample with some large fragments

of clear quartz and orthoclase.

- 21.9-24.6 A coarse to fine angular sand size sample of clear quartz, pink or cream orthoclase and some biotite in approximately equal proportions.
- 24.6-27.3 As above - water continuing to enter borehole.
- 27.3-30.1 A light grey coarse angular sand sized sample of dominantly clear quartz and biotite.
Problems with collapse in the borehole at this depth.
- 30.1-32.8 As above - biotite forms an increasing proportion of the sample.
- 32.8-35.6 A fine to coarse sand size sample of clear quartz and biotite making up about 85% of the sample. The remaining 15% is a fresh yellow to pink orthoclase.
- 35.6-38.3 As above - No fresh rock encountered.

Notes.

The standing water level was 4.56m at the end of drilling.

The yield on air lift was 3.25 m³/hr with a drawdown of 9.1m.

APPENDIX C

Resistivity profile section algorithm

C1 Description of the algorithm

General

The algorithm has been written based upon the work of Dey (1976) and Dey + Morrison (1979).

The version of the program which is included in this Appendix is based upon a mesh of 185 x 16 nodes. A central portion of the mesh is used for the modelling and 41 electrode positions are modelled. The graphical output routines included have been written for a maximum number of 41 source terms.

The mesh numbers, intervals, scaling factors, electrode positions and transform (ky) values can all be altered, however, in the input data shown, these have been selected as appropriate for producing profile sections as shown. However, the algorithm could also be used for many other applications, such as different electrode configurations on the surface, or for down hole electrodes.

The first four input data cards do not have to be changed once the scaling factor is decided for the model in question.

The model resistivity distribution is input for each model run and the last three data cards, or sets of cards, are altered accordingly for each model. Card five contains the column number that the model resistivity distribution commences at, and similarly the column number for which the resistivity distribution input ends at. From the boundaries in x to these values the resistivity distribution is assumed to be equal to the 'edge' values specified below.

The sixth data card contains the resistivity coding information.

The seventh to twenty second cards carry the 15 rows of the re-

sistivity model codes.

If more than 90 columns of data are to be input then the two sets of 15 cards are separated by a dummy card for convenience. The algorithm then reads the coding data for the first half of the columns and then the second half of the columns.

An example of a data set is included after the algorithm coding.

An example of the data output for the same set is also included.

Required run time and storage.

One run of the program requires 65 seconds of time on the Manchester Regional Computer Centre CDC 7600.

Level 2 storage is required on this machine, however the total storage required for an 185 x 16 array is 175_{10}^k words, assuming 1 word of storage for each array element (some machine structures require 2 words for each array element).

C2 Algorithm structure

Main Program

The main program includes a brief description of the theoretical approach and the program structure.

The variables and arrays used are also described.

The spacing of the x nodes are obtained from a data statement although the z node spacing is read on the third data card and can therefore be varied as this is of value during modelling.

The dimensions of the various arrays are also defined by the variables IVS, IVKY, LN, NN, and NN2. If the model is to be run with different dimensioning then these variables must be changed as they carry the array size information through to subroutines.

The main program reads the data and compiles the required 2D mesh grid. The coding for resistivity is converted to conductivity values and assigned to the mesh intervals. The input data is then output for checking.

The finite difference approximation, and the solution of the matrix equation are repeated for different values of the wave number. Only the required transform potentials as defined by the electrode position, are stored - all other potentials are discarded.

An option is included to examine the transform potential response at each electrode. The parameter ICHECK on the first data card should be read as zero for the data to be output.

The transformed potentials are converted to a response in XYZ space and the $IS \times IS$ array of potential response for each source position is then printed.

The potentials are combined together into apparent resistivity results and these results then printed.

Finally, if the parameter IPLOT is not equal to zero on the first data card, then the graphical output is prepared.

The main subroutines are described below, however, if the structure of the program is to be altered it is strongly recommended that the two key references be studied first, so as to obtain an appreciation of the program logic.

SUBROUTINE FINDIF

This routine performs the finite difference approximation to Equation 4.19 for the wave number value contained in WAVE.

An area discretisation is used, and the mesh stretched in the $x = -$, $x = +$ and $z = +$ boundary directions. Special conditions are established around the boundaries. The Neumann condition applies to the top surface, whereas at all other boundaries a mixed condition has been used (Dey + Morrison, 1979b).

Subroutine FINDIF forms the capacitance matrix of the finite difference coupling coefficients required.

SUBROUTINE INVERT.

This routine inverts the capacitance matrix using the Cholesky decomposition technique.

SUBROUTINE SOLVE

This routine performs the back substitution of the inverted matrix with the required source terms as defined by the electrode positions requested.

SUBROUTINE REVERT.

This routine performs the reverse Fourier transformation of the transform potentials for each source position required. A 3D array

is used and, in effect, the transform potentials collapsed along one dimension to leave a 2D array of potentials as described above.

This routine could be easily altered to provide the response at any distance off the x-z plane. The value of Y in the routine is set to zero however for the production of profile section data. To obtain potential data off the x-z plane the dimensioning would require alteration.

SUBROUTINE PROFIL

This routine performs the correct calculation of potentials to produce alpha apparent resistivity data. The form of the statements beginning VA, etc. is the same as that given in Equations 4.15. This illustrates well how the scalar potentials are simply added to produce the required response.

The alpha, beta and gamma response for the first electrode spacing required is printed out.

Due to the approximation inherent in the finite difference technique it is necessary to correct the data for a given set of scaling factors. The values held in array FACTOR perform this correction. The values are empirically found from several trial runs of the program over a uniform half space. The values in FACTOR are selected as zero while the optimum wave numbers are found (but see also Dey + Morrison, op. cit).

Subroutine PROFIL may be readily altered to apply to any electrode configuration where the electrodes are based upon equal distances, or multiples of equal distances. Dipole dipole pseudo section or Schlumberger profile responses could therefore be accommodated as easily.

SUBROUTINE FIPILOT.

This routine plots out the profile section response onto an A4 sheet. Any number of source terms to a maximum of 41 can be plotted, although as the plotting instructions are all contained within DO LOCPS, only a small change would be required to increase this number.

C 3 Resistivity profile section algorithm.

C 4 Input data

C 5 Output data

Sections C3, C4 and C5 follow below.

PROGRAM 'MODEL' CALCULATES THE POTENTIAL DUE TO A POINT SOURCE OF CURRENT USING A FINITE DIFFERENCE APPROXIMATION TO THE FIELD AS DESCRIBED BY DEY AND MORRISON (GEOPHYSICS, 1979)

THE POTENTIAL IS CALCULATED OVER A 3-D CONDUCTIVITY DISTRIBUTION ALLTHOUGH NO VARIATION IN CONDUCTIVITY IS ALLOWED IN THE 'Y', OR STRIKE DIRECTION.

THE CONDUCTIVITY IN THE X-Z PLANE MAY BE VARIED THROUGHOUT THE CENTRAL PORTION OF THE MESH.

A FOURRIER TRANSFORM OF THE 3-D POTENTIAL DISTRIBUTION IS USED SO THAT THE FINITE DIFFERENCE APPROXIMATION CAN BE MADE IN 2-D SPACE OF A LIMITED NUMBER OF VALUES FOR KY, THE WAVE NUMBER.

A MATRIX INVERSION TECHNIQUE, CHOLESKY DECOMPOSITION, IS USED TO INVERT THE POSITIVE DEFINITE SYMETRIC HALF BAND CAPACITANCE MATRIX PRODUCED BY THE FINITE DIFFERENCE DISCRETISATION. AFTER EACH DECOMPOSITION THE INVERTED MATRIX IS BACK-SUBSTITUTED WITH A NUMBER OF USER DEFINED SOURCE TERMS REPRESENTING INDIVIDUAL CURRENT ELECTRODE POSITIONS. THE TRANSFORM POTENTIALS AT EACH ELECTRODE POSITION ARE THEN STORED AND THE REMAINING POTENTIALS DISCARDED.

WHEN THE TRANSFORM POTENTIALS HAVE BEEN CALCULATED FOR 'LWNO' WAVE NUMBERS, THE TRANSFORM RESPONSE AT EACH ELECTRODE IS INVERTED BACK TO A 3-D RESPONSE.

AN (IS*IS) ARRAY OF POTENTIALS AT EACH ELECTRODE IN THE X-Z PLANE IS PRODUCED. THIS ARRAY CONTAINS THE (IS-1) POTENTIALS DUE TO A CURRENT SOURCE AT ONE POSITION, THE PROCESS HAVING THEN BEEN REPEATED FOR A CURRENT POSITION AT EACH ELECTRODE POSITION IN TURN. IN THIS WAY THE APPARENT RESISTIVITY RESPONSE FOR ANY ELECTRODE CONFIGURATION MAY BE CALCULATED.

OUTPUT INCLUDES THE CONTENTS OF THE (IS*IS) ARRAY AND THE APPARENT RESISTIVITIES FOR THE CONFIGURATION OF ELECTRODES CHOSEN. GINO ROUTINES ARE ALSO USED TO PRODUCE GRAPHICAL OUTPUT FOR A NUMBER OF SPECIFIC ELECTRODE CONFIGURATIONS.....

FOR PROFILE RESULTS AN 185*16 ARRAY IS USED WITH 41 SURFACE ELECTRODE POSITIONS.

DEFINITIONS OF VARIABLES

=====

L = NO. OF NODES IN X DIRECTION

N = NO. OF NODES IN Z DIRECTION

XSCA = SCALING FACTOR IN X

ZSCA = SCALING FACTOR IN Z

LWNO = NO. OF VALUES OF KY (USUALLY 8)

LIN = NO. OF SPACES BETWEEN NODES IN X

NIN = NO. OF SPACES BETWEEN NODES IN Z

LYREG = BEGINNING OF AREA OVER WHICH CONDUCTIVITY IS VARIED

LXEND = END OF THIS AREA

DEFINITIONS OF ARRAYS

=====

X(LL) NODES IN X

Z(NN) NODES IN Z

DELX(LLIN) NODE SPACINGS IN X

DELZ(NNIN) NODE SPACINGS IN Z

IDELXR(LLIN) RATIO OF NODE SPACINGS IN X

IDELZR(NNIN) RATIO OF NODE SPACINGS IN Z

AMRX(LLNN,NN1) CAPACITANCE MATRIX

CXZ(LLIN,NNIN) CONDUCTIVITY BETWEEN NODES SUCH THAT
CXZ(I,K) REPRESENTS THE CONDUCTIVITY
ROUNDED BY NODES X(I),Z(K) X(I+1),Z(K)

X(I),Z(K+1) X(I+1),Z(K+1)

ICCODE(LLIN,NNIN) ARRAY OF CODE VALUES 0-9 FOR RESISTIVITIES

RESIST(10) ARRAY OF RESISTIVITY CODE VALUES

XS(LLNN) VECTOR TO CONTAIN SOURCE TERMS AND RESPONSES.

TKY(IVKY) TRANSFORM VALUES, MAX. NUMBER OF TEN....

S(50) WORKSPACE

RHO(10,IVS) APPARENT RESISTIVITY VALUES.

VKY(IVKY,IVS,IVS) TRANSFORM RESPONSE POTENTIALS IN X-Z

V(IVS,IVS) 3-D RESPONSE POTENTIALS IN X-Z PLANE.

ISNODE(IVS) ELECTRODE POSITIONS AS DEFINED BY NODE NUMBERS

DIMENSION TKY(10),RESIST(10),S(50),RHO(10,41)

DIMENSION VKY(10,41,41),V(41,41),ISNODE(41)

DIMENSION X(185),DELX(184),IDELXR(184),Z(16),DELZ(15),IDELZR(15)

DIMENSION AMRX(2960,17),CXZ(184,15),ICCODE(184,15),XS(2960)

COMMON AMRX

LEVEL 2,AMRX

READ IN SPACINGS.IDELXR SHOULD HAVE (L-1) TERMS

DATA IDELXR/1000,100,20,4,1,1,1,1,1,1,1,1,1,1,1,1,1,1,1,1,1,1,
11,
21,
31,
41,
51,
6100,1000/

ISNODE SHOULD HAVE 41 OR LESS TERMS

DATA ISNODE/13,17,21,25,29,33,37,41,45,49,53,57,61,65,69,73,
177,81,85,89,93,97,101,105,109,113,117,121,125,129,133,
2137,141,145,149,153,157,161,165,169,173/

ZZ=1.E-50

READ(5,100) L,N,IS,LWNO,ICHECK,IPLOT

100 FORMAT(6I5)

IVS=41

IVKY=10

LL=185

NN=16

LLIN=LL-1

```

NNIN=NN-1
LLNN=LL*NN
NN1=NN+1
NN2=50
LN=L*N
LIN=L-1
NIN=N-1
N1=N+1
N2=2*N+1
READ(5,101) XSCA,ZSCA
101 FORMAT(2F10.0)
102 FORMAT(20I4)
READ(5,102)(IDELZR(K),K=1,NIN)
DO 10 I=1,LIN
CQ=FLOAT(IDELXR(I))
10 DELX(I)=XSCA*CQ
DO 11 K=1,NIN
CQ=FLOAT(IDELZR(K))
11 DELZ(K)=ZSCA*CQ
X(1)=0.0
Z(1)=0.0
DO 12 I=2,L
12 X(I)=X(I-1)+DELX(I-1)
DO 13 K=2,N
13 Z(K)=Z(K-1)+DELZ(K-1)
PI=3.141592653
C
C READ IN KY TRANSFORM VALUES
READ(5,103)(TKY(I),I=1,LWNO)
103 FORMAT(10F8.0)
C
C READ IN AREA OVER WHICH CONDUCTIVITY IS TO BE MODELLED
READ(5,104) LXBEG,LXEND
104 FORMAT(2I5)
READ(5,105)(RESIST(I),I=1,10)
105 FORMAT(10F8.0)
LXR=LXEND-LXBEG+1
IF(LXR.GT.80) GO TO 29
DO 14 K=1,NIN
14 READ(5,106)(ICODE(I,K),I=LXBEG,LXEND)
106 FORMAT(80I1)
GO TO 28
29 LXMID=LXBEG+79
DO 30 K=1,NIN
30 READ(5,106)(ICODE(I,K),I=LXBEG,LXMID)
LXMID1=LXMID+1
C
C READ SEPARATOR CARD
READ(5,107)NEXT
107 FORMAT(I2)
DO 31 K=1,NIN
31 READ(5,106)(ICODE(I,K),I=LXMID1,LXEND)
28 CONTINUE
C
DO 15 K=1,NIN
DO 15 I=1,LIN

```



```

      IF(I.LT.LXBEG)ICODE(I,K)=ICODE(LXBEG,K)
      IF(I.GT.LXEND)ICODE(I,K)=ICODE(LXEND,K)
      ICX=ICODE(I,K)+1
15  CXZ(I,K)=1.0/RESIST(ICX)
C
C
C
C      WRITE OUT RESISTIVITY CODING FOR THE HALF SPACE
C
      WRITE(6,1000) L,N
1000 FORMAT(1H1,25X,35HRESISTIVITY PROFILE MODELLING USING,
15X,I5,5X,24RY,5X,I5,5X,5HSPACE)
      WRITE(6,1001)(RESIST(I),I=1,10)
1001 FORMAT(1H0,30X,23HRESISTIVITY CODE VALUES/(1X,10F10.1))
      DO 22 K=1,NIN
      WRITE(6,1002)(ICODE(I,K),I=34,153)
1002 FORMAT(1X,120I1)
      22 CONTINUE
C      WRITE OUT DELX, AND X DISTANCES
      WRITE(6,1013)
1013 FORMAT(1H0,30X,27HDISTANCES BETWEEN NODES)
      WRITE(6,1008)(DELX(I),I=1,LIN)
      WRITE(6,1014)
1014 FORMAT(1H0,30X,27HRELATIVE POSITIONS OF NODES)
      WRITE(6,1008)(X(I),I=1,L)
      WRITE(6,1013)
      WRITE(6,1008)(DEL7(K),K=1,NIN)
      WRITE(6,1014)
      WRITE(6,1008)(Z(K),K=1,N)
      WRITE(6,1007)(TKY(I),I=1,LWNO)
1008 FORMAT(1H0,10F10.1/(1X,10F10.1))
1007 FORMAT(1H0,20X,16HTRANSFORM VALUES/(8F15.10))
C
      WRITE(6,1010)(ISNODE(I),I=1,IS)
1010 FORMAT(1H0,10X,31HSURFACE POSITIONS OF ELECTRODES//
1(1X,50I4))
C
C
C
C      COMPUTE CAPACITANCE MATRIX FOR DIFFERENT WAVE NUMBERS
C
      DO 999 KY=1,LWNO
      WAVE=TKY(KY)
      CALL FIDIF(WAVE,CXZ,L,LIN,N,NIN,DELX,Y,DELZ,Z,AMRX,LN,
1N1,N2,S,ZZ,LLNN,NN1,LL,NN,LLIN,NIN,NN2)
      IER=0
C
C      INVERT THE CAPACITANCE MATRIX
      CALL INVERT(AMRX,LN,N,D1,D2,N1,IER,LLNN,NN1)
      WRITE(6,1003) IER
1003 FORMAT(1H0,35X,29HMATRIX SOLUTION ERROR INDEX =,5X,I2)
      WRITE(6,1015) D1,D2
1015 FORMAT(1H0,5HD1 = ,1PE15.6,5X,5HD2 = ,1PE15.6)
C
      IF(IER.NE.0) GO TO 999
C      SOLVE INVERTED MATRIX FOR VECTORS CONTAINING SOURCE TERMS

```

```

DO 998 ISOUR=1,IS
ISN=ISNODE(ISOUR)
IN=(ISN-1)*N+1
DO 17 J=1,LN
17 XS(J)=0.0
XS(IN)=FI

C
C BACKSUBSTITUTE COLUMN VECTOR XS CONTAINING SOURCE TERM WITH
C INVERTED MATRIX
C
CALL SOLVE(AMRX,XS,LN,N,N1,LLNN,NN1)

C
C SORT OUT REQUIRED SOLUTIONS AND PLACE INTO VKY
DO 18 IRESP=1,IS
ISI=ISNODE(IRESP)
INI=(ISI-1)*N+1
18 VKY(KY,IRESP,ISOUR)=XS(INI)

C
C ZERO ELEMENTS OF VECTOR XS AND LOAD WITH NEXT SOURCE TERM
DO 19 IJ=1,LN
19 XS(IJ)=0.0
998 CONTINUE
999 CONTINUE

C
C ARRAY VKY NOW CONTAINS THE TRANSFORM RESPONSE VALUES FOR
C IS NUMBER POTENTIAL ELECTRODE POSITIONS DUE TO THE SAME
C NUMBER OF CURRENT ELECTRODE POSITIONS...
C
C
C VKY IS A THREE DIMENSIONAL ARRAY WITH THE ELEMENTS STORED AS
C ((VKY(I,J,K),I=1,LWNO),J=1,IRESP),K=1,ISOUR)
C
C
C IF(ICHECK.NE.0) GO TO 26

C
C WRITE OUT TRANSFORM VALUES IN VKY
C FOR EACH SOURCE TERM
C
DO 23 ISOUR=20,25
WRITE(6,1004) ISOUR
1004 FORMAT(1H0,20X,13HSOURCE NUMBER,5X,15)
IBEG=1
IEND=9
IF(IEND.GE.IS) IEND=IS
25 WRITE(6,1011)(ISNODE(IJ),IJ=IBEG,IEND)
1011 FORMAT(1H0,10HWAVE VALUE,2X,9I12)
DO 24 I=1,LWNO
24 WRITE(6,1012) TKY(I),(VKY(I,J,ISOUR),J=IBEG,IEND)
IF(IEND.EQ.IS) GO TO 23
IBEG=IBEG+9
IEND=IEND+9
IF(IEND.GE.IS) IEND=IS
GO TO 25

```

```

23 CONTINUE
1012 FORMAT(1X,1P10E12.4)
C
26 CONTINUE
C
CALL REVERT(VKY,IS,LWNO,TKY,V,IVS,IVKY)
THIS ROUTINE WILL PERFORM THE REVERSE FOURIER TRANSFORM
C
DO 20 IJ=1,IS
WRITE(6,1005) IJ,(V(IJ,I),I=1,IS)
1005 FORMAT(1H0,35X,15HSOURCE POSITION,IS,5X,
124HPOTENTIALS AT ELECTRODES//(1X,1P10E11.4))
20 CONTINUE
C
APRANGE POTENTIALS TO PRODUCE LINES OF PROFILE RESULTS
FOR MULTIPLES OF ELECTRODE SPACING.
CALL PROFIL(V,IS,ISNODE,X,L,RHO,IVS,A,LL)
DO 21 I=1,IS
WRITE(6,1006)(RHO(I,J),J=1,IS)
21 CONTINUE
1006 FORMAT(1H0,5X,1P10E12.2/(6X,1P10E12.2))
IF(IPLCT.NE.0) GO TO 27
C
PLOT OUT DATA FROM PROFIL ROUTINE USING GINO-F
CALL PLOT(RHO,ICODE,7,PESIST,LIN,NIN,L,N,A,IS,
1 IVS,LL,ON,LLIN,ONIN)
27 CONTINUE
STOP
END

```

```

FUNCTION AK1(X)
IF(X .GE. 2.00) GO TO 100
T=X/3.75
T2=T*T
T4=T2*T2
T6=T4*T2
T8=T6*T2
T10=T8*T2
T12=T10*T2
B=0.50+C.87890594*T2+C.51498869*T4+C.15084934*T6+C.02658733*T8+
10.00301532*T10+C.00032411*T12
BI1=X*3
T=X*0.5
T2=T*T
T4=T2*T2
T6=T4*T2
T8=T6*T2
T10=T8*T2
T12=T10*T2
AA=X*ALOG(T)*BI1+1.00+C.15443144*T2-C.67278579*T4-C.19156897*T6-
10.01919402*T8-C.00110404*T10-C.00004686*T12
AK1=AA/X
RETURN
100 AK1=1.0
RETURN
END

```

```
SUBROUTINE INVERT(A, LN, N, D1, D2, N1, IER, LLNN, NN1)
```

```
SUBROUTINE PERFORMS THE MATRIX INVERSION OF THE CAPACITANCE  
MATRIX USING CHOLESKY DECOMPOSITION
```

```
DIMENSION A(LLNN, NN1)
```

```
LEVEL 2, A
```

```
IER=0
```

```
R=1.0/(LN*16.0)
```

```
D1=1.0
```

```
D2=0.0
```

```
DO 10 I=1, N
```

```
DO 10 J=1, N
```

```
K=N1-J
```

```
10 A(I, K)=0.0
```

```
DO 11 I=1, LN
```

```
IN1=I-N1
```

```
I1=MAX(1, 1-IN1)
```

```
DO 11 J=I1, N1
```

```
L=IN1+J
```

```
I2=N1-J
```

```
SUM=A(I, J)
```

```
J1=J-1
```

```
IF(J1) 12, 12, 13
```

```
13 DO 14 K=1, J1
```

```
I:=I2+K
```

```
SUM=SUM-A(I, K)*A(L, I)
```

```
14 CONTINUE
```

```
12 IF(J.NE.N1) GO TO 15
```

```
IF(A(I, J)+SUM*R.LE.A(I, J)) GO TO 16
```

```
A(I, J)=1.0/SQRT(SUM)
```

```
D1=D1*SUM
```

```
17 IF(ABS(D1)-1.0) 18, 18, 19
```

```
19 D1=D1*0.0625
```

```
D2=D2+4.0
```

```
GO TO 17
```

```
18 IF(ABS(D1)-0.0625) 20, 20, 11
```

```
20 D1=D1*16.0
```

```
D2=D2-4.0
```

```
GO TO 18
```

```
15 A(I, J)=SUM*A(L, N1)
```

```
11 CONTINUE
```

```
GO TO 21
```

```
16 IER=1
```

```
21 CONTINUE
```

```
RETURN
```

```
END
```

```

SUBROUTINE FINDIF(WAVE,CXZ,L,LLIN,N,NNIN,DELX,X,DELZ,Z,AMRX,
1LN,N1,N2,S,Z7,LLNN,NN1,LL,NN,LLIN,NNIN,N2)

```

```

DIMENSION CXZ(LLIN,NNIN),DELX(LLIN),DELZ(NNIN),AMRX(LLNN,NN1),
1 X(LL),Z(NN),S(NN2)

```

```

SUBROUTINE CALCULATES THE COEFFICIENTS FOR THE MATRIX EQUATION
USING A CENTRE POINT FINITE DIFFERENCE DISCRETISATION
LEVEL 2,AMRX

```

```

JB=1
JF=N1-1
JABEF=N1
JE=N1+1
JA=N2

```

```

DO 14 IJ=1,N2
14 S(IJ)=0.0
DO 10 I=1,L
DO 10 K=1,N
IN=(I-1)*N+K
IF(I.EQ.1.OR.I.EQ.L) GO TO 11
IF(K.EQ.N) GO TO 12
IF(K.EQ.1) GO TO 13

```

```

COEFFICIENTS FOR INTERIOR NODES

```

```

S(JA)=-((DELZ(K-1)*CXZ(I,K-1)+DELZ(K)*CXZ(I,K)) /
1(2.0*DELX(I)))

```

```

S(JB)=-((DELZ(K-1)*CXZ(I-1,K-1)+DELZ(K)*CXZ(I-1,K)) /
1(2.0*DELX(I-1)))

```

```

S(JE)=-((DELX(I-1)*CXZ(I-1,K)+DELX(I)*CXZ(I,K)) /
1(2.0*DELZ(K)))

```

```

S(JF)=-((DELX(I-1)*CXZ(I-1,K-1)+DELX(I)*CXZ(I,K-1)) /
1(2.0*DELZ(K-1)))

```

```

AK=WAVE*WAVE*(CXZ(I-1,K-1)*DELX(I-1)*DELZ(K-1)+CXZ(I,K-1)*
1DELX(I)*DELZ(K-1)+CXZ(I,K)*DELX(I)*DELZ(K)+CXZ(I-1,K)*DELX(I-1)*
2DELZ(K))/4.0

```

```

S(JABEF)=-((S(JA)+S(JB)+S(JE)+S(JF)-AK)

```

```

DO 15 IJ=1,N1

```

```

15 AMRX(IN,IJ)=S(IJ)

```

```

GO TO 10

```

```

13 CONTINUE

```

```

COEFFICIENTS FOR NODES ON THE SURFACE--NEUMANN CONDITION

```

```

AK=WAVE*WAVE*(CXZ(I-1,K)*DELX(I-1)*DELZ(K)+CXZ(I,K)*DELX(I)*
1DELZ(K))/4.0

```

```

S(JA)=-DELZ(K)*CXZ(I,K)/(2.0*DELX(I))

```

```

S(JB)=-DELZ(K)*CXZ(I-1,K)/(2.0*DELX(I-1))

```

```

S(JE)=-((DELX(I)*CXZ(I,K)+DELX(I-1)*CXZ(I-1,K)) /
1(2.0*DELZ(K)))

```

```

S(JF)=0.0

```

```

S(JABEF)=-((S(JA)+S(JB)+S(JE)+S(JF)-AK)

```

```

DO 17 IJ=1,N1

```

```

17 AMRX(IN,IJ)=S(IJ)

```

GO TO 10
12 CONTINUE

COEFFICIENTS FOR NODES ON THE BOTTOM SURFACE

AK=WAVE*WAVE*(CX7(I-1,K-1)*DELX(I-1)*DELZ(K-1)+CXZ(I,K-1)*
1DELX(I)*DELZ(K-1))/4.0
CALL PAD(X,Z,L,N,ALF,ARG,I,K,ZZ,WAVE,THE,LL,NN)
S(JA)=-DELZ(K-1)*CX7(I,K-1)/(2.0*DELX(I))
S(JB)=-DELZ(K-1)*CX7(I-1,K-1)/(2.0*DELX(I-1))
S(JE)=0.0
S(JF)=-((DELX(I)*CXZ(I,K-1)+DELX(I-1)*CXZ(I-1,K-1))/
1(2.0*DELZ(K-1)))
CZ=-S(JF)*DELZ(K-1)*WAVE*COS(ALF)*ARG
S(JABEF)=-S(JA)+S(JB)+S(JE)+S(JF)-AK)+CZ
DO 19 IJ=1,N1
19 AMRX(IN,IJ)=S(IJ)
GO TO 10
11 CONTINUE
IF(I.EQ.L) GO TO 20
IF(K.GT.1.AND.K.NE.N) GO TO 22
IF(K.EQ.N) GO TO 23

COEFFICIENTS FOR TOP LEFT HAND CORNER

AK=WAVE*WAVE*(CXZ(I,K)*DELX(I)*DELZ(K)/4.0)
CALL PAD(X,Z,L,N,ALF,ARG,I,K,ZZ,WAVE,THE,LL,NN)
S(JA)=-DELZ(K)*CX7(I,K)/(2.0*DELX(I))
S(JB)=0.0
S(JE)=-DELX(I)*CXZ(I,K)/(2.0*DELZ(I))
S(JF)=0.0
CZ=-S(JA)*DELX(I)*WAVE*ARG
S(JABEF)=-S(JA)+S(JB)+S(JE)+S(JF)-AK)+CZ
DO 24 IJ=1,N1
24 AMRX(IN,IJ)=S(IJ)
GO TO 10
22 CONTINUE

COEFFICIENTS FOR THE LEFT SIDE

AK=WAVE*WAVE*(CX7(I,K-1)*DELX(I)*DELZ(K-1)+CXZ(I,K)*
1DELX(I)*DELZ(K))/4.0
CALL PAD(X,Z,L,N,ALF,ARG,I,K,ZZ,WAVE,THE,LL,NN)
S(JA)=-((DELZ(K)*CXZ(I,K)+DELZ(K-1)*CX7(I,K-1))/
1(2.0*DELX(I))
S(JB)=0.0
S(JE)=-DELX(I)*CXZ(I,K)/(2.0*DELZ(K))
S(JF)=-DELX(I)*CX7(I,K-1)/(2.0*DELZ(K-1))
CZ=-S(JA)*DELX(I)*WAVE*COS(THE)*ARG
S(JABEF)=-S(JA)+S(JB)+S(JE)+S(JF)-AK)+CZ
DO 25 IJ=1,N1
25 AMRX(IN,IJ)=S(IJ)
GO TO 10
23 CONTINUE

COEFFICIENTS FOR THE BOTTOM LEFT CORNER

```

C
AK=WAVE*WAVE*(CX7(I,K-1)*DELX(I)*DELZ(K-1))/4.0
CALL RAD(X,Z,L,N,ALF,ARG,I,K,ZZ,WAVE,THE,LL,NN)
S(JA)=-DELZ(K-1)*CXZ(I,K-1)/(2.0*DELX(I))
S(JB)=0.0
S(JE)=0.0
S(JF)=-DELX(I)*CXZ(I,K-1)/(2.0*DELZ(K-1))
CZ=-(S(JF)*DELZ(K-1)*COS(ALF)+S(JA)*DELX(I)*COS(THE))*
1WAVE*ARG
S(JABEF)=-((S(JA)+S(JB)+S(JE)+S(JF)-AK)+CZ
DO 26 IJ=1,N1
26 AMRX(IN,IJ)=S(IJ)
GO TO 10
20 CONTINUE
IF(K.GT.1.AND.K.NE.N) GO TO 27
IF(K.EQ.N) GO TO 28

```

```

C
C
C
COEFFICIENTS FOR TOP RIGHT CORNER

```

```

AK=WAVE*WAVE*(CX7(I-1,K)*DELX(I-1)*DELZ(K))/4.0
CALL RAD(X,Z,L,N,ALF,ARG,I,K,ZZ,WAVE,THE,LL,NN)
S(JA)=0.0
S(JB)=-DELZ(K)*CX7(I-1,K)/(2.0*DELX(I-1))
S(JE)=-DELX(I-1)*CXZ(I-1,K)/(2.0*DELZ(K))
S(JF)=0.0
CZ=-S(JB)*DELX(I-1)*WAVE*ARG
S(JABEF)=-((S(JA)+S(JB)+S(JE)+S(JF)-AK)+CZ
DO 29 IJ=1,N1
29 AMRX(IN,IJ)=S(IJ)
GO TO 10
27 CONTINUE

```

```

C
C
C
COEFFICIENTS FOR THE RIGHT SIDE

```

```

AK=WAVE*WAVE*(CX7(I-1,K-1)*DELX(I-1)*DELZ(K-1)+CX7(I-1,K)*
1DELX(I-1)*DELZ(K))/4.0
CALL RAD(X,Z,L,N,ALF,ARG,I,K,ZZ,WAVE,THE,LL,NN)
S(JA)=0.0
S(JB)=-((DELZ(K)*CX7(I-1,K)+DELZ(K-1)*CXZ(I-1,K-1))/
1(2.0*DELX(I-1)))
S(JE)=-DELX(I-1)*CXZ(I-1,K)/(2.0*DELZ(K))
S(JF)=-DELX(I-1)*CXZ(I-1,K-1)/(2.0*DELZ(K-1))
CZ=-S(JB)*DELX(I-1)*WAVE*COS(THE)*ARG
S(JABEF)=-((S(JA)+S(JB)+S(JE)+S(JF)-AK)+CZ
DO 30 IJ=1,N1
30 AMRX(IN,IJ)=S(IJ)
GO TO 10
28 CONTINUE

```

```

C
C
C
COEFFICIENTS FOR THE RIGHT BOTTOM NODE

```

```

AK=WAVE*WAVE*(CX7(I-1,K-1)*DELX(I-1)*DELZ(K-1))/4.0
CALL RAD(X,Z,L,N,ALF,ARG,I,K,ZZ,WAVE,THE,LL,NN)
S(JA)=0.0
S(JB)=-DELZ(K-1)*CXZ(I-1,K-1)/(2.0*DELX(I-1))
S(JE)=0.0

```

```

S(JF)=-DELX(I-1)*CXZ(I-1,K-1)/(2.0*DELZ(K-1))
CZ=-(S(JF)*DELZ(K-1)*COS(ALF)+S(JB)*DELX(I-1)*
10COS(THF))*WAVE*ARG
S(JBEF)=-((S(JA)+S(JB)+S(JE)+S(JF)-AK)+CZ
DO 31 IJ=1,N1
31 AMRX(IN,IJ)=S(IJ)
10 CONTINUE
RETURN
END

```

```

SUBROUTINE PAD(X,Z,L,N,ALF,ARG,I,K,ZZ,WAVE,THE,LL,NN)
DIMENSION X(LL),Z(NN)
LMID=(L+1)/2
DIST=ABS(X(I)-X(LMID))
R=SQRT(DIST*DIST+Z(K)*Z(K))
ARGX=WAVE*R
ARG1=AK1(ARGX)
ARG2=AK0(ARGX)
IF(ARG1.LT.ZZ.AND.ARG2.LT.ZZ) ARG=1.0
IF(ARG1.GE.ZZ.OR.ARG2.GE.ZZ) ARG=ARG1/ARG2
IF(K.EQ.1) GO TO 10
ALF=ATAN(DIST/Z(K))
IF(I.EQ.LMID) GO TO 10
THE=ATAN(Z(K)/DIST)
10 RETURN
END

```

```

FUNCTION AK0(X)
IF(X.GE.2.0) GO TO 10
T=X/5.75
T=T*T
B1=1.0+T*(3.5156229+T*(3.0890424+T*(1.2067492+T*(0.2659732+T*(
10.0360768+T*0.0245813))))))
T=0.5*X
Y=T*T
AK0=-ALOG(T)*B1-0.57721586+Y*(0.42278420+Y*(0.23069756+Y*
2(0.03482590+Y*(0.00262698+Y*(0.00010750+Y*0.00000740))))))
RETURN
10 AK0=1.0
RETURN
END

```



```
SUBROUTINE SOLVE(A,X,LN,N,N1,LLNN,NN1)
```

```

C
C
C
C
SUBROUTINE PERFORMS THE BACKSUBSTITUTION OF VECTOR X WITH
MATRIX .....
```

```
DIMENSION A(LLNN,NN1),X(LLNN)
```

```
LEVEL 2,A
```

```
L1=0
```

```
L=0
```

```
DO 10 I=1,LN
```

```
SUM=X(I)
```

```
IF(N.LE.0) GO TO 11
```

```
IF(L1.EQ.0) GO TO 12
```

```
L=L+1
```

```
IF(L.GT.N) L=N
```

```
K=N1-L
```

```
KL=I-L
```

```
DO 13 J=K,N
```

```
SUM=SUM-X(KL)*A(I,J)
```

```
13 KL=KL+1
```

```
GO TO 11
```

```
12 IF(SUM.NE.0) L1=1
```

```
11 X(I)=SUM*A(I,N1)
```

```
10 CONTINUE
```

```
14 X(LN)=X(LN)+A(LN,N1)
```

```
IF(LN.LE.1) GO TO 15
```

```
NL=LN+1
```

```
DO 16 I=2,NL
```

```
K=NL-I
```

```
SUM=X(K)
```

```
IF(N.LE.0) GO TO 17
```

```
KL=K+1
```

```
K1=MIN0(LN,K+N)
```

```
L=1
```

```
DO 18 J=KL,K1
```

```
SUM=SUM-X(J)*A(J,N1-L)
```

```
18 L=L+1
```

```
17 X(K)=SUM*A(K,N1)
```

```
16 CONTINUE
```

```
15 CONTINUE
```

```
RETURN
```

```
END
```

```
SUBROUTINE REVERT(VKY,IS,LWNO,TKY,V,IVS,IVKY)
```

```
ROUTINE TO PERFORM REVERSE FOURIER TRANSFORM
```

```
ORDER OF ARRAY VKY IS WAVE NUMBER,RESPONSE,SOURCE.....
```

```
DIMENSION VKY(IVKY,IVS,IVS),TKY(IVKY),V(IVS,IVS)
```

```

DO 10 ISOUR=1,IS
DO 11 IRESP=1,IS
VA=VKY(1,IRESP,ISOUR)*TKY(1)
DO 12 IKY=2,LWNO
IK1=IKY-1
XK1=TKY(IK1)
XK2=TKY(IKY)
Y1=VKY(IK1,IRESP,ISOUR)
Y2=VKY(IKY,IRESP,ISOUR)
IF(Y1.LT.1.0E-30.OR.Y2.LT.1.0E-30) GO TO 13
A=-ALOG(Y2/Y1)/(XK2-XK1)
GO TO 14
13 A=0.0
14 CONTINUE
Y=0.0
IF(A.EQ.0.0) GO TO 15
VA=VA+(Y1*(A*COS(XK1*Y)-Y*SIN(XK1*Y))-Y2*
1(A*COS(XK2*Y)-Y*SIN(XK2*Y)))/(A*A+Y*Y)
GO TO 16
15 VA=VA+Y1*(XK2-XK1)
16 CONTINUE
12 CONTINUE
V(ISOUR,IRESP)=VA*2.0
11 CONTINUE
10 CONTINUE
RETURN
END
```

```

SUBROUTINE PROFIL(V,IS,ISNODE,X,L,RHO,IVS,ASF,LL)
C
  DIMENSION X(LL),V(IVS,IVS),ISNODE(IVS)
  DIMENSION RHO(10,IVS),FACTOR(9)
  DATA FACTOR/.9654,.9709,.99,1.0455,1.0267,
11.0504,1.0741,1.0977,1.1223/
  PI=3.141592653
  DO 10 I=1,IS
  DO 10 J=1,10
10 RHO(J,I)=0.0
  DO 11 I=1,IS
  IA=ISNODE(I)
11 RHO(1,I)=X(IA)
  IEND=1
  DO 12 I7=2,10
  IEND=IEND+3
  IP=(IEND-1)/3
  IF(IEND.GT.IS) GO TO 99
  DO 13 I=IEND,IS
  IC1=I-3*IP
  IP1=I-2*IP
  IP2=I-IP
  IC2=I
  K1=ISNODE(IP1)
  K2=ISNODE(IP2)
  A=X(K2)-X(K1)
  IF(I.EQ.4) ASP=A
C
C
C
C
  VA=(V(IC1,IP1)-V(IC2,IP1))-(V(IC1,IP2)-V(IC2,IP2))
  VB=(V(IC1,IC2)-V(IP1,IC2))-(V(IC1,IP2)-V(IP1,IP2))
  VC=(V(IP1,IP1)-V(IP2,IP1))-(V(IC1,IC2)-V(IP2,IC2))
C
C
C
  IF(IEND.EQ.4) GO TO 99
  V1=VA*FACTOR(1)*A/PI
  V2=VB*FACTOR(1)*A/PI*3.0
  V3=VC*FACTOR(1)*A/PI*1.5
  WRITE(6,1000) V1,V2,V3
1000 FORMAT(10X,1P3E14.4)
  98 CONTINUE
C
C
  RHO(I7,IP1)=VA*A/PI
  13 CONTINUE
  12 CONTINUE
  99 DO 14 J=2,10
  DO 14 I=1,IS
  14 RHO(J,I)=RHO(J,I)*FACTOR(J-1)
  RETURN
  END

```

```
SUBROUTINE FIPL0T(RHO,IC0DE,7,RESIST,LIN,NNIN,L,N,A,IS,
1IVS,LL,M,LLIN,NNIN)
```

```
ROUTINE USES GINO ROUTINES TO PLOT OUT THE PROFILE
SECTION ON A4 SIZE.....
```

```
DIMENSION RHO(10,IVS),RESIST(10),7(LL),IC0DE(LLIN,NNIN)
```

```
THE CODE IS DESIGNED FOR A MAXIMUM NUMBER OF 41. ELECTRODE POSITION
```

```
CALL CM925
```

```
CALL DEVPAP(320.0,250.0,1)
```

```
CALL WINDOW(2)
```

```
CALL CHASIZ(3.0,4.5)
```

```
CALL ITALIC(15.0)
```

```
CALL MCVT02(18.0,172.0)
```

```
CALL CHAHOL(31HRESISTIVITY PROFILE SECTION*.)
```

```
CALL ITALIC(0.0)
```

```
CALL MCVT02(18.0,167.5)
```

```
CALL CHASIZ(2.0,3.0)
```

```
CALL CHAHOL(66HC*CALCULATED FROM THE MODEL RESISTIVITY DISTRIBUTIO
IN SHOWN BELOW*.)
```

```
CALL CHASIZ(1.0,1.5)
```

```
Y1=156.0
```

```
Y2=154.0
```

```
X1=17.75
```

```
X2=14.50
```

```
NUMBER=0
```

```
DO 10 I=1,IS
```

```
CALL MCVT02(X1,Y1)
```

```
CALL CHAHOL(5H-X-*.)
```

```
CALL MCVT02(X2,Y2)
```

```
CALL CHAINT(NUMBER,2)
```

```
NUMBER=NUMBER+1
```

```
X1=X1+5.0
```

```
X2=X2+5.0
```

```
10 CONTINUE
```

```
CALL MCVT02(95.0,161.5)
```

```
CALL CHASIZ(2.0,2.75)
```

```
CALL CHAHOL(24HELECTRODE POSITIONS *.)
```

```
CALL MCVT02(160.0,161.5)
```

```
IA=IFIX(A)
```

```
CALL CHAINT(IA,3)
```

```
CALL MCVT02(170.0,161.5)
```

```
CALL CHAHOL(15METRES APART*.)
```

```
X1=25.5
```

```
IR=1
```

```
X=25.5
```

```
IE=IS
```

```
Y=139.0
```

```
CALL CHASIZ(1.0,1.5)
```

```
DO 40 J=2,8
```

```
IR=IR+1
```

```

IE=IE-2
J1=J-1
IAX=IA*J1
CALL MCVT02(12.0,Y)
CALL CHAHOL(SHA=*. )
CALL MCVT02(14.5,Y)
CALL CHAINT(IAX,3)
DO 31 I=IR,IE
CALL MCVT02(X,Y)
IR=IFIX(RHO(J,I))
CALL CHAINT(IR,4)
X=X+5.0
31 CONTINUE
Y=Y-10.0
X1=X1+7.5
X=X1
40 CONTINUE
CALL CHASIZ(2.0,3.0)
CALL MCVT02(230.0,130.0)
CALL CHAHOL(19HMODEL RESISTIVITY*. )
CALL MCVT02(230.0,125.0)
CALL CHAHOL(14HDISTRIBUTION*. )
CALL CHASIZ(1.8,2.5)
CALL MCVT02(230.0,120.0)
CALL CHAHOL(21HCODE VALUES*. )
CALL CHASIZ(1.0,1.5)
CALL MCVT02(255.0,117.5)
CALL CHAHOL(14H(OHM-METRES)*. )
X=232.0
X1=255.0
Y=115.0
CALL CHASIZ(1.8,2.1)
DO 13 I=1,10
I1=I-1
CALL MCVT02(X,Y)
CALL CHAINT(I1,2)
CALL MCVT02(X1,Y)
R1=RESIST(I)
CALL CHAFIX(R1,6,1)
Y=Y-2.5
13 CONTINUE
CALL MCVT02(20.0,65.0)
CALL CHASIZ(2.5,3.0)
CALL CHAHOL(32HCODED RESISTIVITY DISTRIBUTION*. )
X=20.0
Y=60.0
CALL CHASIZ(1.25,2.0)
DO 20 J=1,NIN
DO 21 I=13,172
CALL MCVT02(X,Y)
IC=ICODE(I,J)
CALL CHAINT(IC,1)
X=X+1.25
CALL MCVT02(X,Y)
21 CONTINUE
Y=Y-3.0

```

```
X=20.0  
20 CONTINUE
```

C

```
CALL CHASIZ(2.5,3.5)  
CALL MOVT02(250.0,75.0)  
CALL CHAHOL(8HDEPTH*.)  
CALL MOVT02(252.0,70.0)  
CALL CHAHOL(10H(METRES)*.)
```

```
X=245.0
```

```
X1=260.0
```

```
Y=60.0
```

```
CALL CHASIZ(2.0,2.5)
```

```
DO 30 I=1,NIN
```

```
D1=Z(I)
```

```
D2=Z(I+1)
```

```
CALL MOVT02(X,Y)
```

```
CALL CHAFIX(D1,6,1)
```

```
CALL MOVT02(X1,Y)
```

```
CALL CHAFIX(D2,6,1)
```

```
Y=Y-5.0
```

```
30 CONTINUE
```

C

```
CALL DEVEND
```

```
RETURN
```

```
END
```


APPENDIX D

Travel time data from seismic refraction surveys.

A six channel Bison 1580 signal enhancement siesmograph was used with a hammer source and a chart recorder.

Appendix D1

Travel Time data - seismic refraction example 1.

x (m)	t_g (ms)	t_g (ms)	t_g (ms)	t_g (ms)	t_g (ms)
0	-	27.0	34.2	-	56.7
10	15.8	28.8	34.2	-	56.7
20	17.3	22.7	33.1	-	55.6
30	18.0	18.4	28.8	-	51.3
40	21.6	12.9	29.2	-	51.7
50	27.0	-	27.0	36.0	49.2
60	25.2	14.4	25.5	34.2	47.4
70	27.3	19.8	23.4	32.8	46.0
80	28.8	23.1	19.8	31.2	44.9
90	32.1	25.9	12.6	28.8	42.0
100	34.2	29.2	-	27.0	40.5
110	39.5	32.1	12.2	25.2	37.5
120	41.01	36.0	20.9	23.8	35.3
130	41.0	36.0	28.8	16.6	29.2
140	42.9	32.0	27.0	12.6	29.2
150	44.0	36.0	30.6	-	30.6
160	47.0	-	31.7	-	32.4
170	49.2	-	33.9	-	24.5
180	50.6	-	35.3	-	21.6
190	54.2	-	38.9	-	18.0
200	56.3	-	41.0	-	-

Appendix D2.

Travel Time data - seismic refraction example 2.

x (m)	tg (ms)	tg (ms)	tg (ms)	tg (ms)	tg (ms)
0	-	17.5	33.4	47.5	56.0*
10	5.6	12.2	31.8	46.8	55.0*
20	8.5	10.5	30.6	45.8	54.0*
30	11.6	9.0	29.3	42.7	50.0*
40	14.0	6.8	27.4	40.6	48.7*
50	17.2	-	27.9	38.2	46.6
60	19.4	5.7	22.3	36.3	44.4
70	21.3	10.6	16.4	34.6	42.6
80	26.8	16.6	10.8	34.2	42.2
90	31.3	22.8	5.5	32.0	40.0
100	33.0	27.8	-	30.0	38.0
110	36.0	28.0	8.0	26.5	35.4
120	37.6	29.5	15.6	22.2	33.0
130	40.4	32.0	22.0	11.5	30.6
140	43.5	35.0	26.0	4.5	28.2
150	47.3	38.0	30.4	-	22.0
160	50.5*	40.0	33.4	10.6	20.7
170	57.8*	42.6	34.7	17.0	17.0
180	51.5*	42.7	34.7	20.6	12.5
190	54.0*	45.2	36.8	22.9	9.0
200	55.5*	46.5	38.2	22.8	-

Note * denotes data projected from underlying branch of the t x graph.

Appendix D3

Travel time data - seismic refraction example 3.

x (m)	tg (ms)	tg (ms)	tg (ms)	tg (ms)	tg (ms)
0	-		60.5		
10	11.5		58.7		
20	14.4		54.0		
30	30.6		48.6		
40	33.8		45.0		
50	41.0		43.6	58.5	
60	48.3	16.0	39.6	54.0	
70	51.2	24.8	33.1	52.2	
80	54.0	30.2	27.7	50.8	
90	58.7	37.1	19.8	49.4	
100	60.5	43.6	-	44.6	68.0
110		50.4	16.8	40.0	77.0
120		55.8	27.6	32.4	63.0
130		58.0	35.0	23.7	52.2
140		58.4	40.0	17.3	43.9
150		58.7	43.2	-	43.0
160			50.4	11.6	33.1
170			57.7	24.0	27.0
180			61.2	30.2	24.5
190			67.2	37.1	-
200			68.0	43.6	-

Appendix D4 200m long line with shot points every 75m.

x (m)	tg (ms)	tg (ms)	tg (ms)	tg (ms)	tg (ms)
0	-	40.4	60.5	67.0*	81.0*
5	7.3	40.6	61.4	67.9*	81.9*
10	7.7	40.0	60.9	67.4*	81.4*
15	14.7	38.7	59.4	65.9*	79.9*
20	17.3	38.6	58.8	65.3*	79.3*
25	21.4	37.9	59.9	66.4*	80.4*
30	22.6	35.3	59.7	66.2*	80.2*
35	22.6	33.2	59.2	65.7*	79.7*
40	24.8	29.1	56.5	63.0*	77.0*
45	28.4	27.5	59.2	65.7*	79.7*
50	28.5	34.3	58.6	65.1*	79.1*
55	28.3	29.1	55.0	61.5*	75.5*
60	34.0	31.2	55.4	61.9*	75.9*
65	36.6	23.0	54.4	60.9*	74.9*
70	41.3	15.1	53.7	60.2*	74.2*
75	40.3	-	50.5	58.5*	72.5*
80	40.4	12.5	?	59.0	73.0*
85	45.9	18.7	50.1	57.0	71.0*
90	46.2	24.6	48.7	?	?
95	47.8	27.8	48.2	54.9	66.3
100	57.2	31.5	47.6	53.9	68.4
105	52.8	31.7	46.0	53.2	67.3
110	55.4	33.2	45.5	53.4	67.8
115	57.1	39.4	43.9	51.8	67.3
120	58.2	43.1	38.7	53.9	65.3
125	56.6	46.6	38.7	49.7	64.5
130	57.6	46.6	37.6	49.1	63.2
135	58.5	47.6	32.0	47.7	60.1
140	59.2	49.2	32.0	47.6	59.6

APPENDIX D5

x (m)	t _g (ms)	t _g (ms)	t _g (ms)	t _r (ms)	t _g (ms)
0	-	39.0	51.8	63.8	74.5
5	12.2	37.0	48.3	61.7	71.1
10	17.8	34.3	46.1	60.2	71.0
15	22.6	31.1	45.1	60.7	71.0
20	25.7	29.5	43.0	58.6	70.5
25	27.7	28.5	40.8	56.0	68.4
30	28.8	25.8	38.7	53.9	-
35	31.7	21.2	39.8	53.9	-
40	34.3	15.3	37.1	51.3	63.3
45	37.4	10.9	36.6	49.7	60.7
50	39.0	-	36.1	49.2	56.5
55	41.9	-	34.8	47.6	-
60	42.4	17.1	33.2	47.1	54.4
65	46.1	22.8	30.6	45.5	53.9
70	49.1	25.8	-	44.0	53.4
75	49.7	28.0	27.4	40.8	54.9
80	50.1	28.4	23.2	39.8	52.2
85	-	30.6	21.1	36.6	51.7
90	50.2	32.2	16.9	35.6	49.0
95	51.3	34.3	9.7	35.6	48.0
100	51.8	36.1	-	34.2	46.4
105	53.4	36.5	9.6	31.8	45.9
110	53.4	37.0	15.1	29.2	43.2
115	54.9	38.1	21.4	27.1	43.3
120	57.0	38.6	23.0	25.9	41.8
125	58.6	40.2	24.3	24.0	40.7
130	59.6	42.8	26.1	22.4	38.6
135	59.6	45.9	28.7	19.8	37.6
140	60.7	47.0	29.8	16.2	36.0
145	60.7	49.1	32.4	11.0	33.9
150	63.8	50.6	34.2	-	33.5
155	65.6	52.9	37.0	10.8	31.9
160	66.7	53.4	37.0	16.6	30.3
165	-	57.1	39.7	20.0	29.3
170	68.7	56.6	40.2	22.2	28.3
180	71.0	62.3	42.5	26.7	20.4

145	59.7	49.7	12.7	45.5	59.0
150	59.6	50.7	-	43.5	58.5
155	60.6	47.2	12.0	40.4	58.0
160	63.2	48.8	22.7	37.8	56.9
165	62.3	50.9	26.6	36.7	48.7
170	63.2	?	29.5	34.7	47.7
175	61.2	50.4	35.7	23.7	48.7
180	64.9	50.5	37.3	32.6	48.2
185	64.2	51.0	38.3	30.0	46.6
190	63.7	53.0	41.0	29.5	46.6
195	65.8	57.1	42.0	28.0	42.5
200	63.2	55.1	42.5	23.8	41.4
205	64.7	57.1	42.0	21.2	41.9
210	66.8	58.2	42.5	18.6	43.5
215	67.3	58.7	42.8	17.6	46.4
220	?	58.2	43.5	9.8	37.3
225	66.8	58.0	44.0	-	31.5
230	63.4*	56.8	41.4	10.5	32.8
235	65.8*	58.0	43.8	14.7	32.0
240	66.2*	59.7	44.2	16.8	27.4
245	68.3*	61.4	46.3	19.8	30.7
250	71.3*	62.2	49.3	24.4	29.4
255	70.4*	61.6*	48.4	23.1	27.4
260	72.5*	63.7*	50.5	27.8	27.4
265	75.5*	66.7*	53.5	27.4	23.1
270	?	?	?	29.4	18.9
275	78.8*	70.0*	56.6	30.0	21.0
280	76.7*	67.9*	54.7	?	19.4
285	78.8*	70.0*	56.8	27.0	14.7
290	80.1*	71.3*	58.1	28.7	14.3
295	76.8*	70.0*	56.8	33.0	13.9
300	80.5*	71.7*	56.5	31.0	-

Note Data marked with an asterisk has been calculated from a lower t - x curve.

185	72.6	61.9	44.6	28.3	17.3
190	73.1	64.5	45.7	28.8	13.6
195	73.8	66.7	45.1	30.4	13.8
200	74.7	68.2	47.2	31.9	-

APPENDIX E

Description of the water balance algorithm

E1 Description of the algorithm

General.

The algorithm has been written in Fortran-4 to perform an annual calculation of the water balance within a small catchment. The model is a one dimensional black box model and its main features have been described in Section 5.3 and Section 6.3. Figures 5.10, 6.4 and 6.5 summarise many of the essential components of the model.

The Monteith equation is used to calculate a daily value of actual evapotranspiration which is then combined with any rainfall which has occurred to produce a value of the soil moisture change (DELS) for that day. Antecedent soil moisture conditions are used to control the calculation of evapotranspiration.

The algorithm produces both graphical and ordinary output. Examples of the graphical output are included as Figures 6.6 - 6.8. The written output prints values for all variables on a daily basis, and from this output the various agro-climatological parameters of interest, such as growing season length, soil saturation, etc., may be ascertained.

Any number of consecutive daily data sets may be submitted. The graphical output is produced every two years on a convenient A4 size sheet.

It is necessary to assume initial conditions for the various variables such as soil moisture deficit etc.

E2 Algorithm structure

Main program.

Certain aspects of the main program are identical to that of the

evaporation algorithm described in Appendix A. In particular, the daily values for the sun's declination and the sun's radius vector, have been edited from the program source text which follows.

The main program contains information necessary to present the data in the written output on a calendar month basis.

The required initial conditions are set in the main program and can be varied as necessary by editing. This is to avoid changing one or two lines of data on a data source file which may contain more than 3000 lines and is stored remotely.

The main program sets up the required calendar timing, and performs the water balance whose structure may be seen in Figure 5.10. Various sub-totals are added to as the program reads through the data for one year. At the end of a year, totals are printed and the program then returns to read the first card of the next year's data. Card 3 of the input sequence which contains the input data conversion information is read at the beginning of each subsequent year of data.

The program may be started on the first day of any month as specified by the first reading of card 3.

SUBROUTINE BPLOTT.

This routine uses Gino-F and Ginograf routines from the C.A.D.C. library to plot the graphical output. The routines are device independent and are widely available on most main frame computers. The output is described in Section 5.3.

SUBROUTINE TOTALP.

This routine is a subset of the previous routine and plots out the annual totals at a position specified by BPLOTT.

SUBROUTINE DISCHG.

This routine calculates the quantity of water lost daily from the groundwater table as seepage. A simple one dimensional darcyian relationship is assumed between the hydraulic conductivity of the aquifer material and the elevation of the water table above the stream base level. The value of hydraulic conductivity is assigned within the routine. All other variables are passed through from the main program. The routine is called each day from the main program if the groundwater level (GLEV) is higher than the minimum level (GLEVIN).

SUBROUTINE UNITS.

This routine is called each day from the main program and performs the corrections to the daily climate data as specified by the control options on card 3, or the first card of each subsequent years data. The control options are described in the text at the beginning of the main program. It follows therefore, that the input data is required to be of a consistent type for one year, or part of a year if it is the first or last year included in the data run.

SUBROUTINE DDCWN.

This routine is called from the main program and distributes the calculated value of evapotranspiration (ETA), or the lowest value of ETA during the dry season (ETADRY) if a zero flux plane is present (SMS = 0), between losses from soil moisture (SMDI) or from the groundwater level (GLEW) depending upon the value of SMDI. The relationship used is presented graphically in Figure 6.5.

It is anticipated that the conditions in this routine would be varied under different climatic circumstances. Such changes can be readily programmed to this routine.

SUBROUTINE PEN.

This routine is called daily from the main program and calculates a value of evapotranspiration for the day in question. The routine also acts as a calling program for various aspects of the calculation.

The Monteith relationship is used to calculate ETA.

A value of daily net radiation in watts m^{-2} is returned from the RADIAT SUBROUTINE.

A value of RS is returned from the RESIST SUBROUTINE.

A value of ZO is returned from the VEG SUBROUTINE.

A value of RA is returned from the ROUGHS SUBROUTINE.

Values of ETA, IGROW and RS are returned to the main program.

SUBROUTINE RADIAT.

This routine has the same structure as the similarly named routine described in Appendix A and will not be described further here, other than to point out that the routine can return a value of incoming radiation or net radiation for any locality at any latitude.

In this way the program can be used for environments outside the savanna.

SUBROUTINE RESIST.

This routine calculates an assessment of the RS term in the Monteith equation based upon the soil moisture deficit data available. The relationships are based on Equation 5.6 and the information shown in Figures 6.4 and 6.5.

The relationships are empirical and it is envisaged that further developments will permit a refinement of the simple linear changes presented here.

SUBROUTINE VEG.

This routine calculates the value of Z0 based upon the length of the growing season. A maximum value of Z0 is allowed of 110.0, corresponding to a vegetation height of 1.1m overall. This value is reached after 110 days in which there is sufficient moisture in the soil to permit germination and growth. The value of IGROW represents the length of the growing season and is returned from SUBROUTINE ALB. A minimum value of Z0 of 6mm is assumed.

As for the previous routine the relationship described here is empirical and further development will produce modifications. However, the value of ETA is sensitive to Z0 and by allowing Z0 to increase from an initial small value, the early wet season conditions are better represented.

SUBROUTINE ROUGHES.

This routine calculates the value of RA based upon Equation 5.7. The value of Z0 is returned from SUBROUTINE VEG as described above. There is similarly likely to be modifications to this routine as the method is developed. A value of mean wind speed in metres per second is calculated from the daily value of wind run at the climate station.

SUBROUTINE GROUND.

This routine calculates the value of GPLUX which is used to modify the net radiation calculated by SUBROUTINE RADIAT. If 100% of the available net radiation were used to calculate ETA throughout the year, an overestimate would be produced.

Eighty percent of net radiation is used during the wet season and this falls to 25% during the dry season. The relationship is shown graphically in Figures 6.4 and 6.5.

SUBROUTINE ALB.

This routine calculates a daily value of albedo used in SUBROUTINE RADIAT which is applicable to the time of year and the soil moisture conditions.

During the dry season a value of 0.35 is assumed. As the rains begin, this rapidly falls to 0.25. The growth of a luxuriant vegetation cover during the wet season means that a high proportion of net radiation is absorbed by the vegetation surfaces. As the wet season progresses, the albedo falls to 0.15 after 70 days and remains at this level until the soil moisture deficit approaches the root constant value at the end of the growing season. A gradational change back to 0.35 is then allowed. The relationship of albedo to SMD is shown in Figures 6.4 and 6.5.

E3 Specification of variables.

General.

Throughout the algorithm, individual variable names are given which readily allow identification of their purpose. Where variables have been named in Appendix A, then the names have been retained.

The names of arrays have been retained from Appendix A with the exception that DAT has been increased in size to 40 elements, and an array introduced to store the two years of data for the plotting routines GB (731,9).

The following variables are used.

GLEV	Height of the water table.
GLEVMN	Minimum depth to the water table.
GLEVMX	Maximum depth to the water table.
ROOTM	Maximum value of the root constant.
ROOT	Value of the root constant during the growing season.
SMD1	Soil moisture deficit beneath a zero flux plane.
SMD2	Soil moisture deficit above a zero flux plane.
SMS	Soil moisture store.

SMDA1	SMD value at which the albedo begins to change
SMDA2	SMD value at which albedo change is completed.
SMDG1	SMD value at which ground flux begins to change.
SMDG2	SMD value at which ground flux completes change.
SY	Specific yield.
SMSA1	SMS value at which albedo begins to change.
SMSA2	SMS value at which albedo change is completed.
SMDMX	Maximum value of SMD.
IGROW	Length of growing season.
SEEP	Quantity of seepage.
RECH	Quantity of recharge.
ROFF	Quantity of runoff.
DELS	Change in soil moisture.
ETA	Value of evapotranspiration.
ETADRY	Minimum dry season value of ETA.
DELH	Value of hydraulic head.
HCOND	Value of hydraulic conductivity.
FALL	Daily reduction in level of water table.
ROOTA	Value of SMD at which short rooted vegetation wilts.
SVP	Saturated vapour pressure.
GFLUX	Proportion of net radiation lost to processes other than ETA.

E4 Listing of the Fortran Δ program.

A listing of the program is given below.

```

C
DIMENSION DAT(40),Y(9),RADIUS(366),DECLIN(366),PANE(4)
DIMENSION MONTH(12),PNAME(12),DEC1(133),DEC2(133),DEC3(133)
DIMENSION RAD1(133),RAD2(133),RAD3(133)
DIMENSION GR(731,9)

```

```

C
GLEV=4560.0
ROOTM=100.0
SMD1=105.0
SMD2=0.0
SMS=0.0
SMDA1=ROOTM-20.0
SMDG1=SMDA1
SY=0.03
GLEVMN=1750.0
GLEVMX=3800.0

```

```

C
CALL CN925
CALL DEVPAP(320.0,250.0,1)

```

```

C
PROGRAM CALCULATES A WATER BALANCE ++++++

```

```

C
BASED UPON MONTEITH EQUATION TO CALCULATE ACTUAL ETA, AND THE USE OF
C
OF A SOIL MOISTURE POTENTIAL MODEL DESCRIBED IN THE TEXT++

```

```

C
ANY NUMBER OF CONSECUTIVE DAILY RECORDS MAY BE USED++++

```

```

C
PROGRAM PLOTS A WATER BALANCE AFTER EVERY TWO YEARS OF DATA++

```

```

C
IT IS NECESSARY TO SET INITIAL CONDITIONS FOR BALANCE, VIZ:
C
GLEV,GLEVMN,GLEVMX
C
SMD1,SMD2,SMS

```

```

C
ROOTM IS THE MAXIMUM VALUE OF THE ROOT CONSTANT+++
C
SY IS THE VALUE OF SPECIFIC YIELD ++++

```

```

C
THE PROGRAM HAS BEEN CONSTRUCTED SO THAT ANY OF THE ASSUMED
C
RELATIONSHIPS MAY BE SIMPLY CHANGED IN THE SUBROUTINES+++

```

```

C
DESCRIPTION OF THE DATA CONTROL CARDS
C
=====

```

```

C
CARD 1 (I3,I4,6A6)

```

```

C
I3 NO. OF RECORDS

```

```

C
I4 YEAR IN WHICH TO START DATA RUN

```

```

C
6A6 STATION NAME - UP TO 36 CHARACTERS

```

```

C
CARD 2 (5F6.0,2F5.0)

```

```

C
THE STATION ELEVATION, AVERAGE AMBIENT PRESSURE (MB)

```

```

C
LATITUDE (DEGREES), VALUES OF A AND B, AND PENMAN

```

```

C
CONSTANTS Y(1),Y(9) IN THE FIRST SEVEN FIELDS.

```

```

C
CARD 3 (6I1,1I2,1I1)

```

```

C
THIS CARD DETERMINS NATURE OF DATA INPUT

```

```

C
A 1 IN COL 1 CONVERTS FARENHEITE TO CENTIGRADE

```

```

C
A 1 IN COL 2 CONVERTS MILES TO KILOMETER

```

```

C
A 1 IN COL 3 CONVERTS INCHES TO MM

```

```

C
A 0 IN COLS 1-3 GIVES DEFAULT VALUES FOR THE

```

CALCULATION

A 1 IN COL 4 IF DATA IS NET RADIATION IN CAL/CM/MIN
 A 0 IN COL 4 IF RADIATION VALUES TO BE
 CALCULATED FROM FIRST PRINCIPLES
 A 1 IN COL 5 IF TEMP IS AN AVERAGE OF DRY BULB
 A 0 IN COL 5 IF DATA IS MAX AND MIN
 A 1 IN COL 6 IF HUMIDITY DATA IS WET BULB TEMP
 A 0 IN COL 6 IF RELATIVE HUMIDITY DATA ONLY
 COLS 7-8 OF THE THIRD CARD HOLD THE MONTH TO
 START THE DATA RUN IN. IT IS ASSUMED THAT RUN
 BEGINS AT START OF THE MONTH

DESCRIPTION OF DATA CARDS

=====

THE DATA CARD FORMAT IS (I3,2X,3F5.0,F7.0,5F5.0)

THE FIRST FIELD HOLDS THE DAY NUMBER
 THE 2 FIELD HOLDS MAX TEMP OR AVERAGE TEMP IN DEG F OR DEG C
 THE 3 FIELD HOLDS MIN IN DEG F OR DEG C
 THE 4 FIELD HOLDS RAINFALL IN INS OR MM
 THE 5 FIELD HOLDS DAILY WIND RUN IN MILES OR KILOMETRES
 THE 6 FIELD HOLDS THE PICHE DATA
 THE 7 FIELD HOLDS RELATIVE HUMIDITY OR WET BULB DATA
 THE 8 FIELD HOLDS THE OBSERVED SUN HOURS
 THE 9 FIELD HOLDS THE PAN DATA
 THE 10 FIELD HOLDS GUNN BELLANI DATA IN $^{\circ}$ OR INCOMING
 RADIATION IN CALS/CM**2/DAY

IF ANY DATA IS NOT AVAILABLE THE FIELD IS LEFT BLANK

SUN'S RADIUS VECTOR VALUES

DATA RAD1/0.98324,

AS FOR EVAPORATION PROGRAM+++++

DATA Y/L.95,0.56,0.08,0.10,0.90,0.26,1.00,1.00,1.00/

DATA MONTH/31,28,31,30,31,30,31,31,30,31,30,31/

DATA MNAME/7HJANUARY,8HFEBRUARY,5HMARCH,5HAPRIL,3HMAY,
 14HJUNE,4HJULY,6HAUGUST,8HSEPTEMBER,7HOCTOBER,8HNOVEMBER,
 28HDECEMBER/

KOUNT=0

DO 64 I=1,731

DO 64 J=1,9

64 GR(I,J)=0.0

ICOUNT=0

JCOUNT=0

26 IF(JCOUNT.GT.1) GO TO 61

READ(5,100) N,IYEAR,(NAME(I),I=1,6)

100 FORMAT(2I4,6A6)

READ(5,200) ELEV,ANRPPS,ALAT,A,R,Y(1),Y(9)

200 FORMAT(5F6.0,2F5.0)

61 READ(5,300) L1,L2,L3,L5,L6,L7,L4

300 FORMAT(6I1,I2)

IF(L4.EQ.0) L4=1

RYEAR=FLOAT(IYEAR)

RY=RYEAR/4.0

IRY=IFIX(RY)

RIPY=FLCAT(IRY)

IF((RY-RIPY).LT.1.0E-5) MONTH(2)=29

IF(JCOUNT.GT.1) GO TO 61

SMSA1=5.0


```

SMSA2=30.0
SMDRX=RCOTM+35.0
SMDA2=RCOTM+20.0
SMDG2=SMDA2

```

C

```

WRITE(6,4000) SMD1,SMD2,SMDG1,SMDG2,SMDRX
4000 FORMAT(1H1,5X,26H SOIL MOISTURE DEFICIT DATA/(5X,5F10.2))
WRITE(6,4001) SMS,SMDA1,SMDA2,SMSA1,SMSA2
4001 FORMAT(1H0,10X,24H SOIL MOISTURE STORE DATA/(5X,5F10.2))
WRITE(6,4002) ROOTM,GLEV,SY,GLEVNY,GLEVNX
4002 FORMAT(1H0,15X,25H GROUNDWATER RESPONSE DATA/(5X,6F10.2))
DO 10 I=1,366
IF(I.GT.133) GO TO 11
DECLIN(I)=DEC1(I)
RADIUS(I)=RAD1(I)
GO TO 10
11 IF(I.GT.266) GO TO 12
DECLIN(I)=DEC2(I-133)
RADIUS(I)=RAD2(I-133)
GO TO 10
12 DECLIN(I)=DEC3(I-266)
RADIUS(I)=RAD3(I-266)
10 CONTINUE

```

C

C

C

C

```

WRITE OUT HEADINGS
WRITE(6,1000) (NAME(I),I=1,6),ELEV,AMBPRS,ALAT
1000 FORMAT(1H0,10X,20H CLIMATE STATION NAME/12X,6A6/
111X,17H STATION ELEVATION,3X,F6.2,2X,6H METRES/
211X,24H AVERAGE AMBIENT PRESSURE,2X,F6.2/
3 11X,16H STATION LATITUDE,2X,F6.2)
WRITE(6,2000) A,R,(Y(I),I=1,9)
2000 FORMAT(1H0,16H PENMAN CONSTANTS/1X,2HA=,F5.3,5X,2HR=,F5.3/
1 1X,3HY1=,F4.2,2X,3HY2=,F4.2,2X,3HY3=,F4.2,2X,3HY4=,F4.2/
2 1X,3HY5=,F4.2,2X,3HY6=,F4.2,2X,3HY7=,F4.2,2X,3HY8=,F4.2,2X,
3 3HY9=,F4.2)

```

C

C

```

IGROW=5
ALBEDO=0.2
60 CONTINUE
SEPT=0.0
ETADRY=C.5
RECHT=0.0
ROFFT=0.0
ETAT=0.0
RAINT=0.0
ICOUNT=ICOUNT+1
ETADRY=C.5
DO 13 K=L4,12
LX=MONTH(K)
WRITE(6,3001) MNAME(K),IYEAR
3001 FORMAT(1H0,10X,A8,5X,I4)
WRITE(6,3002)
3002 FORMAT(1H0,9X,4HRAIN,5X,3HETA,4X,4HSMD1,4Y,4HSMD2,4X,4HDELS,5X,
13HSMS,4X,4HGLEV,4X,4HRECH,4X,4HROFF,5X,5HISNOW,4X,4HSEPT,5X,
26HALBEDO,3X,5HGFUX,6X,2HRS)
DO 14 KJ=1,LX
DO 2 I=1,40

```

```

20 DAT(I)=0.0
   READ(5,500) IDAY,(DAT(I),I=1,9)
500 FORMAT(I3,2X,3F5.0,F7.0,5F5.0)
   KOUNT=KOUNT+1
   JCOUNT=JCOUNT+1
   CALL UNITS(DAT,Y,AMPPRS,L1,L2,L3,L5,L6,L7)
C
   IF(IGROW.LT.5.00 .OR. IGROW.GT.60) GO TO 62
   PFR=(1.0-0.25)/60.0
   AIGROW=FLOAT(IGROW)
   ROOTF=AIGROW*RMR+0.25
   ROOT=RCOTH*ROOTF
   GO TO 63
62 ROOT=RCOTH
63 CONTINUE
C
C   BALANCE CALCULATION STARTS HERE+++++++
C
   PECH=0.0
   SEEP=0.0
   ROFF=0.0
   IF(GLEV.LT.GLEVMX) CALL DISCHG(GLEV,GLEVMX,SEEP,SY)
   IF(SMS.GT.0.1) GO TO 30
   CALL PER(ETA,DAT,IDAY,Y,A,B,ELEV,AMPPRS,ALMT,RADIUS,DECLIN,
1SMS,SMSA1,SMSA2,SMD1,SMDG1,SMDG2,SMDA1,SMDA2,ROOT,IGROW,
2L5,ALREDO)
   IF(DAT(3).LT.0.1) ETADRY=ETA
C
   ETADRY=AFIN1(ETADRY,ETA)
C   COMPUTE SOIL MOISTURE BALANCE
C
   DELS=DAT(3)-ETA
   IF(DELS.LT.0.0) GO TO 40
   IF(SMD1.GT.0.0) GO TO 41
   RECH=DELS
   GO TO 42
41 IF((SMD1-DELS).GT.0.0) GO TO 43
   RECH=DELS-SMD1
   SMD1=0.0
42 CONTINUE
   IF((GLEV-RECH/SY).LT.GLEVMN) GO TO 44
   GLEV=GLEV-RECH/SY
   GO TO 25
44 ROFF=PECH-(GLEV-GLEVMN)*SY
   GLEV=GLEVMN
   GO TO 25
43 IF(SMD1.GT.SMDG1) GO TO 45
C
C   THIS CONDITION SETS UP A ZERO FLUX PLANE+++++
C
   SMD1=SMD1-DELS
   GO TO 25
45 SMS=DELS
   SMD2=0.0
   GO TO 25
40 CALL DDOWN(DELS,GLEV,SY,SMD1,ROOTM,SMDMX,SMS,SMDA1,SMDA2)
   GO TO 25
C
C   COMPLETES ALL CONDITIONS WITHOUT A ZERO FLUX PLANE+++
C

```

3. CONTINUE

```

C
C   EVAPORATION CONTINUES BENEATH THE ZERO FLUX PLANE AT A
C   VALUE EQUIVALENT TO THE -VE POTENTIAL ESTABLISHED.
C
C   CALL DDOWN(ETA DRY, GLEV, SY, SMD1, ROOTX, SMDX, SMS, SMDA1, SMDA2)
C
C   MOISTURE REDISTRIBUTED TO BALANCE SMD1
C
C   CALL FEN(ETA, DAT, IDAY, Y, A, P, ELEV, AMPRS, ALAT, RADIUS, DECLIN,
1SMS, SMDA1, SMDA2, SMD2, SMDG1, SMDG2, SMDA1, SMDA2, ROOT, IGROW,
2LS, ALPEDO)
C   DELS=DAT(3)-ETA
C   IF(DELS.LT.0.0) GO TO 52
C   SMS=SMS+DELS
C   SMD2=SMD2-DELS
C   IF(SMD2.LE.0.0) SMD2=.0
C   IF(SMS.GE.SMD1) GO TO 53
C   GO TO 25
53 RECH=SMS-SMD1
C   SMD1=0.0
C   SMS=0.0
C   GO TO 42
52 CONTINUE
C   SMS=SMS+DELS
C   SMD2=SMD2-DELS
C   IF(SMS.LT.0.0) SMS=0.0
C   IF(SMS.EQ.0.0) SMD2=0.0
C
C   NO RECHARGE OCCURRED AND SMD2 NOW EQUAL SMD1
C
C   IF(SMD2.GT.SMD1) GO TO 54
C   GO TO 25
54 SMD2=0.0
C   SMS=0.0
25 CONTINUE
C
C   BALANCE CALCULATION ENDS HERE+++++
C
C   GR(KOUNT,1)=ETA
C   GR(KOUNT,2)=DAT(3)
C   GR(KOUNT,3)=GLEV
C   GR(KOUNT,4)=RECH
C   GR(KOUNT,5)=SMD1
C   GR(KOUNT,6)=SMD2
C   GR(KOUNT,7)=SMS
C   GR(KOUNT,8)=ROFF
C   GR(KOUNT,9)=SEEP
C   SEEPT=SEEPT+SEEP
C   RECHT=RECHT+RECH
C   ROFFT=ROFFT+ROFF
C   ETAT=ETAT+ETA
C   RAINI=RAINI+DAT(3)
C   DAT(20)=ETA
C   DAT(21)=SMD1
C   DAT(22)=SMD2
C   DAT(23)=DELS
C   DAT(24)=SMS
C   DAT(25)=GLEV
C   DAT(26)=RECH

```

```

DAT(27)=ROFF
DAT(29)=SEEP

```

```

C
C WRITE OUT DATA PRODUCED BY BALANCE
WRITE(6,3000) IDAY,DAT(3),(DAT(I),I=20,32)
3000 FORMAT(1X,I3,2X,14F8.2)
14 CONTINUE
13 CONTINUE
WRITE(6,5000) IYEAR
WRITE(6,5001) ETAT,RAINT,RECHT,ROFFT,SEEPT
5000 FORMAT(1H0,25X,15HTOTALS FOR YEAR,5X,I4)
5001 FORMAT(1H0,15X,24HTOTAL EVAPOTRANSPIRATION,5X,F10.1/
116X,14HTOTAL RAINFALL,5X,F10.1/
216X,14HTOTAL RECHARGE,5X,F10.1/
316X,12HTOTAL RUNOFF,5X,F10.1/
416X,13HTOTAL SEEPAGE,5X,F10.1)

```

```

C
IF(ICOUNT.EQ.2) CALL BPLOT(GB,ICOUNT,KOUNT,ROOTY,IYEAR,SY)
IF(N-JCOUNT)23,23,24
24 L4=1
IYEAR=IYEAR+1
RYEAR=FLOAT(IYEAR)
RY=RYEAR/4.0
IRY=IFIX(RY)
RIPY=FLCAT(IRY)
IF((RY-RIPY).LT.1.0E-5) GO TO 21
MONTH(2)=28
GO TO 22
21 MONTH(2)=29
22 CONTINUE
GO TO 26
23 CONTINUE
CALL DEVEND
STOP
END

```

```

FUNCTION SVP(T)
SVP=0.003*(T/5.0-3.0)**4+0.163*(T/5.0-3.0)**3+3.776*
1(T/5.0-3.0)**2+5.487*(T/5.0-3.0)+17.044
RETURN
END

```

```

FUNCTION DEL(T)
DEL=(0.012*(T/5.0-3.0)**3+0.189*(T/5.0-3.0)**2+
11.55*(T/5.0-3.0)+5.487)/5.0
RETURN
END

```

```

SUBROUTINE RPLOT(G5,ICOUNT,KOUNT,ROOT,LYEAR,SY)
DIMENSION IHOL(12),GP(731,9),DAY(731)
DIMENSION G1(731),G2(731),G3(731),G4(731),G5(731),G6(731),
1G7(731),G8(731),G9(731)
DATA IHOL/3HJAN,3HFEB,3HMAR,3HAPR,3HMAY,3HJUN,3HJUL,3HAUG,
13HSEP,3HOCT,3HNOV,3HDEC/
CALL WINDOW(2)

C
C
C
C
C
G1=ETA G2=RAIN G3=GLEV G4=RECH G5=SMD1 G6=SMD2 G7=SMS G8=ROFF
C
C
C
C
PLACE DATA IN SEPARATE ARRAYS

SMD1M=0.0
SMD2M=0.0
SMSM=0.0
DO 10 I=1,731
DAY(I)=FLOAT(I)
G1(I)=GP(I,1)
G2(I)=GP(I,2)
G3(I)=GP(I,3)/1000.0
G4(I)=GP(I,4)
G5(I)=GP(I,5)
G6(I)=GP(I,6)
G7(I)=GP(I,7)
G8(I)=GP(I,8)
G9(I)=GP(I,9)
IF(G7(I).GT.SMSM) ISMS=I
SMSM=AMAX1(SMSM,G7(I))
IF(G6(I).GT.SMD2M) ISMD2=I
SMD2M=AMAX1(SMD2M,G6(I))
IF(G5(I).GT.SMD1M) ISMD1=I
SMD1M=AMAX1(SMD1M,G5(I))
10 CONTINUE

C
CALL MOVTO2(0.1,0.1)
CALL LINTO2(0.1,210.1)
CALL LINTO2(297.1,210.1)
CALL LINTO2(297.1,0.1)
CALL LINTO2(0.1,0.1)
CALL POVTO2(26.0,22.5)

C
SEEPT1=0.0
RECHT1=0.0
RAINT1=0.0
ETAT1=0.0
ROFFT1=0.0
DO 12 I=1,365
RECHT1=RECHT1+G4(I)
RAINT1=RAINT1+G2(I)
ROFFT1=ROFFT1+G8(I)
SEEPT1=SEEPT1+G9(I)
12 ETAT1=ETAT1+G1(I)
SEEPT2=0.0
RECHT2=0.0
RAINT2=0.0
ETAT2=0.0
ROFFT2=0.0
DO 13 I=366,730
RECHT2=RECHT2+G4(I)
SEEPT2=SEEPT2+G9(I)

```

```

    RAIN2=RAIN2+G7(I)
    ROFF2=ROFF2+G8(I)
13  ETAT2=ETAT2+G1(I)
    DO 14 I=1,730
14  G8(I)=G8(I)+G9(I)
    IYEAR=IYEAR-1
    CALL CHASIZ(2.0,2.5)
    CALL CHAINT(IYEAR,4)
    CALL MCVT02(155.5,22.5)
    IYEAR=IYEAR+1
    CALL CHAINT(IYEAR,4)
    CALL CHASIZ(1.5,2.0)
    CALL AXIPOS(1,25.0,30.0,250.0,1)
    CALL AXISCA(5,24,0.0,730.0,1)
    CALL AXILAB(1HOL,12,3,1,21.0,-1)
    CALL AXISCA(3,146,0.0,730.0,1)
    CALL AXIDRA(1,1,1)
    CALL AXISCA(5,730,0.0,730.0,1)
    CALL AXIPOS(1,25.0,30.0,50.0,2)
    CALL AXISCA(3,8,0.0,80.0,2)
    CALL AXIDRA(-2,-1,2)

C
C
C
    PLOT RAINFALL++++++++++++++++

C
C
C
    CALL GRAHIS(G2,730,3.1)
    CALL AXIPOS(1,275.0,30.0,50.0,2)
    CALL AXISCA(3,10,0.0,10.0,2)
    CALL AXIDRA(-2,1,2)

C
C
C
    PLOT ET++++++++++++++++

C
C
C
    CALL PENSEL(2,0,0)
    CALL GRAPOL(DAY,61,730)
    CALL PENSEL(1,0,0)
    IYEAR=IYEAR-1
    X=30.0
    Y=60.0
    CALL TOTALP(Y,Y,RAIN1,RECHT1,ROFF1,SEPT1,ETAT1,IYEAR)

C
C
C
    IYEAR=IYEAR+1
    X=156.0
    Y=60.0
    CALL TOTALP(X,Y,RAIN2,RECHT2,ROFF2,SEPT2,ETAT2,IYEAR)

C
C
C
    CALL MCVT02(30.0,75.0)
    CALL CHASIZ(2.5,3.5)
    CALL CHAHOL(10HRAINFALL*.)
    CALL MCVT02(35.0,72.0)
    CALL CHASIZ(1.5,2.0)
    CALL CHAHOL(10H(MM/DAY)*.)
    CALL MCVT02(225.0,75.0)
    CALL CHASIZ(2.5,3.5)
    CALL CHAHOL(20HEVAPOTRANSPIRATION*.)
    CALL MCVT02(245.0,72.0)
    CALL CHASIZ(1.5,2.0)
    CALL CHAHOL(10H(MM/DAY)*.)

C
C
C
    CALL MCVT02(18.0,174.0)
    CALL CHASIZ(2.5,3.5)
    CALL CHAHOL(20HSOIL MOISTURE DATA*.)

```

```

CALL MCVT02(20.0,174.0)
CALL CHAHOL(18HROOT CONSTANT = *.)
CALL MCVT02(135.0,174.0)
IROOT=JFIX(ROOT)
CALL CHAJNT(IROOT,3)
CALL MCVT02(180.0,174.0)
CALL CHAHOL(18HSPECIFIC YEILD =*. )
CALL MCVT02(228.0,174.0)
CALL CHAFIX(SY,5,3)
CALL CHASIZ(1.5,2.0)
CALL AXIPOS(1,25.0,114.0,250.0,1)
CALL AXISCA(3,365.0,0.0,730.0,1)
CALL AXIDRA(-1,0,1)

CALL AXIPOS(1,25.0,114.0,18.0,2)
CALL AXISCA(3,8,0.0,40.0,2)
CALL AXIDRA(1,-1,2)

PLOT SEEPAGE DATA+++++++

CALL AXIPOS(1,275.0,114.0,18.0,2)
CALL AXISCA(3,8,0.0,40.0,2)
CALL AXIDRA(-2,0,2)
CALL GRAPOL(DAY,68,730)
CALL MCVT02(30.0,130.0)
CALL CHASIZ(2.5,3.5)
CALL CHAHOL(18HCOMBINED SEEPAGE*. )
CALL MCVT02(35.0,125.5)
CALL CHAHOL(12HAND RUNOFF*. )
CALL CHASIZ(1.5,2.0)
CALL MCVT02(40.0,122.0)
CALL CHAHOL(13H(MH-EQUIV.)*. )
CALL MCVT02(30.0,108.6)
CALL CHASIZ(2.5,3.5)
CALL CHAHOL(13HGROUNDWATER*. )
CALL MCVT02(30.0,104.2)
CALL CHAHOL(12HHYDROGRAPH*. )
CALL CHASIZ(1.5,2.0)
CALL MCVT02(35.0,101.0)
CALL CHAHOL(14H(M BELOW GL)*. )
CALL MCVT02(254.0,108.6)
CALL CHASIZ(2.5,3.5)
CALL CHAHOL(10HRECHARGE*. )
CALL MCVT02(260.0,105.0)
CALL CHASIZ(1.5,2.0)
CALL CHAHOL(6H(RR)*. )

C
C
C
C
START ROTATIONS+++

CALL SHIFT2(25.0,170.0)
CALL ROTAT3(1,180.0)
CALL AXIPOS(1,0.0,0.0,250.0,1)
CALL AXISCA(3,146,0.0,730.0,1)
CALL AXIDRA(2,0,1)
CALL AXIPOS(1,0.0,0.0,35.0,2)
CALL AXISCA(3,12,0.0,300.0,2)
CALL AXIDRA(2,-1,2)

```

C

```

C      PLOT SMD DATA+++++++
C      CALL GRAPOL(DAY,65,730)
C      Y=SMD1M+3.0
C      X=FLOAT(ISID1)
C      CALL GRAMOV(X,Y)
C      CALL CHAHOL(6HSMD1*.)

C
C
C      PLOT SMS DATA+++++++
C      CALL PENSEL(2,0,5)
C      CALL GRAPOL(DAY,67,730)
C      Y=SMSB+3.0
C      X=FLOAT(ISMS)
C      CALL GRAMOV(X,Y)
C      CALL CHAHOL(5HSMS*.)

C
C      CALL PENSEL(1,0,0)

C
C      PLOT SMD2 DATA+++++++
C
C      CALL GRAPOL(DAY,66,730)
C      Y=SMD2M+3.0
C      X=FLOAT(ISID2)
C      CALL GRAMOV(X,Y)
C      CALL CHAHOL(6HSMD2*.)

C
C      CALL AXIPOS(1,250.0,0.0,35.0,2)
C      CALL AXISCA(3,12,0.0,300.0,2)
C      CALL AXIDRA(-2,1,2)
C      CALL AXIPOS(1,0.0,56.0,250.0,1)
C      CALL AXISCA(3,146,0.0,730.0,1)
C      CALL AXIPOS(1,0.0,56.0,30.0,2)
C      CALL AXISCA(3,12,0.0,6.0,2)
C      CALL AXIDRA(2,-1,2)

C
C      PLOT HYDROGRAPH DATA+++++++
C
C      CALL GRAPOL(DAY,63,730)

C
C      CALL AXIPOS(1,250.0,56.0,25.0,2)
C      CALL AXISCA(3,8,0.0,40.0,2)
C      CALL AXIDRA(-2,1,2)
C      CALL AXIPOS(1,0.0,56.0,250.0,1)
C      CALL AXISCA(5,730,0.0,730.0,1)

C
C      PLOT RECHARGE DATA AS HISTOGRAM+++
C
C      CALL GRAHIS(64,730,0.1)

C
C      CALL ROTAT3(1,-180.0)
C      CALL SHIFT2(-25.0,-170.0)
C      CALL PICCLE
C      ICOUNT=0
C      KOUNT=0
C      DO 11 I=1,731
C      DO 11 J=1,9
11  GR(I,J)=0.0

C
C      RETURN
C      END

```



```
SUBROUTINE TOTALP(X,Y,R,RE,RO,S,E,IYEAR)
```

C

```
CALL MOVT02(X,Y)
CALL CHAS17(1.5,2.5)
CALL CHAHOL(12HTOTALS FOR*. )
Y=Y-3.0
X1=X+3.0
CALL MOVT02(X1,Y)
CALL CHAINT(IYEAR,4)
Y=Y-2.5
CALL CHAS17(1.25,1.75)
CALL MOVT02(X,Y)
CALL CHAHOL(8HRRAIN =*. )
X1=X+10.0
CALL MOVT02(X1,Y)
CALL CHAFIX(R,6,1)
Y=Y-2.5
CALL MOVT02(X,Y)
CALL CHAHOL(7HETA =*. )
X1=X+8.75
CALL MOVT02(X1,Y)
CALL CHAFIX(E,6,1)
Y=Y-2.5
CALL MOVT02(X,Y)
CALL CHAHOL(12HRECHARGE =*. )
X1=X+15.0
CALL MOVT02(X1,Y)
CALL CHAFIX(RE,6,1)
Y=Y-2.5
CALL MOVT02(X,Y)
CALL CHAHOL(10HRUNOFF =*. )
X1=X+12.5
CALL MOVT02(X1,Y)
CALL CHAFIX(PO,6,1)
Y=Y-2.5
CALL MOVT02(X,Y)
CALL CHAHOL(11HSEEPAGE =*. )
X1=X+13.75
CALL MOVT02(X1,Y)
CALL CHAFIX(S,6,1)
RETURN
END
```

```
SUBROUTINE DISCHG(GLEV,GLEVMX,SEEP,SY)
```

C

C

C

C

C

C

C

```
ROUTINE CALCULATES QUANTITY OF DAILY SEEPAGE++++
HCOND = HYDRAULIC CONDUCTIVITY OF SOIL ("/DAY)
HCOND=1.8E-3
DELH=(GLEVMX-GLEV)/1000.0
CALCULATE FLOW IN M**3 THROUGH SOIL, FOR A UNIT AREA..
FLOW=HCOND*DELH
FALL=FLOW/SY*1000.0
GLEV=GLEV+FALL
SEEP=FALL*SY
RETURN
END
```

```

SUBROUTINE UNITS(DAT,Y,AMBPRS,L1,L2,L3,L5,L6,L7)
DIMENSION DAT(40),Y(9)
IF(L1.EQ.1) DAT(1)=(DAT(1)-32.0)*5.0/9.0
IF(L1.EQ.1) DAT(2)=(DAT(2)-32.0)*5.0/9.0
IF(L2.EQ.1) DAT(4)=DAT(4)*1.6129
IF(L3.EQ.1) DAT(3)=DAT(3)*25.4
DAT(4)=DAT(4)*Y(9)
IF(L5.EQ.0) GO TO 10
DAT(11)=DAT(1)
DAT(1)=0.0
10 IF(L7.EQ.0) GO TO 14
IF(L6.EQ.1.AND.L7.EQ.1) DAT(6)=(DAT(6)-32.0)*5.0/9.0
14 CONTINUE
IF(L6.EQ.1) GO TO 12
DAT(11)=(DAT(1)+DAT(2))*0.5
12 CONTINUE
DAT(12)=SVP(DAT(11))
IF(L7.EQ.0) GO TO 13
C COMPUTE VALUE OF ED FROM WET BULB DATA
EW=SVP(DAT(6))
IF(DAT(6).LT.0.0) GO TO 11
DAT(13)=EW-7.99E-4*AMBPRS*(DAT(11)-DAT(6))
GO TO 15
11 DAT(13)=EW-7.20E-4*AMBPRS*(DAT(11)-DAT(6))
GO TO 15
13 DAT(13)=(DAT(6)*DAT(12))/15.0
15 CONTINUE
DAT(19)=DAT(13)/DAT(12)*100.0
C
RETURN
END

```

```

SUBROUTINE PFC(ETA,DAT,IDAY,Y,A,R,ELEV,AMBPRS,ALAT,RADIUS,
1DECLIN,SMS,SHSA1,SHSA2,SKD,SKDG1,SKDG2,SKDA1,SKDA2,ROOT,IGROW,
2LS,ALBEDO)
DIMENSION Y(9),RADIUS(366),DECLIN(366),DAT(40)
C
C SUBROUTINE COMPUTES THE VALUE OF
C ACTUAL EVAPOTRANSPIRATION
C
7FACT=8.64E04/2.47E06
GAMMA=AMBPRS*6.574E-04
DELTA=DEL(DAT(11))
IF(L5.EQ.0) GO TO 10
RADNET=DAT(9)/(59.0*7FACT)
GO TO 12
10 CALL PADIAT(DAT,RADIUS,DECLIN,ALAT,SKD,RADNET,A,R,SKDG1,
1SKDG2,SKDA1,SKDA2,SMS,IDAY,Y,SHSA1,SHSA2,IGROW,ALBEDO)
12 RHOCF=1.2*1.01E03
CALL RESIST(DAT,ROOT,SKDA1,SKDA2,RS,IGROW,SKD)
CALL VEG(IGROW,Z0)
CALL PUGH(S(DAT,RA,Z0))
X=2.47E06*(DELTA+GAMMA*(1.0+RS/RA))
FACT1=8.64E04*DELTA/X
FACT2=RHOCF*8.64E04/X
AERO=FACT2*(DAT(12)-DAT(13))/RA*(Y(7)+ELEV*5.0-5)
RADNET=RADNET*FACT1
ETA=RADNET+AERO
DAT(22)=IGROW
DAT(32)=RS
RETURN
END

```

```
SUBROUTINE DOWN(ETA, GLEV, SY, SMD, ROOTH, SMDMX, SMS, SMDA1, SMDA2)
```

```
ETA=ABS(ETA)
```

```
ROOTA=80.0
```

```
IF(ROOTA.GE.(ROOTH-35.0)) ROOTA=ROOTH-35.0
```

```
C
C
C
C
```

```
ROUTINE DISTRIBUTES ETA BETWEEN SOIL MOISTURE LOSS AND
EVAPORATION FROM THE GROUNDWATER TABLE++++++
```

```
IF(SMD.GT.SMDMX.OR.SMS.GT.0.1) GO TO 10
```

```
IF(SMD.LT.ROOTA) GO TO 12
```

```
IF(SMD.LT.SMDA1) GO TO 14
```

```
IF(SMD.LT.SMDA2) GO TO 13
```

```
AM=(1.0-0.85)/(SMDMX-SMDA2)
```

```
FALL=(SMD-SMDA2)*AM+0.85
```

```
GO TO 20
```

```
13 BM=(0.85-0.35)/(SMDA2-SMDA1)
```

```
FALL=(SMD-SMDA1)*BM+0.35
```

```
GO TO 20
```

```
14 CM=0.35/(SMDA1-ROOTA)
```

```
FALL=(SMD-ROOTA)*CM
```

```
20 GLEV=GLEV+FALL*ETA/SY
```

```
SMD=SMD+(1.0-FALL)*ETA
```

```
GO TO 11
```

```
12 SMD=SMD+ETA
```

```
GO TO 11
```

```
10 GLEV=GLEV+ETA/SY
```

```
SMD=SMD-ETA
```

```
11 IF(SMD.GT.SMDMX) SMD=SMDMX
```

```
RETURN
```

```
END
```

```
SUBROUTINE RESIST(DAT, ROOT, SMDA1, SMDA2, PS, IGROW, SFD)
```

```
DIMENSION DAT(40)
```

```
C
C
C
C
C
C
```

```
PURPOSE OF THIS SUBROUTINE IS TO MAKE AN ASSESSMENT
OF THE PS TERM IN THE MONTEITH EQUATION BASED ON SOIL
MOISTURE DEFICIT DATA
```

```
IF(IGROW.LT.1) GO TO 10
```

```
IF(IGROW.GT.50) GO TO 10
```

```
GM=FLOAT(IGROW)*(200.0/50.0)
```

```
PL=200.0-GM
```

```
GO TO 11
```

```
10 IF(SMD.LT.60.0) GO TO 14
```

```
BM=250.0/(100.0-60.0)
```

```
PL=(SMD-60.0)*BM
```

```
GO TO 11
```

```
14 PL=0.0
```

```
11 RC=50.0
```

```
IF(SMD.LT.SMDA1) GO TO 12
```

```
IF(SMD.GT.SMDA2) GO TO 13
```

```
AM=5000.0/(SMDA2-SMDA1)
```

```
PH=(SMD-SMDA1)*AM
```

```
GO TO 20
```

```
12 PH=0.0
```

```
GO TO 20
```

```
13 PH=5000.0
```

```
20 PS=RC+PH+PL
```

```
IF(DAT(1).GT.20.0) PS=0.0
```

```
RETURN
```

```
END
```

```

SUBROUTINE RADIAT(DAT,RADIUS,DECLIN,ALAT,SMD,RADNET,A,B,
1SMDG1,SMDG2,SMDA1,SMDA2,SMS,IDAY,Y,SMSA1,SMSA2,IGROW,ALBEDO)
DIMENSION DAT(40),RADIUS(366),DECLIN(366),Y(9)

```

```

SUBROUTINE CALCULATES THE RADIATION BALANCE AT THE
SITE AS MODIFIED BY A VARYING ALBEDO AND VARYING QUANTITY
OF HEAT LOSS TO THE GROUND. BOTH MODIFICATIONS ARE ONLY
EMPIRICAL.+++++++

```

```

DAT(19)=RADIUS(IDAY)
DAT(18)=DECLIN(IDAY)
X=0.0174532925
ABS=273.12
RLAT=ALAT*X
HR=ACOS(-1.0*TAN(RLAT)*TAN(DAT(18)))
DAT(15)=24.0*HR/(X*180.0)+0.11

```

```

COMPUTE INCOMING RADIATION

```

```

DAT(17)=1.3579E8/(X*180.0*(DAT(19)**2))*
1(HR*SIN(RLAT)*SIN(DAT(18))+COS(RLAT)*
2COS(DAT(18))*SIN(HR))

```

```

COMPUTE BACK RADIATION TERM

```

```

DAT(16)=((ABS+DAT(11))**4*5.67E-8)*
1(Y(4)+Y(5)*DAT(7)/DAT(15))*
2(Y(2)-Y(3)*SQRT(DAT(13)))*Y(1)

```

```

CALL GROUND(SMD,SMDG1,SMDG2,GFLUX)
CALL ALF(SMDA1,SMDA2,SMD,IGROW,ALBEDO,SMS,SMSA1,SMSA2)

```

```

RADNET=DAT(17)*(A+B*DAT(7)/DAT(15))*(1.0-ALBEDO)
RADNET=(RADNET-DAT(16))*(1.0-GFLUX)
DAT(30)=ALBEDO
DAT(31)=GFLUX
RETURN
END

```

```

SUBROUTINE GROUND(SMD,SMDG1,SMDG2,GFLUX)

```

```

SUBROUTINE CALCULATES THE PERCENTAGE OF NET RADIATION USED
FOR HEATING THE GROUND. IT IS ASSUMED THAT THIS CAN BE
AS HIGH AS 75% FOR VERY DRY SOIL CONDITIONS. SMDG1 AND
SMDG2 ARE VALUES OF SMD BETWEEN WHICH GFLUX CHANGES
BETWEEN 20 AND 75%.+++++++

```

```

AM=(0.75-0.20)/(SMDG2-SMDG1)
IF(SMD.GE.SMDG2) GO TO 11
IF(SMD.LE.SMDG1) GO TO 10
GFLUX=(SMD-SMDG1)*AM+0.20
GO TO 12
11 GFLUX=0.75
GO TO 12
10 GFLUX=0.20
12 RETURN
END

```

```
SUBROUTINE ALP(SMDA1,SMDA2,SMD,IGROW,ALBEDO,SMS,SMSA1,SMSA2)
```

```
SUBROUTINE CALCULATES THE ALBEDO OF THE SURFACE TO BE USED IN  
FINDING INCOMING RADIATION. BASED ON AN SMD AND SMS MODEL
```

```

C
C
C
C
I=0
IF(SMS.GT.SMSA1) GO TO 14
IF(SMD.GT.SMDA2) GO TO 14
IF(SMD.LT.SMDA1) GO TO 15
AM1=(0.35-0.15)/(SMDA2-SMDA1)
ALBEDO=(SMD-SMDA1)*AM1+0.15
IGROW=0
I=I+1
GO TO 13
14 ALBEDO=0.35
IGROW=0
I=I+1
GO TO 13
10 IF(SMS.LT.SMSA2) GO TO 11
15 IF(ALBEDO.GT(0.25) ALBEDO=0.25
ALBEDO=ALBEDO-0.0015
I=I+1
IF(ALBEDO.LT.0.15) ALBEDO=0.15
IGROW=IGROW+1
GO TO 13
11 AM2=(0.35-0.25)/(SMSA2-SMSA1)
ALBEDO=0.35-(SMS-SMSA1)*AM2
IGROW=IGROW+1
I=I+1
13 IF(I.EQ.0) ALBEDO=0.20
RETURN
END

```

```
SUBROUTINE VEG(IGROW,Z0)
```

```

C
C
C
C
ROUTINE CALCULATES Z0 PARAMETER REQUIRED FOR CALCULATION OF  
THE RA RESISTANCE TERM. CALCULATION BASED UPON TIME SINCE  
GROWING SEASON BEGAN+++++++
IF(IGROW.LT.1) GO TO 10
Z0=6.0+FLOAT(IGROW)
GO TO 11
10 Z0=6.0
11 IF(Z0.GT.110.0) Z0=110.0
RETURN
END

```

```
SUBROUTINE ROUGHS(DAT,RA,Z0)
```

```

C
C
C
C
SUBROUTINE CALCULATES THE VALUE OF RA, THE AERODYNAMIC  
RESISTANCE TERM+++++++
DIMENSION DAT(40)
U=DAT(4)*1000.0/2.64E04
RA=(ALG((2.0E03-0.0)/Z0))**2/(.41**2*U)
RETURN
END

```